Nanotechnologically modified cements

Effects on hydration, microstructure and physical properties

Papatzani, Styliani

Award date:
2015

Awarding institution:
University of Bath

Nanotechnologically modified cements: Effects on hydration, microstructure and physical properties

by

Styliani Papatzani

A thesis submitted for the degree of Doctor of Philosophy

University of Bath

Department of Architecture and Civil Engineering

December 2014

Nanotechnologically modified cements: Effects on hydration, microstructure and physical properties

Styliani Papatzani

A thesis submitted for the degree of Doctor of Philosophy

University of Bath

Department of Architecture and Civil Engineering

December 2014

ACKNOWLEDGEMENTS

To begin with, I would like to thank my two supervisors, Dr. K. Paine and Prof. P. Walker for giving me the opportunity to investigate the limits of my concrete will and nanomodified cement pastes. I owe special thanks to my first supervisor, Dr. K. Paine for allowing me the freedom to experiment with no hesitation. I believe that our collaboration was memorable and wish that our paths will cross again in the scientific field in the near future.

I would like to acknowledge the European Commission (FIBCEM project, grant number 262954) for funding of this research and the collaboration UKIERI for inviting me to India to carry out experiments and give a talk at the international meeting in New Delhi. Thank you Dr. K. Paine for nominating me for this event.

Furthermore, I would like to acknowledge the contribution of the following members of staff at the University of Bath:

Dr. J. Calabria-Holley for the time shared in the concrete labs during the first months of the FIBCEM project

Dr. A. Heath for his precious comments on XRD analysis and clay minerals

Mr. D. Stacey, our subject librarian, and the interlibrary loans' team

Dr. R. J. Ball for enriching my understanding in TEM crystallography and lime putty reactions

Dr. Nigel Treweeke for coping with my computers

Dr. J. Mitchels and Mrs. U. Potter for their precious guidance in the Microscopy and Analysis Suite

Prof. M. Weller for introducing me to the world of XRD & Dr. G. Kociok-Konh for carrying out the XRD tests of my samples

Prof. S. T. Newman for providing necessary insights

Dr. R. Kurchania for introducing me to the Indian culture in Bhopal

Mr. F. Acosta for introducing me to the world of TGA and MIP

Mr. D.A. Montoya for testing samples on the MIP

The king of the concrete labs, Mr. W. Bazeley, Mrs. S. Hayward, Mr. D. Williams and Mr. R. Dyer whose assistance was greatly appreciated

Arriving at this point, of writing the acknowledgements of my PhD thesis, has been a lengthy process, much longer than the actual duration of this research. Therefore, it is the right moment to remember and thank the following people in chronological order:

My influential teachers at state and private schools in Crete, my birthplace

My Cardiff University professors who laid the foundations for my future career and in particular Prof. R.A. Falconer, my tutor and the late Dr. T. Roberts, whose student I am proud to have been

Prof. H. Gulvanessian CBE, my Imperial College MSc dissertation supervisor and mentor; "Professor, thank you and your family from the font of my heart"

Prof. M. Loizidou and Prof. M. Kotsovos the supervisors of my other two MSc dissertation theses, at the National Technical University of Athens

Prof. I. Vaias and Prof M. Aftias for the research carried out at the National Technical University of Athens

Prof. R.D. Hooton for his support

My fellow colleagues and friends; Dr. Vaia Adamaki, my companion-in-arms in our expedition in India who made the whole trip absolutely memorable and Dr. S. Malek, A. Azzouz, A. Zografou and M. Nuño

In addition, I would like to say a profound "thank you guys" to G.P., A.M., K.V., K.K., G.G., S.T., S.D. and E.S. who have supported me from miles away.

Education is one thing, but what gives flavour and persistence in life is **upbringing** and having experienced **unconditional love**, making everything possible... For this, I owe gratitude to my family and especially to my mother.

[1]

Yours,

Stella

[1] Broken sample after a compressive strength test – shape 100% accidental!

ANTI THE PROLOGUE FROM THE WRITER

In this ocean of gnosis and systems' dynamics

the Socratic paradox persists: "I know one thing: that I know nothing[2]*".*

… One cannot know everything with absolute certainty no matter how far science is leading us. However, thorough investigation, can offer significant confidence in specific findings…

[2] In: Plato, Apology 21d or Plato, The Socratic Dialogues

ABSTRACT

Cement science and industry aim at the design of cement formulations with minimum Portland cement content. At the same time, nanotechnology is offering a combination of solutions towards stronger, less permeable and more durable cement.

In this research two different types of nanoparticles; nanosilica, nS, (aqueous and carboxylic nanosilica suspension) or nanoclay, nC, (inorganic and organomodified nanoclay dispersions and undispersed nanoclay powder) were implemented. Both, nS and nC were characterised with different techniques. Particularly the nC particles, were developed exclusively for the FIBCEM[3] project and, as an effect, their properties were investigated with XRD, TEM crystallography, TGA and SEM/EDX. The differences between the three fundamentally dissimilar types were identified and discussed. Furthermore, their nanostructure and characteristics were associated with expected performance in terms of mechanical strength and pozzolanic activity in cement pastes. Three different formulations constituted the reference pastes [containing Portland cement (PC), limestone (LS), fly ash (FA) (and microsilica only in combination with nS)]; (i) 60%PC/40%LS, (ii) 60%PC/20%LS/20%FA and (iii) 43%PC/20%LS/37%FA by mass of binder. The w/b ratio was generally kept constant at 0.3. The nS and nC particles were added to the reference pastes, creating ternary, quaternary or quinary (i) cement pastes, (ii) fibre cement pastes and (iii) mortar formulations.

The combined effect that the addition of the nanoparticles had on the strength was studied with a series of compressive or flexural strength tests at different ages. The effect that nS or nC had on the hydration products and microstructure of the nanomodified pastes was investigated with the help of XRD, TGA, SEM or FESEM, MIP, relative density measurements and impermeability tests at various ages.

The limits to the usage of the nanoparticles were drawn and the most advantageous combinations were discussed. In specific, it was found that the nS addition to blended or composite cement pastes should not exceed 0.5% of solids by mass of binder, especially in the presence of high quantities of FA. With the addition of up to 0.5% nS, both strength gain and microstructure of pastes can be enhanced. The nC particles showed significant diversity amongst them due to their high structural and chemical complexity. In most pastes, 1% nC solids by mass of binder addition was identified as the upper limit. The nCs were found to be partially pozzolanic, consuming $Ca(OH)_2$ to produce additional C–S–H. The OMMTs contained an excess of organomodifier, weakening their beneficial effects in Portland cement formulations. However, inorganic nC dispersions, although neglected for long, could offer new possibilities to cement science. In fact, the shape of the nC particles can even alter traditional characteristics of cement, by providing ductility to the pastes and can offer significant enhancements particularly in flexural strength. With the advancement

[3] FIBCEM: is a project funded by the European Commission under the 7th Framework Programme. The full project title is: Nanotechnology Enhanced Extruded Fibre Reinforced Foam Cement Based Environmentally Friendly Sandwich Material for Building Applications. The FIBCEM Consortium, led by Cembrit Holding A/S, consists of 10 project partners from 5 different European countries (United Kingdom, Spain, Italy, Lithuania and Denmark).

of nanostructural investigation techniques, more conclusive and innovative results are to be expected by the nanomodification of Portland cement blends.

KEYWORDS

Clay/Nanoclay /Organoclay/organomodified clay/inorganic nanoclay

Silica/Microsilica/Nanosilica

Limestone Portland cement

Nanomodified Portland cement formulations

Cement hydration

Microstructure

Porosity

Durability

Mechanical properties

ABBREVIATIONS

Paste constituent materials/chemicals/others

PC: Portland cement

OPC: ordinary Portland cement

LPC: limestone Portland cement

LS: limestone

μS: microsilica

nS: nanosilica

nC: nanoclay

nCs: nanoclays

MMT: Montmorillonite

OMMT: Organomodified MMT

SP: Superplasticizer

nC1: nC1 dispersion

nC2: nC2 dispersion

nC3: nC3 dispersion

nC4: nC4 powder

PVA: Poly Vinyl Alcohol

Stdv: standard deviation

Cement chemistry notations

P: Portlandite, calcium hydroxide, $Ca(OH)_2$

CC: Calcium Carbonate: $CaCO_3$

C–S–H: Calcium Silicate Hydrate

C–A–H: Calcium Aluminate Hydrate

S: SiO_2

w/b: water to binder mass ratio

w/c: water to cement mass ratio

CO_2: carbon dioxide

RH: relative humidity

Characterization techniques

TGA: Thermogravimetric Analysis

XRD: X-Ray Diffraction

SEM: Scanning Electron Microscopy

TEM: Transmission Electron Microscopy

MIP: Mercury Intrusion Porosimetry

FESEM: Field Emission SEM

TABLE OF CONTENTS

LIST OF FIGURES

LIST OF TABLES

LIST OF EQUATIONS

LIST OF CEMENT FORMULATIONS

Below is a list of the total number of pastes and mortars created in order to demonstrate the magnitude of the work carried out for the completion of this thesis. The analysis is covered in the relevant chapters.

10 binary and ternary starting cement pastes

6 μS enhanced quaternary cement paste formulations

15 nC enhanced ternary cement paste formulations

4 LnS enhanced ternary cement paste formulations

7 GnS enhanced quaternary cement paste formulations

4 LnS enhanced quaternary cement paste formulations

4 LnS & μS enhanced quinary cement paste formulations

4 GnS & μS enhanced quinary cement paste formulations

4 nC enhanced ternary fibre cement paste formulations

11 nC enhanced quaternary fibre cement paste formulations

4 nC enhanced quinary fibre cement paste formulations

7 nanomodified lime putty paste combinations

42 nanomodified mortar combinations

LIST OF EXPERIMENTS

Further to the previous list, the total number of tests for the completion of this thesis is presented below. All tests have been carried out and analysed by the author except for the MIP, PSD and XRD tests which were only analysed by the author.

Compressive strength tests: > 1500 samples in total

Approximately 20 x 4 x 6 + 20 = 500 cylindrical samples at different ages just for ternary nanomodified cement series

Approximately 20 x 4 x 6 + 20 = 500 cylindrical samples at different ages for quaternary and quinary nanomodified cement series

46 x 12 = 552 cubical samples at different ages for nanomodified mortar series

Flexural strength tests: > 230 samples in total

Arrest of hydration > 400 samples

XRD: 85 samples

FESEM: 24 samples

Impermeability: >20 samples

TEM: 8 samples of nS and nC

SEM/EDX: 8 samples of nS and nC

SEM: >40 samples

MIP: 26 samples on nC modified samples

Density: 208 samples in total

46 x 3 = 129 samples for nanomodified mortars

21 x 3 = 63 samples for nanomodified cements

8 x 2 = 16 fibre and nC reinforced samples

Particle Size Distribution: 4 samples

TGA: > 300 samples in total

20 lime putty + 20 bases + 18 ternary with μS + 45 ternary with nC + 50 ternary with LnS + 35 quaternary with GnS + 25 quaternary with LnS + 38 quinary with LnS+ μS/ GnS+ μS

+ 50 with fibres

LIST OF PUBLICATIONS/PRESENTATIONS

Papers 1 to 4 have been published, paper 5 has been accepted (1 to 5 are attached in Appendix-B) and the report (item 6) has been accepted by the EC.

1. **Papatzani S**, Paine K, Calabria-Holley J. 2015. A comprehensive review of the models on the nanostructure of calcium silicate hydrates. Construction and Building Materials; 74, 219–234.
2. **Папатзани, С**., Пэйн, К. & Калабрия-Холли, Д. 2014. Прочность и микроструктура цементного камня с добавками коллоидного sio2 (strength and microstructure of colloidal nanosilica enhanced cement pastes (in russian)). Цемент и его применение (Cement and its Applications), 4, 80-85.
3. Calabria-Holley J, Paine K, **Papatzani S**. 2014 Effects of nanosilica on the calcium silicate hydrates in Portland cement-fly ash systems. Advances in Cement Research.;26:1-14.
4. **Papatzani S**, Paine K, Calabria-Holley J, 2014 The effect of the addition of nanoparticles of silica on the strength and microstructure of blended Portland cement pastes. 2014 International Concrete Sustainability Conference, Boston.
5. **Papatzani S** & Paine K. Dispersed and modified montmorillonite clay nanoparticles for blended Portland cement pastes: Effects on microstructure and strength. NICOM5, Chicago, 2015; Accepted.
6. Calabria-Holley J, **Papatzani S**, Paine K. Fibcem deliverable D8.1 – FRC Skin Technical Report, 2014, approved by the E.C.

The following presentations have been carried out:

1. **Papatzani S**, (2013). Nanotechnologically modified cements: Effects on hydration, pore structure and physical properties. Invited speaker. International workshop on green building and sustainable technologies, New Delhi, 7-12-2013.
2. **Papatzani S**, (2014). The effect of the addition of nanoparticles of silica on the strength and microstructure of blended Portland cement pastes. 2014 International Concrete Sustainability Conference. Boston 2014.
3. **Papatzani S**, (2013). FIBCEM project meeting September 2013, Bath: nanoclay modification of fibre reinforced cements - supervised by EU representative.
4. **Papatzani S**, (2014) FIBCEM project meeting January 2014, Bath: New findings on nanoclay modification of fibre reinforced cements - supervised by EU representative.
5. **Papatzani S**, (2014). FIBCEM project meeting May 2014, Madrid: nanoclay modification of fibre reinforced cements and nanoclay modifications of Potland limestone cements - supervised by EU representative.

1 INTRODUCTION

1.1 Background

Cement production has raised environmental concerns with regards to the amount of CO_2 emitted during Portland cement clinkering. The total contribution of the cement industry to the global manmade CO_2 emission reaches 8%, not taking into account the energy consumed for the rest of the industrial processes (Olivier *et al.*, 2012; Meyer, 2009; Mindess and Young, 1981). It has, therefore, become a priority to develop cements in which Portland cement clinker is limited to the maximum, primarily by substituting it with materials, such as fillers, for instance limestone, and/or pozzolanic by-products, for example fly ash or microsilica.

The need for sustainability in construction is calling for more durable and more eco-friendly concretes and consequently cements. Knowing the application for which a concrete is intended (exposure conditions, use, availability of raw materials, and others), the cement paste, which is a highly engineered material, can be designed to meet specific requirements in terms of properties and performance. It can therefore become "greener" not only through the process of replacing Portland cement by supplementary cementitious materials but also by creating a novel blend of constituents that improves the durability and the life span of structures. In this way, cement science can provide the bridge between structural design and protection of natural resources especially taking into consideration the world-wide concern with respect to the deterioration of concrete structures and the need to preserve them for longer periods. This requirement has sparked research towards understanding the internal structure of cement and investigating the modifications applicable in the sub-micron to nanolevel.

Recent research has demonstrated that using nanoparticles, has a significant effect on the chemical reactions taking place during cement hydration with effects at the macro level; that is to say, mechanical characteristics and durability of the hardened cement paste. The main reason for such modifications in the material behaviour as it decreases to the nanosize so that the specific surface area is multiplied. The nanoparticles are more chemically reactive, since a greater surface area is available for reactions (Lim *et al.*, 2012; Oltulu and Sahin, 2011; Björnström *et al.*, 2004) or they strengthen the nanostructure by minimising the nanosized pores (0.5 to 5 nm wide) within the calcium silicate hydrates or both (Bi *et al.*, 2012; Al-Otaibi, 2012; Aly *et al.*, 2011; Vera-Agullo *et al.*, 2009; Morsy *et al.*, 2009; Sobolev *et al.*, 2009a; Chang *et al.*, 2007).

The field of science focusing on the study, experimentation and observation of phenomena and modification of materials at atomic and molecular level is known as "*nanoscience*", whereas the design, characterisation, manufacturing and application of materials limited to the nano-size is termed, "*nanotechnology" (Arivalagan et al., 2011).* As for the definition of nanomaterial or nanoparticles, the European Commission in 2011 specified that: "'*Nanomaterial' means a natural, incidental or manufactured material containing particles, in an unbound state or as an aggregate or as an agglomerate and where, for 50 % or more of the particles in the number size distribution, one or more external dimensions is in the size range 1 nm-100 nm. In specific cases and where warranted by concerns for the environment, health, safety or competitiveness the number size distribution threshold of 50% may be replaced by a threshold between 1 and 50 %."(Commission, 2011, p.40).* Other definitions are given on the grounds of surface area which should not be greater than $6x10^7$ m^2/m^3, stressing the criticality of this parameter (Napierska *et al.*, 2010).

The addition of nanomaterials in cement formulations opens a new horizon to the research and industry; to the extent that many researchers consider nanotechnology as bringing about the next industrial revolution (Sobolev *et al.*, 2006). This is because the manipulation of matter at the nanolevel has been achieved and the observation of the resulting changes at the nanolevel, can also be realized. In light of this, nanotechnologically enhanced cement composites can be engineered to exhibit improvements in strength and durability (Raki *et al.*, 2009). Some of the nanoparticles more extensively researched in the cement industry are nano titanium dioxide (nano-TiO_2) (Lee and Kurtis, 2010), nano-Fe_2O_3 (Li *et al.*, 2004a), nanoalumina (nano-Al_2O_3) (Li *et al.*, 2006), nanosilica (nano-SiO_2) (Rashad, 2014; Papatzani *et al.*, 2014), nano-clays (Chang *et al.*, 2007; Kuo *et al.*, 2006), nanolimestone (nano-$CaCO_3$) (Camiletti *et al.*, 2013; Liu *et al.*, 2012) and others. With the evolution of nanotechnology researchers have gained more insight into the parameters affecting the products of cement hydration, the structure of which is nanosized. Therefore, one of the most stimulating questions to be answered, is what effect would the addition of nano-particles have on the hydration of cement? Are some nanoparticles pozzolanic materials in their own right and therefore produce additional calcium silicate hydrate (C–S–H) responsible for the mechanical strength and the durability of the paste or do they primarily act as nucleation centres or as catalysts for cement hydration? This subsequently raises more questions, such as how does the hydration chemistry change, how are the mechanical properties modified and what would, then, be the optimal proportions in such novel blended cement formulations?

1.2 Aims and objectives

This research was designed to add to the fundamental knowledge on the mechanisms activated by the addition of two types of nanoparticles, nanosilica and nanoclay, in blended cement formulations. Whilst there has been some research on the use of nanosilica particles, as revealed in the literature review (Chapter 2), there is much inconsistent or contradictory

research on its effects and limits when blended with Portland cement. Adding to this, the greater the number of constituents in a cement formulation, the more complicated it is to investigate and interpret the effect the nanoparticles have within this complex matrix. As far as the nanoclay particles are concerned, very few papers have been published on their use in cement formulations, most of which are targeted at uses other than structural applications of cement (e.g. road paving or pollutant absorption). Furthermore, the nanoclay particles used in this research, were specially developed for the FIBCEM project and as an effect, they have never been used before. For the two streams of study evolved (emerging through the addition of two different types of nanoparticles), it was of particular interest, to (i) define their potentials (e.g. pozzolanic materials or nanofillers) by characterizing them, (ii) devise a methodology by which they would be incorporated in the formulation and (iii) investigate their effect on, firstly, the hydration of the cement formulation, secondly, the microstructure and thirdly the relation of the two latter ones with the mechanical properties of blended cement pastes. These parameters were compared with non-nanomodified formulations.

The specific aims and objectives, as unfolded in each chapter, are outlined below:

i. to define the state of the art on the potentials of nanomodifications of cement pastes and main factors affected (Chapter 2)
ii. to identify the umresolved issues with respect to the addition of nanosilica and nanoclay particles (Chapter 2)
iii. to select the appropriate experimental tools to study the identified issues (Chapter 2)
iv. to select the parameters to be studied with the experimental tools; and to carry out characterization and preliminary assessment of the potentials of the selected nanomaterials (Chapter 3)
v. to devise a sequence of formulations with which the various parameters will be investigated (Chapter 4)
vi. to obtain information on the behaviour of non-nanomodified blended cement formulations (Chapter 5)
vii. to identify possible competing constituents in high order cement formulations (Chapter 5)
viii. to evaluate the effect the addition of nanoparticles has on the hydration, microstructure and mechanical properties of the blended cement formulations, as compared with the non-nanomodified ones (Chapters 6-9)
ix. to draw limits on the amounts of both types of nanoparticles used in the formulations (Chapters 6-9)
x. to identify possible competing constituents with the nanoparticles (Chapters 6-9)
xi. to extend the application to fibre cement pastes and analyse the effect on the three main parameters; hydration, microstructure and mechanical properties (Chapter 9)
xii. to define interesting areas of further research (Chapter 10)

1.3 Outline of thesis

This research work is comprised of ten chapters in total:

Chapter 2 constitutes the literature review. Four distinctive areas have been covered; Firstly, cement hydration, from the viewpoint of calcium silicate hydrate (C–S–H) production and a concise discussion on the models suggested to describe C–S–H until present, is made. Secondly, the state of the art on the influence of the addition of nanosilica particles in Portland cement formulations is presented. Thirdly, the state of the art on the influence of the addition of nanoclay particles in Portland cement formulations is discussed. Contradictions and omissions in literature have been identified. Fourthly, the experimental techniques employed for this research program are outlined.

In Chapter 3 the material characterization methods and the material preparation methods according to the techniques they will be tested with are described. Next, the characterization of the constituent micro and nanosized materials used, with an initial estimation of their possible effects when added to cement formulations is also included.

In Chapter 4, the programme of work is exhibited. Due to the number and variety (cement pastes, fibre reinforced cement pastes and mortars) of formulations investigated, an analytical presentation on the sequence of their design and testing is made, along with the reasoning behind the selection of the specific combinations to be produced and tested. Chapter 4 also contains the methodology followed for mixing, casting and demoulding.

In Chapter 5, the compressive strength and microstructural characteristics of binary, ternary and quaternary, non-nanomodified, Portland cement blends are presented and discussed.

In Chapter 6, the compressive strength, hydration and microstructural characteristics of ternary nanosilica modified cement formulations is discussed.

In Chapter 7, the ternary blends of Chapter 6 are taken two levels of complexity further, by studying the performance of quaternary and quinary nanomodified formulations. Two different types of nanosilica solutions are used, tested, analysed and compared. Some of the compressive strength results of the cement pastes are also reinforced by the equivalent results of the mortars. In the quinary formulations the performance of nanosilica and microsilica modified cement formulations, is investigated with respect to the same criteria (compressive strength, hydration and microstructural characteristics).

In Chapter 8, the performance of ternary nanoclay modified cement formulations is discussed in terms of compressive strength, hydration and microstructural characteristics. Three different types of nanoclays are used, tested, analysed and compared. The results on the compressive strength of the cement pastes are also reinforced by the equivalent results of the mortars.

In Chapter 9 an application of the nanoclay modification is developed in ternary and quaternary fibre cement pastes. A full series of results is presented and analysed. Lastly, an investigation of flexural strength of quinary nS and nC modified fibre cement combinations is carried out to facilitate the discussion on the future research suggestions.

In the last chapter, 10, the main conclusions are summarized and the future research suggestions are made.

2 LITERATURE REVIEW

2.1 Introduction

In this section, the history of the evolution of cement towards the era of nanotechnology is presented, with a thorough investigation of the characteristics and properties the traditional materials and nanomaterials possess, and the effect they induce when combined. The most distinctive chemical processes are discussed, and a state of the art is presented on how the cement hydration process can be enhanced with the use of nanotechnology. Inconsistencies, omissions and discrepancies between the published studies were also identified.

2.2 Constituents of traditional blended cements and combinations:

2.2.1 Portland cement

Cementing materials have been used over the millennia, however, according to Hewlett (2004) based on earlier work, the Great pyramid was constructed by burning gypsum and the actual use of lime can be traced back to the prehistoric Crete. This bronze age civilization that flourished in Crete, the Minoans, was also acquainted with the use of crushed potsherd to add to the hydraulicity of the lime mortar. The knowledge was passed to ancient Greeks and Romans who later used volcanic deposits such as volcanic tuff from the island of Santorini in Greece or the Pozzuoli area of Italy (Hewlett, 2004; Neville, 1995). One of the better preserved ancient buildings, the Pantheon, built in approximately 200 A.D. was built of concrete (Mindess and Young, 1981). The evolution of techniques and mixing compositions brought us through the Middle Ages to 1824, when Joseph Aspdin patented ‘Portland cement’. This constituted a milestone in the cement history, as it was the first cement produced by a mixture of finely-ground clay and limestone in a heated furnace in which CO_2 had been burnt off. In 1945 Isaac Johnson, increased the heating temperature and literally burnt a mixture of clay and chalk until clinkered, forming a strong cementing mix. Since then, a number of multiple manufacturing processes have evolved, details of which, such as clinkering temperature and duration, phase equilibria, emissions and others can be studied in the literature (Ylmén, 2013; Sorrentino, 2011; Hewlett, 2004; Mindess and Young, 1981). Moreover, the basic characteristics of clinkering in the kiln, CO_2 emission and naming on the basis of Portland cements are, nowadays, established and standardised. Portland cement nowadays is made by grinding clinker and a little added gypsum. Clinker is a nodular material before it is ground up and the nodules can be anything from 1 mm to 25 mm in diameter.

As far as the composition of Portland cement (PC) is concerned, lime, silica, alumina and iron oxides are the main components (Table 2-1) forming anhydrous crystalline compounds (Table 2-2), the silicate phases of which, are alite (impure C_3S) and belite (impure C_2S). The impurities in the silicate phases emerge from the clinkering process, in which iron and alumina are also present in the raw materials. For this reason, the impurities do not have a negative connotation, but are referred to as the first reason for the variability of PC.

Table 2-1: Ideal oxide composition limits of PC clinker (Neville, 1995)

Name of Oxide	Chemical formula	Cement science notation	Mass (%)
Calcium oxide	CaO	C	60-67
Silicon dioxide	SiO_2	S	17-25
Aluminium oxide	Al_2O_3	A	3-8
Ferric oxide	Fe_2O_3	F	0.5-0.6
Sulfate	SO_3	Š	2-3.5
Magnesium Oxide	MgO	M	0.5-4.0
Alkalis	Na_2O and K_2O	N,K	0.3-1.2

Table 2-2: Typical compound composition of PC clinker (Neville, 1995)

Cement science notation	Chemical formula of compound	Name of Compound	Mineral Phase	Mass (%)
C_3S	3 CaO • SiO_2	Tricalcium silicate	Alite	45-75
C_2S	2 CaO • SiO_2	Dicalcium silicate	Belite	7-32
C_3A	3 CaO • Al_2O_3	Tricalcium aluminate	Aluminate	0-13
C_4AF	4 CaO • Al_2O_3 • Fe_2O_3	Tetracalcium alumino ferrite	Ferrite	0-18

The two silicate phases constitute approximately 75% of the PC clinker and it is these two phases and particularly alite, which are responsible for the majority of the environmental impact of modern PC. In fact, alite is formed last and contains more calcium, therefore more energy is required for its clinkering. As an effect, the higher the alite content in a cement mix, the greater the environmental impact it has. Cement science is, hence, focusing on the design of low CO_2 footprint PC based cements by (i) either reducing the C_3S content (MIT, 2013) in PC or (ii) by reducing the amount of PC itself in the cement paste formulations, with the use of supplementary cementitious materials (SCM), creating blended cements (Lothenbach *et al.*, 2011). In fact, 27 products incorporating SCMs are identified by the European Standardization Committee in the family of Portland cements and are presented in Table 2-3.

In this thesis the second strategy was adopted. On top of that, alongside trying to reduce CO_2 footprint, the work presented herein, was also aimed at increasing performance, to achieve durability, hence Long-term energy savings. Of the various SCMs available, namely, fly ash, silica fume, limestone, ground granulated blastfurnace slag, metakaolin, and others, the first two and in some cases the third, as well, were selected for the design of the cement paste formulations, as according to researches, fly ash (FA) and limestone (LS) have the lowest CO_2 footprint (Jones *et al.*, 2011; MPA, 2011). The SCMs are broadly divided into two categories; filler aggregates and pozzolanas.

Table 2-3: The family of common cements (CEN, 2000)

Main types	Notation of the 27 products (types of common cement)		Composition [percentage by mass [a)]]										
			Main constituents										Minor additional constituents
			Clinker	Blast-furnace slag	Silica fume	Pozzolana		Fly ash		Burnt shale	Limestone		
						natural	natural calcined	siliceous	calca-reous				
			K	S	D [b)]	P	Q	V	W	T	L	LL	
CEM I	Portland cement	CEM I	95-100	–	–	–	–	–	–	–	–	–	0 to 5
CEM II	Portland-slag cement	CEM II/A-S	80 to 94	6 to 20	–	–	–	–	–	–	–	–	0 to 5
		CEM II/B-S	65 to 79	21 to 35	–	–	–	–	–	–	–	–	0 to 5
	Portland-silica fume cement	CEM II/A-D	90 to 94	–	6 to 10	–	–	–	–	–	–	–	0 to 5
	Portland-pozzolana cement	CEM II/A-P	80 to 94	–	–	6 to 20	–	–	–	–	–	–	0 to 5
		CEM II/B-P	65 to 79	–	–	21 to 35	–	–	–	–	–	–	0 to 5
		CEM II/A-Q	80 to 94	–	–	–	6 to 20	–	–	–	–	–	0 to 5
		CEM II/B-Q	65 to 79	–	–	–	21 to 35	–	–	–	–	–	0 to 5
	Portland-fly ash cement	CEM II/A-V	80 to 94	–	–	–	–	6 to 20	–	–	–	–	0 to 5
		CEM II/B-V	65 to 79	–	–	–	–	21 to 35	–	–	–	–	0 to 5
		CEM II/A-W	80 to 94	–	–	–	–	–	6 to 20	–	–	–	0 to 5
		CEM II/B-W	65 to 79	–	–	–	–	–	21 to 35	–	–	–	0 to 5
	Portland-burnt shale cement	CEM II/A-T	80 to 94	–	–	–	–	–	–	6 to 20	–	–	0 to 5
		CEM II/B-T	65 to 79	–	–	–	–	–	–	21 to 35	–	–	0 to 5
	Portland-limestone cement	CEM II/A-L	80 to 94	–	–	–	–	–	–	–	6 to 20	–	0 to 5
		CEM II/B-L	65 to 79	–	–	–	–	–	–	–	21 to 35	–	0 to 5
		CEM II/A-LL	80 to 94	–	–	–	–	–	–	–	–	6 to 20	0 to 5
		CEM II/B-LL	65 to 79	–	–	–	–	–	–	–	–	21 to 35	0 to 5
	Portland-composite cement [c)]	CEM II/A-M	80 to 94	<---------- 6 to 20 ---------->									0 to 5
		CEM II/B-M	65 to 79	<---------- 21 to 35 ---------->									0 to 5
CEM III	Blastfurnace cement	CEM III/A	35 to 64	36 to 65	–	–	–	–	–	–	–	–	0 to 5
		CEM III/B	20 to 34	66 to 80	–	–	–	–	–	–	–	–	0 to 5
		CEM III/C	5 to 19	81 to 95	–	–	–	–	–	–	–	–	0 to 5
CEM IV	Pozzolanic cement [c)]	CEM IV/A	65 to 89	–	<---------- 11 to 35 ---------->					–	–	–	0 to 5
		CEM IV/B	45 to 64	–	<---------- 36 to 55 ---------->					–	–	–	0 to 5
CEM V	Composite cement [c)]	CEM V/A	40 to 64	18 to 30	–	<-------- 18 to 30 ------>			–	–	–	–	0 to 5
		CEM V/B	20 to 38	31 to 50	–	<-------- 31 to 50 ------>			–	–	–	–	0 to 5

a) The values in the table refer to the sum of the main and minor additional constituents.
b) The proportion of silica fume is limited to 10 %.
c) In Portland-composite cements CEM II/A-M and CEM II/B-M, in Pozzolanic cements CEM IV/A and CEM IV/B and in composite cements CEM V/A and CEM V/B the main constituents other than clinker shall be declared by designation of the cement (for example see clause 8).

2.2.2 Filler aggregates

Filler aggregates, commonly known (and here also referred to as fillers) are finely ground materials believed to be chemically inert which due to their fineness, have a beneficial effect on consistence, permeability, packing, bleeding or cracking tendency. LS, the most extensively used filler, is a sedimentary rock, consisting mainly of the minerals calcite and aragonite, the two most common crystal forms of calcium carbonate ($CaCO_3$). LS, when used as a filler, has a specific surface area of about 800 m^2/kg, depending on the fineness. It can have a nucleation role for cement hydration, especially if combined with smaller than 1 μm particles of FA and it can also form part of the calcium silicate hydrate (C–S–H) (Neville, 1995, p.88). An interesting remark is provided by Neville (1995), who suggested that since the addition of LS is provoking mainly physical effects, if the paste contains high proportions of LS, the cement should be finer than typical. However, an opposing view has been provided by Vuk *et al.* (2001) who concluded that limestone addition in traditional mixes is more influential with respect to the clinker type rather than cement fineness. Portland limestone cements are broadly used in Europe and as can be seen in Table 2-3 two classes exist in EN 197-1; CEM II/A-L and CEM II/B-L in which the maximum contents of LS are 20 and 35% respectively. Two further distinctions have also been made with respect to the total organic carbon (TOC); LL: when TOC does not exceed 0,20 % by mass and L: when TOC does not exceed 0,50 % by mass (CEN, 2000).

2.2.3 Pozzolanas

Any inorganic material containing silica or alumina in a reactive form that hardens in water when mixed with materials containing calcium hydroxide or with materials that release $Ca(OH)_2$, is termed a pozzolana (Hewlett, 2004). The pozzolanic reaction results in the production of additional C–S–H, but as a counterpart the early strength gain and setting is retarded (Mindess and Young, 1981). For silica to be reactive it must be amorphous, or glassy. ASTM 618-94a gives a more detailed description of pozzolanas as “a siliceous or siliceous and aluminous material which, in itself, possesses little or no cementitious value but which will, in finely divided form and in the presence of water, react chemically with calcium hydroxide at ordinary temperature to form compounds possessing cementitious properties” (ASTM, 2012).

Fly Ash

Fly ash (FA) is one of the most common synthetic pozzolanas. It is an industrial by-product, a residue generated by the combustion of coal. The quantities of FA produced vary with demand for electricity (Dhir et al., 2002). In the UK, coal-based FA production is predicted to partially give way to biomass FA (Heath et al., 2013). Where coal-based FA needs to be disposed of, significant costs are incurred. Particularly in the UK just 55% of FA is suitable for binders (McCarthy et al., 2008). FA is a glassy silicate, its particles are spherical (with a typical diameter of about 20 μm) and has a high specific surface area (typically between 300 - 500 m^2/kg) rendering it highly reactive. Due to this, water demand and intrinsic

permeability is minimized (Dhir *et al.*, 1997), as an effect, bleeding, segregation and consistence are improved (Dhir et al., 2002). Moreover, FA can assist with chloride resistance, as increase in the FA content can result in up to 50% increase in chloride binding (Dhir *et al.*, 1997). However, pastes in which FA has been added, exhibit a low rate of strength gain, averting its use in cases were early strength is a prerequisite (McCarthy and Dhir, 2005; Dhir et al., 2002). It should be noted that when added to cement, the product is nearly always darker, because of the unburnt carbon component, which could be important if aesthetics is an issue (Neville, 1995).

Microsilica

Microsilica is referred to as silica fume in BS EN 197-1. However, in this research, microsilica was the preferred term and was abbreviated as μS, to denote the scale difference with nanosized particles of silica. Microsilica is often a by-product of the silicon industry and it is one of the most expensive additions, due to the improvement it brings about in strength and durability when added in cement combinations. It is produced in powder form, has a spherical shape with an average diameter of about 0.1 μm and is 100 times finer than ordinary cement with a specific surface area of approximately 20,000 m^2/kg. Its colour is light grey and it consists of at least 85% amorphous SiO_2. It can be mixed in three forms: undensified, densified or pelletized (Hewlett, 2004). It exhibits a dual action of a pozzolana and of a filler material. As far as the former is concerned, the highly reactive amorphous silica it contains undergoes a rapid reaction with $Ca(OH)_2$ during cement hydration, as discussed in paragraph 2.3.4 and as far as the latter is concerned, the very small spherical particles fill the pores of the paste, improving particle packing. As a result, the mechanical properties and durability of concretes in which μS is added, are enhanced (Bi *et al.*, 2012). It is interesting to note that financial savings can be achieved as the addition of small amounts μS in the mix can save larger amounts of cement, for the same properties (Fares and Khan, 2013). As seen in Table 2-3 the amount of μS allowed in European cements cannot exceed 10%.

2.3 Blended cement hydration

The reaction of anhydrous cement powder with water is termed hydration, a process inducing several chemical reactions taking place with time, transforming cement paste into a firm, hard and insoluble mass. Most of the principal properties of the hardened cement paste are attributed to the hydration products, and for this, the study of the related process is of utmost importance. In this section a short presentation of the main characteristics of Portland cement hydration, is given and the main differences brought about by the addition of limestone, pozzolanas or nanoparticles are discussed, leading the discussion to more complex issues such as the structure of the cement hydration product at the nanolevel.

2.3.1 Portland cement hydration

When the two major compounds of cement, that is to say the silicate phases (C_3S and C_2S), react with water two very significant products are formed; crystalline calcium hydroxide and an almost amorphous calcium silicate hydrate, abbreviated as C–S–H, which comprises over 60% of the hydration products in total. The hyphens imply that the stoichiometry is not constant. The specific surface area of C–S–H ranges between $7x10^4$ and 10^5 m^2/kg of dry paste measured by the small angle scattering method (Jennings *et al.*, 2008) and for this it is usually described as gel. However, there are many reasons for calling C–S–H a gel and surface area is not the main one. Under X-ray diffraction C–S–H is amorphous, which in fact could constitute another criterion, as discussed later. Furthermore, the setting and hardening of cement is primarily determined by the physical properties of the C–S–H. In particular, the setting time and the early strength development of cement is attributed to the hydration of alite, whereas the strength development up to one year is related to the hydration of belite (Ridi *et al.*, 2011). It should be noted that the hydration of these two major compounds, the silicate phases, is often considered individually, for simplicity. Effectively, strength, shrinkage and durability of the hardened cement paste can be attributed to the C–S–H (Ridi *et al.*, 2011; Alizadeh, 2009; Neville, 1995).

The chemical formulas expressing the hydration of alite and belite can only be approximated, respectively, as (Brouwers, 2003);

$$C_3S + (3 - x + y)\,H \rightarrow C_xSH_y + (3 - x)\,CH \qquad \text{Equation: 2-1}$$

$$C_2S + (2 - x + y)\,H \rightarrow C_xSH_y + (2 - x)\,CH \qquad \text{Equation: 2-2}$$

Where x, y are not necessarily integers, C = CaO, Si = SiO_2, H = H_2O, CH = $Ca(OH)_2$ and x = C/S.

Apart from C–S–H, the second main hydration product is calcium hydroxide ($Ca(OH)_2$). Due to the presence of impurities during its production, the mineralogical term, portlandite, is often adopted. The monitoring of the portlandite level is significant, as it can yield information on the reactivity of pozzolanas (Dyer *et al.*, 1999).

The hydration of belite produces a C–S–H, different to the one produced by the hydration of alite in terms of (i) the C/S ratio and (ii) the chemically bound water (Bye, 2011).

The molar ratio of calcium to silicon (C/S) is one of the most determinant parameters for the structure of C–S–H. This ratio ranges from 0.7 to 2.1. The higher values may be obtained under extreme hydration or curing conditions and the lower values in presence of supplementary cementitious materials (Lothenbach *et al.*, 2011). C–S–H has been historically classified according to the C/S value. In fact, Taylor (Taylor, 1950) suggested

an average value of 1.5, dividing C–S–H in two categories; C–S–H (I), when C/S < 1.5 and C–S–H (II) when C/S > 1.5. Nonat (Nonat and Lecoq, 1998), further divided the first category into two; C–S–H (α) for C/S < 1.0 and C–S–H (β) for 1 < C/S < 1.5. C/S is affected by the clinker components and their particle size distribution, degree of hydration of PC (and curing conditions), age of the paste (Alizadeh, 2009; Yang, 2006) and addition of supplementary cementitious materials (Lothenbach *et al.*, 2011). A reduction in C/S, causes an increase in the mean length of the silicate chains and the interlayer distance, affecting C–S–H structural morphology.
The products of hydration are summarized in the table below:

Table 2-4: Hydration Products

Abbreviation	Chemical formula of compound	Name or Mineral Phase
CH	$Ca(OH)_2$ or $CaO \cdot H_2O$	Calcium hydroxide/ **portlandite**
C–S–H	$2(CaO) \cdot SiO_2 \cdot 0.9\text{-}1.25(H_2O)$, and/or; $0.8\text{-}1.5(CaO) \cdot SiO_2 \cdot 1.0\text{-}2.5(H_2O)$	Calcium Silicate Hydrate
C-A-H	not clearly defined	Calcium Aluminate Hydrate
AFt	$C_3A\check{S}_3H_{30\text{-}32}$	Aluminate Ferrite trisulfate/ **ettringite**
AFm	$C_2A\check{S}H_{12}$	Aluminate Ferrite monosulfate/ monosulfate
C_3AH_6	$3CaO \cdot Al_2O_3 \cdot 6\ H_2O$	Hydrogarnet

The inherent versatility in the stoichiometry of hydration products, the chemical reactions involved and the time sequence in which they are taking place has made the study of the stages of hydration process a very challenging topic, along with the study of the structure of C–S–H and its evolution. Ridi et al (2011), Bye (2011), Vogt (2010), Dyer *et al.* (1999) and Neville (1995) provided schematic representation of the phases, with slight differences in the models suggested. In essence, the stages are identified with respect to the heat released with time, defined primarily by isothermal conduction calorimetry. This method also allows for the study of retardation or acceleration of PC hydration according to the composition of the paste (Dyer *et al.*, 1999).

The stages are presented in the following graphs:

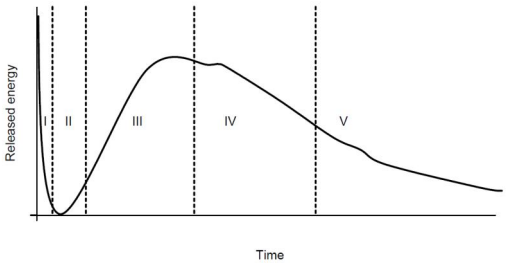

A. Phases of hydration (Vogt, 2010)

I: the induction period, II: the dormant period
III: the acceleration period, IV: the deceleration period, steady period

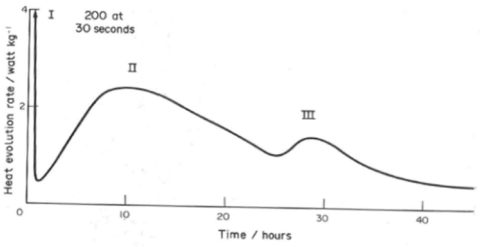

B. Hydration of PC (w/b=0.4) (Bye, 2011)

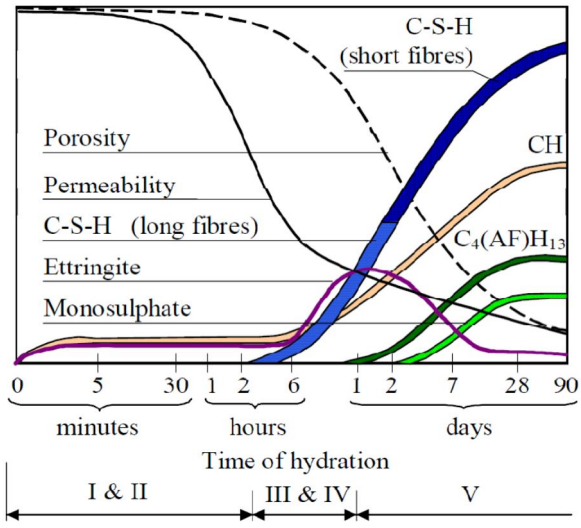

C. Microstructure development (Vogt, 2010)

Figure 2-1: Phases of hydration and microstructure development-hydrate phase formation in the main hydration phases

Amongst the various models that have been published, Ridi et al (2011), Vogt (2010) and Hewlett have adopted the five phase model, depicted in Figure 2-1.A, which will be described in short. Neville (1995) and Bye (2011) distinguish three peaks, Figure 2-1.B, which divide the stages but in practice, phase I is combined with II and phase III with IV, according to the classification provided by the formerly referenced researchers. When water is added to cement the highest amount of heat is released and the induction period starts with aluminate and alite reacting instantly, to produce ettringite and $Ca(OH)_2$, respectively. The dissolution of alite provokes saturation, further hydration is impeded and after 0.5 to 1 hours the dormant period (II) begins. In phase II, in a period of 5-15 hours the first long needle-like C–S–H and ettringite are formed around clinker particles, creating a shell-like structure and further slowing down hydration. In phase III the released energy is increased, reaching a peak, as the hydration products, that is to say portlandite and needle like C–S–H and ettringite, are interacting. Specifically, densification and setting is initiated as portlandite fills the space between the clinker particles which in turn are surrounded by a larger C–S–H shell. In the deceleration period, as is implied by its name, reactions slow down again, while the remaining C_2S and C_4AF are depleted and the products of hydration diffuse through the pores. In the steady period the remaining clinker particles hydrate and monosulfate is formed. According to Bye (2011) not all cements can create the third peak shown in his model, Figure 2-1.A. In Vogt's thesis other models are also discussed, associating hydration with pH values (Vogt, 2010). Lastly, the model of Ridi *et al.* (2011) exhibits an abrupt decrease in heat evolution in the deceleration period.

2.3.2 Cement paste microstructure

Having touched upon the topic of hydration products, a short reference to the microstructure of the hardened cement paste is necessary. The hydrated cement paste consists of solids, voids and water. In Table 2-4 the solid hydration products are listed. Residual unhydrated cement should also be regarded in the solids of the paste. The strength of the paste is highly affected by the amount of pores present and their distribution. As a matter of fact, cylinder compressive strength (f_c) and porosity (p) are inversely related (Kurtis, 2007):

$$fc = k(1-p)^3 \qquad \text{Equation: 2-3}$$

Where k = strength of voidless mortar (~ 234 MPa)

It is acknowledged that a number of different definitions exist with respect to the pore sizes and characteristics. The water-filled pores in the fresh paste are called capillary pores and the water is termed capillary water, whereas the nanosized pores in the interlayer space within the gel itself are called gel pores. The latter have a nominal diameter of 0.5-3 nm, while the former lie in a range of 1 μm to 100 nm and have an irregular shape. In capillaries of diameter up to 50 nm, removal of water results in shrinkage because new attractive forces can form between the C–S–H surfaces. In capillaries of diameter from 50 to 100 nm, water is in the form of "free water", it is not attracted by forces on the surface of solids and its removal does not yield volume changes. Capillary pores are created from the excess of water in the paste; they are interconnected and largely responsible for the permeability of the hardened paste and its susceptibility to freezing and thawing. As hydration progresses (affected by curing time, temperature or relative humidity) the volume of the capillary pores is reduced (Figure 2-2). Gel pores occupy about 28% of the total volume of gel. Unlike capillary pores, the gel pores' volume is independent of the water/cement ratio or the degree of hydration. As the total volume of gel increases, the volume of the relevant pores increases, too. In general, the micropores (<50 nm) are significant for drying shrinkage and creep, while the macropores (> 50 nm) affect strength and permeability (Bye, 2011). Last but not least, there is entrained air (purposely trapped air in the mix, usually with the help of admixtures) in the form of spherical voids of 70-500 μm in size, that mainly increase freeze/thaw resistance and irregular voids of entrapped air (air trapped due to, for example, inadequate compaction), varying in size (often larger than 1 mm), usually exhibiting a distorted shape and accounting for 1-2% in most concrete mixes (Alizadeh, 2009; Neville, 1995; Kurtis, 2007).

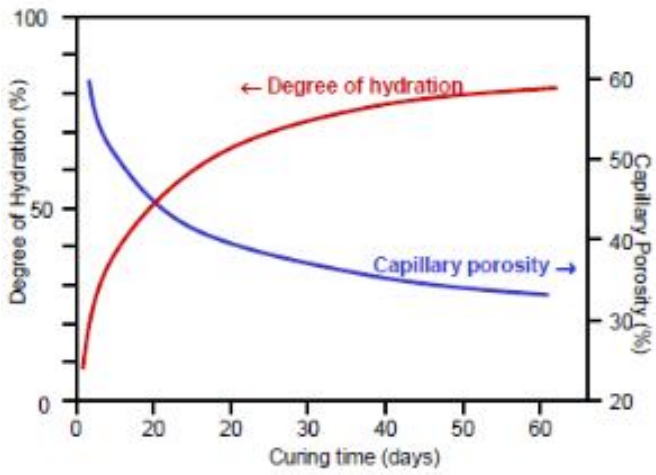

Figure 2-2: Development of capillary porosity with degree of hydration (Kurtis, 2007)

The third significant component of the hardened cement paste is water. Apart from the capillary water which has already been mentioned, there is also the adsorbed water. Most of the hydration products are colloidal, hence, according to Jennings (2000) the surface area of C–S–H expands during hydration and adsorbs free water, which for this it is termed adsorbed water. The layers of adsorbed water are held by hydrogen bonding and can be removed, if the hydrated cement paste is dried to below 30% relative humidity, causing shrinkage. Furthermore, some other water molecules are trapped within the interlayers of C–S–H, comprising the interlayer water, a monomolecular layer strongly held by hydrogen bonding. If the interlayer water is lost (only under severe drying), collapse of the C–S–H layers at 11% relative humidity, occurs. Lastly, the chemically combined water, which is water in molecular combination with the hydration products, cannot be removed by drying, but can be decomposed on heating.

2.3.3 Effect of limestone on cement hydration

Although initially, LS was regarded by some scientists (Sprung and Siebel, 1991) as a chemically inert material, which has only physical filler effects on cement hydration, recent evidences suggest that it can also form hydration products in the form of carboaluminate hydrates (De Weerdt *et al.*, 2011a; Ipavec *et al.*, 2010; Lothenbach *et al.*, 2008) or interact with alite, accelerating its hydration and altering the C/S ratio. Vogt (2010) summarized the effect of the addition of LS in three key points. Firstly, it can accelerate hydration as it provides nucleation sites for the products. Secondly, the amount of heat released increases with the fineness and the quantity of LS added. Thirdly, both hydration and setting start sooner with more and finer LS. However, pastes containing 50%PC and 50%LS by mass have been found to decrease compressive strength at 28 days by 50%, while increasing porosity by a factor of 3 compared to the reference paste of CEMI-42.5R at w/b ratio of 0.36 (Barluenga *et al.*, 2012).

2.3.4 Effect of pozzolanas on cement hydration

The effect of the addition of pozzolanic particles in cement pastes, has been studied through a series of tests, such as heat of hydration, compressive strength, shrinkage, frost resistance, microstructural characterisation and has been found to accelerate the hydration of cement, through the creation of nucleation sites assisting the depletion of Ca and Si in the pore solution (Vogt, 2010).

During the process of hydration, pozzolanas consume one of the hydration products, portlandite, producing supplementary C–S–H or C–A–H or Calcium-Alumina-Silicate hydrates (C–S–A–H) (Mendoza and Tobón, 2013; McCarthy and Dhir, 2005). The consumption of CH and alkalis causes the lowering of the pH of the paste. There is a maximum proportion of μS that is allowed to be added in the mix, based on the quantity of $Ca(OH)_2$ available. In broader terms, the hydration of C_3A is delayed, whereas the hydration of C_3S is accelerated (Vogt, 2010).

The chemical formulas representing the reactions taking place with the addition of μS, in the paste are as follows (Vogt, 2010):

$$2\,Ca(OH)_2 + SiO_2 + H_2O \rightarrow C-S-H\ (1) \qquad \text{Equation: 2-4}$$

$$C-S-H\ (1) + SiO_2 \rightarrow C-S-H\ (2) \qquad \text{Equation: 2-5}$$

The secondary C–S–H (2) produced by the reaction of additional μS with the primary C–S–H (1) exhibits a lower C/S. According to Vogt the higher the μS content the slower the compressive strength gain, since at high concentrations there will not be enough $Ca(OH)_2$ to react with μS. Adding to this, higher shrinkage and autogeneous shrinkage values are also expected for higher proportions of μS. On the positive side, packing density is improved, enhancing frost resistance. It has also been observed that with the addition of μS the capillary porosity is reduced because the additional C–S–H produced by the pozzolanic reaction is much denser (Lindgreen *et al.*, 2008).

The effect of the addition of FA depends on the amorphous phase of FA; in general the reaction is not as fast as the one with μS. The particle size distribution and the exact oxide composition of FA has a significant influence on the hydration procedure. Grains greater than 10 μm can act as fillers, while those smaller than 10 μm can accelerate the hydration of C_3S. Adding to this Al_2O_3 and SiO_2 present in FA also participate in the pozzolanic reaction.

Studies have been presented with the addition of a combination of FA and μS particles to PC. Addition of the FA with the aim to address consistence issues when μS is present, and addition of μS with the aim to counterbalance the low early strength gain and total porosity induced by FA (Barbhuiya *et al.*, 2009), as compared by Supit and Shaikh (2014). Their results indicate that the introduction of even finer particles, i.e. nanoparticles, could be even more promising.

2.3.5 Composite cement hydration: combined effect of pozzolanas and limestone

Qualitative characteristics of the hydration products resulting from the binary combinations of PC with either FA or µS or LS can be observed in Figure 2-3 and studied in greater detail in Lothenbach *et al.* (2011).

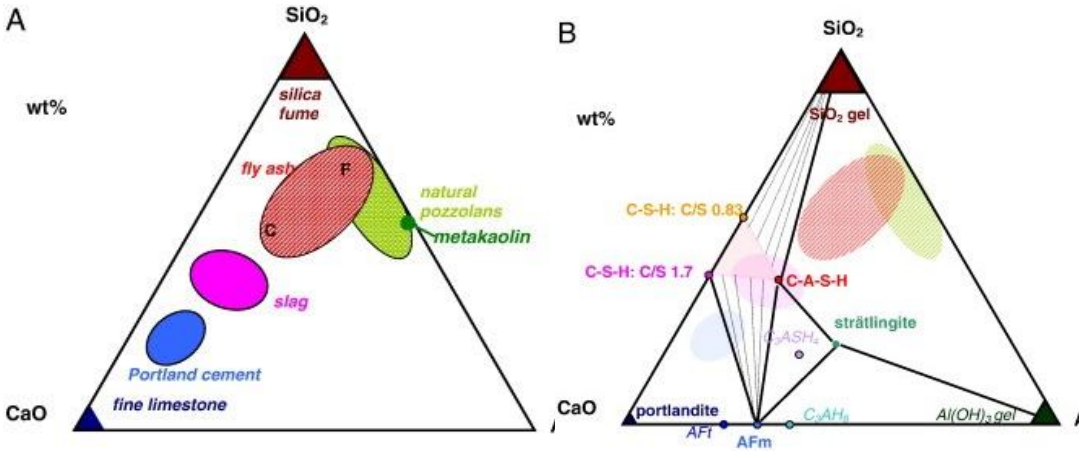

Figure 2-3: A) $CaO–Al_2O_3–SiO_2$ ternary diagram of cementitious materials, B) hy phases in the $CaO–Al_2O_3–SiO_2$ system (Lothenbach *et al.*, 2011)

Although there are many publications on binary systems, i.e. studies on various contents of FA or µS or LS Portland cements, there are very few published researches on ternary systems. It has been found that in ternary cements containing PC, FA and LS, LS played a dual role; LS (i) contributed as a filler and (ii) participated in chemical reactions with the aluminate hydrates from the PC hydration (De Weerdt *et al.*, 2011a; De Weerdt *et al.*, 2011b). Adding to this, after a study of eight different combinations of FA and LS content combined with PC, this team of researchers concluded that the consumption of $Ca(OH)_2$ was more pronounced for the 30%FA 5%LS and 65%PC blend rather than the 35%FA and 65%PC blend and was related to carboaluminate formation. Lastly, with respect to compressive and flexural strength they inferred that although a 5% replacement of cement by LS reduced the strength of the formulation, a 5% addition of LS to a 30%FA and 65%PC blend, will not cause strength reduction.

Furthermore, several researches have reported a number of benefits of the combined effect of FA and µS on Portland cement blends such as increased early age compressive strength and slump of concretes (Wongkeo *et al.*, 2013). Moreover, the C/S ratio decreased with increasing µS content, which effectively caused an increase in compressive strength. Lastly, the maximum strength was obtained for the PC50FA40µS10 formulation.

It is interesting to note that although very few studies have been reported on ternary cement blends, no studies have been found on quaternary cement blends including all the above mentioned elements, that is to say PC, FA, LS and µS.

2.4 Nanostructure of C–S–H:

2.4.1 Introductory section

Taking into consideration the perspective that "many of the mechanical properties of the hardened cement depend not so much on the chemical composition of the hydrated cement as on the physical structure of the products of hydration, viewed at the level of colloidal dimensions" (Neville, 1995, p.25) or the belief that the way to enhance the macroscopic mechanical properties of cement is by understanding and modifying the structure of the C–S–H gel at the nanolevel (Selvam *et al.*, 2009) one can imagine the possibilities nanotechnology can offer in cement technology, as the addition of nanoparticles fundamentally modifies the nanostructure of the hydration products.

Having referred to the hydration products and the related phases forming the hydrated cement microstructure, at this point, it is necessary to go one level down and provide some insight to the nanostructure of C–S–H and lay the path for the understanding of the mechanisms affecting it when nanoparticles are added in the different cement formulations. Discussion presented in this subsection comprises a summary of a journal paper (Papatzani *et al.*, 2015).

The atomic structure of C–S–H is still not fully determined and the nanostructure of the C–S–H is currently being researched and is still being debated (Alizadeh, 2009; Selvam *et al.*, 2009). Adding to this, there is still controversy and dispute as to whether C–S–H is made of globules (Jennings, 2008; Jennings *et al.*, 2007; Allen *et al.*, 2007; Thomas and Jennings, 2006; Tennis and Jennings, 2000) particles of 5x30x60 nm^3 size (Plassard *et al.*, 2004), disks of 5 nm thickness (Pellenq *et al.*, 2008) or a morphology derived from a foil-like growth mechanism (Bullard, 2009). Consequently, the following questions are pertaining; is the structure of the C–S–H colloidal or continuous, amorphous and up to what scale, "very poorly crystalline" or nanocrystalline and how has it emerged? What is the role of water in the C–S–H, what are the characteristics of the different forms in which it is encountered and how do humidity changes at the nanolevel affect the macroscopic behavior of pastes? To address the issue of the nanostructure of the C–S–H in the hydrated cement paste, only the key features of the proposed models over the decades will be summarized, which are in full agreement amongst the aforementioned researchers. Adding to this, the historical evolution of the models will be presented on the basis of the structural characteristics and the form in which water is found in the nanopores, an aspect of particular importance.

2.4.2 The first colloidal model

The beginning of the discussions started in 1918, at the Faraday Society meeting in London, but it was not until 1946-7 that the first ever hydrated cement paste model, the "P-B" model, was published by Powers and Brownyard (1946-7). Their model recognized the colloidal characteristics of the hydrated cement paste and suggested C–S–H consisted of three phases: (i) capillary water (thus, unreacted water), (ii) unreacted cement and (iii) cement gel or "colloidal gel" or "colloidal hydrous silicate" of "calcium silicate hydrate" (consisting of water-filled gel pores and hydrated cement particles) (Figure 2-4). The water in the gel pores was named gel, absorbed or evaporable water. The capillary water was visualized as free water. The total water equaled the sum of the non-evaporable plus gel water. Furthermore, a distinction was made between gel and capillary porosity. However, one of the limitations of the model was the fact that the size of the colloidal gel particles could not be determined directly. Another limitation stemmed from the fact that a number of the adsorption isotherms obtained by Powers and Brownyard showed irreversibility, which they attributed to shrinkage, without providing any further justification. These issues were resolved in 1966, by Feldman and Sereda.

Brouwers (2005, 2004) recently revisited Powers and Brownyard's study and contributed by determining the molar reactions of the calcium silicate phases, the two hydration products (C–S–H and $Ca(OH)_2$) and the molar reactions of the aluminates (C_3A and C_4AF) and the sulfates. Moreover, the density and porosity of the C–S–H was measured for C/S=1.7, providing assumptions for cases where C/S≠1.7.

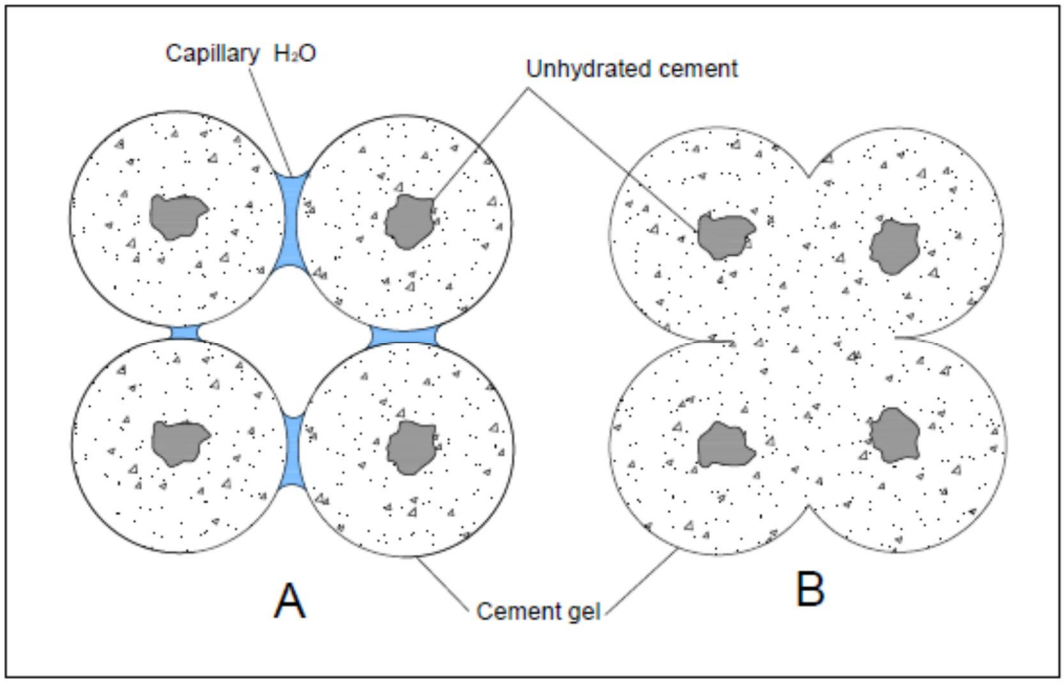

Figure 2-4: Main constitunts of hydrated cement paste [after (Powers and Brownyard, 1946-7)]

2.4.3 First layered models

The first layered model was introduced by Bernal in 1952, who produced two synthetic products; C–S–H (I) and (II) by hydrating C_3S. The layered structure was similar to the naturally occurring tobermorite crystal, in the sense that layers of CaO reinforced by (theoretically) infinite silicate chains was inferred by Bernal *et al.* (1952) based on XRD data performed on C–S–H type (I). Still this model could not address the shrinkage issue, resolved later by Feldman and Sereda.

The model of the structure of C–S–H developed by Powers and Brunauer in 1962-1970 adopted the layered structure similar to the tobermorite and jennite and it was based on porosimetry and adsorption tests. The product of the hydration of C_3S and C_2S was named "tobermorite gel" and was identified as having a high surface area. It was suggested by Brunauer (following Bernal's misconception) that C–S–H in hydrated paste, although layered, collapses on drying and water cannot reenter the layers. In other words the system, after initial drying, is considered to be reversible on subsequent wetting and drying cycles. As an effect, the Brunauer–Emmett–Teller (BET) theory was considered applicable to the water adsorption isotherm (Brunauer *et al.*, 1967; Powers, 1965; Kantro *et al.*, 1962; Brunauer, 1962). Not only has this argument been proven wrong by subsequent research by Helmuth (Helmuth, 1965), Feldman (Feldman, 1972b) and Daimon (Daimon *et al.*, 1977), but also, being based on nitrogen and water sorption, the failure of nitrogen to enter all pores did not allow this model to give a direct answer to the arrangement of the pores in the C–S–H gel and consequently address the issues of creep and shrinkage.

2.4.4 The Feldman and Sereda model and Daimon's improvements

The Powers and Brunauer model was further modified by Feldman and Sereda leading to the F-S model in 1966-1970 (Figure 2-5) with the novel introduction of the concept of a *layered structure with pores* between the layers. Adding to this, the concept of the *interlayer water* was firstly introduced in the model under consideration. The importance of interlayer water was stressed by the fact that creep and shrinkage were attributed to the transportation characteristics of water in various forms within the paste. The F-S model suggested that if the collapsed layer is exposed to water, water will re-enter the pores rendering the system irreversible (Helmuth, 1965; Feldman, 1972b; Daimon *et al.*, 1977). Therefore, instead of using water as a medium for sorption isotherms, they employed helium, methanol, lime solution isotherms at 11% relative humidity (Feldman, 1972b) or, N_2 adsorption isotherms (Daimon *et al.*, 1977) or sorption and length-change isotherms (Feldman, 1969) for porosity and density measurements for d-drying or prolonged drying at 110°C. The harshness of the drying conditions employed by Feldman (1969) has been criticized by later researchers (Brouwers, 2004), because it causes partial removal of water from the gel. As pointed out by the initial studies of Powers, the theory on the irreversibility of the process was established along with the fact that the pores were not bottle necked or

of fixed dimensions. Furthermore, the F-S model provided further insight into the structure of C–S–H gel, describing the interlayer water as being part of the C–S–H "colloid", affecting creep and shrinkage and ascribing the "external" surface available to nitrogen as the "valid" surface for surface area measurements. Still, the F-S model could not account for the measurement of the internal surface area, i.e. the surface area of the inner C–S–H (Feldman, 1972a), a matter addressed by Daimon and his collaborators (Daimon *et al.*, 1977).

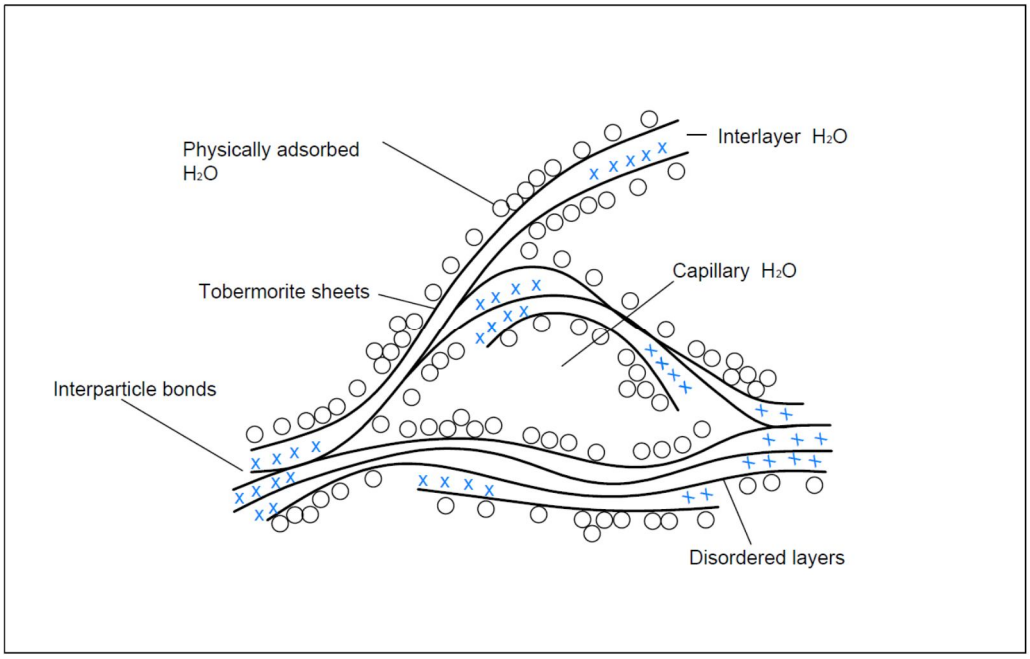

Figure 2-5: Feldman and Sereda Model [after (Feldman and Sereda, 1968)]

The F-S model was further improved by Daimon *et al.* (1977) who investigated the pore structure of C–S–H by N_2 and water adsorption isotherms. It was deduced that the actual pore size is smaller than that measured because the inner C–S–H can be encapsulated by $Ca(OH)_2$ making it difficult for the adsorbate to reach the pores and capillary condensation occurs at higher relative pressure. They postulated that more accurate results can be obtained if a $Ca(OH)_2$ extraction treatment was used. The porosity they measured was the "intergel particle porosity", that is to say the space between the gel particles that can be found in the inner C–S–H (Figure 2-6). According to the Daimon model, two other types of pores existed within the gel particle and subsequently the intragel pore, that is to say, (i) the "intra-crystallite pores", which are similar to the F-S interlayer space, but are not as ordered as clays, and (ii) the "inter-crystallite pores", which are similar to the Brunauer micropore, but with swelling characteristics. Still the magnification available by the electron microscopy at that time was not sufficient to confirm the characteristics of the intragel pore, water and solid matter.

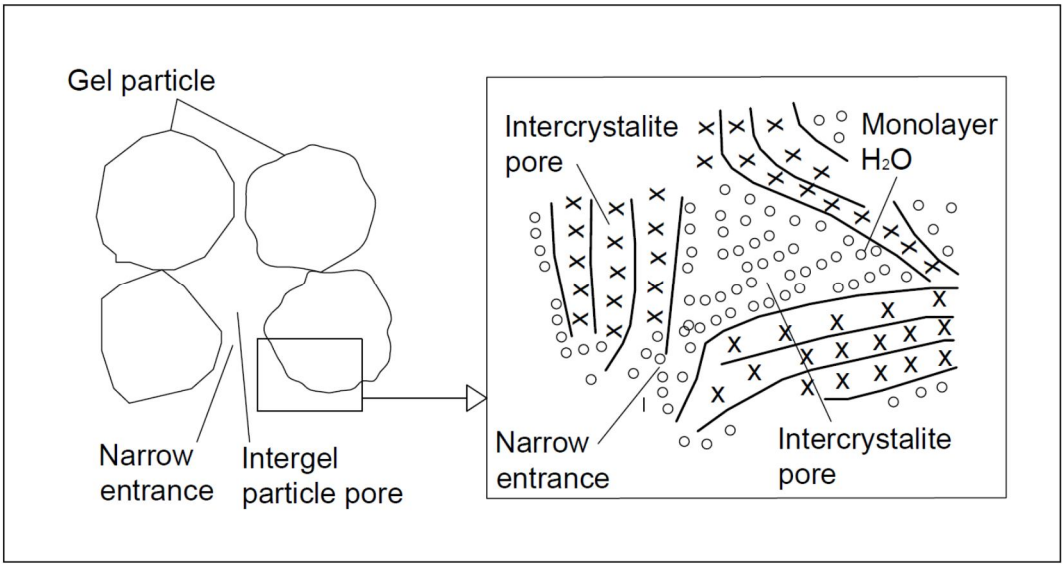

Figure 2-6: Pore model of the C–S–H gel [after (Daimon et al., 1977)]

2.4.5 Taylor's dreierkettes and the *3n-1* rule

Taylor (1986) suggested that the structure of C–S–H comprises of two types of innumerable disordered layers, resembling a) imperfect 1.4 nm tobermorite and b) jennite-like structures. As far as the tobermorite structure is concerned, theoretically, the silicate chains are infinitely long and are formed by groups of dreierkettes. In each dreierkette, two oxygen atoms are paired and the third (bridging tetrahedron) forms the link between two adjacent pairs (Figure 2-7-A). Some oxygen ions are replaced by OH^- (Figure 2-7-S).

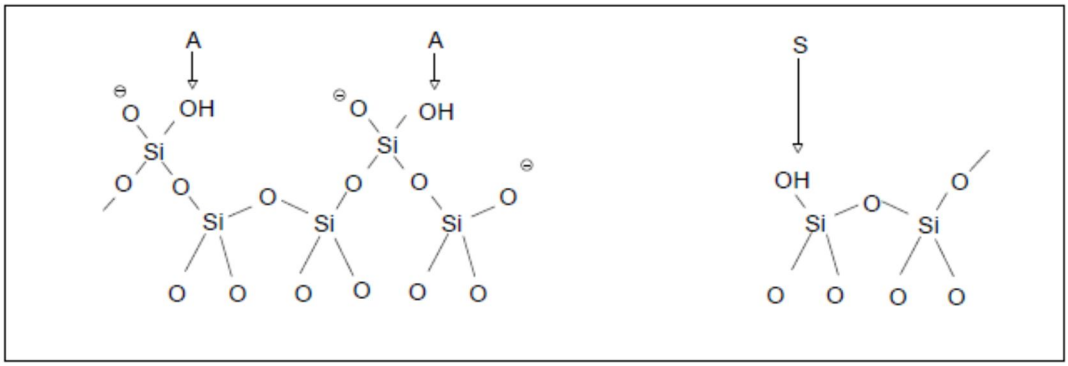

Figure 2-7: Dreierkette-based models [after Taylor (1986)]

In the same research the C/S ratio in the C–S–H was linked to the C/S ratio in the dimeric 1.4 nm tobermorite and jennite structures but water in the interlayer was only hypothesized (Ridi *et al.*, 2011).

The length of these chains or in cement science terminology "the polymerisation of silicates", as well as the surface area of the C–S–H depends on the C/S ratio of the C–S–H and is determined by the number of silicon atoms, given by the 3n-1 rule. It was experimentally observed in 1986 by XRD, TG and density analysis by Taylor (1986) and confirmed by EDX enhanced TEM and electron microprobe analyses of Richardson and Groves (1993) that the silicate anions could be found in 2, 5, 8, …, 3n-1 chain lengths, creating dimers, pentamers, octamers and so on. They also categorized C–S–H in the inner (formed within the boundary of the original particles) and the outer (formed in the originally water filled space). The inner hydration product consisted primarily of "single-phase" C–S–H and was often found to encapsulate $Ca(OH)_2$. As will be discussed in paragraphs 2.6 and 2.6, the extent of pozzolanic reactivity (and subsequently the amount of C–S–H formed, its C/S ratio and the length of the silicate chains) is proportional to the surface area available for reactions when nanoparticles are added (Jo *et al.*, 2007b).

A more general model was, still, needed to cover the *3n-1* rule and both types of C–S–H. With a number of XRD studies, the crystal structure of the 1.1 nm tobermorite was resolved in 1981 by Hamid (Hamid, 1981) and the model suggested by Merlino *et al.* (2001) corrected the misaligned and separated Si–O chains of the former (Skinner *et al.*, 2010). A model for the crystal structure of 1.4 nm tobermorite was suggested by Bonaccorsi *et al.* (2005). The difference between the 1.1 tobermorite by Hamid and the 1.4 nm tobermorite by Merlino has been identified by Selvam *et al.* (2009) as being "the bonding scheme in the silica chains", as in the latter's model the silicon tetrahedra bond together in between interlayers. In 2000 the crystal structure of jennite was also resolved by Merlino, believed to be describing the C–S–H (II). The structure of jennite was also further developed by Bonaccorsi *et al.* (2004), and so was the crystal structure of tobermorite (2005). A comparison between these dreierkette models, their purposes and experimental methods on which they were based and their structural evolution as a function of the C/S ratio, was made by Richardson (2008).

Taylor (1986) and Plassard *et al.* (2004) both noted that some bridging tetrahedral could be omitted in order to increase the C/S ratio. In this case, the structure is referred to as a *defect tobermorite structure*. It was also suggested that there is the interlayer locus between the calcium sheets, in which water, calcium cations and hydroxide anions are present. Shrinkage and swelling is attributed to this water being dried out and reappearing due to wetting. An extension to this model was provided by Cong and Kirkpatrick (1996a, b) whose results corroborated that the presence of Ca–OH and Si-OH in the C–S–H is affected by the C/S ratio. They supported the model of disordered C–S–H with missing tetrahedra and added that the chains formed are short and can be rotated and inclined, explicating the versatility in the stoichiometry of C–S–H. Pellenq *et al.* (2009) also increased the C/S ratio to deliver shorter silicate chains beginning with the 1.1 nm tobermorite. They concluded that within the mass of the C–S–H there are "both glass-like short-range order and

crystalline features of the mineral tobermorite" (Ridi *et al.*, 2011, p.261). Further discussion on the models and their limitations can be found in (Papatzani *et al.*, 2015a).

2.4.6 Contemporary models - CMI

All these models have provided precious qualitative and quantitative information with regards to the nanostructural characteristics shape, size, arrangement of elements, shrinkage and water movement and their relation with the mechanical properties of the paste. Recent years have found colloidal models of the C–S–H gaining acceptance. One of the first studies in this area, after the P-B model, was carried out by Wittman (1976) with his "Munich" model (Figure 2-8). The role of water in the spaces between the particles was also stressed in this model and the disjoining pressure between the particles was addressed. However, the proposed model did not resolve the phenomena related to creep under load or drying shrinkage induced by changes in the nanopores of the C–S–H. Ten years later, in 1986, Allen and collaborators observed the microstructure of the paste right after the induction time by SANS (small angle neutron scattering) analysis and concluded that gel globules of 5 nm in size conglomerate forming structures of about 40 nm in length (Ridi *et al.*, 2011, p.261). This study constituted the precursor of the modern theories on the colloidal models and marked the shift of C–S–H classifications from using C/S as the main criterion, to using packing characteristics.

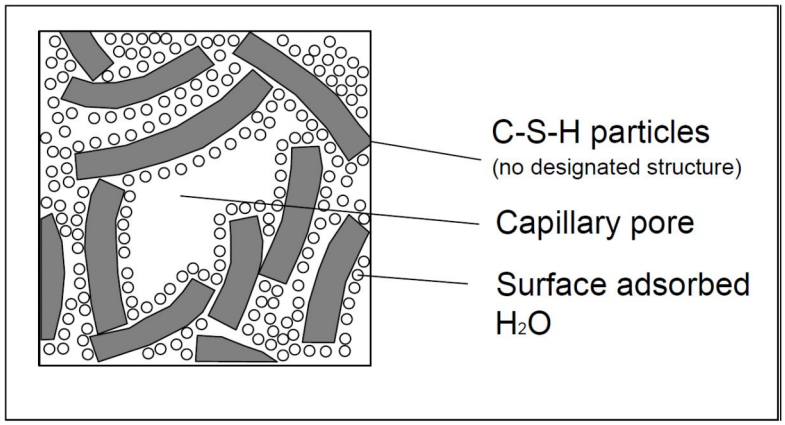

Figure 2-8: Colloidal C–S–H model: Munich model [after (Wittmann, 1976)]

Further work on the colloidal nature of C–S–H was carried out by Jennings and his team from 2000 to 2011. Initially, Jennings (2000) through a series of SANS and SAXS (small angle X-ray scattering) analyses within a size range of 1 to 100 nm determined the shape of the C–S–H particles in Colloidal Model I (CM-I) as being almost spherical and approximately 5 nm diameter. Tennis and Jennings (2000) presented a model, validated with the help of nitrogen sorption. It could quantitatively predict the volumes of the phases (Figure 2-9) and the pore structure in terms of density, gel porosity accessible by the nitrogen, and surface area of the C–S–H. The basis of the model was the separation of the

C–S–H in two distinct forms, the low density (LD) C–S–H and the high density (HD) C–S–H.

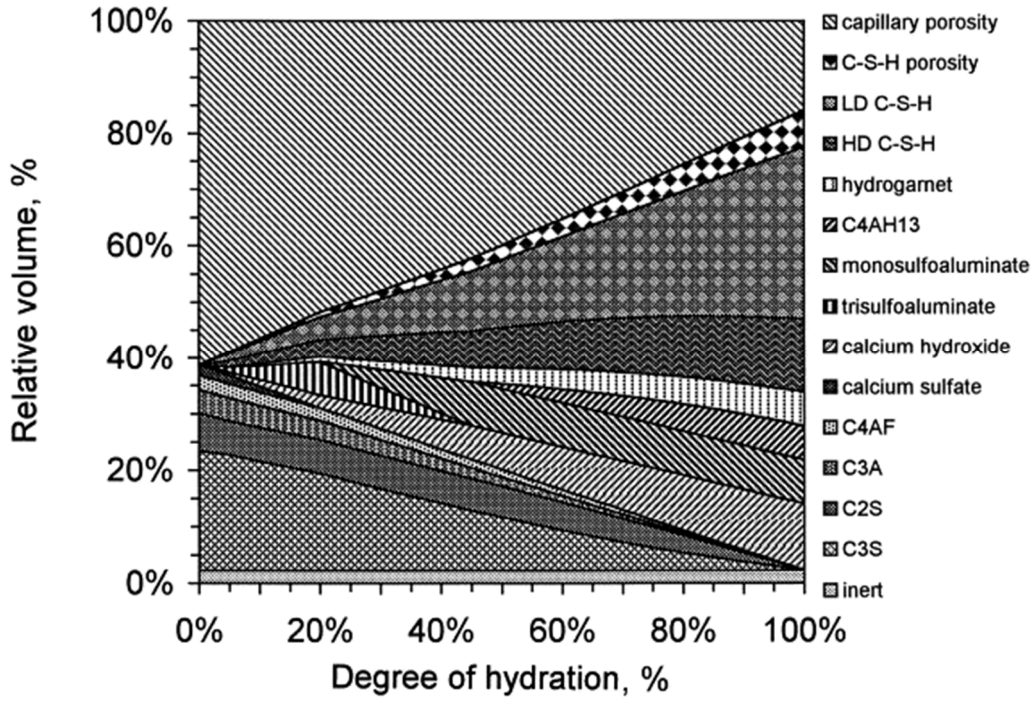

Figure 2-9: Product generation with degree of hydration (Tennis and Jennings, 2000)

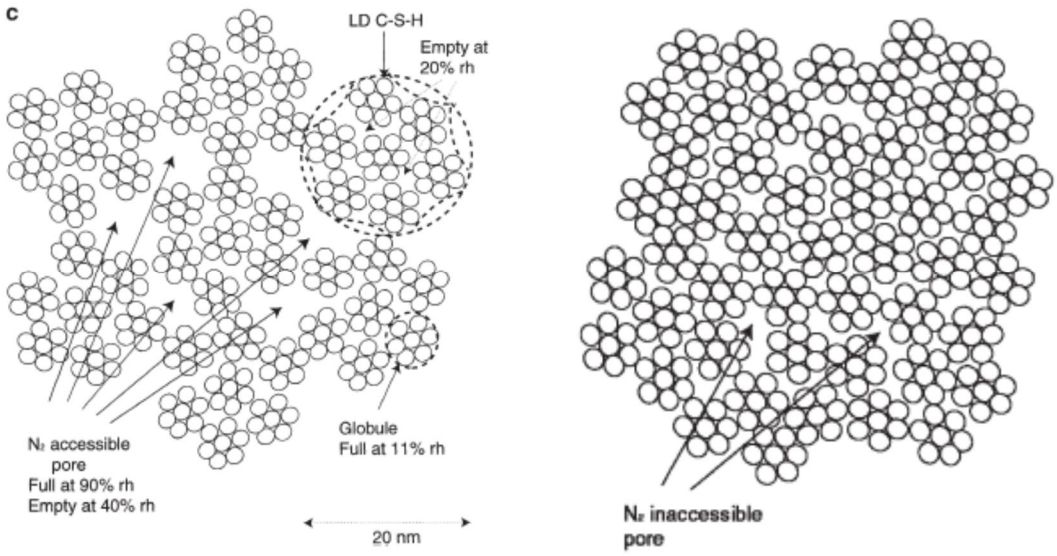

Figure 2-10: 2-D schematic of LD C–S–H (left) and HD C–S–H (right) for w/b=0.4 as formed by the late stage and/or by drying (Jennings, 2000)

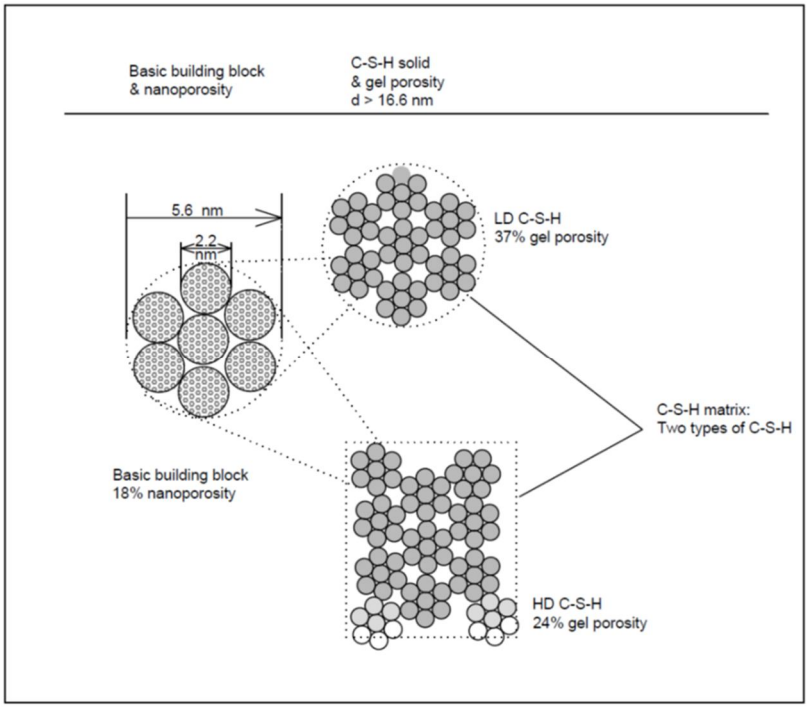

Figure 2-11: Colloidal structure of the C–S–H [after (Jennings, 2000)]

As seen in Figure 2-10, Figure 2-11, and Figure 2-12 the basic units are the small spheres of approximately 2.2 nm diameter, which cluster together (flocculate) to form the globules or else, "basic building blocks" of about 5-5.6 nm in diameter (Alizadeh, 2009). It is these basic units, the smallest ones, that are tobermorite-like or jennite-like particles, since their dimensions (2.2 nm diameter) correspond to the largest lattice dimension of the tobermorite unit cell, which is equal to 2.2 nm (Selvam *et al.*, 2009; Thomas and Jennings, 2006). With CM-I different, physical properties; densities, porosities and specific surface areas, were measured.

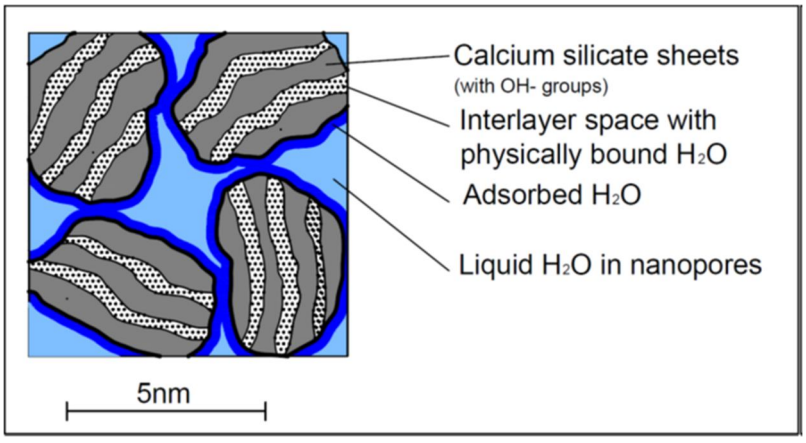

Figure 2-12: 5 nm globules [after (Allen *et al.*, 2007)]

One of the limitations of the CM-I, is that the pores within the globules are filled with water and are excluded in the porosity measurements. In other words, LD C–S–H is considered as the primary contributor to the specific area estimations, since it is more accessible to nitrogen than HD C–S–H. The latter remained undetectable by SANS or nitrogen adsorption. It was, therefore, suggested that the contribution of HD C–S–H to the SSA could be ignored (Lindgreen *et al.*, 2008). This simplification constitutes a significant weakness of the model. In fact, computational studies (González-Teresa *et al.*, 2010) suggested that the computational counterpart of the "experimentally inaccessible HD C–S–H" could also contribute to the specific surface area measurements. This computational model provided significant convergence with the LD C–S–H SSA measured by SANS (Allen and Thomas, 2007). These findings and hypotheses concerning the detectability of the HD C–S–H surface remain to be proven experimentally. Quantifying the SSA of the HD C–S–H is to be achieved. Is the HD C–S–H SSA substantially different from the LD C–S–H phase? The C–S–H solid is essentially the same but particle packing or degree of polymerisation could change, causing variations in surface area. In any case the outer surface of the "stacked" layers would most certainly be accessible to nitrogen.

Moreover, with respect to CM-I, since the globule is about 5 nm in diameter, this nanoporosity is filled with so-called "structural" water and has been measured to be in the order of 18% of the total volume fraction irrespective of the type of C–S–H. However, the physico-chemical and mechanical behaviour of cement has not been linked to a "structural" role of this water, a fundamental difference between colloidal and layered models. In fact, the F-S model can be used to explain experimental results on pure C–S–H phases (11% RH to the dry state) that clearly indicate a structural role for interlayer and surface adsorbed water as no capillary pore water is present. In addition, it is not related to the gel porosity, which is larger than 5 nm and differs according to the C–S–H density. In this idealized structure, LD C–S–H has a gel porosity of roughly 37% and stiffness of about 22 GPa and HD C–S–H has a gel porosity of 24% (both LD and HD C-S-C porosities exclude porosity in the globules) and stiffness of about 29 GPa, as shown in Figure 2-11 (Jennings, 2000; Jennings *et al.*, 2007). Moreover, the structure suggested, was favouring the reversibility of the model, involving restructuring of the globules towards denser arrangements. This has been proven wrong by Feldman. As an effect CM-I is unable to address thermodynamic sorption and e.g. explain the relationship between elastic or viscoelastic behaviour of the paste and relative humidity. However, it is interesting to note that this model connects the structure of C–S–H, its density and its SSA at different nanometric scales. At 1 nm the density was measured to be equal to 2450 kg/m^3 and the surface area to 1000 m^2/g. The fact that at different scales different readings in surface area and density are taken, could also imply a fractal structure, a hypothesis revisited in later studies, as well (Jennings *et al.*, 2007). A molecular dynamics predictive model should also be developed to have the strength and the nature of the bonds between the C–S–H particles in both areas determined. All in all, it can be argued that CM-I is essentially a hybrid structure, in which C–S–H layers of C–S–H stack together to form the "globules" (Raki *et al.*, 2010).

2.4.7 Contemporary models - CMII

The Colloidal Model-II (CM-II) suggested by Jennings (2008) was significantly different from CM-I. It constituted a morphological combination of the F-S model, with the colloidal model, as it brought a layer-like model into the colloidal-like model. The model was considered to be "granular" and its purpose was to interpret the water sorption isotherms under different moisture environments and to provide a deeper understanding of the structure of the globules. The structure of the paste is drawn in Figure 2-13. The basic globule resembles a disc of 4 nm thickness, with an internal layered structure analogous to the tobermorite and jennite. Advancing Daimon's model, water in CM-II can be found in the interlamellar spaces and in the intraglobular pores (IGP). The latter have a dimension of less than 1 nm. Two other types of pores are created by the stacking of the globules: the small gel pores (SGP) of 1-3 nm and the large gel pores (LGP) of 3-12 nm. As pointed out by Alizadeh (2009), the structure of the interlayer water in the CM-II model is not specifically described and therefore it is not clear if it comprises a layer on its own or of several molecular layers. Adding to this, the mechanical behaviour of the paste is influenced by sorption, which in turn, is related to the structural role of the interlayer water, still, not addressed by CM-II. As an effect, drying shrinkage, ageing and creep cannot be justified. For example, creep is attributed to sliding of globules with respect to each other causing their rearrangement and C–S–H is considered to behave as a granular material. The F-S model accounted for the role of interlayer water in the creep process, the removal of which affects the properties of C–S–H. As far as the assumption of the nanogranular nature of the phase is concerned, it is still under debate (Nguyen *et al.*, 2014; Nguyen *et al.*, 2013) since the packing factors were calculated with respect to water porosity, equating in this way the interlayer water with pore water, which is not correct. Notwithstanding, a milestone in the modern colloidal models has been met with this study of the sub-nanometric porosity, relating the structure of C–S–H and the mechanical properties of the paste.

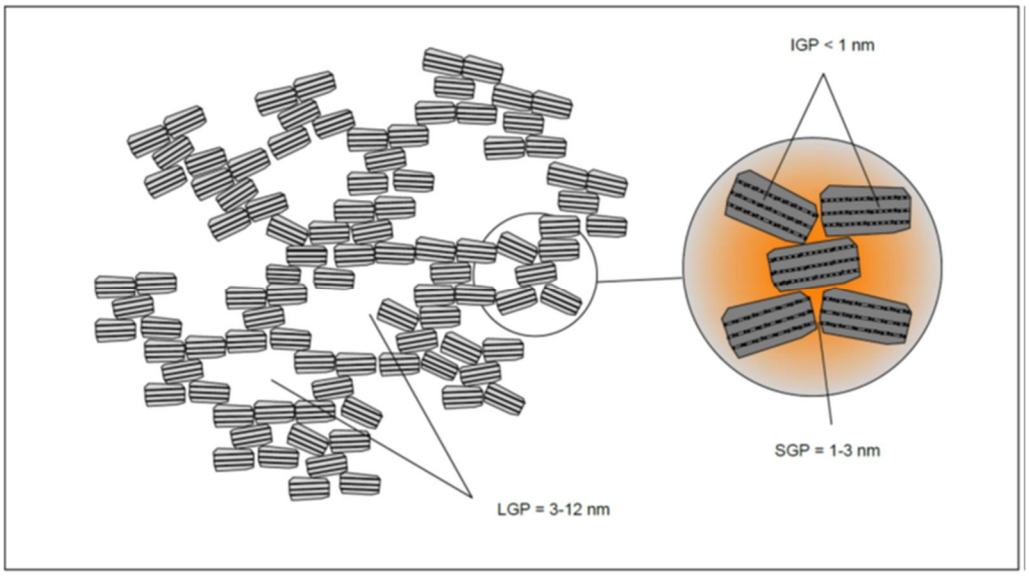

Figure 2-13: CM-II model [after (Jennings, 2008)]

2.4.8 Novel techniques for the verification of the contemporary models - nanoindentation

A novel approach has been suggested by Ridi *et al.* (2009), who studied the confinement of water in the paste from time zero of mixing to 2 months of curing. The different exothermic temperature peaks were assigned to water being confined in the SGP or in the LGP and signs of IGP water were also monitored using low temperature differential scanning calorimetry (LT-DSC) and low temperature Near-Infrared Spectroscopy (LT-NIR). Findings suggest that water confined in this nanometric porosity undergoes significant changes after 8 hours of hydration.

Nowadays, nanoindentation is broadly used as a method to assess the mechanical properties at the nanolevel. The basis of the technique is that a metallic thin probe perforates the surface of the material and by studying the response of the indented material its mechanical properties can be determined and most importantly, this technique can be applied even in highly heterogeneous (due to porosity) materials such as cement paste (Ulm, 2012). As mentioned earlier, the work carried out by Jennings and his team proved the existence of two distinct phases of the C–S–H, which are different in terms of structure but similar with respect to chemical composition; the high density C–S–H phase (HD) and the low density C–S–H phase (LD) (Jennings, 2008; Jennings, 2004; Jennings, 2000). The existence of the two types of C–S–H is questioned by Nguyen *et al.* (2014) who have claimed that the conformance of the density measurement with the pycnometric method and with the use of crystallographic data imply that if the form of the C–S–H changes because of C/S, compositionally it will be similar since the density variation is marginal.

At the same time as Jennings and his team were developing CM-I, Constantinides and Ulm (2004) through a series of nanoindentation experiments also confirmed the existence of the two phases and proved that the elastic property and hardness, which were determined quantitavely do not depend on the composition of the mix, but rather constitute an intrinsic property associated with the C–S–H packing density. As the latter increases, so do stiffness and hardness, and therefore, HD C–S–H has higher values of these properties, compared to LD C–S–H. Only the proportions between LD and HD C–S–H change with mix composition. Selvam *et al.* interestingly noted that similar values of the elastic modulus were also obtained by the nanoindentation experiments carried out by Acker (Selvam *et al.*, 2009, p.22).

These findings are also related, in some analogy, to the latest work of Plassard and his team (2007) who carried out nanoindentation experiments and determined the elastic properties of synthetic C–S–H nanoparticles. The discrepancies observed between the elastic properties' results provided by Plassard *et al.* (2007) and Constantinides and Ulm (2004) were attributed to the sample used, which in the former case it was a single C–S–H crystal (derived from the synthetic C–S–H), whereas in the latter one, it was a network of C–S–H (derived from PC paste), enclosing, gel porosity. Both teams concluded that the elastic modulus of C–S–H increased with the C/S ratio. Their results were in direct conflict with

the results presented by Alizadeh *et al.* (2011) who investigated the properties of synthetic C–S–H, hydrated PC paste and glass at low porosity values (30%) with dynamic mechanical analysis (DMA) finding the exact opposite, that the elastic modulus decreased with increasing C/S ratio (0.8 to 1.5). Moreover, it was recognised by all three approaches that the interlayer and adsorbed water play a significant role in the elastic properties of the C–S–H and that in any case the latter is dependent on the C/S ratio. It should be noted that the first experiments in the area of elastic properties of C–S–H were carried out by Beaudoin *et al.* (1986) who presented density, surface area, silica polymerisation and microindentation and microhardness results on synthetic and compacted C–S–H powders of C/S ranging from 0.68 to 1.49. They suggested that the elastic properties (but not the chain polymerisation) are independent of the C/S ratio, recognizing differences due to the microstructural variability of C–S–H, demonstrating how much the currently available techniques such as nanoindentation, have contributed to the better understanding of the C–S–H phase performance.

In recent work, Sarris and Constantinides (2013) proved that two factors should be taken into consideration as far as nanoindentation is concerned. These are the effect of hydrostatic pressure on the plasticity response and the effect of the contact friction between the indenting probe and the material. These two parameters were quantified for the first time and the elastic and plastic modulus of LD and HD C–S–H and the contact friction were determined with the use of finite element method. The simulations they carried out have shown the elastic modulus (E) to be within +15% and the hardness values (c) to be up to +50% with respect to past studies, which determined that E = 21 GPa and c = 50 MPa for LD C–S–H and E = 31 GPa and c = 97 MPa for HD C–S–H. The calculation of the area of contact is very significant as it constitutes the primary parameter affecting the measurement of the indentation hardness and consequently the evaluation of the strength of the C–S–H. The two researchers concluded that more advanced parametric studies will be necessary as the knowledge progresses.

Recent work by Ulm *et al.* (Ulm, 2012; Vandamme et al., 2010) on different w/c ratios has provided evidence as to the existence of a further distinct phase in the C–S–H; an ultra-high density phase (UHD) that is in addition to the LD and HD. UHD was determined to be compositionally similar to HD and LD and dependent on the packing density distributions. Adding to this, they deduced that the increase of water in the mix, and the simultaneous increase in gel porosity acts in favour of the formation of more LD against HD, whereas the volume of UHD remained constant (approximately 20%) above w/c=0.2. For w/c=0.3, it was calculated that the volume of LD was 30% and that of HD was 52%. However, evidence for the existence of a single phase UHD C–S–H has been questioned since a suite of nanoindentation and SEM/EDX analyses suggest that the presence of embedded nano-$Ca(OH)_2$, leads to much higher values of elastic modulus and hardness than those measured for LD and HD C–S–H (Chen *et al.*, 2010).

A number of computational models for the molecular reconstruction of C–S–H have also been suggested over the years. Reference to them is beyond the scope of this research. However, some information can be traced indicatively in Papatzani *et al.* (2015a), Fonseca *et al.* (2011) or Selvam *et al.* (2009).

2.4.9 Summary of key findings

The most interesting disparities and key findings will be summarized at this stage (Papatzani et al., 2015);

- The bricks of CM-I were abandoned in favour of the globules of CM-II, which have not yet been experimentally probed. The two colloid models, which classified C–S–H with respect to packing density (LD and HD C-S-H), cannot fully address shrinkage phenomena, as the role of water has not been incorporated in the models. However, several bulk properties (densities, porosities, specific surface areas) of C–S–H have been explained.

- While the discussion was directed towards the fractal/nanogranular models, Viehland and Xu (Xu and Viehland, 1996; Viehland *et al.*, 1996) experimentally and Skinner *et al.* (2010) analytically, identified nanocrystalline C–S–H structure of 3.5 nm diameter by X-ray scattering experiments on synthetic C–S–H. C–S–H is a phase changing, polycrystalline material at the nanolevel, hence it can be highly disordered at the micron level but exhibiting crystalline areas at the nanolevel in agreement with Plassard *et al.* (2004).

- According to work presented by Beaudoin *et al.* (2010) attention is still focused on the layered models of C–S–H, which seem to be providing answers to the pertaining issues (shrinkage, role and different categories of water in the C–S–H, structural and compositional characteristics and others).

2.5 Effect of nanoparticles on hydration and microstructure

As seen from the previous section, C–S–H is nanosized, and within the hydrated cement paste, apart from the nanostructured solids, there are also nanopores filled with water and nano air voids. Therefore, nanotechnology can offer a twofold advantage by (i) providing nanosized constituent materials and by (ii) allowing the study of the chemical and structural modifications induced by the addition of nanomaterials at the nanometric scale range.

The introduction of nanoparticles in cement matrices affects hydration, strength, durability and microstructure in a number of ways, as nanoparticles may play the role of:

- nanofillers, reducing the nanoporosity within the hydrated paste and extending the concept of particle packing (Scrivener, 2009; Jo *et al.*, 2007a)
- nanoreinforcements, increasing the tensile and flexural strength and consistence of the paste (Sobolev *et al.*, 2009a; He and Shi, 2008)
- catalysts due to their high surface area (Figure 2-14) (Birgisson and Dham, 2011; Björnström *et al.*, 2004)
- nucleation sites for the reaction products due to their high specific surface area and the unsaturated bonds on the surface of the particles (Birgisson *et al.*, 2012; He and Shi, 2008)
- highly reactive pozzolanas, consuming $Ca(OH)_2$ to produce additional C–S–H (Sobolev and Gutiérrez, 2005a) and as
- counter balance against high amounts of supplementary cementitious materials (such as reduction in the early strength gain with high amounts of FA or need for superplasticizers with large quantities of μS (Scrivener, 2009))

They are, therefore, expected to react rapidly and enhance the precipitation of hydrates, resulting in a denser matrix (Sobolev and Sanchez, 2012; Lin *et al.*, 2012; Al-Otaibi, 2012; Balaguru and Chong, 2006; Li *et al.*, 2004a; Li *et al.*, 2004b). However, different nanoparticles, show different combinations of the abovementioned properties, therefore a number of studies have concluded contradicting results, as identified in the next two sections.

Knowing the composition, the structure, the variables that affect C–S–H and how in turn C–S–H affects the hardened cement properties, material scientists and cement technologists can now engineer new cements, which are highly durable, with savings on maintenance costs. Adding to the above, the cost of nanosized silica containing particles is significantly lower than the cost of μS, especially in the case of montmorillonite (MMT) which is provided naturally, since they are clays or nS, which is produced from the extraction of silica sand avoiding the μS industrial processes (Bi *et al.*, 2012). It is interesting to note that nS characteristics and reactivity are affected by the production method used and the same is valid with nanoclay (nC), which on top of that, being produced by generic clays also have

a significant variability according to the place they are collected from. All these will be discussed extensively in the following subsections.

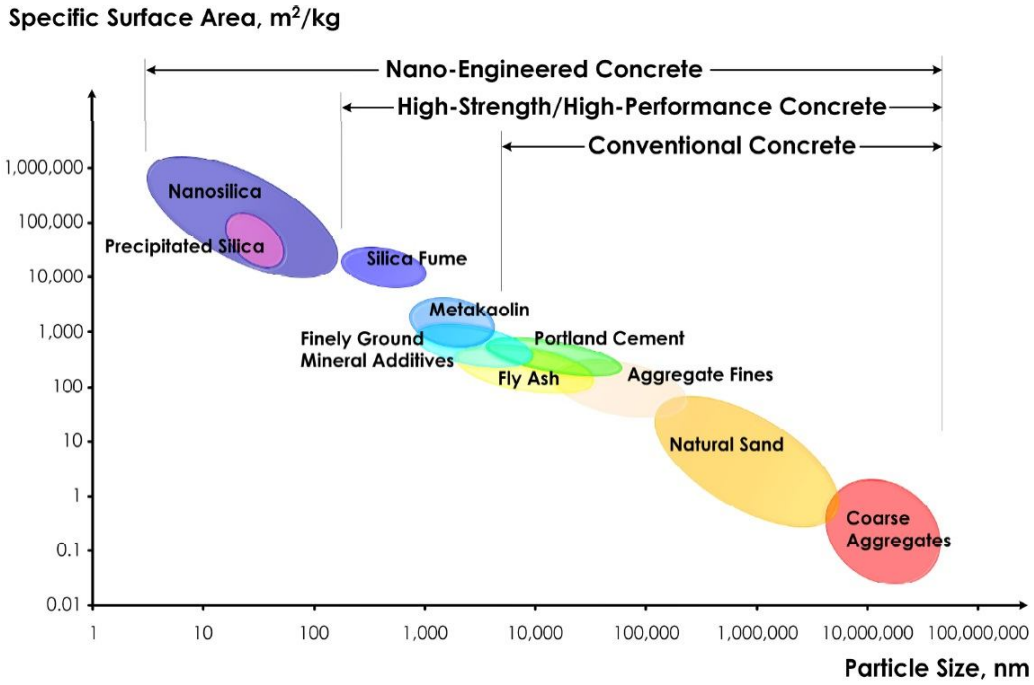

Figure 2-14: Particle size and specific surface area scale related to concrete materials (Sobolev *et al.*, 2009b)

The common drawback being reported by most researchers is the tendency of the nanoparticles to conglomerate before and/or after mixing, particularly when in contact with water (Fares and Khan, 2013; Bi *et al.*, 2012). Although it is more predominant in higher loadings, it can be observed even at lower concentrations, minimizing the benefits of the nanosize and creating unreacted pockets and therefore, potential localized stress points within the paste (Sanchez and Sobolev, 2010). Various suggestions have been proposed as a way to overcome this limitation. The general concept that governs these methodologies, however, is that the repulsive forces between the nanoparticles must be increased, so that they remain dispersed. This subject will be analytically discussed in the next paragraphs.

In this study the effect of the addition of two types of nanoparticles, namely nanosilica (nS) and nC, was investigated. Both nanoparticles attract the attention due to the innumerable abilities they offer, if used appropriately, for the production of low carbon-footprint cement with enhanced properties leading to sustainability, which could be practically achieved. The former was selected due to the fact that although it has been used in several studies a number of inconsistencies have been observed calling for a holistic understanding of the effect it has on C–S–H formation while simultaneously discussing (i) the optimal dosage of nanoparticles, (ii) the limits of their reactivity in blended cement pastes, (iii) potential competition with supplementary cementitious materials and (iii) use of superplasticizers in the pastes. Research was needed to provide an insight into the synergistic effect in the

microstructure and mechanical characteristics of low embodied CO_2 cements and nS in the fresh and hardened state. At the same time, no former study had been presented with the specific type of nC with respect to the same parameters; modification in the microstructure and mechanical properties of cement pastes, optimal dosage, reactivity, limitations of use. The nC modified pastes were compared with the nS nanomodified ones, in terms of these parameters.

2.6 Addition of nanosilica particles to cement pastes

2.6.1 On the production of nanosilica particles

According to Fares and Khan (2013) the foreseen global need for silica (natural, biogenic or synthesized) for concrete will reach 2.7 million tonnes with a total cost estimation approaching 3.9 billion British pounds (GBP) by 2014. nS is essentially nanosized silica, produced by reducing the particle size of silica powder to the nanometric level through a number of different processes. Silica has the chemical formula of silicon dioxide; SiO_2. Every atom of Si is connected with four atoms of oxygen, creating tetrahedra, the basic building block. Hence, silicate chains are produced by oxygen sharing silicate tetrahedra. In crystalline silicas, there is some long range order with chains formed by siloxane bonds (≡Si–O–Si≡). Amorphous SiO_2 has no long range order. In both cases, the Si atom is unsaturated on its outer side, allowing for reactions with water leading to the creation of silanol groups (≡Si–OH), governing adsorption and surface reactivity of silica (Oertel, 2013). In terms of physical properties, nS compared with μS, has the following typical characteristics:

Table 2-5: Material characteristics of commercially available nS compared to μS

	Particle size	Specific surface	Form
μS	200-1000 nm	15-20x10^3 m^2/kg	Dried powder (or in solution)
nS	1-150 nm	20-1000 x10^3 m^2/kg	In solution

Different synthesis processes have been suggested, believed to have an effect, in turn, on the reactivity of nS (Soleymani, 2012). The nS particles delivered are either hydrophilic or hydrophobic, with respect to the condition of the OH– group on the surface of the nS particle. There are two major nS production methods used, encompassing thermal treatment or not; pyrogenic or non-pyrogenic, accordingly (Fares and Khan, 2013; Napierska *et al.*, 2010). Amorphous nS particles are produced by polymerization of monomers and can be classified in six major categories, depending on the method of production (Figure 2-15). These are (i) colloidal or sol with uniformly shaped hydrophilic particles of diameter ranging from 1 to 1000 nm, (ii) Stöber silica with spherical hydrophilic particles of diameter ranging from 10 to 1000 nm, (iii) silica gel with hydrophilic particles of diameter of 0.5-5

nm, (iv) precipitated silica with hydrophilic particles of diameter of 5-6 nm, (v) mesoporous silica with hydrophobic particles of diameter of 50-1000 nm, and (vi) pyrogenic/fumed silica with hydrophobic particles of diameter of 2-50 nm (Fares and Khan, 2013). Overall, the use of dry powders in concrete can only be achieved with the use of superplasticizers as dispersion mediums. For practical reasons, therefore, colloidal silica is more often preferred by cement scientists. More information on the synthesis of amorphous nS, as well as the synthesis of crystalline silica and their relative properties can be traced in Napierska *et al.* (2010). Production costs in terms of energy requirements can be reduced through nS production by the dissolution of olivine $(Mg, Fe)_2SiO_4$, a promising technique, since the Si–O–Si bonds it contains can be easily broken. However, this is still at an experimental level (Lazaro *et al.*, 2012).

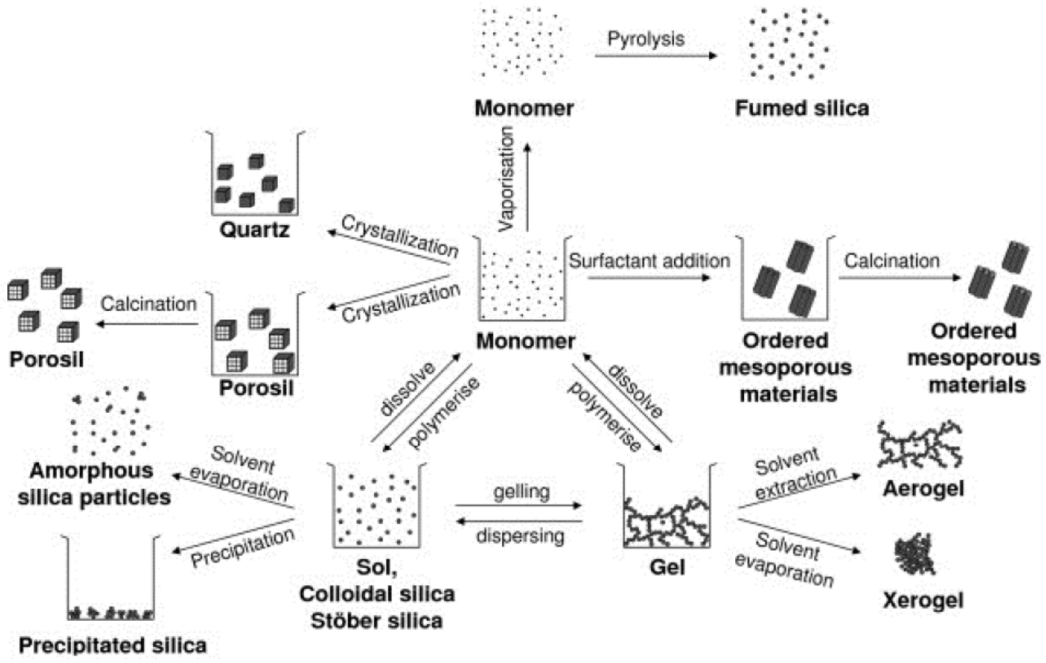

Figure 2-15: Methods of production of nS and classification (Fares and Khan, 2013)

2.6.2 Optimum dosage of nanosilica particles

Different optimum proportions have been suggested by various researchers and contradictions have been observed. Some researchers managed to maximize compressive strength by keeping nS substitution to a minimum, for example (i) less than 1% (Sobolev *et al.*, 2009a; Sobolev and Gutiérrez, 2005a, b; Stefanidou and Papayianni, 2012) (ii) between 1-3% nS (Qing Ye *et al.*, 2007; Ye *et al.*, 2006), 0.5, 1, 1.5 or 2% (Soleymani, 2012) or (iii) up to 10% nS by weight of cement (Li *et al.*, 2004b). The justification provided was on the grounds that at higher dosages the nS particles conglomerate and dispersion is inhibited. Others recommended even higher percentages of replacement for best results. For example Bi *et al.* (2012) tested concrete specimens containing 3, 5, 10 and 15% nS and compared them against similar specimens which contained 5% of μS in addition, in a study

discussed in detail later. In another study, Mondal *et al.* (2010) in a nanoindentation and ^{29}Si MAS-NMR spectra analyses compared pastes containing 6 and 18% by mass of colloidal nS and found that the higher the percentage of nS the more the HD C–S–H (38% for the sample containing 6% of nS and 50% for the sample of 18% of nS) is formed against LD C–S–H. According to this finding, the higher the nS replacement the more durable the product is (since more high-stiffness C–S–H which is more resistant to calcium leaching is produced). One of the research objectives is hence, to engineer and suggest an optimum mix, containing colloidal nanosilica, for compressive strength and durability enhancement as revealed in the following paragraphs.

2.6.3 Pozzolanic activity of nanosilica particles

In a comparative study presented by Lim *et al.* (2012) the pozzolanic reactivity of nS in mixes containing nS dispersion at 5% replacement by mass of cement was confirmed through thermogravimetric analysis (TGA), X-ray diffraction (XRD) and compressive strength tests. Importantly, the fact that the addition of nS increases the thermal stability of the paste was affirmed. Two series of samples were prepared (with and without nS) and were cured in an environmental chamber at 25ºC and 100% relative humidity for 28 days. They, then, underwent different cycles of heat treatment, ranging from 105 to 500ºC. To ensure the validity of results six specimens were used for the heat treatment and three specimens for control. TGA showed a 5% mass loss related to the $Ca(OH)_2$ consumption for the sample containing nS. The observed reduction in $Ca(OH)_2$ for the specific samples supports the opinion of the enhanced pozzolanic reaction that nS is offering, a conclusion also confirmed by the XRD analyses. It is interesting to note that the XRD showed that the percentage of nS was insufficient for the full transformation of $Ca(OH)_2$ into C–S–H. The compressive strength of the samples with nS was always higher by 10-20% with maximum performance achieved for the sample with the highest heat treatment. Still in this research the optimum content was not investigated, TG analyses were carried out only up to 500ºC and tests were presented only for day 28, not allowing further conclusions to be drawn.

2.6.4 Effect of nanosilica particle size also related to pozzolanic activity

Al-Otaibi (2012) compared the effect of two different sizes of nS: a 15nm (fine) nS and an 80nm (coarse) nS to cement mixes. 1, 2, 3, 4 and 5% replacement of PC was investigated. XRD, scanning electron microscopy (SEM), TGA and compressive strength tests were carried out at 7 and 28 days. Some results for the 3% and 5% replacement were presented. Overall, the addition of nS was found to increase hydration products and accelerate the reaction. The microstructure was once again improved. Conclusions would have been more robust if supported by later ages and all percentages of nS.

A similar comparison, although this time using colloidal nS, was carried out by Kawashima *et al.* (2012) who blended nS in FA mortars. nS is believed to counteract the negative effects that the addition of FA has on the early-age properties of pastes. The importance of incorporating nS in the mix is then enhanced since, in parallel, it allows for greater

substitutions of cement by greener replacements. Their intention was to combine the high consistence provided by FA with high early strength gain provided by nS. The slump flow was determined for mortars containing 0, 2.25 or 5% nS together with 20, 40 or 60% FA. Fluidity increased with increasing FA and decreased with more nS. At the same time compressive strength of later ages was also slowed down. Microscopic analyses showed that this effect can be attributed to the consumption of most of the $Ca(OH)_2$ by nS at early ages, leaving small amounts of $Ca(OH)_2$ for the hydration of FA. However, some FA particles exhibited a thick coating of hydration products comprised of two layers with a low C/S ratio, lower than that of the adjacent C–S–H, implying that this double-coating is acting as an "ion penetration barrier" not allowing the hydration of these FA particles. They also concluded that the higher FA and nS contents are, the more insufficient the amount of $Ca(OH)_2$ is likely to be. In this study, arrest of hydration was carried out with the use of acetone, which is not the most recommended alcohol for this procedure, as will be discussed in Chapter 3. Oltulu and Şahin (2014) studied the effect of powder nS on PC mortars containing 15% by mass FA and concluded that increase in compressive strength can be expected if nS addition is limited to 1.25% by mass when FA is present. A 2.25% nS addition led to reductions in compressive strength due to agglomeration of the nanoparticles as suggested by SEM analysis.

2.6.5 Effect of nanosilica on blended cements

Colloidal nS produced by sol-gel and stabilized with sodium was added to cement and calcium hydroxide to study the effects on cement hydration and C–S–H gel properties in early and later ages by Hou *et al.* (2013b). Binary mixes containing up to 5% nS and up to 5% μS was also developed for comparison at a w/b ratio of 0.4. Specimens were demoulded one day after casting and were stored in a lime-water curing tank for 3, 7, 28 and 84 days (Figure 2-16). For the microstructural characterisation the samples were crushed, the hydration was arrested with acetone and then they were oven-dried at 105ºC for 4h. Once again, it was confirmed that the pozzolanic reaction of nS was nearly finished after 7 days, but for μS a month was needed. In agreement with Ye *et al.* (2007), they attributed this difference in the chemical structure of the two materials; nS having many unsaturated Si–O bonds [due to high surface area, there are more terminations of the silica network at the surface, which can, in turn, extend pozzolanic reactivity (and subsequently the amount of C–S–H formed) (Jo *et al.*, 2007b)], whereas μS has saturated ones, slowing down the reactions. The compressive strength tests on mortars having additionally 40% of FA as cement replacement revealed that nS has a stronger effect at early ages. Indicatively, for the 5% nS mix the 7 day strength was enhanced by 45%. However, the 5% nS and μS mix exhibited a 10% reduction for the same age. They also concluded that nS accelerated cement hydration due to the nucleation sites created. The severe pozzolanic reaction that is taking place when nS is added leads to the depletion of $Ca(OH)_2$, an effect responsible for the high early age reactivity of nS and catching up of μS mixes with the nS ones at later ages. As also pointed out in an earlier study of Hou's team (Kawashima *et al.*, 2012) backscattered SEM image analysis confirmed this finding, while revealing a coating of

hydrates surrounding unhydrated cement particles. This coating of very low permeability is not allowing alite's hydration. For this reason only 89.4% of cement with 5% nS added participated in the 8-month hydration. However, the possibility of $Ca(OH)_2$ depletion will be extensively discussed in this thesis, in addition to findings suggesting antagonism between FA and nS (Calabria-Holley *et al.*, 2014).

Lastly, nanoindentation tests showed that the addition of nS cause a reduction of LD C–S–H in favour of the HD C–S–H, as also proven by Mondal *et al.* (2010).

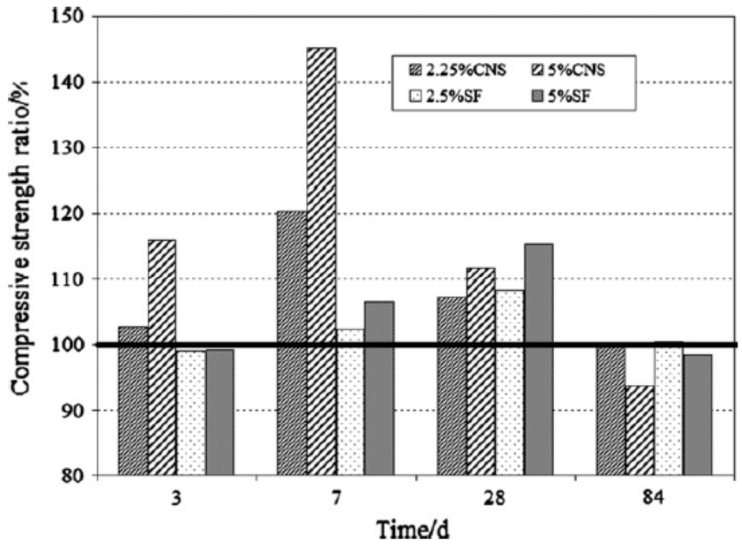

Figure 2-16: Improvement in compressive stength with the addition of nS or μS (Hou *et al.*, 2013b)

2.6.6 Effect of conditioning, grinding and mechano-chemical activation

Soleymani (2012) investigated the effect that curing in saturated limewater or plain water or a combination of both has on pastes where PC is replaced by 0.5, 1, 1.5 and 2% of nS powder by mass of cement. Water to binder (cement + nS) ratio was held constant at 0.4. Compressive strength tests were carried out on mortars at day 7, 28 and 90. The optimal mix cured in water contained 1% nS, where the 2% nS mix was less strong than the 0.5% nS mortar. Overall the highest strengths were achieved by the 2% nS mortar cured for the first 28 days in limewater and from then on, in plain water.

At this stage, special attention should be given to the preparation method followed for the addition of nS to the mix. Various methods have been studied in an effort to accelerate hydration and avoid clustering of the nanoparticles. Stirring the solutions in an ultrasonic sonicator seems to be one of the most effective mitigation measures (Bhattarai, 2006). Very recently, Elkady *et al.* (2013) presented a study on the effect of different de-agglomeration techniques (sonication, homogenization and stirring) on the compressive strength and workability of nS concrete. The specimens were water cured and tested at day 7 and 28. Five minutes sonication proved to be the most effective method, enhancing the compressive

strength by 23%, and the concrete workability, using only 1% of nS (as opposed to 0, 1.5 and 2% of nS), substituting cement. Sonication was considered to have increased the surface area and the nucleation sites. The sonicated nS exhibited a higher pozzolanic activity.

Lastly, apart from super-fine grinding of the materials or ultrasonic stirring or high speed mixing at different stages, Lin *et al.* (2012) presented a study of mortars prepared with nanomilling and mechano-chemical activation (MCA). They created a slurry believed to be "mechano-chemically activated" (AC: Activated Cement Slurry), containing colloidal nS at 10-20% cement replacement and superplasticizer. AC was then tested in standard mortars as replacement of PC, cured at room temperature, at ages 1, 3, 7 and 28 days, again lacking the study of the effect at later ages. Adding to this, two specimens were reported to be tested for each mix. The results showed that the MCA did not reduce the binding characteristics of cement and in effect nanocement can be used as slurry for the design of concrete mixes. The early age compressive strength of cement can be improved by the proposed method as well as the microstructure of the cement thanks to the higher densification of the nanoparticles.

2.6.7 Limitation on the addition of nanosilica particles - consistence

Another divergence of findings is related to consistence. According to several studies consistence is enhanced by nS (Sobolev *et al.*, 2009b; Sobolev and Gutiérrez, 2005a; Li, 2004). More recent studies proved that with increasing amounts of nS additional water and/or superplasticizers are needed (Bi *et al.*, 2012; Sanchez and Sobolev, 2010; Sobolev *et al.*, 2006). Senff *et al.* (2010b), after testing samples containing 0-7% nS (in suspension having 30% of solids by weight), μS of 0-20% and water to binder ratio of 0.35-0.59 found that the maximum unrestrained shrinkage increased 80% for the 7-day old nS mortars and 54% for the 28-day old ones, compared against the μS mortars. Moreover, the maximum proportion of nS yielded the maximum water absorption and porosity. It is necessary therefore, to clarify the effect the addition of various percentages of nS has on the consistence of cement pastes.

2.6.8 Mitigating limitations – use of superplasticizers and other additives

Bi *et al.* (2012) produced a reference concrete mix, including μS, and the admixture Viscocrete 10 ex® by Sika and compared its compressive strength, permeability and microstructure against four mixes containing 3, 5, 10 and 15% nS by mass of cement and 4 mixes containing 3, 5, 10 and 15% nS together with 5% μS by mass of cement. Testing was carried out only at ages 1, 3, 7 and 28 days, as shown in Figure 2-17 therefore the effect nS has on the mixes at later ages, which is of high importance and interest, was not reported. The 10% nS with 5% μS mix showed the highest compressive strength and the lowest permeability and chloride ion penetration. The highest amount of nS (with or without μS) showed a decrease in the compressive strength, and a dramatic increase in permeability and chloride ion penetration, a fact attributed by the authors to the agglomeration of the

particles, implying that excessive nS does not allow μS to react as intended. It is of interest to note, though, that the lower dosage of nS (3% nS and 5% μS) exhibited very high values on permeability and chloride ion penetration and that for higher amounts of nS the water/binder ratio and dosage of viscocrete was increased, proving once again the point that workability would have been reduced with higher dosages of nS if superplasticizers had not been employed.

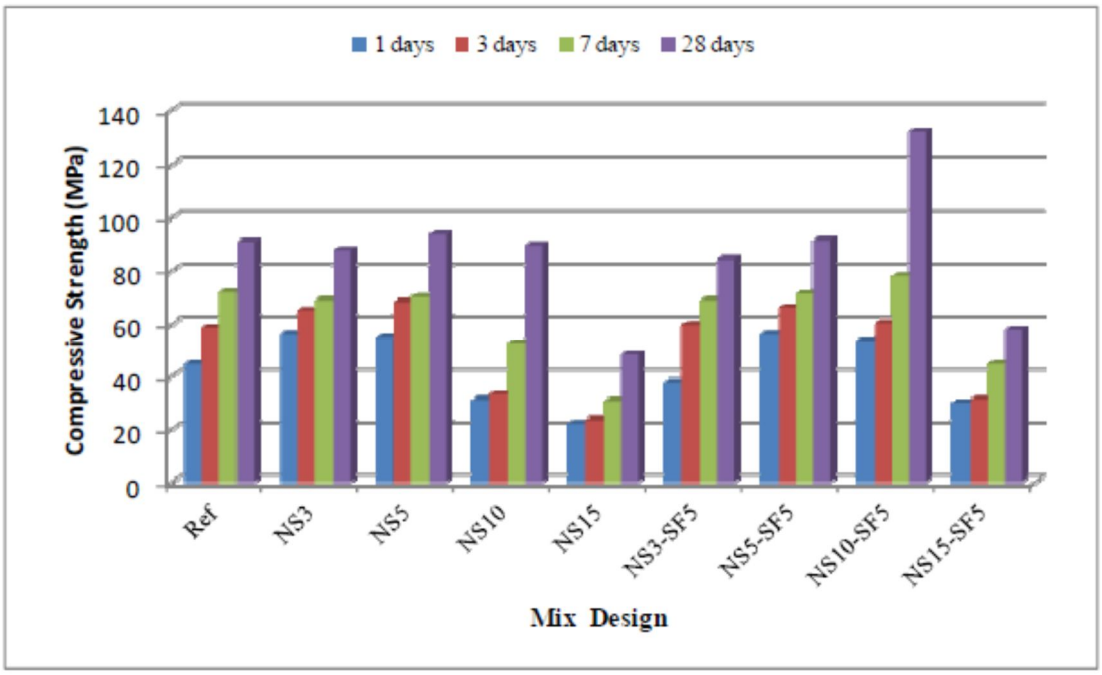

Figure 2-17: Compressive strength results (Bi *et al.*, 2012)

Oltulu and Sahin (2011) compared the compressive strength and capillary permeability of cement mortars combined with one, two or three nanoparticles of nS, nano-Al_2O_3, nano-Fe_2O_3 in powder form and μS. It is worth noting that a water reducing agent (commercially available as Viscocrete PC-15®) was added in the mix at 0.75% by mass of the binder, as well as a defoamer at 1% by mass of the binder. After mixing, compacting and demoulding a day later, the specimens (three for each mix and age) were cured in lime-water at 20±2ºC. In the single combinations, only nS was added at 0.5%, 1.25% and 2.5% of the binder by mass. In the binary combinations, apart from nS, μS was added at 5% of the cement, keeping the water/binder ratio constant and equal to 0.4. Compressive strength was tested at day 3, 7, 28, 56 and 180. In all mixes higher values were achieved with age, the later ones being marginal. Best results were achieved for the 1.25% nS mortar. Specifically, both compressive strength and capillary permeability were greatly enhanced, in both single and binary combinations compared to the control specimen (mortar of CEMI+5% μS by weigh of cement). In contrast, a strength reduction between 43% and 60% and an increase of the capillary permeability of the mortar by 54% compared to the control specimen was observed for the 2.5% nS mortar. The general increase in compressive strength and reduction in "capillary permeability" [as a function of (i) the amount of water absorbed by immersed in water specimens, (ii) the area of the specimen in contact with water and (iii)

the time elapsed] was attributed to the effective filling of the micro and nanopores of the paste by the nanoparticles, supported by SEM images. There is a threshold, though, that if exceeded, the permeability of the mortar instead of being further decreased, as intended and expected due to the filler effect, is reduced. This was attributed to agglomeration of the nanoparticles that took place at higher concentrations (2.5% nS) due to their very high specific surface area, which in turn caused uneven dispersion of the nanoparticles in the mortar. Hence, the two researchers brought attention to the fact that this threshold must be determined in all efforts of improving the pore structure of pastes.

It is a fact though, that superplasticizers have been used in older studies, too. For instance, Ye *et al.* (2007) kept a constant w/b ratio of 0.22 and a superplasticizer content of 2.5% by mass of cement to compare mixes with 3% nS or 3% μS content. They concluded that nS, due to its high specific surface area, increases the amount of adsorbed water and the wettable surface area, producing a denser paste. They also concluded that due to the great number of unsaturated ≡Si-O- and ≡Si- bonds, nS accelerates hydration, as was also expected by Bye (2011), specifically with regards to the reaction with $Ca(OH)_2$ according to the following formulas:

$$\equiv Si - O - \ + H - OH \ \rightarrow \equiv Si - OH \ (rapid\ reaction) \qquad \text{Equation: 2-6}$$

$$\equiv \text{Si} - \ + \text{OH} \ \rightarrow \equiv \text{Si} - \text{OH (rapid reaction)} \qquad \text{Equation: 2-7}$$

$$\equiv Si - OH \ + \ Ca(OH)_2 \ \rightarrow \ C - S - H \qquad \text{Equation: 2-8}$$

As opposed to the hydration reactions taking place in mixes containing only μS, which has many saturated siloxane bonds (≡Si-O-Si≡) at the surface:

$$\equiv Si - O - Si \equiv \ + H - OH \ \rightarrow \equiv Si - OH \ (slow\ reaction) \qquad \text{Equation: 2-9}$$

$$Si - OH \ + \ Ca(OH)_2 \ \rightarrow \ C - S - H \qquad \text{Equation: 2-10}$$

Lastly, they present compressive strength results, including ages at 1, 3, 28 and 60 days. Ye *et al.* (2007) also concluded that compressive strength increases with increasing percentage of nS addition, as opposed to μS, which had an adverse effect for 1 and 3 day old samples.

Li *et al.* (2004b) tested the mechanical properties and produced SEM images of cement mortars containing 3, 5 and 10% nS by weight of cement mixed with cement, sand defoamer and UNF-water reducing agent. In research by Li *et al.* (2004a) the mixing procedure for the pre-mentioned mortars is described as follows: the defoamer and the water reducing agent were dissolved in water, then, nS was added and the mix was stirred for 2 minutes at high rotation. Next, cement was added and mixed for 1 minute at low speed in a mortar mixer. Sand was added last and mixed again at low speed for 1.5 minutes. At a constant

water/binder ratio of 0.5 (the binder being considered as the sum of cement and nanoparticles), the three different mixes showed an enhancement in both 7 and 28 days compressive and flexural strength, with values increasing with the nS content. The conglomeration ability and the formation of nuclei were once again observed with the use of SEM. Furthermore, it was confirmed that nanoparticles may prevent the growth of $Ca(OH)_2$ crystals and although they are indeed capable of filling the nanopores, in cases where they are not well dispersed (such as at high nanoparticle contents) they create weak zones, an opinion also shared by Sobolev (2009a). At the same time, they claimed that at lower nS contents, even if nS is not well dispersed, the weak zones will be prevented, as the nS will be consumed for the production of C–S–H. They argued that the addition of nS had an overall enhancing effect, providing mortars with higher compressive strength for the pastes containing higher nS percentage, whereas flexural strength was found to be inversely proportional to the nS content. It should be stressed that these two researches were carried out for the ages of 7 and 28 days, hence still lacking the later age effect.

2.6.9 Discussion and further research

To sum up, it is still uncertain what is the optimum dosage of nS in cement, with researchers suggesting dosages ranging from 0.5% (Soleymani, 2012), to 1% (Qing Ye *et al.*, 2007; Sobolev *et al.*, 2009b) and even as high as 10% by mass of cement (Li *et al.*, 2004b). Furthermore, a maximum limit on nS addition in blended cements has not been determined. Adding to this, some researchers are reporting pozzolanic reactivity of the nS particles, whereas others are supporting the seeding effects of nS. Therefore, the way the nS particles affect cement pastes, both at early and later ages is still uncertain. It is necessary therefore that in a single research programme the effect of different percentages of colloidal nS are studied in blended and composite Portland cement pastes in an effort to define (i) the limits of nS addition, (ii) the competing constituents in the formulations, (iii) the role the nS particles play within the hydrating pastes and (iv) optimal engineered formulations towards more sustainable Portland cement blends.

2.7 Addition of nanoclay particles to cement pastes

2.7.1 Supply of natural clays

After an extensive number of studies in the field of clay-polymer nanocomposites, clay-cement nanocomposites have gained momentum as a cutting-edge alternative to the engineering of sustainable modern construction materials. A nanoclay is essentially a clay whose layers have been separated and are individually available for reactions. The popularity of clays as additions to cement is due to their vast surface area, which lies in the order of 10 – 800x10^3 m^2/kg (Xi, 2006; Utracki, 2004), since it has been proven that the extent of pozzolanic reactivity (and subsequently the amount of C–S–H formed) is proportional to the surface area available for reactions (Jo *et al.*, 2007b). Unlike most nanoparticles, clays are naturally occurring minerals, therefore their use is the most economical amongst most nanoparticles (De Paiva *et al.*, 2008). Clays are classified in two categories with respect to the geographical location they are extracted/excavated/mined from; residual and transported clays. The former are the result of rock weathering and are found where they were created. They are usually formed by either disintegration of volcanic ash or by the hydrothermal modification or solution of volcanic rocks (Briell, 2000). The latter category encompases all clays naturally removed from the site they were created and deposited elsewhere (Uddin, 2008). The main constituents of clays are silica and alumina. Clays can also be classified with respect to their structure into four main groups: smectites [comprising of montmorillonites (MMT) and others], kaolinites, illites and chlorites. The latter is classified by some scholars as a separate phyllosilicate group (Briell, 2000). Smectites are groups of clay minerals, with a general chemical formula: $(Ca,Na,H)(Al,Mg,Fe,Zn)_2(Si,Al)_4O_{10}$ $(OH)_2$. nH_2O (Uddin, 2008). Montmorillonite (MMT) is a specific mineral, which took its name after the place where it was discovered, Montmorillon, in the Vienne prefecture of France, in 1847. Bentonite, also known as Wyoming bentonite, was given its name by Wilbur C. Knight in 1898, after the cretaceous Benton shale near Rock River, Wyoming. The Wyoming bentonite is an impure clay soil, containing a number of minerals the majority of which (about 80%) is MMT (Utracki, 2004). Through purification processes with the use of sodium cations, MMT can also be derived from bentonites, justifying its second name, “sodium bentonite”, as discussed later.

Both the Montmorillonite clay and the MMT coming from purified bentonite were used in the present study.

2.7.2 Nanostructure of clays

In order to understand how nC is produced, the structure of natural MMT clay will be discussed first. MMT clay is a two-dimensional hydrophilic nanoparticle. It is composed of crystalline layers or platelets stuck together. each layer is composed of a “sheet” of octahedra of AlO_6, which is bounded at the top and bottom by a “sheet” of tetrahedra of SiO_2. The silicon-oxygen tetrahedra share three corners with neighbouring SiO_2 tetrahedra

to form hexagonal networks, whereas the fourth corner is bonded with the octahedra of AlO_6 (Uddin, 2008). The total thickness of this 2:1 ratio, structure, also known as 2:1 layer silicate (Figure 2-18) is estimated to range from about 0.95 nm to 1 nm (Dalir *et al.*, 2012; Sapalidis *et al.*, 2011; Jahromi *et al.*, 2010; Utracki, 2004). The lateral dimensions varying from a few nanometers to a few hundreds of micrometers (Sapalidis *et al.*, 2011).

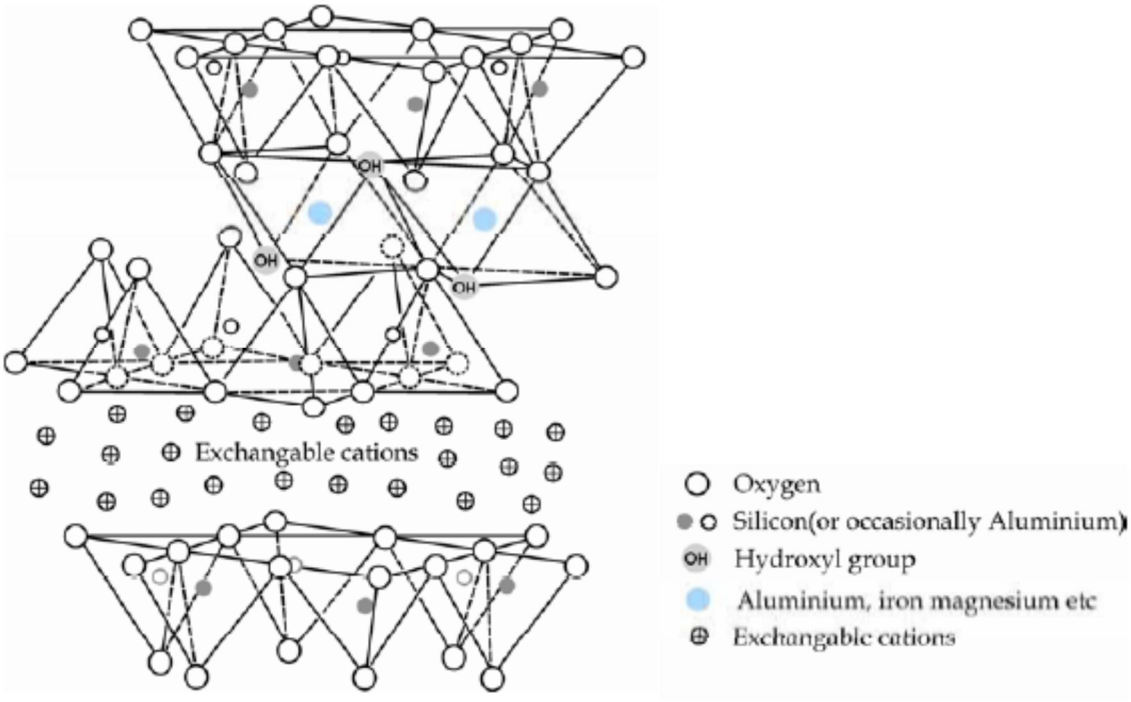

Figure 2-18: The structure of montmorillonite (Sapalidis *et al.*, 2011)

2.7.3 Production of nanoclay particles

The agglomeration of the nanosized layers in MMT is due to the surface attraction between them (Batra *et al.*, 2011). A certain number of layers can be held together by electrostatic force, by hydrogen bonding, by interlayer cations or by van der Waals forces, inhibiting the solubility or miscibility (Dalir *et al.*, 2012). However, these forces are moderately weak forces in MMT (Dalir *et al.*, 2012; Uddin, 2008). Clays can only be considered to comprise of individual nanoparticles, charged for reactions, if and only if the bonds bridging the layers are weakened to the extent of separation of the layers. This happens usually in two steps; (a) purification of the MMT through washing with distilled water and shearing/vigorous stirring leading to the delamination of the particles (Vazquez *et al.*, 2008) (heating being another or additional method for delamination which is mostlty used for the expansion of metakaolin) and (b) introduction of either a modifier, within the "galleries", i.e. the interlayer spaces in clays, having a chemical effect by causing an exchange of cations, hence a change in the charge of the molecules inducing electrostatic repulsion of the platelets and hence, a furter separation of the layers or/and of a surfactant, introducing surface tension and repulsion of the platelets. The addition of either of the two should be followed by vigorous striring, reflux or other processes.

MMT particles are naturaly agglomerated inorganic, hydrophilic nanoparticles and they are considered incompatible to use in cement because the clay will swell in presence of water (Birgisson and Dham, 2011). For this reason, significant research has been dedicated to the modification of the clay to an organophilic material, compatible with cement, which is the case if the modifier is organic. The clay is then said to be organomodified (e.g. OMMT = organomodified MMT), becoming organophilic, therefore, hydrophobic by cation exchange. The cation exchange mechanism can be explained as follows: Si and Al are bonded with oxygen molecules. Molecules of OH^- are also found at the edges of the octahedral sheet. Since each of the layers is charged, including their edges, a major feature of the MMT is the fact that ion exchange can take place within their structure affecting the properties of the clay. Specifically, mostly Na, Mg, Al or Ca cations can be exchanged for organic cations between the interlayer to produce the OMMT. When only Na^+ cations are used for the modification, the clay is known as sodium-MMT or, else, bentonite, with chemical formula: $Na_{0.33}[(Al_{1.67}Mg_{0.33})(O(OH))_2(SiO_2)_4)]$ (Luckham and Rossi, 1999). A number of studies on the preparation of OMMT are mentioned in De Paiva *et al.* (2008). Theoretically, most MMT have a total total content of SiO_2 and Al_2O_3 equal to 92% and the SiO_2/Al_2O_3 ratio is equal to 2.6. These values for the sodium-MMT, however, are 83.6% and 4.79 respectively, indicating greater amounts of SiO_2.

The degree of expansion in the OMMT is reflected by the number of cations exchanged between the layers of the crystal which is termed the cation exchange capacity (CEC). MMT has a CEC in the order of 80 to 120 meq/100g (Jahromi *et al.*, 2010).

MMTs are preferred due to their high CEC, their high surface area and the relatively easy "expansion" in water. The fact that they can form stable suspensions in water allows for exploration of many potential applications, since, in any case, they must be dispersed in water before added to cement mixes. However, the higher the concentration of the nC particles in these aqueous solutions, the greater the possibility of flocculation.

This technology of modifying clay into a highly absorptive, organophilic material with enormous specific surface area has been extensively implemented in sea water pollutant removal applications or remediation of contaminated soils (Xi, 2006; Xi *et al.*, 2005). Notwithstanding the significant research involved in the expansion and separation of the platelets in the presence of organomodifiers, there is one issue pertaining; for certain industrial applications the organomodified clay may need to be dispersered in aqueous solutions. Since it has become hydrophobic, though, it is incompatible with water, causing extensive flocculation of particles. This difficulty can be overcome with the use of surfactant technology. The surfactants, are amphiphilic compounds, that is to say, they contain both a water-insoluble component and a water-soluble component. They can surround the platelets, increase the surface tension and allow the dispersion of the nanoclay platelets in aqueous solutions. However, if used in organomodified clays, the product becames even more chemically complex. This technology is of particular importance as it can potentially keep the platelets dispersed without the need for organomodification, possibly allowing the use of inorganic nC. At the same time it can be utilized in OMMT

dispersions. It should be noted that some modifiers may act as surfactants, as well, but the surfactants cannot act as modifiers as chemically they are not designed to facilitate cation exchange.

Kuo *et al.* (2011) have stressed the need for the organo-modification of clays by cation-exchange in order to prepare the clay for mixing with water and consecutively with cement. Along the same lines, Alizadeh (2009) and De Paiva *et al.* (2008) also suggest organomodification for easier interaction in an organic polymer matrix.

2.7.4 Intercalated or exfoliated nanoclay particles

The organomodification and subsequent expansion of the platelets can yield three different states (Sinha Ray and Okamoto, 2003). The first one, which is the flocculation/phase-separation, results into a microcomposite (Figure 2-19a). In this case, layers of clay are mixed with a polymer but the two phases are weakly interacting with each other. As a result, the modifier or surfactant cannot enter in the clay galleries and the composite exhibits poor mechanical properties. The next two modification techniques produce nano-sized particles of clay: the intercalation and the exfoliation (or delamination), schematically represented in Figure 2-19b, c, respectively.

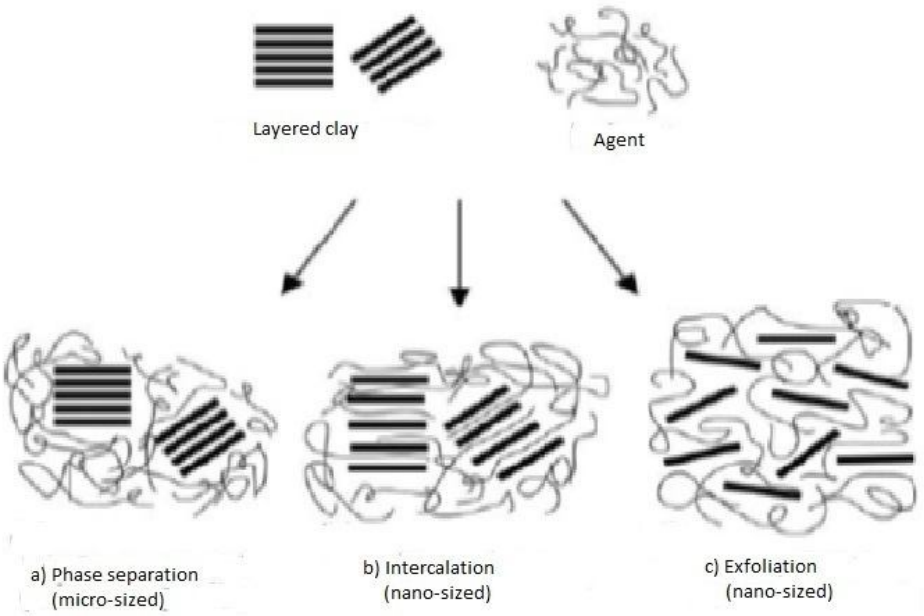

Figure 2-19: MMT modification techniques (Bhat et al., 2008)

Through the process of intercalation, the silicate platelets shown in Figure 2-20 can be forced apart by the selected modifier/surfactant, but still remain at regular, orderly distances. When the agent is very reactive, the platelets are completely separated and randomly dispersed, they are exfoliated as shown in Figure 2-21, transforming a small mass

of MMT in multiples of platelets, therefore, creating a material with very large surface area. Once it is exfoliated the interlaminar distance increases, reaching 5 to 10 or more nm (Sapalidis *et al.*, 2011) and the environment is transformed to hydrophobic (organophilic) (Jahromi *et al.*, 2010; Kuo *et al.*, 2006; Xi, 2006), facilitating the nanoclay dispersion in water (since water will not be absorbed causing subsequent agglomeration of particles). When added to cement, the hydrophobic nanoclay is expected to inhibit water from entering the interlayer space, lowering the water demand. Simultaneously, OMMT nanoparticles are expected to contribute to permeability reduction by surrounding the capillary pores and impeding diffusion. Adding to this, Xi (2006) noted that the basal spacing of the exfoliated nC is also significantly expanded. It is generally acknowledged that composites with exfoliated clays perform better in terms of mechanical properties than system with intercalated clays (Sapalidis *et al.*, 2011). This is because the specific surface area when the platelets are fully separated (exfoliation) increases drastically relative to the intercalated clay. This condition renders the nanoclay highly reactive.

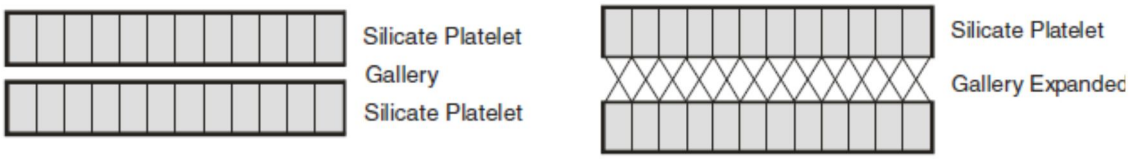

Figure 2-20: Platelets before and after adding expanding agent (Birgisson and Dham, 2011)

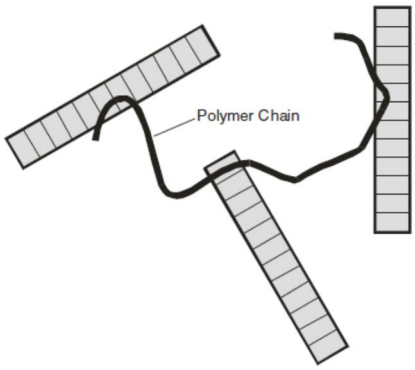

Figure 2-21: Exfoliation (separation) of the silicate layers (Birgisson and Dham, 2011)

Furthermore, there are some other arrangements that may occur (Figure 2-22b-d), apart from exfoliated-dispersed (or in other words highly separated and suspended in water) Figure 2-22(a). Aggregation of the nC platelets is represented by Figure 2-22(b) the distance being less than 2 nm. This face to face (FF) arrangement reduces the strength of the nC gel, as a smaller surface area is available for reactions. Moreover, FF stacking appears to be the preferred inherent arrangement of the nanolayers rendering their dispersion in monolayers challenging (LeBaron *et al.*, 1999). Additionally, it could induce stress paths at the nanolevel. The other two arrangements are typical of nC flocculation forming a continuous gel like structure in the nC dispersions. Other arrangements have also been suggested (Luckham and Rossi, 1999).

According to De Paiva *et al.* (2008) the lead commercial suppliers of organoclays are Laviosa Chemica Mineraria (Dellite®), Nano-cor (Nanomer®), Southern Clay Products (Cloisite® and Garamite®), Süd Chemie (Nanofil®) and Elementis Specialites (Bentone®Nanoclays) [20]. Laviosa Chimica Mineraria, Southern Clay Products and Elementis Specialities produce organoclays based only on quaternary alkylammonium salts, also known as quats, modified MMT.

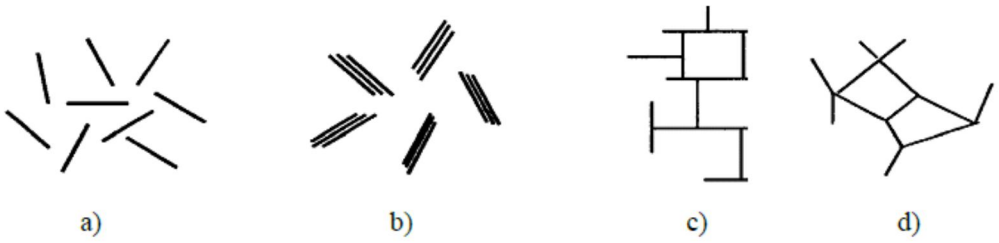

Figure 2-22: Arrangements of nC: (a) dispersed, (b) face to face, (c) edge to face and (d) edge to edge (Luckham and Rossi, 1999)

2.7.5 Effect of modifiers/surfactants and optimum content of nanoclay particles

Various modifiers/surfactants have been utilized in the different studies. For example Birgisson and Dham (2011) used dehydrogenated tallow quaternary ammonium chloride (also known as Cloisite Na^+ or sodium MMT) and concluded that the amount of modifier/surfactant must be carefully chosen with the use of zeta potential, by which the electrostatic repulsion between near and similarly charged particles in a dispersion can be determined. If the zeta potential is high the dispersion is considered stable, i.e. resists conglomeration. This condition can lead to the increase of the compressive strength of cement pastes. However, if the surfactant is excessive, the zeta potential will indicate and electrically destabilized suspension whose particles tend to agglomerate and create weak zones. After studying different samples, containing 0, 2, 5, 9 and 13% of OMMT by mass of cement, they reached the conclusion that 5% exhibited the highest compressive strength. Kuo *et al.* (2006) used dimethyl, dihydrogenated tallow, quaternary ammonium chloride as organic modifier and assessed the effect that 0, 0.5 and 2% of OMMT had on the strength and coefficient of permeability of cement mortars for different w/b ratios: 0.4, 0.48, 0.55. They concluded that in dosages larger than 1% by mass the OMMT particles tend to conglomerate. They suggested that the optimal amounts are less than 1%, depending on the w/b ratio. Furthermore, they clarified that the OMMT particles surround the capillary pores and impede the diffusion of pore solution, reducing the permeability. In a later study Kuo *et al.* (2011) used the same organic modifier as before. They compared the effect different dosages of OMMT: 0, 0.25, 0.5, 0.75, 1 and 2% by weight of cement replaced and different w/b ratios: 0.485 and 0.6 have on the microstructure and mechanical properties of cement mortars. Mercury intrusion porosimetry (MIP) tests proved that the pore size distribution is greatly affected by the addition of OMMT with a significant reduction of the pores between 0.1 and 0.2 μm. It should be stressed though, that they also recorded an increase in the total volume of the larger pores (> 0.2 μm) which could be attributed to the agglomeration of the

OMMT particles while they were dispersed in water. Adding to that, they found that the compressive strength and the elastic moduli initially increase when OMMT was added as the proportions of OMMT increase further, it drops. For this, the ideal dosage was found to be about 0.5% for the lower w/b and about 0.75% for the higher one. According to their results, compressive strength can be increased by more than 33% of equivalent plain cement mortars and elastic moduli can be increased over 65%, which in combination with the total porosity and intermediate pore reduction justify the use of OMMT for the enhancement of the properties of cements. Chang *et al.* (2007) added OMMT to cement at 0, 0.2, 0.4, 0.6 and 0.8% by weight of cement at affixed w/b ratio of 0.55. The highest compressive strength was achieved by the 0.6% nanoclay mix in a twofold manner: OMMT acted as filler, reducing the porosity of the microstructure and as a catalyst-pozzolana forming supplementary hydration products. The lowest permeability coefficient was derived for the 0.4% mix. The microstructural analyses revealed a denser structure with more stable bonds.

In a review produced by De Paiva *et al.* (2008) it was stated that one of the most frequently used cationic surfactants are quats, having as a major advantage the reduction of the density of the dispersed particles due to the large amount of organic material. These organic compounds comprise four functional groups covalently linked to a central nitrogen atom. Of the four functional groups, there is one or more long chain alkyl group and the remaining are either benzyl of methyl groups. Different compounds induce different basal spacings.

2.7.6 Pozzolanic activity of nanoclay particles

Moreover, two further studies with interesting findings will be referred to, for a different purpose. Jahromi *et al.* (2010) used an organic surfactant quaternary ammonium salt with alkyl chains to modify OMMT and disperse it in a bitumen matrix. Aly *et al.* (2011) created waste-glass cement mortars of different dosages with 2.5% of OMMT (Cloisite® 30B) modified with quaternary ammonium salt. The flexural and compressive strength were enhanced. The thermogravimetric analyses they ran, proved that the nanoclay acted as a catalyst-pozzolana. In the mix with the nanoclay most of the $Ca(OH)_2$ was consumed for the production of supplementary C–S–H. As a result a very strong increase in the C–S–H formation (strong increase in the first peak- dehydration) at the expense of $Ca(OH)_2$ (dramatic decrease in the second peak- loss of carbon dioxide from the inorganic compound) was observed. The improvement of the microstructure due to the packing effect of OMMT was also confirmed by Scanning Electron Microscopy (SEM) analysis.

2.7.7 Discussion and further research

It is evident from this literature review that the optimal dosage of nC for possible increase in compressive strength has yet to be defined. It would also be interesting to clarify the role of nC within the cement matrix; is it primarily acting as a nanofiller, a pozzolana or both? Additionally, the effect on flexural strength development is another area of research, since the different arrangements that the platelets may take could act as nanoreinforcement of the paste. Furthermore, the long-term effect of nC in strength is worth being studied since some

researchers claim reductions in strength over time. Up to what proportions on nC by mass of binder can strength increase be maintained? Although much has been discussed about organomodified MMT, research seems to have been extended only in one direction, that of inserting organic modifiers in MMT to transform it to hydrophobic in fear of its swelling capabilities if allowed to maintain its natural characteristics in a cement paste. However, the fact that the organomodified intercalated or exfoliated nC particles should be dispersed in an aqueous solution and remain dispersed until insertion in the cement paste constitutes an additional difficulty. A comparison, therefore, with inorganic nC, in which only surfactants and no modifiers are present, could shed more light in the reactions taking place during cement hydration when nC are present in the formulation. Would a naturally hydrophilic material, absorb water in the cement paste and cause the theoretically expected expansion in its bulk structure (Aly *et al.*, 2011)? Lastly, if modified but undispersed nC is used what differences would it incur?

2.8 Summary

The main conclusion derived from the literature review, can be summarised as follows:

- The hydration product of PC is nanosized and can be manipulated at nanolevel by adding nanoparticles.
- Adding a component whose size is reduced to the nanolevel, yields a cement product whose properties such as chemical reactivity, mechanical characteristics, porosity and durability are remarkably altered compared to cement pastes containing materials at the micro level.
- Nanoparticles can significantly enhance the properties of low carbon cements.
- Nanoparticles can produce sustainable cements.
- The effect the addition of nS or nC has on the microstructure and hydration of cement pastes is still unclear. So is the optimal dosage.
- The combined effect of the addition of nS and μS on the properties of cement pastes is still unresolved.
- There is plenty room for improvements of ternary (PC/LS/FA) formulations and the study of nanomodified quaternary (PC/LS/FA+nanoparticles) formulations has not been covered.
- There have not been reported studies on quaternary formulations (PC/LS/FA/μS), let alone nanomodified quinary (PC/LS/FA/μS+nanoparticles) formulations.
- The effect on Long-term strength of nS and nC is still to be examined.
- nCs are extremely complicated constituents, due to the chemistry and physics involved in their production. It is still believed that the organomodified nCs can offer advantageous solutions, whereas the inorganic nCs can be detrimental.
- The effect of inorganic nC on cement paste hydration and strength has not been investigated.

- A comparison between organically and inorganically modified nC has not been investigated.
- A comparison between dispersed and undispersed nC has not been studied, either.

3 METHODS & MATERIALS (MICRO & NANOSIZED)

3.1 Introductory section

In this chapter the programme of work is described (Figure 3-1). Furthermore, the material preparation and the elaboration of the results of the characterization methods used in this thesis are presented. Next, the characteristics of the constituent materials and nanomaterials are given. The nanostructural characteristics were linked to possible behaviour when added to cement pastes.

3.2 Programme of work

To begin with, it is acknowledged that according to the "Guidance on the use of terms relating to cement and concrete" (BCA, 2003), fly ash should not be abbreviated and instead of the term microsilica, silica fume should be used. Notwithstanding, for reasons of brevity, fly ash was, indeed, abbreviated as FA and silica fume was abbreviated as μS, the latter to denote the scale difference with nanosilica, abbreviated as nS. Limestone was abbreviated as LS and Portland cement as PC.

As shown in Figure 3-1, the first step was to characterize the constituent materials and ascertain their properties. CEMII/A-L was a pre-blended Portland limestone cement, therefore it was important to define the limits of the LS content. FA can contain various impurities depending on the power plant it was taken from. The particle size and the purity of FA, LS and μS had to be determined. For this purpose, several techniques were implemented, the theoretical background of which was given in Chapter 2. Furthermore, all techniques and methods employed for the investigation of the material properties were elaborated upon in this chapter, along with the sample preparation suitable for the various testing procedures.

Next the nanomaterials were characterised by specific methods. The two different types of nS investigated are commercially available. However, verification of the characteristics of the products was necessary in terms of particle size, level of dispesion, other materials present, etc. Additionally, three different nC dispersions were prepared by partners of the FIBCEM project. These dispersions are unique and have never been used before. Any possible agglomeration had to be detected and the particle size and reactivity of the nC in the dispersion had to be defined. According to the literature review some nCs may be expected to have pozzolanic characteristics. This had to be checked before mixing with cement. A novel approach was implemented, which gave significant indications. A fourth type of nC, commercially available, was also characterized as it was chosen to be used in some formulations for comparison purposes.

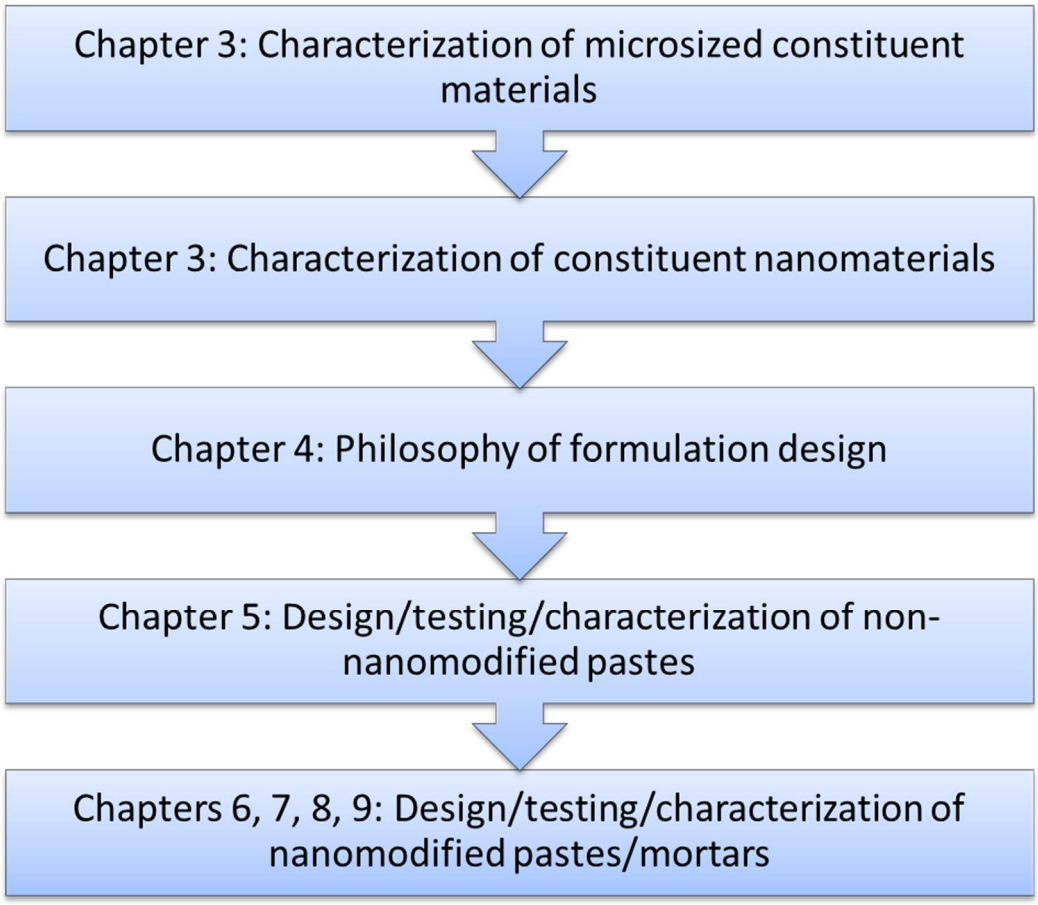

Figure 3-1: Steps of research programme

Once the constituent microsized materials and nanomaterials were characterized, the cement formulations had to be developed. The philosophy behind the cement paste and mortar formulations is addressed in Chapter 4. In Chapters 5, 6, 7 and 8 the various pastes were characterized and main conclusions were drawn.

3.3 Test Methods

Reference will be made to the analytical techniques selected for the characterization of nanoclays, nanosilicas and nanomodified blended cement pastes in this thesis. Various experimental methods have evolved in the past decades and can serve for the observation or manipulation of cementitious materials. The ones implemented in this research are referred to below, including some basic information on their capabilities and limitations. More details can be studied in literature (Sanchez and Sobolev, 2010; Alizadeh, 2009; Scrivener and Kirkpatrick, 2008).

3.3.1 Preparation of materials

For the characterization of the pastes, arrest of hydration was performed following two different methodologies. In brief, if images were to be generated and the microstructure to be evaluated, such as SEM/FESEM and MIP, solvent exchange was the technique employed for the arrest of hydration. The samples were crushed and immersed in isopropanol for 48 hours. Isopropanol was selected as the most appropriate solvent according to Zhang and Scherer (2011) and Bye (2011). The samples were, then, vacuum dried for 24 hours. The cement paste samples were examined uncoated at the SEM (Figure 3-2).

Figure 3-2: Uncoated samples prepared for SEM

For experiments in which chemical reactions would occur or where the chemical composition had to be evaluated, such as TGA, XRD, the oven drying technique was adopted as explained in detail in Calabria-Holley et al. (2014). In these studies the samples were crushed and placed in the oven at 60^{o}C for up to 24 hours. Then, they were ground and sieved through a 125 μm sieve and placed back in the oven at 60^{o}C for another 24 hours. All samples were placed in the desiccator in a labelled air-tight container until they were analysed.

In Chapter 3, for SEM imaging and EDX elemental composition analyses the specimens were uncoated. All nanomaterials in dispersions were dried and pulverized. Samples were placed on molybdenum foil to carry out unbiased elemental analyses. A matrix of 5 x 5 spectra was acquired and the median of the elemental composition was presented. In the case of nC, the Si/Al ratio was also calculated and the standard deviation shown.

In Chapter 6 and beyond, for secondary electron imaging of the pastes the solids were sputter coated with Quorum Q 150T with a layer of chromium 5 nm thick.

In Chapter 5 and beyond, for the compressive strength tests, the three samples prepared for each paste formulation were removed from the curing tank a few minutes before being tested. Any uneven surfaces were levelled with a diamond saw, avoiding capping. Consecutively, the specimens were weighed and measured.

In Chapter 9, for the flexural strength tests, at least three samples were prepared for each formulation and were removed from the curing tank a few minutes before being tested.

In Chapter 5 and beyond, for the mortar compressive strength tests, at least three samples were prepared for each formulation and were removed from the curing tank a few minutes before being tested.

3.3.2 Micro and nanostructural characterization techniques

Themogravimetric analyses (TGA)

Thermogravimetric analysis (TGA) is the technique by which the mass change of a sample is monitored as a function of temperature change. A typical analysis comprises of heating up a sample from room temperature to 1000°C at a rate of 10°C/min. Three phases are distinguished; (i) the dehydration of C–S–H, ettringite and monosulfate occurring approximately between 100°C and 180°C, (ii) the dehydration of $Ca(OH)_2$ taking place approximately between 400°C and 500°C and (iii) the decomposition of $CaCO_3$ between 600°C and 800°C. These temperature ranges were selected after a further search in literature, from which a tabulated literature review on TGA was also developed (Appendix-A). The technique is offering an approximation of the C–S–H produced, the $Ca(OH)_2$ consumed, the extent of pozzolanic reaction and evidence of carbonation of the samples (DeJong and Ulm, 2007; Scrivener *et al.*, 2004; Dyer *et al.*, 1999) (Table 3-1 and Table 3-2).

Themogravimetric analyses (TGA) were carried out using a Setaram TGA92 instrument. Approximately 20 mg of each sample were placed in an alumina crucible and heated at a rate of 10°C/min from 20°C to 1000°C under 100 mL/min flow of inert nitrogen gas. Mass change, differential mass change and heat flow measurements were recorded and analysed using the built-in software. The differential thermogravimetric curve (dTG) was derived by the TG curve. The first derivative curve was produced for the various samples tested and was used for comparisons instead of the mass loss curve, as it yields sharp distinctive peaks. The precision of the specific refurbished thermogravimetric analyser can reach two decimal points (Lawrence *et al.*, 2006).

Three broad areas, can be distinguished by the TGA, as also shown in the tabulated TGA in Table 3-1. According to Ramachandran *et al.* (2002):

The first one is related to the dehydration of C–S–H, ettringite and monosulfate, between 100°C and 200°C. It can be postulated that the greater the loss measured the greater the amount of C–S–H and ettringite was produced by the hydration of the paste.

The second area of interest is associated with the dehydration of $Ca(OH)_2$ between 400°C and 510°C (as described by Equation: 3-1).

$$Ca(OH)_2 \rightarrow CaO + H_2O \uparrow \qquad \text{Equation: 3-1}$$

The amount of $Ca(OH)_2$ present in the paste at different ages can be computed by the stoichiometric elaboration of the mass loss results within the specific temperature range (Equation: 3-2).

$$Ca(OH)_2 = \frac{Ca(OH)_2\ related\ H_2O\ mass\ loss \times 74}{18}$$ Equation: 3-2

Where, 18 = atomic mass unit of H_2O and 74 = atomic mass unit of $Ca(OH)_2$.

The third area of interest is the decomposition of $CaCO_3$ occurring between 700°C and 810°C according to the following chemical reaction:

$$CaCO_3 \rightarrow CaO + CO_2 \uparrow$$ Equation: 3-3

The amount of $CaCO_3$ present in the paste at different ages can be computed by the stoichiometric elaboration of the mass loss results within the specific temperature range. If it is greater than the limestone content of the reference paste, it constitutes an indication of sample carbonation.

$$CaCO_3 = \frac{CaCO_3\ related\ CO_2\ mass\ loss \times 100}{44}$$ Equation: 3-4

Where, 100 = atomic mass unit of $CaCO_3$ and 44 = atomic mass unit of CO_2.

Particularly for the quantification of $Ca(OH)_2$, TGA is considered a very accurate technique (Scrivener *et al.*, 2004), especially if coupled with XRD.

The dehydration temperatures of monosulfate, ettringite and other compounds are given in Table 3-1.

Table 3-1: Decomposition temperatures of hydration products of non-nanomodified hydraulic pastes

	He *et al.* (2012) effect of SP on hydration products	Esteves (2011) effect of SP and µS, on CEMI	DeJong and Ulm (2007) at elevated temperatures	Lawrence *et al.* (2006) tested 20°C/min	(Ramachandran and Beaudoin, 2001)	(Papadakis, 1999) low Ca-FA and PC
Compound	Decomposition temperature (°C)					
Calcium silicate hydrate: C–S–H	100-180	20-150	105-300	95-120	<200	110-140
Ettringite: C_4ASH_{12}	90-170	n/m[4]	n/m	125-135	n/m	90-170
Monosulfate: C_6ASH_{32}	n/m	n/m	n/m	185-195	n/m	270-380
Syngerite: K_2CaS_2H	n/m	n/m	n/m	265-275	n/m	n/m
Gypsum (dihydrate): CSH_2	n/m	n/m	n/m	160-186 (2 peaks)	n/m	n/m
Calcium sulfate hemihydrate: $CSH_{1/2}$	n/m	n/m	n/m	185	n/m	Gehlenite: 140-200
Calcium aluminates: CAH_{10}, C_2AH_8 C_3AH_6	n/m	n/m	n/m	110-130 175-185 280-320	n/m	Tetracalcium aluminate hydrate: 200-270
Calcium hydroxide: $Ca(OH)_2$	390-500	410–550	400-600	n/m	450–550	n/m
Calcium carbonate: $CaCO_3$	500-750	~800	n/m	n/m	750-900	n/m
Carboaluminate	n/m	>800	n/m	n/m	n/m	n/m

[4] n/m: not mentioned

Table 3-2: Decomposition temperatures of hydration products of nanomodified pastes & major conclusions

Binder analysed	Purpose of TGA	Sample preparation / Gas used / Sample weight & heating rate	Temperature intervals	Results & comments	Reference
PC60FA40 **PC57.5FA40+2.5nS** **PC55FA40+55.0nS** **Mortars @ 0.5w/b**	Measure pozzolanic activity in terms of $Ca(OH)_2$ content	Samples were oven dried @ 105 ºC for 4h Atmospheric pressure About 20mg 15ºC/min	Weight loss between 440 and 510 ºC due to decomposition of $Ca(OH)_2$	OPC + type F FA + Colloidal nS of 20 nm & 10 nm average particle size Depletion of $Ca(OH)_2$ at high FA and nS content pastes, cured in water at 70ºC for 7 days, did not allow further hydration of FA. In general decrease in hydration degree of FA at later ages due to the low $Ca(OH)_2$ content	(Kawashima *et al.*, 2013)
20g of $Ca(OH)_2$ content + 5g of colloidal nS compared with 20g of $Ca(OH)_2$ content + 5g of µS at **both @2w/b**	$Ca(OH)_2$ content at different ages	Limewater curing Hydration arrested with acetone &oven – dried at 105 ºC for 4 h.	@ 440 -510 ºC: decomposition of $Ca(OH)_2$	$Ca(OH)_2$ contents were calculated on the ignited basis at 950ºC for 30 min Pozzolanic reaction of nS was completed by day 7, however, for µS, over one month was needed.	(Hou *et al.*, 2013a)
1%, 2% and 3% Halloysite nanoclay by mass replacement of CEMI in mortar 95%CEMI-32.5+5%µS @0.45w/b +2%SP – limewater curing	Check $Ca(OH)_2$ consumption	n/m	Peaks: @105-120: decomposition of C–S–H @105-120: decomposition of Gehlenite hydrate (C_2SAH_6) @295-320: decomposition of hydrogarnet (C_3SAH_6) @480-490ºC: dehydroxylation of $Ca(OH)_2$	DSC at 28 days showed consumption of $Ca(OH)_2$ towards formation of C–S–H	(Farzadnia *et al.*, 2013)

OPC + 0.5%,1%,1.5% & 2% nS by mass replacement of OPC in mortar	Check pozzolanic activity	Saturated LS curing for 28d. Then in water until day 90. N_2 4ºC/min, From 100-650ºC	n/m	The loss in weight of the specimens is increased by increasing the nano content in concretes, maybe due to more formation of hydrated C–S–H gel	(Soleymani, 2012)
5% nS by mass replacement of OPC mix, 7 and 28 day old	Hydration of OPC paste and 5%nS paste	n/m From 20 to 1000ºC	@ 120-190 ºC: evaporation of capillary water, decomposition of C–S–H @450-500ºC: dehydroxylation of $Ca(OH)_2$ @700-780ºC: Decarboxylation of $CaCO_3$	Increased hydration with use of nS	(Al-Otaibi, 2012)
5% nS by mass replacement of OPC	Study of decomposition of hydration products	n/m N_2 10 ºC /min 20-1000ºC - held @105 ºC for 2hours to remove free water	@20- 105 ºC: loss of free water and decomposition of ettringite @105- 400 ºC: gradual mass loss due to dehydration of C–S–H &loss of interlayer, absorbed and chemically bound water @ 450 ºC: dehydroxylation of $Ca(OH)_2$	Reduction in amount of $Ca(OH)_2$ in sample with nS shows evidence of pozzolanic reaction	(Lim *et al.*, 2012)
1, 2, 3, 4 and 5% nS by mass replacement of OPC + 1%SP @0.4w/b **nS was dispersed in the SP**	Study of decomposition of hydration products	n/m N_2 4ºC/min From 110 to 650ºC	110 - 650ºC: dehydration of hydrated products	Powder 99.9% pure nS of 15 nm average particle size After 28 days of curing, mass loss of samples increased with increasing nS content up to 4% by mass SP: polycarboxylate with condensate defoamer base admixture	(Nazari and Riahi, 2010)
CEMI-52.5R+SP1.2 **PC80µS20+SP1.2** **PC96.5nS3.5+SP3** **PC87.8µS12.2+ SP1.2** **PC87.8µS10.2nS2+SP1.2** **All@0.35w/b** **SP: carboxylic acid** **nS: 30% solids by mass**	To study the effect of MS and NS and their combined use	Water curing at 21 ºC for 7, 28 and 90 days, samples with w/b ratio of 0.35 N_2 From 27 to 1000ºC. 10ºC/min	@~100ºC: evaporation of water @ 115–125ºC: partial dehydration of C–S–H @ 120–130ºC: partial dehydration of Aft @ 180–200ºC: partial dehydration of AFm @ 450–550ºC: dehydration of $Ca(OH)_2$	For 7 and 28 days (up to 400 ºC), samples with 3.5%nS and 2+10.2%nS+ µS showed a higher weight loss when compared to 0%nS and 0+12.2%nS+ µS, while for 20% µS, it was lower than that of 0% µS.	(Senff *et al.*, 2010a)

			@ ~800ºC: decarboxylation of $CaCO_3$		
2%, 4%, 6% and 8% nanometakaolin (NMK) by mass replacement of CEM-I mortars @0.5w/b	To study the effect of NMK	20ºC/min N_2	Peaks @ 105-110ºC: decomposition of C–S–H @ 160ºC: decomposition of gehlenite @ 350ºC: decomposition of hydrogarnet @470ºC: dehydroxylation of $Ca(OH)_2$ @580ºC: decomposition of quartz	DSC analyses – the addition of NMP led to the consumption of $Ca(OH)_2$ and its transformation from well crystalline to ill-crystalline phases.	(Morsy *et al.*, 2009)
0.2%, 0.4%, 0.6% and 0.8% OMMT by mass replacement of ASTM-I PC **@0.55w/b**	n/m	n/m up to 1400 ºC	Peaks @ 100 ºC: capillary water evaporates @ 470 ºC: dehydroxylation of $Ca(OH)_2$ @ 720 ºC: decarboxylation of $CaCO_3$ @ 1300 ºC: glass transition temperature transforming the cement from powder into a melted material.	DSC analyses	(Chang *et al.*, 2007)
0%, 0.5% and 2% of OMMT nC by mass replacement of type I PC **mortars @ 0.4, 0.485, 0.55w/b**	Verification of organomodification of OMMT	n/m	@ 150 ºC: partial dehydration of C–S–H @ 300-400 ºC: the organomodifier decomposed	Verification of organomodification of clay particles	(Kuo *et al.*, 2006)

Scanning electron microscopy/ X-ray energy dispersive spectroscopy (SEM/EDX)

Scanning and transmission electron microscopy (SEM and TEM) with the additional feature of X-ray energy dispersive spectroscopy (EDX) can assist in differentiating the hydrated phases, their chemistry and their evolution. The thickness of the elements present in the phases can be measured and high resolution images of over 100,000 times magnification can be captured. However, densities or volume of pores cannot be measure. Imaging of the surface topography and morphology of the pastes has also been rendered possible with modern SEMs (Ylmén *et al.*, 2009). C/S be calculated with the use of EDX.

For Chapter 3, SEM/EDX the three nC dispersions were at first vacuum dried for three days at a pressure of 10^{-2} mbar (100 Pa). The dried samples from the three nC dispersions along with the three powder (initial state) nC/clays were placed on a sheet of molybdenum, an element not contained in the nanoclays, so that the elemental analyses would remain unbiased. The SEM was calibrated with a standard 1:1 Si/Al ratio steel stud. The scale bar was optimized with copper.

Moreover, the surface morphology was observed with SEM in Chapters 5 to 9. Back scattered micrographs of uncoated samples at various magnifications were obtained using a Jeol 6480 LV scanning electron microscope. The elemental distribution was studied using SEM/EDX (X-ray energy dispersive spectrometry) at different beam currents.

Field emission electron microscopy (FESEM)

Secondary electron imaging of the pastes described in Chapter 6 was generated using a field emission electron microscope (FESEM) Jeol JSM 6301F at 2.4 kV, spot size of 7 and working distance of 16 mm. FESEM allowed capturing images at low voltage and high analysis, and indeed was the only microscope which would allow the nC to be distinguished.

Transmission electron microscopy (TEM)

For Chapter 3, TEM image analysis and crystallographic diffraction analysis of samples initially dispersed or in powder form, 10 μl of each nC and nS dispersion or 10 mg of the powder were diluted in 100 ml of distilled water and small drops of the diluted solutions were dripped on copper mesh grids coated with a thin carbon film. Grids were dried at 25°C prior to the insertion in the instrument. Samples were examined at a voltage of 120 kV and micrographs were acquired with GATAN Jeol view camera.

A polycrystalline structure, with randomly oriented grains, forming rings was detected. Having the camera constant known, the calculation of the lattice spacing was allowed according to the following formula adapted from Goodhew (1975):

$$\frac{r}{2L} = \frac{\lambda}{d} \rightarrow d = \frac{2\lambda L}{r} \qquad \text{Equation: 3-5}$$

Where L: the camera length and λ: the electron wavelength, which are independent of the specimen and constant for the TEM instrument and d = d-spacing and r = distance of the ring from the diffraction centre. Since d is inversely proportional to r, the largest d-spacing is obtained by the innermost ring. For the specific TEM diffraction analysis, $\lambda L = 1$. These results could be compared with d-spacing measured by XRD, where available. The only variable measured with the help of the TEM software was r, manually taken to be equal to the distance between the centre of the diffraction and the centre of each individual ring. As an effect, greater error is expected if compared to d-spacings measured by XRD.

Particle size distribution analysis (PSD)

Particle size distribution analysis with optical system can provide the PSD of a wide range of scales of particles from 10 nm to 3 mm. Particle size distribution analysis, for Chapter 3, was carried out at the MANIT laboratory, Bhopal, India, using a Laser Scattering Particle Size Distribution Analyzer Horiba LA950.

X-ray diffraction (XRD)

X-ray diffraction (XRD) is used for the characterization of crystalline phases and detection of chemicals in the cement pastes and became broadly available for these purposes since the 1950's. By utilizing Bragg's law the d-spacing or basal spacing (distance between planes of atoms) of the crystalline materials can also be determined. In principle, if the structure is amorphous, the x-rays cannot be diffracted and a plateau may be observed in the graph of the intensity of the x-rays versus 2θ, angle of diffraction. Still, the plateaus of the amorphous phases detected with XRD are correlating well with other methods, e.g. mass balance calculations (Scrivener *et al.*, 2004). The XRD measures mass fraction and with Rietveld analysis (also known as Quantitative XRD – QXRD) the quantification of the phases and the determination of their individual contribution in PC hydration is also possible (Peterson, 2003). The technique is frequently paired with TGA, which is also providing mass fraction measurements, as in the case of a recent research by which the PC phase distributions were determined by combined QXRD/TGA studies (Soin *et al.*, 2013).

The state and extent of dispersion - exfoliation of the nC can be examined by XRD and TEM analysis. Apart from mineralogical analysis, XRD is used to probe the structure and measure the interlayer spacing by monitoring the basal reflection of the silicate layers. Changes in basal spacing offer an indication of the intercalation of the nC. TEM and in specific the study of diffraction patterns can clarify the extent of dispersion or exfoliation of the nC. For example, if the nC is polycrystalline a series of rings will be observed or if it is highly crystalline a spot pattern will emerge.

Powder flat plate XRD measurements for Chapters 3 to 8 were performed using a D8 ADVANCE x-ray diffractometer with CuK_α radiation controlled by a Dell PC. Spectra were obtained in the range $4^o < 2\theta < 60^o$. Analysis of peaks and d-spacing [according to Bragg's law ($n\lambda = 2d\sin\theta$) (Ramachandran and Beaudoin, 2001)] was carried out using EVA software.

In Chapter 3, Flat plate XRD semi-quantitative analysis was also performed for the pozzolanic study of nCs on the grounds of comparisons of the integrated areas under the two adjacent peaks of $Ca(OH)_2$ at 28.7º2θ and $CaCO_3$ at 29.4º2θ.

Mercury intrusion porosimetry (MIP)

In mercury intrusion porosimetry (MIP) the size of a pore system is inversely proportional to the pressure needed to force mercury into the pore system. Hence, MIP can provide information on porosity at the nanolevel and is particularly useful at comparative assessments of the pore refinement that may be taking place in the modified cement pastes (Wild, 2001). The total amount of pores, the median pore area diameter and the average pore diameter may be estimated, although studies have suggested that MIP pore size distribution estimates are actually unreliable (Diamond, 2000). Moreover, the samples need to be dried prior to the execution of the measurement and drying procedures generally influence the results and only relatively small samples can be analysed, therefore, not necessarily representative of the bulk.

Porosity at the nanolevel was investigated by MIP. The mercury intrusion porosimeter used was an Autopore III - Model unit 9420 supplied by Micromeritics, Hexton, Herts, UK. Stems of 3 ml capacity were filled with solids of the arrested hydration paste.

MIP allows for the measurement of both bulk and apparent density. In bulk density the open (interconnected) and closed porosity are included, while in apparent density the open porosity is excluded. Subsequently, the apparent porosity provides an estimate of the open pores (Adamaki, 2015).

Long-term relative density

Long-term relative density measurements for the pastes and mortars are significant, as possible variations in porosity at very late ages can be detected.

Long-term relative density for the pastes and mortars characterized in Chapters 6 to 8 were carried out in accordance with BS EN 12390-7:2000. Volume was obtained by water displacement

$$V = \frac{m_a - m_w}{\rho_w} \qquad \text{Equation: 3-6}$$

Where, m_a = the mass of the specimen in air, in kg, m_w = the apparent mass of the immersed specimen in water, in kg, ρ_w = is the density of water, at 20 °C, taken as 998 kg/m³.

$$D = \frac{m_a}{V} \qquad \text{Equation: 3-7}$$

Where, D is the relative density in kg/m^3.

Water impermeability

Water impermeability tests can be carried out to assess the water absorbing characteristics of the nC modified pastes and to compare the effect the different types on nC can have depending on their hydrophobic or hydrophilic nature.

Water impermeability test was modified by Dr. J. Calabria-Holley for the FIBCEM project to account for the much smaller specimen used in this research (slabs 120 mm x 40 mm and 10 mm thickness) and were carried out in accordance with BS EN 492:2012. A transparent tube of 250 mm length was used as water column with an internal bore of 29 mm diameter. A control water column was also adopted to monitor possible water evaporation in the laboratory testing environment (Figure 3-3). The results of these tests are discussed in Chapter 9.

Figure 3-3: Example of the water impermeability test

3.3.3 Mechanical properties testing

To begin with, the strength of the supplied cement was validated according to BS EN 196-1.

Compressive and flexural strength tests were carried out in accordance with BS EN 196-1 and BS EN 12467, respectively. All samples were tested at a loading speed of 0.5MPa/s on a Dartec 100kN servo hydraulic machine. Mean strength values of the specimens tested were calculated.

- Cylindrical specimens of 60 mm height and 30 mm diameter were tested for compression.

- Slabs 100 x 40 x 10 mm were tested for flexure.
- Cubes of mortars 40 x 40 x 40 mm were tested for compression.

Prior to any testing material preparation was necessary and was carried out as described in section 3.3.4.

3.3.4 Other calculations

CO_2 footprint

Preliminary estimation of the CO_2 footprint of the initial pastes was derived from compressive strength of cement pastes (MPa) evaluated against embodied CO_2. (ECO_2). The levels of ECO_2 have been agreed in the UK and are evaluated in terms of kg CO_2 per tonne of binding material (BCA, 2009).

- PC = 930 kg CO_2/ tonne
- FA if a waste from coal burning power generation = 4 kg CO_2/ tonne
- LS = 32 kg CO_2/ tonne

It can be seen that in terms of CO_2 footprint the use of FA as a supplementary cementitious material is beneficial. This is the reason why it was used in the formulation design despite its shortage in the UK.

Additionally,

- μS = 14 kg CO_2/ tonne (Grist *et al.*, 2013)

Error estimation

The error provided in some graphs was estimated according to the following formula

$$e = \bar{x} \pm (stdv) \qquad \text{Equation: 3-8}$$

Where $\bar{x}$ is the mean value and *stdv* the standard deviation (Urdan, 2010).

3.4 Characterization of microsized constituent materials

The following materials and any commercially available data are listed below. These materials were characterized with a selection of the techniques stated in Figure 3-4, before implemented in the various cement paste combinations:

- Portland limestone cement: CEM II/A-L conforming to BS EN 197-1, Blaine density = 525 kg/m^3, absolute density = 3060 kg/m^3, bulk density = 1100 kg/m^3, clinker composition: 70% C_3S, 4% C_2S, 9% C_3A, 12% C_4AF
- LS filler conforming to BS EN 197-1 – no information on specific surface area due to confidentiality issues
- FA (siliceous) conforming to BS EN 450 – oxide composition: 53.5% SiO_2, 34.3% Al_2O_3, 3,6% Fe_2O_3, 4.4% CaO– no information on specific surface area due to confidentiality issues
- µS conforming to BS EN 13263 – specific surface area = 15-30x10^3 m^2/kg, mean particle size = 0.15 µm

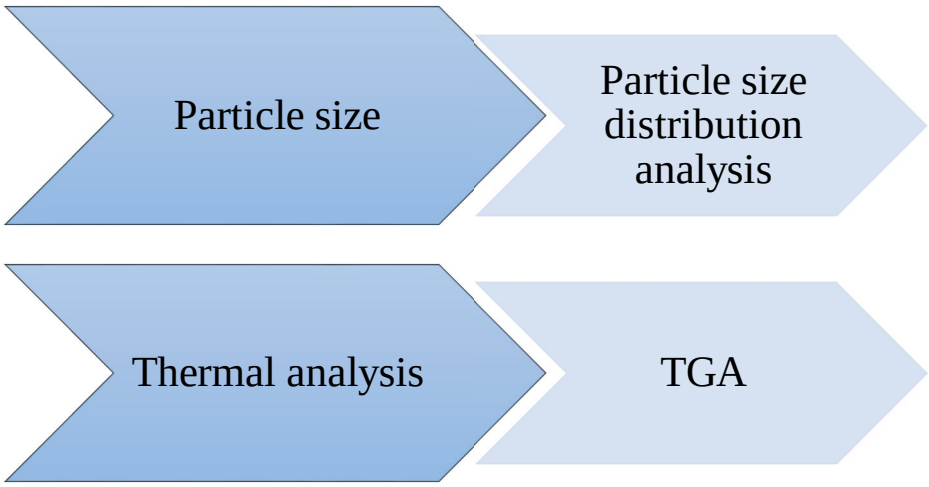

Figure 3-4: Property tested and technique used for characterization of CEMII, FA, LS and µS

3.4.1 PSD results of CEM II/LS/FA/ condensed µS

The particle size distribution results of the four constituent materials reacted with water were prepared by colleagues in MANIT, India and are presented below. As can be seen in Figure 3-8, µS seems to be two-graded.

Table 3-3: PSD results

	Mean size (µm)	Mode size (µm)	Median size (µm)	Diameter at 10% (µm)	Diameter at 90% (µm)
CEMII	11.38	2.74	3.25	1.40	22.16
LS	12.14	2.44	3.21	1.36	31.89
FA	9.09	2.14	2.53	1.46	10.13
µS	9.65	3.66	5.05	2.41	22.03

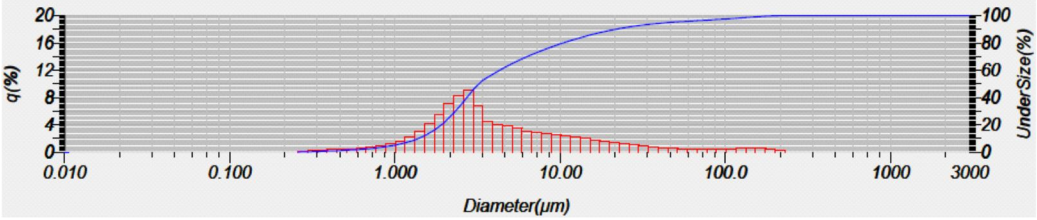

Figure 3-5: Normal distribution of CEMII

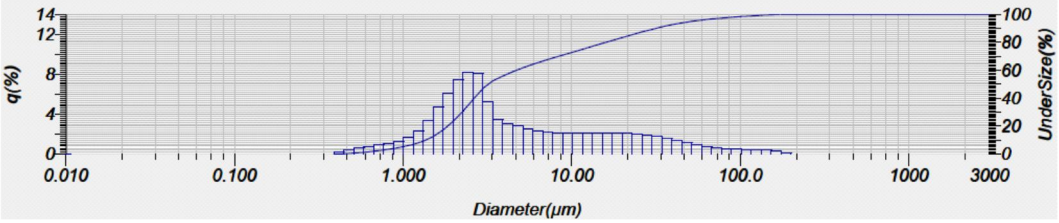

Figure 3-6: Normal distribution of LS

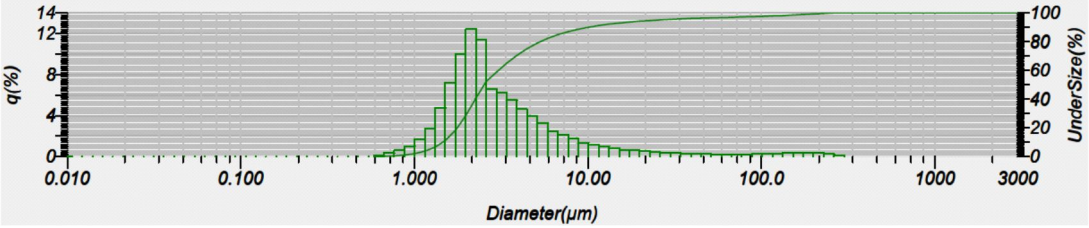

Figure 3-7: Normal distribution of FA

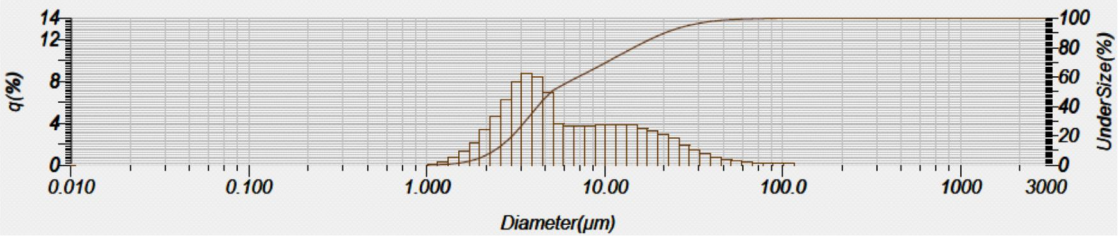

Figure 3-8: Normal distribution of condensed µS

3.4.2 TGA results of CEM II/LS/FA/µS

The thermogravimetric analyses results of the four constituent materials are presented below:

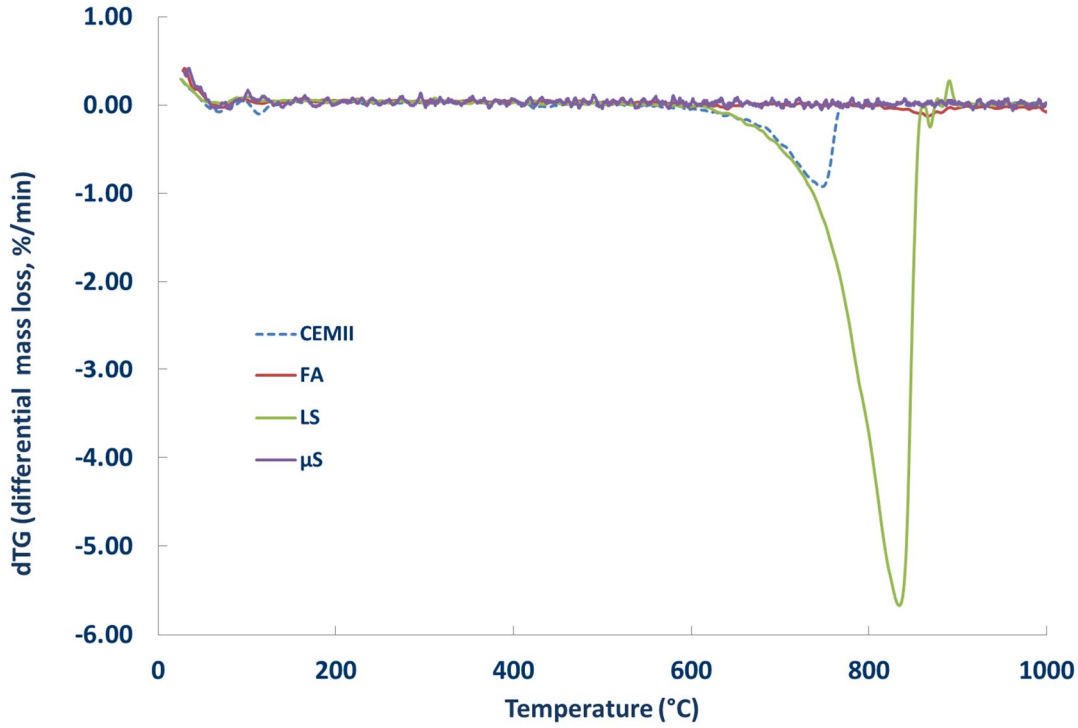

Figure 3-9: Differential mass loss of microsized constituent materials

It can be seen in Figure 3-9 that practically the only mass loss upon heating is observed for, CEMII and LS, the differential mass loss of which was measured to be 42.4% and 5.95%, respectively. The initial amount of $CaCO_3$ present is given by Equation: 3-2, yielding 14% of $CaCO_3$ present in CEMII and 97% in LS. Therefore the LS powder is considered to be almost pure $CaCO_3$ and the composition of CEMII is considered as 86% PC and 14% LS. The minor mass loss of FA with a peak at about 850°C can be attributed to the volatile matter in the unburnt coal (Xu *et al.*, 1993).

3.4.3 XRD and SEM/EDX results of FA

Moreover, the different minerals present in the FA powder were determined by XRD crystallographic analysis (Sobolev *et al.*, 2013). As shown in Figure 3-10, mullite, quartz, hematite, lime and calcium carbonate are present.

Lastly, 20 spectra were acquired via the SEM/EDX carried out on a FA sample, five of which are indicatively shown in Table 3-4. The presence of sulfur which has been reported to increase the ettringite formation during cement hydration was confirmed (Tishmack *et al.*, 1999).

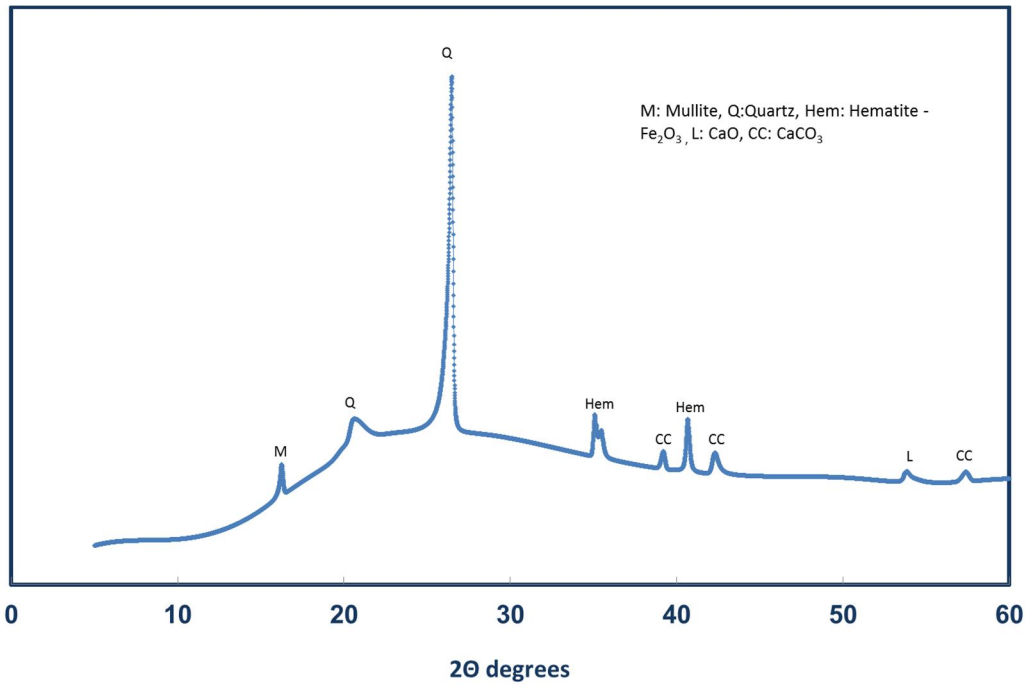

Figure 3-10: XRD diffraction pattern of FA

Table 3-4: SEM/EDX counts summary (% atomic) of FA

FA - All results in atomic % normalized to 100%													
Spectrum	C	O	Na	Mg	Al	Si	P	S	Cl	K	Ca	Ti	Fe
(1,1)	16.73	55.58	0.49	0.74	8.84	13.62	0.00	0.14	0.04	0.82	1.06	0.28	1.66
(2,1)	18.86	52.35	0.06	0.72	12.23	13.31	0.01	0.10	0.02	0.33	1.23	0.02	0.80
(3,1)	15.07	55.63	0.36	0.7	11.54	12.52	0.07	0.19	0.02	0.52	1.26	0.69	1.48
(4,1)	5.41	60.94	0.67	0.96	10.96	16.5	0.17	0.19	0.06	1.07	1.15	0.33	1.70
(5,1)	8.57	59.8	0.35	0.52	12.34	15.08	0.1	0.09	0.05	0.60	1.45	0.21	0.94
Total mean	16.97	55.1	0.52	0.77	8.13	12.62	0.09	0.21	0.01	0.62	1.35	0.20	3.42
Stdv	6.48	3.05	0.17	0.52	2.37	2.36	0.08	0.21	0.05	0.18	1.55	0.14	3.29

As can be observed in Table 3-4, the carbon content in FA is particularly high.

3.5 Characterization of constituent nanomaterials

The various methodologies existing for nS and nC preparation can lead to variable properties and reactions. Therefore, the characterization of the following nanomaterials with different combinations of the techniques stated in Figure 3-11 before implemented in the various cement paste combinations was necessary:

A) Two nanosilica dispersions:

- Carboxylic dispersion of nanosilica, denoted as GnS: commercially available.
- Aqueous dispersion of nanosilica, denoted as LnS: commercially available.

B) Three clay and nanoclay powders:

- Purified (unmodified/inorganic) MMT clay powder (from which the inorganic dispersion evolved), commercially available as Dellite HPS.
- Organomodified bentonite nanoclay powder (from which the two organomodified dispersions evolved), denoted as nCX.
- Organomodified MMT nanoclay powder, commercially available. This form of nC was used undispersed in cement paste formulations and denoted as nC4.

C) Three nanoclay dispersions:

- Aqueous dispersion: nCX dispersed with a non-ionic fatty alcohol, denoted as nC1: supplied by the UK Materials Research Institute (MaTRI).
- Aqueous dispersion: nCX dispersed with an anionic alkyl aryl sulphonate, denoted as nC2: supplied by UK MaTRI.
- Aqueous dispersion: (inorganic) Dellite HPS dispersed with sodium tripolyphosphate, denoted as nC3: supplied by UK MaTRI.

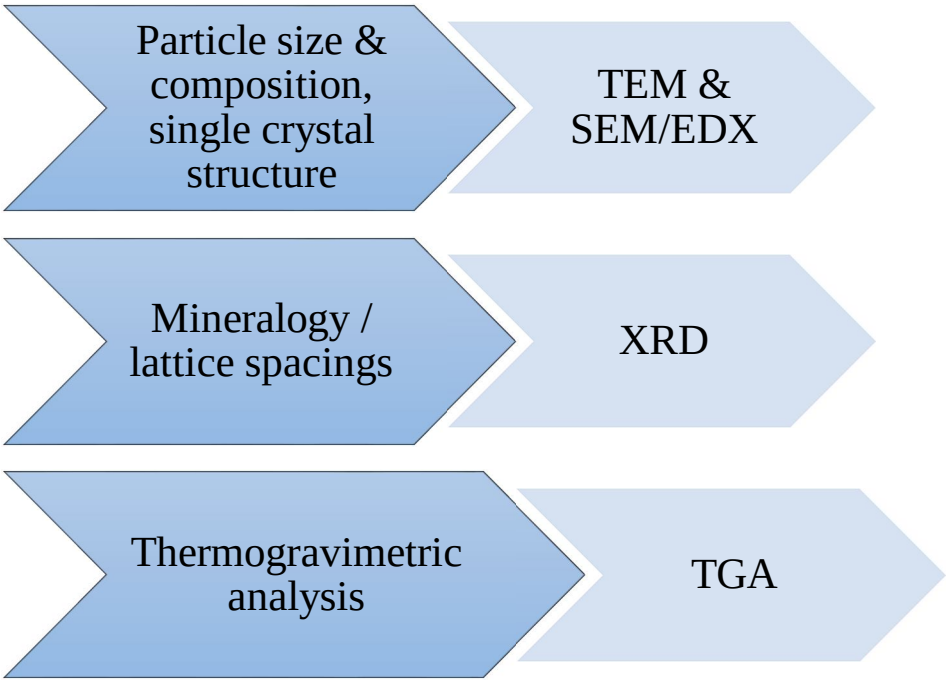

Figure 3-11: Property tested and technique used for characterization of nanomaterials

3.5.1 Nanosilica dispersions (GnS & LnS)

The particle size of GnS in the colloidal solution was investigated by transmission electron microscopy (TEM). TEM analysis showed that the diameter of the GnS particles was about 5-8 nm (Figure 3-12-A). However, it is shown by the 10000 times magnification TEM micrograph (Figure 3-12-B) that there are some large agglomerations of about 100 nm diameter.

TEM analysis showed that the diameter of the LnS particles ranged from 8 nm to 50 nm (Figure 3-13-A) and that they were homogenously dispersed and highly concentrated layers of nS on top of other layers of nS (Figure 3-13-B).

Table 3-5 and Table 3-6 contain indicatively the first 5 spectra from the 5 x 5 matrix of spectra collected in each elemental analysis (SEM/EDX). Adding to this, in Figure 3-14 the comparison of the elemental compositions of the two different nS dispersions is showing that GnS has traces of SiO_2 and over 70% (normalized atomic) carbon content. It could therefore be more appropriately described as carboxylate dispersion with limited quantities of nS particles. Adding to this, in GnS, the hydrocarbon present is more prone than the nS itself to have significant effects on the cement pastes. LnS, however, comprises of almost pure SiO_2 and therefore expected to perform as a pure, aqueous nS dispersion, exploiting the benefits of nanoparticles discussed before such as the high surface area or (due to the high SiO_2) increase in the C–S–H, when added to cement paste formulations.

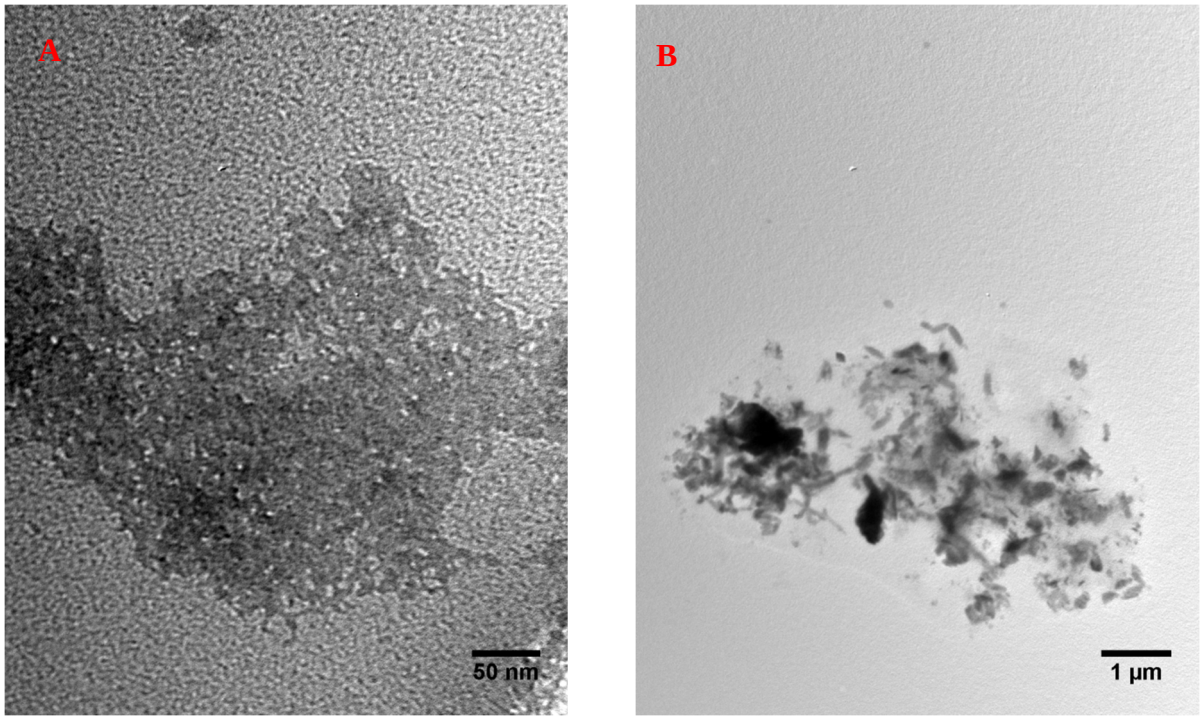

Figure 3-12: TEM micrograph of GnS (A) @ 100000x and (B) @ 10000x

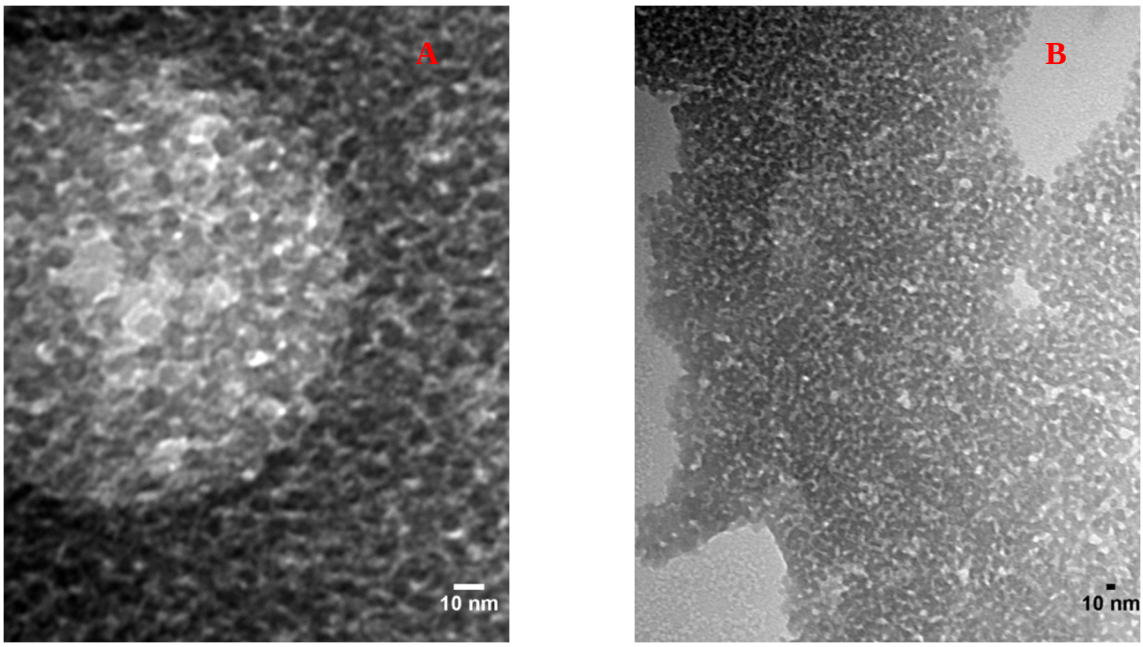

Figure 3-13: TEM micrograph of LnS (A) @ 500000x and (B) @ 150000x

Table 3-5: SEM/EDX counts summary (% atomic) of GnS

GnS - All results in atomic % normalized to 100%					
Spectrum	C	O	Na	Si	S
(1,1)	70.58	28.43	0.48	0.12	0.40
(2,1)	70.74	28.38	0.37	0.09	0.42
(3,1)	70.83	28.18	0.40	0.11	0.47
(4,1)	69.19	29.32	0.40	0.21	0.88
(5,1)	72.04	25.15	0.21	0.19	2.41
Total mean	71.42	26.66	0.41	0.23	1.28
Stdv	1.29	2.04	0.12	0.2	1.37

Table 3-6: SEM/EDX counts summary (% atomic) of LnS

LnS - All results in atomic % normalized to 100%				
Spectrum	C	O	Na	Si
(1,1)	10.37	61.57	0.97	27.08
(2,1)	7.57	63.00	1.05	28.38
(3,1)	6.5	62.87	1.00	29.63
(4,1)	5.63	64.02	1.02	29.33
(5,1)	7.34	63.57	1.00	28.10
Total mean	6.11	62.74	0.98	30.17
Stdv	1.31	1.61	0.07	1.74

As can be observed in Table 3-5 and in Table 3-6, the carbon content in both GnS and LnS is particularly high.

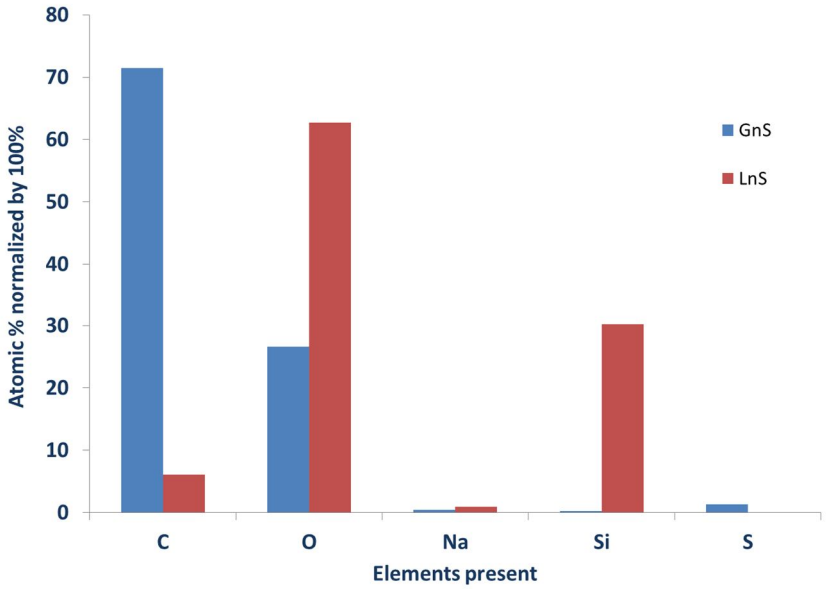

Figure 3-14: Comparison of the elemental composition of GnS and LnS

3.5.2 Clay (Dellite HPS) and nC powders (nCX & nC4)

The dispersions of two types of clays were used in this research. Dellite HPS, which is a purified montmorillonite, was used for the production of the inorganic dispersion and supplied by Laviosa Chimica Mineraria S.p.A.

The second type of clay was a purified bentonite, also supplied by Laviosa Chimica Mineraria S.p.A. It was organomodified with methylbenzyl di-hydrogenated tallow ammonium chloride (Noramonium MB2HT) by Lietuvos Energetikos Institutas (LEI) at a modifier to clay ratio of 1:1 by mass. Although other quaternary alkylammonium salts (quats) have been employed by other researchers for the organomodification of clays, as discussed in Chapter 2, Noramonium MB2HT, has never been used so far as a clay organomodifier, and hence no studies on the effect of the specific OMMT in cementitious matrices have been published.

The optimal salt dosage for the organomodification of the MMT, the original and modified property characterization and the processes involved are included in four reports, produced by LEI for the FIBCEM project (Lukošiūtė and Čėsnienė, 2012, 2013a, c, b).

Notwithstanding, selected characteristics and findings of high relevance to the addition of the nC in cement pastes are summarized below:

- In a perfect MMT structure the ratio SiO_2 to Al_2O_3 (Si/Al) is 2.6. In Na-bentonite the ratio can increase to 4.79
- Unmodified Dellite HPS properties: CEC = 128 meq/100g, BET surface area = $89x10^3$ m^2/kg, particle size = 6-8 μm, specific weight = 2.2 g/cm^3, bulk density = 0.65 g/cm^3, XRD crystallite size = 11.4 nm and d-spacing = 1.255 nm (interplanar d_{001}) at approximately 7°2θ
- Unmodified purified bentonite suspension properties: CEC = 105 meq/100 g, BET surface area = $66x10^3$ m^2/kg, XRD crystallite size = 5.6 nm and d-spacing = 1.238 nm at approximately 7°2θ
- Organomodified bentonite suspension (nCX) properties: d-spacing = 3.85 nm at approximately 1.9°2θ , BET surface area = 6.4 $x10^3$ m^2/kg
- Particle size analysis of the organomodified bentonite showed that about 80% particles had a shape between 9 - 11 nm

i. Clay powder (Dellite HPS)

The clay with which the inorganic dispersion was produced, was received separately in powder form and was characterized for verification purposes. The d-spacing received by the XRD measurement (Figure 3-15) was equal to 1.22 nm, hence, lower than its predefined value (1.26 nm), indicating a monolayer of water ((He *et al.*, 1996)). The broader diffraction peaks at 20.0, 35.0 and 54.1°2θ are attributed to the OMMT showing the amorphous and poorly crystalline structure of the aluminosilicate (Chang *et al.*, 2007). The peak at 26.8°2θ is associated to quartz, the peak at 28.7°2θ is associated to feldspar and the one at 29.6°2θ to calcite (He *et al.*, 1996). The intermediate peaks between 40 and 55°2θ can be associated to a Mg-Al-silicate according to He *et al.* (1996). It is acknowledged that calcite has a peak between 29.3-29.4 and quartz at about 26.6-26.7, indicating an angular error on the diffraction traces. Applying a 0.2°2θ correction to the data presented in Figure 3-15, a d-spacing of about 1.255 nm is extrapolated, which, in this case, is close to the predefined value.

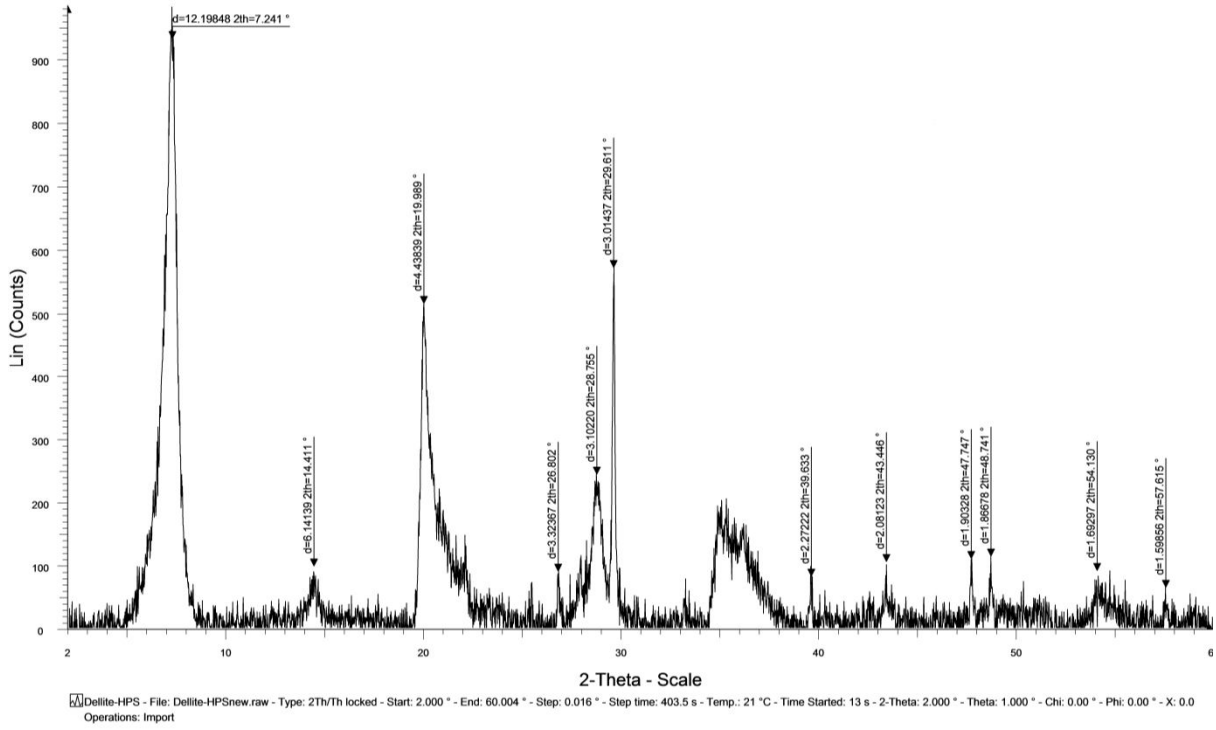

Figure 3-15: XRD pattern of the Dellite HPS clay

For statistical reliability of the elemental analysis a matrix of 5 x 5 randomly selected spectra was collected. Indicatively, the first five are presented in Table 3-7. The elemental composition of Dellite HPS as acquired by the SEM/EDX measurement (Figure 3-21) showed that this starting clay contained only small quantities of C, and significant quantities of Si (16.4%), Al (6.4%) and O (70.0%). The Si/Al ratio of Dellite HPS clay was found to be between 3.24 and 3.64 with a median of 3.53 and a standard deviation of 0.09 (Figure 3-22).

Table 3-7: SEM/EDX counts summary (% atomic) of Dellite HPS

Dellite HPS - All results atomic & normalized by 100%										
Spectrum	C	O	Na	Mg	Al	Si	K	Ca	Ti	Fe
(1,1)	5.59	70.83	1.10	1.53	5.66	13.95	0.08	0.50	0.08	0.67
(2,1)	7.51	68.04	0.83	1.53	5.65	14.61	0.17	0.61	0.15	0.88
(3,1)	4.08	66.70	0.68	1.63	6.88	17.79	0.24	0.72	0.14	1.13
(4,1)	4.21	67.45	0.89	1.43	6.52	17.41	0.13	0.81	0.10	1.03
(5,1)	5.99	66.41	0.77	1.58	6.47	17.01	0.14	0.61	0.11	0.92
Total mean	2.78	69.96	0.82	1.58	6.35	16.4	0.19	0.75	0.14	1.02
Stdv	3.68	2.57	0.16	0.11	0.67	1.91	0.09	0.18	0.07	0.23

TEM imaging (Figure 3-16-A and B) showed an already reasonably exfoliated type of clay (a result of the industrial purification of the MMT by Laviosa Chimica Mineraria S.p.A.) with some unexfoliated particles in the bulk.

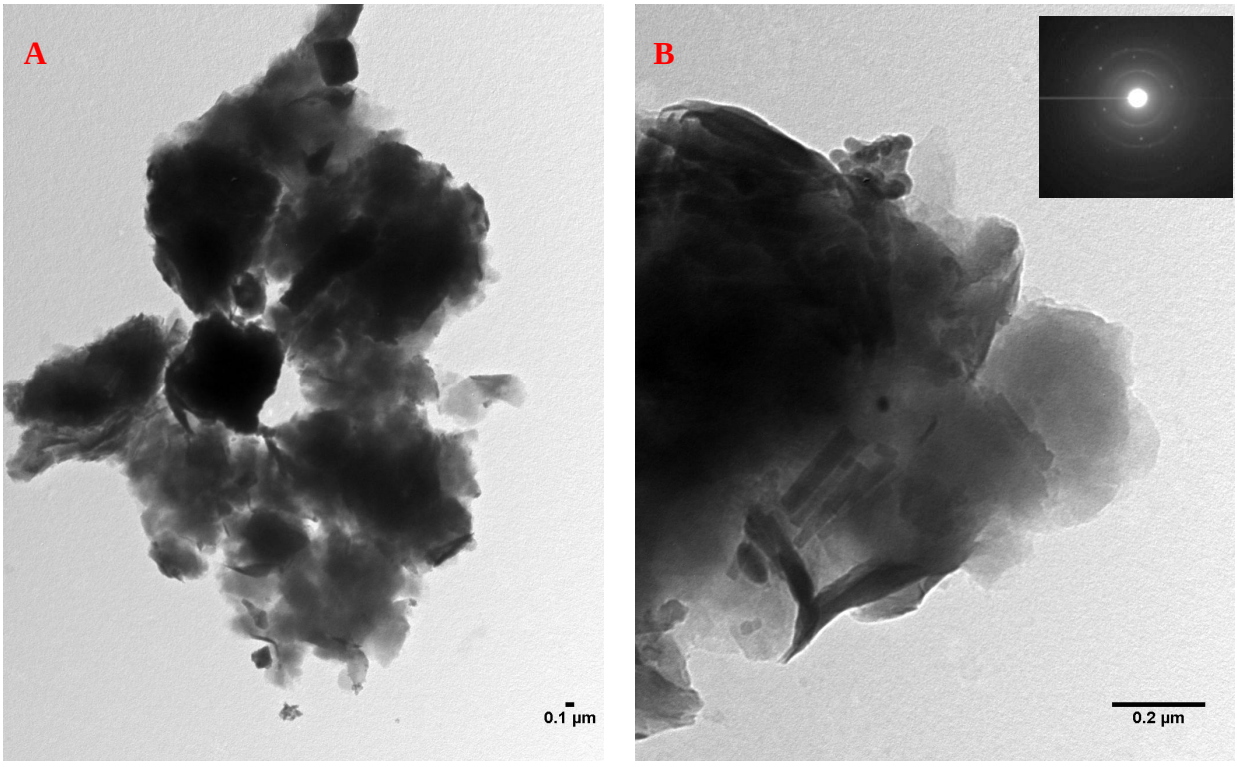

Figure 3-16: TEM micrograph of Dellite HPS clay (A) @ 75000x and (B) @ 100000x

The diffraction pattern of Dellite HPS showed a polycrystalline structure, since rings are present. The many bright spots present, represent many scattered crystals in different planes (Figure 3-23), enforcing the view that this clay was partly exfoliated. The grouping of these spots indicates an extremely ordered single crystal, which does not belong to the nC and

could be calcite. The various d-spacings were calculated by the diffraction pattern according to Equation: 3-5:

d from diffraction pattern A1

d_1= 2 x 1/1.76 = 1.14 nm

d_2= 2 x 1/3.57 = 0.56 nm

d_3= 2 x 1/5.26 = 0.38 nm

d_4= 2 x 1/6.25 = 0.32 nm

d_5= 2 x 1/7.14 = 0.28 nm

ii. Nanoclay powder (nCX)

The organomodified clay with which the two organic dispersions were produced, was received separately in powder form and was characterized for verification purposes. The d-spacing received by the XRD measurement (Figure 3-17) was equal to 3.55 nm at 2.5°2θ, hence, again lower than its specified value (3.85 nm, as measured by Lukošiūtė and Čėsnienė (2012)). This could be attributed to variations in the different laboratories and diffractometers. However, since the X-ray diffractometers were calibrated, the difference could possibly be attributed to low stability of the material. The broader diffraction peaks at 19.9, 34.9 and 54.0°2θ are attributed to the nano bentonite showing the amorphous and poorly crystalline structure of the aluminosilicate (Chang *et al.*, 2007). The peak at 27.44°2θ is associated to quartz or feldspar and the one at 29.9°2θ to calcite (Fernandez *et al.*, 2011; He *et al.*, 1996).

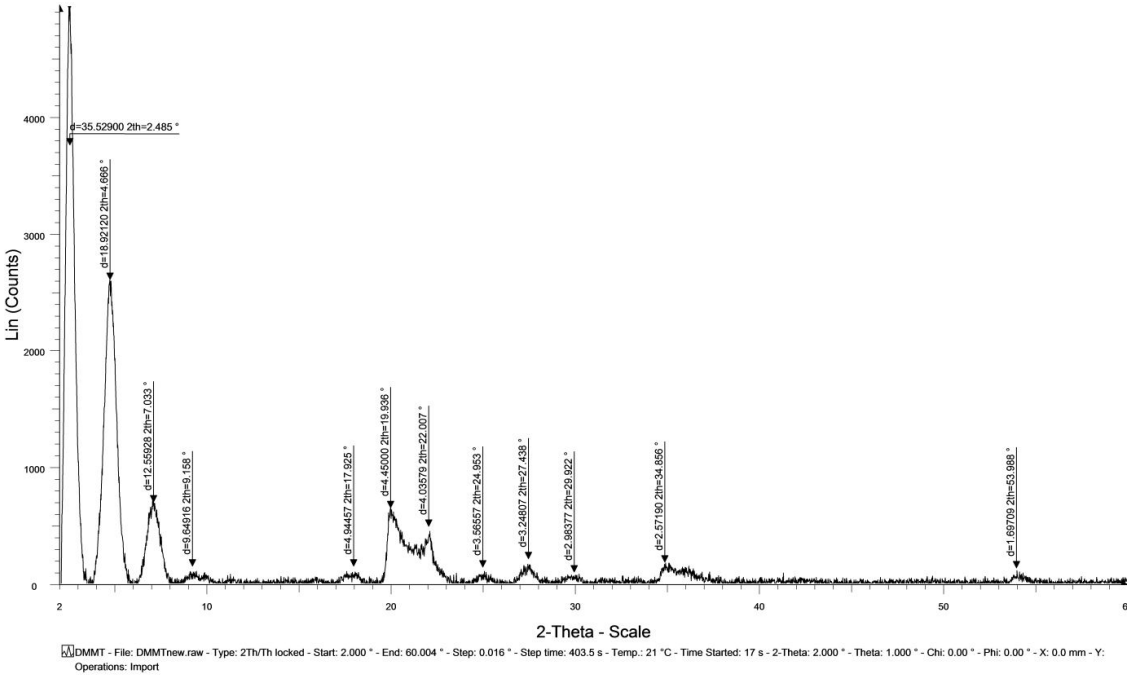

Figure 3-17: XRD pattern of the organomodified nCX

For statistical reliability of the elemental analysis a matrix of 5 x 5 randomly selected spectra was collected. Indicatively the first five are presented in Table 3-8. The elemental composition of nCX as acquired by the SEM/EDX measurement (Figure 3-21) showed that this organomodified bentonite contained high quantities of C (median 60.5% and standard deviation of 1.9), and low quantities of Si (5.7%), Al (2.0%) and O (31.0%). The Si/Al ratio of nCX was found to be between 4.38 and 3.67 with a median of 3.88 and a standard deviation of 0.18, much higher than that of Dellite HPS, hence expected to show further variations when dispersed (Figure 3-22).

Table 3-8: SEM/EDX counts summary (% atomic) of nCX

nCX - All results atomic & normalized by 100%											
Spectrum	C	O	Na	Mg	Al	Si	P	S	Cl	Ca	Fe
(1,1)	59.85	32.89	nd[5]	0.33	1.76	4.76	nd	nd	0.17	nd	0.25
(2,1)	62.03	27.28	nd	0.35	2.58	6.90	nd	nd	0.30	nd	0.56
(3,1)	56.26	36.28	0.15	0.35	1.81	4.73	nd	nd	0.11	0.08	0.23
(4,1)	64.49	27.03	nd	nd	1.80	5.16	nd	nd	nd	nd	1.51
(5,1)	64.60	23.52	nd	nd	2.35	7.26	nd	0.43	0.37	nd	1.47
Total mean	60.46	31.06	0.14	0.36	2.02	5.70	0.10	0.43	0.25	0.08	0.45
Stdv	1.90	6.30	0.02	0.20	1.44	4.46	nd	nd	0.30	0.00	0.50

[5] The SEM-EDX analyses did not deliver a value of elemental composition in various spectra. Peaks were **not detected** (denoted by "nd" from this point onwards) and quantified unless the diffraction over satisfied the 3 sigma threshold for quantification (according to the normal distribution statistics).

TEM of nCX showed large overlapping clusters. The areas created were so dense that it was difficult for transmission to get through (Figure 3-18-A and B). The distinctive spots shown in Figure 3-18-B represent the organic matter.

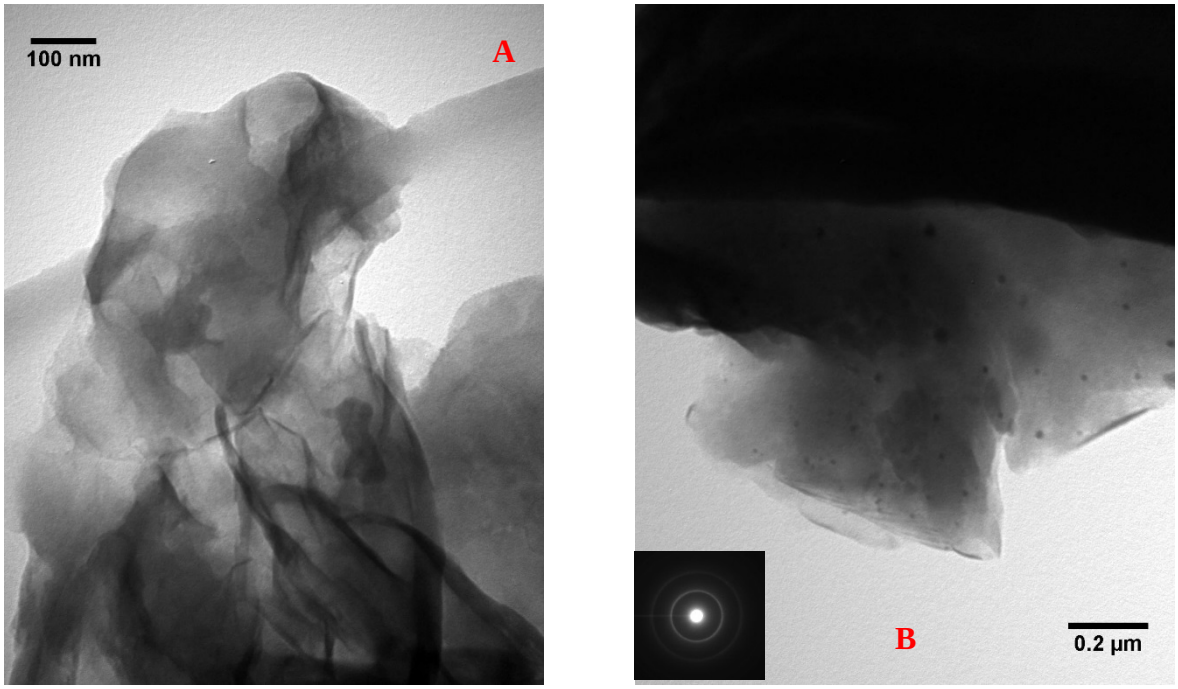

Figure 3-18: TEM micrograph of nCX (A) @ 100000x and (B) 60000x

The diffraction pattern of nCX showed a poorly crystalline structure, with a few rings present. Neither bright spots were present, indicating scattered crystals in different planes (Figure 3-24), enforcing the view that this clay was most probably intercalated but not exfoliated. The various d-spacings were calculated by the diffraction pattern according to Equation: 3-5:

d from diffraction pattern B1

d_1= 2 x 1/0.54 = 3.7 nm

d_2= 2 x 1/0.7 = 2.86 nm

d_3= 2 x 1/1.27 = 1.57 nm

d_4= 2 x 1/2.18 = 0.92 nm

d_5= 2 x 1/2.5 = 0.8 nm

iii. Nanoclay powder (nC4)

Lastly, a commercially available OMMT modified with approximately 27.5% by total mass of powder methyl dihydroxyethyl hydrogenated tallow ammonium with density = 200 - 500 kg/m^3 and size $\leq$ 20 micron was also characterized before introduced to cement pastes. XRD analysis yielded a d-spacing of 1.8 nm (Figure 3-19), which is more than expected in unmodified nC.

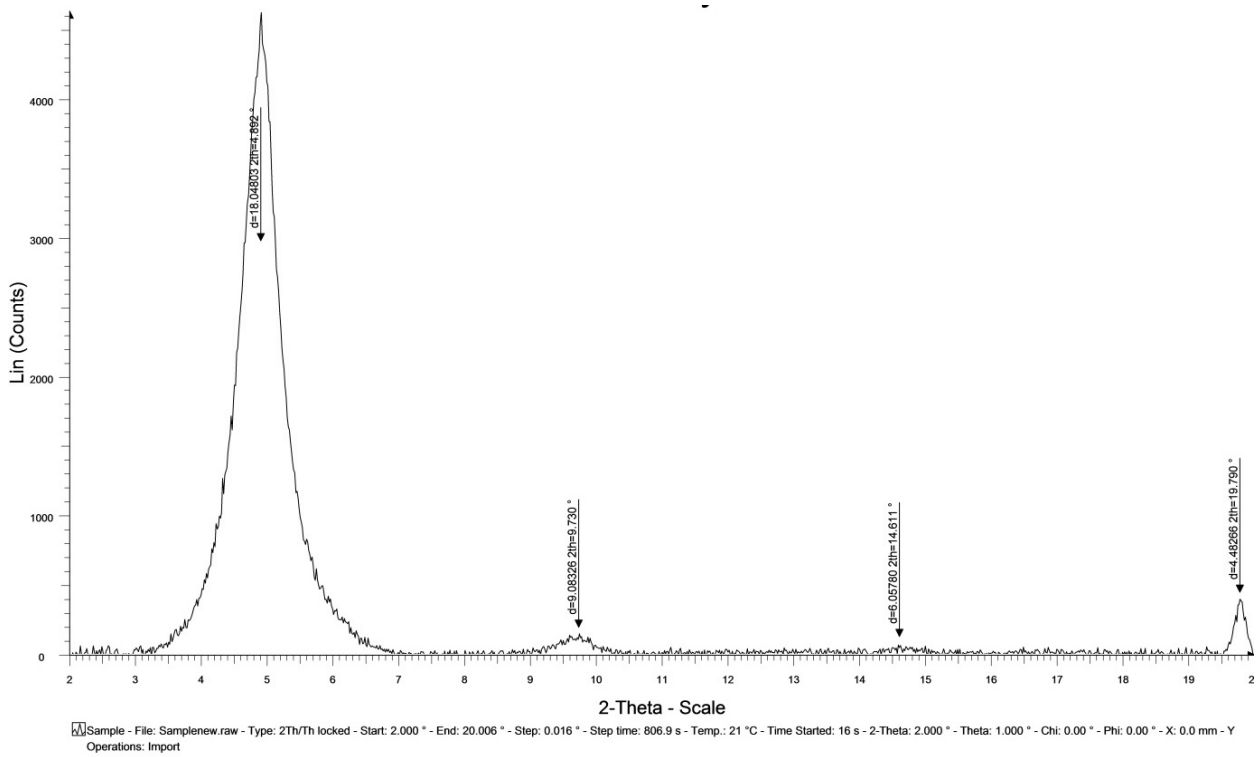

Figure 3-19: XRD pattern of nC4

Again, a matrix of 5 x 5 randomly selected spectra was collected (Table 3-9). The elemental composition of this OMMT showed that nC4 contained lower quantities of C (with a median of 41% with a standard deviation of 2.95) and higher quantities of Si (8.3% as opposed to 5.7% for nCX), Al (3.4% as opposed to 2.0% for nCX) and O (46.0%). Furthermore, it comprised of fewer elements (Figure 3-21). The Si/Al ratio of nC4 was found to be between 3.31 and 3.67 with a median of 3.48 and a standard deviation of 0.10, similar to that of nCX (Figure 3-22).

Table 3-9: SEM/EDX counts summary (% atomic) of nC4

Initially Undispersed nC -All results in atomic % normalized by 100%						
Spectrum	**C**	**O**	**Mg**	**Al**	**Si**	**Fe**
(1,1)	38.63	49.13	0.55	3.29	8.01	0.40
(2,1)	39.31	45.63	0.62	3.94	9.95	0.54
(3,1)	37.94	48.55	0.60	3.70	8.74	0.47
(4,1)	39.87	48.95	0.47	2.86	7.40	0.44
(5,1)	38.78	47.83	0.55	3.54	8.83	0.47
Total mean	41.01	45.56	0.51	3.37	8.30	1.25
Stdv	2.95	2.95	0.08	0.52	1.47	0.99

TEM micrographs showed good intercalation of nC4. Soft edges can be observed in Figure 3-20-A and –B. Moreover, nC4 agglomerated less in water dispersion and showed significant differences in terms of particle shape and size, with platelets reaching the size of 300 nm.

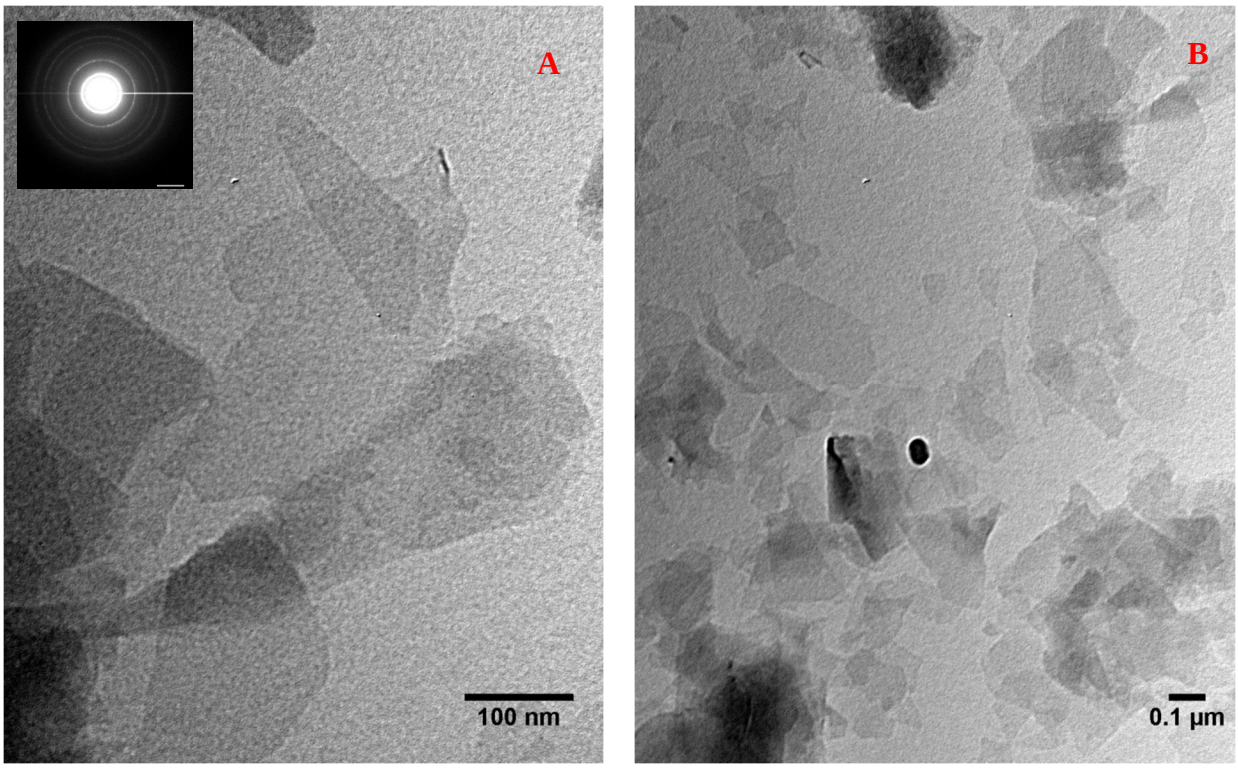

Figure 3-20: TEM micrograph of nC4 (A) @ 150000x and (B) 50000x

The diffraction analysis was carried out according to Equation: 3-5:

d from diffraction pattern C1

d_1= 2 x 1/0.96 = 2.08 nm

d_2= 2 x 1/1.83 = 1.09 nm

d_3= 2 x ½.63 = 0.76 nm

d_4= 2 x 1/1.26 = 0.63 nm

These values clearly indicate that some platelets were intercalated and some exfoliated. The different d-spacing (1.8 nm) given by analysis XRD can be attributed to the fact that TEM diffraction analysis is carried out on a single crystal, whereas XRD in the bulk of the powdered sample. Moreover, a greater error is expected on the TEM results, inherent to the technique adopted to extract the *r* parameter.

The comparative graphs of the elemental composition (Figure 3-21), the Si/Al ratio (Figure 3-22) and TEM diffractograms (Figure 3-23 to Figure 3-25) of the unmodified MMT (Dellite HPS) and the organomodified bentonite (nCX) and organomodified MMT (nC4) are presented below. In summary, these figures allow for the following conclusions are drawn:

- There are high amounts of carbon present in the organomodified nC, nCX.
- There are many impurities present in nCX, a fact confirmed by SEM/EDX, XRD and TEM, and this could lead to significant variations in the performance of cement binders enhanced with the dispersions evolved from nCX.
- Dellite HPS has higher potential to form additional C–S–H, due to the higher quantities of silica and better exfoliation.
- Compared with nCX, the commercially available nC4 was better exfoliated, showed less variation in Si/Al and more polycrystalline phases.

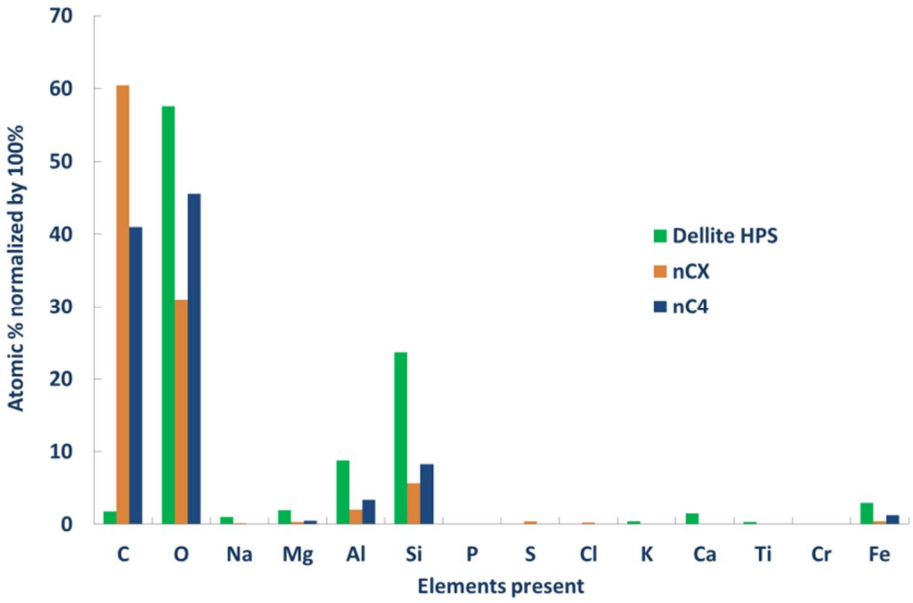

Figure 3-21: Comparison of the elemental composition of the unmodified MMT (Dellite HPS), the organomodified bentonite (nCX) and organomodified MMT (nC4)

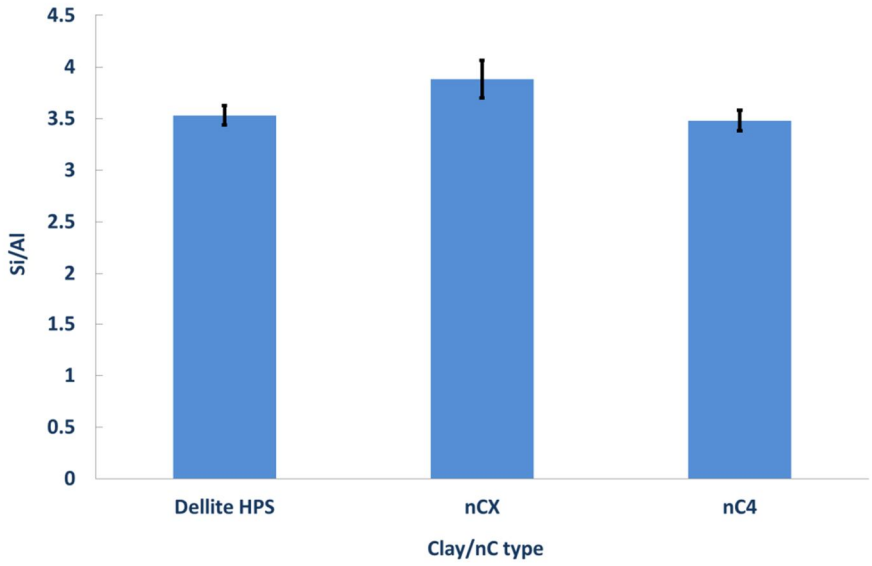

Figure 3-22: Comparison of the Si/Al ratios of the unmodified MMT (Dellite HPS), the organomodified bentonite (nCX) and organomodified MMT (nC4)

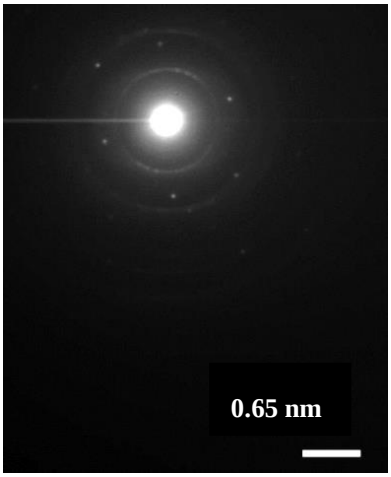

Figure 3-23: TEM-Diffraction pattern A Dellite HPS

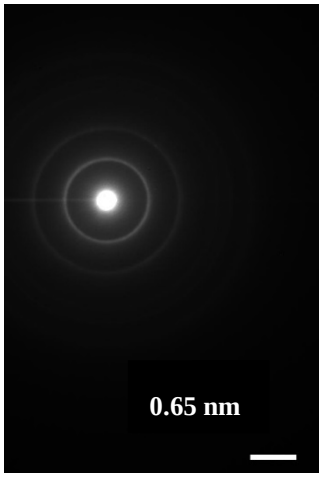

Figure 3-24: TEM-Diffraction pattern I nCX

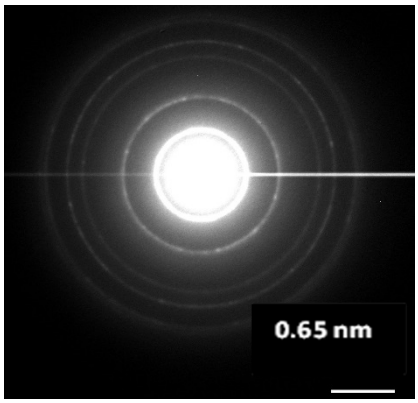

Figure 3-25: TEM-Diffraction pattern C1 of nC4

iv. TG analyses of Dellite HPS, nCX and nC4 powders

TG analyses was carried out for each of the three powders and plotted in a single, comparative graph (Figure 3-26). As expected, the inorganic clay, Dellite HPS (Table 3-10) exhibited the most substantial mass loss (approximately 10%) at around 110°C representing the loss of adsorbed and interlayer water. A second loss, representing the decomposition of the MMT, took place between 600-800°C (Xi *et al.*, 2005).

Table 3-10: Mass loss (%) of Dellite HPS between different temperatures

	0-100ºC	100-400ºC	600-800ºC
Powder Dellite HPS	10.33	0.25	4.45

Thermal analysis of organomodified nCs is more complex because the modifiers used, change the physical and chemical characteristics of the nCs. A more elaborate analysis was

carried out for nCX, to assist with the thermal analyses of the two organic dispersions which will follow in later sections of this chapter. The first observation derived from Figure 3-26 is that the organomodification has taken place; nCX and nC4 became hydrophobic, therefore, the amount of adsorbed water was only a fraction of that of inorganic clays and therefore, the related mass loss much smaller, as can be seen below 200°C (Nie *et al.*, 2012).

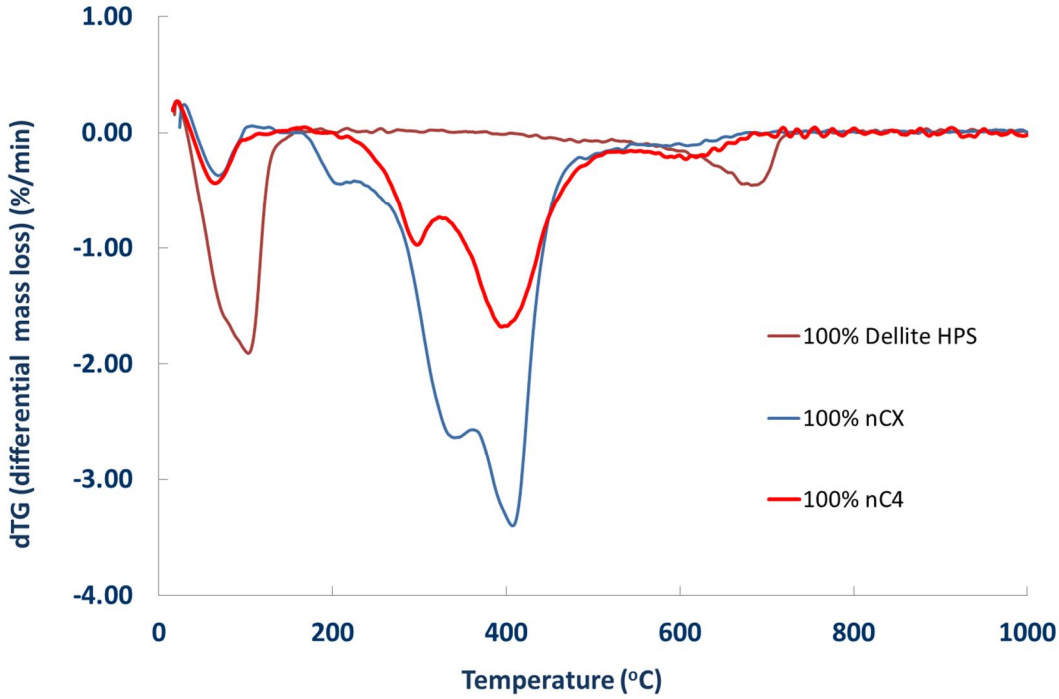

Figure 3-26: Comparison of dTG of of the unmodified MMT (Dellite HPS) and the organomodified bentonite (nCX) and organomodified MMT (nC4)

The modifier used for nCX was methylbenzyl dihydrogenated tallow ammonium chloride.

TGA/dTG carried out on the modifier by Lukošiūtė and Čėsnienė (2012) has revealed that:

- At 41°C melting of materials commences
- At 105°C evaporation of solvents takes place
- At 185°C, 321°C and 414°C decomposition of the modifier is completed
- By 450°C, 88.9% of the total material was decomposed

As an effect the mass loss at these temperatures is attributed to the aforementioned reactions related to the organomodifier.

TG analysis of the modified bentonite (Figure 3-27), used for nC1 and nC2 was carried out by Lukošiūtė and Čėsnienė (2012) has revealed that:

- In the temperature range of 180-280°C, with two distinct peaks at 210°C the decomposition of the modifier occurred at a mass change of 4.1%.
- In the temperature range of 280-380°C with a distinct peak at 340°C the decomposition of modifier bound to neighbouring molecules took place at a mass change of 16.2%.
- In the temperature range of 380-480°C with a distinct peak at 420°C the deconstruction of the modifier bound to the bentonite was completed at a mass change of 21.3%.
- Overall, in the temperature range of 280-480°C, the first peak at 340°C could also be described as a left shoulder of the major peak at 420°C and the total mass change was 37.5%.
- By 480°C, 41.6% (4.1%+37.5%) of the modifier bound in the interlayer of bentonite was decomposed.
- Between 500 and 900°C, a remaining 4% of the modified bentonite was decomposed.

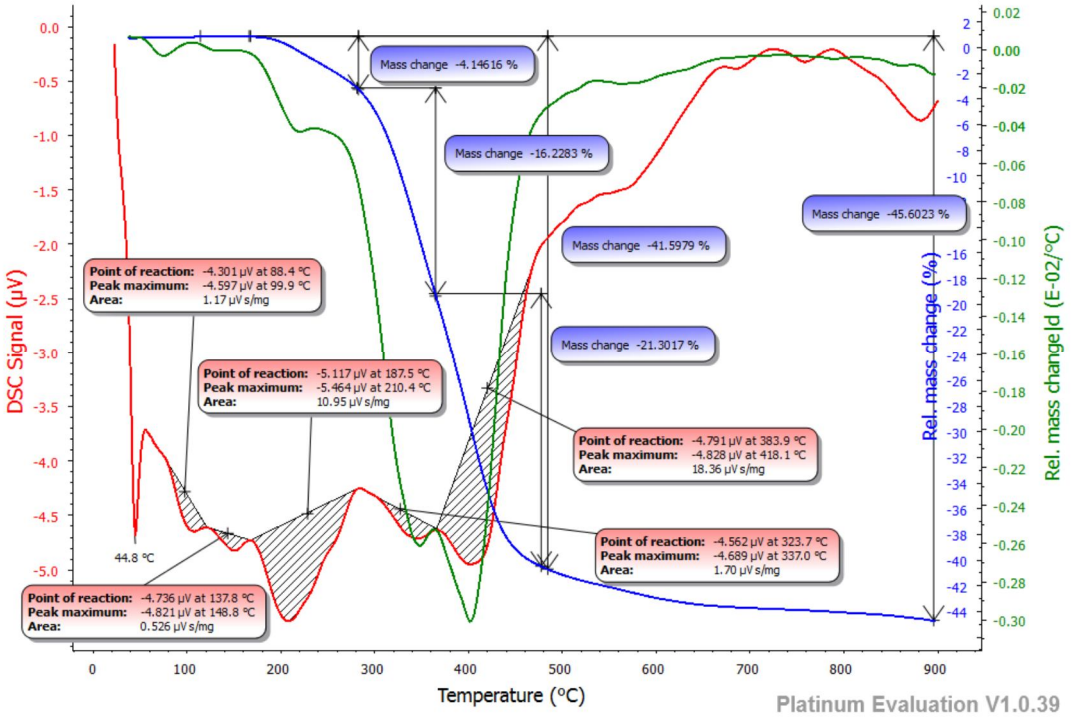

Figure 3-27: TG analysis of the modified bentonite suspension as received by Lukošiūtė and Čėsnienė (2012)

The results reported by Lukošiūtė and Čėsnienė (2012) (Figure 3-27) are in general agreement with the separate TG analyses carried out by the author for comparison and verification (Figure 3-26 and Table 3-11). The fact that the mass loss up to 180°C is minor is another proof that the organomodification was successful rendering the starting clay hydrophobic. However, the most significant mass losses related to the performance of the nC, in the two temperature bands 280-380ºC and 380-480ºC (mass losses underlined and

in bold in Table 3-11) seem to be alternated. A possible reason for this, was the low stability of the nC or variations emerging from the modification process. It could also be attributed to the high amounts of carbon used for the modification, causing some semi-permanent saturation in the nC galleries, followed up by chemical instabilities. It is acknowledged, however, that these differences could be attributed to the use of different instruments and therefore can be ignored.

Table 3-11: Mass loss (%) of nCX – Bath compared with LEI TG analyses

	0-100ºC	**100-180ºC**	**180-280ºC**	**280-380ºC**	**380-480ºC**	**480-900ºC**
nCX	0.93	0.10	4.42	**21.08**	**17.89**	2.11
LEI dTG measurements	-	4.10	-	**16.20**	**21.30**	4.00

As far as nC4 was concerned, the TG analysis carried out, showed four mass loss peaks (Figure 3-26 and Table 3-12):

- In the temperature range of 30-130°C, with a distinct peak at 67°C attributed to the loss of surface and interlayer water.
- In the temperature range of 200-330°C with a distinct peak at 295°C the decomposition of modifier bound to neighbouring molecules took place
- In the temperature range of 330-530°C with a distinct peak at 396°C the deconstruction of the modifier bound to the bentonite was.
- In the temperature range of 570-700°C with a distinct peak at 600°C the remaining OMMT was decomposed.

Table 3-12: Mass loss (%) of nC4

	0-100ºC	**100-250ºC**	**250-400ºC**	**400-500ºC**	**500-700ºC**
nC4	1.33	0.31	13.63	8.00	2.86

3.5.3 Nanoclay dispersions (nC1, nC2 & nC3)

The organomodification created a hydrophobic nC, which is incompatible with water, causing extensive flocculation of particles, when dispersed. This fact was overcome with the use of surfactant technology. From a range of over twenty surfactants, two different ones were selected (steric stabilisers non-ionic and anionic) to facilitate dispersion as discrete nanoparticles in aqueous solution by the UK Materials Research Institute (MaTRI). As an effect, two different organomodified nanoclay (nC) aqueous dispersions were prepared with the same organomodified nC as the base: nC1 and nC2.

In addition, the inorganic, unmodified montmorillonite clay, Dellite HPS, is by nature compatible with water. However, the electrostatic interaction of particles does not allow high clay loading in aqueous solutions. For this reason, the introduction of inorganic dispersant was considered necessary. After a study of various inorganic dispersants sodium polyphosphate (STPP) was selected by Naden *et al.* (2013) for the dispersion of the inorganic nC, called nC3 in this research.

The proportions and exact processes of the addition of surfactants for the dispersion of the nC are included in a confidential report (Naden *et al.*, 2013). However, selected elements of high relevance to the introduction of the nC1, nC2 and nC3 in cement pastes are outlined in Table 3-13, which also serves as a summary of the processes required to result into the three different types of nC dispersions. Some further element of the research carried out by Naden *et al.* (2013) are listed below:

- The surfactant used in nC1 was an ethoxylated fatty alcohol added at 5% by mass, which additionally necessitated the inclusion of a defoaming agent. This was expected to affect the foaming performance of the cement pastes in which nC1 would be added.
- The surfactant in nC2 was a commercially available alky aryl suphonate added at 5% by mass. The concentrated dispersion showed evidence of phase separation; however, very small clay particle size was achieved.
- The inorganic dispersant, STPP has a chemical formula of $Na_5P_3O_{10}$ added at 5% by mass.
- The highest clay loading achieved in water was 15%. Setting a barrier on the nC solids to be included in cement pastes depending on the w/b ratio.
- All three suspensions were optimized in a simulated cement environment in terms of pH and electrolyte concentrations.
- nC3 particles carry an electrostatic charge in aqueous solutions, which provides a stabilizing mechanism for the particles. At low pH the edge to face attractive forces create a “house of cards” structure between the platelets (type (c) arrangement of Figure 2-21 discussed in Chapter 2). At high pH the positive charge on the edges decreases and a parallel (face to face as shown in Figure 2-21) configuration is adopted by the platelets. Hence, the nC3 was sensitive to pH and electrolyte

concentration changes, but complete re-dispersion can take place by shaking the flocculated samples.

- High values of pH and electrolyte concentration had little effect on the OMMT (nCX), but the viscosity was significantly increased.
- Lastly, it was stated by Naden *et al.* (2013) that long-term stability should not be a problem in cement because particles would be immobilized.

All nC properties are summarized in the following table:

Table 3-13: Summary of the sequence of nC development and related properties

	Initial conditions			Organo modification		Dispersion	
Sequence of evolution of the nC	**Initial Clay**	**Initial d-spacing (nm)**	**Initial Si/ Al**	**Modifier @ modifier to clay ratio of 1:1 by mass**	**Modified clay d-spacing (nm)**	**Dispersant**	**Final nC**
From purified bentonite to nC1	Purified bentonite	1.24	2.6	Noramonium MB2HT → producing **nCX**	3.85	5% by mass fatty alcohol & 1% by mass defoaming agent	Modified/ dispersed in aqueous solution. Clay loading 15% by mass. →**nC1**
From purified bentonite to nC2	Purified bentonite	1.24	2.6	Noramonium MB2HT → producing **nCX**	3.85	5% by mass alkyl aryl sulphonate	Modified/ dispersed in aqueous solution. Clay loading 15% by mass. → **nC2**
From purified MMT to nC3	Dellite HPS (MMT)	1.26	2.6	n/a	n/a	Sodium polyphosphate	Unmodified/ dispersed in aqueous solution. Clay loading 15% by mass. → **nC3**

Once the three dispersions were received at the University of Bath, they were characterized by the author in terms of pH, level of exfoliation and single crystal structure (via TEM), elemental composition (via SEM/EDX), bulk crystallographic characteristics (via XRD) and pozzolanic activity (via TGA) as shown in Figure 3-11, before being implemented in the design of cement formulations. All three nC slurries were vacuum dried for three days

and crushed to fine powder, passing the 125 μm sieve before being tested using XRD, TGA and SEM/EDX. For the TEM image analysis the procedure described in paragraphs 3.3.1 and 3.3.2 was adopted. The three nC dispersions exhibited physical and chemical differences. Figure 3-28-A, B and C show the physical appearance of the different dispersions and the pH measurement taken. As can be seen, the nC1 had a pH of 8.65, the nC2 of 9.84 and the nC3 of 8.30, prior to mixing in the cement pastes. It should be stressed that the dispersions showed small pH variations at subsequent measurements, but were all designed to maintain stability at the higher pH of hydrating cement. Lastly, for values of pH above 9, a small error is always expected ("alkaline error").

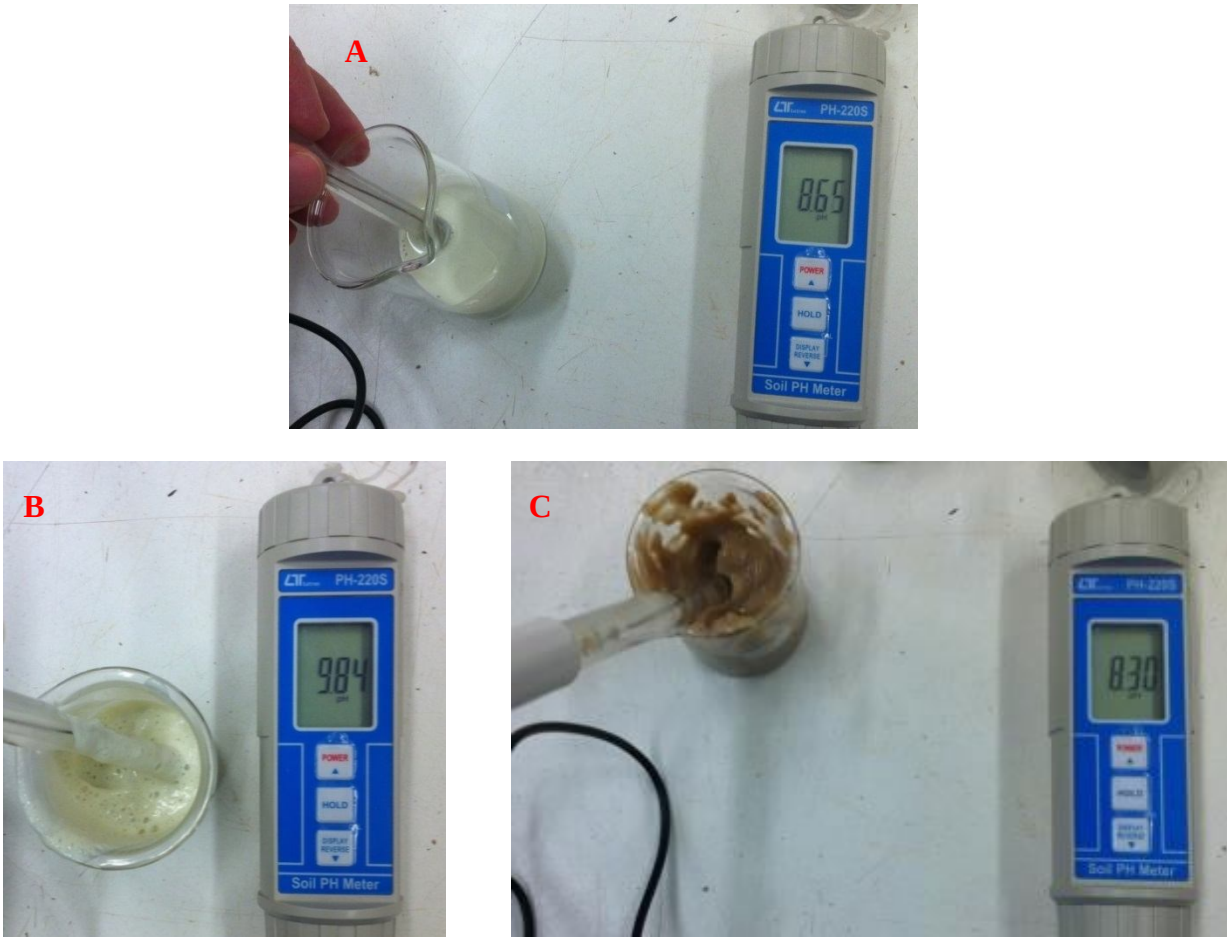

Figure 3-28: pH measurement of (A) nC1, (B) nC2 and (C) nC3

i. Organic dispersion nC1

The diffraction pattern, the TEM micrograph and the XRD of nC1 indicate that it was possibly intercalated, but not exfoliated and particles tend to conglomerate back together locally. The nC1 layers were covered with organic matter, possibly coming from the surfactant and were stacking on top of each other, possibly in a combination of primarily face to face arrangement (type b in Figure 2-19) and edge to edge or face to edge arrangements. This arrangement does not allow the reactive sides to be exposed, hence no seeding effect can be expected and additionally this could initiate localized shear failures in the materials with cracks propagating between the stacks of platelets (Figure 3-30A and B). As a result, cement pastes formulated with nC1 were predicted to have lower compressive strengths due to poor bonding, and presence of significant amounts of impurities.

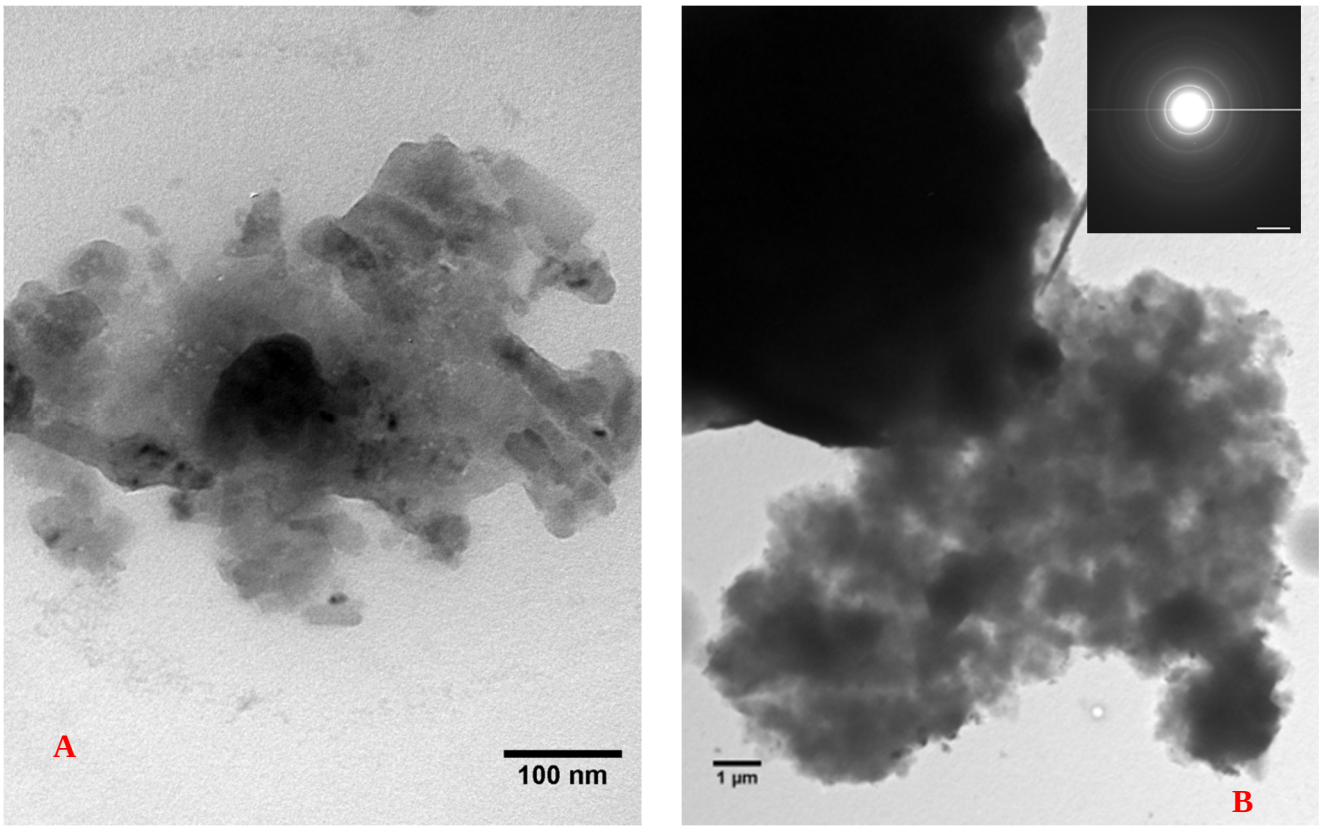

Figure 3-29: TEM micrograph of nC1 (A) @ 150000x and (B) @ 6000x

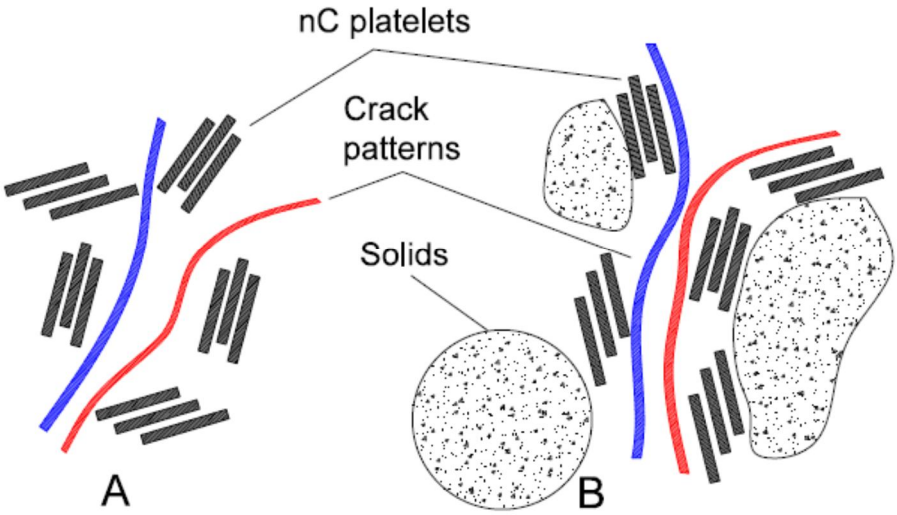

Figure 3-30: A: Possible shear failure as a result of the arrangement of nC platelets, B: possible nanocrack propagation path around LS or PC solids

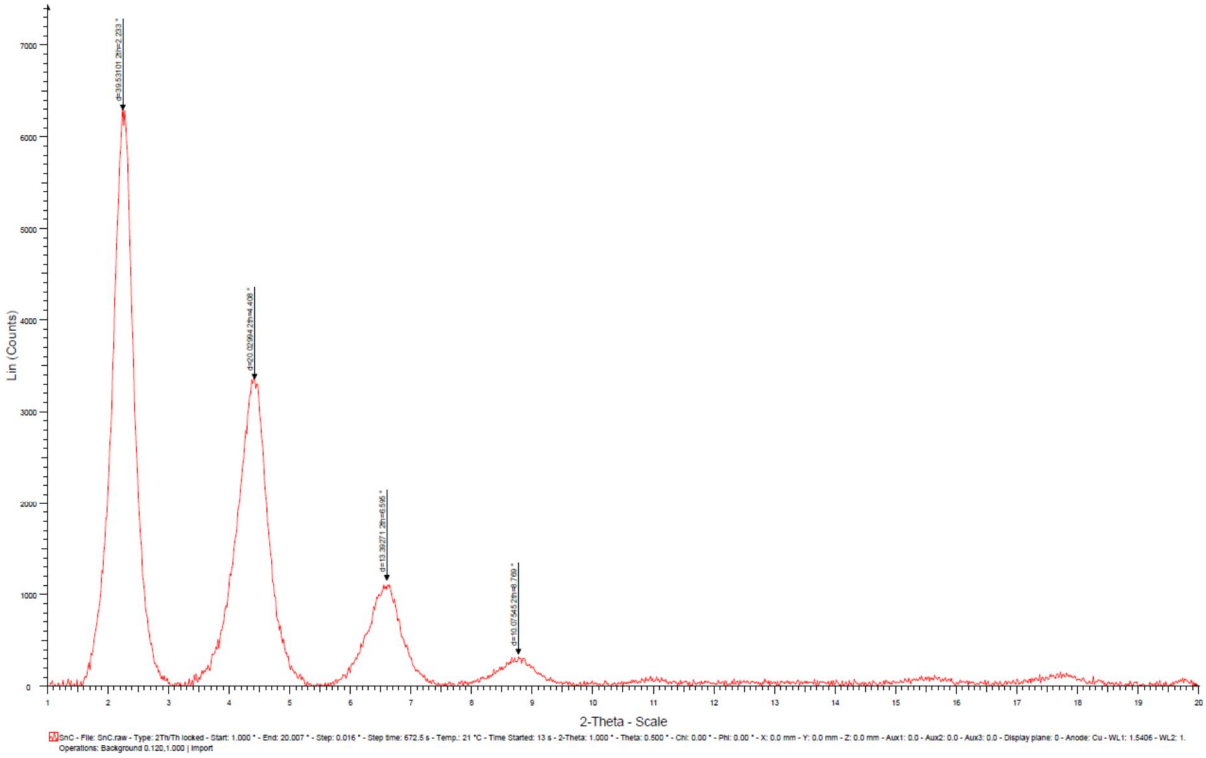

Figure 3-31: XRD pattern of nC1 dispersion

The XRD analysis of the nC1 showed a marginal increase in the d spacing of the 001 plane. From 3.85 nm achieved by the modification, it was increased to 3.95 nm by the dispersion.

For high statistical reliability of the elemental analysis a matrix of 5 x 5 randomly selected spectra was collected. Indicatively the first five are presented in Table 3-14, whereas in

Figure 3-35 a comparison of the elemental composition in terms of the median of the atomic percentage normalized by 100% is presented. For nC1 the Si/Al ratio was found to be between 4.02 and 4.48 with a median of 4.23 and a standard deviation of 0.12, significantly higher than the ratio obtained for the modified only nC. The carbon content was found to be significantly high (44-55% atomic). Knowing that the amount of organic modifier added to the nC was equal to 41% by mass, the difference could be attributed to the presence of the organic surfactant. The high carbon content could possibly lead to formation of carboaluminates when nC1 would be added to the cement paste. Indicatively, the elemental analysis of the first five spectra is shown in Table 3-14.

The diffraction pattern of nC1 shows a polycrystalline structure, with randomly oriented grains, since rings are present. Two diffraction patterns were collected and the various d-spacings were calculated according to Equation: 3-5:

d from diffraction pattern A1	*d* from diffraction pattern B1
d_1= 2 x 1/0.65 = 3.08 nm	d_1= 2 x 1/0.701 = 2.85 nm
d_2= 2 x 1/1.25 = 1.60 nm	d_2= 2 x 1/1.22 = 1.64 nm
	d_3= 2 x 1/1.83 = 1.09 nm
	d_4= 2 x 1/2.08 = 0.96 nm
	d_5= 2 x 1/2.41 = 0.83 nm
	d_6= 2 x 1/2.52 = 0.79 nm

Both diffraction patterns had similar d-spacings, however lower than the values obtained by XRD. The reason for this is that XRD is measuring the d-spacing in the bulk of the material, whereas TEM is focused on a single crystal. The particles seem to be agglomerating back together.

Table 3-14: SEM/EDX counts summary (% atomic) of nC1

nC1 - All results atomic & normalized by 100%											
Spectrum	C	O	Mg	Al	Si	P	S	Cl	K	Ca	Fe
(1,1)	53.15	33.68	0.54	2.75	8.87	0.12	nd	0.39	nd	0.08	0.41
(2,1)	53.59	33.69	0.48	2.74	8.64	nd	nd	0.40	nd	0.10	0.38
(3,1)	53.56	33.85	0.54	2.78	8.39	nd	nd	0.36	nd	0.10	0.42
(4,1)	54.60	32.94	0.46	2.73	8.37	nd	nd	0.36	nd	0.11	0.42
(5,1)	54.98	31.08	0.47	2.97	9.51	nd	nd	0.36	nd	0.14	0.47
Total mean	53.29	33.22	0.51	2.92	9.30	0.17	0.13	0.39	0.16	0.10	0.47
Stdv	2.03	2.36	0.07	0.52	1.97	0.04	nd	0.12	nd	0.03	0.15

ii. Organic dispersion nC2

The analysis of nC2 confirmed the findings reported by Naden *et al.* (2013) had much smaller particles. The EDX analysis showed that it contained almost the same amount of carbon as nC1 (about 47-59% normalized atomic) for the same reasons stated before, as indicatively shown in the first five spectra in Table 3-16. The Si/Al ratio was similar to nC1 (Figure 3-40) and was found to be between 3.86 and 4.39 with a median of 4.08 and a standard deviation of 0.14. Figure 3-34-A and –B show areas of agglomeration in the nC2 disperion and areas of crystallization of impurities, but at a more intercalated arrangement than nC1. Consequently, it can be expected to perform better when mixed in cement pastes. XRD of nC2 dispersion was also carried out, showing a d-spacing of 3.95 nm at 2.2°2θ and 2.0 nm at 4.4°2θ (Figure 3-32). Comparing the d-spacing derived from the XRD analyses of the modified nC and of the modified and dispersed nC, it can be assumed that nC2 platelets remained dispersed in the solution, i.e. comprised of discrete nanoparticles within the dispersion having the same d-spacing at approximately the same 2θ angles, since it was the modification that caused the lattice expansion. Adding to this, it seems that both surfactants increased the d-spacing by 0.1 nm. However it is interesting to note that the elemental analysis of nC1 did not show any Na, implying that all Na cations were exchanged as intended during the nC modification. EDX on nC2 showed traces of Na in various spectra and this is because for nC2 an anionic surfactant containing Na, was used, also shown in Figure 3-35.

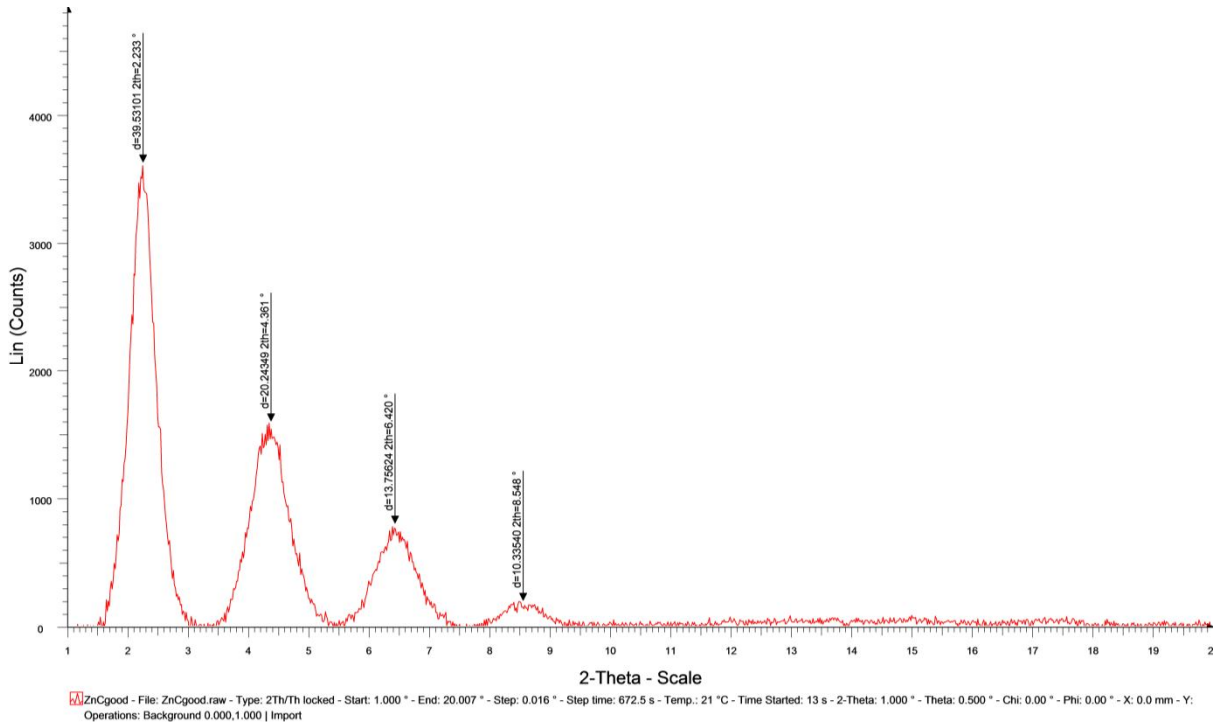

Figure 3-32: XRD pattern of nC2 dispersion

It is known that d-spacing corresponding to the XRD peaks is used as a means of measuring the degree of exfoliation. However, as exfoliation takes place, there should also be a broader spread of different d-spacings present, so the XRD peaks may also be wider. Two approaches could be followed to assess this hypothesis. Either measuring the full-width at half maximum of the peaks or carrying out base line correction and mathematical curve fitting and comparing the full widths. The second technique was adopted, as the WIRE software available could provide exact and mathematically elaborated values. Comparing curve 1 in Figure 3-33 and Table 3-15 nC1 exhibited a smaller width value, while nC2 a greater width value to the starting one of nCX.

Table 3-15: Width and height of XRD peaks of nC1, nC2 as compared to original nCX

nC1				**nC2**			
	Centre	Width	Height		Centre	Width	Height
Curve 1	2.23	0.42	7002.93	**Curve 1**	2.21	0.61	4352.50
Curve 2	4.38	0.57	3200.33	**Curve 2**	4.35	0.71	1440.63
Curve 3	6.55	0.65	1120.55	**Curve 3**	6.44	0.81	778.15
Curve 4	8.75	0.70	299.84	**Curve 4**	8.55	0.85	200.87

nCX			
	Centre	Width	Height
Curve 1	2.49	0.55	4917.99
Curve 2	4.66	0.90	3306.86
Curve 3	7.07	0.93	776.74

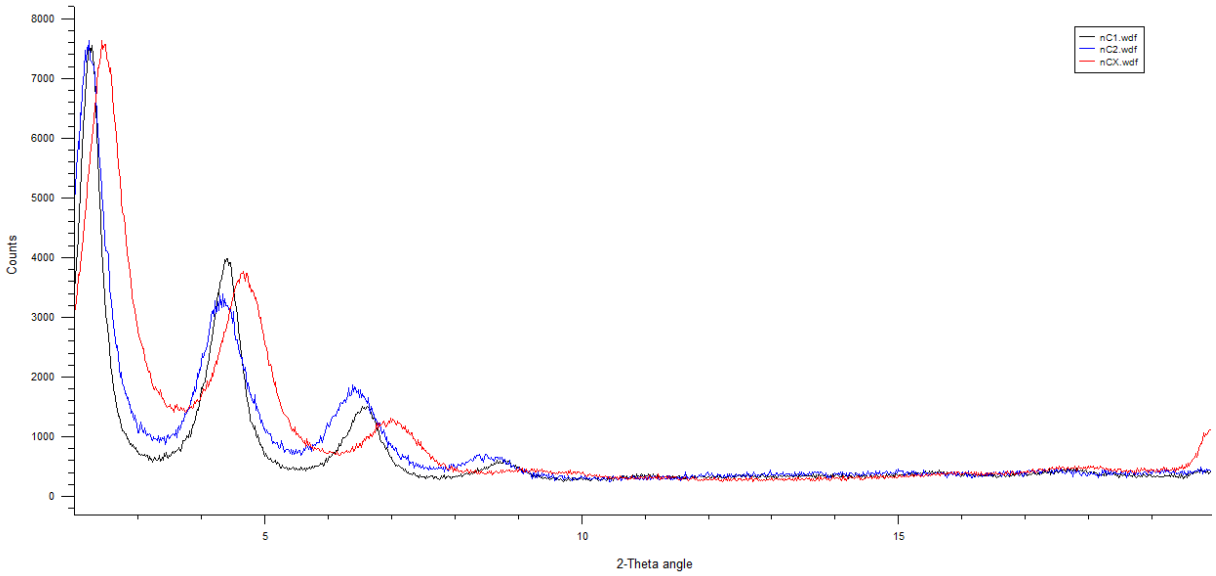

Figure 3-33: Comparison of peak shifts of nC1 & nC2 with addition of surfactants as compared to original nCX

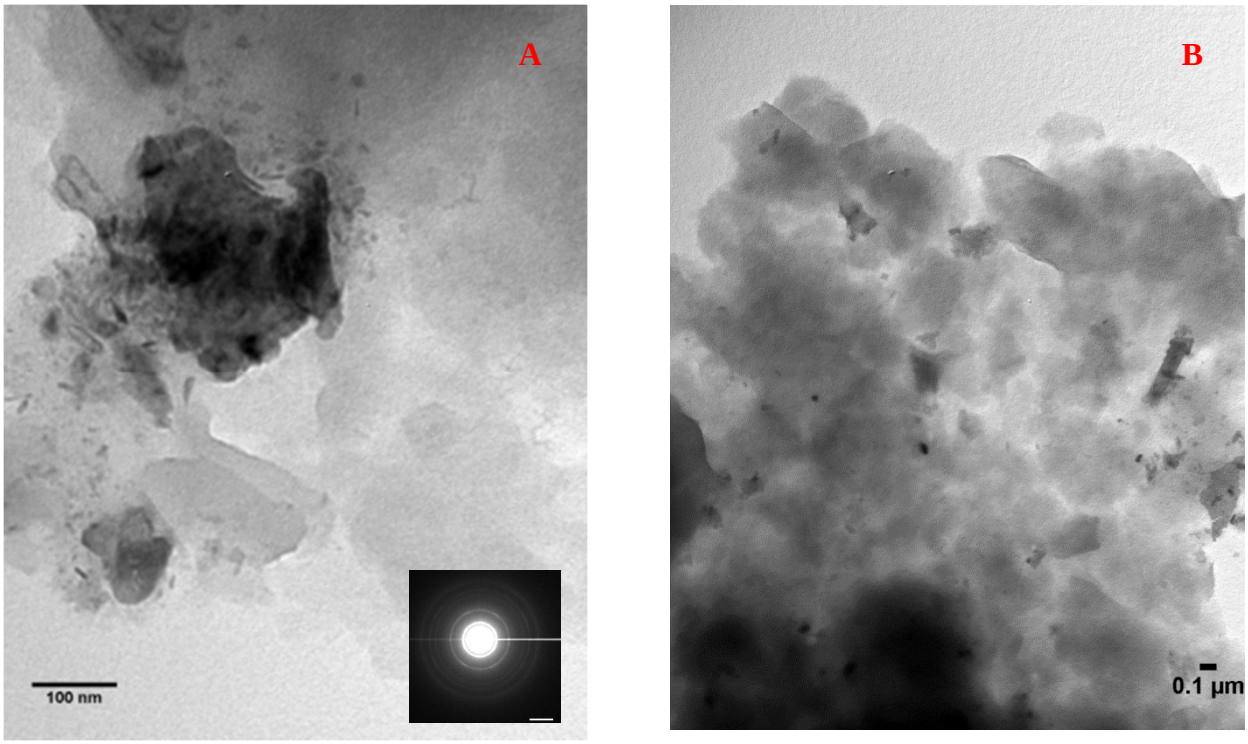

Figure 3-34: TEM micrograph of nC2 (A) @ 120000x and (B) @ 25000x

Table 3-16: SEM/EDX counts summary (% atomic) of nC2

nC2 - All results atomic & normalized by 100%													
Spectrum	C	O	Na	Mg	Al	Si	P	S	Cl	K	Ca	Ti	Fe
(1,1)	58.99	21.83	nd	0.58	3.64	11.6	n/a	2.18	nd	nd	0.26	nd	0.91
(2,1)	55.22	26.96	nd	0.55	3.58	10.97	0.16	1.62	0.11	nd	0.09	nd	0.73
(3,1)	49.43	26.74	nd	0.56	4.29	14.52	0.21	2.66	nd	0.12	0.13	nd	1.33
(4,1)	54.98	28.70	0.15	0.49	3.20	10.06	0.20	1.51	0.07	nd	0.06	nd	0.58
(5,1)	56.06	30.84	nd	0.47	2.70	8.13	0.08	1.13	0.06	nd	0.05	nd	0.48
Total mean	54.30	28.7	0.15	0.54	3.53	10.68	0.15	1.64	0.10	0.08	0.10	0.07	0.76
Stdv	4.22	6.11	0.08	0.19	1.24	4.24	0.04	0.77	0.06	0.02	0.06	0.03	0.32

Two diffraction patterns were collected and the various d-spacings were calculated according to Equation: 3-5:

d from diffraction pattern A2	*d* from diffraction pattern B2
d_1= 2 x 1/0.7 = 2.86 nm	d_1= 2 x 1/0.701 = 2.85 nm
d_2= 2 x 1/1.26 = 1.59 nm	d_2= 2 x 1/1.27 = 1.64 nm
d_3= 2 x 1/1.9 = 1.05 nm	d_3= 2 x 1/1.97 = 1.02 nm
d_4= 2 x 1/2.17 = 0.92 nm	d_4= 2 x 1/2.23 = 0.9 nm
d_5= 2 x 1/2.5 = 0.8 nm	d_5= 2 x 1/2.53 = 0.79 nm
d_6= 2 x 1/2.64 = 0.76 nm	d_6= 2 x 1/2.62 = 0.76 nm

It is interesting to note that the d-spacings calculated from the diffraction patterns of nC2 were almost equal to the ones derived by single crystal analyses of nC1, as expected, since the same modifier was used for both nC.

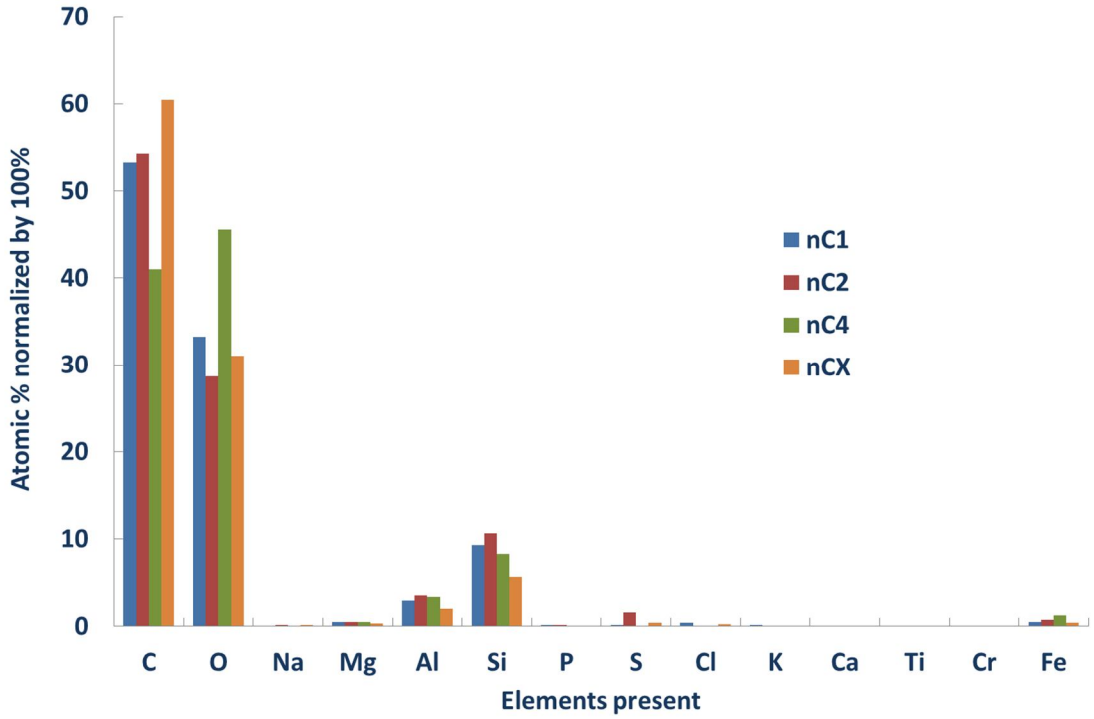

Figure 3-35: Comparison of the elemental composition of all organomodified nC (powder and dispersion)

It is shown in Figure 3-35 that the dispersion was successful leading to nC1 and nC2 with less C and more Si and Al than the initial OMMT, nCX. The commercial nC4 exhibited lower quantities of Si and Al than the two dispersed nC, however it could perform better in a cement paste due to the fact that significantly less C was involved for its organomodification. This observation can be coupled with the TEM image analyses,

showing platelets covered with organic matter for nC1 and nC2, possibly not allowing the nC to perform best.

iii. Inorganic dispersion nC3

Figure 3-36 (A) and (B) shows nC3, very well dispersed in which discrete platelets of nC smaller than 50 nm can be identified, indicating that although the d-spacing is lower than in the organomodified nC, exfoliation has taken place, with some small agglomerates of impurities. Soft, rather than angular edges can be observed, lowering the possibilities of shear failure at the nanolevel. nC3 overall looks the most stable of all three dispersions. EDX showed low carbon content; between 7.8 and 9.0% normalized atomic. The Si/Al ratio was found to be between 2.60 and 3.97 with a median of 2.71 and a standard deviation of 0.08, therefore close to the theoretically expected value for MMT of 2.60 and hence, lower than the ones of OMMT (Figure 3-40). It should also be noted that there is a Ca content ranging from 0.7 to almost 2.0%, which could react in a cement paste towards formation of C–S–H.

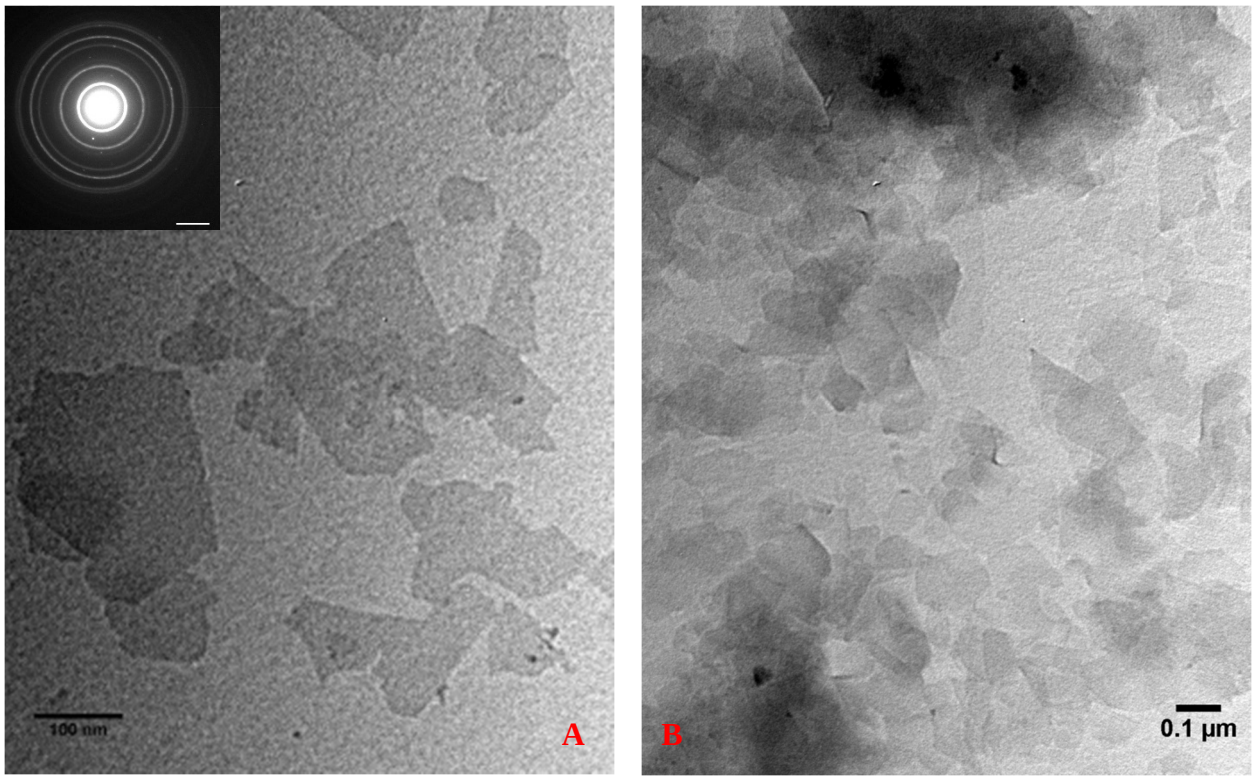

Figure 3-36: TEM micrograph of nC3 (A) @ 120000x and (B) @ 60000x

Two diffraction patterns (Figure 3-43 (A3) and (B3)) were collected, showing a great number or rings, i.e. many diffracting planes and the various d-spacings were calculated according to Equation: 3-5:

d from diffraction pattern A3	*d* from diffraction pattern B3
d_1= 2 x 1/0.72 = 2.78 nm	d_1= 2 x 1/0.85 = 2.35 nm
d_2= 2 x 1/1.36 = 1.47 nm	d_2= 2 x 1/1.54 = 1.3 nm
d_3= 2 x 1/1.95 = 1.03 nm	d_3= 2 x 1/2.31 = 0.86 nm
d_4= 2 x 1/2.2 = 0.91 nm	d_4= 2 x 1/2.64 = 0.76 nm
	d_5= 2 x 1/3.18 = 0.63 nm

In addition to this, XRD of nC3 dispersion was also carried out (Figure 3-37), showing a d-spacing of 1.49 nm at 5.9° 2θ and 0.45 nm at 19.7° 2θ as expected for unmodified MMT. Comparing the d-spacing derived from the XRD and TEM analyses it can be assumed that nC3 remained dispersed in the solution, i.e. comprised of discrete nanoparticles within the dispersion.

Some disparity between TEM and XRD d-spacing measurements and calculation is always expected, as discussed earlier. Additionally, the overall lower d-spacings given by the TEM diffraction analyses could be attributed to the material preparation method; vacuum drying of samples may have caused some imbalance to the nature of the specimens.

Table 3-17: SEM/EDX counts summary (% atomic) of nC3

nC3 - All results atomic & normalized by 100%														
Spectrum	C	O	Na	Mg	Al	Si	P	S	Cl	K	Ca	Ti	Cr	Fe
(1,1)	nd	65.65	4.05	1.46	6.61	18.09	0.86	0.73	nd	0.19	1.01	0.14	nd	1.21
(2,1)	nd	64.19	3.58	1.49	6.89	19.37	0.76	0.77	nd	0.23	1.02	0.20	nd	1.49
(3,1)	nd	65.51	3.52	1.43	6.81	18.44	0.82	0.70	nd	0.21	1.20	0.21	nd	1.16
(4,1)	nd	66.69	3.64	1.45	6.52	18.22	0.69	0.60	nd	0.14	0.83	0.15	nd	1.06
(5,1)	9.33	61.87	3.13	1.22	5.66	14.81	0.57	0.53	nd	0.17	1.48	0.18	nd	1.05
Total	7.81	65.33	3.52	1.49	6.81	18.65	0.73	0.67	0.07	0.23	0.91	0.18	0.18	1.17
Stdv	0.89	1.36	0.26	0.34	0.39	1.25	0.11	0.08	nd	0.11	0.28	0.03	nd	0.17

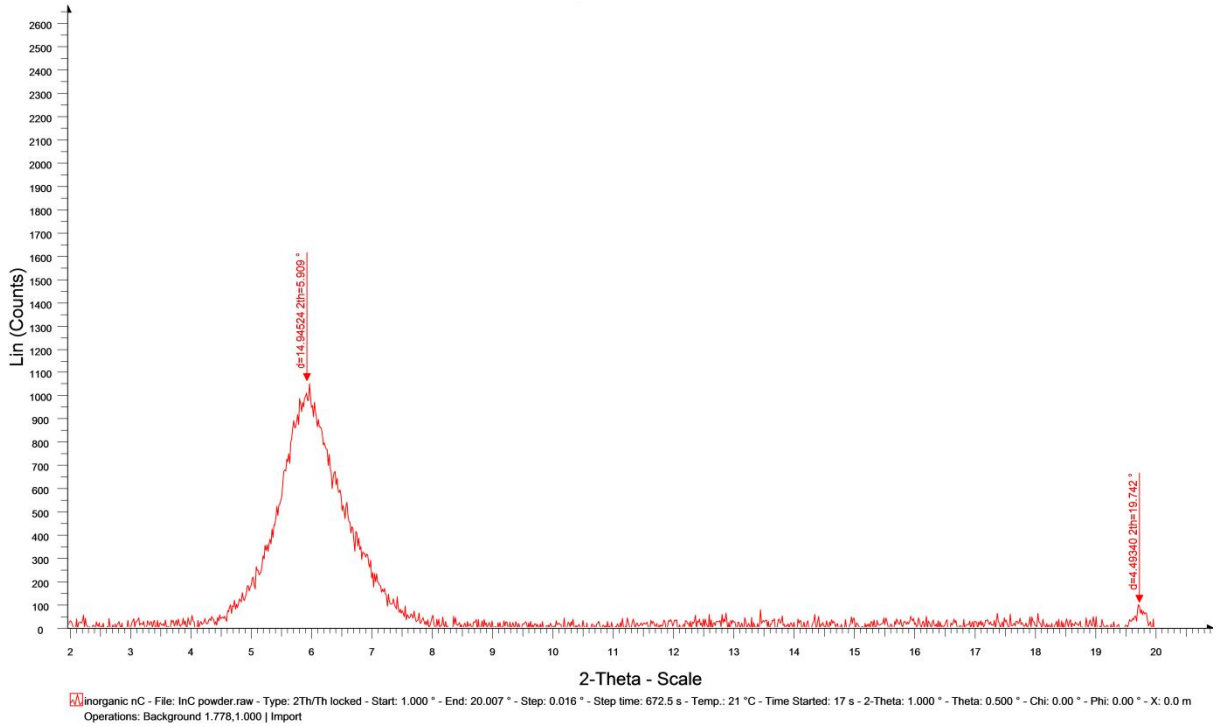

Figure 3-37: XRD pattern of nC3 dispersion

As discussed in the case of nC1, nC2 and nCX with regards to the comparative XRD analyses, the peak shift and difference in width between nC3 and the starting nC, HPS is also presented. As shown in Figure 3-38 and Table 3-18 the width of the first peak was almost equal in both samples, whereas the peak of nC3 was shifted towards lower 2θ angle.

Table 3-18: Width and height of XRD peaks of nC3 as compared to original HPS

nC3				**HPS**			
	Centre	Width	Height		Centre	Width	Height
Curve 1	5.98	1.18	900.41	**Curve 1**	7.33	1.22	909.47
Curve 2	19.76	0.24	76.18				

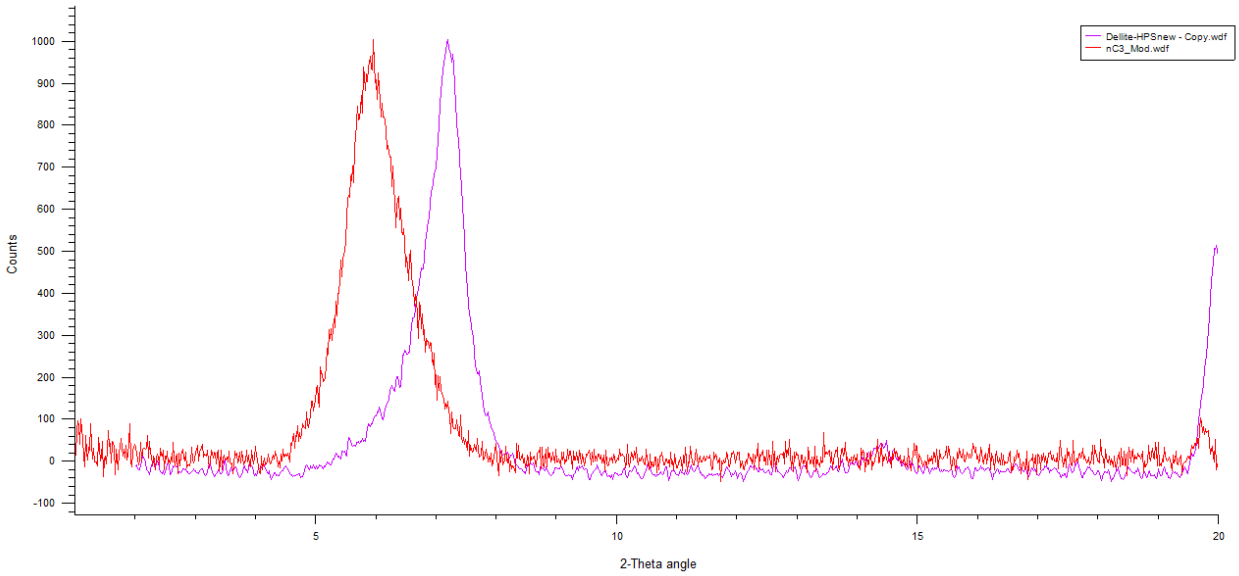

Figure 3-38: Comparison of peak shifts of nC3 with addition of surfactants as compared to original HPS

The comparison of the elemental composition acquired by the SEM/EDX between nC3 and Dellite HPS, from which the former was developed, showed that both the original clay and the dispersed nC contain only small quantities of C, compared to nC1 and nC2 and significant quantities of Si, Al and O (Figure 3-39). Apparently, the dispersant increased the carbon content.

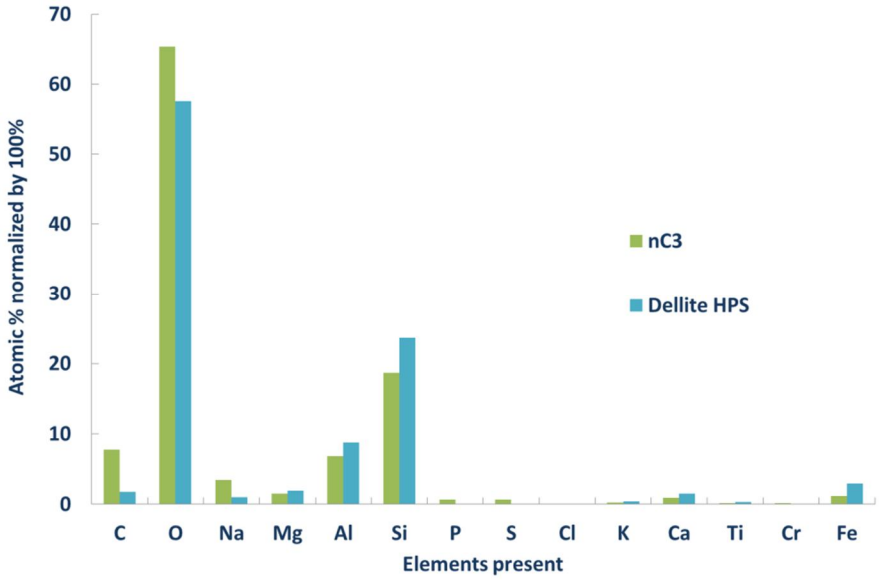

Figure 3-39: Comparison of elemental composition of original/unmodified powder Dellite HPS and unmodified/dispersed nC3

The comparison of the Si/Al ratios of the three dispersions provided another evidence of the variation observed in the organomodified dispersions since the standard deviation of these samples was higher than that of the inorganic dispersion (Figure 3-40).

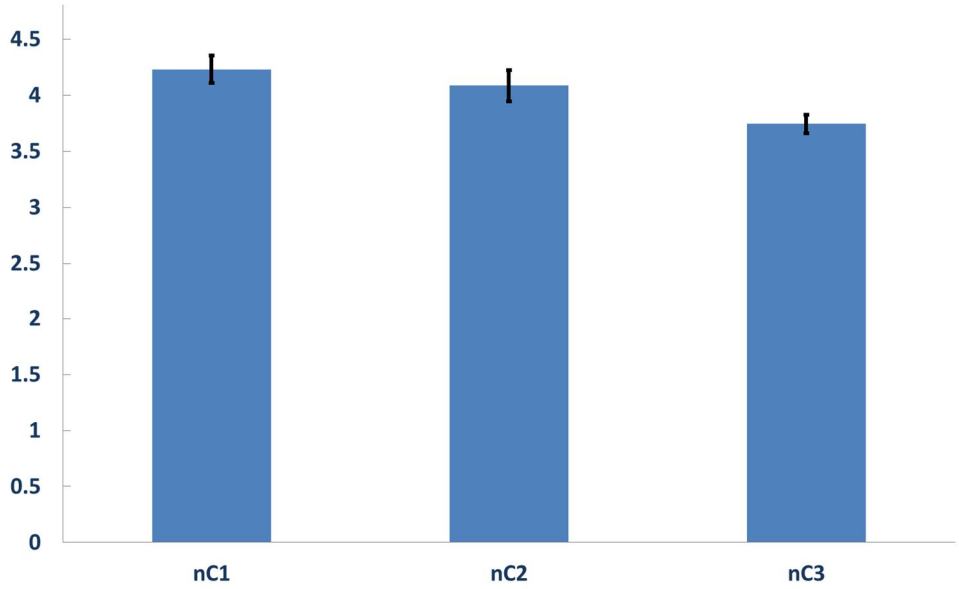

Figure 3-40: Comparison of the Si/Al ratios of the organomodified & dispersed nC and the unmodified & dispersed nC

Furthermore, the TEM diffraction patterns of the three dispersions, showed more rings, therefore, more polycrystalline structures than the starting nC but not as many randomly scattered crystals for nC1 and nC2. However, again, the TEM diffraction patterns of nC3 showed more exfoliated crystals and greater homogeneity.

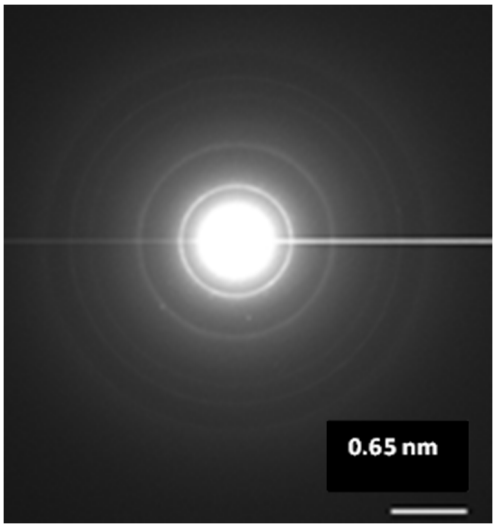

Figure 3-41: TEM-diffraction pattern A1 of nC1

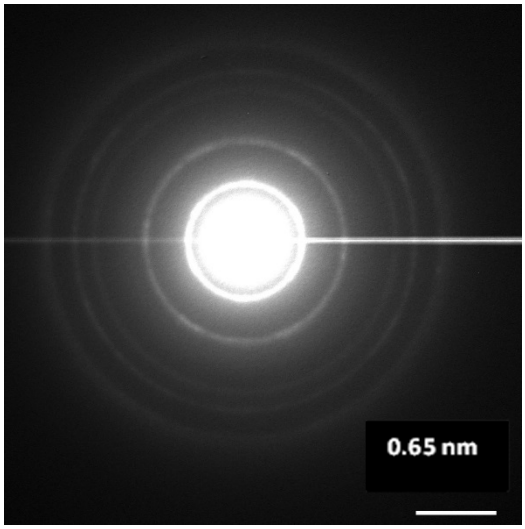

Figure 3-42: TEM-diffraction pattern A2 of nC2

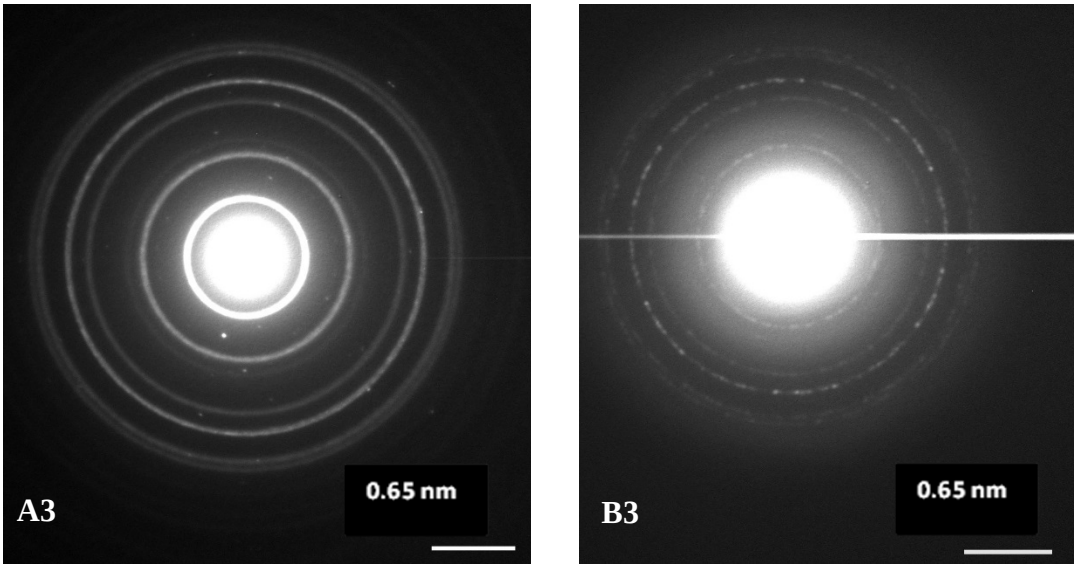

Figure 3-43: TEM-diffraction pattern of nC3 (A3) and (B3)

iv. TG analyses of nC1, nC2 and nC3 dispersions

Continuing from the thermal analysis of the starting clay and nanoclay, the dispersed nCs were thermogravimetrically analysed in order to assess any changes within the structure of the dispersions, after the addition of the surfactants. For this, the three nanoclay dispersions were vacuum dried for three days, then ground and sieved through a 125 μm sieve. Consecutively, the TG analyses were carried out. As can be seen in Figure 3-44 to Figure 3-46 and also numerically expressed in Table 3-19, nC1, nC2 and nC3 exhibited three mass loss peaks. The organomodified samples were totally decomposed by 500°C.

Table 3-19: TGA of nC decomposition temperatures

nC1	nC2	nC3
70°C	70°C	85°C & shoulder at 110°C
198°C	213°C & shoulder at 360°C	656°C
360°C & shoulder at 411°C	410°C	750°C

Moreover, comparing the results of the nCX and the organomodified and dispersed nC1 and nC2 (Figure 3-44) the first peak at 70°C of nCX occurred at the same temperature for nC1 and nC2. The second peak at 210°C of nCX was shifted by a few degrees lower for nC1, but for nC2 it occurred at the same temperature. The third peak of nCX occurred at the same temperature for nC2, but for nC1 it was shifted at lower temperatures and comprised of two curves; one at 360°C with greater mass loss and the second, a right shoulder at 410°C. Overall, nC2 seemed to be more stable with respect to the starting nCX, possessing similar shape including the left shoulder with a peak at about 360°C and the major peak, at 10°C higher temperature than nCX. These two elements suggest that the surfactant used in nC2 had better affiliation in the dispersion. In a way this result was expected, taken that the alkyl aryl sulphonate is anionic, therefore, causes charge interaction as opposed to the surfactant used in nC1 which was non-ionic. It is possible that in the complex chemistry of the organomodified and dispersed nC the anionic surfactants contribute to the formation of stronger bonds, in agreement with Xi *et al.*(2005) who used an ion-exchange bromide as surfactant and modifier.

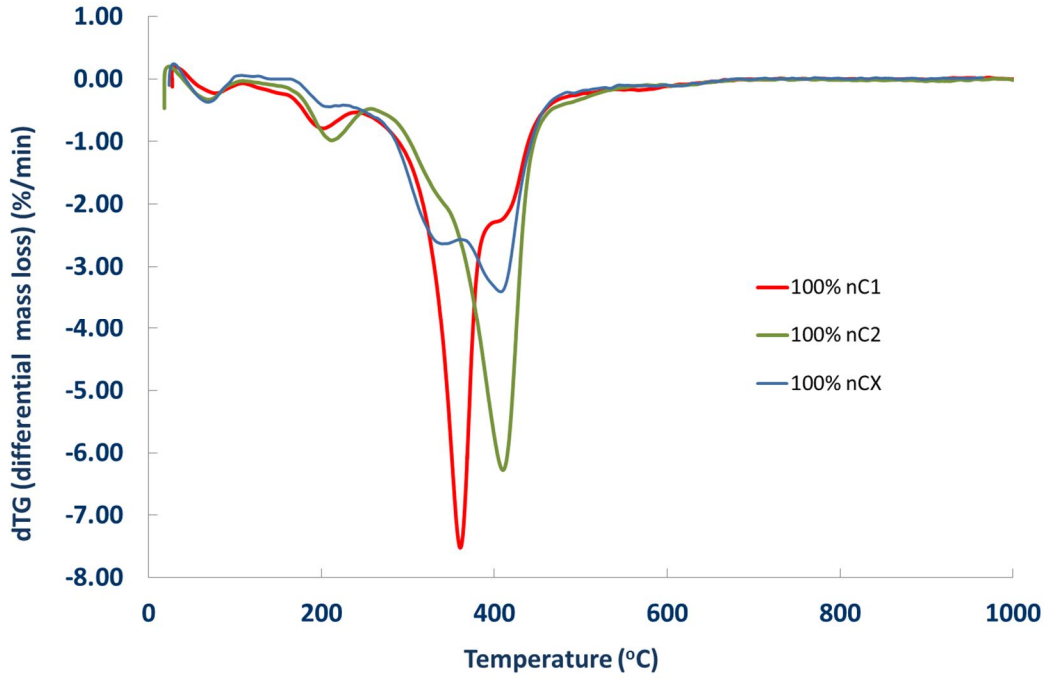

Figure 3-44: dTG curves of modified and dispersed organoclays (nC1 & nC2) compared to the starting modified but undispersed nCX

Table 3-20: Mass loss (%) of nC1 & nC2 dispersions

Specimen	0-100°C	100-180°C	180-280°C	280-400°C	400-500°C	500-1000°C	Note
Dried 100% nC1	0.68	2.63	6.73	35.34	9.48	2.17	1
Dried 100% nC2	1.02	1.82	6.52	25.95	20.14	2.29	2

Note 1: For nC1 the mass loss between 280-500°C is equal to 35.34+9.48 = 44.82% > 41.6%, which was the total mass loss of nCX within this temperature range.

Note 2: For nC2 the mass loss between 300-500°C is equal to 25.95+20.14 = 46.09% > 41.6%, as expected.

The quantitative analysis of the differential mass losses of nC1 and nC2 (Table 3-20) at the different temperature ranges, yielded a number of interesting observations:

In closer observation, most of nC1 decomposed within the 280-400°C temperature range, whereas for the decomposition of nC2 greater energy was required. Although the organomodification was designed in such a way that the decomposition of the modifier bound to the bentonite occurred at 380-500°C (mass loss of 21.3% with a peak at 400°C) the surfactant used in nC1 possibly produced a less stable dispersion; whereas the surfactant used in nC2 produced a more stable dispersion, enhancing the structure of nCX.

Above 500ºC almost the same amount of clay residues were found in both nC.

It was also interesting to compare nC1 and nC2 with the undispersed nC4 (Figure 3-45). Two things can be noted:

- The modifier used for nC4 decomposes at greater temperatures (by 100°C).
- Possibly, some clay particles remained unreacted with the modifier and this is why a mass loss was recorded within 570-700°C.

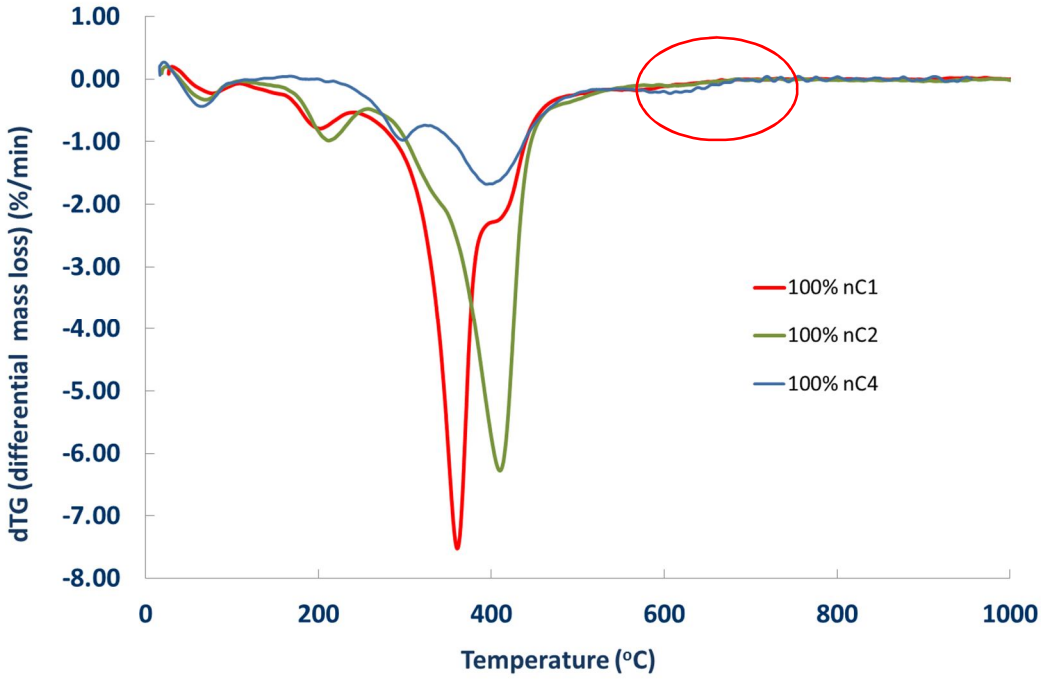

Figure 3-45: dTG curves of modified and dispersed organoclays (nC1 & nC2) compared to modified and undispersed nC4

Lastly, the dispersed inorganic nC3 showed a typical decomposition behaviour with three primary mass losses (Table 3-21). The first significant one occurred at around 100°C and was attributed to the loss of the adsorbed interlayer water (Figure 3-46). This loss was much greater than that of Dellite HPS, the original clay, as expected since according to literature clays adsorb water if directly dispersed in aqueous solutions. Furthermore, two other mass losses were recorded for nC3 with peaks at 650 and 750°C attributed to the calcite mass loss of the bentonite. Dellite HPS exhibited one significant peak at 684°C.

Table 3-21: Mass loss (%) of nC3 dispersion

Specimen	0-100ºC	100-180ºC	180-300ºC	300-600ºC	600-800ºC	800-1000ºC	Note
Dried 100% nC3	10.82	5.34	1.00	1.00	3.30	1.13	3

Note 3: although the nC3 dispersion was dried, pulverized and tested, it can be seen that a great percentage of the mass of non organomodified nanoclay was water bound on the surface of its platelets, as suggested by the 10.82% of mass loss within 0-100ºC.

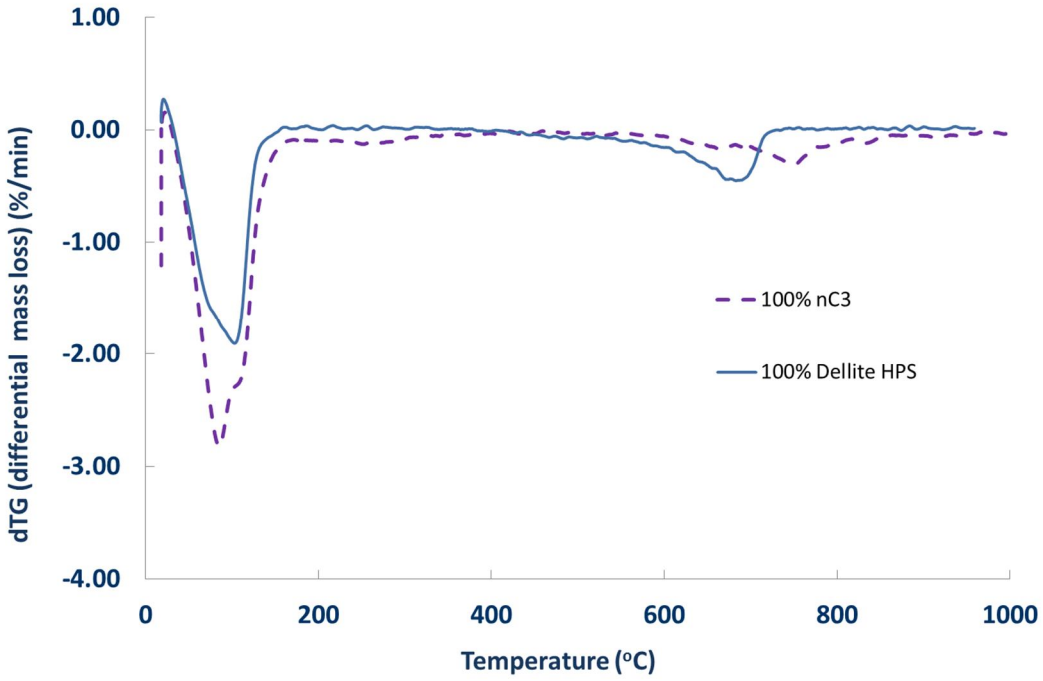

Figure 3-46: dTG curves of purified MMT (Dellite HPS) and dispersed unmodified inorganic clay nC3

v. Pozzolanic study of nC1, nC2 and nC3 dispersions

An additional study was carried out in order to assess possible pozzolanic activity of the three nC dispersions in terms of consumption of $Ca(OH)_2$. Thermogravimetric analyses results cannot be conclusive on their own and hence, were coupled with XRD results. Moreover, as discussed in Chapter 5, the results of the pozzolanic study were in agreement with results derived from the addition of the nC dispersions in the cement paste formulations.

Materials and methods:

Initially a reference sample of lime putty (LP) was prepared by vigorous whisking of the material with a pallet knife until it was homogenized. 20 gr of the sample were sealed in a vial. Next, six compositions were realized as shown in Table 3-22. It should be noted that in this section, the mix proportions of nC refer to the nC dispersion rather than nC solids only. Materials were manually mixed with spatula for 1 minute and the pastes were placed in vials. All vials were immediately sealed, extra protected with tape and secured in a sealed, airtight bag to avoid contact with the air and consequently carbonation.

Samples were kept in the vials for two different periods: (i) 6 days and (ii) 8 months at room temperature. Only the LP + nC3 dispersion set immediately, whereas the remaining four formulations were still liquid after 6 days, as can be seen in Figure 3-47 (A denotes the 50% nC dispersion content and B, the 80% nC dispersion content by mass); a first indication that nC3 exhibited a stronger pozzolanic activity.

Table 3-22: Composition of lime putty+nC dispersion pastes

Sample	**LP content (%)**	**nC dispersion content (%)**
100% LP	100	0
50% LP + 50% nC1 dispersion	50	50
50% LP + 50% nC2 dispersion	50	50
50% LP + 50% nC3 dispersion	50	50
20% LP + 80% nC1 dispersion	20	80
20% LP + 80% nC2 dispersion	20	80
20% LP + 80% nC3 dispersion	20	80

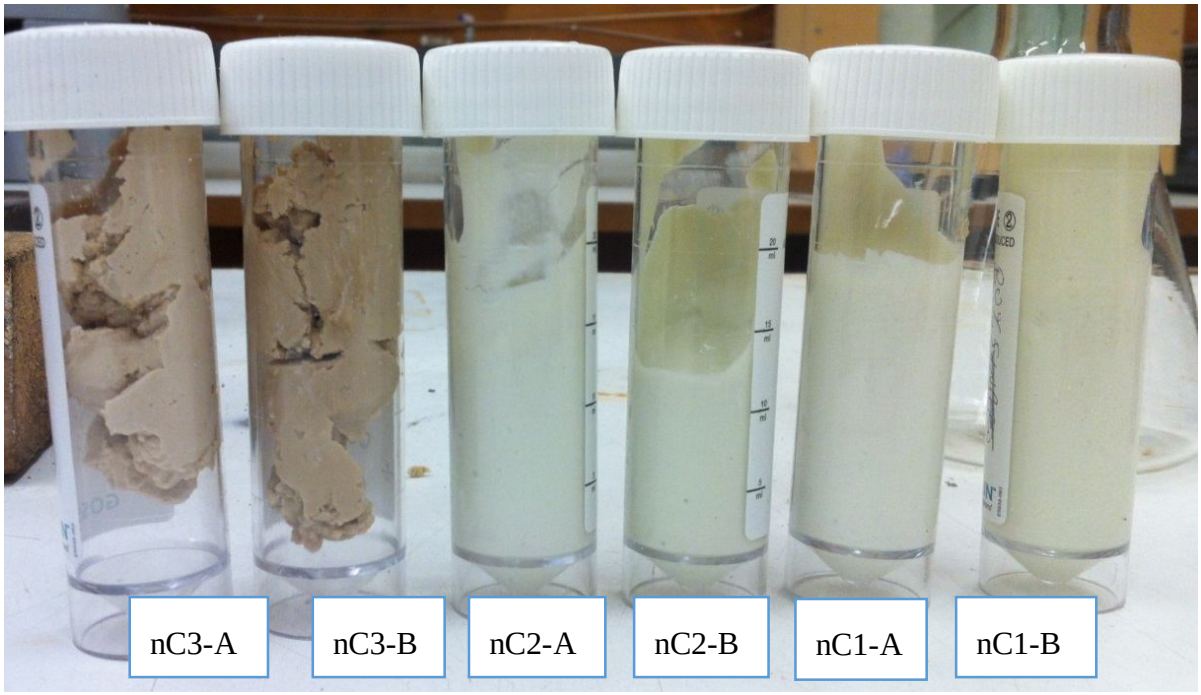

Figure 3-47: Physical appearance of lime putty+nC dispersion pastes at six days

When the six day period had passed, the seven specimens were allowed to dry in an oven at 60ºC for 24 hours.

A separate sample of the reference lime putty was also dried at a higher temperature, 100ºC, to detect any differences in $Ca(OH)_2$ or surface water content.

After the first 24h, the samples were crushed to powder passing through a 125μm sieve. It should be noted that the lime putty+nC2 as well as the LP+nC1 were extremely soft upon grinding. As a matter of fact, the powder produced by these pastes was so fine that they gave a sense of mist when poured in the vial. On the contrary, the LP+nC3 were very hard to break and to grind. Ground powdered samples were allowed to dry for a further 12h in a desiccator placed in the oven at 60ºC.

The procedure was repeated 8 months later for the study of the ageing process of the same LP+nC dispersion pastes.

TGA was carried out on the 8th day starting from the moment of mixing for the first series of pastes and on the 8th month for the aged series of pastes.

It is worth noting that once the TGA was completed the powder remains were totally incoherent and loose, therefore no sintering had taken place.

With respect to the reference (pure LP) paste, the TG analyses (Figure 3-48 and Table 3-23) revealed the following:

Pre-drying the lime putty at 100°C almost drained it from surface water, therefore the TGA showed marginal mass loss up to 100°C. However, slightly greater amount of surface water was lost up to 100°C on TGA for the lime putty pre-dried at 60°C. Pre-drying at either temperatures did not affect the detection of pure $Ca(OH)_2$ content with was found to reach almost 90% by mass. In agreement with the study of Margalha *et al.* (2013) in which, one month old lime putty lost free and adsorbed water (3.5%) up to 300°C, the chemically bound water (21.5%), related to $Ca(OH)_2$ content up to 500°C and above 600°C mass loss (2.3%) related to $CaCO_3$, in this study the mass losses were recorded at similar temperature ranges and exhibited almost equal mass losses related to $Ca(OH)_2$ and $CaCO_3$ content.

The mass loss within the temperature range of 600-800°C is attributed to the decomposition of $CaCO_3$. Although researches carried out on undispersed montmorillonites and bentonites claim that they decompose at this temperature range (Xie *et al.*, 2001), in the particular analysis this cannot be the case since the TGA of nC1 and nC2 exhibited no mass losses between 600-800°C. It is clear that the samples have carbonated. This is certainly true for the sample 20% LP + 80% nC1 dispersion (Figure 3-49) and from the XRD results probably for the 50% LP + 50% nC1 dispersion and 50% LP + 50% nC3 dispersion, as well. Mass loss after 800°C can be attributed to the formation of high temperature silicate minerals e.g. cristobalite, mullite, spinel or carbonaceous residues (Hedley *et al.*, 2007), however after 800°C no mass losses were recorded.

Overall, the pozzolanic activity in terms of $Ca(OH)_2$ consumption as shown in Table 3-23 and Figure 3-48 to Figure 3-50 was more pronounced for the better dispersed nC particles. A qualitative interpretation of the results shown in the following two figures is that both nC1 and particularly nC2 dispersions are capable of forming new stronger bonds in presence of $Ca(OH)_2$ signalled by the new peaks at about 460°C.

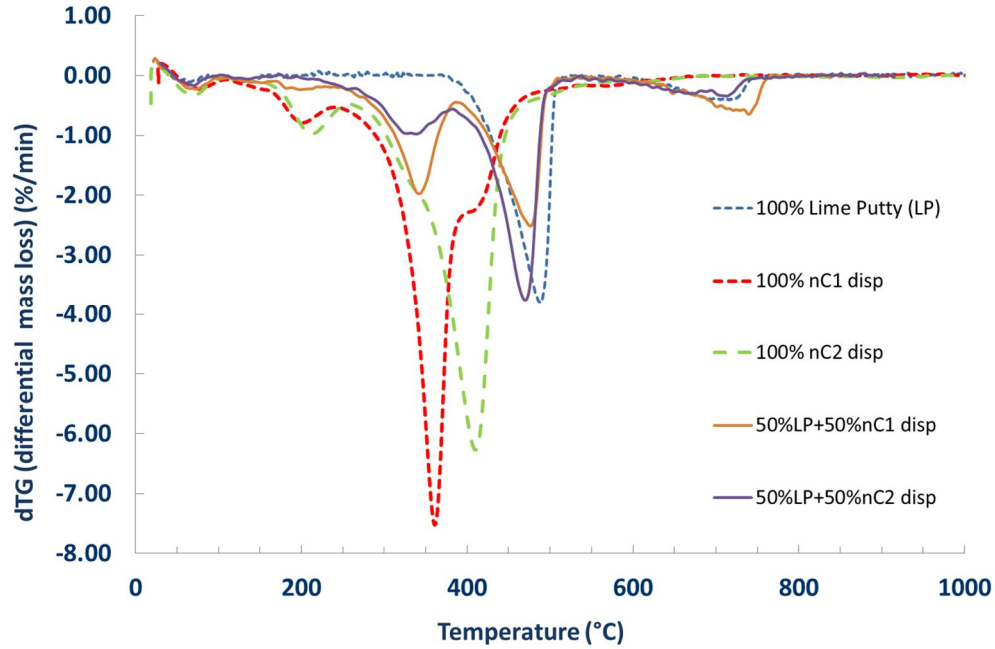

Figure 3-48: Investigation of pozzolanic activity: 50% LP + 50% nC1 dispersion & nC2 dispersion -1 week old

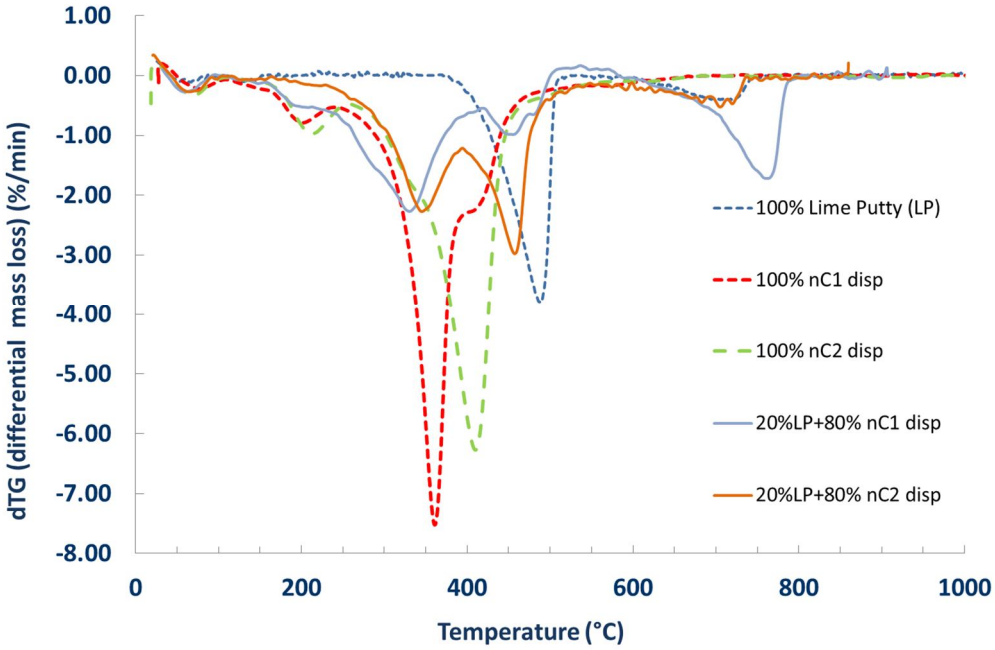

Figure 3-49: Investigation of pozzolanic activity: 20% LP + 80% nC1 dispersion & nC2 dispersion -1 week old

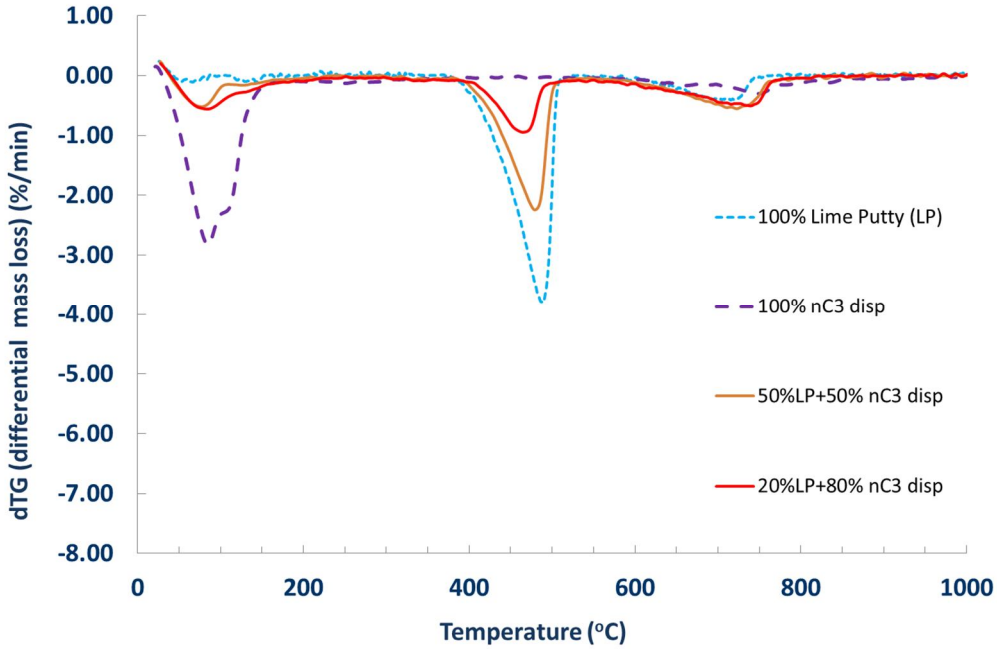

Figure 3-50: Investigation of pozzolanic activity: LP + nC3 dispersion -1 week old

The mass loss related to $Ca(OH)_2$ was calculated in Table 3-23 and Table 3-24 according to the following formula:

Mass loss related to $Ca(OH)_2$ =

[Mass loss of LP+nC paste recorded between 400-500°C] – [mass loss recorded between 400-500°C of dried nC (taken from Table 3-20 or Table 3-10)] x [% of nC present in the paste (50% or 80%)]. Equation: 3-9

As shown in Table 3-23, the higher nC1 concentrations favoured the formation of compounds, decomposing at over 700°C. It can be assumed that the nC has reacted and part of its mass has been chemically bound with these compounds. Hence, this mass, excluding the equivalent produced by the lime putty should be added to nC content which would then be:

For nC1: 15.96+6+11.29-3.8 x 20% = 34.28% ~ 80% x 47.5% = 38% (47.5% is the mass loss observed within the specific temperature range due to 100% nC1 decomposition). The discrepancy can be again attributed to the low stability of nC1.

For nC2: 15.54+16.11+6.46-3.8 x 20% = 37.35% = 80% x 46.09% (100% nC2 decomposition mass loss).

Table 3-23: Mass loss (%) of 1 week old lime putty, nC dispersions and LP +nC dispersion pastes

Sample	0-100ºC	100-200ºC	200-300ºC	300-400ºC	400-500ºC	600-1000ºC	Note
Dried 100% LP		0.33		20.20		3.52	1
Dried 50% LP + 50% nC1	0.64	1.06	2.8	10.53	13.97	5.93	2 & 2A
Dried 50% LP + 50% nC2	0.36	0.20	2.04	7.35	18.63	4.19	3 & 3A
Dried 50% LP + 50% nC3	2.34	0.60		0.56	8.88	11.73	4
Dried 20% LP + 80% nC1	0.86	1.80	7.90	15.96	6.00	11.30	5
Dried 20% LP + 80% nC2	0.74	0.46	3.30	15.54	16.11	6.46	6
Dried 20% LP + 80% nC3	4.13	2.34		0.83	3.60	9.00	7

Note 1: At 100% LP, the mass loss related to $Ca(OH)_2$ was 20.2%, therefore for 50% LP it would be 10.1% and for 20% LP, the mass loss would be 4%.

Note 2: for the mass loss observed within 400-500ºC: 13.97% – 9.48%x50% = 9.23% < 10.1%, therefore some reduction of $Ca(OH)_2$ was achieved by 50% nC1.

Note 3: for the mass loss observed within 400-500ºC: 18.63% – 20.14%x50% = 8.56% < 10.1%, therefore significant reduction of $Ca(OH)_2$ was achieved by 50% nC2.

It is interesting to add the two underlined mass losses observed between 400-500ºC:

Note 2A: 10.53 + 13.97 = 24.5% ~ 50% x 44.8 % = 22.4% (50% nC1 decomposition mass loss - Table 3-20).

Note 3A: 7.35 + 18.63 = 25.98% ~ 50% x 46 % = 23% (50% nC2 decomposition mass loss Table 3-20).

Note 4: for the mass loss observed within 400-500ºC: 8.88% – 1.0%x50% = 8.38% < 10.1%, therefore significant reduction of $Ca(OH)_2$ was achieved by 50% nC3.

Note 5: for the mass loss observed within 400-500ºC: 15.96% – 9.48%x80% = 6.7% >4%, therefore no reduction in $Ca(OH)_2$ was achieved by 80% nC1.

Note 6: for the mass loss observed within 400-500ºC: 16.11% – 20.14%x80% = 8.56% > 4%, therefore no reduction in $Ca(OH)_2$ was achieved by 80% nC2.

Note 7: for the mass loss observed within 400-500oC: 3.6% – 1.0%x80% = 2.8% > 4%, therefore significant reduction of $Ca(OH)_2$ was achieved by 80% nC3.

In fact, the nC enhanced putties were dried and tested after 8 months by TGA (Figure 3-51 to Figure 3-53). All samples have carbonated. Furthermore, the pozzolanic performance of nC3 is more pronounced at 8 months, with elimination of the $Ca(OH)_2$, at 80% nC3 dispersion content. Analytical elaboration of the results at 8 months is presented in Table 3-24.

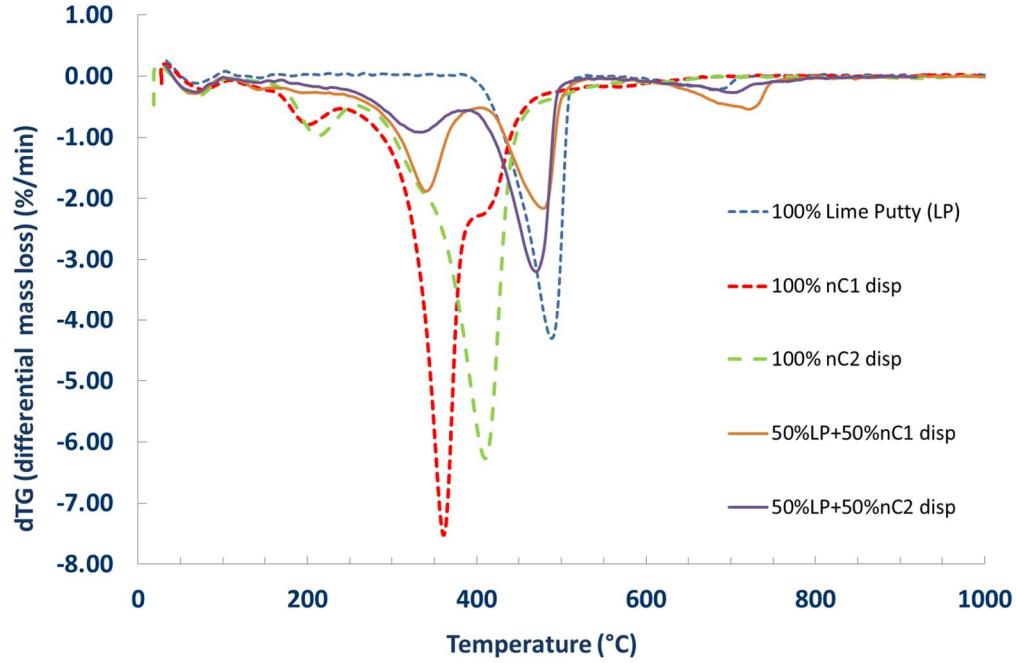

Figure 3-51: Investigation of pozzolanic activity: 50% LP + 50% nC1 dispersion & nC2 dispersion - 8 months old

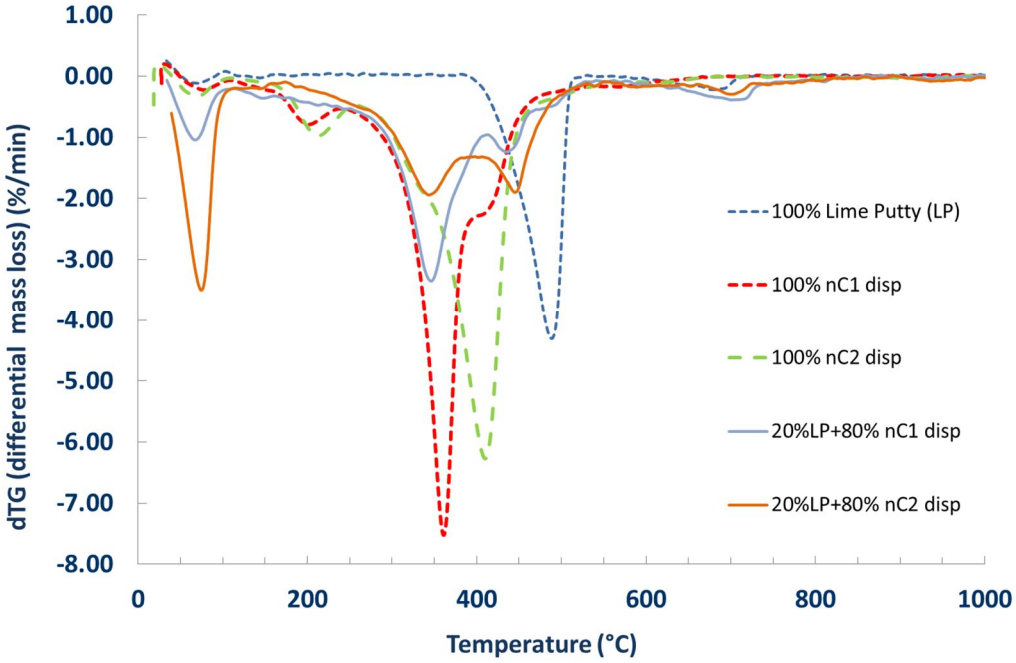

Figure 3-52: Investigation of pozzolanic activity: 20% LP + 80% nC1 dispersion & nC2 dispersion - 8 months old

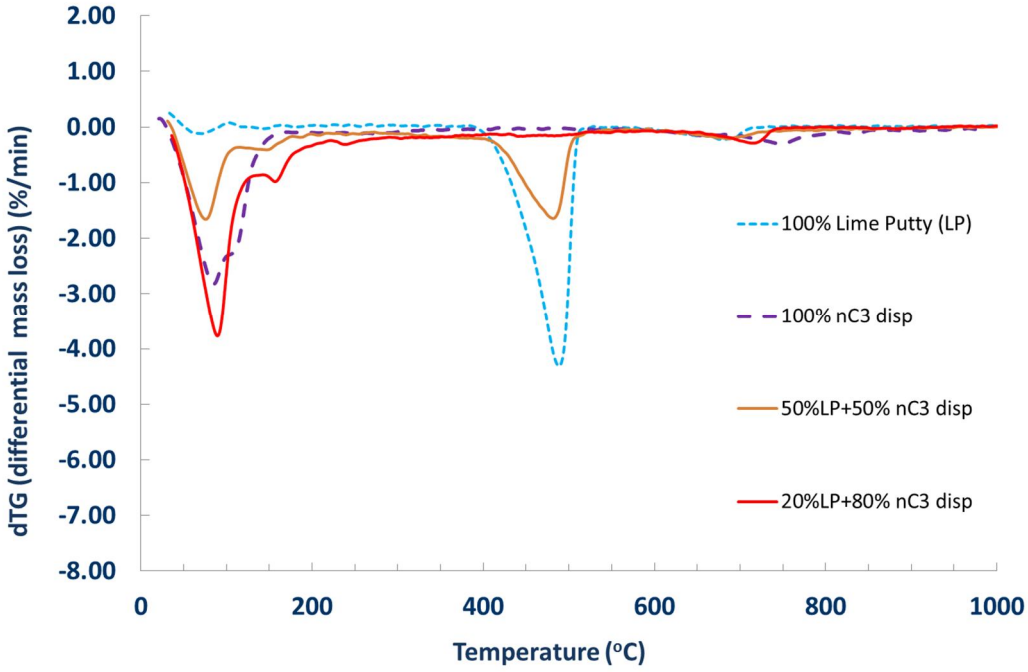

Figure 3-53: Investigation of pozzolanic activity: LP + nC3 dispersion - 8 months old

Table 3-24: Mass loss (%) of 8 month old lime putty, nC dispersions and LP+nC dispersion pastes

Sample	0-100ºC	100-200ºC	200-300ºC	300-400ºC	400-500ºC	600-1000ºC	Note
Dried 100% LP		0.33		21.24		1.62	1
Dried 50% LP + 50% nC1	0.83	1.55	3.71	10.93	12.47	5.57	2 & 2A
Dried 50% LP + 50% nC2	0.81	0.76	2.86	6.90	17.26	3.40	3 & 3A
Dried 50% LP + 50% nC3	5.43	2.38		0.66	9.23	2.94	4
Dried 20% LP + 80% nC1	3.46	2.70	5.81	20.68	8.10	5.50	5
Dried 20% LP + 80% nC2	10.18	1.45	4.34	14.46	11.37	4.93	6
Dried 20% LP + 80% nC3	13.45	6.65		3.96	1.42	3.00	7

Note 1: At 100% LP, the mass loss related to $Ca(OH)_2$ was 21.24%, therefore for 50% LP it would be 10.6% and for 20% LP, the mass loss would be 4.2%.

Note 2: for the mass loss observed within 400-500ºC: 12.47% – 9.48%x50% = 7.73% < 10.6%, hence some reduction of $Ca(OH)_2$ was achieved by 50% nC1.

Note 3: for the mass loss observed within 400-500ºC: 17.26% – 20.14%x50% = 7.19% < 10.6%, therefore significant reduction of $Ca(OH)_2$ was achieved by 50% nC2.

In addition it is interesting to add the two underlined mass losses:

Note 2A: 10.93 + 12.47 = 23.4% ~ 50% x 44.8 % = 22.4% (50% nC1 decomposition mass loss - Table 3 8).

Note 3A: 6.9 + 17.26 = 24.16% ~ 50% x 46.09 % = 23.5% (50% nC2 decomposition mass loss Table 3 8).

Note 4: for the mass loss observed within 400-500ºC: 9.23% – 1.0%x50% = 8.73% < 10.6%, therefore significant reduction of $Ca(OH)_2$ was achieved by 50% nC3.

Note 5: for the mass loss observed within 400-500ºC: 8.1% – 9.48%x80% = 0.52% <4.2%, therefore almost elimination of $Ca(OH)_2$ was achieved by 80% nC1.

Note 6: for the mass loss observed within 400-500ºC: 11.37% – 20.14%x80% = 0% < 4.2%, therefore elimination of $Ca(OH)_2$ was achieved by 80% nC2.

Note 7: for the mass loss observed within 400-500ºC: 1.42% – 1.0%x80% = 0.62% < 4.2%, therefore almost elimination of $Ca(OH)_2$ was achieved by 80% nC3.

In addition, the higher nC1 concentrations favour the formation of compounds, decomposing at over 700ºC. It can be assumed that the nC has reacted and part of its mass has been chemically bound with these compounds. Hence, this mass, excluding the equivalent produced by the lime putty should be added to nC content which would then be:

For nC1: 20.68+8.1+ 5.5 - 3.8 x 20% = 33.52% ~ 80% x 47.5% = 38% (47.5% is the mass loss observed within the specific temperature range due to 100% nC1 decomposition). The discrepancy can be attributed to the low stability of nC1.

For nC2: 14.46+11.37+4.93 - 3.8 x 20% = 30% ~ 80% x 46.09% = 37.3% (100% nC2 decomposition mass loss).

The first part of the pozzolanic reaction is the consumption of $Ca(OH)_2$. The second part is the production of C–S–H, the decomposition of which takes place between 100 and 200ºC. With similar calculations, it could be argued that nC1 and nC3, particularly after the 8 months produced more C–S–H, although it is acknowledged that molar calculations are difficult in this region due to the simultaneous decomposition of the modifier.

However, since carbonation has occurred, the total mass related to $Ca(OH)_2$ must be recalculated. The related molar masses, as a percentage of the initial mass of the sample tested with TG were estimated as follows:

Mass of $Ca(OH)_2$ = (TGA recorded mass loss between 400-500ºC) / 0.24 (equation 3-9)

Mass of $CaCO_3$ = (TGA recorded mass loss between 600-800ºC) / 0.44

By assuming that all of this calcium carbonate was once calcium hydroxide:

$Ca(OH)_2 + CO_2 \rightarrow CaCO_3 + H_2O$

Which in mass terms is: 74 + 44 → 100 + 18, therefore:

Mass of $Ca(OH)_2$ that has carbonated = [mass of $CaCO_3$] / [(100/74)]

Therefore:

Total mass of $Ca(OH)_2$ prior to carbonation =

[Mass of $Ca(OH)_2$ as calculated by eq 3.9] + *[mass of $Ca(OH)_2$ that has carbonated (i.e. mass loss after 600ºC)]*. Equation: 3-10

All calculations are presented in Table 3-25.

Table 3-25: Total mass of $Ca(OH)_2$ taking into consideration carbonation

	Calculated (eq. 3.9) mass loss @ 400-500°C		TGA mass loss @ 600-1000 °C		Note	Total mass of $Ca(OH)_2$ (eq. 3.10)		Note
Week/Month	**1**	**8**	**1**	**8**		**1**	**8**	
100% Lime putty (LP)	20.20	21.20	3.52	1.62		90.09	91.05	3
50%LP+50%nC1	9.23	7.73	5.93	5.57		48.44	41.58	
50%LP+50%nC2	8.56	7.19	4.19	3.40		42.71	35.68	
50%LP+50%nC3	8.38	8.73	9.52	0.73	1	50.93	37.61	
20%LP+80%nC1	6.7	0.52	11.3	5.50		46.92	11.42	
20%LP+80%nC2	8.56	0.00	6.46	4.93		46.53	8.29	
20%LP+80%nC3	2.8	0.62	5.42	0.00	2	20.79	2.58	
Particular attention should be given to nC3, which naturally decomposes after 600°C. Therefore, in order to calculate the mass loss related to $CaCO_3$ (due to the carbonation of the samples), the amount of nC3 must be subtracted from the total amount of mass loss within this temperature range;								

Note 1: week1 - At 600-1000°C, the mass loss related to $CaCO_3$ is:11.73-(3.3+1.13)*50% = 9.52
Month 8 - At 600-1000°C, the mass loss related to $CaCO_3$ is: 9.00-(3.3+1.13)*80% = 5.42
Note 2: week1 - At 600-1000°C, the mass loss related to $CaCO_3$ is: 2.94-(3.3+1.13)*50% = 0.73
Month 8 - At 600-1000°C, the mass loss related to $CaCO_3$ is: 3.00-(3.3+1.13)*80% = 0.00
Note 3: week1 – Example of calculations: 20.2/0.24 + [(3.52/0.44)/(100/74)] = 90.09

A graphical representation of the total mass of $Ca(OH)_2$ of the various combinations of LP+nC dispersions is given in Figure 3-54. It can be seen that according to this TG analyses the higher nC concentrations at 8 months can lead to the elimination of $Ca(OH)_2$ and that in all cases nC3 showed the highest pozzolanic activity, followed by nC2.

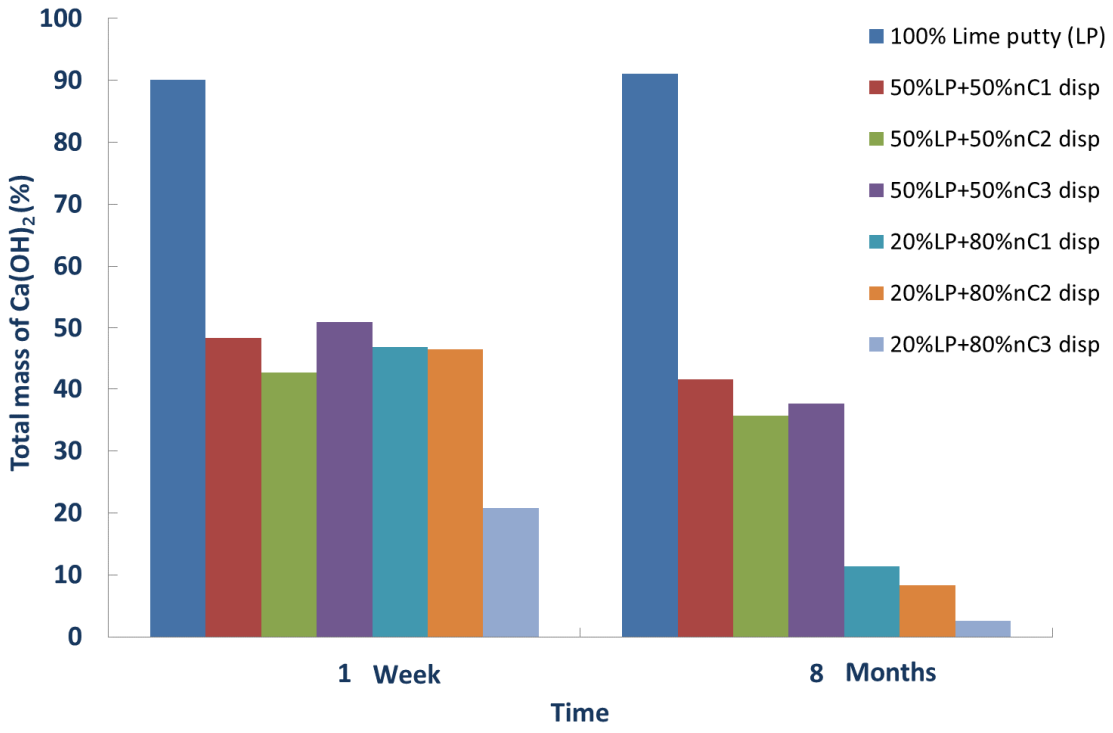

Figure 3-54: Total mass of $Ca(OH)_2$ taking into consideration carbonation of the various combinations of lime putty and nC dispersions

The consumption of $Ca(OH)_2$ was further confirmed by XRD analyses carried out in both 1 week and 8 months powders. As shown in Figure 3-55 and Figure 3-56, the $Ca(OH)_2$ peaks were reduced with increasing nC content and this reduction was more pronounced for nC3.

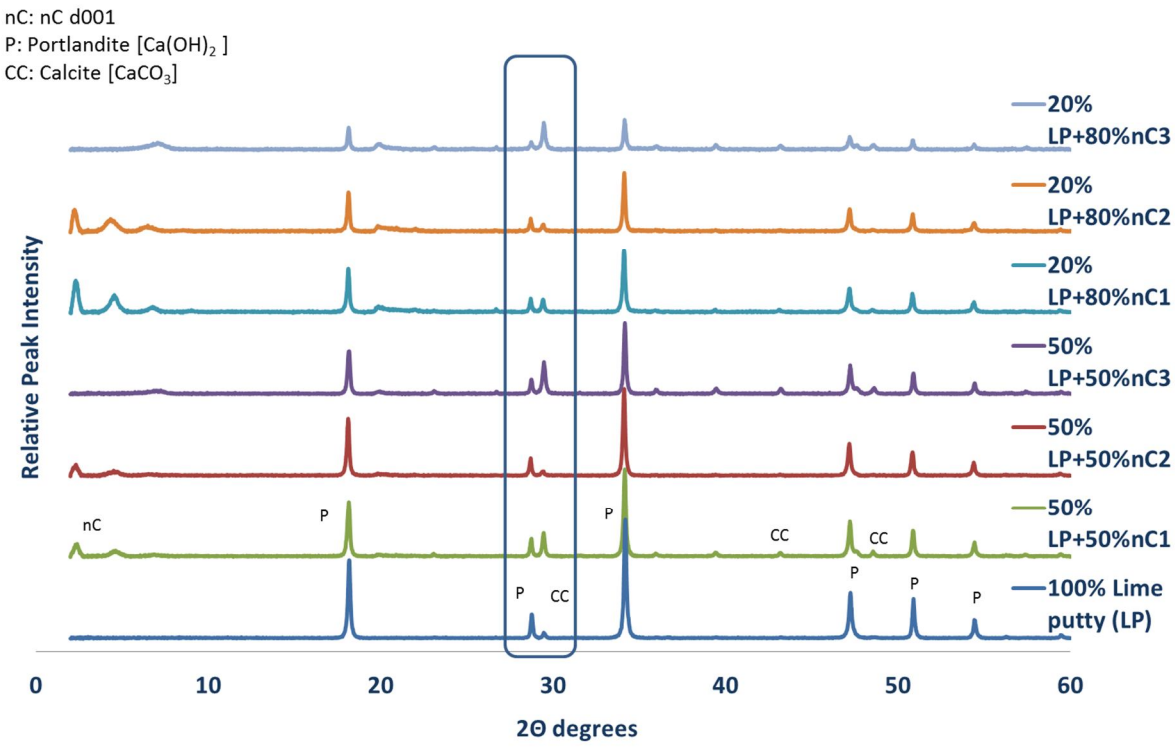

Figure 3-55: Investigation of pozzolanic activity: XRD analyses of LP+nC dispersions -1 week old

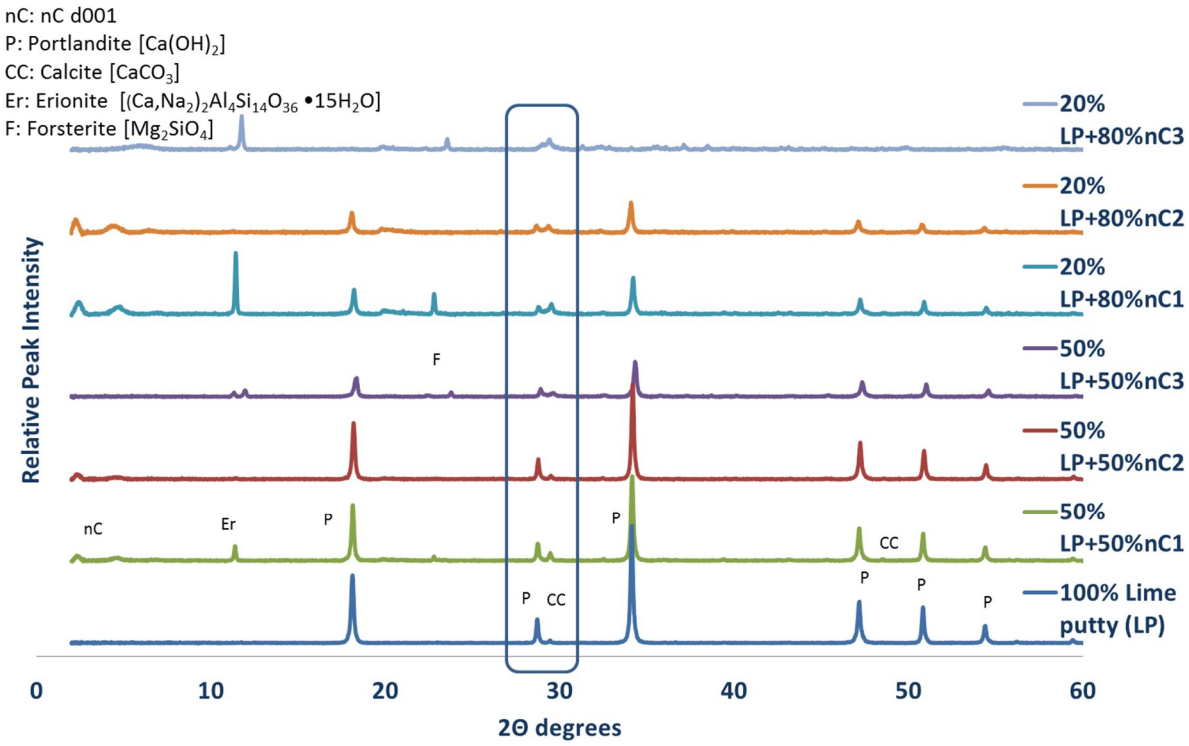

Figure 3-56: Investigation of pozzolanic activity: XRD analyses of LP+nC dispersions -8 months old

Knowing that the C–S–H humps are expected between 20 and 30°2θ (Snellings *et al.*, 2014; Fernandez *et al.*, 2011) the unsmoothened XRD patterns of the 80% nC are presented in Figure 3-57 and Figure 3-58 clearly showing the rise near the nC diffraction peak at approximately 19°2θ.

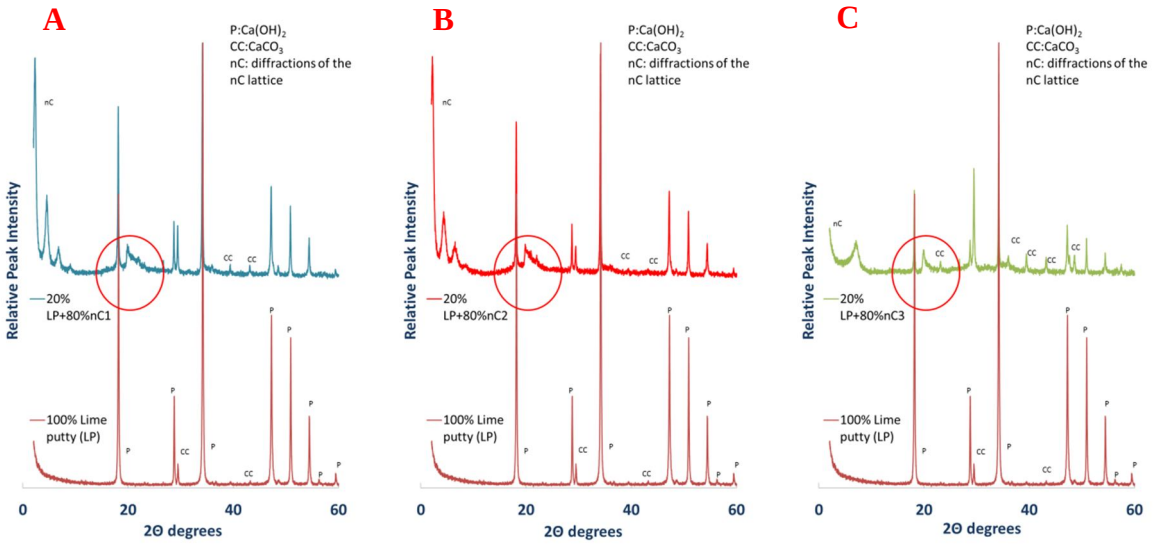

Figure 3-57: 1 week XRD of (A) 20%LP+80% nC1 dispersion, (B) 20%LP+80% nC2 dispersion and (C) 20%LP+80% nC3 dispersion

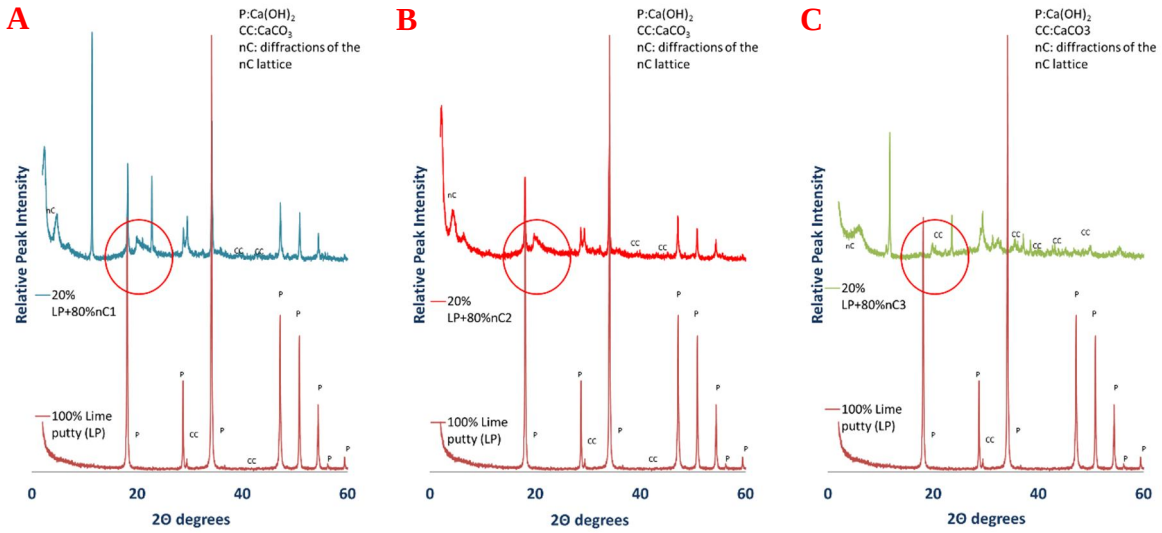

Figure 3-58: 8 months XRD of (A) 20%LP+80% nC1 dispersion, (B) 20%LP+80% nC2 dispersion and (C) 20%LP+80% nC3 dispersion

Furthermore, a semi-quantitative analysis was developed on the grounds of comparison of the integrated areas (blue rectangle in Figure 3-55 and Figure 3-56) under the two adjacent peaks of $Ca(OH)_2$ at 28.7°2θ and $CaCO_3$ at 29.4°2θ.

Mathematical curve fitting was performed for greater accuracy. Figure 3-59 and Figure 3-60 depict the results of these analyses, with the consumption of $Ca(OH)_2$ clearly identified. The two figures provide a measure of how much carbonation has occurred.

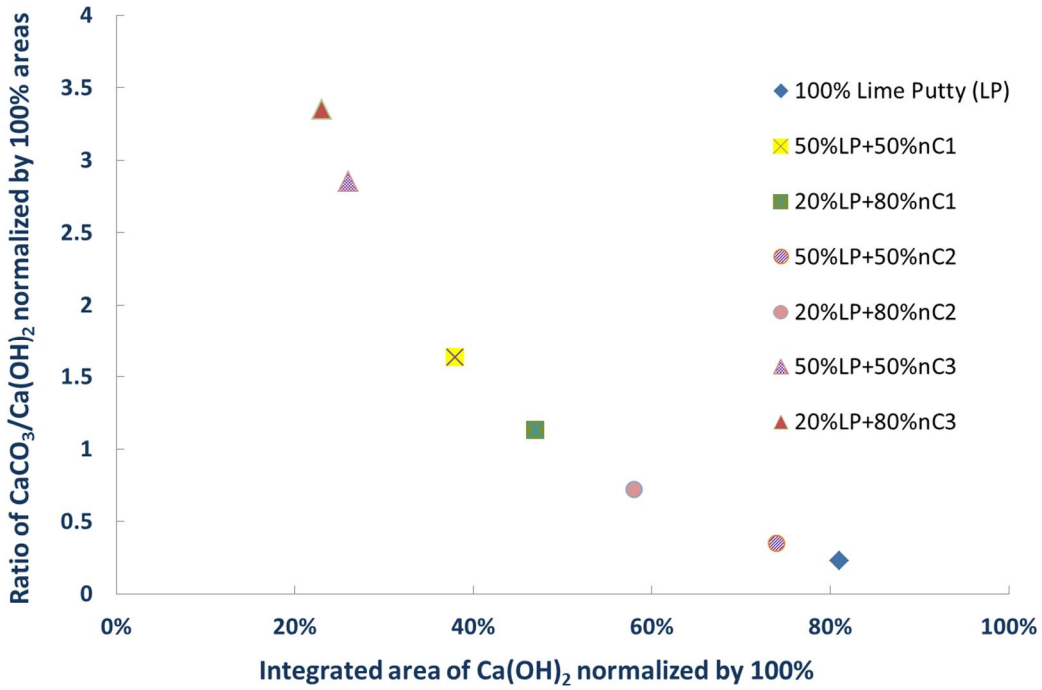

Figure 3-59: Semi-quantitative XRD analyses of LP + nC dispersion - 1 week old

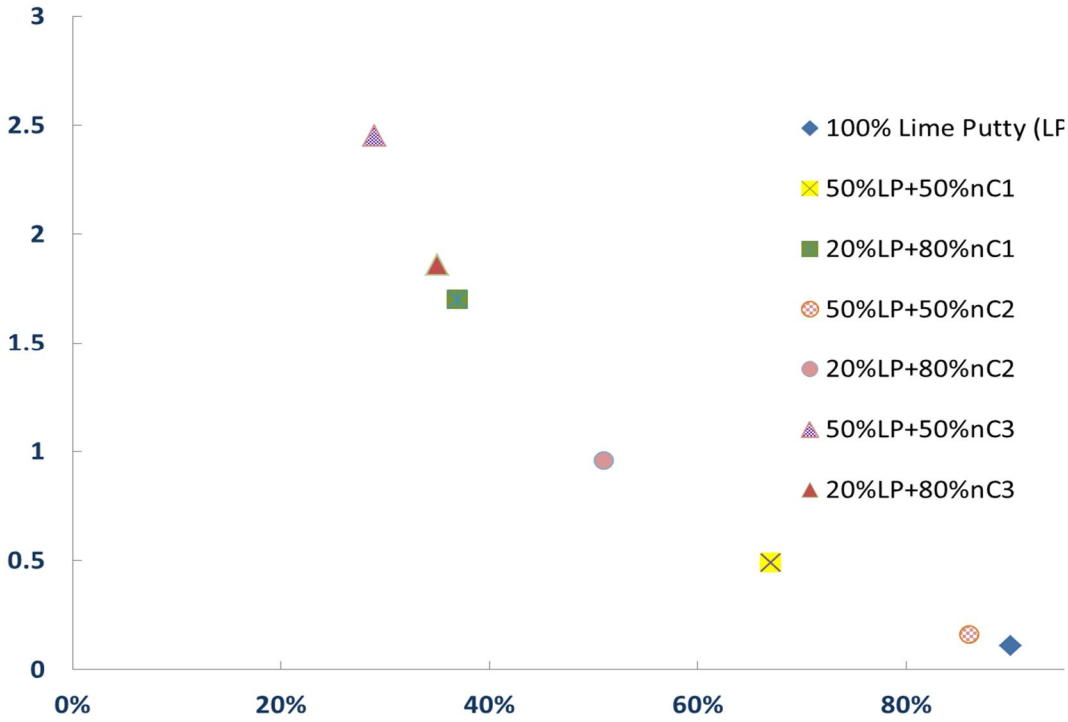

Figure 3-60: Semi-quantitative XRD analyses of LP + nC dispersion - 8 months old

3.6 Further discussion and conclusions

Overall, it can be claimed that nC1 showed pozzolanic activity, increasing with age and higher proportions. nC2 can show pozzolanic activity if allowed time to react and if added in reasonable quantities. nC3 exhibited the highest and most rapid consumption of $Ca(OH)_2$ and due to its simpler chemistry can be expected to consume more $Ca(OH)_2$ when added to cement pastes.

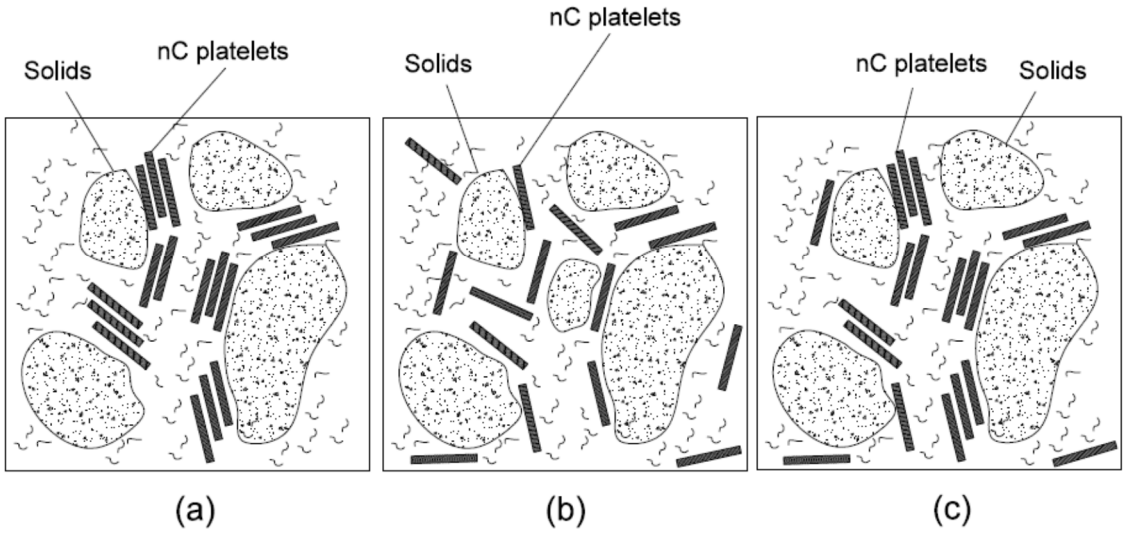

Figure 3-61: Effect of platelet condition within the cement paste- (a) non- exfoliated platelets, (b) exfoliated and dispersed platelets and (c) some platelets exfoliated/some intercalated

Furthermore, the level of intercalation or exfoliation of the nC platelets is predicted to affect the mechanical properties of the cement pastes into which the different nC dispersions will be added. Three different configurations can be suggested for the analysed nC dispersions.

In the first case (Figure 3-61 (a)) the platelets were not exfoliated and possibly remained agglomerated in the volume of the paste. The agglomeration of platelets brought nC1 back to the micron size, hence reduced the variability in the sizes of the particles, within the paste (Figure 3-62 (a)). As an effect, larger voids were expected and cracks could propagate amongst the bigger elements. Although d-spacing between the platelets was similar for nC1 and for nC2, the different surfactants changed the structure of the nC platelets, which could be more prone to splitting apart. This weakness, could in turn attract nanocrack propagation between the platelets, rendering nC1 enhanced pastes **more brittle** and less resistant in either tension or compression.

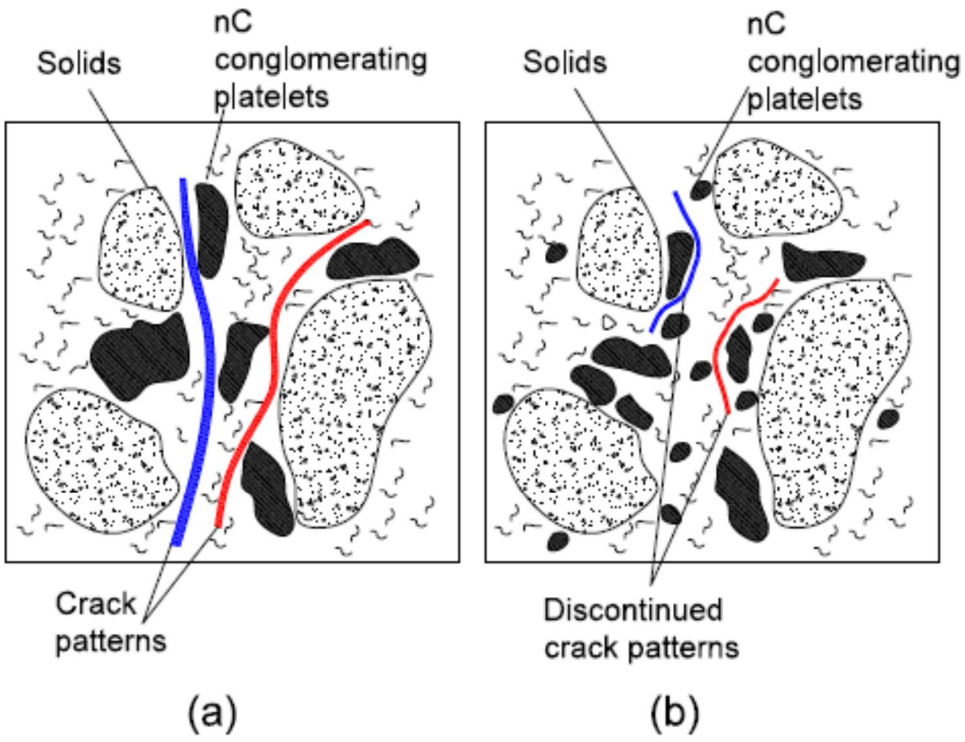

Figure 3-62: Effect of nC exfoliation level on particle size distribution in cement paste – (a) more brittle configuration and (b) less brittle to ductile configuration

In the second case (Figure 3-61 (b)) the exfoliated platelets were dispersed in the volume of the paste acting as nanoreinforcements. The particle size distribution is therefore enhanced, while the nC platelets may also be acting as nanofillers (Figure 3-62 (b)). This configuration also allows for the benefits of increased surface area of the platelets to be delivered. At the same time, individual platelets can bend freely within the paste and can therefore introduce an obstacle to the crack propagation. Such platelet arrangements favour **less brittle** behaviours, hence the addition of nC3 was expected to deliver more ductile cements, nonetheless of lower compressive strength. However, the arrangement depicted in Figure 3-61 (b) is expected to favour flexural strength when added in cement pastes.

In the third case (Figure 3-61 (c)) some platelets were exfoliated and some remained intercalated in the volume of the paste. This case is more representative of nC2, the major difference with nC1 is that some platelets are better dispersed. The different surfactant used in nC2 differentiated the mechanical performance of the nC2 enhanced pastes significantly. In fact, the higher energy bonds do not allow the slippage of the nC platelets, which, then, act as nanoreinforcement stopping the propagation of nanocracks through the nC. This condition can lead to **more ductile** behaviour and increases in flexural strength.

To sum up, the great diversity in modifying and dispersing nanoclays, let alone the preparation methods and origin of the original clay can totally alter the structure and chemistry of the final nC product. In fact, nC are that sensitive that even in cases in which the nCX is exactly the same but the surfactant changes, as in nC1 and nC2 dispersions, variable properties can be achieved and unexpected reactions can take place as the energy within the forming bonds is affected. For this reason, thorough characterization is required to gain more understanding on how the nC perform and how they are structured before allowed to interact with other materials. It was shown that in the process of achieving exfoliated forms inorganic solutions can offer another direction in the near future.

4 PHILOSOPHY OF FORMULATIONS

4.1 Introductory section

In this chapter the reasons behind the design and selection of the various pastes are elucidated. Once a better understanding of the possible performance of the constituents is gained, several non-nanomodified pastes are designed and tested to acquire an insight into the collaboration of, or competition between the constituent materials. Of the initial non-nanomodified pastes, the two best performing in terms of compressive strength and low carbon footprint are selected. Next, with these two formulations as pivotal points, different series of ternary, quaternary and quinary nanomodified formulations are designed. Figure 4-1 and Figure 4-2 were drawn as guidance to the evolution of the nanomodified cement paste formulations and as a key to the remaining chapters of this thesis, since each group of formulations is accompanied by the relevant chapter and section number. Consequently, the exact percentages of the constituents of the pastes are presented and the aims and progressive complexity increase of the formulations are discussed. A separate section is also reserved for the design of the mortars. Lastly, the mixing, casting, demoulding and curing methodology is specified.

4.2 The sequence of formulations

To begin with, the non-nanomodified pastes were produced and tested, mostly until day 28. Ternary pastes contained different combinations of CEMII, LS and FA at a water to binder (w/b) ratio of 0.3 in an effort to minimize the carbon dioxide footprint by minimizing the PC content and increasing the use of supplementary cementitious materials. Consistence and setting time requirements were not considered. It should be noted that any powder material is added in the binder content. Therefore, PC, LS, FA, μS and nS or nC solids will be taken into consideration as binder constituents. Additionally, any possible competition between the different constituents could be more easily detected at this stage, before complicating the design with the addition of nanoparticles. Thirdly, the best performing pastes in terms of compressive strength and carbon dioxide footprint were selected to be enhanced with the use of μS. Some of the pastes were tested until day 28 and others until day 56. The two best combinations of CEMII, LS and FA which had the highest compressive strength and low CO_2 footprint when μS was added, were chosen to be enhanced with nS or nC. In the current research, consistency was not considered, however it is acknowledged that it would be an interesting parameter for future research.

Given that there is a shortage of FA in the UK (Heath *et al.*, 2013) it would be interesting to investigate if in blended cements, the addition of nanoparticles can bring about benefits such as those accredited to the use of FA even in cement formulations that do not contain

any FA. At the same time, one of the most important aspects that had to be examined was whether or not the specific types of nS and nC are active pozzolanas. Hence, the first reference paste should not contain any other pozzolanic materials and still maintain a low CO_2 footprint. The reference paste satisfying these criteria contained 60% by mass PC and 40% by mass LS. Ternary combinations were created when the different nanoparticles were added, again at w/b ratio of 0.3. The amount of nC or LnS solids was deducted from the LS content, so that the $Ca(OH)_2$ produced by the hydration of PC would remain similar in all pastes and any possible fluctuations could then be directly related to the reactivity of the nanoparticles. These pastes were tested at day 1, 7, 28, 56, 90 and 170 in order to determine the Long-term effect of the addition of nanoparticles, which has been another area of diverging discussions.

Consequently, the first quaternary combination was created with the reference paste at the same PC content (60%) but this time having additionally 20% by mass LS and 20% by mass FA. The effect of the second type of nS particles, GnS, was investigated in these pastes at w/b ratio of 0.3, 0.22 and 0.2 until day 28. GnS was found to be a carboxylate dispersion of nS, hence, the aim of this series of pastes was to experiment with the collaboration of the different materials in light of low PC paste design, which was the next step.

At this stage of the research, a low PC content, ternary reference paste was implemented, containing 43% PC, 20% LS and 37% by mass FA. It constituted a challenge, as not only the FA content was high, but the presence of LS caused the decrease of PC content. Different concentrations of GnS and LnS particles were added at a w/b ratio of 0.3, exploring the limits of nanoparticles' addition and possible issues with the collaboration of the constituents. Pastes were tested until day 90.

Then quinary pastes were created and tested containing 43% by mass PC, 37% by mass FA and various quantities of LS, μS and nS. It was of particular interest to investigate the effect of nS particles in such complicated cement matrixes in terms of hydration and compressive strength. LnS and μS modified pastes were tested until day 90, whereas GnS and μS modified pastes were tested until day 56.

This research was completed with the development of a successful application for the nC dispersions. Noticing the scarce improvements in compressive strength, poly vinyl acetate (PVA) fibres and superplasticizer were added initially to the 60% PC and 40% LS paste together with the nC. The performance of the fibre pastes was measured in terms of flexural strength, water impermeability and microstructural enhancement. The amount on nC solids was selected according to the findings of the ternary nC enhanced paste formulations.

The last series of pastes created, tested and analysed was based on 60% PC, 20% LS and 20%FA. PVA fibres, superplasticizer and nC was also added and again performance of the fibre pastes was measured in terms of flexural strength, water impermeability and microstructural enhancement until day 90.

One final series of trial pastes was created, with the combination of two nanoparticles; nC and nS, based on 60% PC, 20% LS, 20%FA, 4% PVA and 2%SP. It was designed to provide some indication for future research suggestions, in Chapter 9.

The findings of the nanomodified pastes were confirmed by compressive strength tests on 56 different mortar combinations performed from day 1 to day 90. The reason behind testing mortars in compression, was to rule out any possible size/shape effects caused by testing in compression cylindrical specimens of cement pastes and to limit autogeneous shrinkage in the cement specimens.

4.3 Design of non- nanomodified cement paste formulations

4.3.1 Non- nanomodified cement formulations: Binary & ternary

The primary constituent is Portland limestone cement, CEMII-42.5, which is a binary combination on its own, since it contains 86% of PC and 14% of LS, as discussed in paragraph 3.4.2. The first specimen produced, then, was named B1 and contained only CEMII. Nine more samples were produced next. B2, B3 and B10 contained LS at 20%, 30% and 40% respectively. B4 to B9 represented ternary formulations of PC, LS and FA. All 10 initial bases were mixed at a w/b ratio of 0.3. The exact proportions are shown in the following table:

Table 4-1: Binary and ternary initial cement paste formulations - Mix Proportions % by total mass of solids

Sample	PC (%)	LS (%)	FA (%)	W/B
B1-PC86LS14	86	14	0.0	0.3
B2-PC80LS20	80	20	0.0	0.3
B3-PC70LS30	70	30	0.0	0.3
B4-PC66LS14FA20	66	14	20	0.3
B5-PC51LS14FA35	51	14	35	0.3
B6-PC36LS14FA50	36	14	50	0.3
B7-PC60LS20FA20	60	20	20	0.3
B8-PC45LS20FA35	45	20	35	0.3
B9-PC30LS20FA50	30	20	50	0.3
B10-PC60LS40	60	40	0.0	0.3

4.3.2 Non- nanomodified cement formulations: Quaternary

B7 and B8 were found to perform best as will be discussed in Chapter 4 and they were further enhanced by the addition of μS. Initially, two quaternary formulations, having 60% PC by mass, in which the μS content was subtracted by the PC content, were designed as shown in Table 4-2.

Table 4-2: Quaternary μS enhanced cement paste formulations - Mix Proportions % by total mass of solids

Sample	PC (%)	LS (%)	FA (%)	μS (%)	W/B
PC60LS20FA20	60	20	20	0.0	0.3
PC55LS20FA20+5%μS	55	20	20	5.0	0.3
PC50LS20FA20+10%μS	50	20	20	10	0.3

Then, a lower PC content paste was designed, containing 43% PC, 20%LS and 37% FA by mass as a reference paste, which was further enhanced by the addition of μS, subtracted by the LS content, this time, in order to maintain a w/b ratio of 0.3, as shown in Table 4-3.

Table 4-3: Quaternary μS enhanced cement paste formulations - low PC - Mix Proportions % by total mass of solids

Sample	PC (%)	LS (%)	FA (%)	μS (%)	W/B
PC43LS20FA37	43	20	37	0.0	0.3
PC43LS17FA37+3% μS	43	17	37	3.0	0.3
PC43LS14FA37+6% μS	43	14	37	6.0	0.3

4.4 Design of nanomodified cement paste formulations

Nanomodifications were applied to two different PC contents; 60% by mass and 43% by mass, as shown in Figure 4-1 and Figure 4-2. A number of different ternary, quaternary and quinary combinations evolved, as explained one by one over the following paragraphs.

4.4.1 nC modified cement formulations - Ternary

Fifteen ternary cement combinations were designed, composed of Portland limestone cement, limestone, and either of the two organomodified nC dispersions or the inorganic nC dispersion. PC60LS40, a non-pozzolanic blended cement paste, containing only PC and LS, was selected as the reference paste, to investigate whether the addition of any of the nC dispersions has a pozzolanic effect. The content of nC solids ranged from 0%, 0.5%, 1%, 2%, 4% and 5.5% by mass. The 5.5% represented the upper limit of nC addition in the cement paste, as the water used in the nC dispersion was considered as available to react

during the hydration of cement and therefore was deducted from the total amount of water to be added according to the w/b ratio which again was constant and equal to 0.3. Furthermore, PC content was kept constant and the content of nC solids was deducted from the LS content. This was done to keep the $Ca(OH)_2$ production during PC hydration comparable in all pastes, so as to detect possible pozzolanic reactivity of the nanoparticles. Therefore, the general formula of the matrix of the ternary cement paste mixes was:

$$PC(60) + LS(40 - x) + nC(x) \qquad \text{Equation: 4-1}$$

Where x = % by mass of nC solids ranging from 0 to 5.5%.

The mix proportions in terms of % of the total mass of binder are shown in Table 4-4 in which the nC content refers to the nC solids content and the matrix of the total formulations in Table 4-6.

Table 4-4: nC modified ternary cement paste formulations - Mix proportions % by total mass of solids

Sample	PC (%)	LS (%)	nC (%solids)	W/B
PC60LS40+0% nC	60	40	0.0	0.3
PC60LS39.5+0.5% nC	60	39.5	0.5	0.3
PC60LS39+1.0% nC	60	39.0	1.0	0.3
PC60LS38+2.0% nC	60	38.0	2.0	0.3
PC60LS36+4.0% nC	60	36.0	4.0	0.3
PC60LS34.5+5.5% nC	60	34.5	5.5	0.3

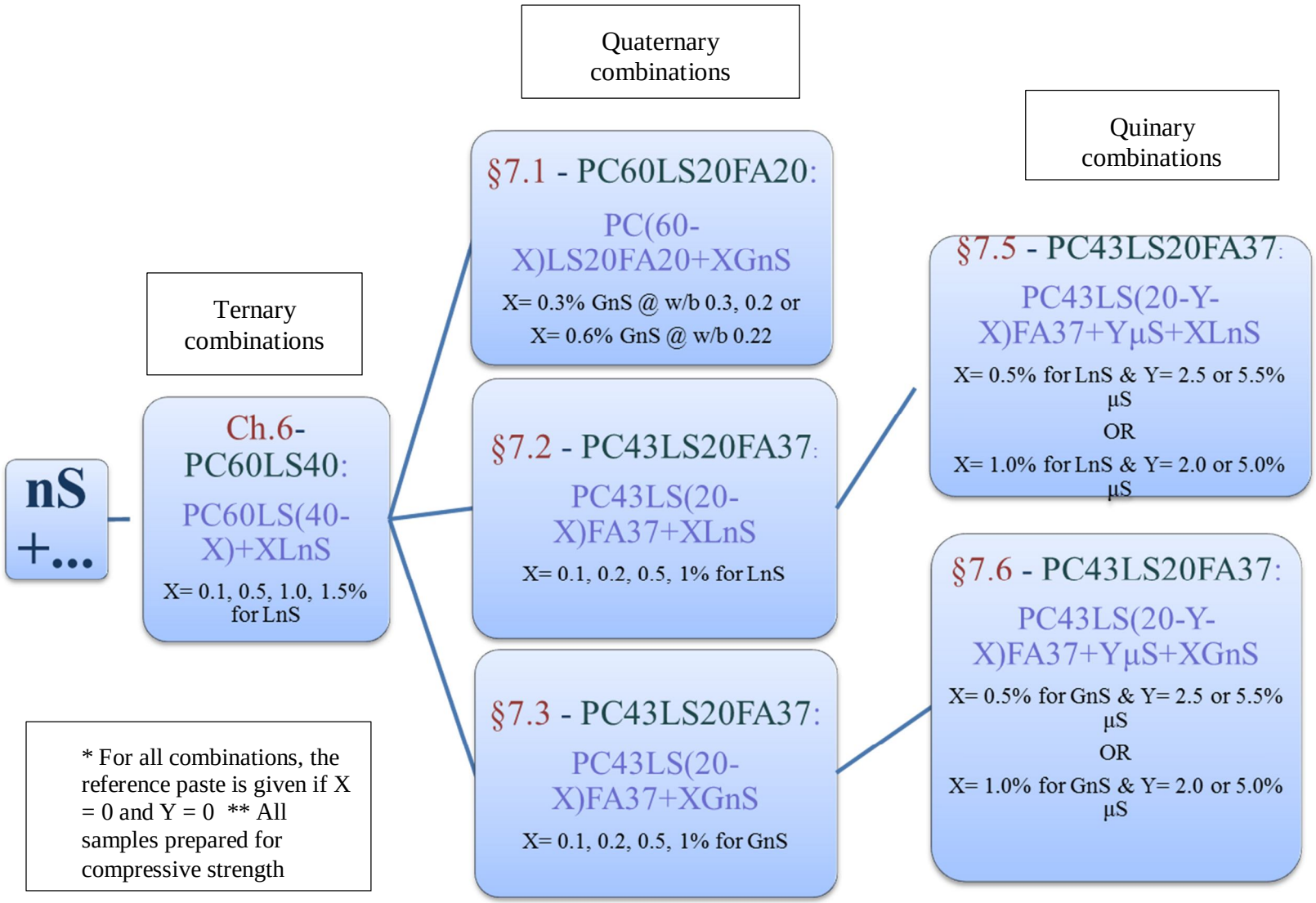

Figure 4-1: Overview of nS modified combinations

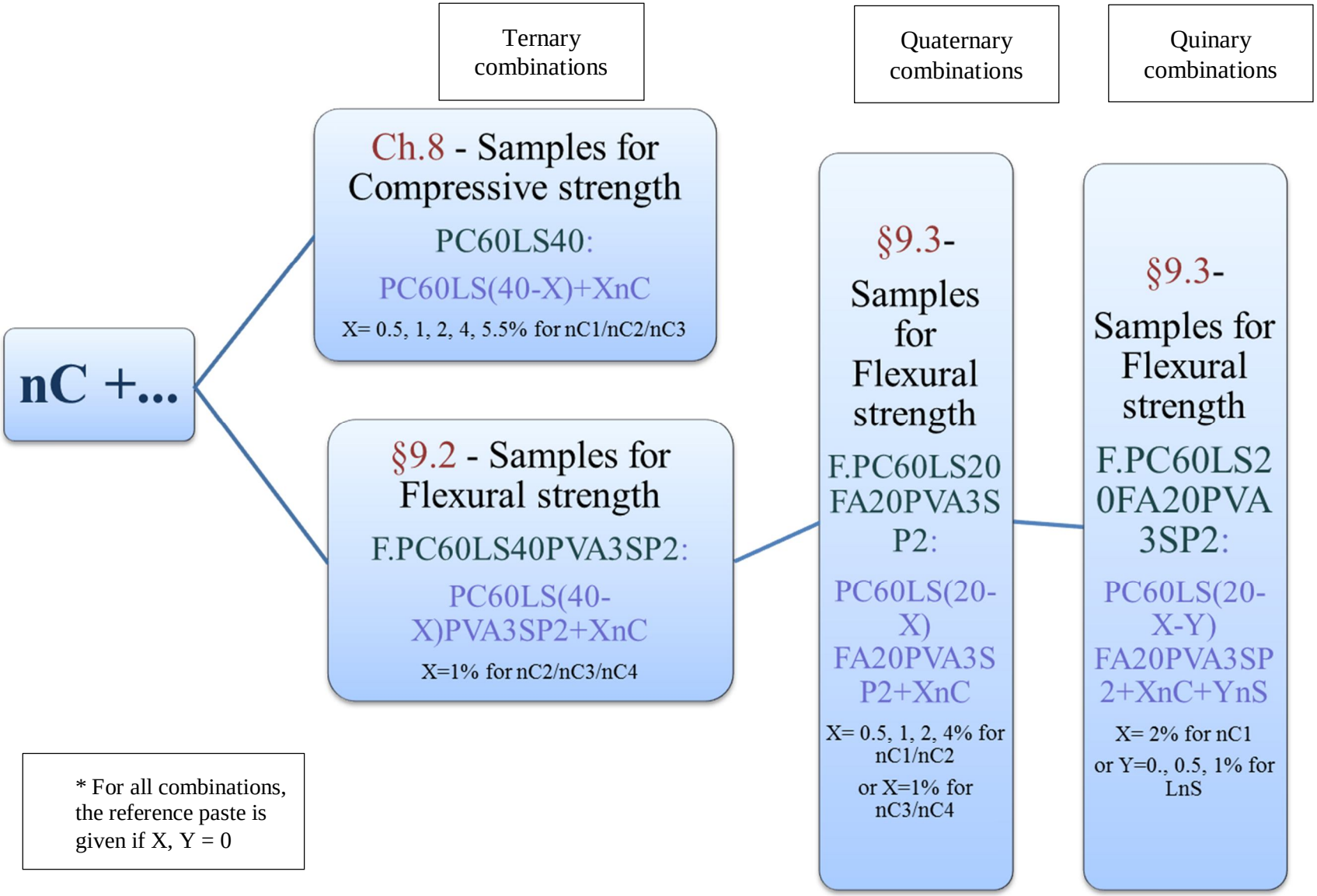

Figure 4-2: Overview of nC modified combinations

4.4.2 LnS modified cement formulations - Ternary

The non-pozzolanic blended cement formulation PC60LS40 was used as the reference to investigate whether the addition of LnS has a pozzolanic effect. The amount of water present in the LnS aqueous solution was subtracted by the total amount of water in order to maintain a constant w/b ratio of 0.3. Again, the PC content was kept constant and the content of LnS solids was deducted from the LS content for the reason mentioned above. Therefore, the general formula for the LnS modified pastes was:

$$PC(60) + LS(40 - x) + LnS(x) \qquad \text{Equation: 4-2}$$

Where x = % by mass of LnS solids, ranging from 0 to 1.5%.

The mix proportions in terms of % of the total mass of binder are shown in Table 4-5 and the matrix of the total formulations in Table 4-6.

Table 4-5: LnS modified ternary cement paste formulations - Mix proportions % by total mass of solids

Sample	PC (%)	LS (%)	nS (%solids)	W/B
PC60LS40+0%LnS	60	40.0	0.0	0.3
PC60LS39.9+0.1%LnS	60	39.9	0.1	0.3
PC60LS39.5+0.5%LnS	60	39.5	0.5	0.3
PC60LS39+1.0%LnS	60	39.0	1.0	0.3
PC60LS38.5+1.5%LnS	60	38.5	1.5	0.3

Table 4-6: Matrix of total ternary nanomodified cement paste formulations

Nanomodifications of PC60LS40			
LnS	nC1	nC2	nC3
	PC60LS39.5+ 0.5%nC1	PC60LS39.5+ 0.5%nC2	PC60LS39.5+ 0.5%nC3
PC60LS39.9+0.1%LnS	PC60LS39+ 1%nC1	PC60LS39+ 1%nC2	PC60LS39+ 1%nC3
PC60LS39.5+0.5%LnS	PC60LS38+ 2%nC1	PC60LS38+ 2%nC2	PC60LS38+ 2%nC3
PC60LS39+1%LnS	PC60LS36+ 4%nC1	PC60LS36+ 4%nC2	PC60LS36+ 4%nC3
PC60LS38.5+1.5%LnS	PC60LS34.5+ 5.5%nC1	PC60LS34.5+ 5.5%nC2	PC60LS34.5+ 5.5%nC3

4.4.3 GnS modified cement formulations - Quaternary

PC60LS20FA20 was nanomodified with GnS at two different concentrations for three different w/b ratios. GnS was commercially described as "water reducing admixture with nS particles", therefore, these initial pastes were designed to assess this piece of information. Moreover, it was recommended by the supplier that the GnS addition should be between 0.5-3.0% by mass of Portland cement, hence for these pastes the lowest GnS content would be 0.3%. The different formulations are shown in the table below:

Table 4-7: GnS modified quaternary cement paste formulations - Mix proportions % by total mass of solids

Sample	PC (%)	LS (%)	FA (%)	GnS (%solids)	W/B
PC60LS20FA20	60.0	20.0	20.0	0.0	0.30
PC59.5LS20.1FA20.1+0.3% GnS @0.3	59.5	20.1	20.1	0.3	0.30
PC59.5LS20.1FA20.1+0.3% GnS@0.2	59.5	20.1	20.1	0.3	0.20
PC58.6LS20.4FA20.4 +0.6% GnS @0.22	58.6	20.4	20.4	0.6	0.22

4.4.4 LnS and GnS modified low PC cement formulations - Quaternary

Another series of specimens containing different quantities of nS solids were added to the reference paste PC43LS20FA37, maintaining the w/b ratio of 0.3 (Table 4-8 and Table 4-9). These pastes were designed with a high content of FA, which permitted an investigation into possible effects of pozzolanic interference between the two different types of nS and other pozzolanic materials. Again, the PC content was kept constant and the content of nS solids was deducted from the LS content for the reason mentioned above. The general formula of the matrix of the quaternary cement pastes was given by the following formula:

$$PC(43) + LS(20 - x) + FA(37) + nS(x) \qquad \text{Equation: 4-3}$$

Where x = % by mass of nS solids, ranging from 0 to 1.0%.

These pastes were also mentioned to as PC/FA=1.16 pastes.

Table 4-8: LnS modified quaternary cement paste formulations - low PC - Mix proportions % by total mass of solids

Sample	PC (%)	LS (%)	FA (%)	nS (%solids)	W/B
PC43LS20FA43 (0% nS)	43	20	37	0.0	0.3
PC43LS19.9FA37 +0.1%LnS	43	19.9	37	0.1	0.3
PC43LS19.8FA37 +0.2%LnS	43	19.8	37	0.2	0.3
PC43LS19.5FA37 +0.5%LnS	43	19.5	37	0.5	0.3
PC43LS19FA37 +1.0%LnS	43	19	37	1.0	0.3

The GnS modified quaternary series of specimens is shown in the following table:

Table 4-9: GnS modified quaternary cement paste formulations - low PC - Mix proportions % by total mass of solids

Sample	PC (%)	LS (%)	FA (%)	GnS (%solids)	W/B
PC43LS20FA37 (0% nS)	43	20	37	0.0	0.3
PC43LS19.9FA37 +0.1%GnS	43	19.9	37	0.1	0.3
PC43LS19.8FA37 +0.2%GnS	43	19.8	37	0.2	0.3
PC43LS19.5FA37 +0.5GnS	43	19.5	37	0.5	0.3
PC43LS19FA37 +1.0%GnS	43	19	37	1.0	0.3

4.4.5 nS and µS modified low PC cement formulations - Quinary

Continuing the enhancement of PC43LS20FA37 four paste formulations were created for each nS type containing in addition µS. Again, the PC content was kept constant and the content of nS solids was deducted from the LS content for the reason mentioned above. The quinary pastes were prepared in the following proportions:

Table 4-10: LnS/GnS and µS modified quinary cement paste formulations - low PC - Mix proportions % by total mass of solids

Sample	PC (%)	LS (%)	FA (%)	µS (%)	nS (%solids)
PC43LS20FA37	43	20	37	0.0	0.0
PC43LS17FA37+2.5% µS + 0.5%nS	43	17	37	2.5	0.5
PC43LS17FA37+2.0% µS + 1.0% nS	43	17	37	2.0	1.0
PC43LS14FA37+5.5% µS + 0.5% nS	43	14	37	5.5	0.5
PC43LS14FA37+5.0% µS + 1.0% nS	43	14	37	5.0	1.0

4.4.6 nC modified fibre reinforced cement paste formulations

In all nC modified fibre cement paste formulations, the PC content was kept constant and the content of nC solids was deducted from the LS content for the reason mentioned above. As shown in the overview of nC modified formulations (Figure 4-2) two more series of the nanoclay enhanced pastes were designed for flexure. The first one was based on F.PC60LS40, containing in addition, 3% PVA fibres (Kuralon H-1: 4mm) and 2% superplasticizer (ViscoCrete 20 HE), provided by SIKA, was enhanced with the use of 1% by mass of solids of nC3 or 1% by mass of solids of nC4 as shown in Table 4-11.

Table 4-11: nC modified and fibre reinforced ternary cement paste formulations - Mix proportions % by total mass of solids

Sample	PC (%)	LS (%)	nC (%solids)	SP (%)	PVA (%)	W/B
F.PC60LS40PVA3SP2	60	40	0	2	3	0.3
F.PC60LS39PVA3SP2+1%nC2	60	39	1	2	3	0.3
F.PC60LS39PVA3SP2+1%nC3	60	39	1	2	3	0.3
F.PC60LS39PVA3SP2+1%nC4	60	39	1	2	3	0.3

Then the paste was enhanced by the addition of FA, and different concentrations of the nC dispersions as shown in Table 4-12. The full series with all four different nC concentrations were created only for nC1 and nC2. For the remaining two other types of nC; nC3 and nC4 only the 1% concentration was implemented.

Table 4-12: nC modified and fibre reinforced quaternary cement paste formulations - Mix proportions % by total mass of solids

Sample	PC (%)	LS (%)	FA (%)	nC (%solids)	SP (%)	PVA (%)	W/B
F.PC60LS20FA20PVA3SP2	60	20	20	0.0	2	3	0.3
F.PC60LS19.5FA20PVA3SP2+0.5%nC	60	19.5	20	0.5	2	3	0.3
F.PC60LS39PVA3SP2+1%nC	60	19	20	1.0	2	3	0.3
F.PC60LS18FA20PVA3SP2 +2%nC	60	18	20	2.0	2	3	0.3
F.PC60LS16FA20PVA3SP2 +4%nC	60	16	20	4.0	2	3	0.3

4.4.7 nS and nC modified fibre reinforced cement paste formulations

The reference paste F.PC60LS20FA20PVA4SP2 was enhanced by the addition of two different nanoparticles; nC1 and LnS as shown in Table 4-13. These series was only tested in flexure and no chemical analysis was carried out. It served as indication for directing future work suggestions.

Table 4-13: nC and LnS modified fibre reinforced quinary cement paste formulations - Mix proportions % by total mass of solids

Sample	PC (%)	LS (%)	FA (%)	nC1 (%solids)	LnS (%solids)	SP (%)	PVA (%)	W/B
F.PC60LS20FA20PVA4SP2	60	20	20	0.0	0.0	2	4	0.3
F.PC60LS19.5FA20PVA4SP2+2.0%nC1	60	19.5	20	2.0	0.0	2	4	0.3
F.PC60LS39PVA4SP2+2.0%nC1+0.5%LnS	60	19	20	2.0	0.5	2	4	0.3
F.PC60LS18FA20PVA4SP2+2%nC+1.0%LnS	60	18	20	2.0	1.0	2	4	0.3

4.4.8 nS and nC modified mortar formulations

Forty two different series of mortars were prepared for the verification of the cement paste results according to EN-196-1 in terms of w/b ratio (0.5), use of distilled water and set mixing procedure.

The inorganic nC dispersion was diluted in the calculated amount of distilled water that was needed for every mortar combination.

nC4 was directly added with the powders, i.e. was not initially dispersed in water before added to the mixer.

GnS was added in the last 30 seconds of high speed mixing.

The various mortar combinations are shown in Table 4-14.

Table 4-14: Mortar combinations

	M.PC100 @0.5w/b	M.PC60FA40 @0.5w/b	M.PC60LS20FA20 @0.5w/b	M.PC60LS40 @0.5w/b	M.PC43LS20FA37 @0.5w/b	M.PC43LS20 FA37 @0.35w/b
..+ 0.25 % GnS	M.PC99.75+ 0.25% GnS	M.PC59.75FA40+ 0.25%GnS	n/a	n/a	n/a	n/a
..+ 0.50 % LnS	M.PC99.5 + 0.5% LnS	M.PC59.5FA40 + 0.5% LnS	M.PC59.5LS20FA20 + 0.5% LnS	M.PC59.5LS40+ 0.5% LnS	M.PC42.5LS20FA37+0.5%LnS	n/a
..+ 1.0 % LnS	M.PC99+ 1.0% LnS	n/a[6]	n/a	n/a	n/a	n/a
..+ 0.50 % GnS @ 0.35w/b	M.PC99.5 + 0.5% GnS @0.35w/b	M.PC59.5FA40+ 0.5% GnS @0.35w/b	n/a	n/a	n/a	M.PC42.5LS20FA37 + 0.5% GnS
..+ 1.0 % nC2	M.PC99+ 1.0% nC2	M.PC59FA40 + 1.0% nC2	M.PC59LS20FA20 + 1.0% nC2	n/a	n/a	n/a
..+ 2.0 % nC2	M.PC98+ 2.0% nC2	M.PC58FA40+ 2.0% nC2	M.PC58LS20FA20 + 2.0% nC2	M.PC60LS38+2% nC2	n/a	n/a
..+ 5.0 % nC2	M.PC95+ 5.0% nC2	n/a	n/a	n/a	n/a	n/a
..+ 1.0 % nC4	M.PC99 + 1.0% nC3	n/a	n/a	n/a	n/a	n/a
..+ 1.4 % nC4	n/a	n/a	M.PC58.6LS20FA20 +1.4% nC4	n/a	n/a	n/a
..+ 2.0 % nC4	M.PC98 + 2.0% nC3	n/a	n/a	n/a	n/a	n/a
..+ 2.8 % nC4	n/a	M.PC57.2FA40 + 2.8% nC4	M.PC57.2LS20FA20+2.8% nC4	n/a	n/a	n/a
..+ 6.9 % nC4	M.PC93.1+ 6.9% nC4	n/a	n/a	n/a	n/a	n/a
..+ 1.0 % nC3	n/a	M.PC59FA40 + 1.0% nC3	n/a	n/a	n/a	n/a
..+ 2.0 % nC3	n/a	M.PC58FA40 + 2.0% nC3	n/a	n/a	n/a	n/a
..+ 2.0 % nC1	n/a		n/a	M.PC60LS38+2%nC1	n/a	n/a
..+ 2.0 % nC2 + 0.25 % GnS	n/a	M.PC57.75FA40 + 2.0% nC2+ 0.25%	n/a	n/a	n/a	n/a
..+ 2.8 % nC4 + 0.50 % LnS	n/a	M.PC56.7FA40 + 2.8% nC4+ 0.5% LnS	M.PC56.7LS20FA20+2.8%nC4+ 0.5% LnS	n/a	n/a	n/a
..+ 2.0 % nC2 + 0.50 % LnS	n/a	M.PC57.5FA40 + 2.0% nC2+ 0.5% LnS	M.PC57.5LS20FA20+2.0%nC2+ 0.5% LnS	M.PC60LS37.5+2%nC2+ 0.5%LnS	n/a	n/a
..+ 2 % nC3 + 0.5% LnS	n/a	M.PC57.5FA40 + 2.0% nC3 + 0.5% LnS	n/a	n/a	n/a	n/a
..+ 2 % nC1 + 0.5 % LnS	n/a	n/a	n/a	M.PC60LS37.5+2%nC1+ 0.5%LnS	n/a	n/a

[6] n/a: not applicable

4.5 Mixing, casting, demoulding, curing

4.5.1 Non-nanomodified and nS or nC modified cement paste formulations

The following methodology was adopted for the mixing procedure:

- Dry mixing of the powders with a spatula by hand.
- For formulations containing nS, the nS suspension was poured in a separate container together with water, stirred with the use of a magnetic stir bar for 1 minute and then added to the mixed powders.
- For formulations containing nC, the nC dispersion was poured in a separate container together with water, stirred with the use of a magnetic stir bar for 1 minute and then added to the mixed powders.
- With the addition of water (and nS or nC where applicable), the paste was mixed by a with an automatic dual shaft mixer at 1150 rpm for 3 minutes for pastes up to 300 g, time increasing with amounts of paste.

In order to imitate pressure exerted through extrusion needed for the FIBCEM project, the non-nanomodified pastes were cast in syringes of approximately 60 mm height and 30 mm diameter and compaction was applied through pressure induced via the syringe piston. Notwithstanding the ingenuity of the idea, the number of samples that were scheduled to be created lead to the adoption of simpler casting techniques.

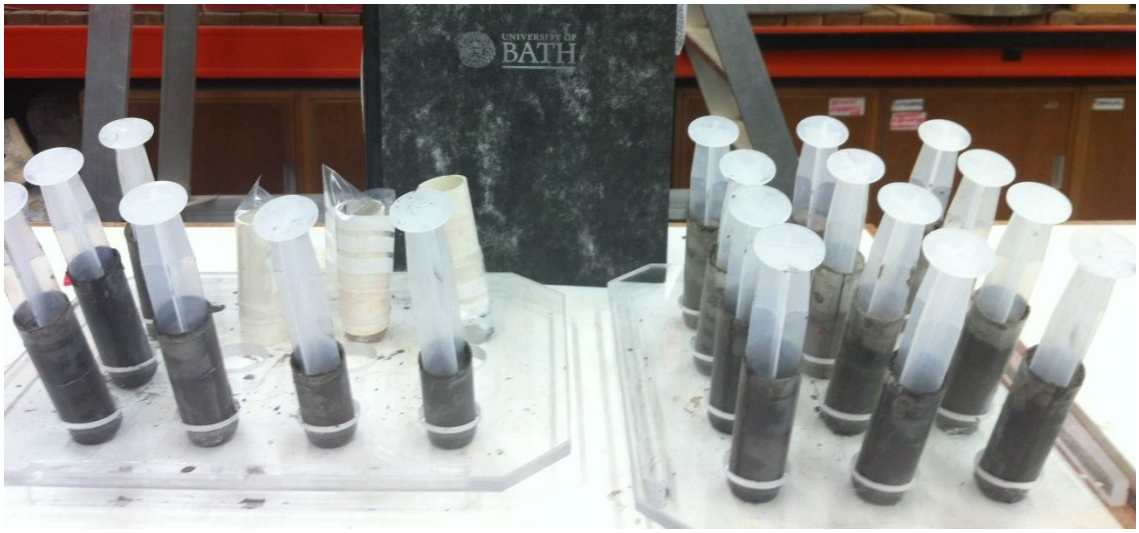

Figure 4-3: Casting technique imitating extrusion

The GnS dispersion did not allow immediate setting of the GnS modified pastes. As shown in Figure 4-4, these pastes were fluid when cast in the moulds. Therefore, the compressive strength at day 1 can be expected to be low.

Figure 4-4: GnS nanomodified cement pastes

All nanomodified pastes, were cast into cylindrical moulds or in the syringes without the application of pressure (Figure 4-5). The dimensions of the moulds and syringes were approximately 60 mm height and 30 mm diameter, so as to secure a height-to-diameter ratio of 2. Specimens were vibrated and were air cured in dry sealed conditions at 20±2ºC for the first 24 hours. Consequently they were demoulded and placed in a curing tank filled with distilled water at 20±2 ºC. To avoid contamination, separate samples of each paste were kept in sealed, airtight bags for the first 24 hours, then filled up with water at 20±2 ºC and kept until the day of arrest of hydration for chemical or microstructural characterisation.

After demoulding the samples were examined for bad compaction and visual porosity (Figure 4-6 and Figure 4-7). It can be observed that for the higher concentrations of either nC or nS particles, the visual pores increased. Hence, the mechanical properties are expected to be lower for the specimens with the highest nC or nS content. The effect is possibly aggravated due to the fact that superplasticizers were not used in these pastes.

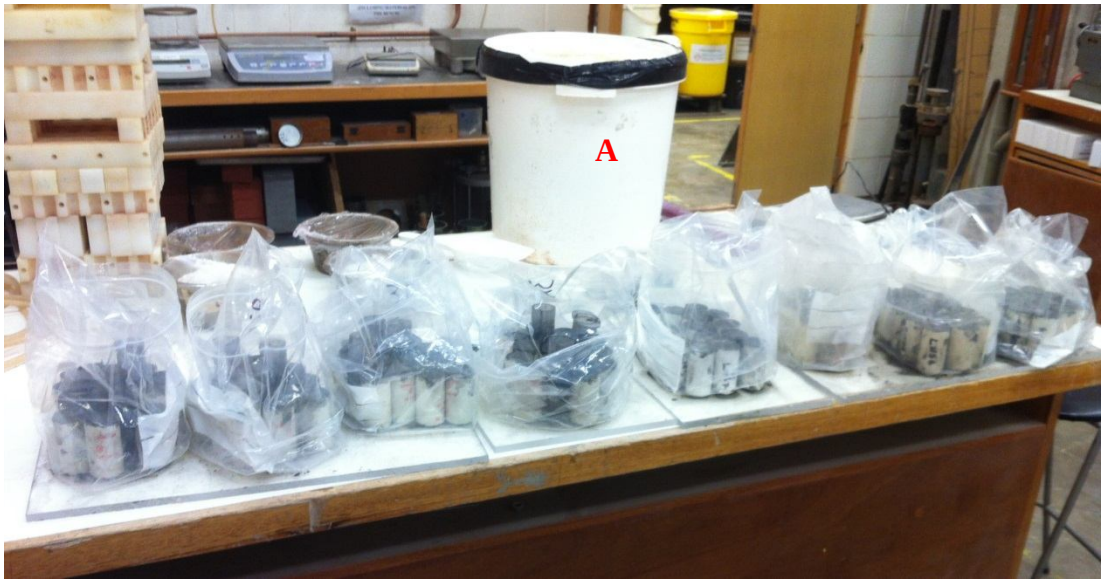

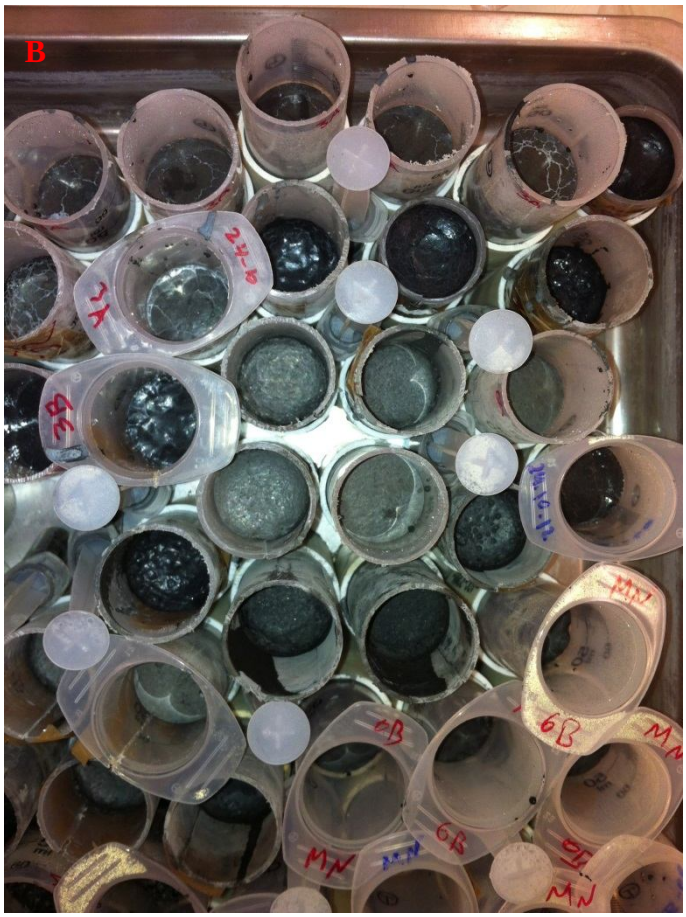

Figure 4-5: (A) & (B) Production of specimens

Figure 4-6: nC modified ternary cement paste specimens

Figure 4-7: nS modified ternary cement paste specimens

4.5.2 nC modified fibre reinforced cement paste formulations

The procedure followed for the preparation of the slabs, was exactly the same as for the pastes however; the PVA fires were added last after they had been manually further separated. Mixing lasted three to four minutes, in the automatic mixer. The higher nC additions were agglomerating within the paste posing difficulty for compaction (Figure 4-8).

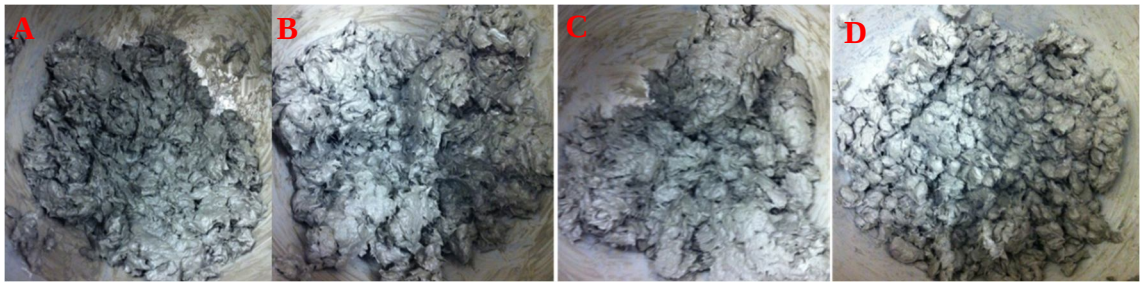

Figure 4-8: (A) 0%, (B) 0.5%, (C)1% and (D) 4% by mass addition of nC2 on F.PC60LS20FA20PVA3SP2

Pastes were cast in two layers (Figure 4-9) in prismatic moulds, of the following dimensions: - 10 mm depth, 40 mm breath and 120 mm length and compacted at a shaking table (Figure 4-10). Samples were demoulded and cured with distilled water after the first 24 hours at 20±2 ºC (Figure 4-11) until the day of flexural strength testing.

Figure 4-9: Placing the nanoclay modified and fibre reinforced cement pastes in the special moulds

Figure 4-10: Compacting pastes at shaking table

Figure 4-11: Curing of samples in distilled water

4.5.3 nS and nC modified mortar formulations

The 46 different mortars formulations were prepared in an automatic mixer complying with EN -196-1 mixing times. The w/b ratio was equal to 0.5, according to the standard. Distilled water and standard sand were used. The proportions by mass according to the standard were: one part of the cement, three parts of CEN Standard sand, and one half part of water (water/binder ratio 0.50). Each batch for three test specimens consisted of:

- ✓ (450 ± 2) g of powders (PC/LS/FA/nC solids/nS solids)
- ✓ (1 350 ± 5) g of sand and
- ✓ (225 ± 1) g of water

Two mortar specimens at w/b = 0.35 were also created to assess the water reducing capacity of GnS.

For the mortars containing GnS, GnS was added in the last 30 seconds of high speed mixing.

For the mortars containing nC, the dispersion was diluted in the calculated amount of distilled water that was needed for every mortar combination. Water and nC were added according to the standard.

Each mortar formulation was poured into the standard moulds, in three layers. It was vibrated and covered for 24 hours (Figure 4-12). Samples were demoulded and kept into water at 20±2ºC thereafter until the day of testing. On the day of testing, cubes of 40 x 40 x 40 mm were cut from the prisms with a diamond saw.

Figure 4-12: nS and/or nC modified mortars

5 NON-NANOMODIFIED CEMENT FORMULATIONS

5.1 Binary and ternary cement formulations

5.1.1 Introductory section

Apart from the pure CEMII paste (B1), seven additional Portland limestone cement initial formulations (B2-8) were designed, containing different proportions of CEMII, limestone and fly ash, as presented in Chapter 4. Preliminary evaluation of the embodied carbon dioxide content was related to compressive strength. The best relations between strength and embodied CO_2 were obtained by B7: PC60LS20FA20 and B8: PC45LS20FA35 delivering 80MPa/t/t and 110MPa/t/t, respectively. Consistence and setting time requirements were not considered. These two formulations were selected to be further optimized. Thermal analyses were also performed on all initial pastes. Consistency and setting time requirements were beyond the scope of this research. All results are presented in the following sections.

5.1.2 Compressive strength of starting pastes

The initial pastes (B1-B10) were tested in compression at day 7, 28 and 56, as shown in Figure 5-1 and Table 5-1.

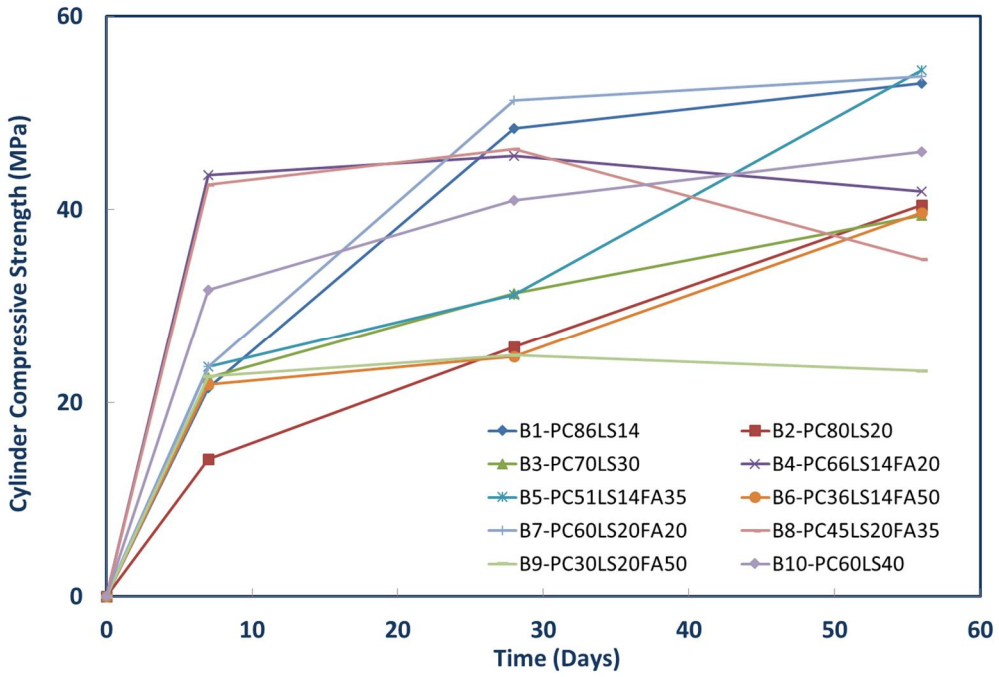

Figure 5-1: Cylinder compressive strength of starting cement pastes

Table 5-1: Cylinder compressive strength of Bases 1-9

Sample	Formulation composition	Cylinder compressive strength (MPa)		
		7 Day	28 Day	56 Day
B1	PC86LS14	21.5	48.4	53.1
B2	PC80LS20	14.2	25.8	40.5
B3	PC70LS30	22.6	31.4	39.4
B4	PC66LS14FA20	43.6	45.6	41.9
B5	PC51LS14FA35	23.7	31.2	54.4
B6	PC36LS14FA50	21.9	24.8	39.7
B7	PC60LS20FA20	23.7	51.3	53.8
B8	PC45LS20FA35	42.6	46.3	34.9
B9	PC30LS20FA50	22.7	24.9	23.3
B10	PC60LS40	31.7	41.0	46.0

The compressive strength tests allowed the rejection of B1, B2 and B3 on the grounds of high PC content and performance that can be achieved with greener combinations, e.g. B5 showed better Long-term performance than B1. B9 was also rejected due to poor performance.

5.1.3 CO_2 footprint of binary and ternary pastes

The starting pastes to be nanomodified were selected according to their sustainability potential, with respect to the embodied CO_2 ($E.CO_2$) of PC (930 kg CO_2/tonne), LS (32 kg CO_2/tonne) and FA (4 kg CO_2/tonne) as discussed in Chapter 3 (Jones *et al.*, 2011; MPA, 2011). The results are presented in Table 5-2.

Table 5-2: Embodied CO_2 (kg/tonne) associated with strength of binary & ternary pastes

Sample	Formulation composition	PC $E.CO_2$	LS $E.CO_2$	FA $E.CO_2$	Total $E.CO_2$	Compres. Strength 28 days (MPa)	Strength/ $E.CO_2$ (MPa/ kg/tonne)
B1	PC86LS14	799.8	4.5	0.0	804.3	48.4	0.06
B2	PC80LS20	744.0	6.4	0.0	750.4	25.8	0.03
B3	PC70LS30	651.0	9.6	0.0	660.6	31.4	0.05
B4	PC66LS14FA20	613.8	4.5	0.8	619.1	45.6	0.07
B5	PC51LS14FA35	474.3	4.5	1.4	480.2	31.2	0.06
B6	PC36LS14FA50	334.8	4.5	2.0	341.3	24.8	0.07
B7	PC60LS20FA20	558.0	6.4	0.8	565.2	51.3	**0.09**
B8	PC45LS20FA35	418.5	6.4	1.4	426.3	46.3	**0.11**
B9	PC30LS20FA50	279.0	6.4	2.0	287.4	24.9	0.09
B10	PC60LS40	559.8	12.8	0.0	572.6	41.0	0.09

By observing the results provided in Table 5-2, it is evident that B6 to B10 had the lowest total E.CO_2. Furthermore, B7, B8 and B10 had the lower environmental impact and exhibited the highest mechanical properties in terms of compressive strength compared amongst the initial pastes. As an effect, B7, B8 and B10 were the three selected bases for further optimisation with the addition of micro and nanosized elements.

5.1.4 Thermal analyses of cement pastes

TG analyses were carried out at 7 and 28 days, the results of which are shown in Figure 5-2 and Figure 5-3. It should be noted that initially the first nine bases were dry cured (B10 was only water cured), as it was later decided to dry cure all samples to avoid their exposure in air. None of the samples had carbonated since the $CaCO_3$ content is lower than the initial LS content in the paste.

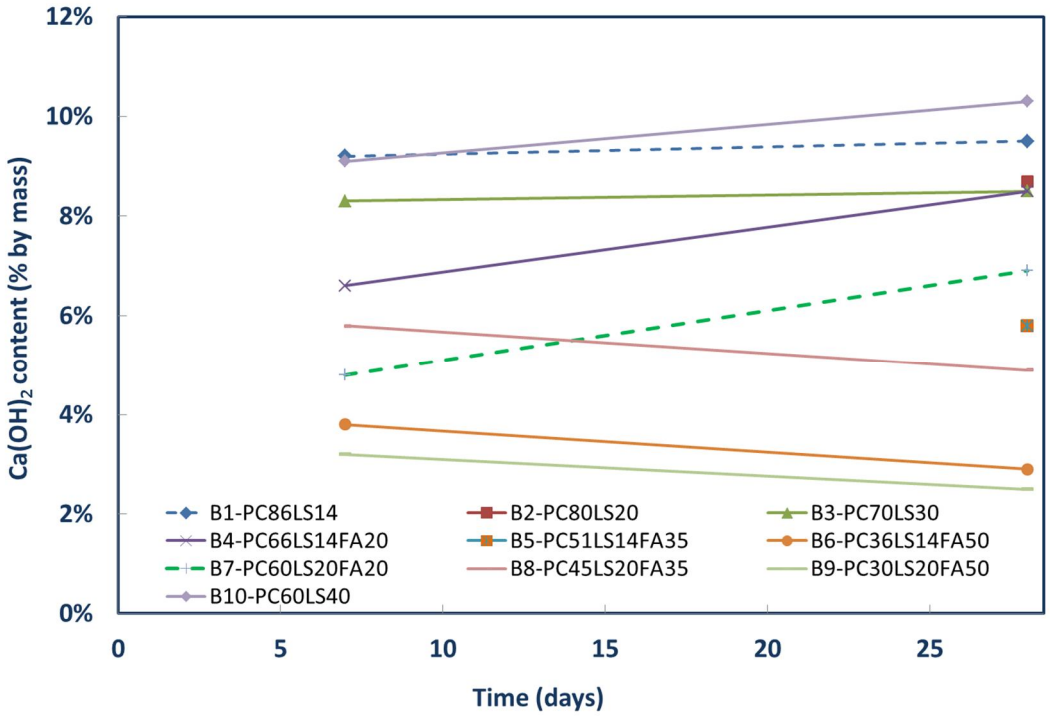

Figure 5-2: $Ca(OH)_2$ content of starting cement pastes

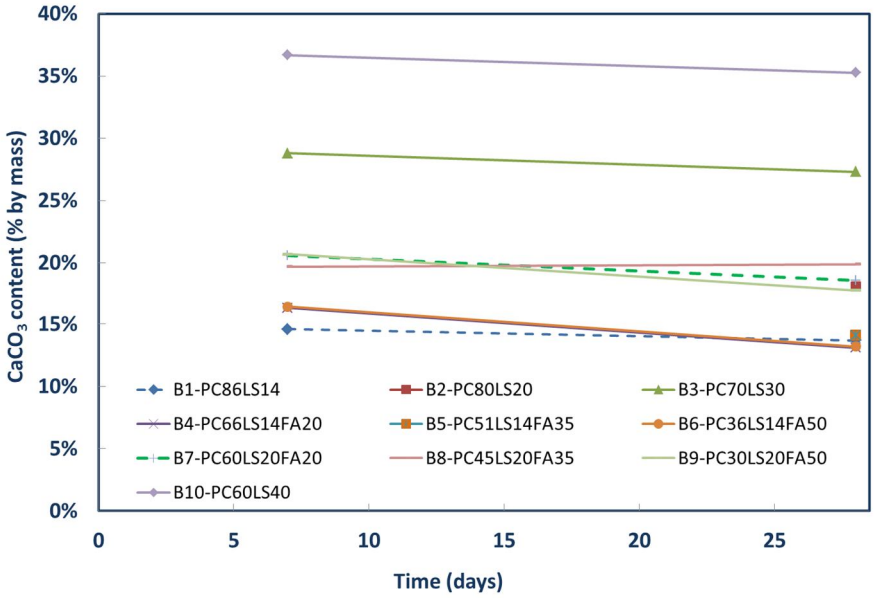

Figure 5-3: $CaCO_3$ content of starting cement pastes

In addition to the thermal analyses carried out at day 7 and day 28, the three selected bases, were reproduced, water cured after day 1 and TG analyses were carried out at day 1, 7, 28 and 56. For PC60LS40, TG analyses were carried out at day 90, as well. At this point, the $Ca(OH)_2$ consumption will be discussed (Table 5-3), to pave the ground for the changes that will be observed due to the nanomodifications. To begin with, it can be noticed that until day 28, that PC continues hydrating, the $Ca(OH)_2$ content of PC60LS40 increased and from then after it remained almost constant. It can be claimed, therefore, that the presence of FA in PC60LS20FA20 increased the consumption of the $Ca(OH)_2$ content significantly over all ages.

Table 5-3: Comparison of the $Ca(OH)_2$ content of the selected bases

	1	7	28	56
PC60LS40	**7.5%**	**9.1%**	**10.3%**	**10.6%**
PC60LS20FA20	**7.2%**	**8.1%**	**8.2%**	**8.1%**
PC43LS20FA37	**4.0%**	**6.0%**	**5.9%**	**1.5%**

As demonstrated in Table 5-3, PC60LS40 at day 1 contained 7.5% $Ca(OH)_2$ and 9.1% at day 7. For the two first pastes, PC60LS40 and PC60LS20FA20, which have the same PC content, the rate of hydration of PC at day 1 and 7 is expected to be essentially unaltered. However, it can be observed that at early ages, the $Ca(OH)_2$ content of PC60LS20FA20 is significantly lower, particularly at day 7. This is a strong indication that the pozzolanic activity of the FA present in this paste had already started by day 7, although it has been claimed that at high FA contents (PC45FA55) other researchers had noticed $Ca(OH)_2$ consumption by day 3 (Feldman *et al.*, 1990). Nonetheless, FA content is one matter and

PC content is another. For this, the author has adopted the PC/FA ratio, which is more representative in thermal analyses, together with the full formulation dosages, since FA is feeding from the $Ca(OH)_2$ produced during cement hydration.

Moreover, a paste containing 43%PC would be expected to generate 43/60x7.5% = 5.4% $Ca(OH)_2$ based on PC60LS40 $Ca(OH)_2$ content at day 1.

Also, a paste containing 43%PC would be expected to generate 43/60x7.2% = 5.2% $Ca(OH)_2$ based on PC60LS20FA20 $Ca(OH)_2$ content at day 1.

As shown in Table 5-3, PC43LS20FA37 contained 4.0% $Ca(OH)_2$ at day 1. This indicates that the pozzolanic activity of a part of the FA present in the paste had already commenced.

Inversely, a paste containing 43%PC would be expected to generate 43/60x9.1% = 6.5% $Ca(OH)_2$ based on PC60LS40 $Ca(OH)_2$ content at day 7.

A paste containing 43%PC would be expected to generate 43/60x8.1% = 5.8% $Ca(OH)_2$ based on PC60LS20FA20 $Ca(OH)_2$ content at day 7.

As demonstrated in Table 5-3, PC43LS20FA37 contained 6.0% $Ca(OH)_2$ at day 7. This indicates that the pozzolanic activity of a part of the FA present in the paste had progressed by day 7, but the reaction of the available FA particles could have been delayed.

Continuing this train of thought, a paste containing 43%PC would be expected to generate 43/60x10.3% = 7.4% $Ca(OH)_2$ based on PC60LS40 $Ca(OH)_2$ content at day 28.

Moreover, a paste containing 43%PC would be expected to generate 43/60x8.2% = 5.9% $Ca(OH)_2$ based on PC60LS20FA20 $Ca(OH)_2$ content at day 28.

PC43LS20FA37 contained 5.9% $Ca(OH)_2$ at day 28 (Table 5-3), implying that almost half of the FA was unreacted by day 28 since the amount of $Ca(OH)_2$ was equal to that of PC60LS20FA20.

Lastly, a paste containing 43%PC would be expected to generate 43/60x10.6% = 7.6% $Ca(OH)_2$ based on PC60LS40 $Ca(OH)_2$ content at day 56.

Also, a paste containing 43%PC would be expected to generate 43/60x8.1% = 5.8% $Ca(OH)_2$ based on PC60LS20FA20 $Ca(OH)_2$ content at day 56.

PC43LS20FA37 contained 1.5% $Ca(OH)_2$ at day 56 (Table 5-3), implying that the remaining unreacted FA was engaged in reaction by day 56. Although no carbonation was detected, as analysed in the following chapters, even if that was the case the amount of $Ca(OH)_2$ at day 56 is that low that any increase due to carbonation would still be negligible.

5.1.5 Microstructural characterisation of cement pastes

Backscattered (BSC) images were developed for PC86LS14 (B1), PC60LS20FA20 (B7) and PC60LS40 (B10) and are presented below.

As illustrated in Figure 5-4, Figure 5-5 and Figure 5-6 the microstructure of the CEMI, PC60LS20FA20 and PC60LS40 exhibited typical characteristics of such pastes at day 28. A number of $CaCO_3$ flakes, $Ca(CO)_2$ crystals and nest-like C–S–H are shown in the PC/LS paste. In Figure 5-6-A hydration products surrounding a reacted FA particle can be identified. In Figure 5-6-B probably a water void can be seen [rather than a common hydrated FA rim known as the "pull-out feature", "reminiscent" of the fully reacted FA particle (Xu and Sarkar, 1994)]. In Figure 5-6-C a number of FA spherical particles can be observed.

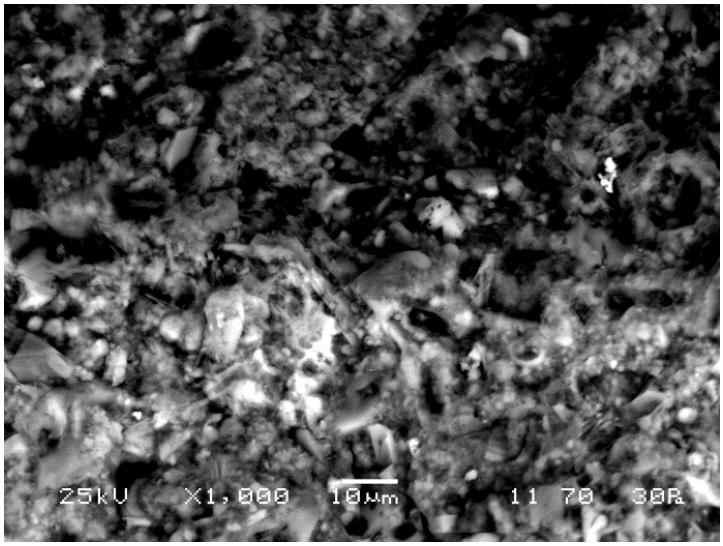

Figure 5-4: BSC micrograph of B10-PC60LS40 28D – 1000x

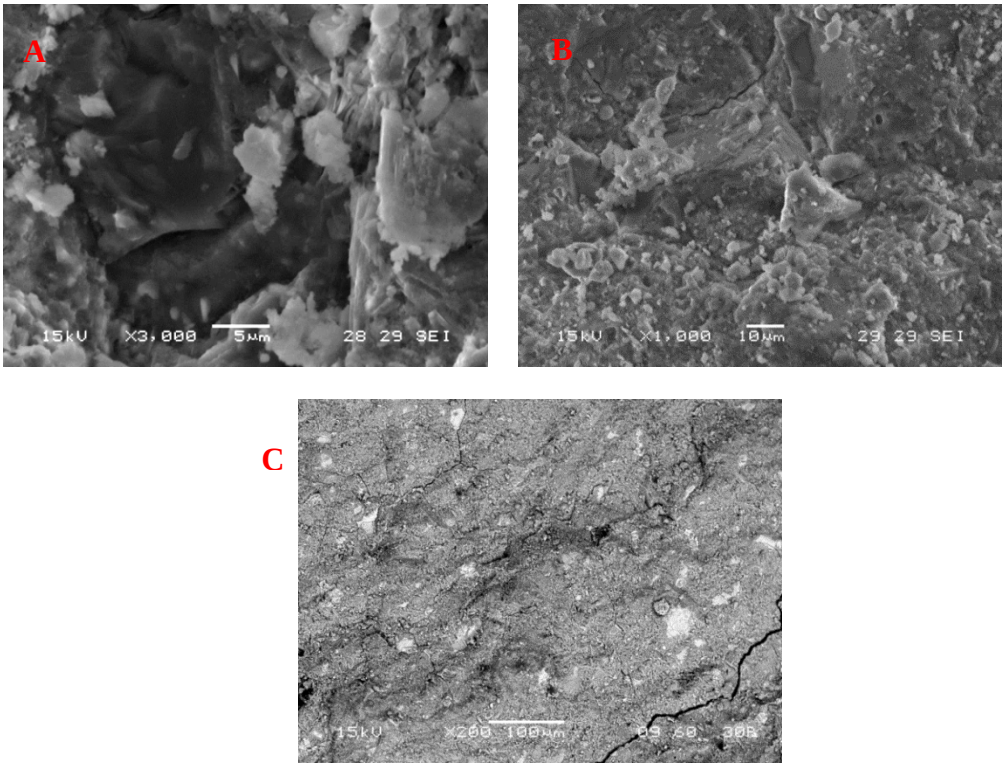

Figure 5-5: BSC micrograph of B1-PC86LS14 28D – (A) 3000x, (B) 1000x and (C) 200x

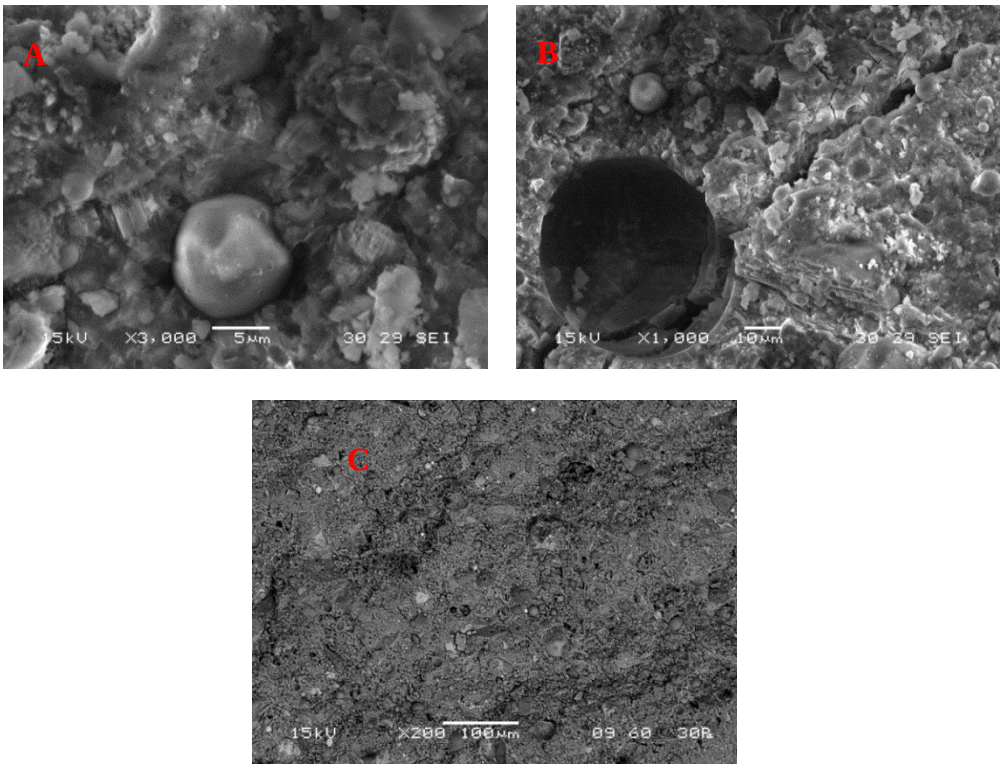

Figure 5-6: BSC micrograph of B7-PC60LS20FA20 28D – (A) 3000x, (B) 1000x and (C) 200x

5.2 Quaternary cement formulations on PC60LS20FA20

5.2.1 Introductory section

The first microstructural enhancement was completed with the addition of two different dosages of μS (5% and 10% by mass) on PC60LS20FA20, creating forth order pastes. The results on compressive strength, $Ca(OH)_2$ consumption and microstructure are shown in the following sections.

5.2.2 Compressive strength of cement pastes

As depicted in Figure 5-7 the addition of μS in pastes containing at least 20% FA by mass of binder is causing a retardation of the strength development, delivering lower compressive strengths. More than that, 10% μS, delay the strength gain by 28 days. These results were expected since according to CEN (2000) the maximum allowable μS content in PC/μS cements is 10% by mass. In other words, for every 1% μS by mass, at least 9% of PC content by mass, is required so that there will be enough $Ca(OH)_2$ produced by PC hydration for the μS to react with. Therefore, the 10% μS addition was excessive and as an effect, unreacted μS particles were predicted to be distinguished by SEM investigations.

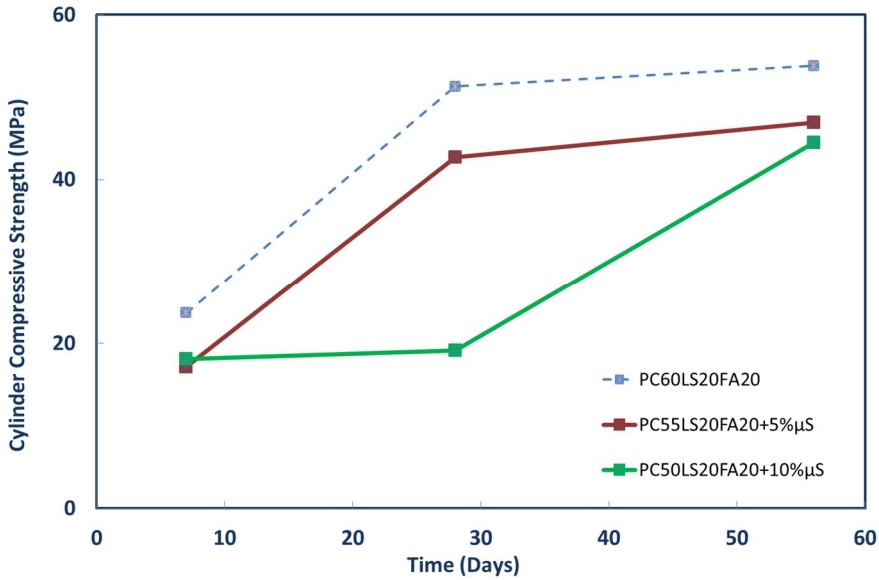

Figure 5-7: Cylinder compressive strength of μS modified cement pastes based on PC60LS20FA20

5.2.3 Thermal and crystallographic analyses of cement pastes

As shown in Figure 5-8 given than the reference paste contained at the various ages approximately 8% $Ca(OH)_2$, a paste containing 55%PC would be expected to generate 7.3% $Ca(OH)_2$ and a paste containing 50%PC would be expected to generate approximately 6.6% $Ca(OH)_2$ Therefore, it can be argued that in all cases the μS addition cause a further $Ca(OH)_2$ consumption. Lastly, as shown in Figure 5-9 no carbonation has taken place as the $CaCO_3$ content is lower than the 20% LS content present in the pastes in all combinations.

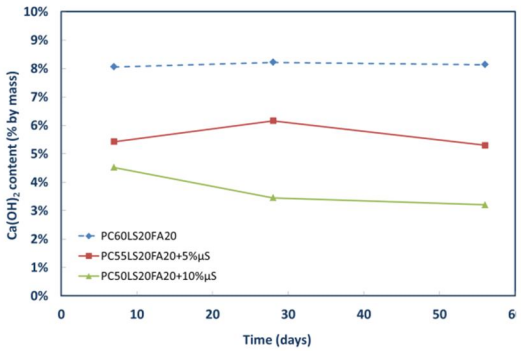

Figure 5-8: $Ca(OH)_2$ content μS modified cement pastes based on PC60LS20FA20

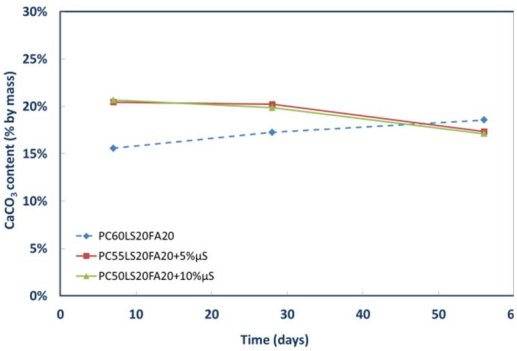

Figure 5-9: $CaCO_3$ content of μS modified cement pastes based on PC60LS20FA20

5.2.4 Microstructural characterisation of cement pastes

Indicatively, four BSC micrographs of PC55LS20FA20+5%μS are shown in Figure 5-10. As discussed earlier in Portland limestone cement pastes with high FA contents except for the needle-like hydration products (Figure 5-10-C and D), $CaCO_3$ flakes and $Ca(OH)_2$ crystals a number of rims and reacted FA particles can be detected. It is interesting to note that the investigation of different areas did not yield indications of unreacted FA particles. A fact correlating well with the TG measurements showing that there was enough $Ca(OH)_2$ still present in the hydrated paste after day 28 and 56 should the FA have needed it to react with. Reacted FA particles are circled in Figure 5-10-B. Furthermore, in Figure 5-10-B the reaction of a FA particle leaving a characteristic mullite sphere (Xu and Sarkar, 1994) was identified (enclosed in the rectangle). It was suggested by Xu and Sarkar that the glass phase in FA has been reacted and the crystalline phase is left almost intact.

Comparing the reference paste PC60LS20FA20 (Figure 5-6) with the 5% μS (Figure 5-10) and the 10% μS (Figure 5-11) enhanced quaternary and particularly the 200 times magnification there is an indication that the μS enhanced pastes are less dense. This cannot be attributed to particle packing that is expected to be enhanced, but to the high amount of FA present. The FA was already feeding from the $Ca(OH)_2$ therefore the more reactive

pozzolanic particles of µS may not be able to access the $Ca(OH)_2$ crystals encapsulated within the reacted FA particles. That is to say, although $Ca(OH)_2$ is not depleted in these quaternary formulations, the µS particles may be deactivated by the inaccessibility of $Ca(OH)_2$ created by the hydration products around the much greater quantities of FA.

It should be noted that further analysis on the microstructureal morphology of the reference paste with respect to its nanomodied combinations will be presented in Chapter 7.

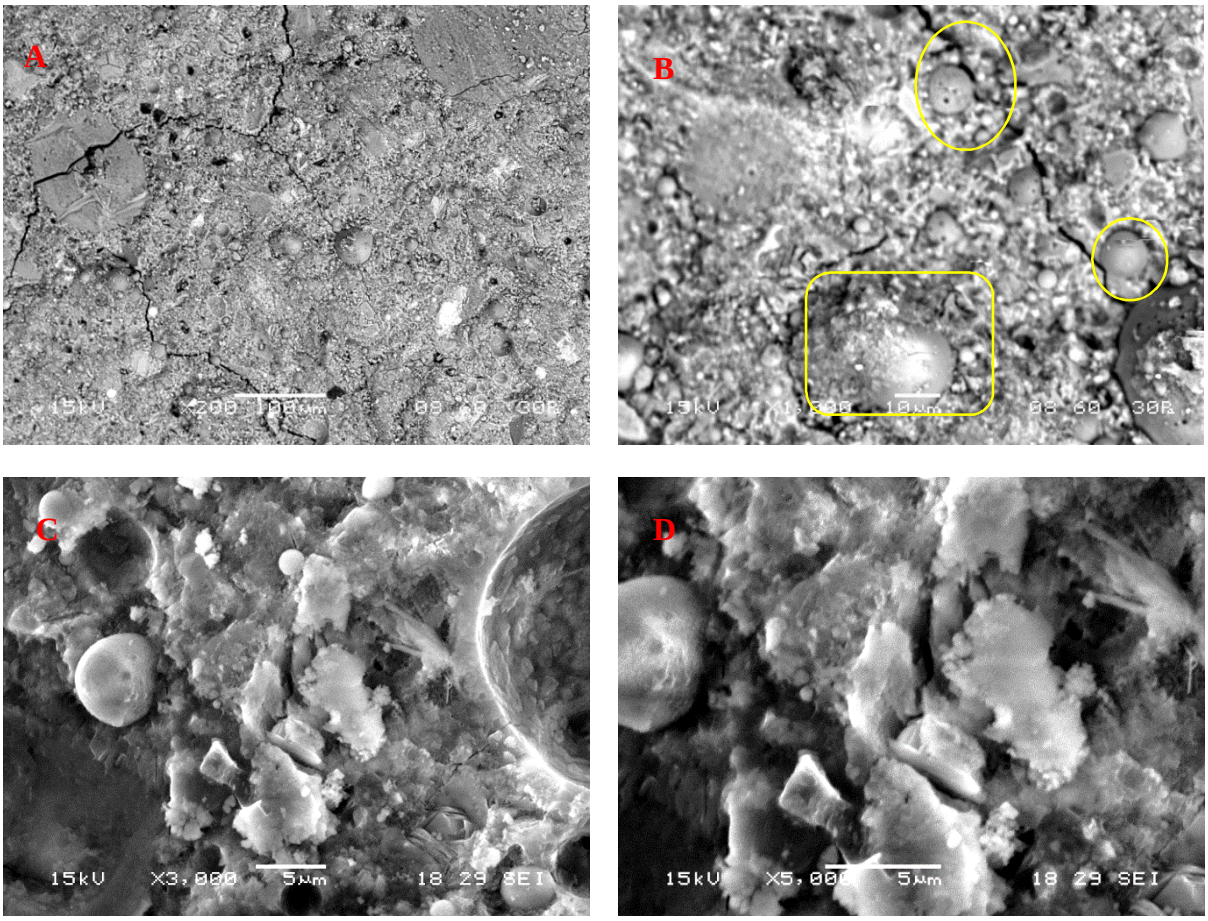

Figure 5-10: BSC micrograph of PC55LS20FA20+5%µS 28D – (A)200x, (B) 1000x, (C 3000x and (D) 5000x

As depicted in Figure 5-11, a similar microstructure to the lower µS content paste can be observed. The only difference being the plethora of needle-like ettringite detected at all magnifications and the many unreacted µS particles (small, spherical bright elements). The typically acicular hydration product of FA in the first 28 days can be seen in Figure 5-11-B (enclosed in a rectangle). Another FA particle with hydration gel around it, is circled in Figure 5-11-C. Reached FA particles are circled in Figure 5-11-C. In agreement with Lothenbach *et al.* (2011), the µS enhanced pastes showed a more refined pore structure, but are expected to deliver higher total porosities. That is to say, capillary pores are expected to be reduced and finer pores slightly increased. Therefore, it was of special interest to add an even smaller particle, of nS, in an effort to increase particle packing and seeding effects

and observe the related changes. This step was taken in Chapter 7, with a concise series of studies on µS and nS enhanced blended cement pastes.

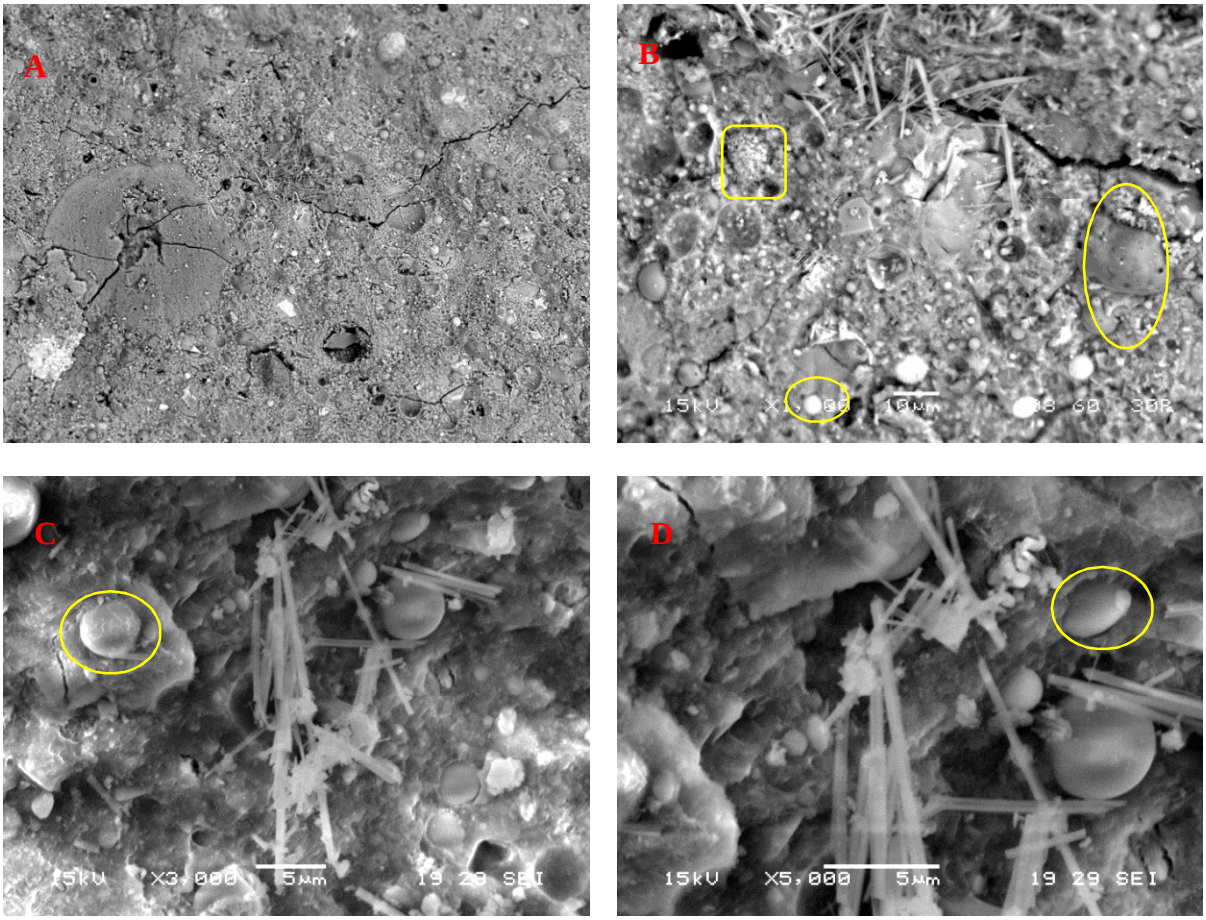

Figure 5-11: BSC micrograph of PC50LS20FA20+10%µS 28D – (A)200x, (B) 1000x, (C) 3000x and (D) 5000x

5.3 Quaternary cement formulations on PC43LS20FA37

5.3.1 Introductory section

Although B8-PC45LS20FA35 showed optimum performance a slightly different paste was adopted for further optimisation; PC43LS20FA37. This was decided in an effort to reduce the PC content even further. Hence, another microstructural enhancement was completed with the addition of two different dosages of μS (3% and 6% by mass) on PC43LS20FA37, creating another series of quaternary pastes. The results with regards to compressive strength and $Ca(OH)_2$ consumption are shown in the following sections.

5.3.2 Compressive strength of cement pastes

As in the case of μS-enhanced PC60LS20FA20, the μS-enhanced low PC content PC43LS20FA37, showed similar compressive strength gain characteristics, although the μS content was lower in both combinations (Figure 5-12).

(i) At day 7 both series had similar starting points (about 21 MPa for PC60LS20FA20 and 25 MPa for PC43LS20FA37), indicating that pozzolanic reactions had already been initiated within the first 7 days.

(ii) After day 28 the compressive strength of the reference paste PC60LS20FA20 (Figure 5-7) is almost equal to the compressive strength of the reference paste PC43LS20FA37 (Figure 5-12). However, the addition of μS offered little improvement. Therefore, although high LS contents are reported to be causing deterioration of the compressive strength at later ages the presence of μS offered a limited (due to the additional presence of FA) enhancement.

A small improvement in strength was also observed at day 1, followed by deterioration at day 28 and 56 with respect to the reference paste. These results were in agreement with other findings, suggesting that the increasing PC replacement is liable for the decrease in both compressive and flexural strengths (De Weerdt *et al.*, 2011b).The limited amount of PC and the high amount of FA present created some antagonism with the μS particles. Moreover, since for 1% μS, at least 9% of PC content by mass is required so that the μS can react with the $Ca(OH)_2$ produced by PC hydration for these series of pastes, the μS content should have been limited to approximately 4.8% by mass. Furthermore, knowing that for high replacements of PC with FA and LS the resulting strengths will be low, it was of particular interest to investigate if the nanoparticles could alter the performance of the low PC content blended cements. This part of the research will be covered in Chapter 7.

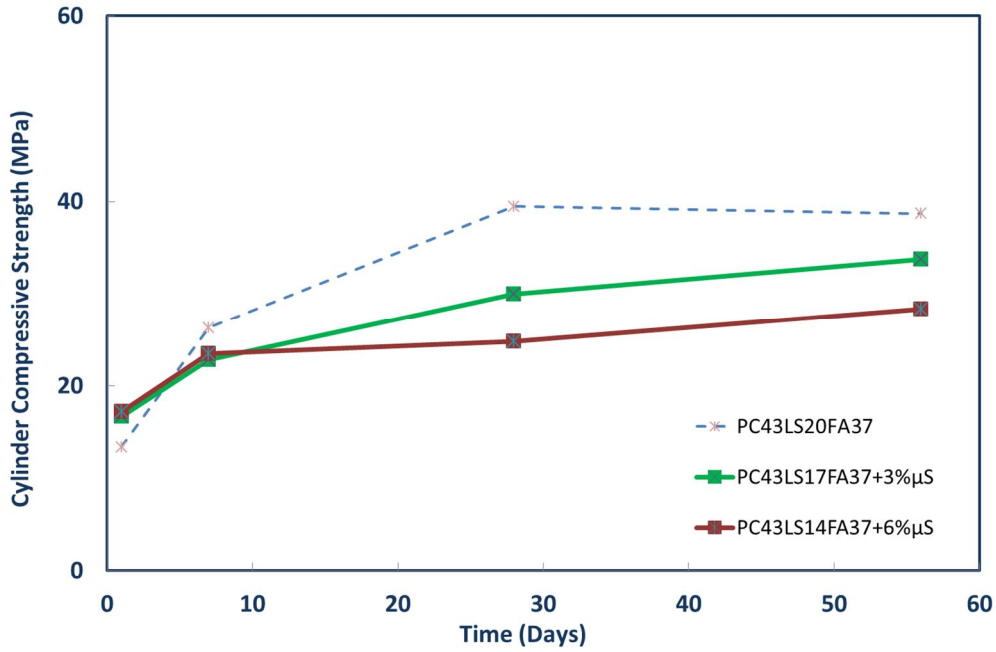

Figure 5-12: Cylinder compressive strength of µS modified cement pastes based on PC43LS20FA37

5.3.3 Thermal analyses of cement pastes

The $Ca(OH)_2$ consumption is depicted in Figure 5-13. It is interesting to note that after day 28 and by day 56, the $Ca(OH)_2$ content in the reference paste reduced to 1.5% by mass. It has been reported that for high PC replacement by FA (> 60%), depletion of $Ca(OH)_2$ may be observed after one year (Lothenbach *et al.*, 2011). Therefore, given more time, $Ca(OH)_2$ in this ternary system is expected to be depleted, if the sample has not carbonated. However, the phenomena observed in composite cements can be more complex. In fact, it has been reported that combinations containing 65% OPC and 35% of a formulation of FA and LS produced similar amounts of $Ca(OH)_2$ after day 1.However, the minimum amount of $Ca(OH)_2$ was reached for the 30% FA and 5% LS formulation and not the 35% FA formulation (De Weerdt *et al.*, 2011b). This was attributed to the synergistic interaction of FA and LS. Although according to De Weerdt *et al.* (2011b) the presence of LS leads to the formation of carboaluminate hydrates, this was not detected by the TG analyses (no mass loss after 890^{o}C) (Figure 5-14), neither by the XRD analyses shown in detail in Chapter 7.

In Figure 5-13 and Figure 5-14 there is fairly strong evidence of a correlation between the increase in $CaCO_3$ and the decrease in $Ca(OH)_2$ consumption, signal of slight carbonation. Since carbonation is fairly consistent in all samples, it is not further discussed.

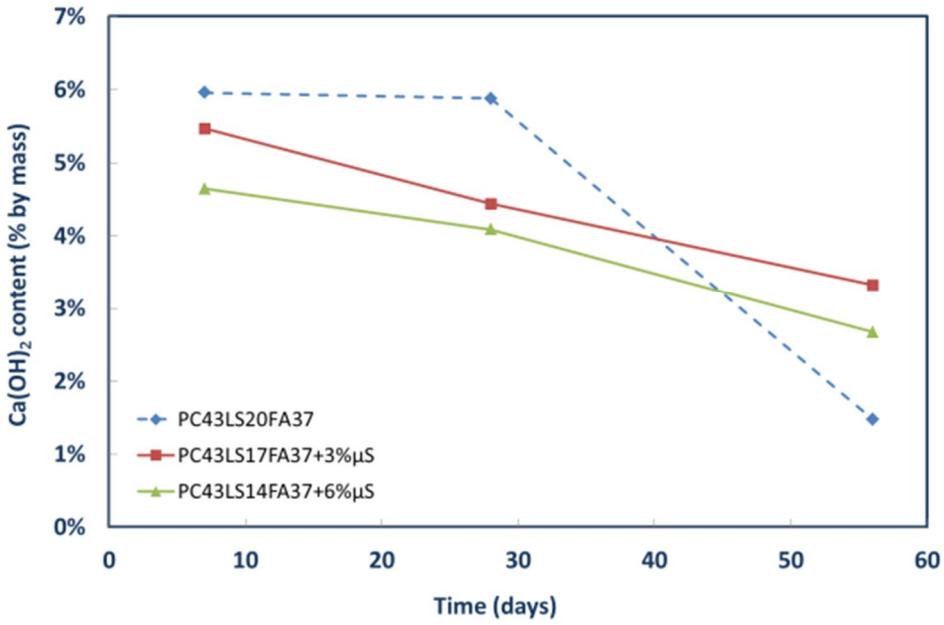

Figure 5-13: $Ca(OH)_2$ content µS modified cement pastes based on PC43LS20FA37

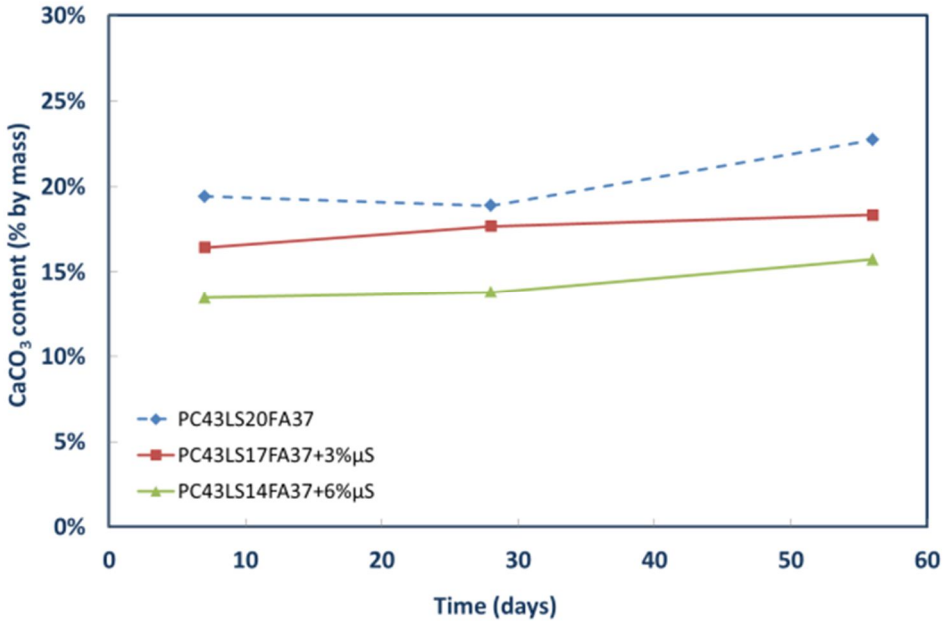

Figure 5-14: $CaCO_3$ content of µS modified cement pastes based on PC43LS20FA37

5.3.4 CO_2 footprint of quaternary pastes

In addition to the $E.CO_2$ values of PC, LS and FA pastes, the $E.CO_2$ of µS modified pastes was also evaluated (taking as µS $E.CO_2$ =14 kg CO_2/tonne according to Grist *et al.* (2013)). The results are presented in Table 5-4.

It is shown in Table 5-4, that the second quaternary series based on PC43LS20FA37 had the lowest total $E.CO_2$. Furthermore, PC43LS20FA37 exhibited the highest mechanical properties in terms of the ratio of compressive strength/ $E.CO_2$. Lastly, for such pastes the lower µS content seems to be delivering the most optimal results.

Table 5-4: Embodied CO_2 (kg/tonne) associated with strength of quaternary pastes

Formulation composition	**PC** $E.CO_2$	**LS** $E.CO_2$	**FA** $E.CO_2$	**µS** $E.CO_2$	**Total** $E.CO_2$	**Compres. Strength 28 days (MPa)**	**Strength/ $E.CO_2$ (MPa/ kg/tonne)**
PC60LS20FA20	558.0	6.4	0.8	0.0	565.2	51.3	0.09
PC55LS20FA20 +5%µS	511.5	6.4	0.8	0.7	519.4	42.7	0.08
PC50LS20FA20 +10%µS	466.5	6.4	0.8	1.4	475.1	19.1	0.04
PC43LS20FA37	401.2	6.4	1.5	0.0	409.1	39.5	**0.10**
PC43LS17FA37 +3%µS	401.2	5.4	1.5	0.4	408.5	30.0	0.07
PC43LS14FA37 +6%µS	401.2	4.5	1.5	0.8	408.0	24.8	0.06

5.3.5 Microstructural characterisation of PC43LS20FA37

The BSC micrographs of PC43LS20FA37 are shown in detail in Chapter 7. However, for completion another BSC image of PC43LS20FA37 at day 28 is presented below.

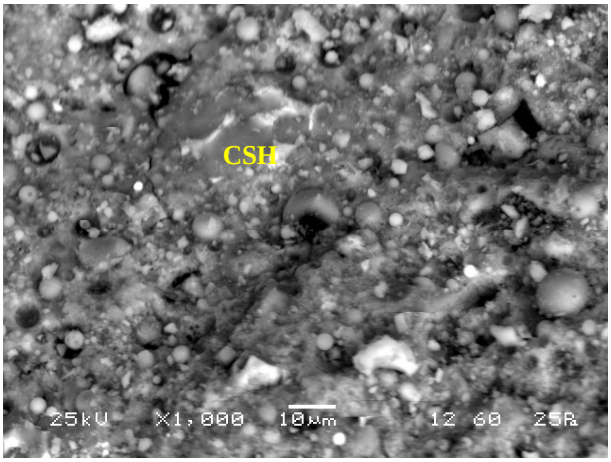

Figure 5-15: BSC micrograph of B10- PC43LS20FA37 28D – 1000x

A number of reacted and unreacted particles, can be observed as expected according to the TG analyses which lead to the conclusion that at this age almost half of the FA particles were still unreacted), $CaCO_3$ flakes and $Ca(OH)_2$ crystals were also present and areas of dense matter, believed to be C–S–H.

6 NANOSILICA MODIFIED TERNARY CEMENT PASTE FORMULATIONS

As discussed in Chapter 2, Portland limestone cements are broadly used in Europe and an upper limit of limestone content ranging from 21% to 35% by mass is specified by the Eurocodes (CEN, 2000). In these series, the envelope was pushed further with the total limestone content of the reference paste reaching 40% by mass. Part of the results extracted from this chapter, have been presented in 2014 International Concrete Sustainability Conference hosted by the MIT and published in the conference proceedings (Papatzani *et al.*, 2014). Another part of the results presented in this chapter have been translated in Russian and published in the Journal Cement and its Applications (Папатзани *et al.*, 2014).

6.1 Ternary cement formulations with LnS on PC60LS40

6.1.1 Introductory section

It should be noted that in these series of experiments only LnS was used, since the analyses carried out in Chapter 3, showed that LnS was a pure aqueous dispersion of nS, whereas GnS contained significant impurities and the certain carboxylates of indeterminate composition.

With the investigation carried out:

(i) the late age performance was identified
(ii) the optimum nS dosage was revealed
(iii) the stagnant compressive strength of the reference paste after 56 days was counterbalanced
(iv) the pozzolanic activity of LnS was confirmed

6.1.2 Compressive strength of cement pastes

One of the reasons for which cement pastes with higher nS contents were designed, was to maximize homogeneity within the pastes. This was expected to minimise the standard deviation (stdv) of compressive strength. The stdv was more significant for the two extreme LnS contents (in the order of 6.6 MPa) and lower for the 1.0% LnS content (approximately 4.9 MPa). The values of stdv are not shown in the Figure 6-1 for reasons of clarity.

Figure 6-1 shows the effect of nS on compressive strength for all pastes as measured between day 1 and day 170. According to previous research, the compressive strength of Portland limestone cements is inversely related to the LS content. Therefore, the more LS the less strong the cement paste at all ages (De Weerdt *et al.*, 2011b). The addition of LnS

led to an improvement in compressive strength in all cases when compared to the reference paste PC60LS40. This confirmed that nS contributed to the early strength gain, with the higher content (PC60LS38.5+1.5% nS) paste having the highest compressive strength gain at early ages, but the lower strength gain over 56 days of age. The 0.1% and 0.5% nS pastes exhibited the largest overall gain in compressive strength.

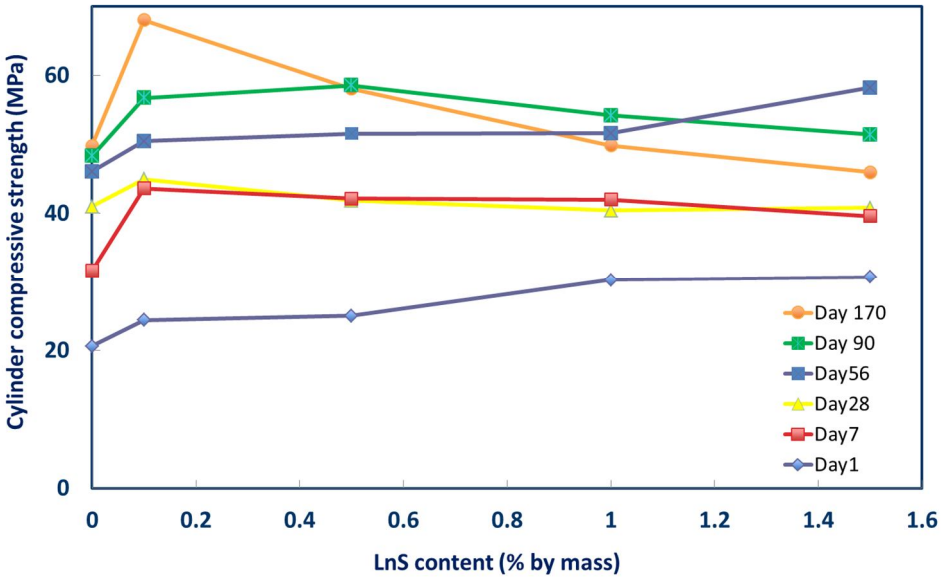

Figure 6-1: Cylinder compressive strength of LnS modified cement pastes based on PC60LS40

6.1.3 Thermogravimetric and crystallographic analyses of cement pastes

TGA results are focused on the mass losses between 100 °C and 200°C, where as discussed before C–S–H and ettringite decompose. TGA results within this temperature range are presented in Figure 6-2 until Figure 6-6 and indicate that the amount of C–S–H present in all LnS enhanced pastes was greater than that in PC60LS40. Hence, it became clear that nS must react with and consume $Ca(OH)_2$ at early ages, including the first 24 hours (Figure 6-2), to produce additional C–S–H in these pastes.

With respect to the $Ca(OH)_2$ content, for PC60LS40, containing only PC and LS, there was an increase in $Ca(OH)_2$ up to approximately 28 days beyond which it remained constant until day 56, before reducing slightly at day 90 and 170 (Figure 6-7). Interestingly the $Ca(OH)_2$ at 1 day was equal to 7.9% by mass, and equated to 75% of all $Ca(OH)_2$ produced by the 56 day old paste. There are evidences of slight carbonation consistent in most samples. It can be argued that for this particular PC, the production of $Ca(OH)_2$ resulting from hydration of alite and belite components of the Portland cement took place rapidly and essentially was completed in the first 28 days, as there was no significant $Ca(OH)_2$ formation after this time. It is worth noting that, $Ca(OH)_2$ consumption amongst the pastes containing over 0.5% LnS was practically the same at day 28, providing further evidence that greater than 0.5% LnS addition will not be able to react in such pastes. Furthermore,

consumption of $Ca(OH)_2$ was practically stabilized by 28 days for the 1% LnS addition and by day 56 for the 1.5% LnS addition, providing a first indication of a limit reached. On the contrary, both of the lower LnS additions, the 0.1% and the 0.5%, exhibited a further 33% consumption of $Ca(OH)_2$ at day 170, relative to day 90. Overall, when LnS was present in the paste the amount of $Ca(OH)_2$ at each age was lower than that of the reference mix (PC60LS40) and the reduction in the $Ca(OH)_2$ content is prominent up to day 28. Given that in PC60LS40 there was no significant $Ca(OH)_2$ formation after 28 days, then it is reasonable to assume that the colloidal LnS has been converted to C–S–H and that there was no further pozzolanic activity after 28 days for the higher LnS content pastes. The rapid consumption of small proportions of LnS has been observed by a number of authors and is unsurprising given the high $Ca(OH)_2$/LnS ratio and the high surface area of SiO_2 available for reactions.

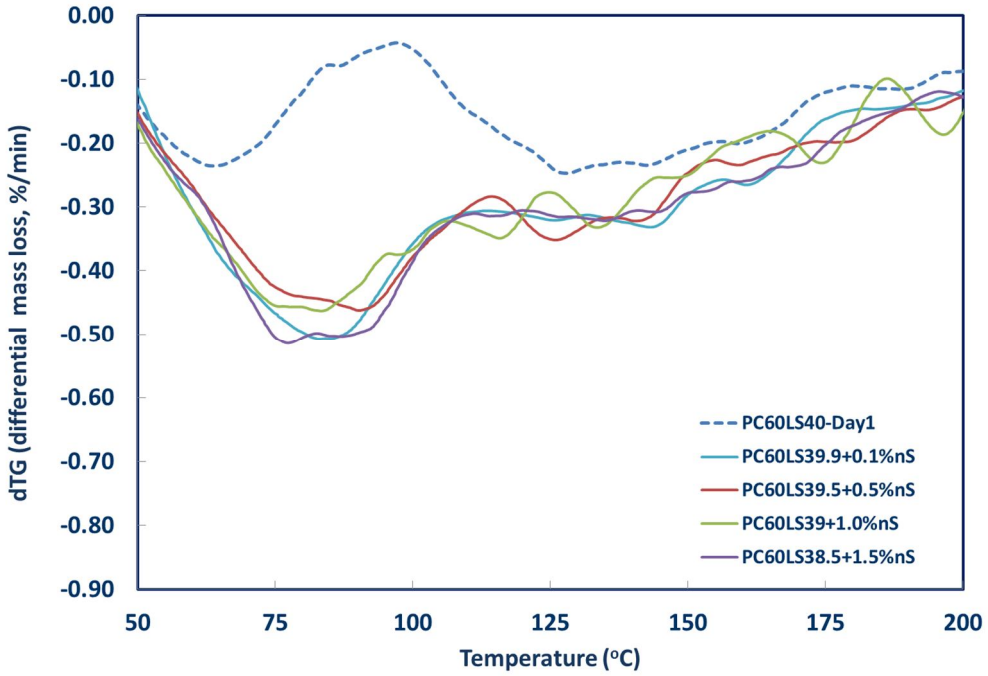

Figure 6-2: Differential mass loss of LnS modified cement pastes based on PC60LS40 between 100-200°C at Day 1

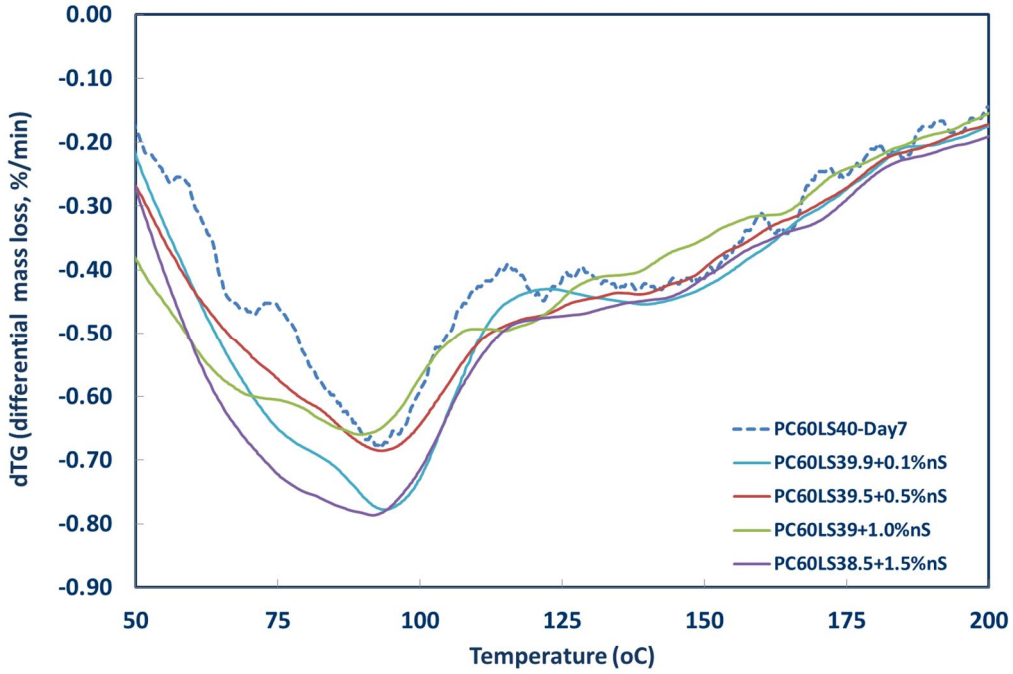

Figure 6-3: Differential mass loss of LnS modified cement pastes based on PC60LS40 between 100-200°C at Day 7

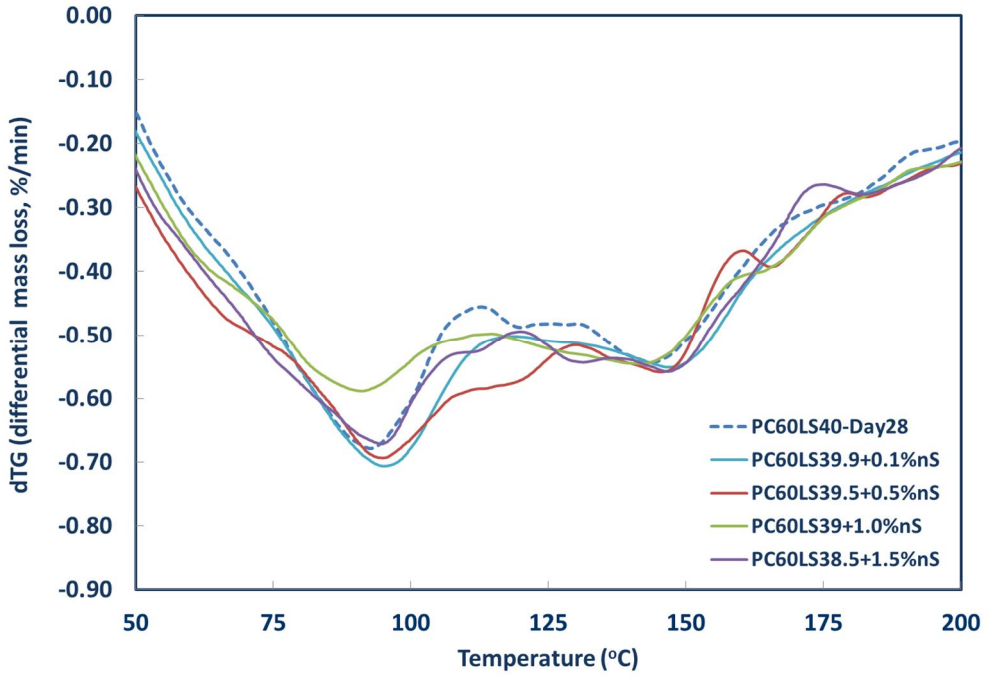

Figure 6-4: Differential mass loss of LnS modified cement pastes based on PC60LS40 between 100-200°C at Day 28

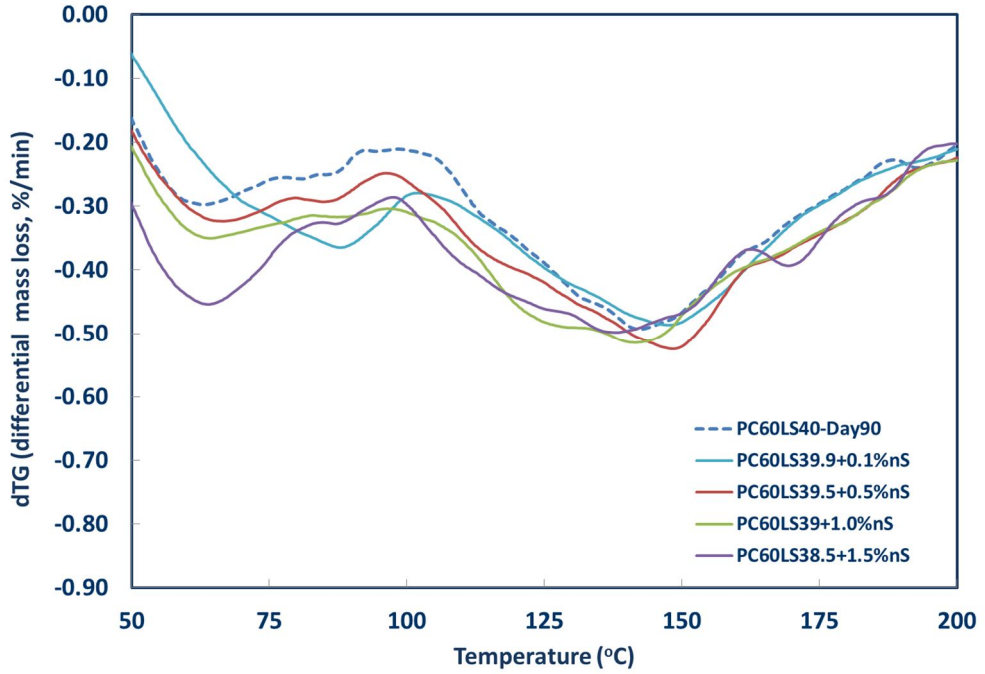

Figure 6-5: Differential mass loss of LnS modified cement pastes based on PC60LS40 between 100-200°C at Day 90

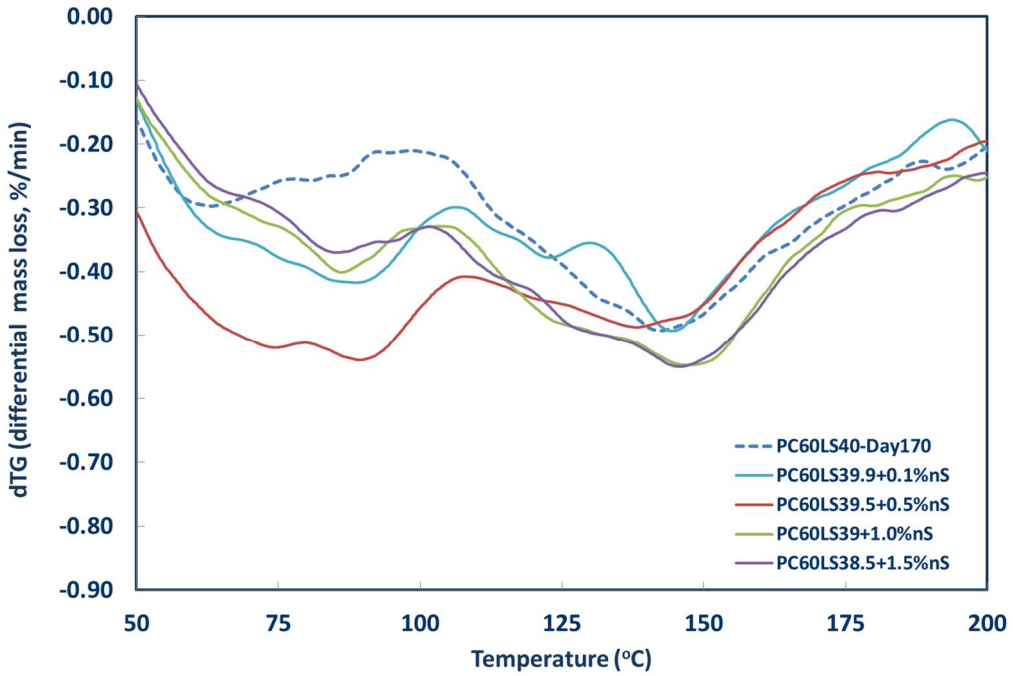

Figure 6-6: Differential mass loss of LnS modified cement pastes based on PC60LS40 between 100-200°C at Day 170

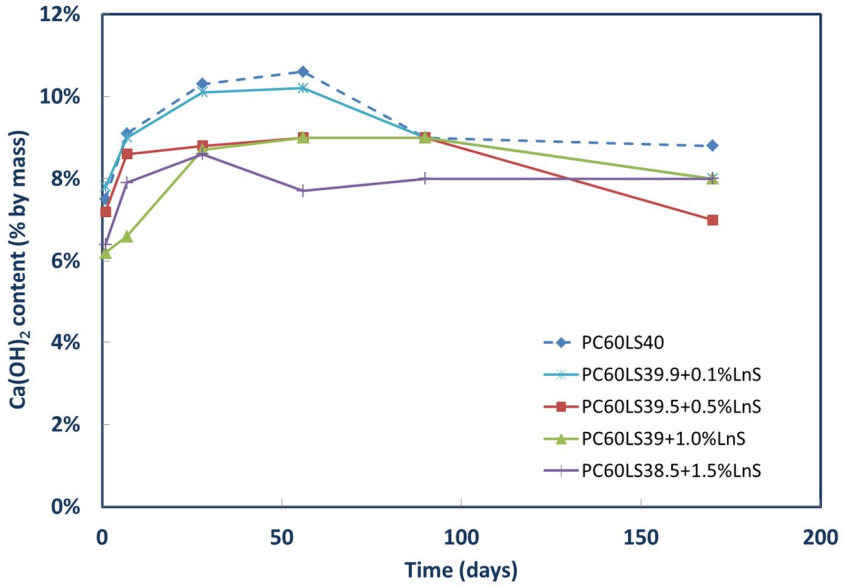

Figure 6-7: $Ca(OH)_2$ content of LnS modified cement pastes based on PC60LS40

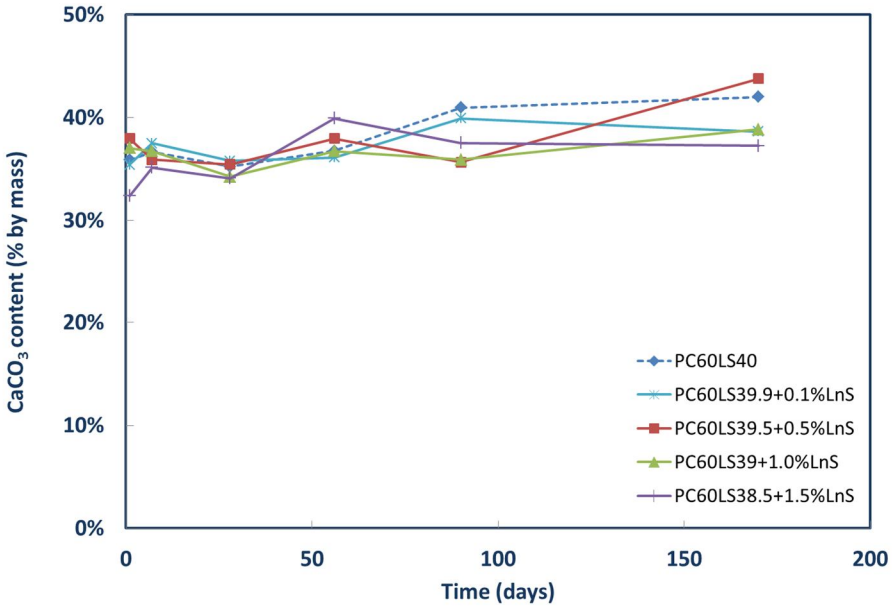

Figure 6-8: $CaCO_3$ content of LnS modified cement pastes based on PC60LS40

The chemical effect reported due to the presence of high contents of LS in the reference paste, which is the formation of hemicarbonate with a diffraction peak at 10.8°2θ or calcium monocarbonate hydrate with a diffraction peak at 11.7°2θ (De Weerdt *et al.*, 2011b; Lothenbach *et al.*, 2008) was not confirmed in this research by the XRD analyses.

However, the consumption of $Ca(OH)_2$ for the production of C–S–H (hump marked within red circle) was observed by the XRD as well, although more evident after day 7 (Figure 6-9 to Figure 6-12). Lastly, the immediate reactivity of LnS was also shown in Figure 6-9 in

which the formation of additional C–S–H can be observed at day 1, when the reference paste had no C–S–H to show.

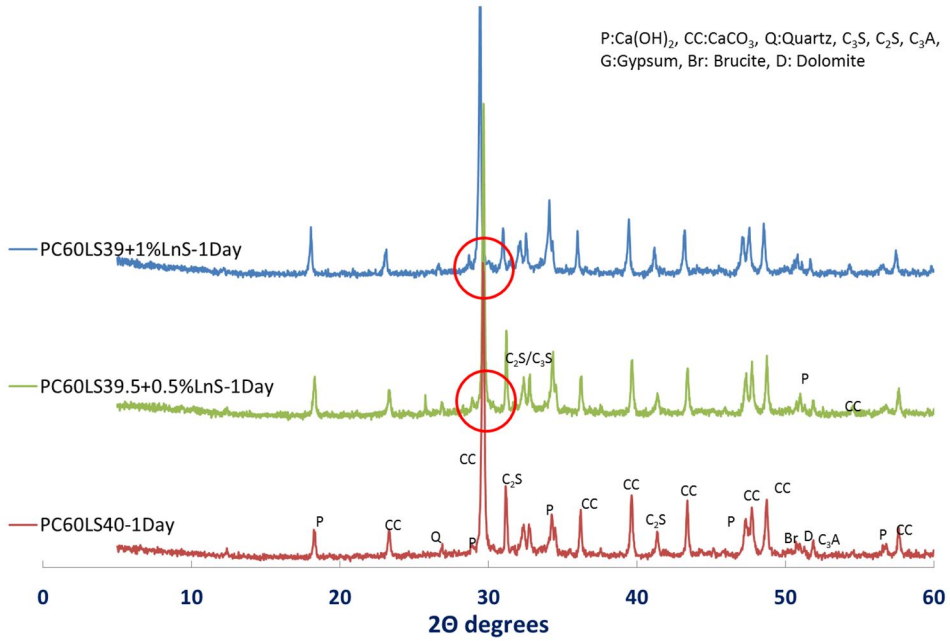

Figure 6-9: XRD pattern of LnS modified cement pastes based on PC60LS40 at Day 1

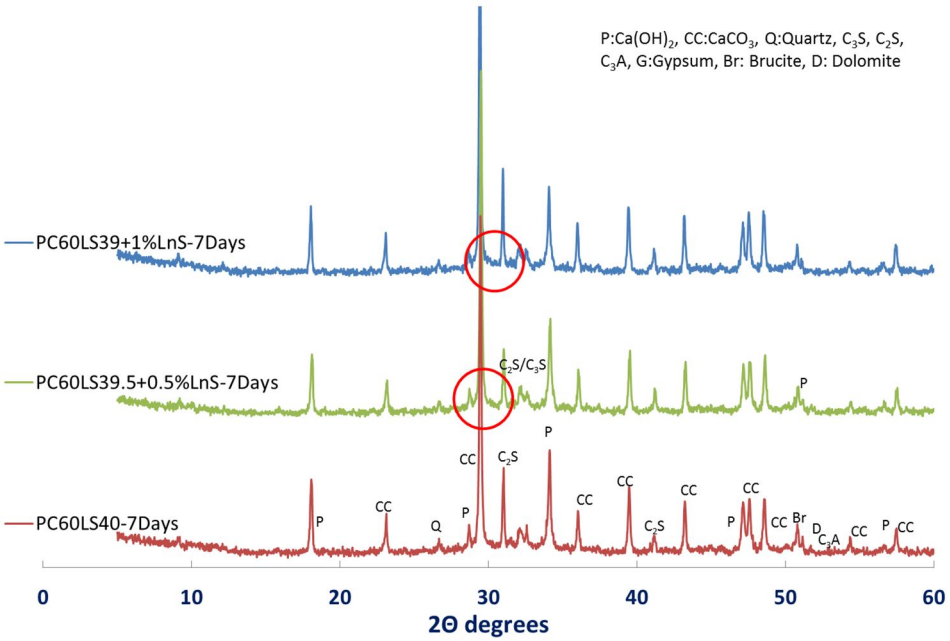

Figure 6-10: XRD pattern of LnS modified cement pastes based on PC60LS40 at Day 7

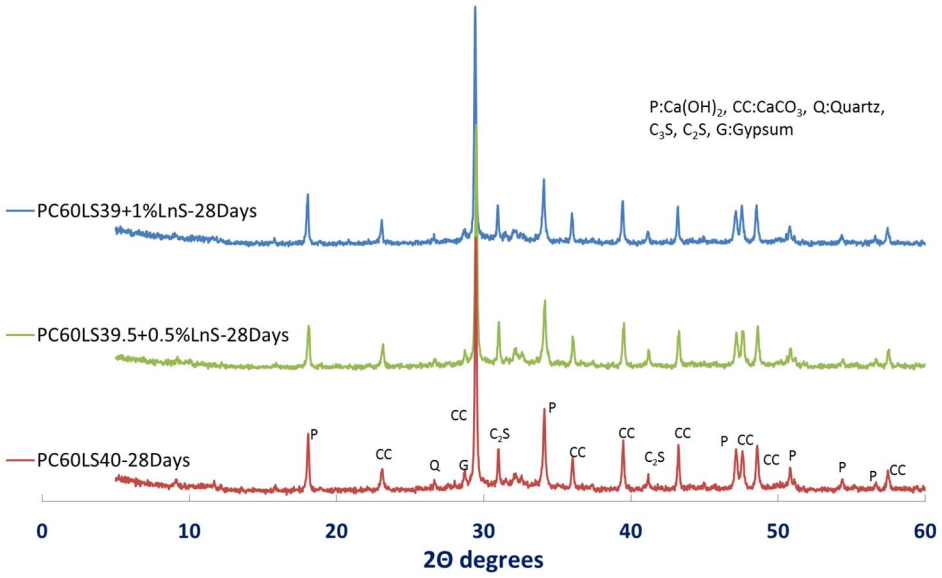

Figure 6-11: XRD pattern of LnS modified cement pastes based on PC60LS40 at Day 28

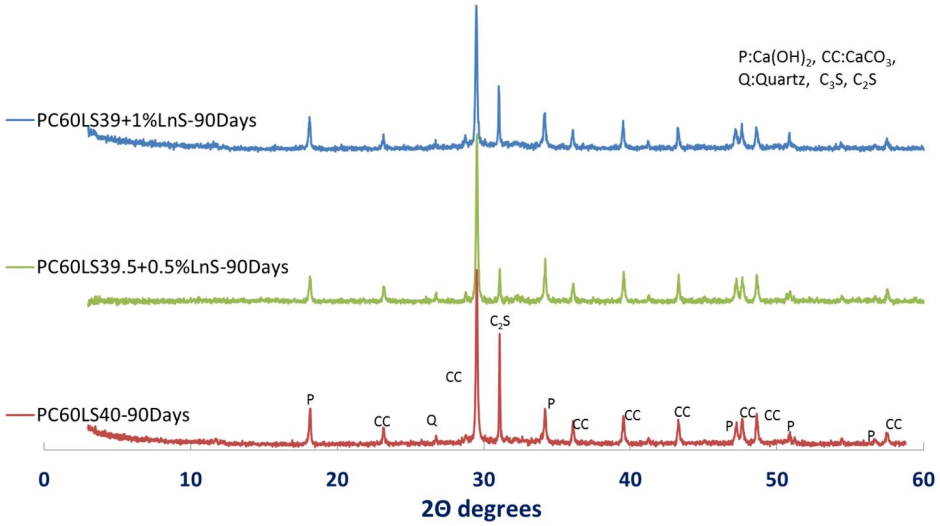

Figure 6-12: XRD pattern of LnS modified cement pastes based on PC60LS40 at Day 90

6.1.4 Microstructural characterisation of cement pastes

The microstructure of PC60LS40, PC60LS39.5+0.5%nS and PC60LS39+1.0%nS was investigated after day 1, 28 and 90, which according to the TGA and compressive strength analyses seemed to be the most critical, as shown from Figure 6-13 to Figure 6-24. All SEM images were backscattered (BSC) and were taken at various magnifications. In most cases, day 1 is presented next to day 90, rather than day 28, to make any differences more evident.

To begin with, at day 1 as depicted in Figure 6-13, Figure 6-15 and Figure 6-19, the nS enhanced pastes exhibited patches of what may be considered denser C–S–H areas compared to PC60LS40. These areas are circled in white. Furthermore, the morphology observed in PC60LS40, resembles more PC60LS39.5+0.5%LnS than PC60LS39+1.0%LnS. In the former, the structure is similar to PC60LS40 in terms of visible porosity and amount of $Ca(OH)_2$ crystals, whereas in the latter, the paste looked denser with less $Ca(OH)_2$ crystals present, an observation correlating well with the formerly presented TGA results.

At day 28, PC60LS40 (Figure 6-14) seemed more densified, with larger areas of C–S–H present, whereas the morphology between the two nS enhanced pastes exhibits a greater similarity. $Ca(OH)_2$ crystals are more prominent in the higher content nS paste, indicating that nS optimum concentration lays between 0.1% and 0.5%, consuming more $Ca(OH)_2$ to form additional C–S–H, supported by TGA and compressive strength results. Particularly in Figure 6-18-D, it can be noticed that the $Ca(OH)_2$ nest is surrounded by denser C–S–H patches (some areas were indicatively circled), possibly rendering its accessibility by nS, difficult. It should be noted that overall, the nS enhanced pastes demonstrated a visibly less porous paste. The observations on the 28 day micrographs, again, correlated well with the TGA results, presented.

Although on BSC-SEM day 1 and day 90 showed subtle differences for the same magnifications, the FESEM micrographs of the 0.5% and 1.0% LnS modified pastes, seemed significantly denser at day 90 than at day 1 (Figure 6-21 to Figure 6-24).

Furthermore, in the FESEM micrographs different formations of the hydration products have been captured. For example intertwined honey comb-like and needle-like hydration products have covered the $Ca(OH)_2$ crystals (Figure 6-21-A to C and Figure 6-23-A to C) already by day 28. As hydration advanced, by day 90, all voids seem to have been filled by the hydration products and the paste densified even further (Figure 6-22-A to C and Figure 6-24-A to C).

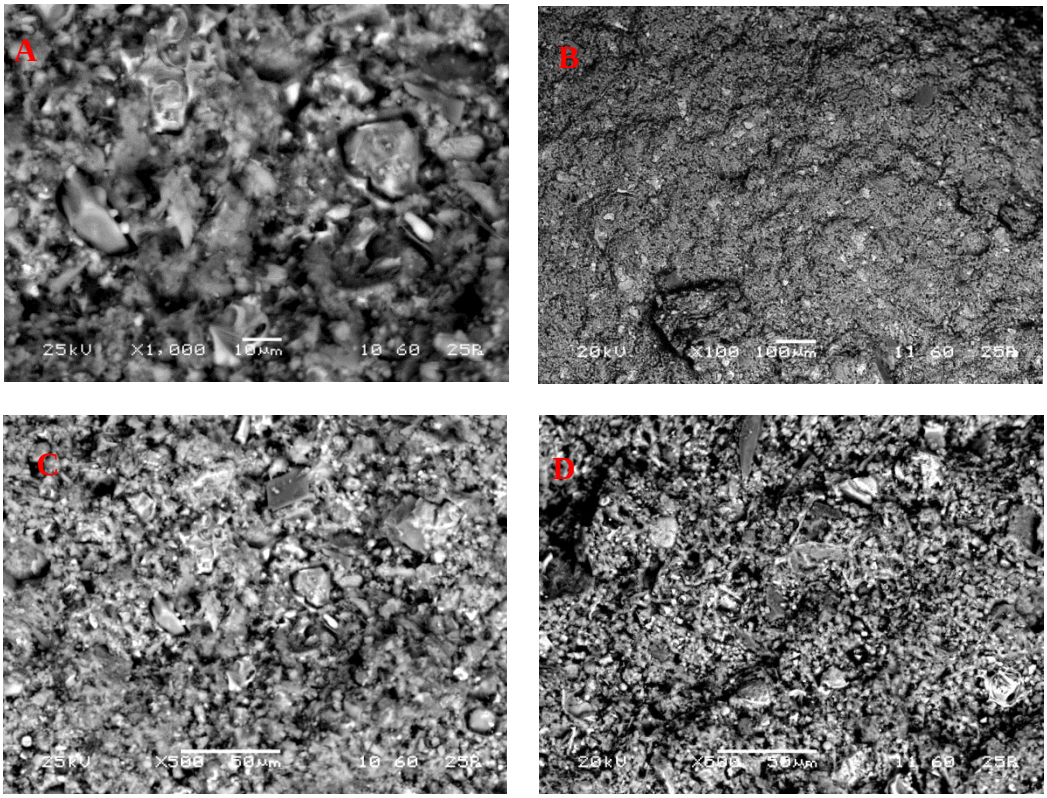

Figure 6-13: BSC micrograph of PC60LS40 - 1D – (A) 1000x, (B) 100x (C) and (D), 500x

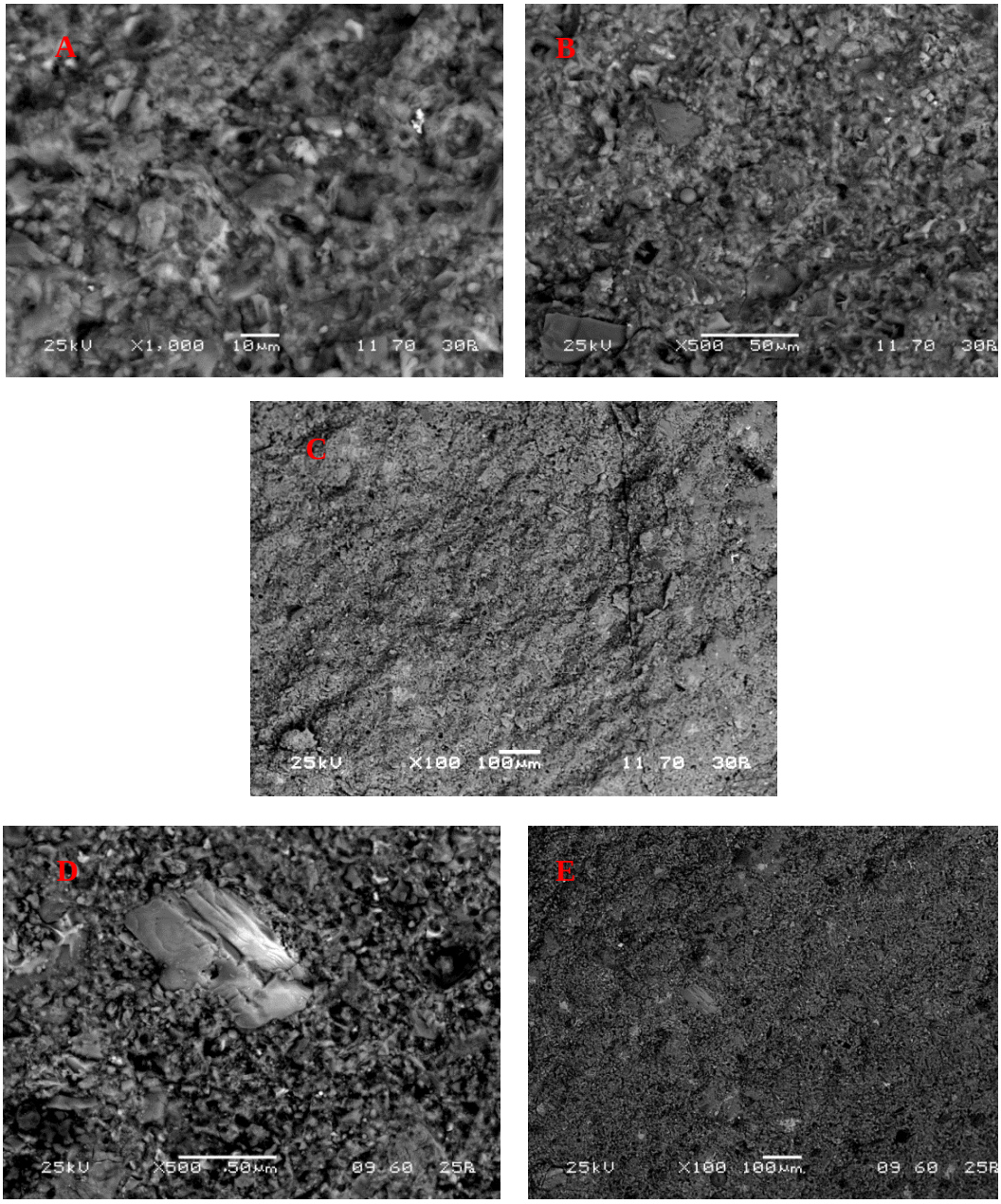

Figure 6-14: BSC micrograph of PC60LS40 - (A) 28D –1000x, (B) 28D –500x, (28D – 100x, (D) 90D – 500x and (E) 90D – 100x

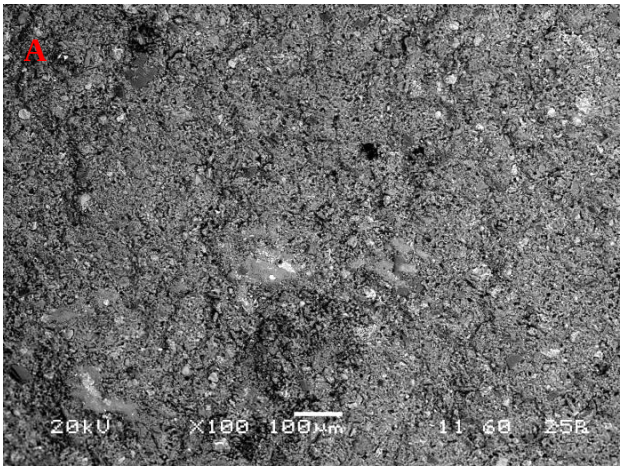

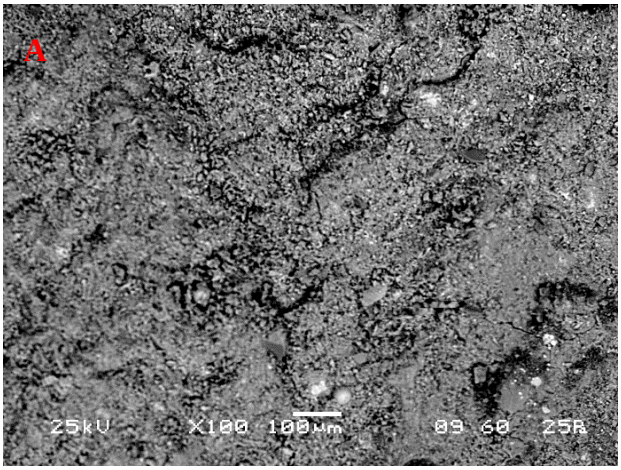

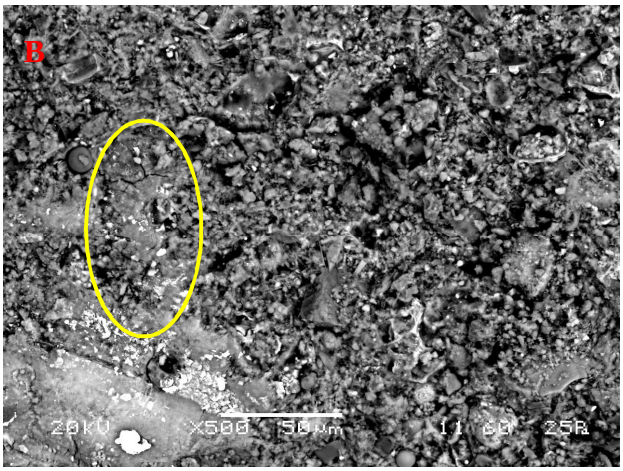

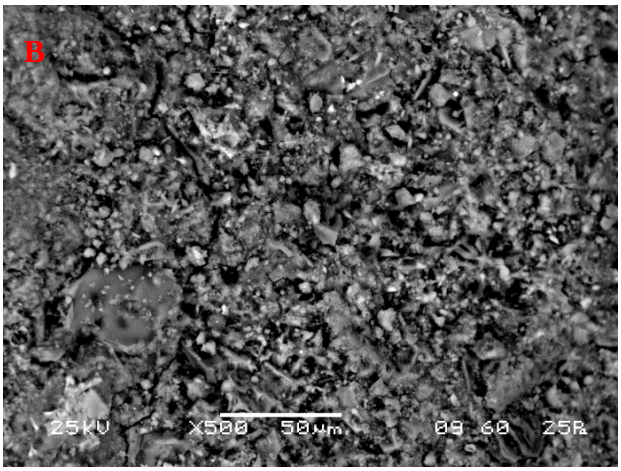

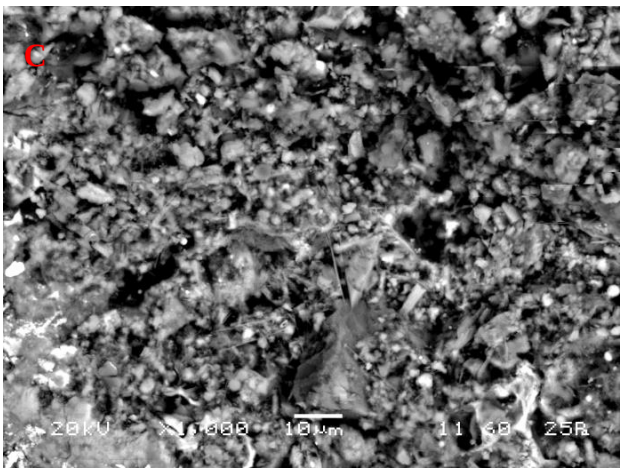

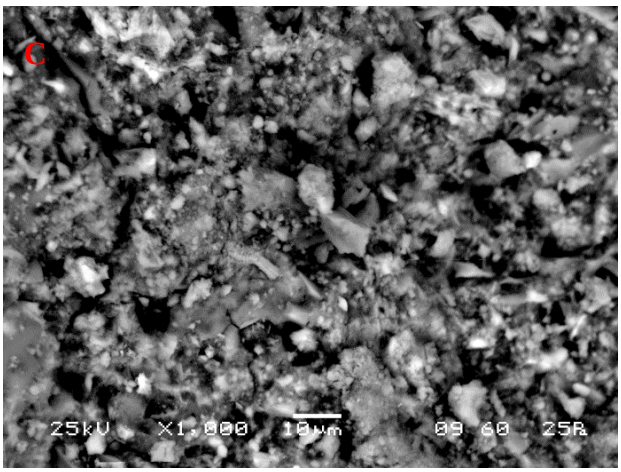

Figure 6-15: BSC micrograph of PC60LS39.5+0.5%nS -1D - (A)100x, (B) 500x and (C) 1000x

Figure 6-16: BSC micrograph of PC60LS39.5+0.5%nS -90D - (A)100x, (B) 500x and (C) 1000x

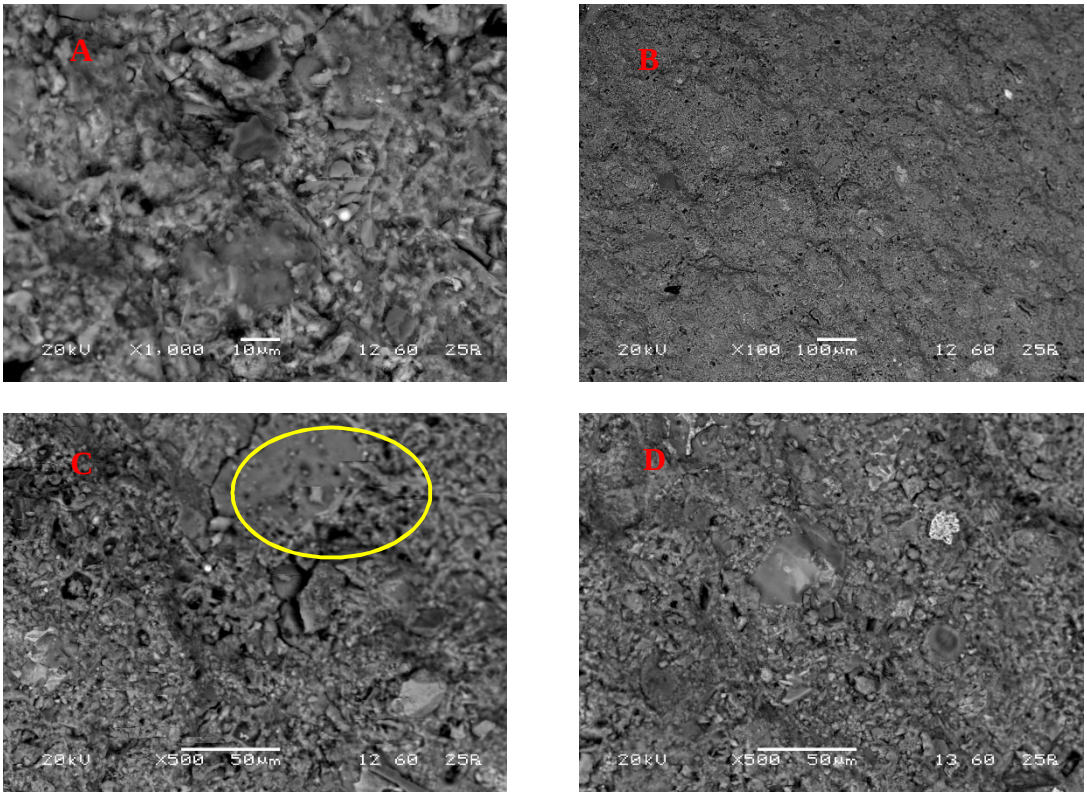

Figure 6-17: BSC micrograph of PC60LS39.5+0.5%nS -28D – (A) 1000x, (B) 100x (C) & (D), 500x

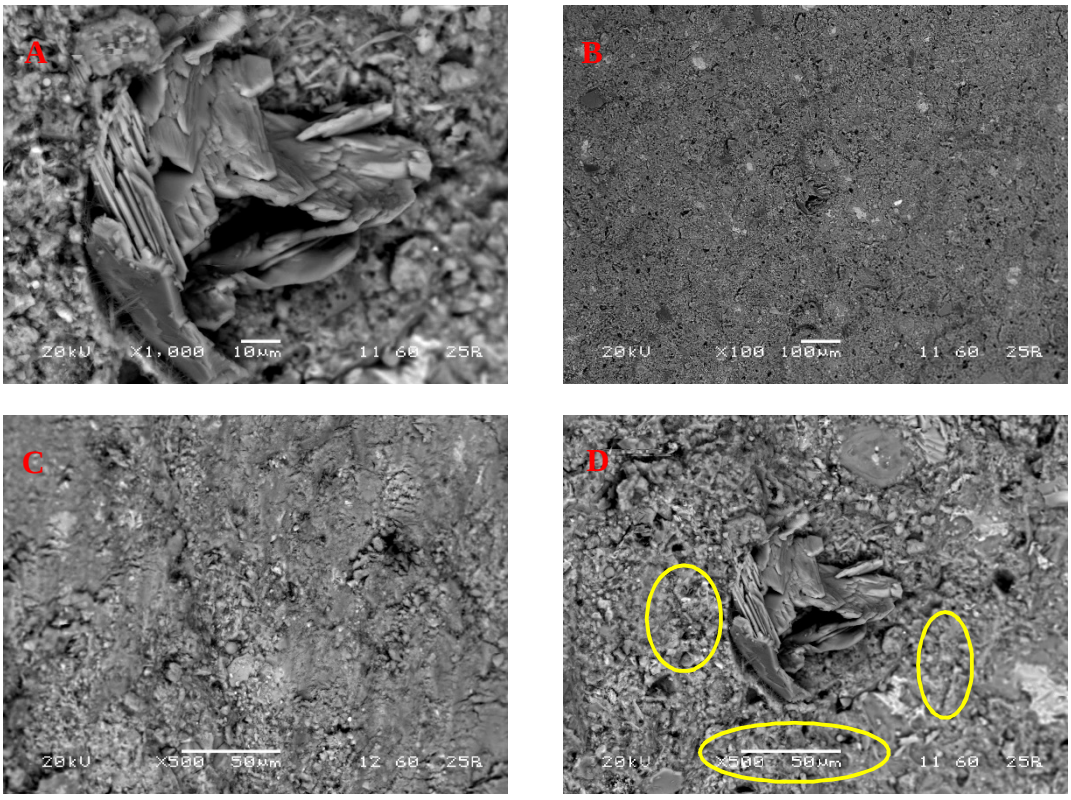

Figure 6-18: BSC micrograph of PC60LS39+1.0%nS -28D–(A)1000x, (B)100x,(C)& (D), 500x

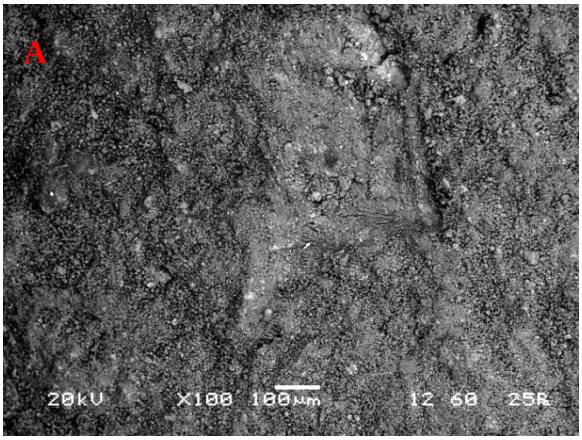

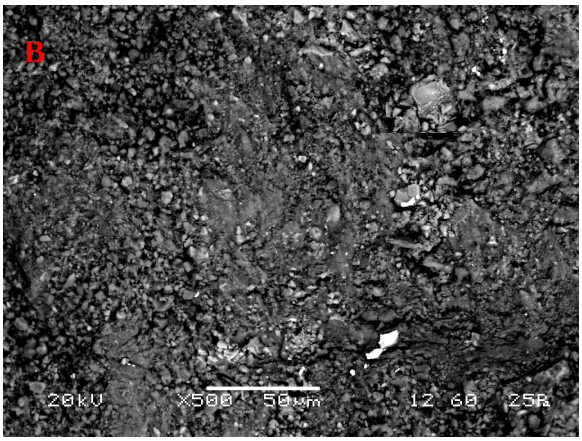

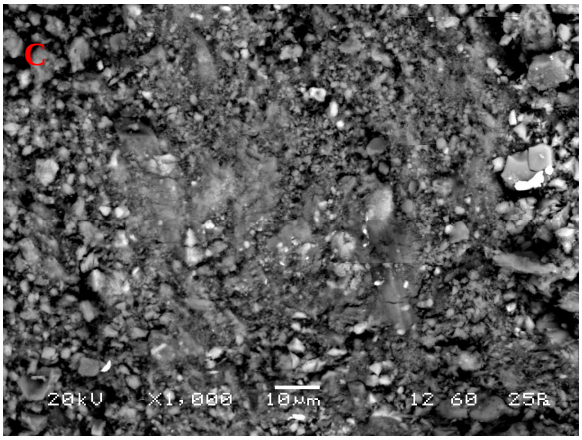

Figure 6-19: BSC micrograph of PC60LS39+1%nS -1D - (A)100x, (B) 500x and (C) 1000x

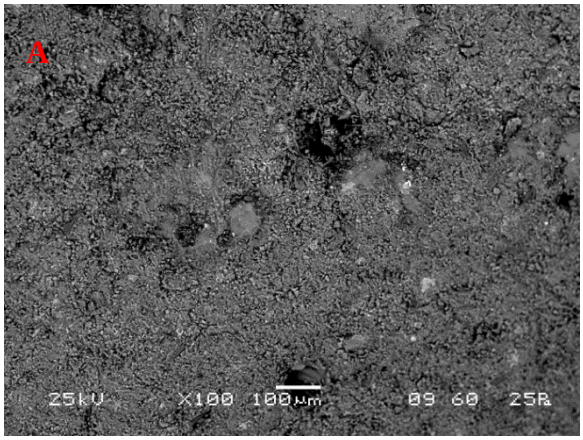

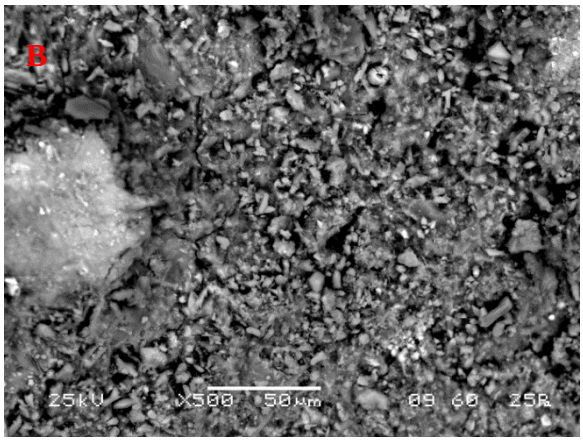

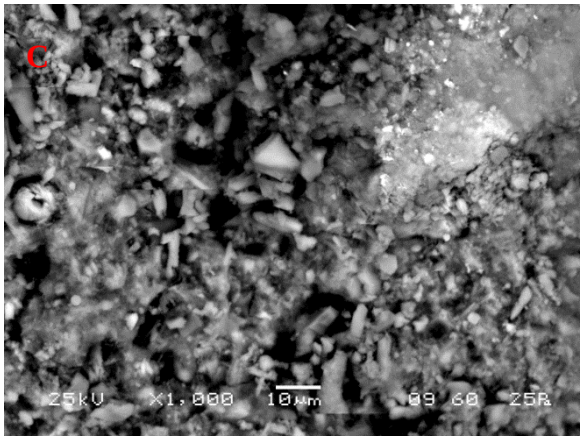

Figure 6-20: BSC micrograph of PC60LS39+1%nS -90D - (A)100x, (B) 500x and (C) 1000x

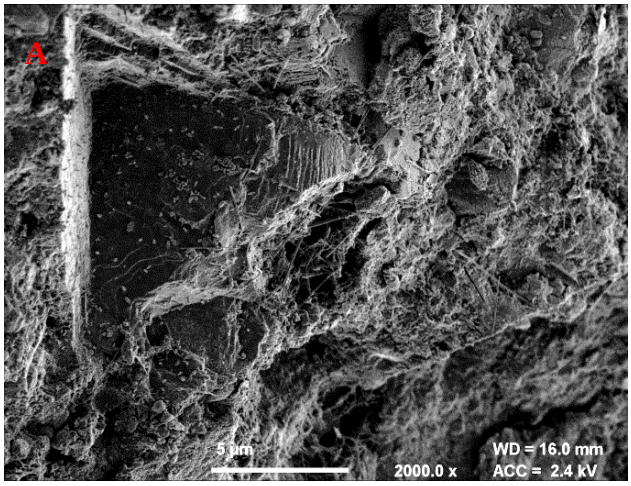

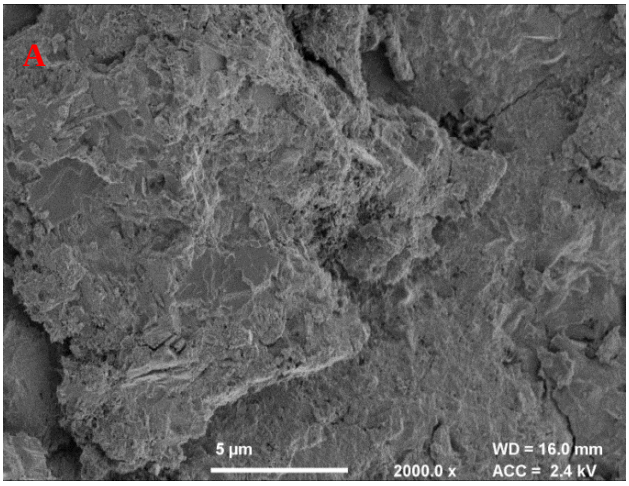

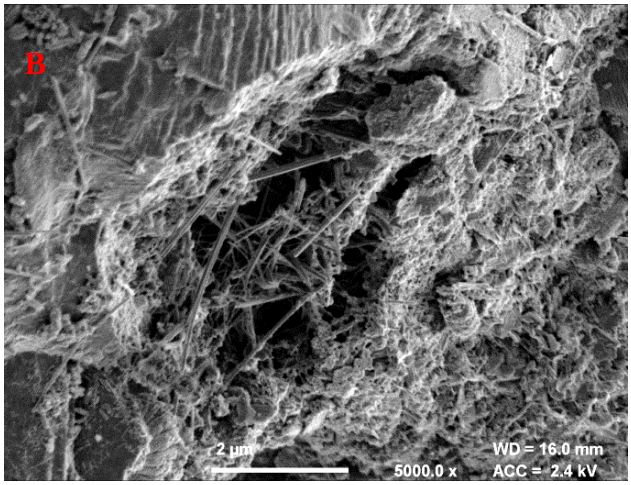

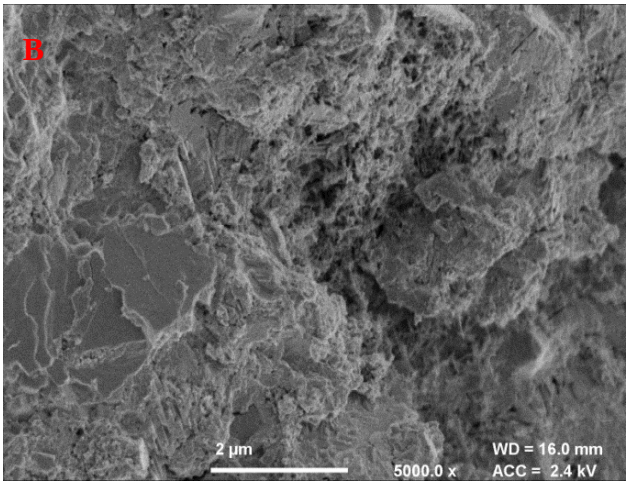

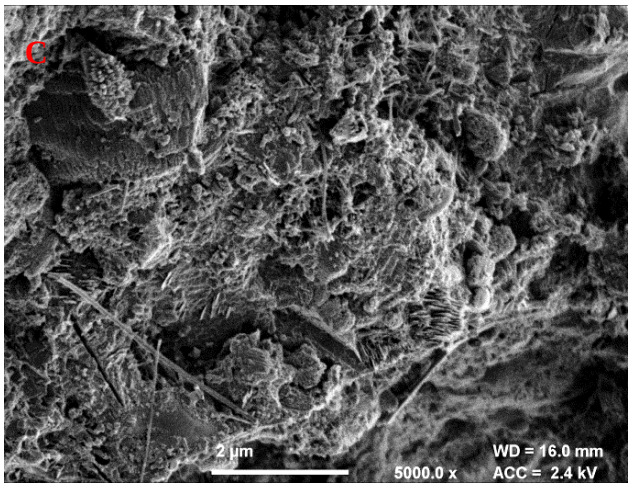

Figure 6-21: FESEM image of PC60LS39.5+0.5%nS-28D – (A) 2000x, (B) & (C) 5000x

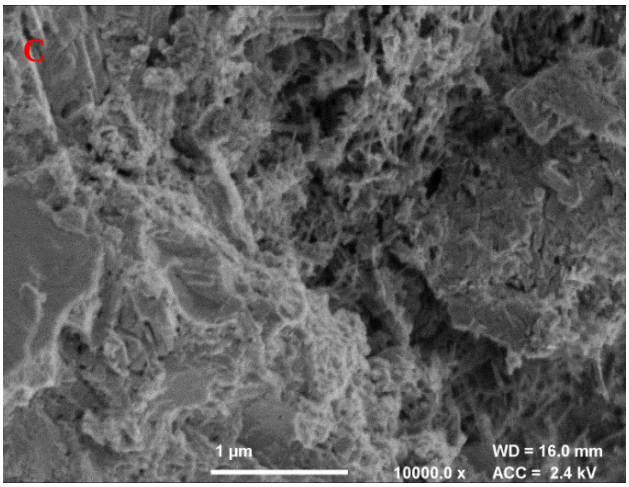

Figure 6-22: FESEM image of PC60LS39.5+0.5%nS -90D – (A) 2000x, (B) 5000x & (C) 10000x

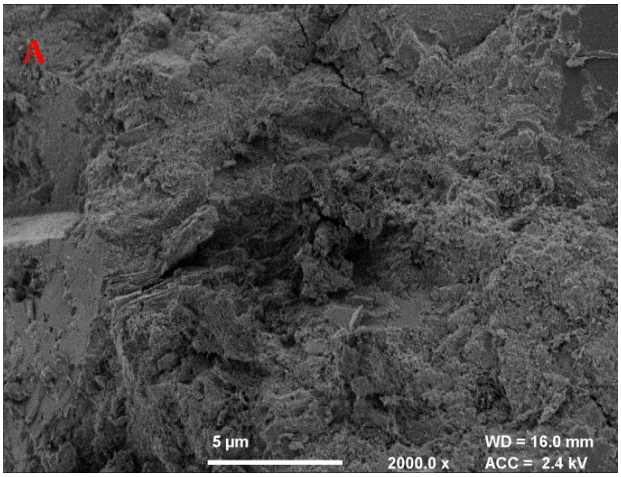

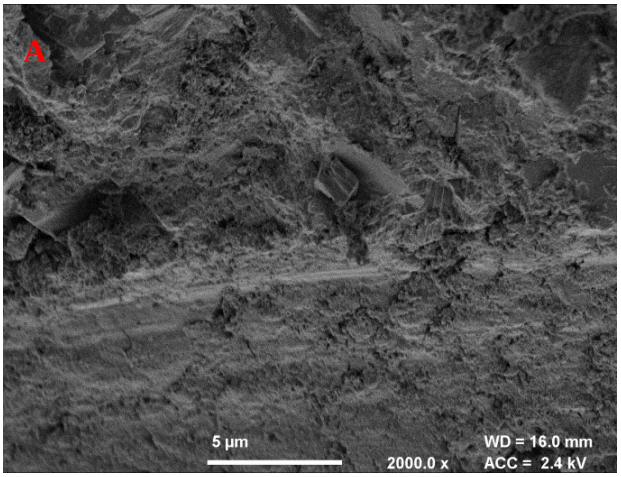

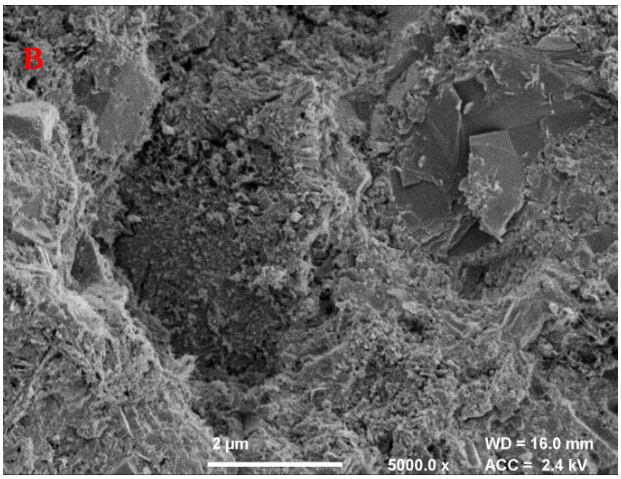

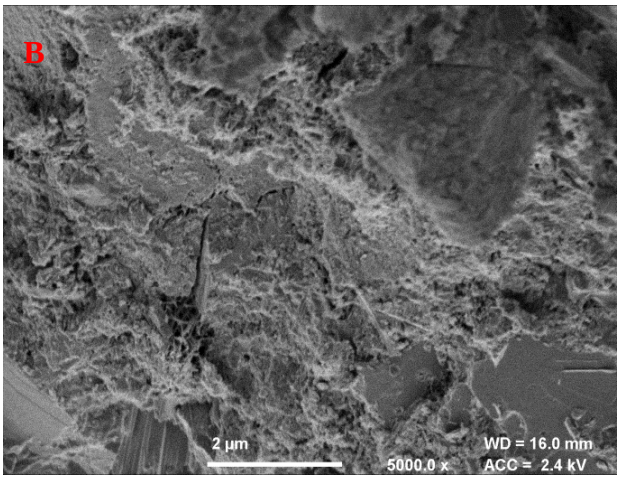

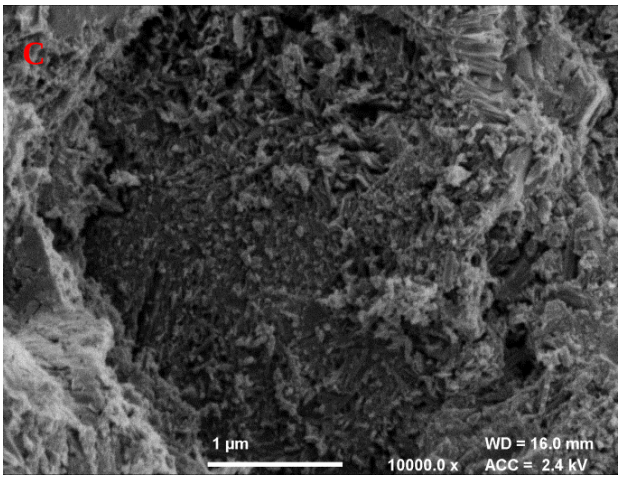

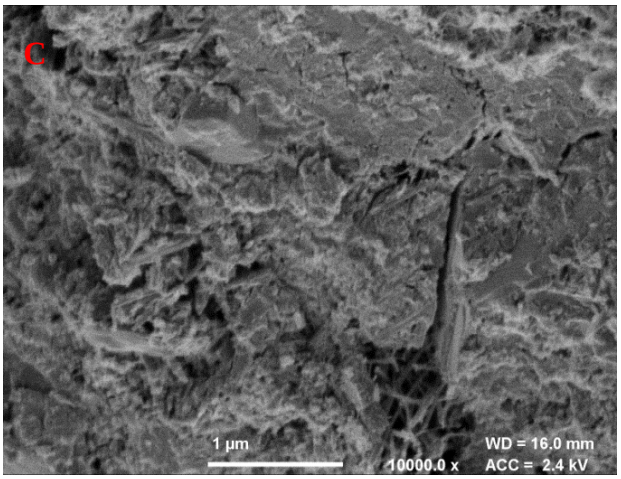

Figure 6-23: FESEM image of PC60LS39+1%nS-28D – (A) 2000x, (B) 5000x & (C) 10000x

Figure 6-24: FESEM image of PC60LS39+1%nS-90D –(A) 2000x, (B) 5000x & (C) 10000x

6.1.5 Relative density and pore structure

Knowing that the theoretical maximum density of PC is 3250 kg/m^3, that of LS is 2800 kg/m^3 and of water 1000 kg/m^3 the theoretical maximum density for 60% PC and 40% LS at w/b = 0.3 was found to be equal to 2072 kg/m^3. Therefore, judging by the late age (after month 6) relative density measured (Figure 6-25) the reference paste did not seem to contain significant pores. Practically there is no difference between the samples. Fluctuations in density values could be attributed to the carbonation of the samples. As also discussed with regards to the micrographs the 1.0% LnS modified paste, which seemed to provide denser morphology, also provided the highest relative density, surpassing the reference paste. The next best performance was given by the lower percentage of replacement, bringing together all the analyses presented above. The visual pores observed in section 4.5.1 of Chapter 4 for the highest nS content are further justified by Figure 6-25. In essence, due to the standard deviation, theoretically, all samples could have the same relative density if the compaction could be optimized. For this, it is the author's opinion that superplasticizers should be used when higher nS contents are considered.

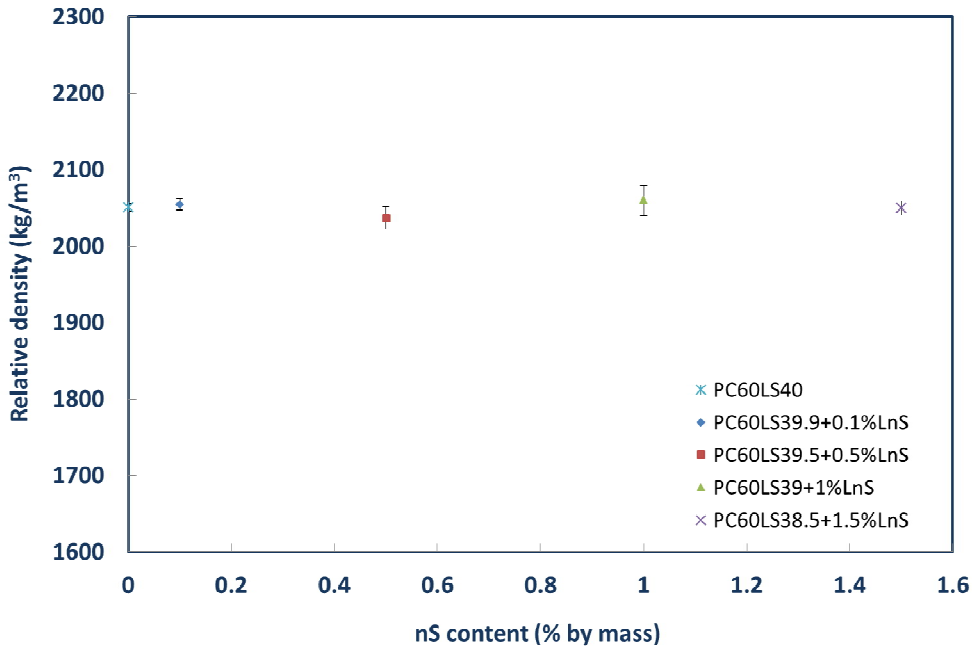

Figure 6-25: Long-term relative density of LnS modified cement pastes

6.1.6 Further discussion and conclusions

Based on the results shown in Chapter 6, it appears reasonable to assume that the nS used in these series was a pozzolanic material that consumed $Ca(OH)_2$, and that the additional products resulting from this pozzolanic activity, most probably C–S–H, gave rise to improvements in early age strength. Furthermore, these strength improvements were maintained at later ages, for the lower (0.1% and 0.5%) nS content pastes. Consequently, nS does not act simply as an accelerator of reactions but plays a role in the development of an enhanced microstructure. There has been much discussion in the literature on the role of nS as providing a nucleation point for C–S–H reactions. Given the research reported in this paper and the significant pozzolanic activity observed, it was not been possible to distinguish between the two mechanisms (nucleation sites/seeding agents and pozzolanic activity) in the early ages. It is very likely that the two mechanisms have taken place at the same time. Further information on the nucleation effects of nS on similar pastes is described in the work by Calabria-Holley *et al.* (2014).

Judging by the TGA and compressive strength results, it can be assumed that a maximum nS content has been identified, particularly with respect to later age performance. It seems reasonable to suggest that nS additions of less than 0.5% by mass of solids can improve early and late age compressive strength of cement pastes.

Clearly more research is required, but these results potentially provide support to the argument that early-age pozzolanic reactions between nS and $Ca(OH)_2$ may inhibit pozzolanic reactions involving higher amount of nS. The reason for this is that nS reacts instantly with $Ca(OH)_2$ produced by cement hydration, forming dense C-S-H. These dense C–S–H areas are formed around unreacted cement particles and $Ca(OH)_2$ particles, acting as ion penetration barriers, impeding homogeneous hydration of the cement paste and consequently further production of $Ca(OH)_2$. As an effect, only a proportion of $Ca(OH)_2$ is available to the pozzolanic reaction, and furthermore, the amount of $Ca(OH)_2$ produced could reduce as nS content increases.

7 NANOSILICA MODIFIED COMPOSITE CEMENT PASTE FORMULATIONS

In this chapter, two different reference pastes were nanomodified. The correlation of microstructural characteristics with compressive strength at the macroscale was particularly interesting in light of a newly introduced ratio for the design of composite cement paste formulations; that of PC to FA content. The importance of this ratio will be demonstrated in this chapter with the analysis of the two series of experiments with respect to this matter. The former analyses were carried out on reference paste PC60LS20FA20 and is presented in section 7.1, for PC/FA = 3. The latter analyses were carried out on reference paste PC43LS20FA37 in sections 7.2 –7.6 representing a much lower ratio, that of PC/FA = 1.16. Lastly, it should be noted that the behaviour of the 0.5% GnS and the 0.5% LnS modified pastes based on PC43LS20FA37 has also been analysed in terms of C–S–H network formation, as studied by SEM/EDX and FTIR (Calabria-Holley *et al.*, 2014). Some of the results presented in this chapter have been compared with the results of PC60LS40 LnS modified pastes and have already been published (Papatzani *et al.*, 2014).

7.1 Quaternary cement formulations with GnS on PC60LS20FA20

7.1.1 Introductory section

Three starting pastes were produced through the GnS modification of PC60LS20FA20. The results presented in this section constituted a preliminary study on the application of GnS in blended cement pastes, as the presence of higher quantity of PC facilitated the interpretation of the results. This study was necessary, since as discussed in Chapter 3 there were some unidentified chemicals in the GnS dispersion, possibly carboxylates. For this reason, apart from the w/b ratio of 0.3 which has been studied throughout this thesis, two lower ones were investigated in section 7.1; w/b 0.2 and 0.22. The main results are presented below.

7.1.2 Compressive strength of PC/FA=3 GnS modified pastes

As can be seen in Figure 7-1 for the same amount of GnS (0.3% by mass) the higher w/b ratio proved to be detrimental. Furthermore, for the lower w/b ratios the higher GnS content exhibited a better performance than the reference paste for the first 28 days. It should be noted at this point, that during the production of the specimens, the ones with the higher w/b ratio exhibited a prolonged setting.

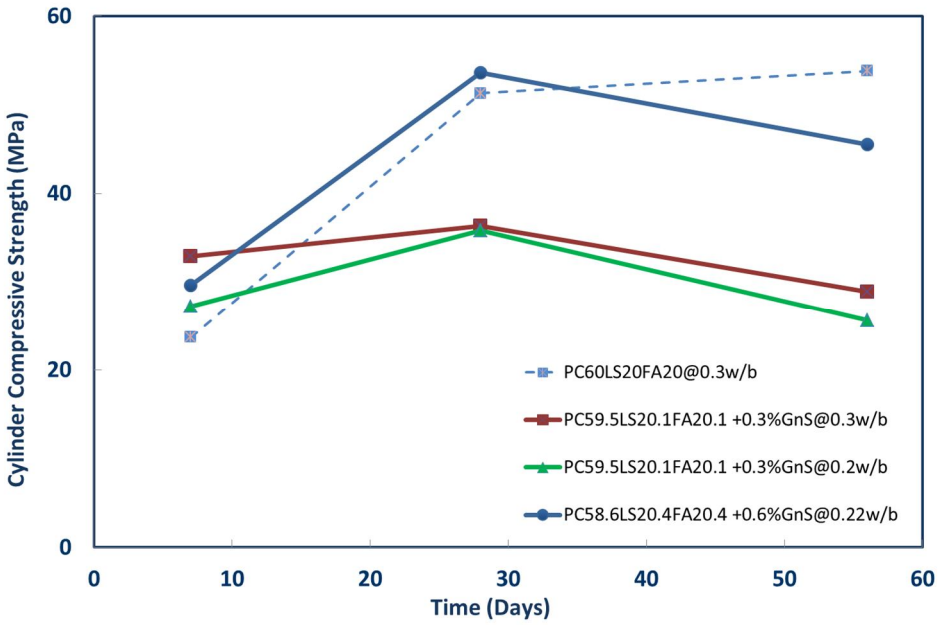

Figure 7-1: Cylinder compressive strength of GnS modified cement pastes based on PC60LS20FA20

7.1.3 Thermogravimetric analyses of cement pastes

As can be observed in Figure 7-2 the $Ca(OH)_2$ content of the reference paste did not change significantly with time except for day 1 to day 7. It can be noted that paste PC59.5LS20.1FA20.1+0.3%GnS@0.3w/b, which did not seem to have consumed any significant quantities of $Ca(OH)_2$ also exhibited the lowest compressive strength. It is also interesting to note that the rate of $Ca(OH)_2$ consumption increased drastically after day 28, presumably because the hydration of PC produced additional quantities of $Ca(OH)_2$ available for reactions. The gradient of the line representing the rate of strength gain of paste PC59.5LS20.1FA20.1 +0.3%GnS @ 0.3w/b was greater, as expected since more water was available for the hydration of cement, which apparently advanced after day 28 in all three GnS modified pastes. Lastly, the $CaCO_3$ content was dramatically increased in the GnS modified pastes (Figure 7-3).

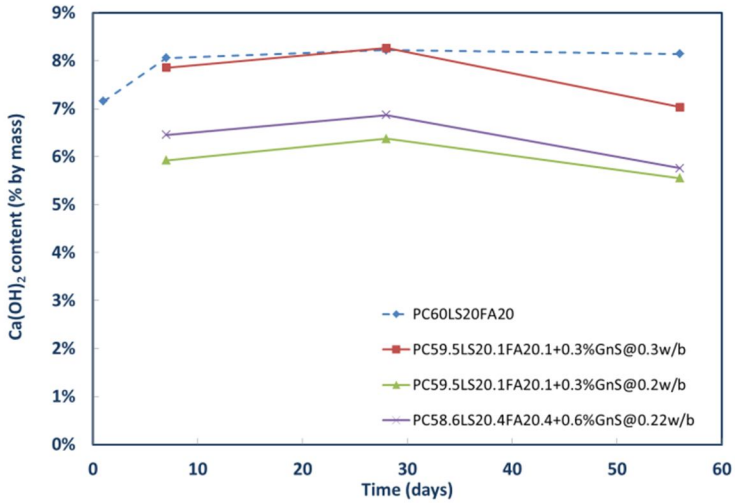

Figure 7-2: $Ca(OH)_2$ content of GnS modified cement pastes based on PC60LS20FA20

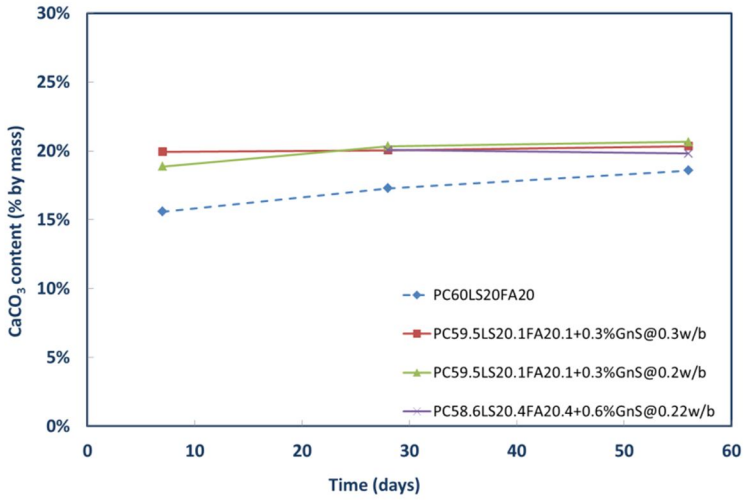

Figure 7-3: $CaCO_3$ content of GnS modified cement pastes based on PC60LS20FA20

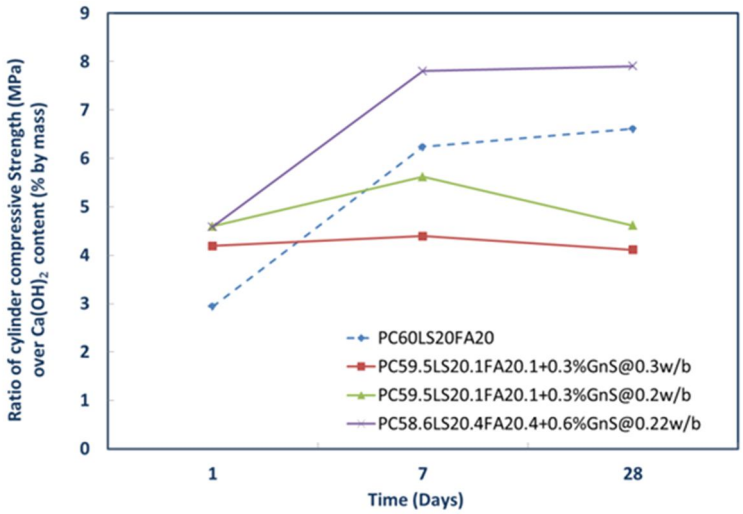

Figure 7-4: Relating microscale characteristics to macroscale performance of GnS modified cement pastes based on PC60LS20FA20

7.1.4 Microstructural characterisation of cement pastes

The microstructural investigations confirmed the findings of compressive strength testing and thermogravimetric analyses. In all cases, denser patches of what seems to be C–S–H were identified and marked (CSH for brevity and clarity), indicatively. In contrast, $Ca(OH)_2$ crystals were not noticeable. It is acknowledged, though, that they may be encapsulated by C–S–H and therefore, not individually visible. Although at a first glance the micrographs bear strong similarities, a number of differences can be identified at more careful observation (Figure 7-5, Figure 7-6 and Figure 7-7):

- The number of microcracks reduced with the addition of higher GnS content or lower w/b ratio.
- Innumerable reacted FA particles, with the characteristics analysed in the previous chapters (darker rims around them and a wrapping of hydration productions around the reacted particles) were present.
- The higher the content of GnS the more extended the development of denser patches of what seemed to be C–S–H.
- Paste PC58.6LS20.4FA20.4+0.6%GnS@0.22, which showed the best mechanical performance, exhibited the densest microstructure with no visible microcracks (Figure 7-7).
- Fibrillar and flake-like formations can be identified and assigned to C–S–H.

From the above, it can be postulated that GnS, if added at a reduced w/b ratio, can offer microstructural enhancement. The latter, in turn is expected to lead to Long-term mechanical performance superior than that of the reference paste, for PC/FA ratio of 3. Moreover, it is possible that greater quantities of GnS can be added in blended cements of PC/FA=3 and that contain 20% FA by mass, as the thermogravimetric analyses showed that there was plenty of $Ca(OH)_2$ available for pozzolanic reactions. However, if the increase of GnS is at the expense of PC content, care should be taken so that the hydration of Portland cement can advance, notwithstanding the reduction of w/b ratio, which is necessary for the greater GnS additions. This limitation is more pronounced with non-aqueous nS dispersions, such as GnS. As was observed in Figure 7-1, for the same w/b ratio (0.3) the addition of even minor (0.3% by mass) carboxylate nS dispersions can be detrimental, probably due to delayed setting and obstruction of the hydration reactions. However, a small reduction in the w/b ratio (0.22) accompanied by an increase in the GnS content (0.6% by mass) proved to be more successful in these pastes than a more drastic reduction in w/b ratio (0.2) and low amount of GnS (0.3% by mass). All in all, in the GnS modified blended cements with PC/FA=3 (PC60LS20FA20), the materials present did not show antagonistic features between their functionalities. For instance, there was still $Ca(OH)_2$ available from the PC hydration for FA and GnS to react with. The only competitive feature of these pastes is the w/b ratio in relation to the GnS content, as discussed.

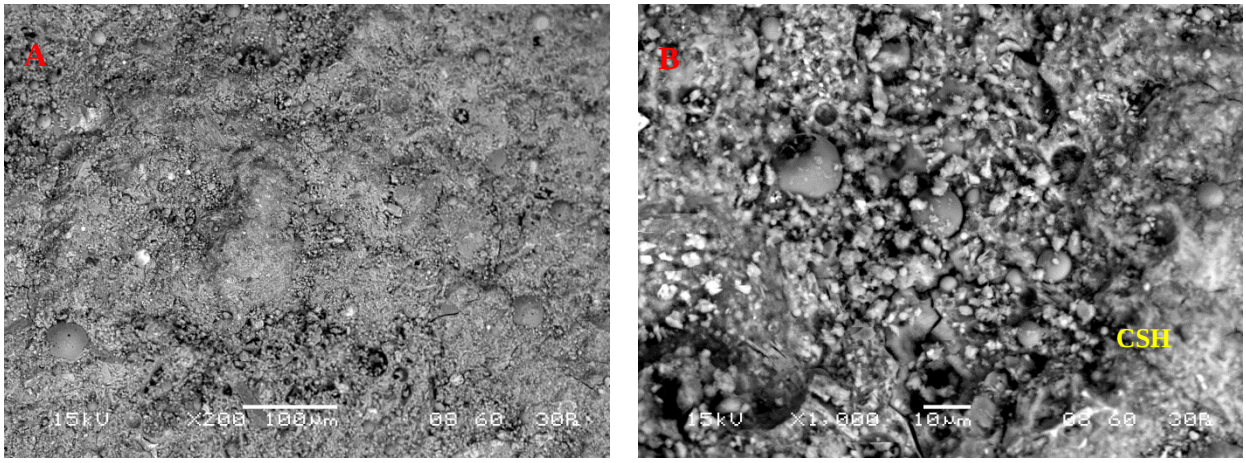

Figure 7-5: BSC micrograph of PC59.5LS20.1FA20.1 +0.3%GnS @ 0.3-28D - (A) 200x and (B) 1000x

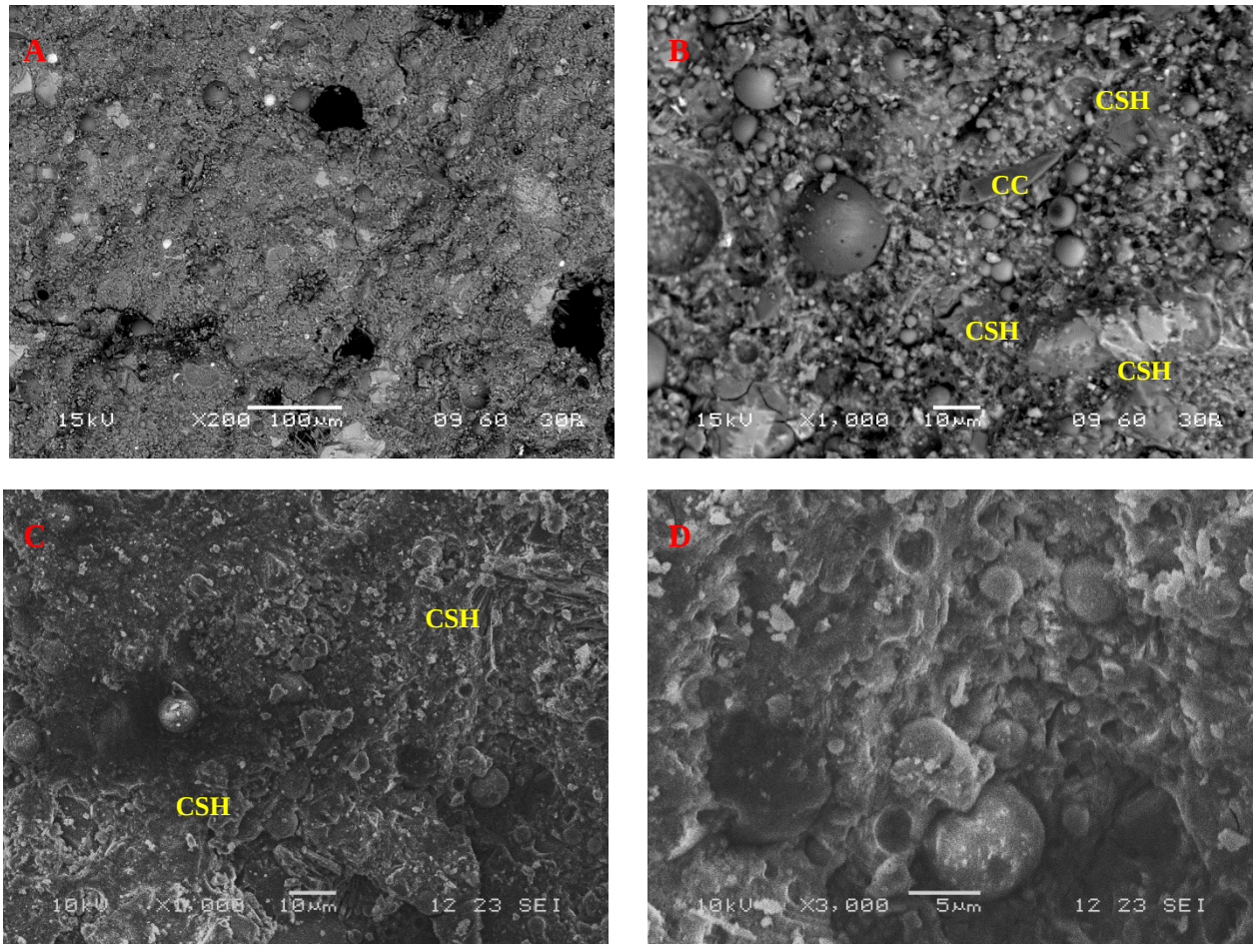

Figure 7-6: BSC micrograph of PC59.5LS20.1FA20.1 +0.3%GnS @0.2-28D - (A) 28D – 200x, (B) 28D –1000x, (C) 28D – 1000x and (D) 28D – 3000x

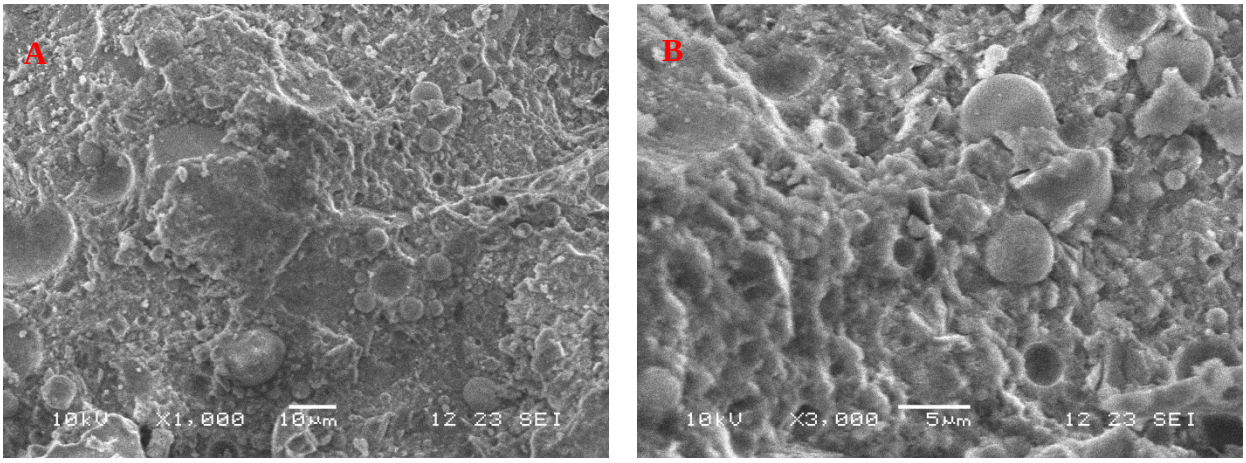

Figure 7-7: BSC micrograph of PC58.6LS20.4FA20.4 +0.6%GnS @0.22-28D - (A) 28D – 1000x, (B) 28D –3000x

7.2 Quaternary cement formulations with LnS on PC43LS20FA37

7.2.1 Introductory section

Having analysed the performance of the GnS modified composite pastes of PC/FA=3 (based on PC60LS20FA20), the analysis of the effects of the nanomodifications on the low PC content series followed. In these series, the PC content was reduced in favour of the FA content, lowering the PC/FA ratio to 1.16. In such composite cements a challenge in the hydration of the PC and FA particles of the reference paste was already created, as discussed in Chapter 5. The main findings of these analyses are presented in the following sections.

7.2.2 Compressive strength of PC/FA=1.16 LnS modified cement pastes

The mechanical performance of nS modified composite cements exhibited multivariate characteristics as can be observed (after month 3) with the PC60LS40 pastes, in the PC43LS20FA43 pastes, LnS did not show immediate reactivity (day 1). Adding to that, the reference paste reached a compressive strength of approximately 40 MPa at day 28, which was maintained thereafter. This could be attributed to delayed PC and FA hydration, a hypothesis revisited and elaborated upon after the thermal analyses. Furthermore, neither did the two lower LnS contents (0.1 and 0.2% by mass) offer improvements in the compressive strength. The highest LnS content had the most detrimental effects on the strength of these series of pastes at later ages. The optimum amount of LnS particles for composite cement pastes with PC/FA ratio of 1.16, seemed to be 0.5% by mass. As discussed in Calabria-Holley *et al.* (2014), Papatzani *et al.* (2014) and Kawashima *et al.*

(2013) it is possible that at higher nS concentrations, the hydration products formed by the immediate reactivity of the nS, have higher C/S ratio in the C–S–H, creating dense wrapping around the FA particles which are found in abundance in the paste. The C–S–H formed in presence of FA has a lower C/S ratio (Feldman *et al.*, 1990) therefore, these "pockets" of dense C–S–H and ettringite may be performing as ion penetration barriers, delaying even further the reaction of a part of the FA. It is the author's opinion that in low PC/FA ratio composite cement pastes, the presence of high contents of nS managed to "deactivate" part of the FA. In support to this argument, a number of unreacted FA particles where identified by the SEM analyses presented in section 7.2.4. This could be the reason why the specific pastes delivered reduced compressive strength. For the lower LnS content pastes their compressive strength is expected to increase further with age, mainly because with the advancement of time the contribution of FA to strength gain and densification of the LnS modified pastes will be more prominent.

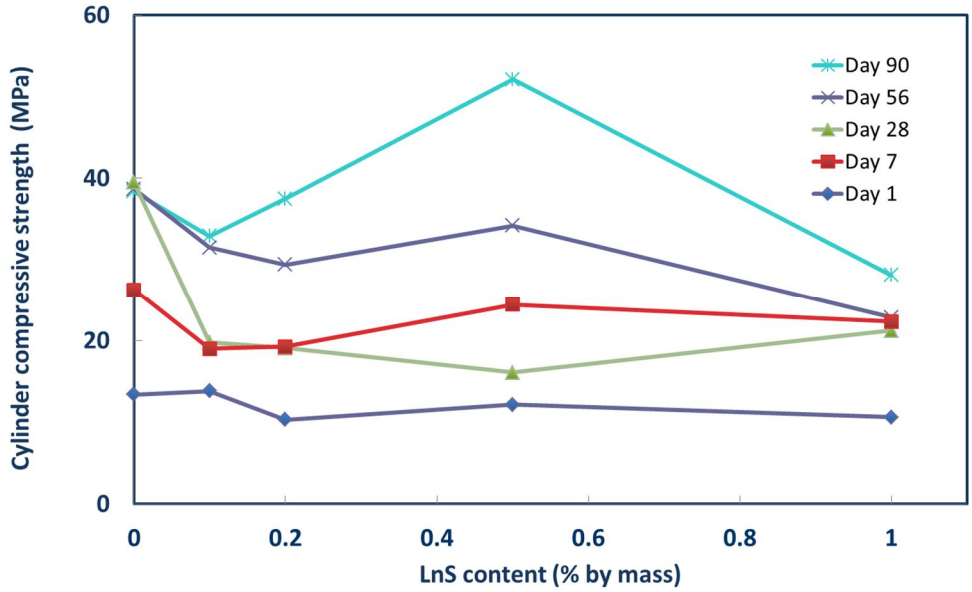

Figure 7-8: Cylinder compressive strength of LnS modified cement pastes based on PC43LS20FA37

7.2.3 Thermogravimetric and crystallographic analyses of cement pastes

The results of the TG analyses on the four different combinations of LnS on PC43LS20FA37 are shown in Figure 7-9 to Figure 7-12. The drastic reduction in the $Ca(OH)_2$ content observed at day 56 in Figure 7-9 could be related to the increase in $CaCO_3$ observed at the same age in Figure 7-10 implying occurrence of carbonation rather than chemical reactivity of the LS present in the paste. In fact, as shown in the XRD analyses that follow (Figure 7-13 to Figure 7-16), monocarbonate or hemicarbonate compounds were not detected. Moreover, the analyses carried out in Calabria-Holley *et al.* (2014) with the help of FTIR on selected pastes did not detect evidence of carbonation of the pastes until day 28. However, carbonation did occur after day 28, but since consistent amongst

specimens is not further elaborated upon. Furthermore, the TGA curves, covering 0-1000°C, presented in Figure 7-11 and Figure 7-12 showed a significant increase in the C–S–H and ettringite directly linked with the consumption of $Ca(OH)_2$ content from day 28 to day 56 and of course the strength gain observed at this ages for specific pastes.

Additionally, the following can be observed in the graphs that follow:

- Significant increase in the $Ca(OH)_2$ content from day 1 until day 7 in agreement with the results on PC65LS05FA30 presented by De Weerdt *et al.* (2011b).
- From day 7 to 28 there were subtle changes in the $Ca(OH)_2$ content.

When PC hydrates it produces about 20-25% by mass $Ca(OH)_2$ at day 28 (Lam *et al.*, 2000). Also, in the same research, the degree of FA reaction has been identified as approximately 13% of the total FA content at day 28, reaching about 25% at day 90, therefore, of the 37% FA, 4.81% is expected to have reacted at day 28.

Moreover, at day 28, 43% by mass PC alone should have produced approximately 10.75% (43x25%) $Ca(OH)_2$. The TG analyses, at day 28, detected 6% $Ca(OH)_2$, therefore very small amount of the reactive by day 28 FA (summing up to ¼ of the total FA content) was left to react after day 28. Theoretically, at day 56, the $Ca(OH)_2$ content detected in the reference paste was expected to be lower than that of day 28. If it is assumed that another 5.5% of FA has reacted by day 56, then the $Ca(OH)_2$ content detected in the reference paste PC43LS20FA37, should be 6-5.5 = 0.5%. The TG analyses showed that there was 1.5% of $Ca(OH)_2$, indicating further hydration of PC and possible delayed reactivity of the FA, certainly, though, no depletion of $Ca(OH)_2$ by the FA. Lastly, it should be acknowledged that some carbonation of the reference paste may have taken place, since a mass loss was detected after 860°C in Figure 7-12. However, the same evidence was present for almost all pastes at day 28 as displayed in Figure 7-11, therefore relative comparisons are valid.

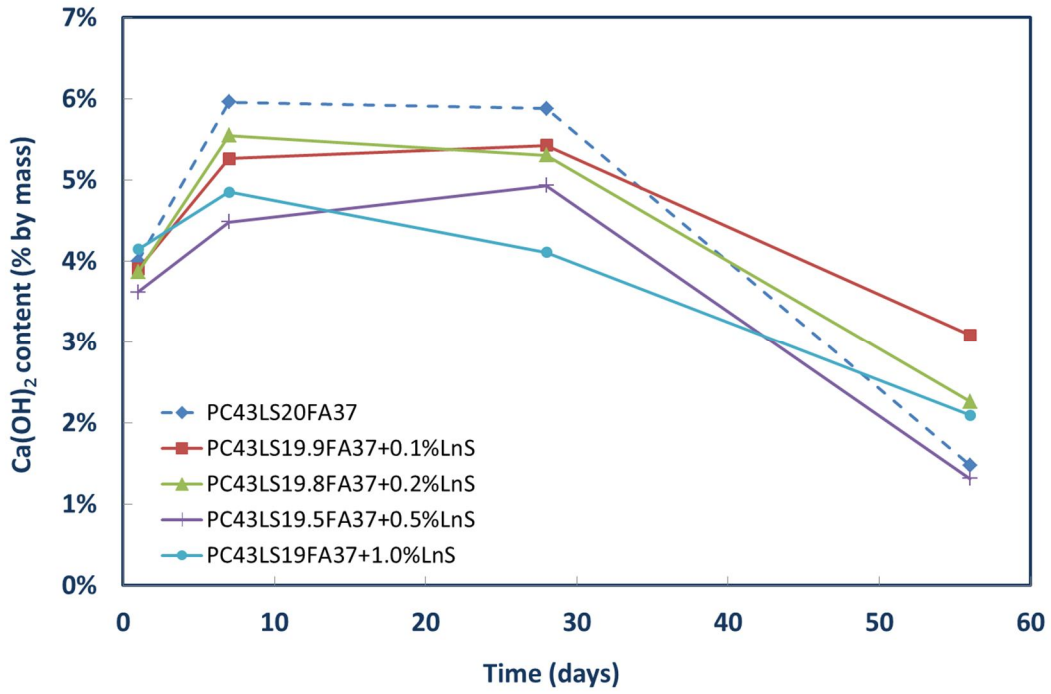

Figure 7-9: $Ca(OH)_2$ content of LnS modified cement pastes based on PC43LS20FA37

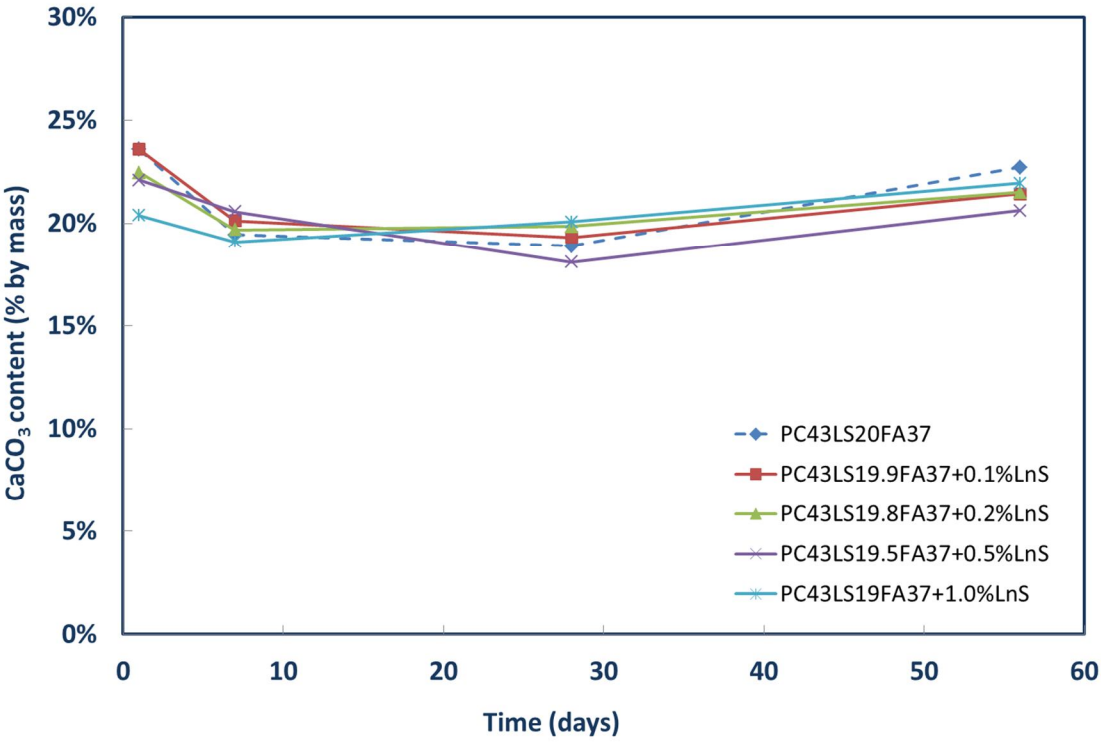

Figure 7-10: $CaCO_3$ content of LnS modified cement pastes based on PC43LS20FA37

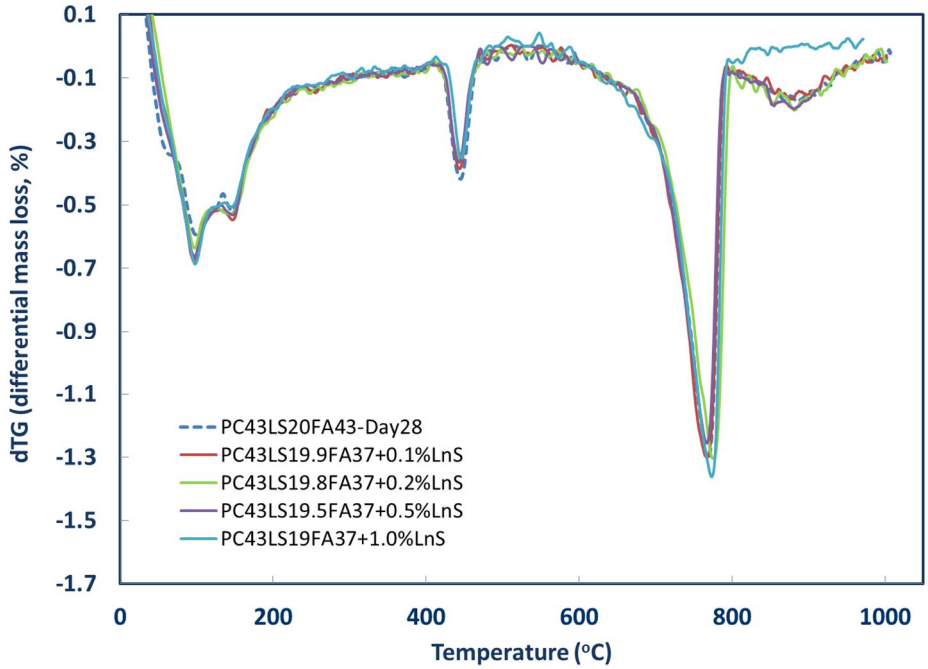

Figure 7-11: Differential mass loss of LnS modified cement pastes based on PC43LS20FA37 between 0-1000°C at Day 28

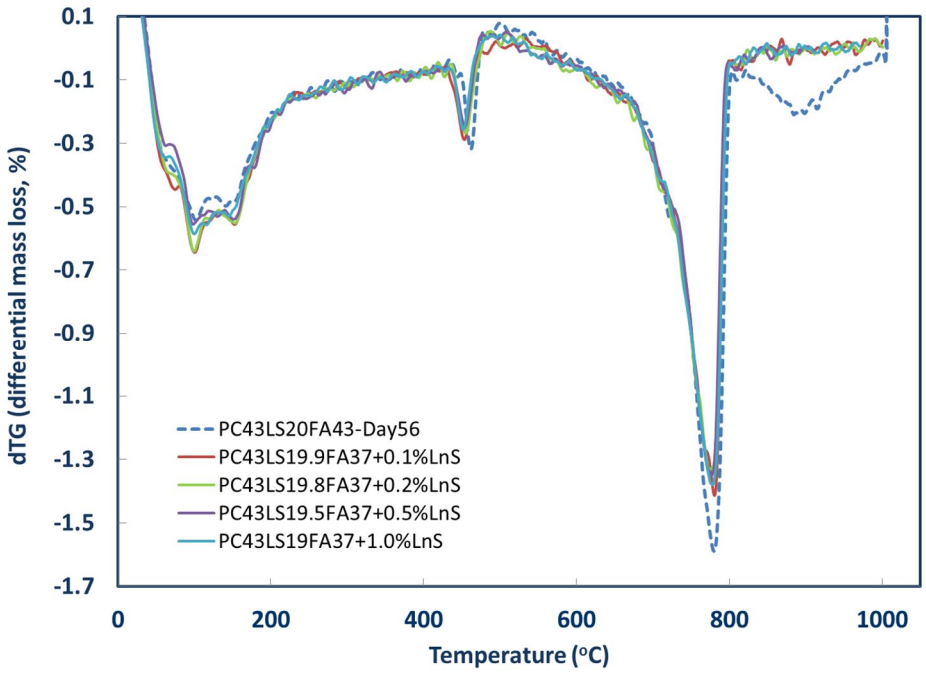

Figure 7-12: Differential mass loss of LnS modified cement pastes based on PC43LS20FA37 between 0-1000°C at Day 56

It is the author's opinion that the evolution of strength gain for these series of pastes could be described in the following chronological sequence:

By day 1 the hydration of PC had started and the LnS particles, being highly reactive, as shown in the less complex pastes in Chapter 6, were immediately engaged in reactions consuming $Ca(OH)_2$ formed by the hydration of cement. The C–S–H produced by LnS reactivity has a lower C/S ratio and a denser nature than the reference paste.

Between day 1 and day 7, PC had further hydrated; the remaining LnS particles were completing their participation expanding the C–S–H network around particles of PC, LS and FA. Moreover, a part of the FA particles had started feeding from the $Ca(OH)_2$ formed by PC hydration. Another part was yet to react, but remained covered by the dense C–S–H formed by LnS.

At day 7 the TG analyses inferred that in such pastes with high FA content, the pozzolanic reactions were the primary consumers of $Ca(OH)_2$, particularly since most of the LnS had already reacted in the lower LnS content nanomodifications.

By day 28, the lower LnS content nanomodifications did not consume any more $Ca(OH)_2$, but neither did the FA particles due to the ion barriers set by the LnS hydration products.

However, as age advanced, possibly lowering the pH of the hydrating paste, the FA attraction of $Ca(OH)_2$, exceeded the strength of the bonds surrounding the FA particles another part of which started to react, consuming the available $Ca(OH)_2$.

By day 56, further strength gain was achieved by the LnS contents up to 0.5% by mass and significant amounts of $Ca(OH)_2$, were, still, noticeable. Therefore, the theory presented by other researches on the depletion of $Ca(OH)_2$ in such pastes was not confirmed in this research. For example, Kawashima *et al.* (2013) who studied ternary nanomodified Portland cement binders of high PC/FA ratio equal to 1.5 found that water cured at 60°C samples showed signs of $Ca(OH)_2$ depletion at day 7.

In contrast to this, the chronological scenario is shedding more light in the complex processes taking place in nanomodified composite cements and is by no means dogmatic. Evidences rendered the theory of competition between FA and nS particles in such pastes more adequate to explain the complex phenomena (Papatzani *et al.*, 2014; Calabria-Holley *et al.*, 2014; Hosseini *et al.*, 2014).

The suggestions should be investigated by the nanoindentation method discussed in Chapter 2, in more nanotechnologically set up laboratories. A series of X-ray tomography (CT) scans could also bridge the relationship between, densification of C–S–H in the presence of lower LnS contents and probable increase in porosity due to the presence of excessive LnS particles.

A short reference to the ettringite formation should also be made. Knowing that the specific FA used, contained impurities and sulfates, it was no surprise that greater quantities of ettringite were formed (De Weerdt *et al.*, 2011b), as can be noticed in Figure 7-11 and Figure 7-12.

The XRD analyses (Figure 7-13 to Figure 7-16) confirmed all the above findings:

- Production of additional ettringite from day 1.
- Production of additional C–S–H from day 1.
- Increase of $Ca(OH)_2$ content at day 1 with subsequent reduction at later ages, leading to elimination of the detectable (non-encapsulated by C–S–H) $Ca(OH)_2$ by day 56.
- Absence of carboaluminates hydrates (expected to give diffractions at 10.8°*2θ*, for hemicarbonate and 11.7°*2θ* for calcium monocarbonate hydrate (De Weerdt *et al.*, 2011b)) even by day 56, a finding which was not totally clear by the TG analyses.

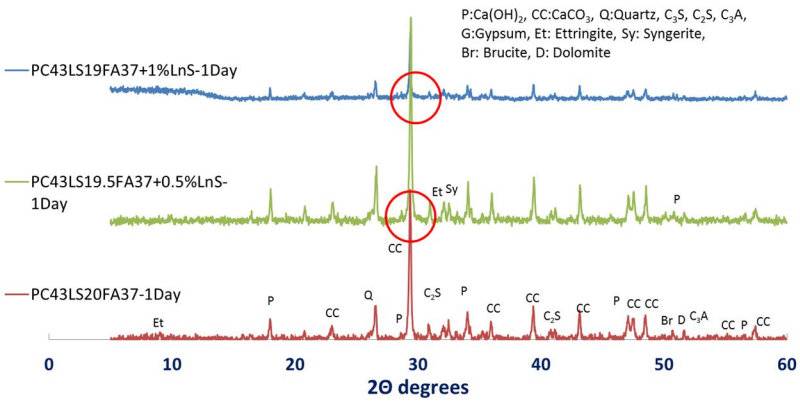

Figure 7-13: XRD pattern of LnS modified cement pastes based on PC43LS20FA37 at Day 1

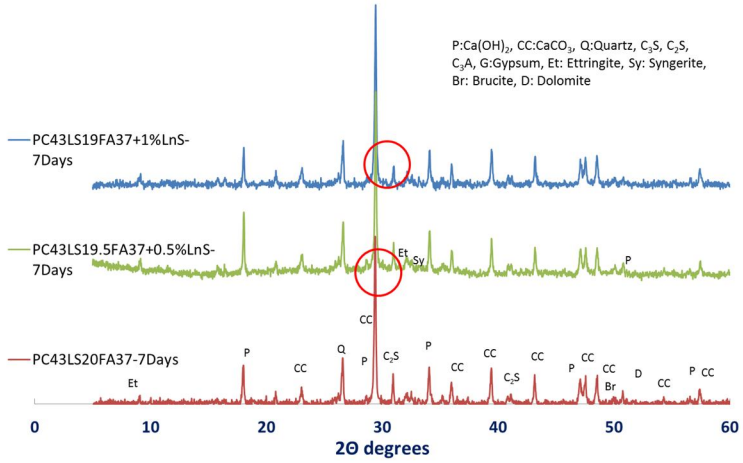

Figure 7-14: XRD pattern of LnS modified cement pastes based on PC43LS20FA37 at Day 7

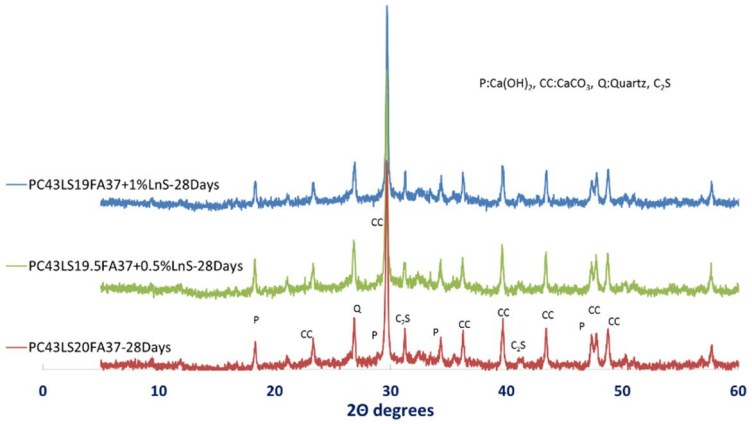

Figure 7-15: XRD pattern of LnS modified cement pastes based on PC43LS20FA37 at Day 28

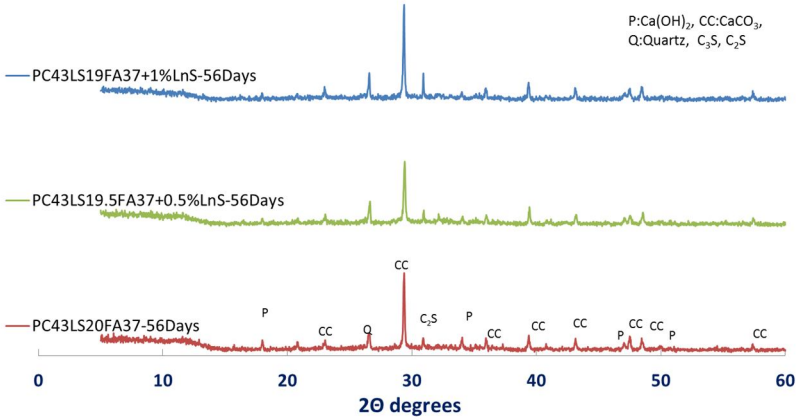

Figure 7-16: XRD pattern of LnS modified cement pastes based on PC43LS20FA37 at Day 56

7.2.4 Microstructural characterisation of cement pastes

In the BSC micrographs that follow, day 1 of the same paste is presented next to day 56 to make differences more distinguishable. As an effect, micrographs of 28 days old pastes are presented separately.
With respect to the reference paste, PC43LS20FA37 the following can be seen in Figure 7-18, Figure 7-19 and Figure 7-17:

i. Densification of the paste, more visible in the 100 time magnification has taken place by day 28 (Figure 7-18-C, Figure 7-19-C and Figure 7-17-C) accompanied by reduction in microcracks.
ii. A number of unreacted FA (denoted by uFA) particles, identified by their light colour and spherical shape are still visible by day 56, enforcing previous arguments.
iii. Reacted FA (denoted by rFA) particles created seeding effect, by attracting needle like hydration products Figure 7-19-A, B, verifying that finding of higher FA activation by day 56.
iv. Dense areas of what seems to be C–S–H (denoted by CSH on the micrographs) were distinguished. The dark rim around the formation was clearly visible.
v. $Ca(OH)_2$ crystals (denoted by P) participating in the seeding effects in agreement with De Weerdt *et al.* (2011b).

In addition to the reference paste the optimal LnS modified paste, PC43LS19.5FA37+0.5%LnS (Figure 7-20 to Figure 7-22) and the less favourable one, PC43LS19FA37+1%LnS (Figure 7-23 to Figure 7-25), were also examined at different ages. With respect to PC43LS19.5FA37+0.5%LnS the following can be noted:

i. A highly densified morphology by day 56, can be observed, possibly denser than that of the reference paste. The presence of microcracks seemed eliminated (Figure 7-20-C to Figure 7-22-C).
ii. Prevalent reacted and unreacted FA particles and $Ca(OH)_2$ crystals.
iii. Extended patches of dense areas of C–S–H can be distinguished.

Lastly, PC43LS19FA37+1%LnS bore great resemblance to the previously discussed paste in terms of hydration products, morphology and pozzolanic activity of the constituents. Qualitative differences were difficult to be identified by SEM.

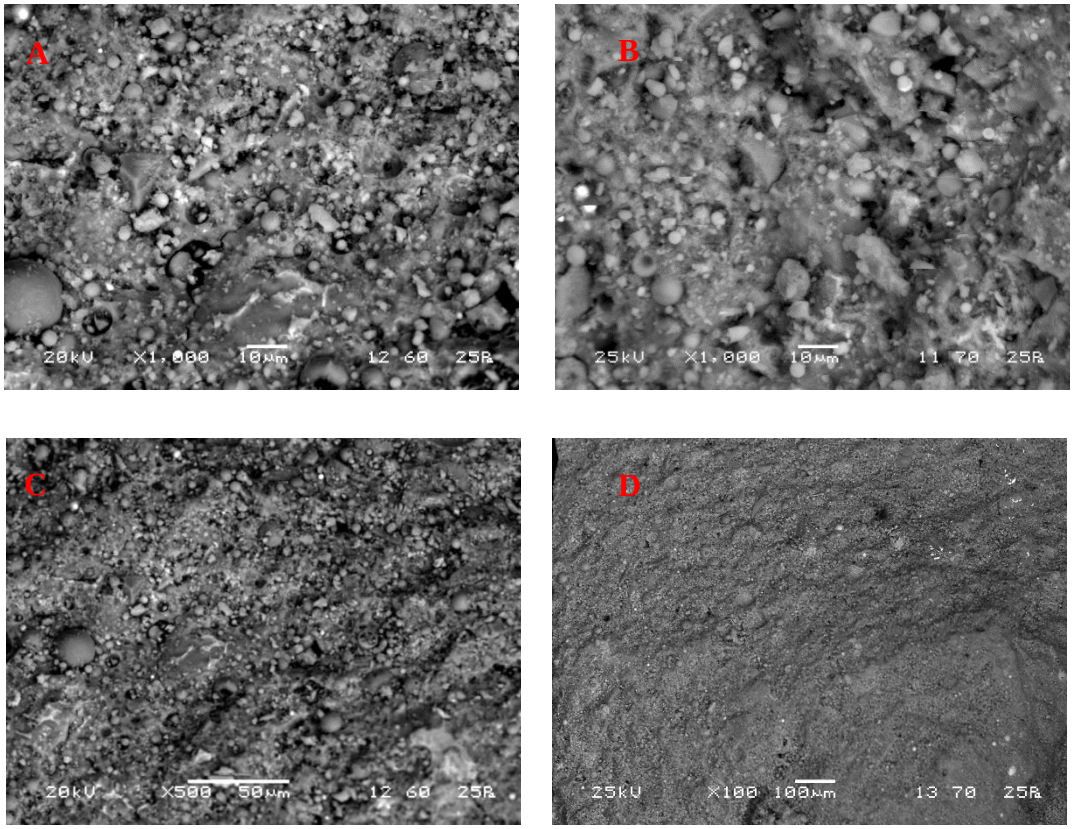

Figure 7-17: BSC micrograph of PC43LS20FA37 -28D – (A) 1000x, (B) 500x and (C) 100x

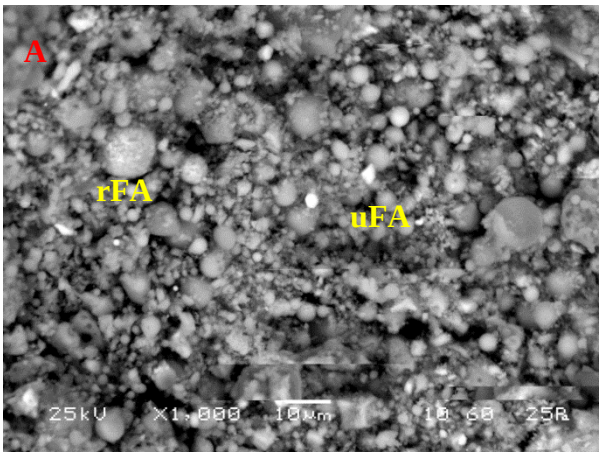

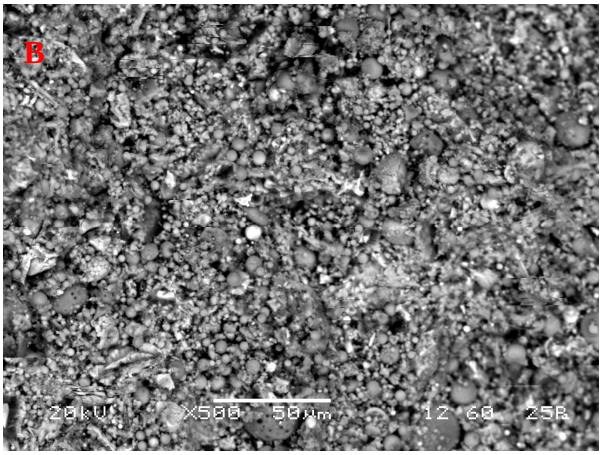

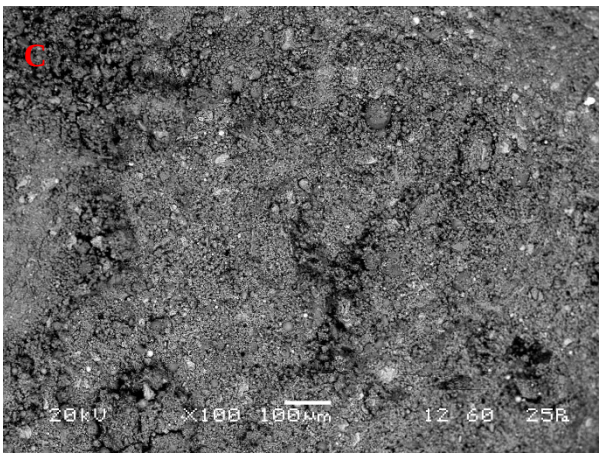

Figure 7-18: BSC micrograph of PC43LS20FA37 -1D - (A) 1000x, (B) 500x and (C) 100x

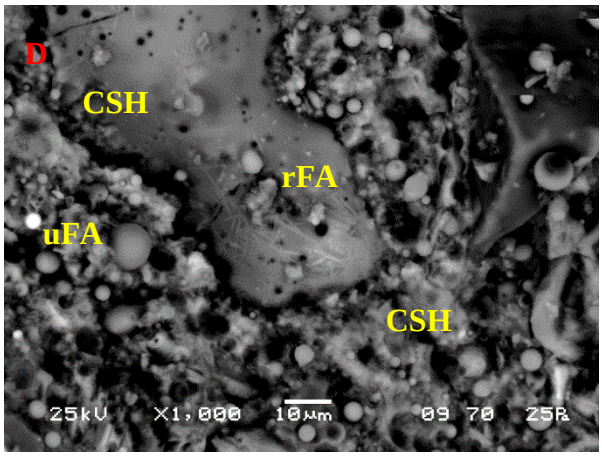

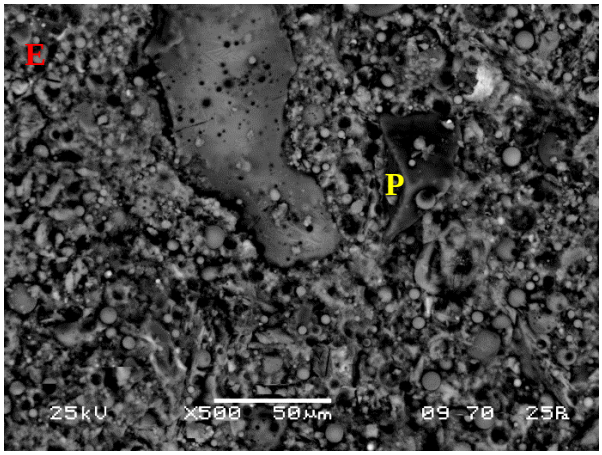

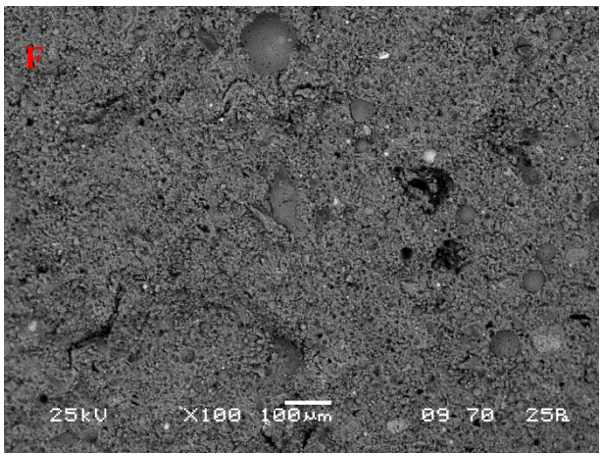

Figure 7-19: BSC micrograph of PC43LS20FA37 -56D - (A) 1000x, (B) 500x and (C) 100x

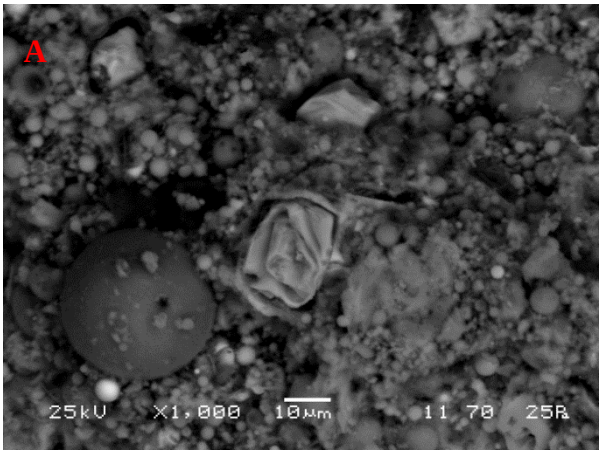

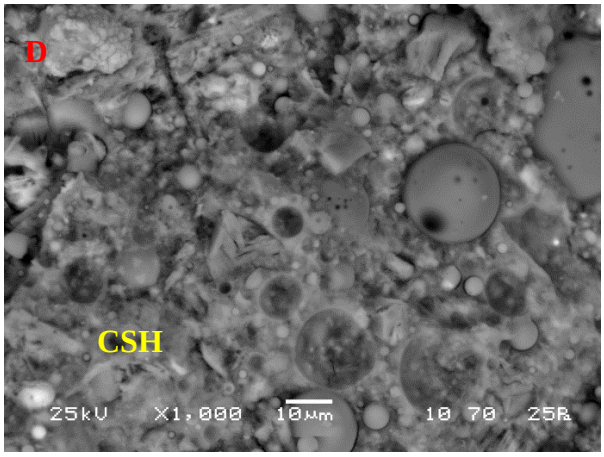

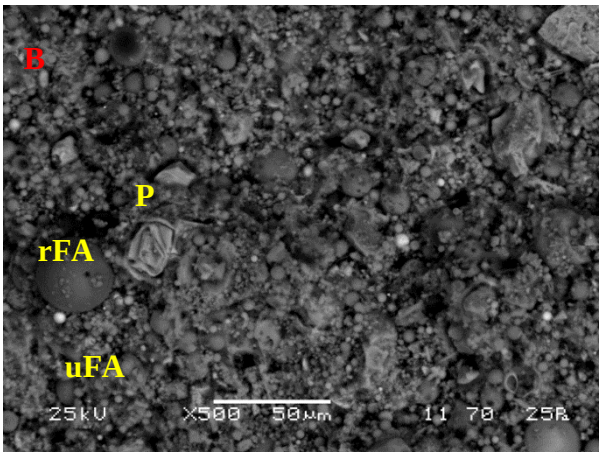

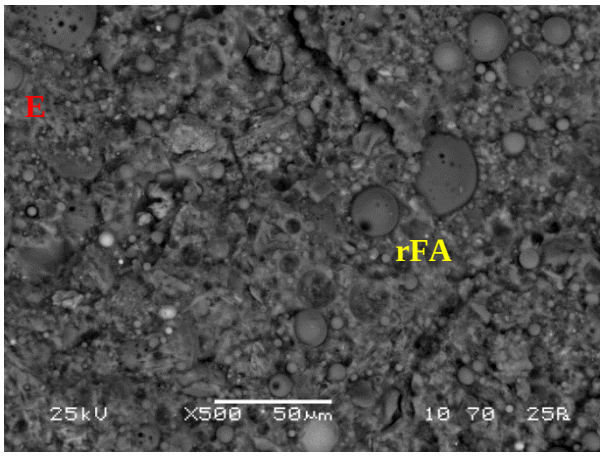

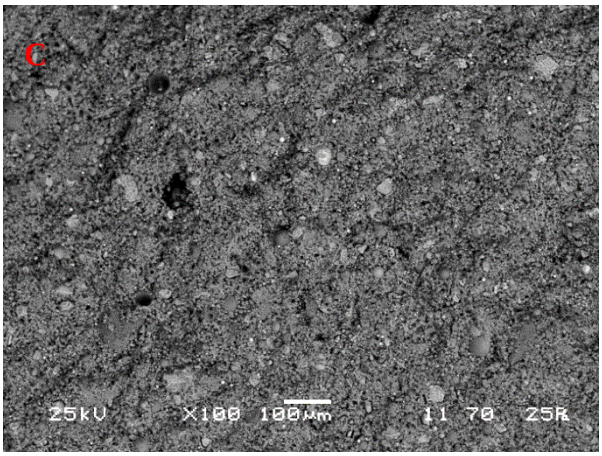

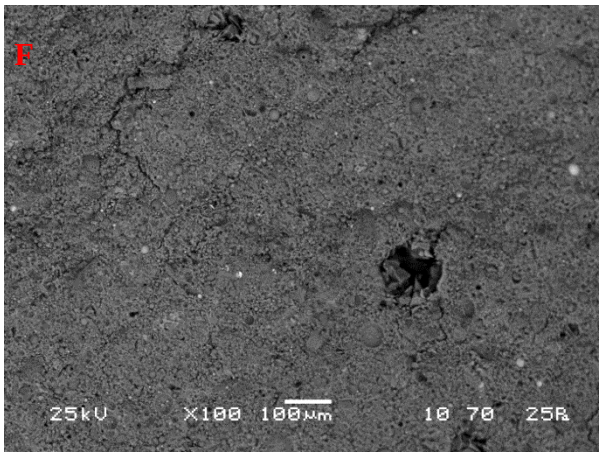

Figure 7-20: BSC micrograph of PC43LS19.5FA37+0.5%LnS 1D– (A) 1000x, (B) 500x and (C) 100x

Figure 7-21: BSC micrograph of PC43LS19.5FA37+0.5%LnS 56D– (A) 1000x, (B) 500x and (C) 100x

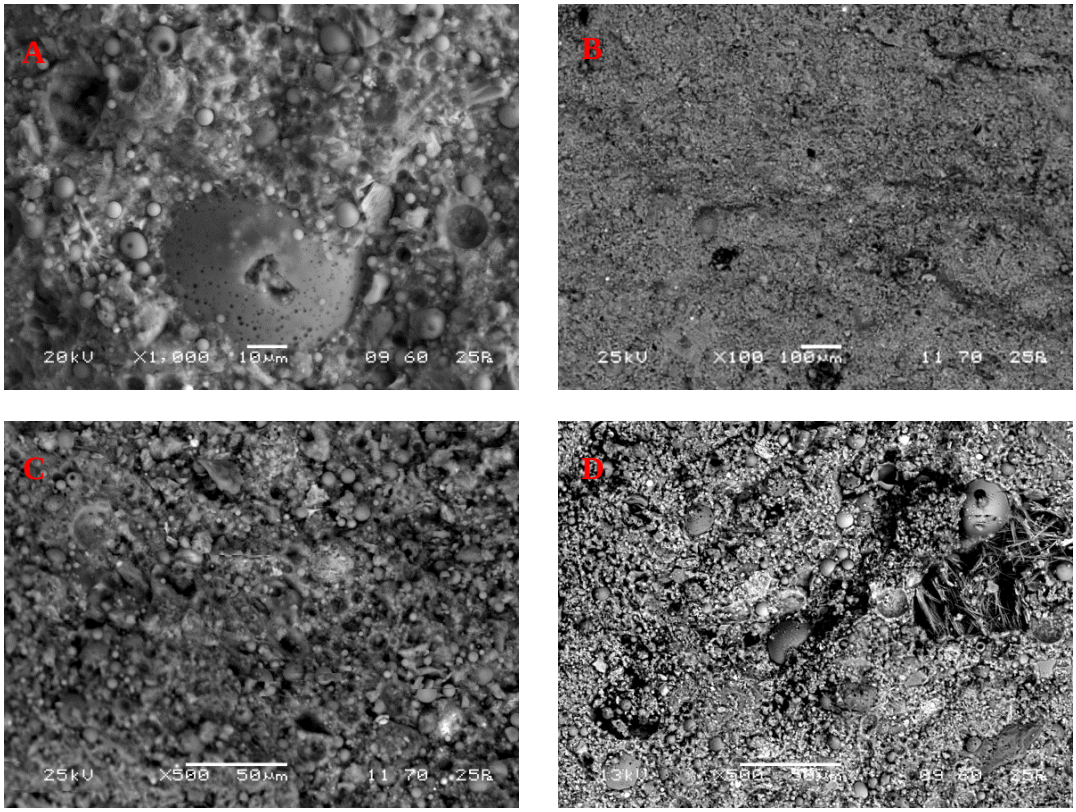

Figure 7-22: BSC micrograph of PC43LS19.5FA37+0.5%LnS 28D– (A) 1000x, (B) 100x (C) 500x and (D) 500x

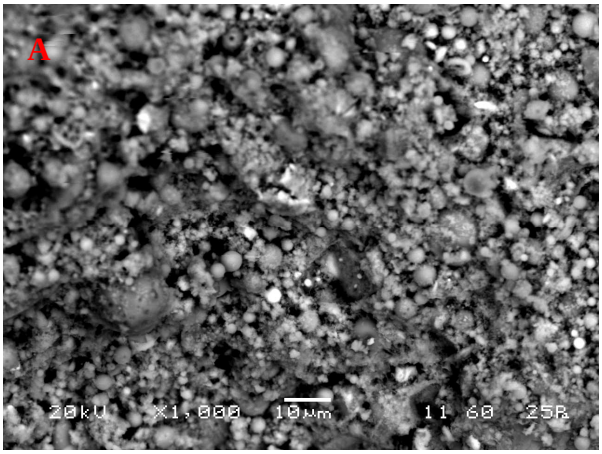

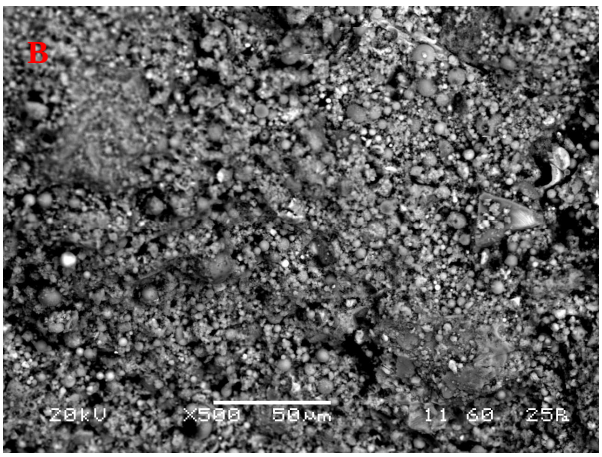

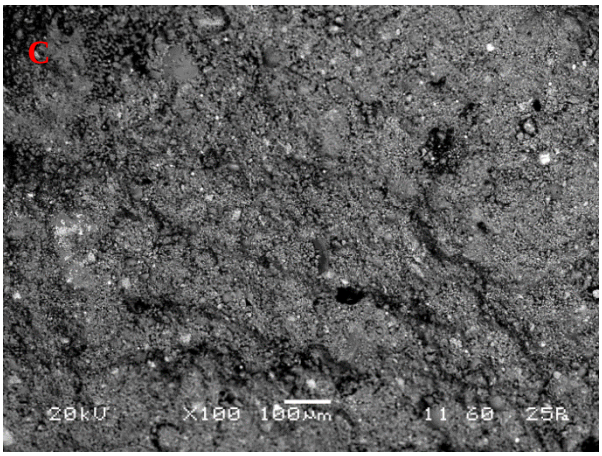

Figure 7-23: BSC micrograph of PC43LS19FA37+1%LnS 1D – (A) 1000x, (B) 500x and (C) 100x

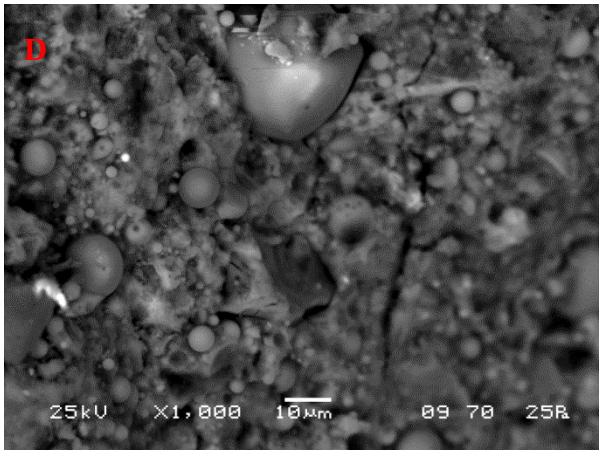

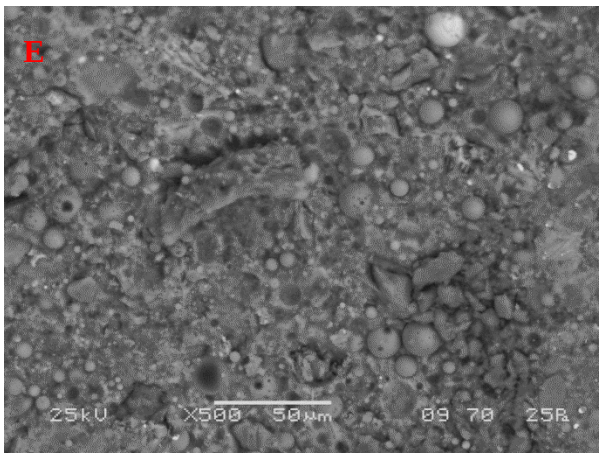

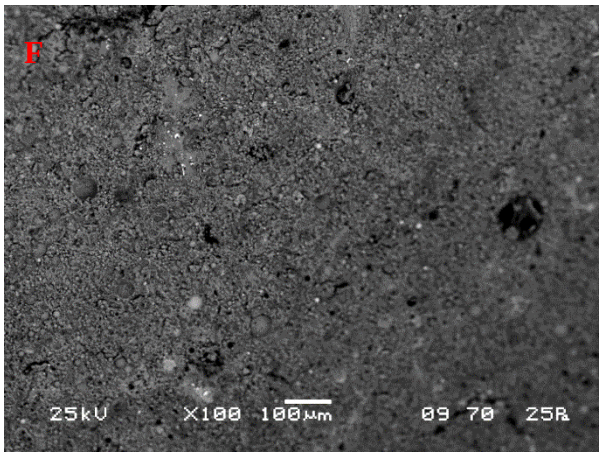

Figure 7-24: BSC micrograph of PC43LS19FA37+1%LnS 56D – (A) 1000x, (B) 500x and (C) 100x

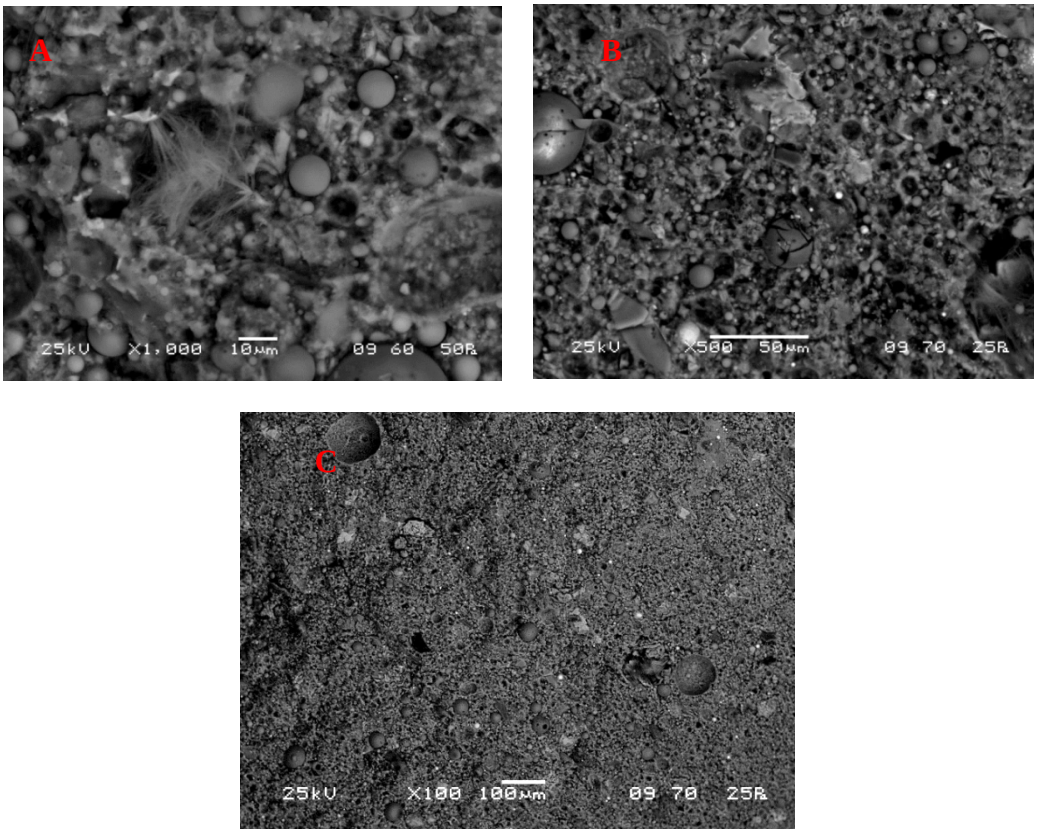

Figure 7-25: BSC micrograph of PC43LS19FA37+1%LnS 28D – (A) 1000x, (B) 500x and (C) 100x

7.3 Quaternary cement formulations with GnS on PC43LS20FA37

7.3.1 Introductory section

In essence similar findings to the ones analysed in section 7.1, can be reported. Indeed, the long-term performance seems to be enhanced by the 0.5% by mass GnS addition. The presence of significant quantities of carbon seemed to have played a role in the performance of the GnS modified pastes, as analysed in the following sections. It should be mentioned that during the production of the specimens, the ones with the higher w/b ratio exhibited prolonged setting.

7.3.2 Compressive strength of PC/FA=1.16 GnS modified cement pastes

As in the case of LnS the highest (1% by mass) GnS addition was proven detrimental and the lowest (0.1% by mass) was beneficial for the early age compressive strength (Figure 7-26). Unfortunately, not enough samples were prepared to allow for testing of the full series (all GnS contents) at day 90.

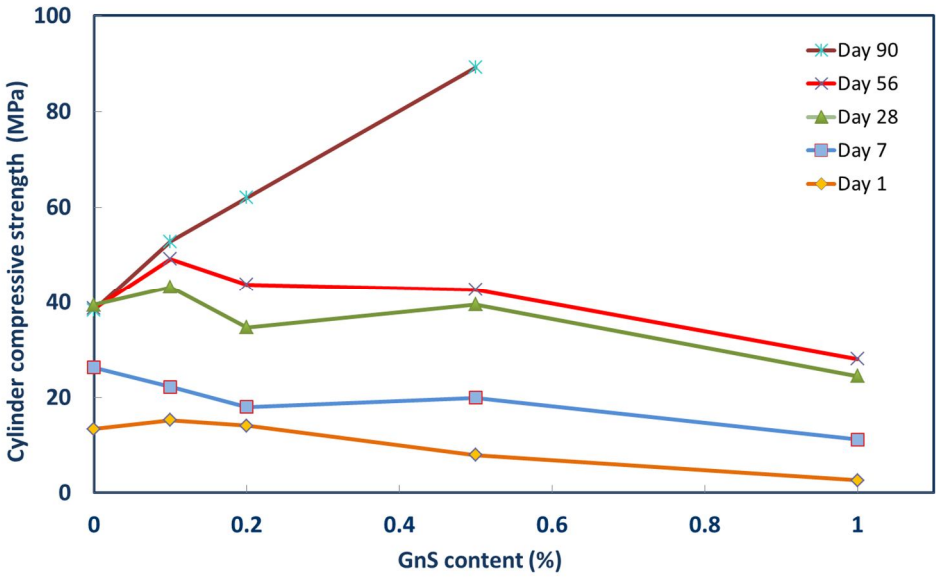

Figure 7-26: Cylinder compressive strength of GnS modified cement pastes based on PC43LS20FA37

7.3.3 Thermogravimetric and crystallographic analyses of cement pastes

As shown in Figure 7-27 and Figure 7-28, the addition of GnS affected the consumption of the $Ca(OH)_2$ content, at day 1 and 7, for the two higher GnS concentrations, whereas its effect was more evident after day 28. The 1% GnS dosage seemed to be carbonating more (greater mass loss in the temperature range between 650-800°C).

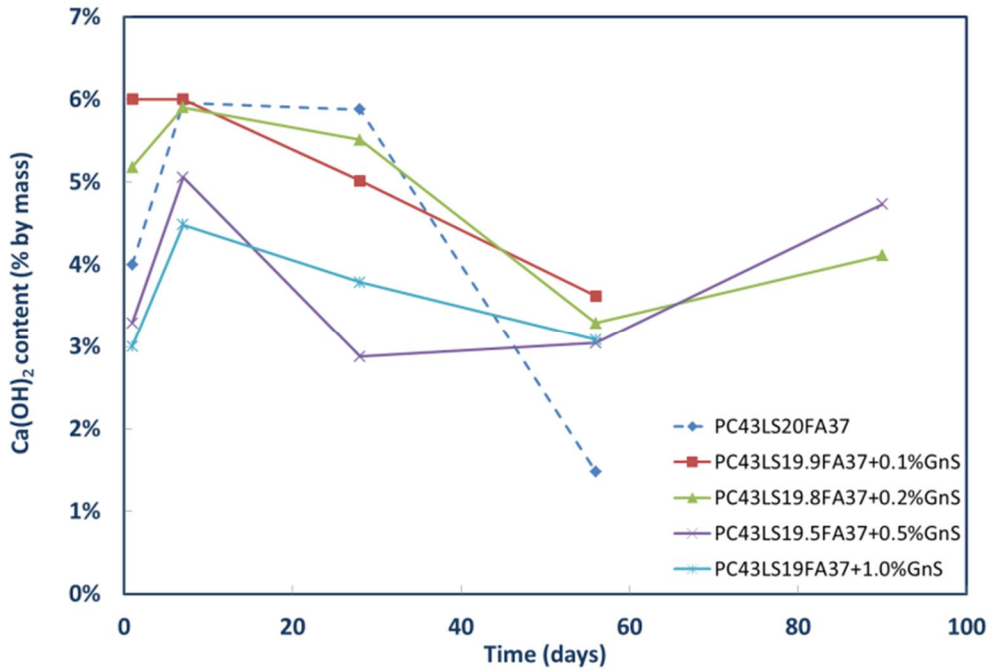

Figure 7-27: $Ca(OH)_2$ content of GnS modified cement pastes based on PC43LS20FA37

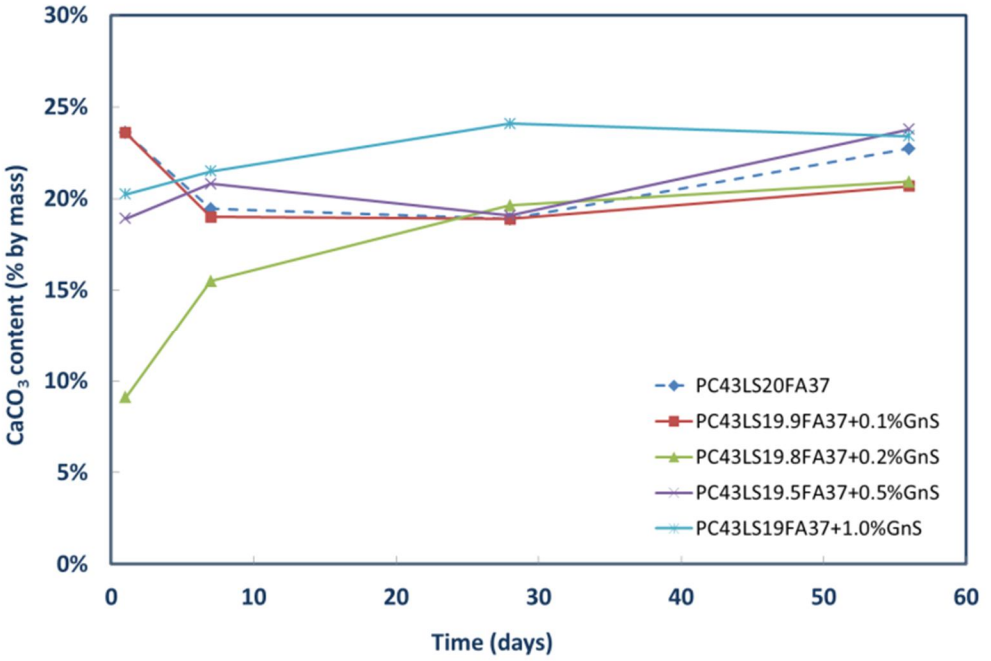

Figure 7-28: $CaCO_3$ content of GnS modified cement pastes based on PC43LS20FA37

7.4 Comparison of the performance of the nS particles

7.4.1 Performance of cement pastes based on PC43FA20LS37

The two following graphs, serve as a summary and comparison of the performance of the 0.1% and 0.5% nS modifications of PC43FA20LS37 at different ages (Figure 7-29 and Figure 7-30). The stagnant compressive strength of the reference paste after day 28 was surpassed by both GnS additions, the 0.5% being the most advantageous. The 0.1% LnS addition delayed the strength gain, which was eventually enhanced only at the 0.5% LnS addition.

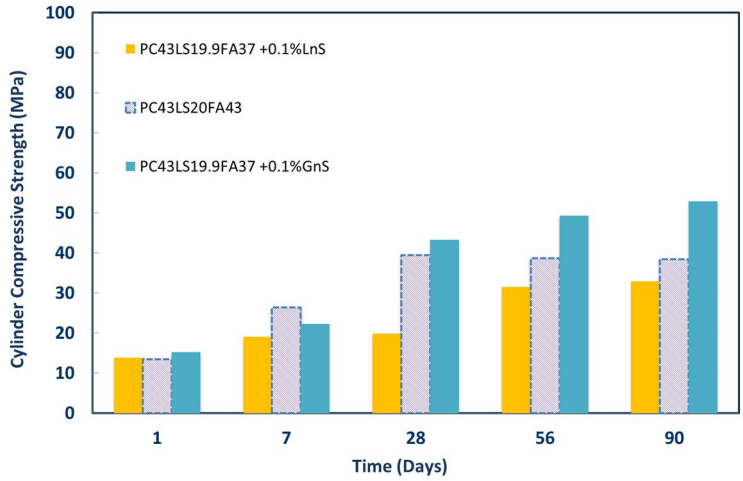

Figure 7-29: Comparison of the 0.1% GnS or 0.1% LnS modification of cement pastes based on PC43LS20FA37

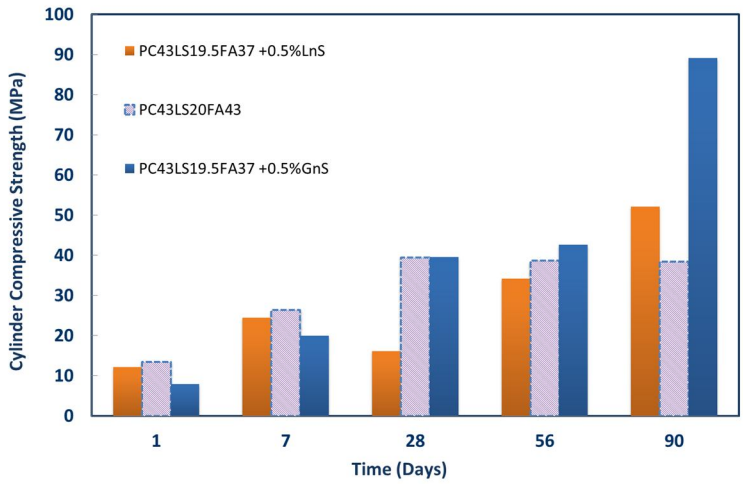

Figure 7-30: Comparison of the 0.5% GnS or 0.5% LnS modification of cement pastes based on PC43LS20FA37

7.4.2 Cube compressive strength and relative density of mortars based on PC100

To confirm the understanding on the behaviour of the nS modified pastes, four series of mortars were nanomodified and tested in compression. To begin with, the simplest combination was developed based on PC100 (denoted as M.PC100) using CEMI-45R, with a w/b ratio of 0.5. Knowing that GnS may be performing as water reducing agent, for the 0.5% GnS addition a reduced w/b ratio was employed. The reference mortar, could not be mixed at lower than 0.5 w/b ratio. As can be seen in Figure 7-31, LnS, offered early age strength increase but the performance at later ages was inferior to the reference mortar's. Furthermore, the 1% LnS addition, was proven to be detrimental. On the contrary, the same dosage 0.5% by mass of GnS, at lower w/b ratio offered significant improvements.

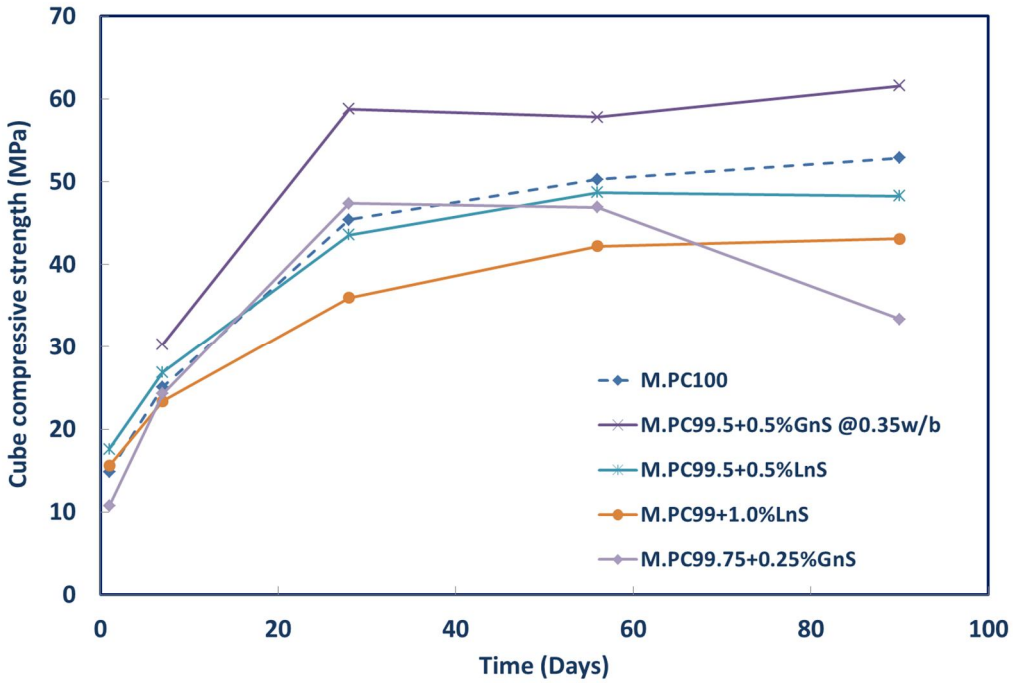

Figure 7-31: Cube compressive strength of nS modified mortars based on PC100

Knowing that the theoretical maximum density of PC is 3250 kg/m^3, that of sand is 2650 kg/m^3 and of water 1000 kg/m^3 the theoretical maximum density for a mortar of 100% PC at w/b = 0.5 was found to be equal to 2600 kg/m^3. Therefore, judging by the late age (after month 6) relative density measured (Figure 7-32) the M.PC100 did not seem to contain significant pores. The nS content of M.PC99+0.5%LnS has been shifted in the graph for ease of the reader. It is important that both types of nS offered higher densities, probably due to the particle packing effect. Notwithstanding, the addition of greater amounts can cause conglomeration of the particles within the hydrating paste and consequently, increase the porosity and relative density. It should be noted that the theoretical maximum density of the nanomodified mortars could not be calculated due to lack of data on the theoretical density of the nanoparticles.

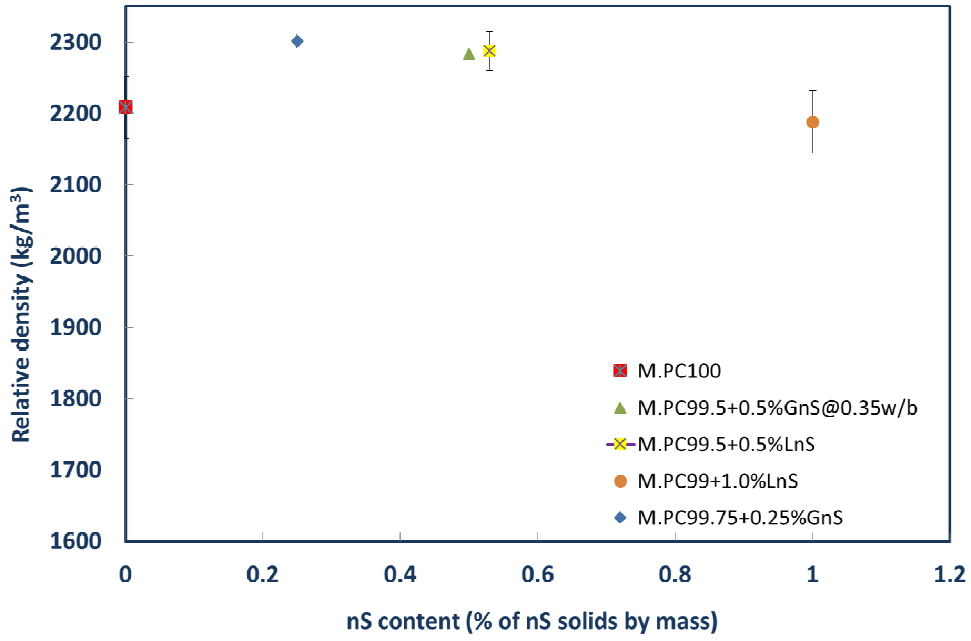

Figure 7-32: Relative density of nS modified mortars based on PC100

7.4.3 Cube compressive strength and relative density of mortars based on PC43LS20FA37

The second series of mortars for the verification of the results on the cement pastes, was based on PC43LS20FA37 and was produced using CEMI-45R. For this series, in order to make the performance of the two different nS dispersions comparable, two reference mortars were created; one at 0.5 w/b ratio, which was nanomodified with LnS and another at 0.35 w/b ratio, which was nanomodified with GnS. In this series LnS did not offer a significant strength increase. In contrast, GnS contributed substantially to strength enhancement at all ages (Figure 7-33). The measured compressive strengths are also presented in the table below.

Table 7-1: Cube compressive strength results on M.PC43LS20FA37

	DAY			
	7	28	56	90
M.PC43LS20FA37@0.5w/b	5.6	15.7	20.9	24.7
M.PC43LS20 FA37@0.35w/b	7.7	10.1	18.9	19.6
M.PC42.5LS20FA37 +0.5 LnS@0.5w/b	5.5	15.1	16	25.4
M.PC42.5LS20FA37 + 0.5%GnS@0.35w/b	11.3	31.1	30.3	27.3

Lastly, the late age relative density measurements of the mortars based on PC43LS20FA37 showed that nS can enhance density, probably through better particle packing (Figure 7-34).

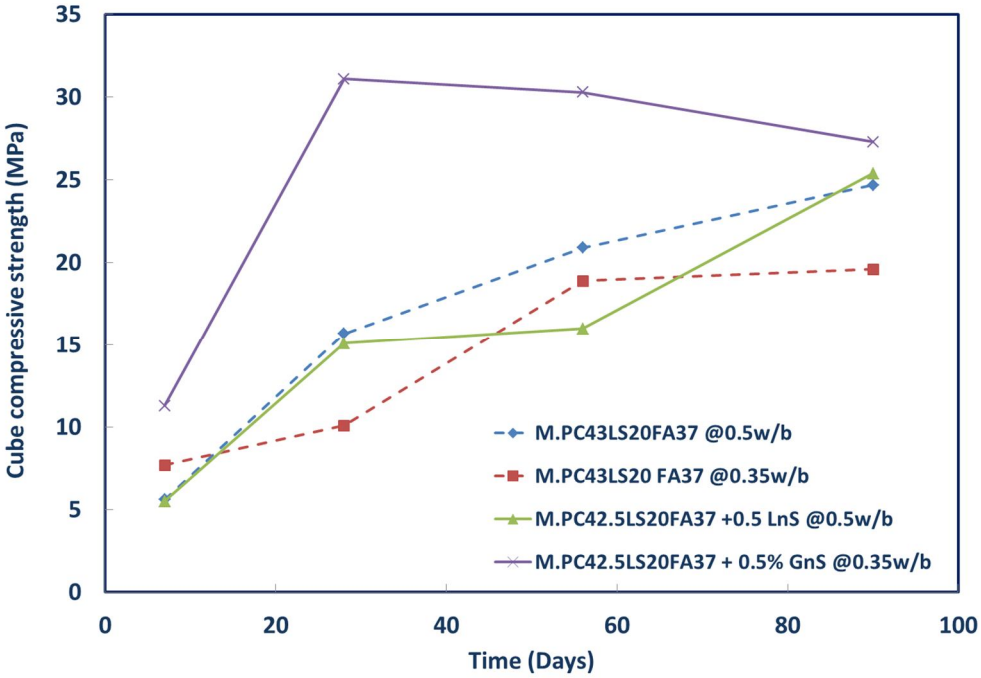

Figure 7-33: Cube compressive strength of nS modified mortars based on PC43LS20FA37

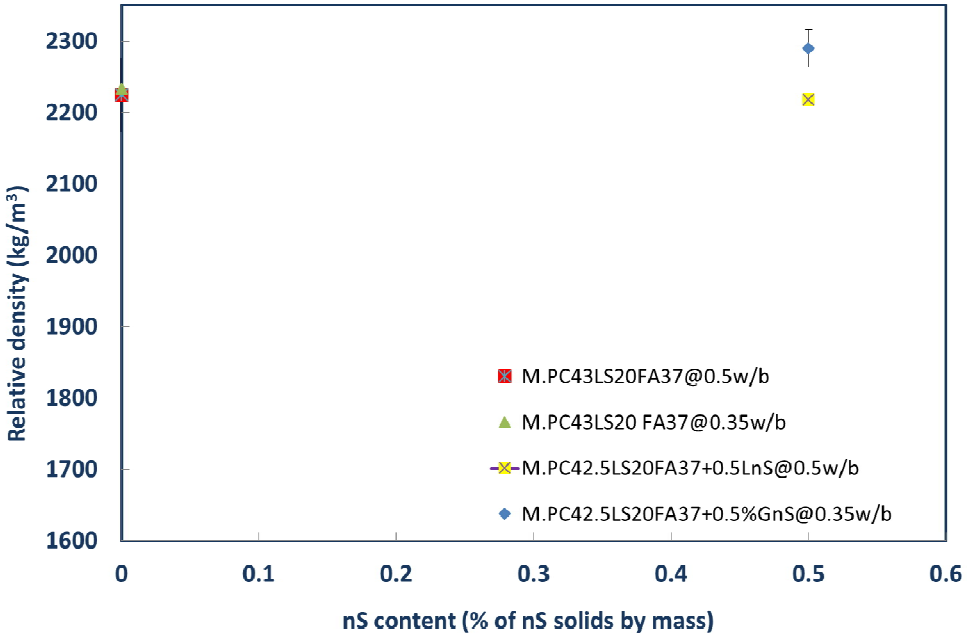

Figure 7-34: Relative density of nS modified mortars based on PC43LS20FA37

7.4.4 Cube compressive strength and relative density of mortars based on PC60LS20FA20 & PC60FA40

Two last series of mortars were finally produced. The first one was based on PC60LS20FA20, and CEMI-45R was used for its production and the second one was based on PC60FA40 using CEMII-42.5R. The results of both series were presented in one graph (Figure 7-35).For the first series, the 0.5% LnS addition offered favourable results, but the 0.25% GnS addition did not. For the second series only the LnS modification was carried out, however without exhibiting strength enhancement. Significant strength variability was observed for the lower GnS content mortar specimens.

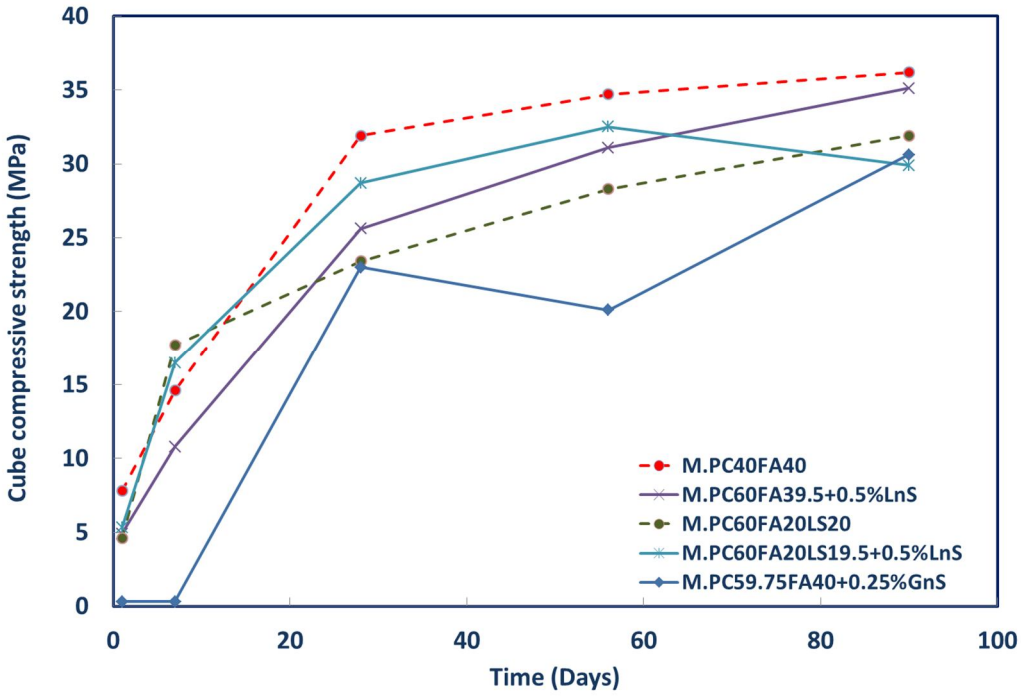

Figure 7-35: Cube compressive strength of nS modified mortars based on PC60LS20FA20 & PC60FA40

For both series, the late age (after month 3) relative density of the mortars was again enhanced by the addition of the nS (Figure 7-36). However, significant relative density variability was observed for the lower GnS content mortar specimens.

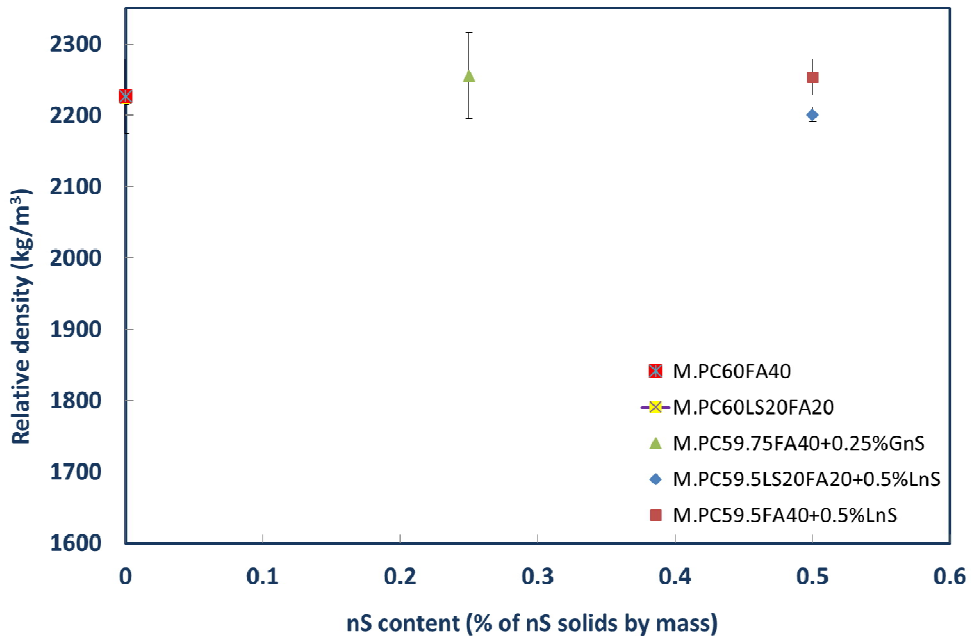

Figure 7-36: Relative density of nS modified mortars based on PC60LS20FA20 & PC60FA40

7.5 Quinary µS and LnS modified cement formulations on PC43LS20FA37

7.5.1 Introductory section

In the last two sections of analyses in this chapter, paragraphs 7.5 and 7.6, the compressive strength and thermogravimetric results of two sets of quinary pastes are presented, both based on PC43LS20FA37. The first was modified by the addition of µS and LnS and the second of µS and GnS. The addition of micro and nanosized silica, has been reported to reduce porosity and improve mechanical properties of cements, although the possibility of use of superplasticizers has also been acknowledged (Gupta, 2014). In this series no superplasticizers were used. The results are presented below.

7.5.2 Compressive strength of PC/FA=1.16 cement pastes

Once again the specimens containing 0.5% nS by mass performed better than those containing 1% nS by mass. As shown in Figure 7-37, LnS exhibited greater potentials with the higher content of µS (5% by mass). However the strength gain was delayed until day 90.

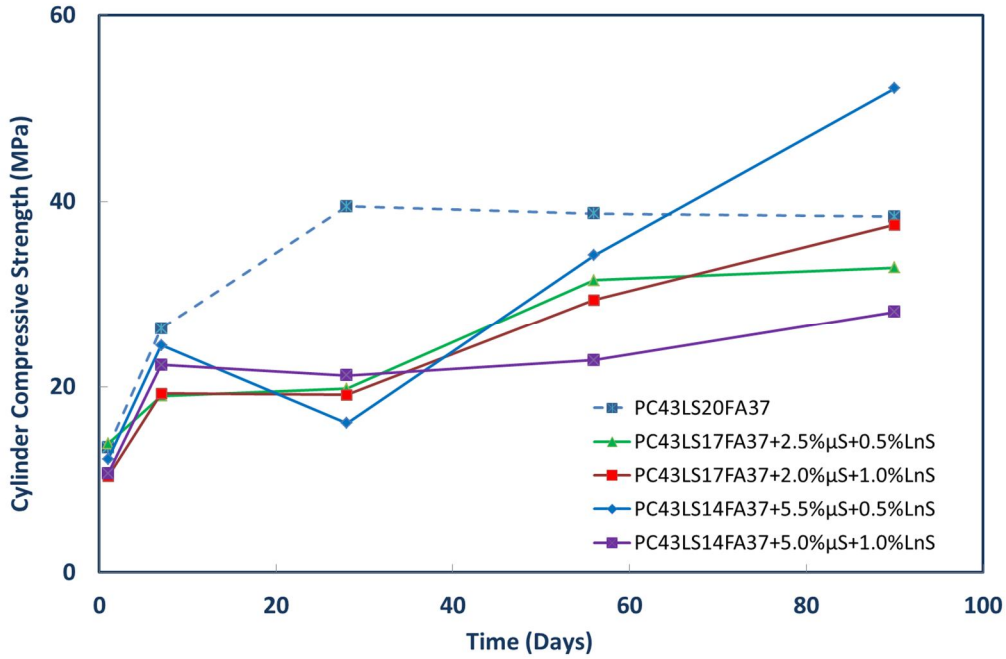

Figure 7-37: Cylinder compressive strength of µS and LnS modified cement pastes based on PC43LS20FA37

7.5.3 Thermogravimetric analyses of cement pastes

It is interesting to note the similarities between the graph depicting the $Ca(OH)_2$ consumption in the LnS modified pastes and the one for the µS and LnS modified pastes (Figure 7-38). The only difference between the two is the slightly greater consumption of the latter, attributed to the µS. Once again the 0.5% LnS combination showed better performance by consuming more $Ca(OH)_2$ at later ages. The samples showed signs of carbonation (Figure 7-39). In fact, for the first two samples at the lower µS content, the LS content was reduced to 17% by mass, and the $CaCO_3$ detected, was of this order. The same was valid for the other two samples at the higher µS content, in which LS was reduced to 14% by mass. Furthermore, the differences in the TG analyses of the 28 day old and 56 day old µS pastes can be observed in Figure 7-40 and in Figure 7-41. The consumption of $Ca(OH)_2$ is evident with simultaneous production of additional C–S–H.

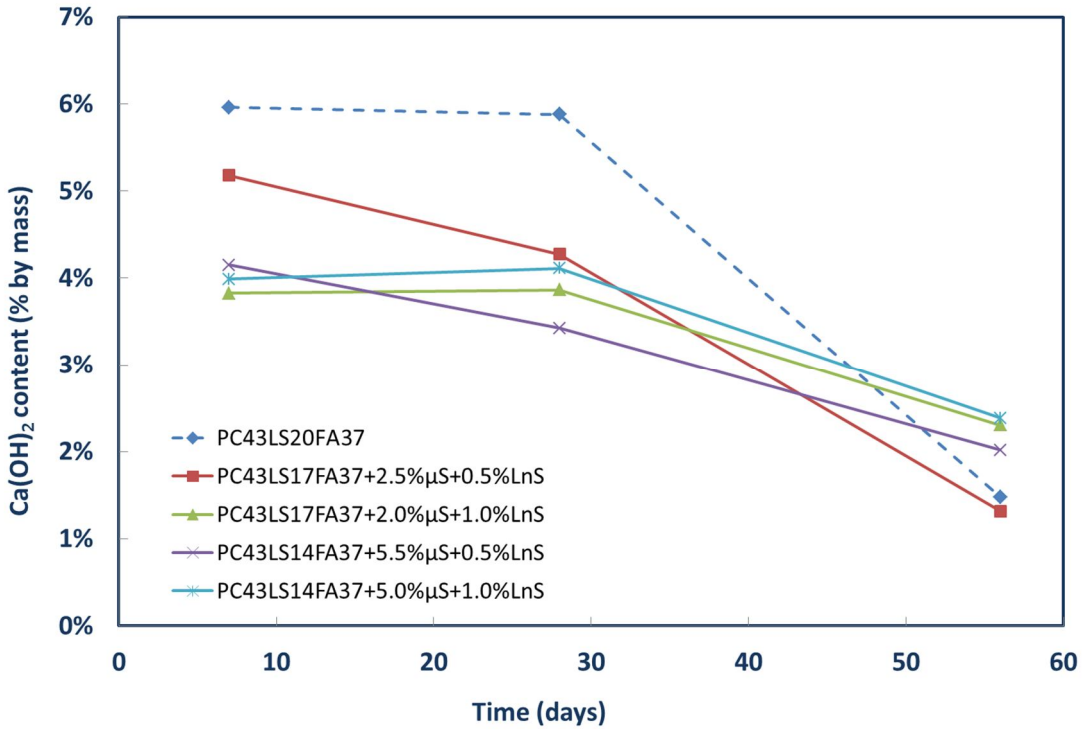

Figure 7-38: $Ca(OH)_2$ content of LnS and µS modified cement pastes based on PC43LS20FA37

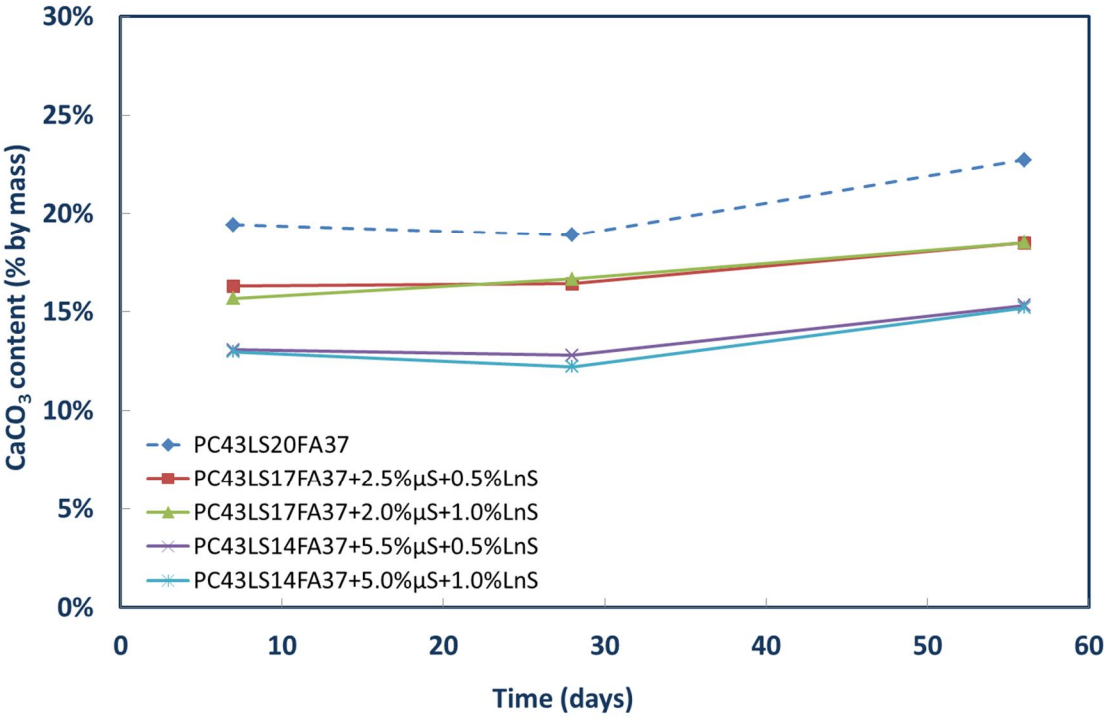

Figure 7-39: $CaCO_3$ content of LnS and µS modified cement pastes based on PC43LS20FA37

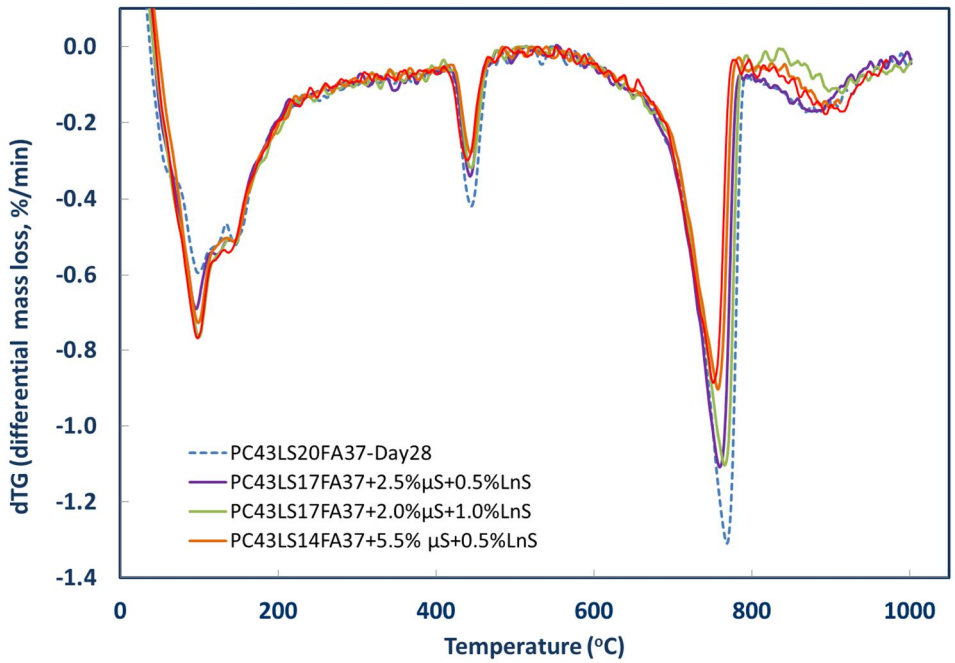

Figure 7-40: Differential mass loss of LnS and µS modified cement pastes based on PC43LS20FA37 between 0-1000°C at Day 28

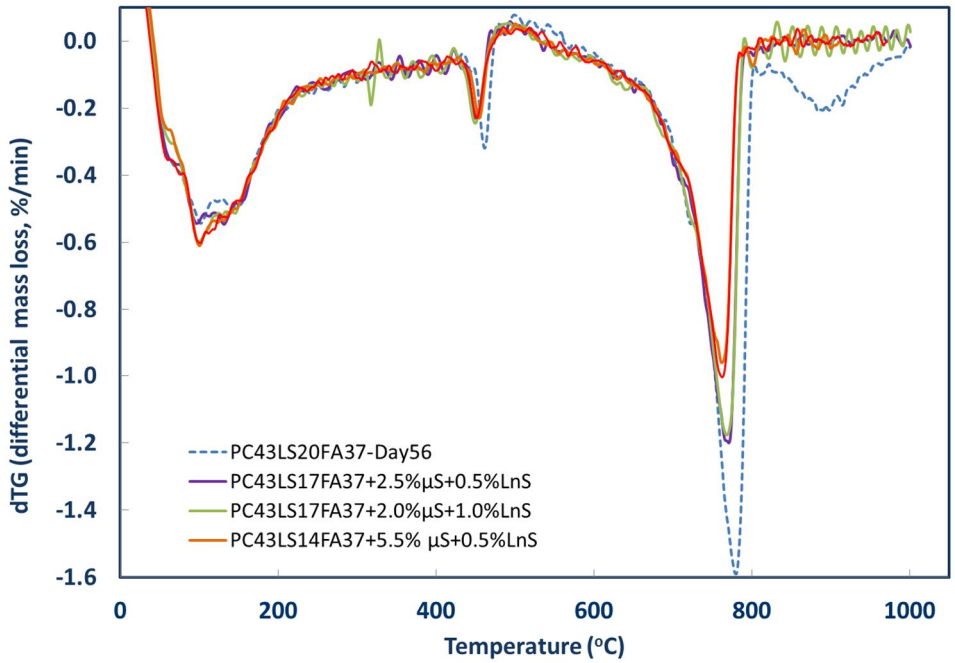

Figure 7-41: Differential mass loss of LnS and µS modified cement pastes based on PC43LS20FA37 between 0-1000°C at Day 56

7.6 Quinary µS and GnS modified cement formulations on PC43LS20FA37

7.6.1 Introductory section

The results presented below bear some similarity to the ones produced through the µS and LnS modification of cement pastes.

7.6.2 Compressive strength of PC/FA=1.16 cement pastes

Once again the specimens containing 0.5% GnS by mass performed better than those containing 1% GnS by mass. As shown in Figure 7-42, GnS performed better in combination with the lower µS content (2.5% by mass). However, even in the case of GnS, superior strength was only achieved after day 56. The FA, µS and nS particles in these quinary formulations compete for the consumption of the $Ca(OH)_2$ produced by cement hydration. Hence, the pozzolanic reactions must have been delayed.

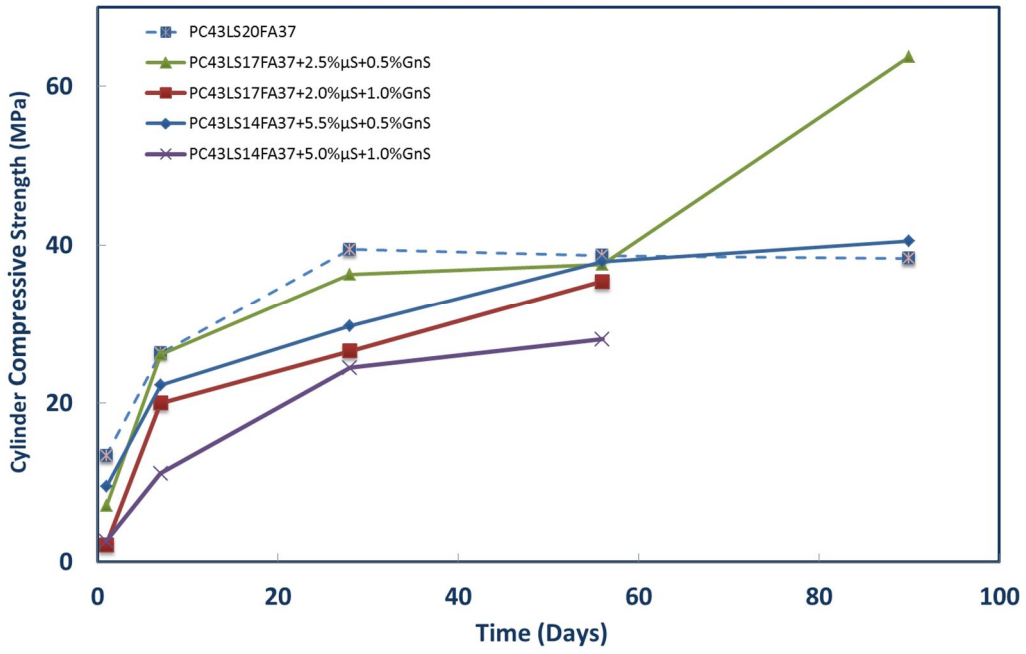

Figure 7-42: Cylinder compressive strength of GnS and µS modified cement pastes based on PC43LS20FA37

7.6.3 Thermogravimetric analyses of cement pastes

The trend in $Ca(OH)_2$ consumption in the μS and GnS modified cement pastes is almost identical to the one delivered by the GnS only modified pastes. The overall consumption is slightly lower, though, due to the reactivity of μS. Two things should be noted: (i) the 0.5% GnS with 2.5% μS paste consumed greater quantities of $Ca(OH)_2$ (Figure 7-43) and (ii) it was this paste that exhibited the best compressive strength performance. Therefore the prementioned criterion of correlation between compressive strength and $Ca(OH)_2$ consumption holds even in this case of very complex pastes. Furthermore, there were no indications of carbonation having taken place (Figure 7-44).

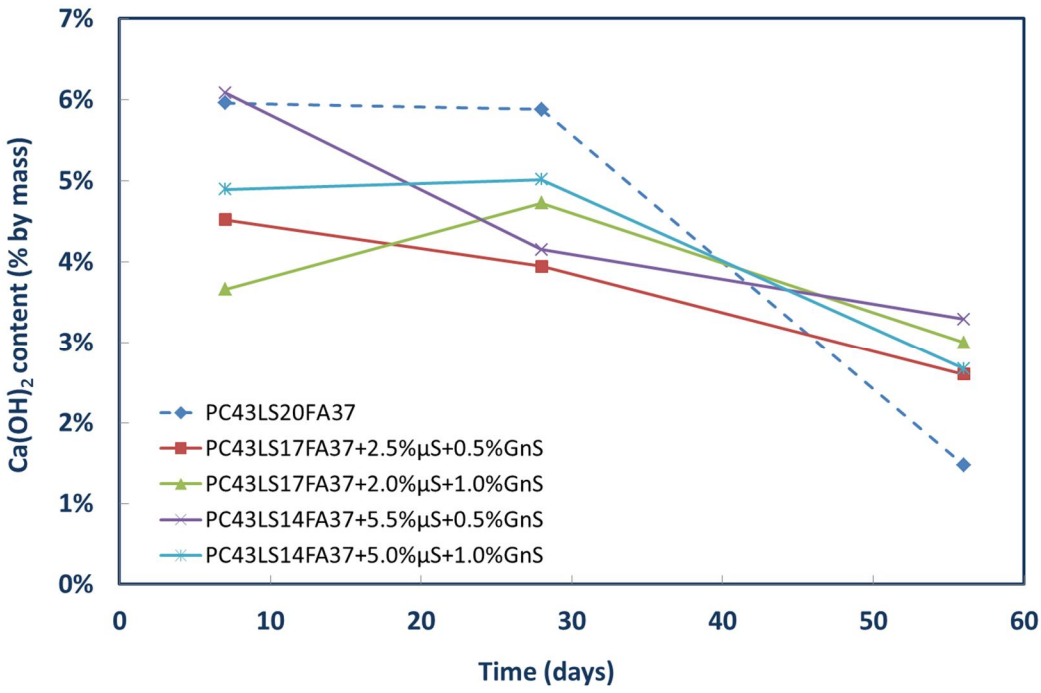

Figure 7-43: $Ca(OH)_2$ content of GnS and μS modified cement pastes based on PC43LS20FA37

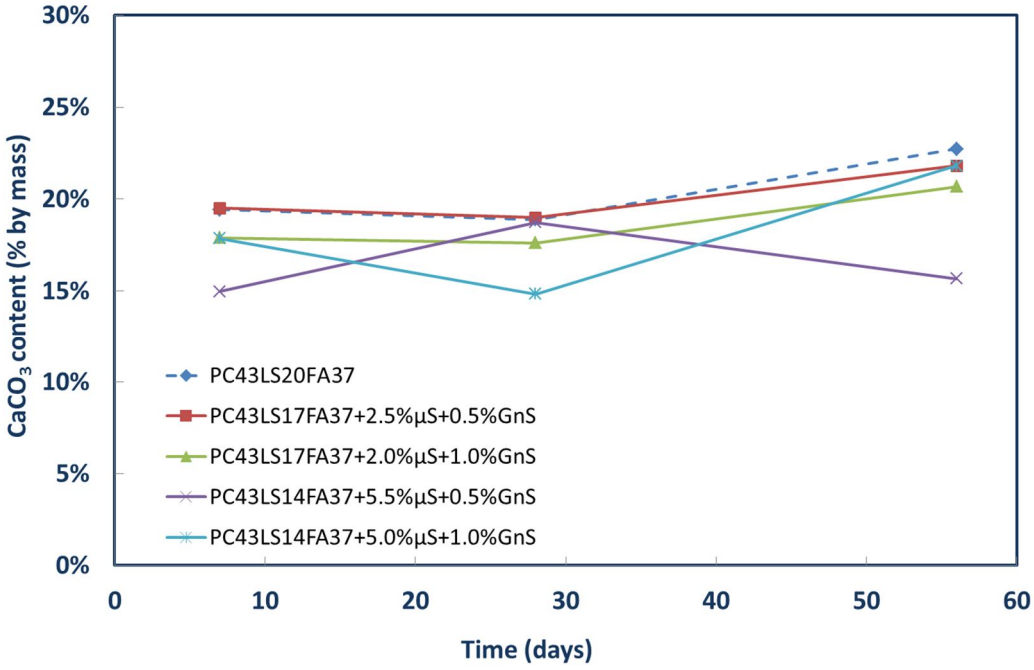

Figure 7-44: $CaCO_3$ content of GnS and µS modified cement pastes based on PC43LS20FA37

7.7 Further discussion and conclusions

In this chapter, five different combinations of nanoparticles of silica were studied. Through a number of interrelated experiments, the optimal dosage was determined to be 0.5% by mass of the binder. The differences that the two dispersions caused within the pastes were discussed in terms of chemical reactions and hydration products, density, strength and microstructure of the pastes. Through a detailed investigation, the results of excessive usage of these nanoparticles were also defined.

All results were also presented in terms of the ratio of PC/FA contents, as it proved to be critical for the evaluation of the performances.

8 NANOCLAY MODIFIED CEMENT FORMULATIONS

8.1 Introductory section

As elaborated upon in Chapter 4, a non pozzolanic reference paste, a Portland limestone cement, was selected to assess the performance of the three different nC dispersions. The nC was added at different proportions resulting eventually, in a total of fifteen, ternary cement formulations. Specimens were prepared according to the specifications given in Chapter 4. The nC modified cement pastes were tested in compression at different ages starting from day 1 and reaching day 170. No significant strength improvements were achieved for any of the dispersions. Characterization of selected pastes allowed for more conclusions to be drawn and links to be formed between nanostructural characteristics and mechanical performances. Finally, a number of standard mortar cubes were also tested in compression with a twofold target; (i) to eliminate any possible size-effects or autogeneous shrinkage which are unavoidable when testing small cylindrical specimens of pastes in compression and since no significant increase in compressive strength was observed in the cement paste samples (ii) to provoke further activation of the nC with the addition of nS in the mortar combinations. In general, the effectiveness of the two organomodified and one inorganic nC dispersion was compared, with respect to compressive strength, additional pozzolanic or hydraulic activation, C–S–H and ettringite formation, porosity and late age density.

Some of the results presented herein have been peer reviewed and accepted for publication at the three yearly international conference NICOM5 in Chicago in May 2015 (Papatzani *& Paine*, 2015).

8.2 Ternary cement formulations with nC

8.2.1 Compressive strength of cement pastes

The standard deviation was computed for all specimens but was not presented in the graphs for reasons of clarity. The standard deviation of the reference paste was 8 MPa. For nC1 it was approximately equal to 3 MPa, for nC2 it reached 3.3 MPa, whereas for nC3 it was about 4.1 MPa. Therefore the addition of nC seemed to have improved the standard deviation of compressive strength of the reference paste. This is an indication of the better packing that nCs can offer within Portland limestone cement pastes, as discussed in Chapters 2 and 3.

The compressive strength results are included in Figure 8-1, Figure 8-2 and Figure 8-3. All three different nC dispersions seemed to be offering marginal improvements in compressive strength and only at the lower substitutions, i.e. for nC solids summing up to 1% by total

mass of solids as suggested in earlier researches (Kuo *et al.*, 2006). The performance was less favourable with the advancement of time. By investigating the limits, it was confirmed that high contents of nC, which since in aqueous dispersions limit the amount of extra water added to the binder, are detrimental to the pastes. At the same time, it can be suggested that 1% of solids is the upper limit for the organomodified nC with no superplasticizer added, whereas the inorganic nC could probably be added at slightly greater amounts.

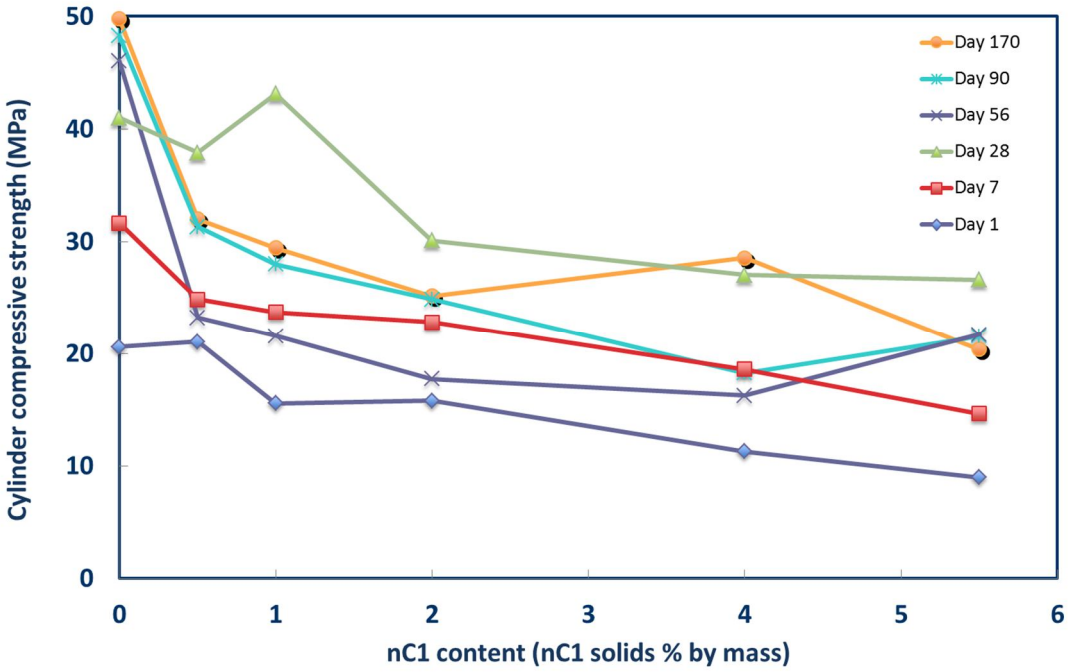

Figure 8-1: Compressive strength of nC1 modified cement pastes

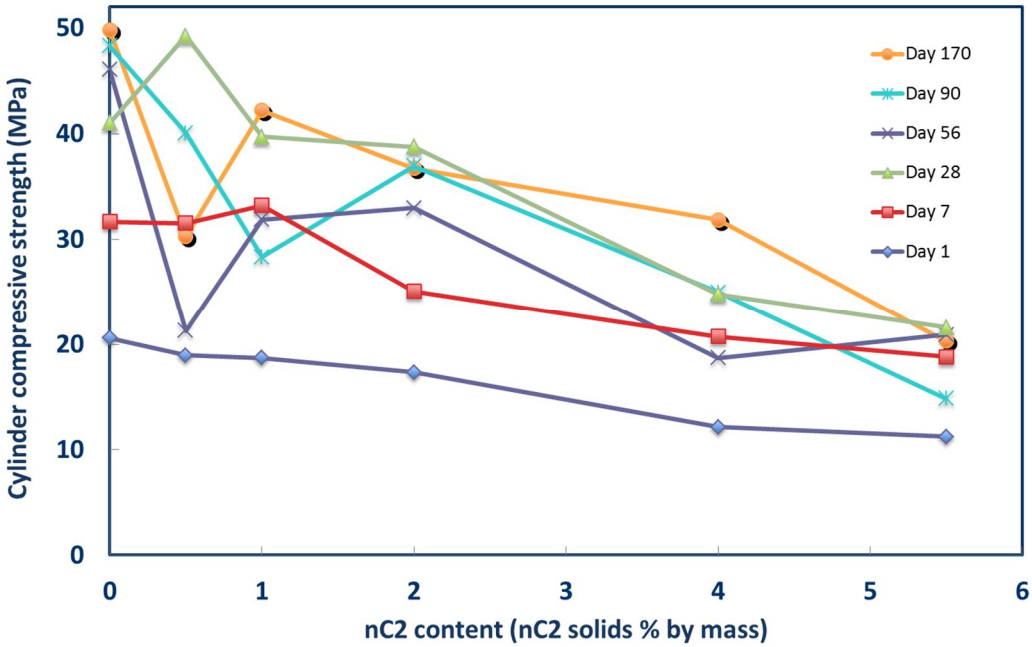

Figure 8-2: Compressive strength of nC2 modified cement pastes

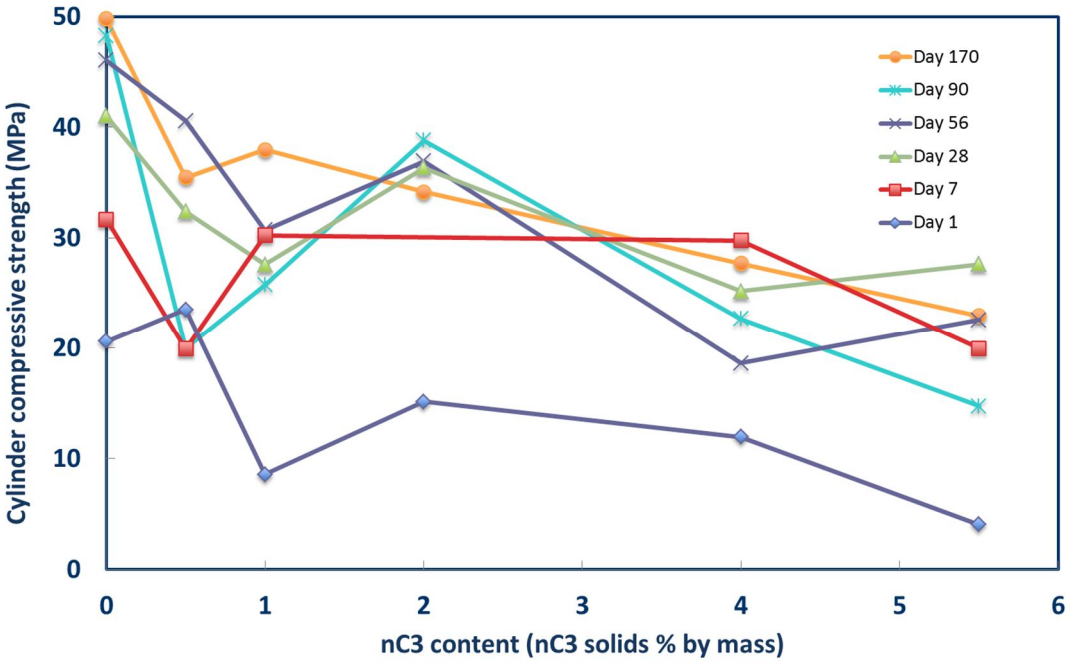

Figure 8-3: Compressive strength of nC3 modified cement pastes

These results were in agreement with the nanostructural characterization of the dispersions, presented in Chapter 3, and with the visual inspection of the specimens, which was reported in Chapter 4. The overall decrease in compressive strength of the nanomodified pastes, as compared with the reference paste can be attributed to the following factors, so far:

i. nC1 was identified as the weakest dispersion, with particles conglomerating. Evidently, this led to the creation of lumps of clay within the paste, acting as weak links and reducing the potentials of variable particle size distribution. Aside from that, nC1 was intercalated, rather than exfoliated, therefore less active as a nanomaterial.

ii. nC2, which was also intercalated with some exfoliated platelets, showed less conglomeration, better abilities for nanostructural packing and was expected to engage in less brittle behaviour. However, these characteristics were still not enough to improve the compressive strength performance of the nC2 modified pastes beyond the control paste. In addition, as shown in Figure 8-4 nC2 exhibited much more ductile behaviour than the reference paste and nC1.

iii. nC3, was better exfoliated and more stable, however, very viscous. Hence, the pastes produced at this low w/b ratio were very stiff and this has caused compaction problems. Nonetheless, as shown in Figure 8-4 nC3, just as nC2, exhibited much more ductile behaviour than the reference paste and nC1.

iv. It was reported in Chapter 4 that visual inspection of the specimens, revealed an increase in visual pores for the higher concentrations of nC, possibly creating inconsistences within the mass of the nC modified pastes. Hence, the microstructure of the modified pastes with high nC content is expected to be more porous.

v. nC2 and nC3 were difficult to handle, therefore they may have not been homogeneously blended with the other two powders and with water.

vi. More mixing time could be prescribed, although the mechanoactivation of the paste could precipitate some water evaporation that could be critical in such pastes.

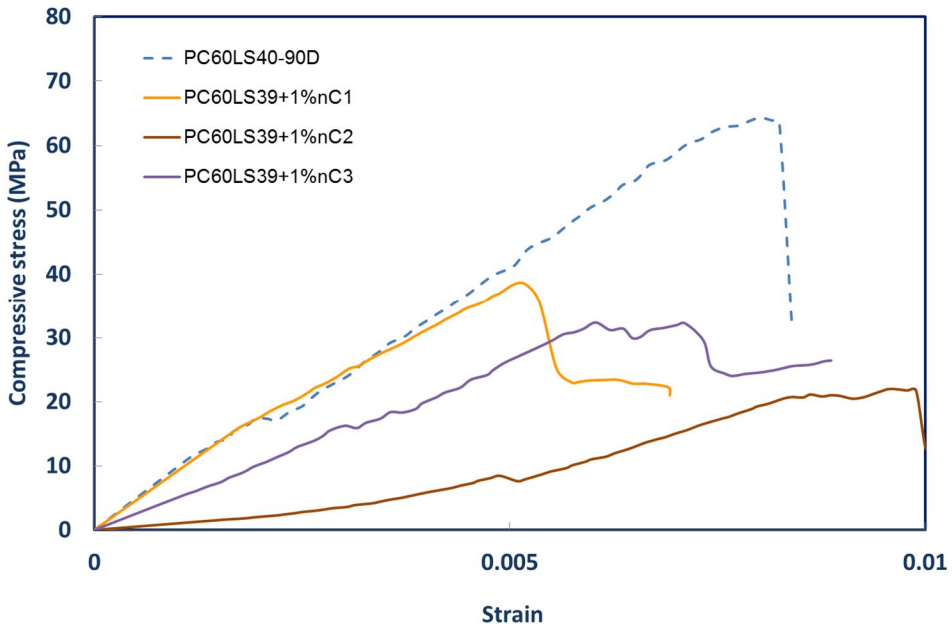

Figure 8-4: Typical compressive stress-strain curves of the nC modified cement pastes at day 90

It is the author's perception that for such low w/b ratio it is possible that the nC modified cement pastes would perform better and could exploit their potentials with the addition of superplasticizers. This is primarily because it would decrease the thixotropy of the paste permitting: (i) mixing for longer time, (ii) better dispersion of the nanoparticles within the paste, (iii) better compaction, therefore, greater homogeneity of the paste and (iv) better particle interaction, limiting air voids.

8.2.2 Thermogravimetric and crystallographic analyses of cement pastes

The thermal analyses and crystallographic investigations carried out in Chapter 3, showed potential for pozzolanic activity for the three dispersions in their own right. Although, within the cement paste, these analyses are complicated, in the first two graphs (Figure 8-5 and Figure 8-6), the $Ca(OH)_2$ content and the $CaCO_3$ content of selected pastes are shown at different ages. It should be noted that the amount of decomposition of the modifier and clay were deducted from the mass loss occurring at the 400-500°C[7] temperature band and the amount of decomposing clay was deducted from the mass loss occurring at the 600-800°C temperature band, according to the analyses carried out in Chapter 3. nC1 and nC3 seem to have consumed $Ca(OH)_2$ (Figure 8-5). It can be considered that carbonation had taken place (Figure 8-6) for most nC concentrations and ages.

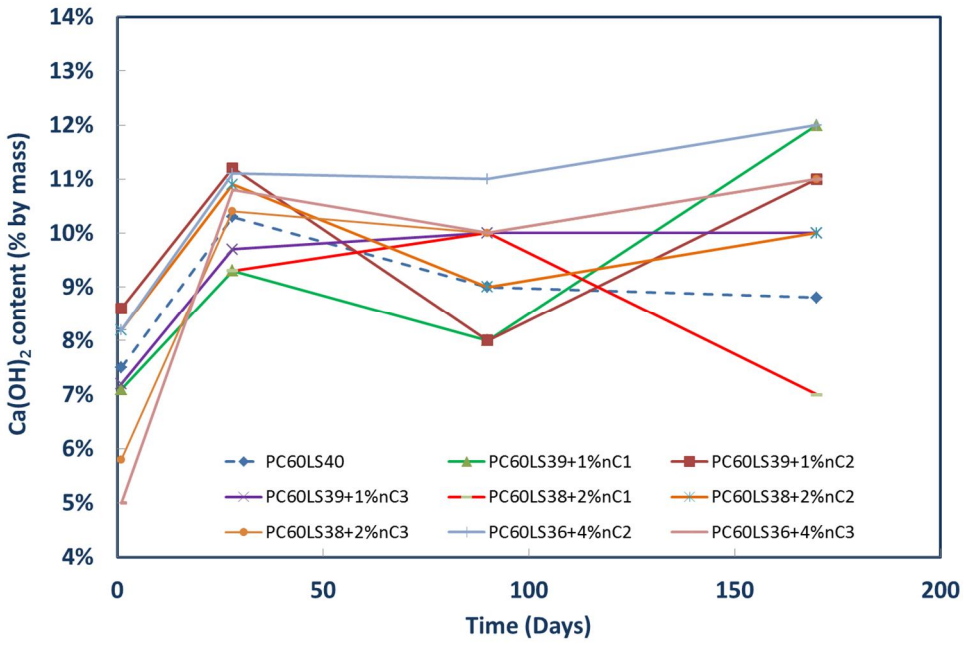

Figure 8-5: $Ca(OH)_2$ content of nC modified cement pastes

[7] The temperature ranges were selected according to a concise, tabulated literature review of TGA results of other researchers, presented in the Appendix.

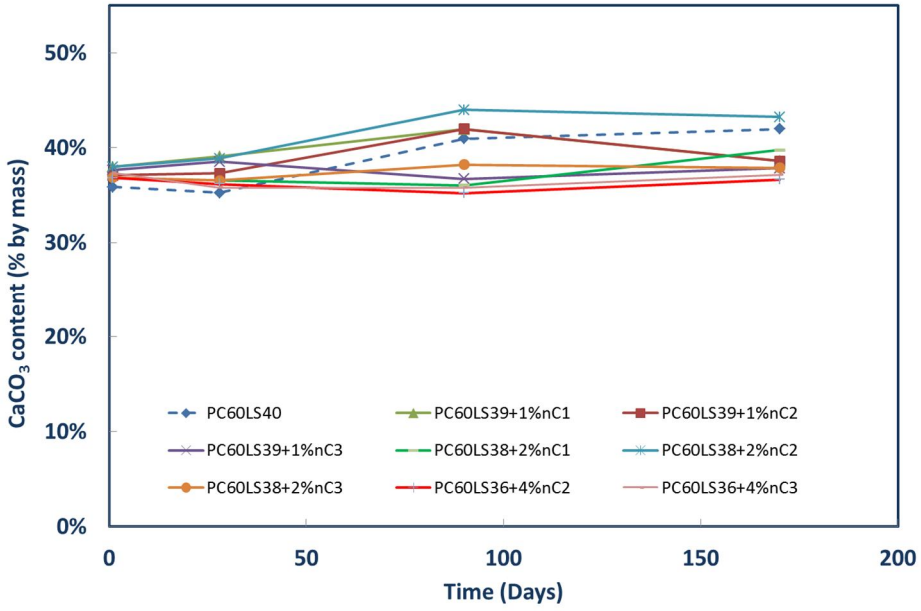

Figure 8-6: $CaCO_3$ content of nC modified cement pastes

The quantitative analysis is limited by the fact that at 400-500°C the decomposition of both, $Ca(OH)_2$ and modifier, takes place. Therefore, a gas detector on the TG analyser or differential scanning calorimeter would help with the identification of the exact phases decomposing within the specific temperature ranges and therefore the exact mass losses would have been computed. For this reason, further analysis was carried out with respect to the temperature range within which ettringite and C–S–H decompose, i.e. at approximately 100-130°C for the former and at approximately 125-180°C for the latter. At the same time it is acknowledged that calcium aluminate hydrates also decompose before 400°C (Appendix A). This comparison is more direct since the percentage of the mass loss of the modifier within this temperature was 2.63% for nC1 and 1.8% for nC2, nC3 lost 5% of adsorbed water in the same temperature range according to the thermal analyses of the vacuum dried slurries in Chapter 3. That is to say, approximately 2% of the amount of solids (1% to 5.5%) decomposed between 100-180°C. Therefore, the contribution of the mass loss of the modifier can be neglected compared to the mass loss due to the dehydration of ettringite and C–S–H[8].

At one day, the reference paste contained significant amounts of water which were lost shortly after the 100-125°C temperature range. This excess of water, however, could be captured within the galleries of the nC and for this reason the mass loss observed in Figure 8-7 is almost double than that of the reference paste. It should be noted, though that this extra mass loss could be also attributed to the decomposition of the surfactants, however,

[8] Minimum contribution of nC to the mass loss between 100-180°C = 1% x 2% = 0.0002 i.e. insignificant
Maximum contribution of nC to the mass loss between 100-180°C = 5.5% x 2% = 0.0011 i.e. insignificant

due to their limited quantity (only 5% by mass of the total quantity of nC) the first hypothesis is more realistic. The results at day 1 are shown for completion rather than further commenting.

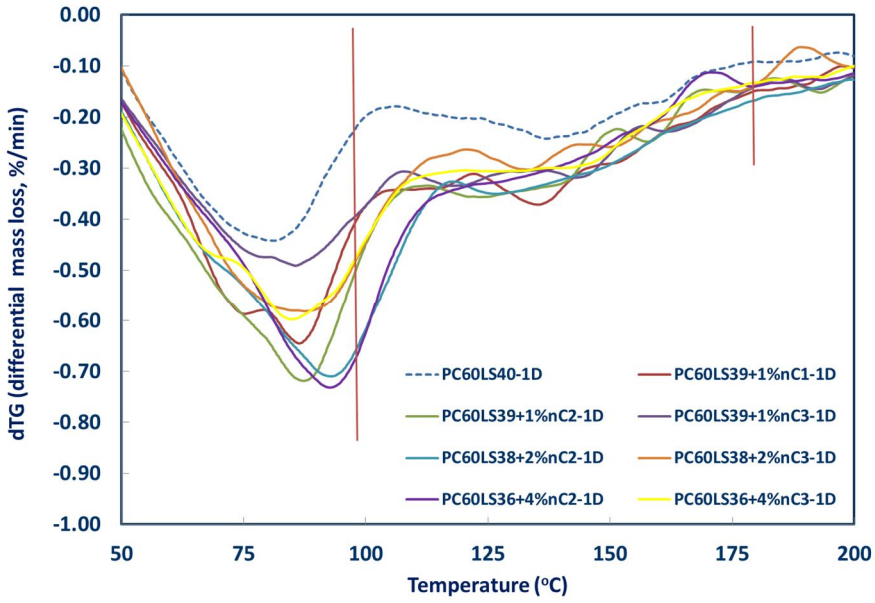

Figure 8-7: Differential mass loss between 100-200°C at Day 1

It can be seen that in the first 28 days (Figure 8-8) nC2 seemed to have produced more ettringite and C–S–H than the reference paste.

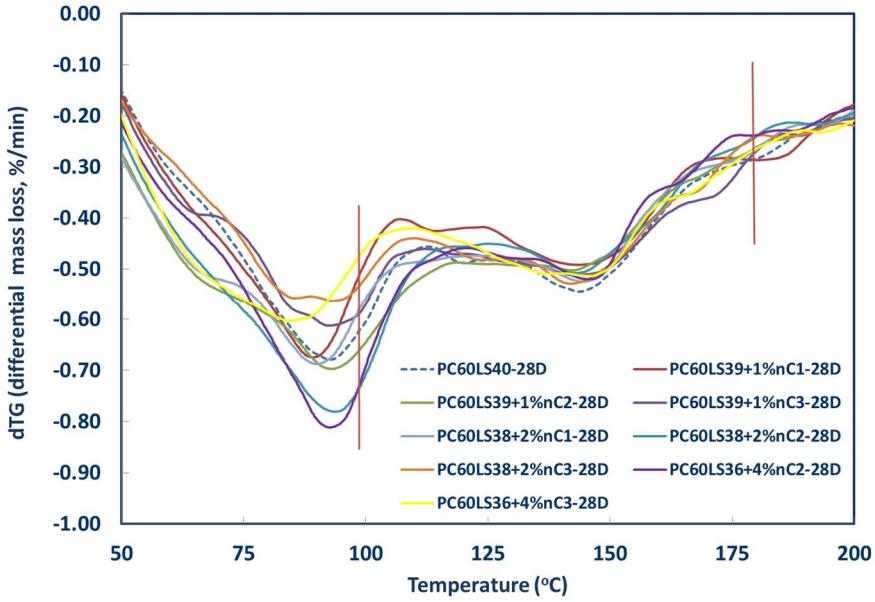

Figure 8-8: Differential mass loss between 100-200°C at Day 28

Figure 8-9 shows that by the first 3 months nC3 was the most active, and the greater the amount of nC3, the greater the production of ettringite and C–S–H. nC2 followed at marginally lower mass losses, validating the findings of the thermal analyses in Chapter 3.

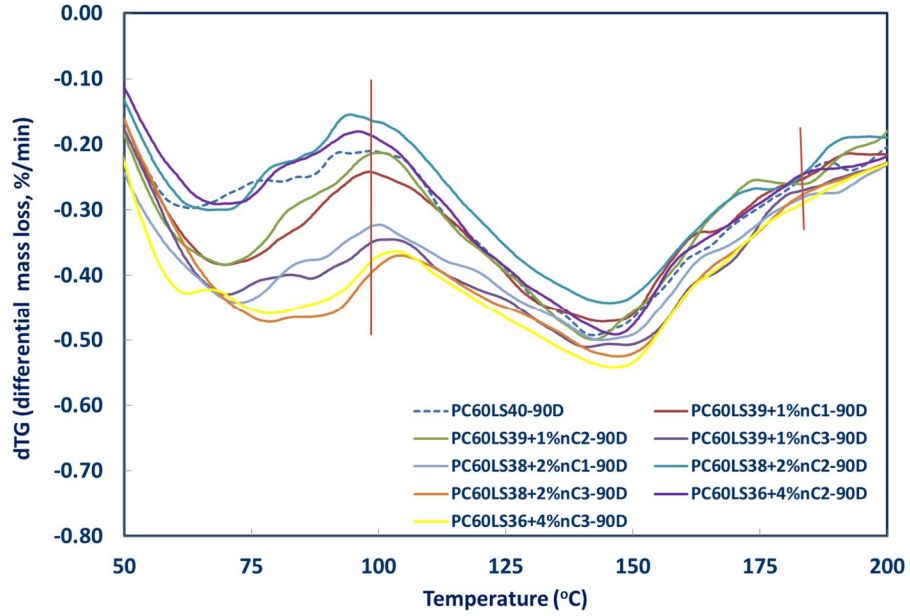

Figure 8-9: Differential mass loss between 100-200°C at Day 90

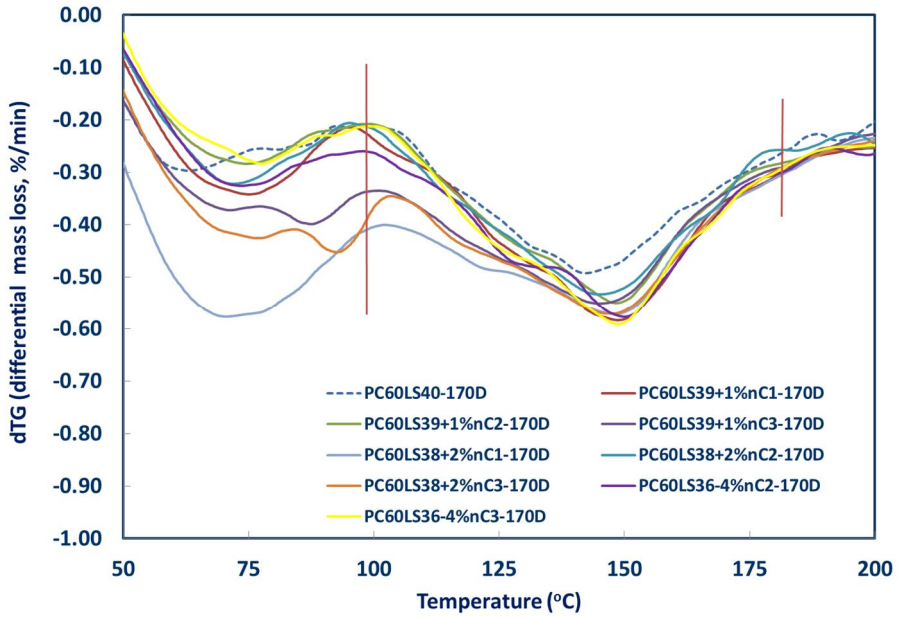

Figure 8-10: Differential mass loss between 100-200°C at Day 170

Figure 8-10 shows the effect of the nCs at almost half a year since the production of the pastes. It is apparent that the mass losses attributed to ettringite and C–S–H have increased significantly, reaching the highest values amongst the different ages of the pastes. nC3 has a more pronounced activity, which can be explained by the fact that it was better dispersed and less conglomerating, therefore the available surface area should be greater than that of the organomodified samples.

In general, the TG analyses of the nC modified Portland limestone cement pastes:

- Confirmed the TGA findings on the nC dispersions presented in Chapter 3 (that nC3 could show greater pozzolanic activity and that given time, nC2 can also engage in pozzolanic reactions).
- Provided a distinct connection between the mechanical performance of the nC modified pastes and the hydration products formed.
- Will be further validated by the crystallographic analyses that follow.

Consequently, to confirm these findings, XRD patterns were developed for 1%nC1, 1%nC2 and 1%nC3 at day 1, 28 and 90. As shown in Figure 8-11, Figure 8-12 and Figure 8-13 there is a significant reduction in the relative intensity of the $Ca(OH)_2$ peak for all nC at all ages with respect to the reference paste, contributing to the hypothesis of pozzolanic reactivity of the nC, in agreement with other researches (Chang *et al.*, 2007). The only exception was nC1, whose diffracted peak intensity corresponding to $Ca(OH)_2$ showed an increase at later ages. Moreover, a significant reduction in the relative intensity of the $CaCO_3$ peak can also be noticed, implying that the samples have, indeed, not carbonated.

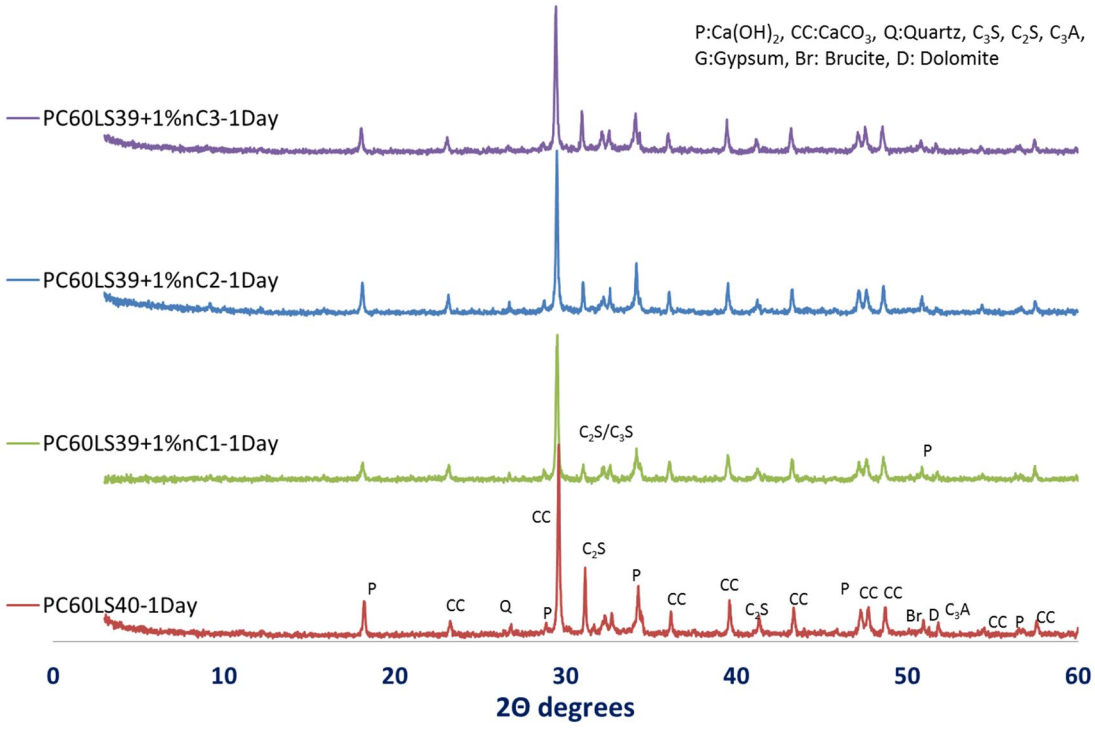

Figure 8-11: XRD pattern of nC modified cement pastes at Day 1

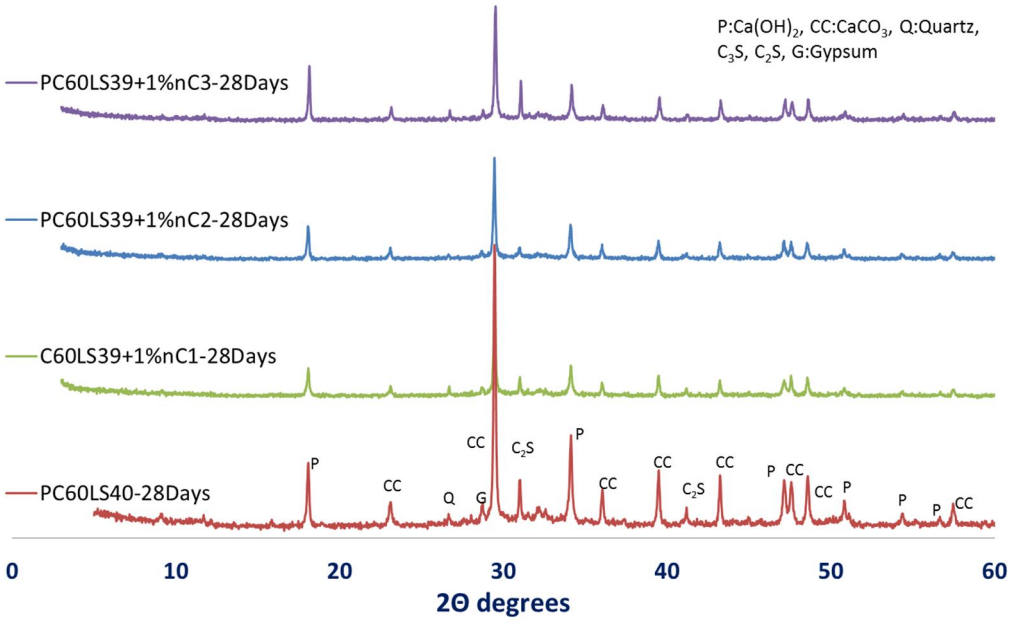

Figure 8-12: XRD pattern of nC modified cement pastes at Day 28

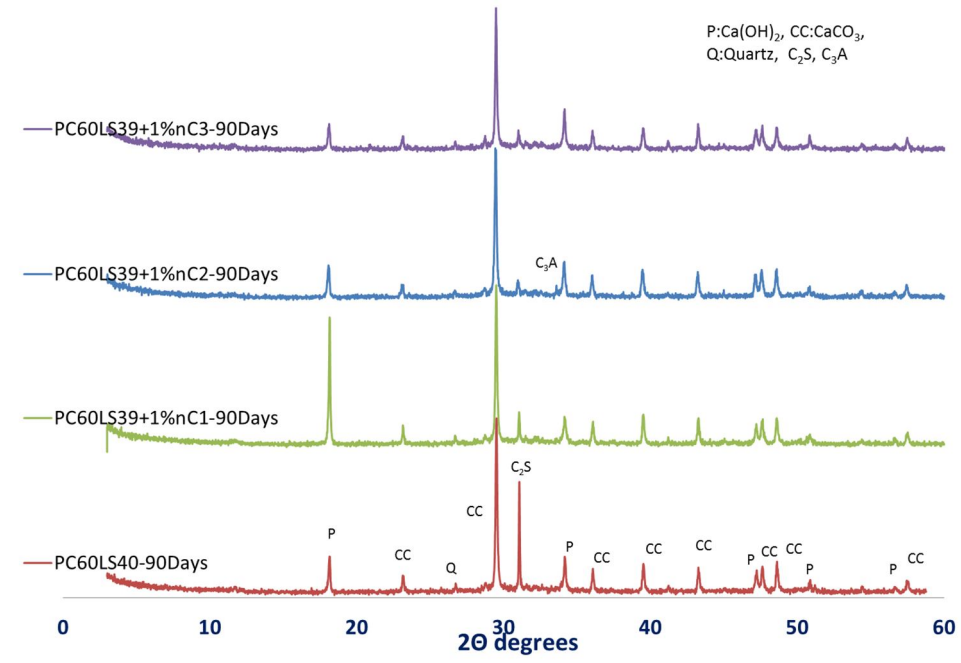

Figure 8-13: XRD pattern of nC modified cement pastes at Day 90

8.2.3 Microstructural characterisation of cement pastes

Initially, field emission SEM imaging was performed on the reference paste at day 28 and 90 at different magnifications (Figure 8-14 and Figure 8-15). The SEM examination of the microstructure revealed the presence of C–S–H in a nest-like honeycomb morphology, $Ca(OH)_2$ plate crystals (marked by the letter P) and ettringite needle shaped crystals. It is evident that the paste became significantly denser and more homogenized with age with the polygonal crystals being covered with C–S–H lamellae.

Consecutively, pastes PC60LS39+1%nC1 (Figure 8-16 and Figure 8-17), PC60LS39+1%nC2 (Figure 8-18 and Figure 8-19) and PC60LS39+1%nC3 (Figure 8-20 and Figure 8-21) were also investigated with FESEM. The micrographs of the nC1 modified pastes revealed many crystals ($Ca(OH)_2$) and characteristic of ettringite spikes, together with a great number of microcracks. Age advancement showed lack of coherence, as suspected by the compressive strength tests on that age. nC2 was the more representative hydrophobic nC and nC3 the hydrophilic nC. As discussed by He and Shi (2008) and more recently by Hosseini *et al.*(2014) the high microstructural regularity captured by the 2000 times magnification especially for nC3 modified pastes (circled area) is attributed to the presence of the exfoliated MMT. nC3 modified pastes seemed to have developed the most dense morphology, while consuming the $Ca(OH)_2$ crystals.

nC2 modified pastes showed a slightly denser paste with greater coherence at day 90 and consumption of $Ca(OH)_2$ crystals. Adding to this, the morphology of the nC2 modified pastes bear close resemblance to the morphologies delivered with the addition of nano-Al_2O_3 as shown in the micrographs produced by Hosseini *et al.*(2014). The reason behind this could be that because nC2 had the highest Si/Al ratio and also the highest Si and Al content, the nC platelets possibly produced greater volume of C–S–H.

Moreover, the reference paste and the 1% nC modified pastes were examined with the help of SEM. PC60LS40 showed a denser with age image (Figure 8-22 to Figure 8-24). PC60LS39+1%nC1 (Figure 8-25) was the less dense of the tree nanoenhanced pastes with many crystals, spikes and unhydrated PC particles present, as also observed with the FESEM. In addition significant microcracks and voids could also be distinguished in the micrograph of the nC1 modified paste. PC60LS39+1%nC2 (Figure 8-26) showed a denser, fibrilar structure with layers in parallel probably created by the nC acting as seeding agents for the hydration products. In this micrograph $Ca(OH)_2$ crystals and ettringite spikes are also present whereas PC60LS39+1%nC3 (Figure 8-27) seemed to be the most dense of the three with a honeycomb structure and less visible crystals and spikes. However, even at day 90 unhydrated cement particles could be identified (enclosed in rectangles).

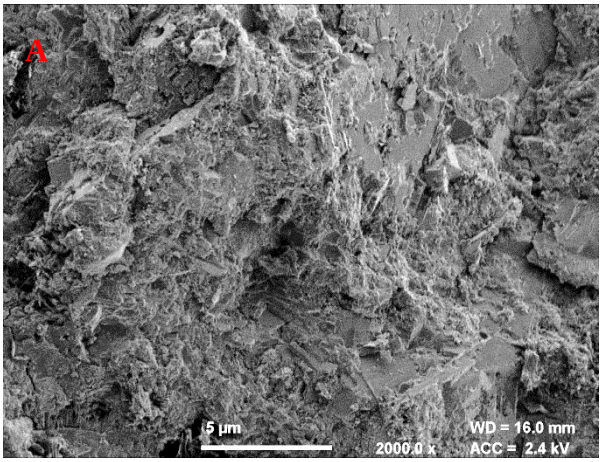

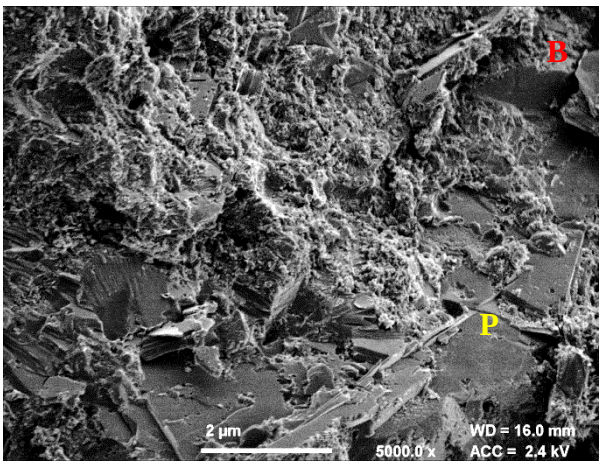

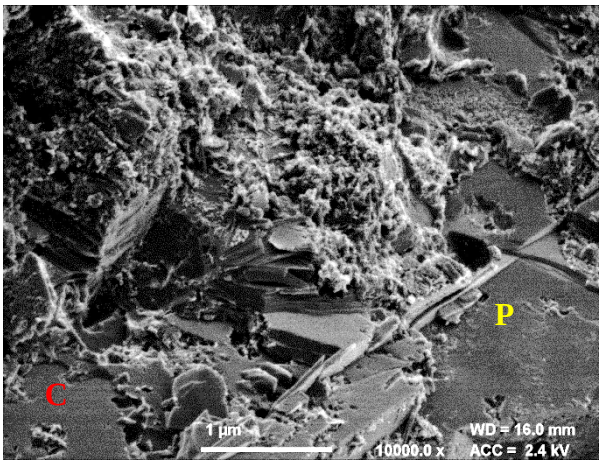

Figure 8-14: FESEM image of PC60LS40 - 28D – (A) 2000x, (B) 5000x and (C) 10000x

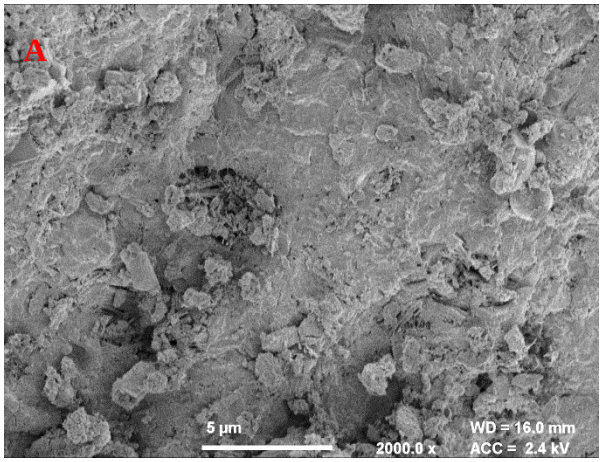

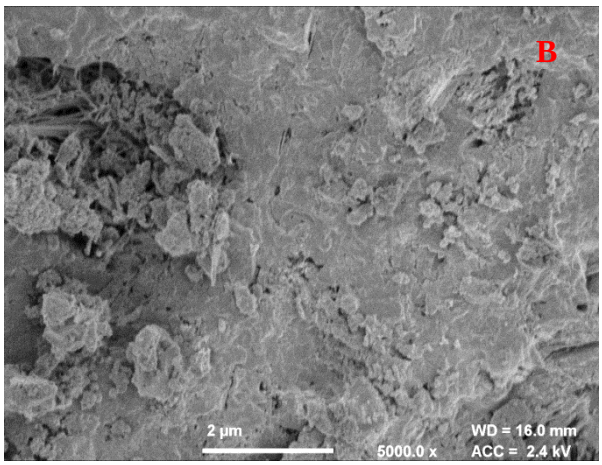

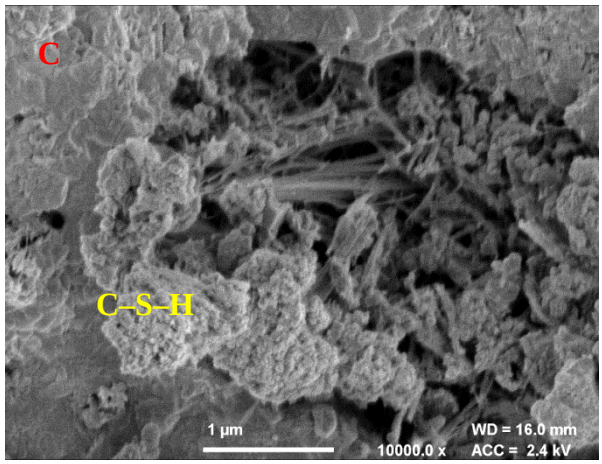

Figure 8-15: FESEM image of PC60LS40 - 90D – (A) 2000x, (B) 5000x and (C) 10000x

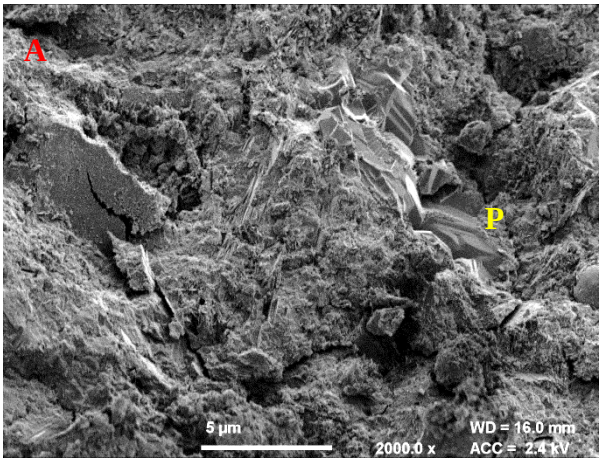

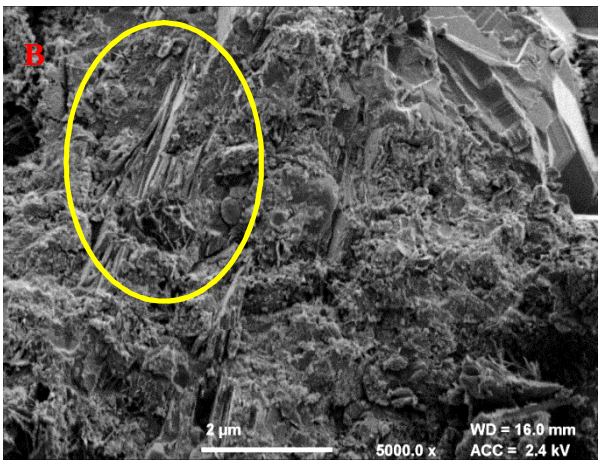

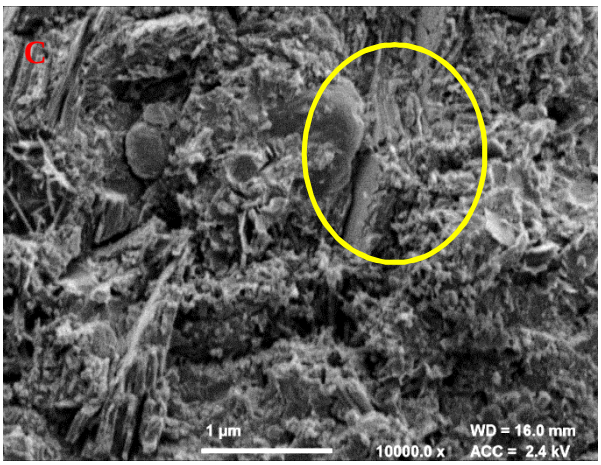

Figure 8-16: FESEM image of PC60LS39+1%nC1-28D – (A) 2000x, (B) 5000x and (C) 10000x

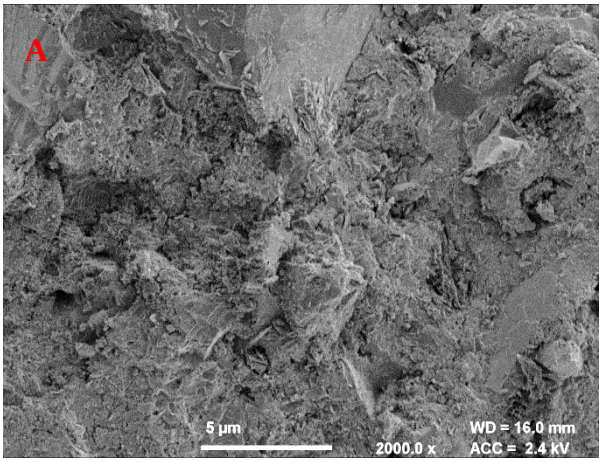

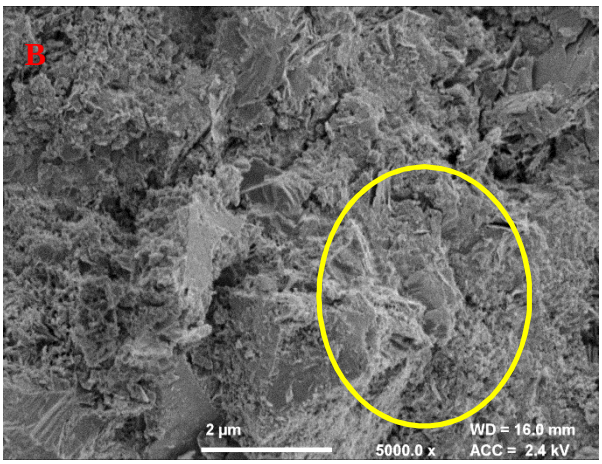

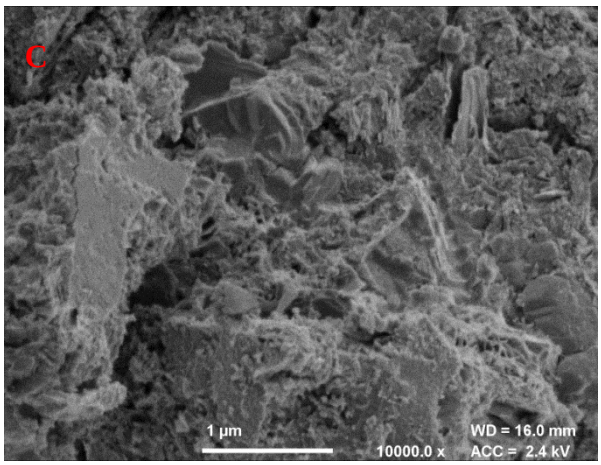

Figure 8-17: FESEM image of PC60LS39+1%nC1-90D – (A) 2000x, (B) 5000x and (C) 10000x

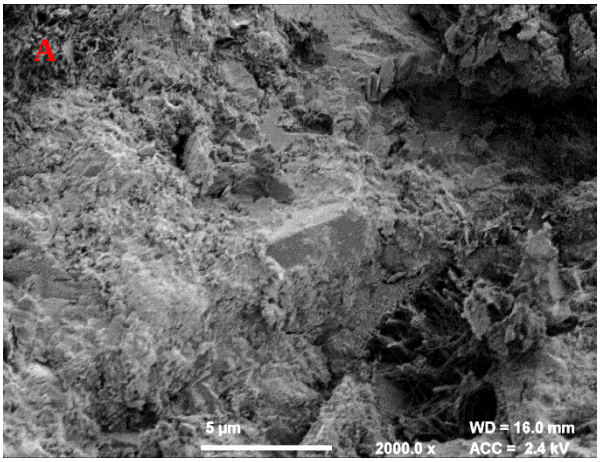

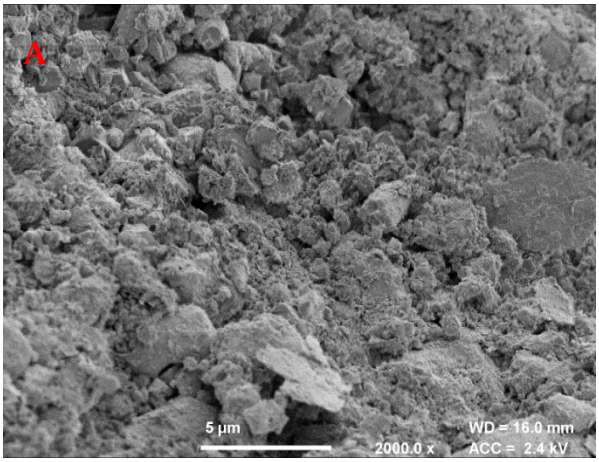

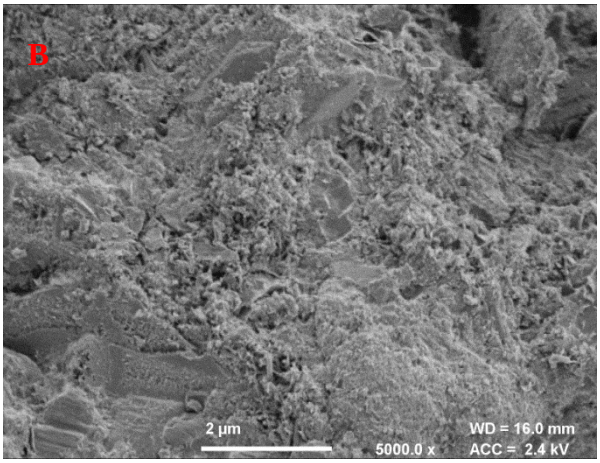

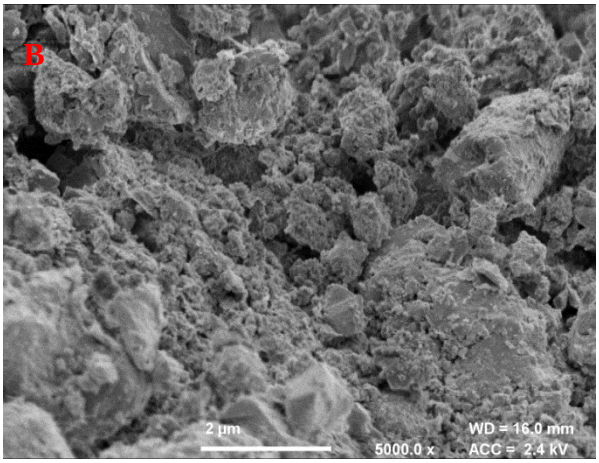

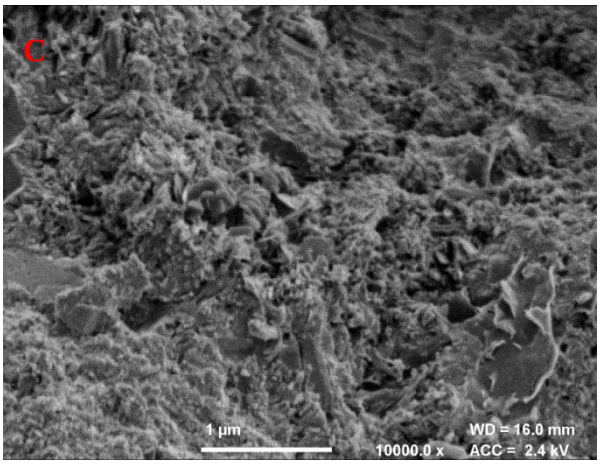

Figure 8-18: FESEM image of PC60LS39+1%nC2-28D – (A) 2000x, (B) 5000x and (C) 10000x

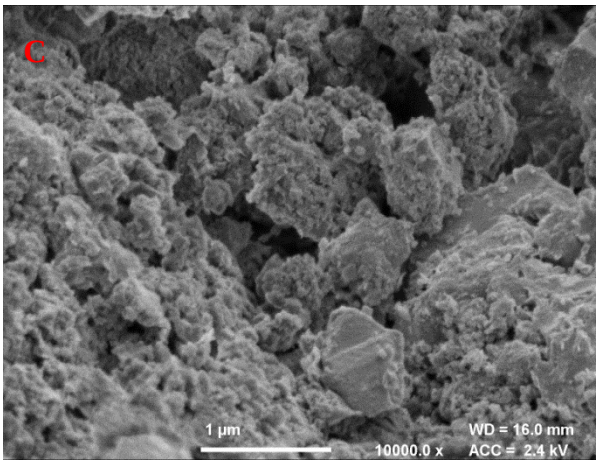

Figure 8-19: FESEM image of PC60LS39+1%nC2-90D – (A) 2000x, (B) 5000x and (C) 10000x

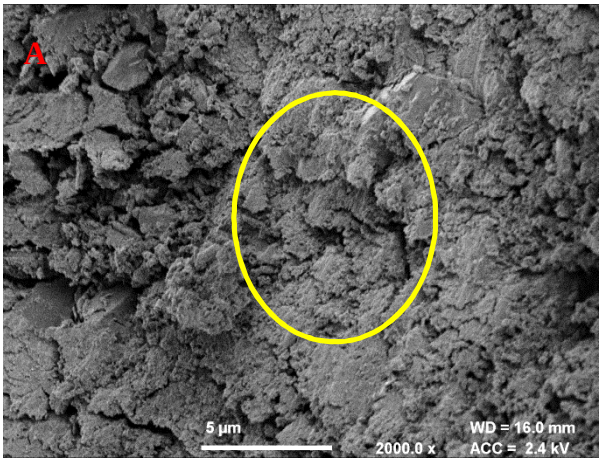

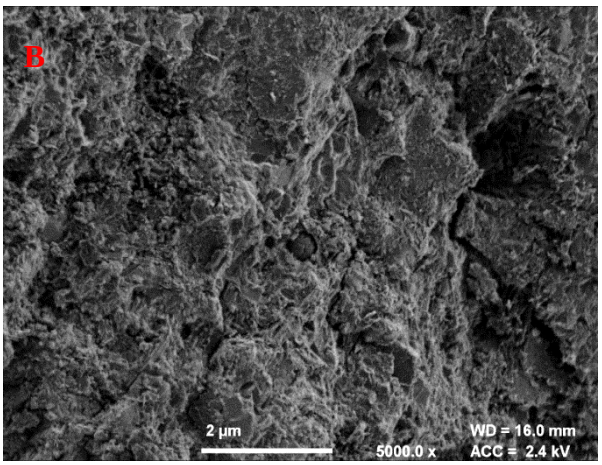

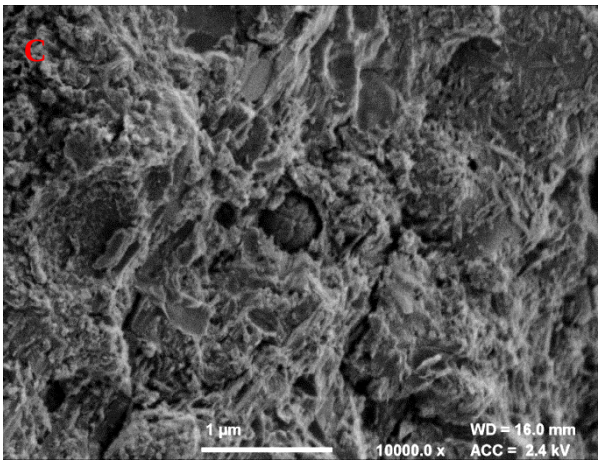

Figure 8-20: FESEM image of PC60LS39+1%nC3-28D – (A) 2000x, (B) 5000x and (C) 10000x

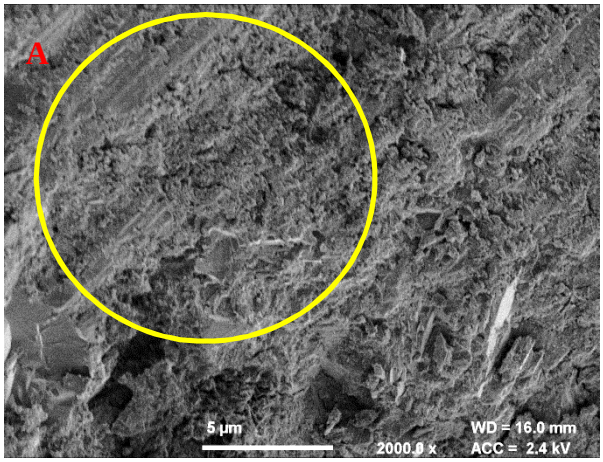

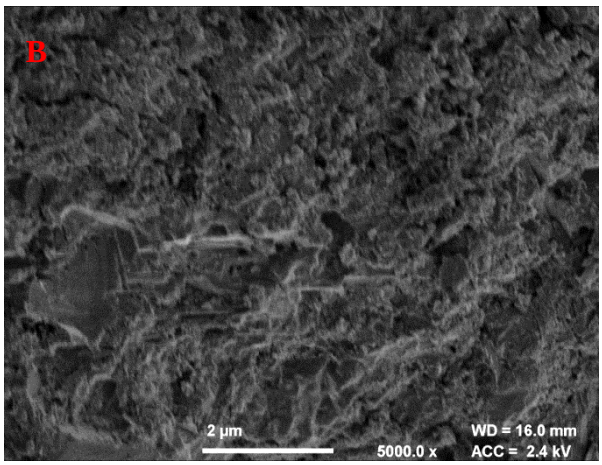

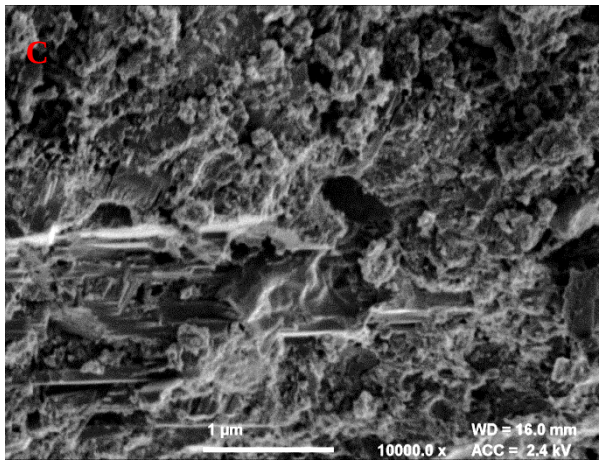

Figure 8-21: FESEM image of PC60LS39+1%nC3 -90D – (A) 2000x, (B) 5000x and (C) 10000x

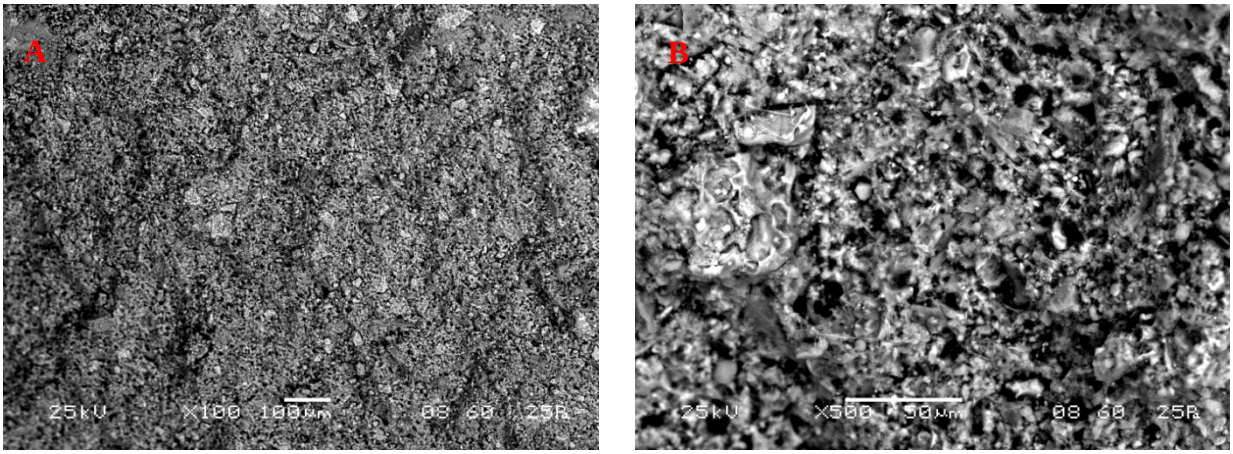

Figure 8-22: BSC micrograph of PC60LS40-1D – (A) 100x and (B) 500x

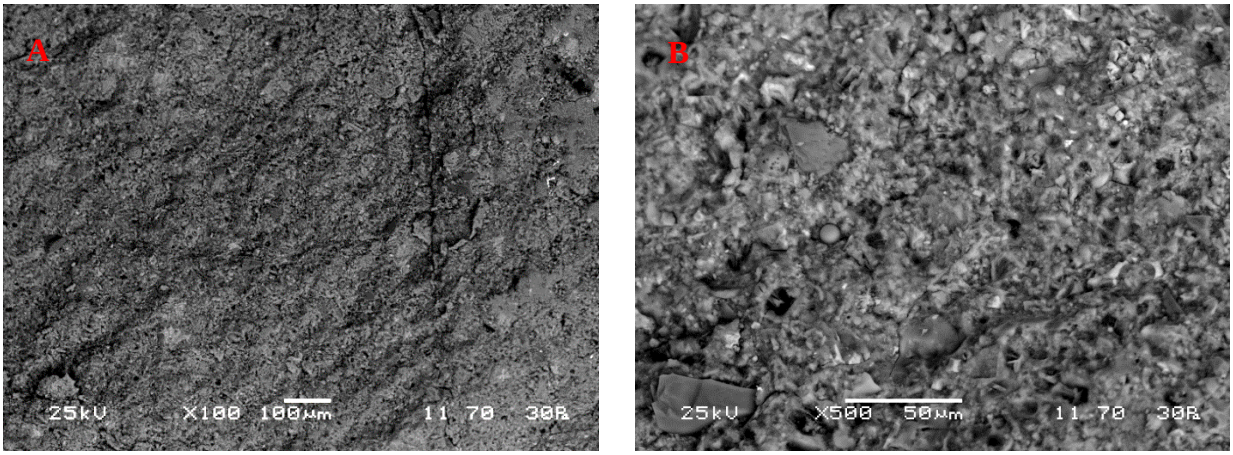

Figure 8-23: BSC micrograph of PC60LS40-28D – (A) 100x and (B) 500x

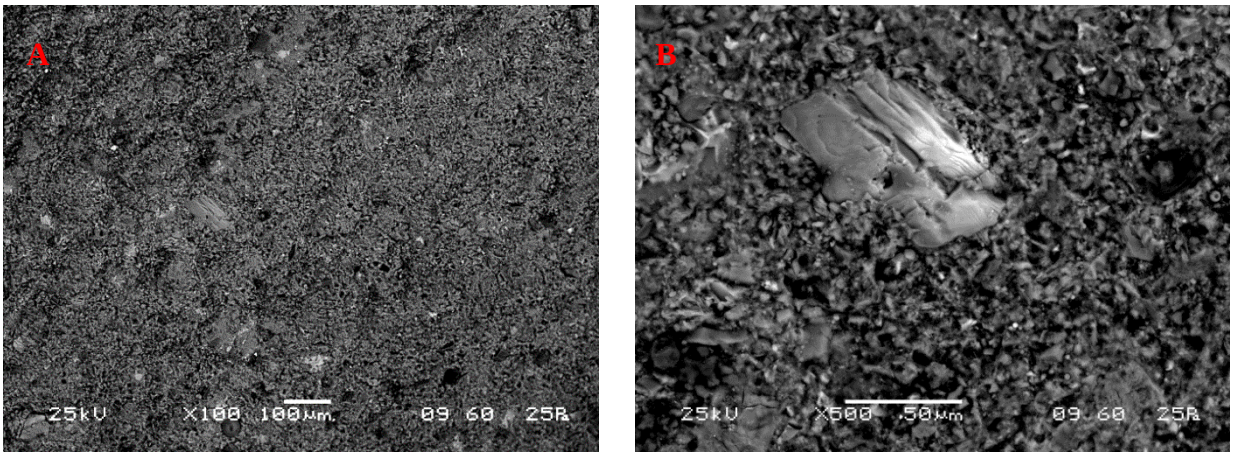

Figure 8-24: BSC micrograph of PC60LS40-90D – (A) 100x and (B) 500x

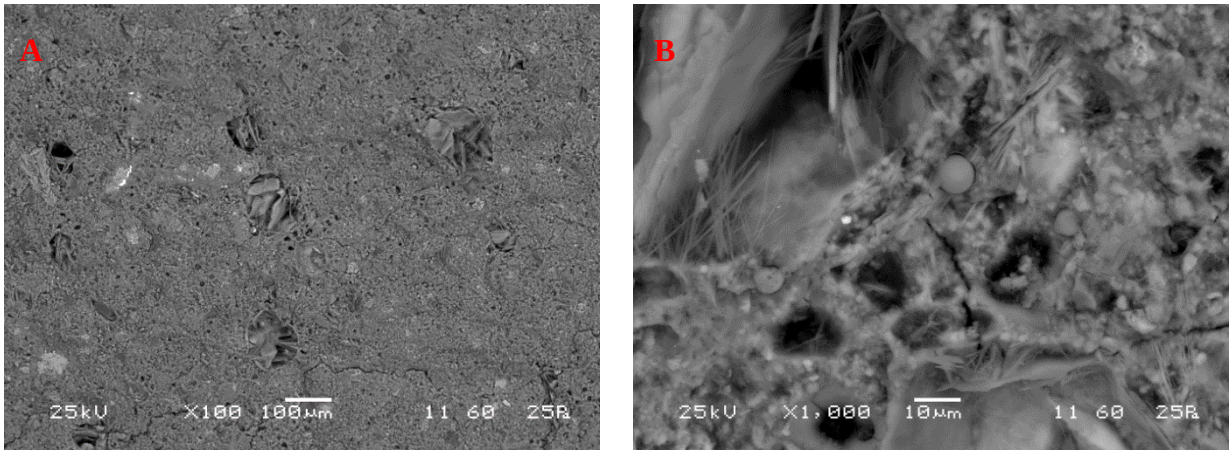

Figure 8-25: BSC micrograph of PC60LS39+1%nC1-90D – (A) 100x and (B) 1000x

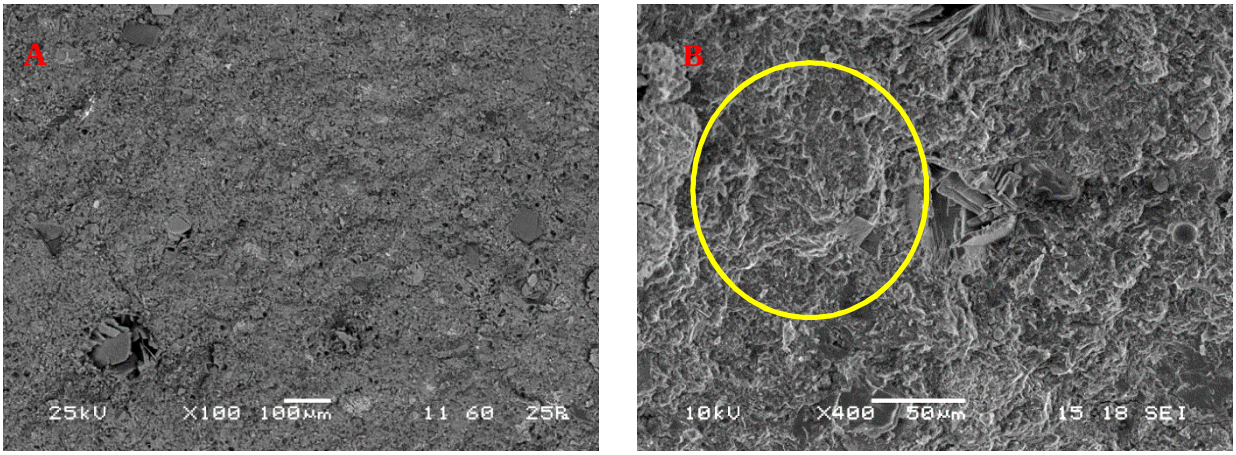

Figure 8-26: BSC micrograph of PC60LS39+1%nC2-90D – (A) 100x and (B) 400x

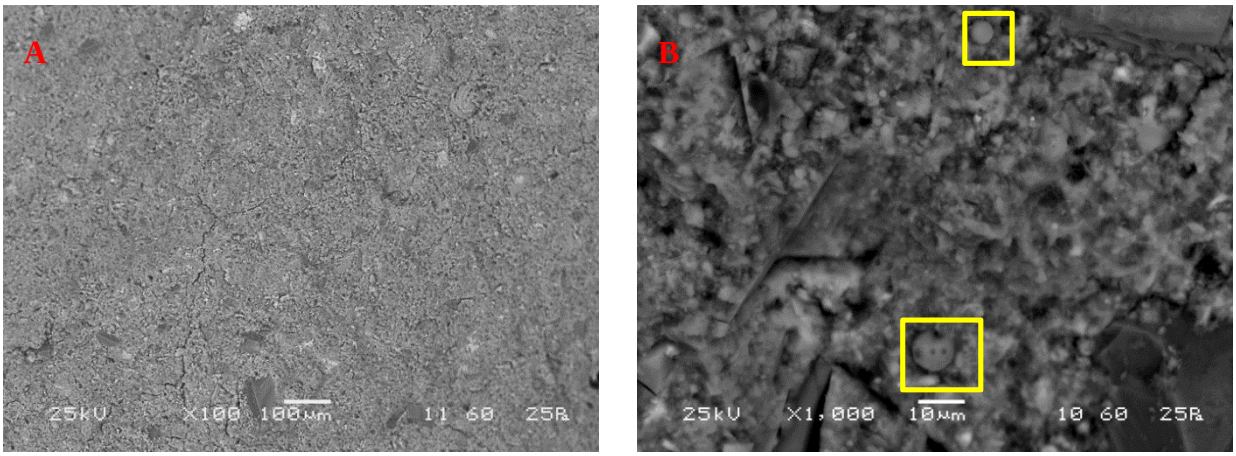

Figure 8-27: BSC micrograph of PC60LS39+1%nC3-90D – (A) 100x and (B) 1000x

8.2.4 Relative density and pore structure

Late age density measurements were taken of the nC modified pastes. All measurements showed a very low standard deviation. As can be seen in Figure 8-28, nC1exhibited lower densities as the amount of nC solids increased. Up to an extent this is expected, since nC has lower particle density. Also, as discussed in section 6.1.6, the theoretical density for 60% PC and 40% LS at w/b = 0.3 was found to be equal to 2072 kg/m^3, therefore equal to the relative density measured. However, the fact that even the lowest nC addition caused a significant reduction could only be attributed to the poor compaction during production, resulting in a less dense paste, and possibly in an increase in the porosity. Hence, in this way, the low compressive strengths delivered by the nC1 addition can be further justified, as well as the visual pores observed in Chapter 4. nC2 showed a better performance in this regard, until the 2% nC addition (Figure 8-29). The 4% and 5.5% nC2 addition was similar to the nC1 density measurements for these percentages of nC (Figure 8-29). nC3 performed best, with densities equal to that of the reference paste for 0.5% and 1% nC3 addition (Figure 8-30). 2%, 4% and 5.5% nC3 performed similar to the former two.

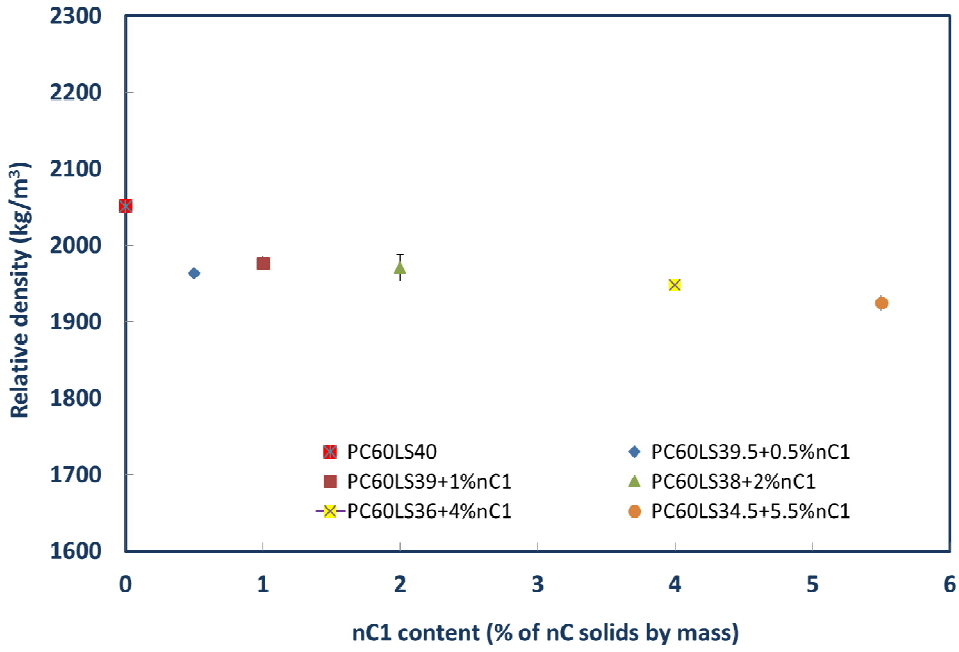

Figure 8-28: Long-term relative density of nC1 modified cement pastes

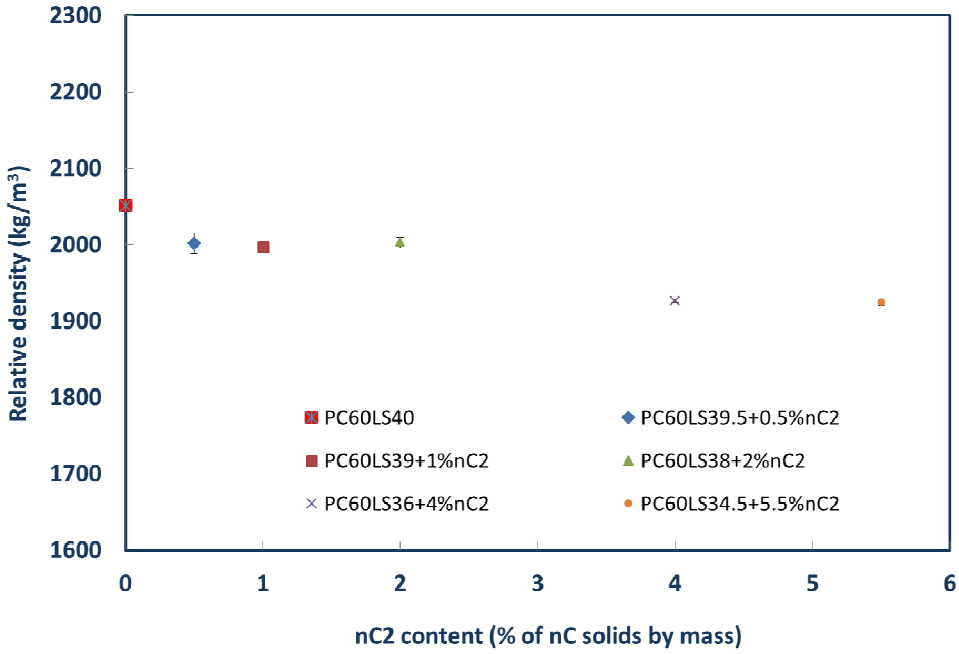

Figure 8-29: Long-term relative density of nC2 modified cement pastes

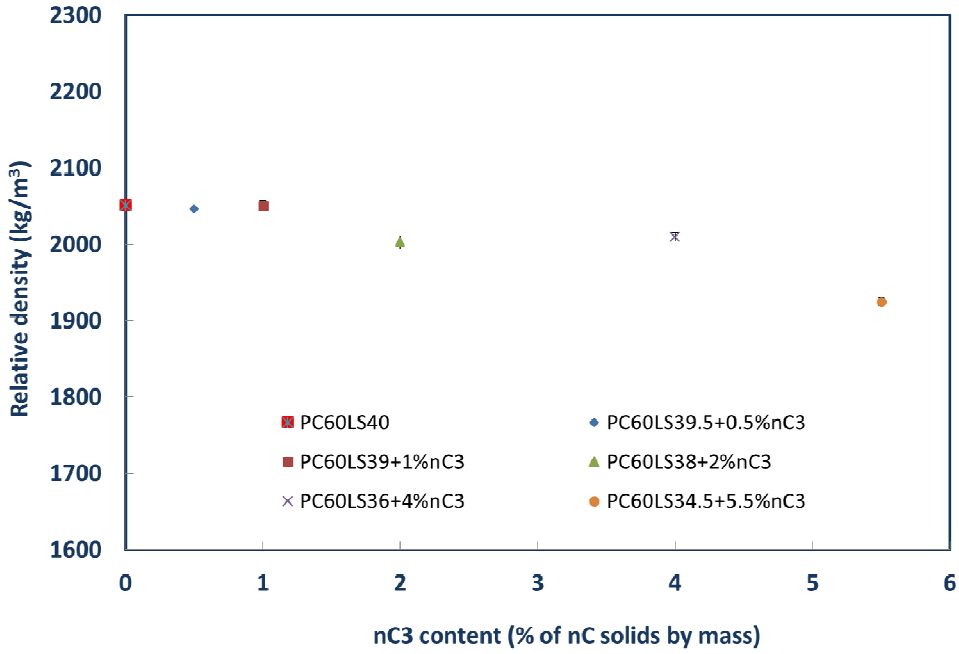

Figure 8-30: Long-term relative density of nC3 modified cement pastes

The accuracy of the MIP has been questioned (Diamond, 2000; Abell *et al.*, 1999) with experimental results suggesting that the MIP, instead of "measuring the size of the pore, is measuring the diameter of the throats, referred as the ink bottle effect". Nonetheless, due to the lack of other porosimeters, eventually, it was not used to deliver standalone results, but

to compare the effect that the three nC dispersions had on (i) the total pore area (Figure 8-31), (ii) average pore diameter (Figure 8-32), (iii) porosity (Figure 8-33), (iv) apparent density (Figure 8-34) and bulk density (Figure 8-35) compared with relevant values of the reference paste. Hence, although there is significant inherent variability in the samples and the method is being challenged, the mere comparison of results can still provide valid scientific evidences. This is the reason why, the MIP results were in good agreement with all the results previously presented in this chapter.

To begin with, nC1 increased porosity, in contrast to some other reported results suggesting that OMMTs act as nanofillers, reducing the porosity (Chang *et al.*, 2007) or the total pore volume (Kuo *et al.*, 2006). In other words, as expected by the relative density results (Figure 8-28), nC1, was the only dispersion that caused an increase in porosity from day 1 to day 90. As also confirmed by the voids observed by FESEM and SEM this could be the major reason for which the compressive strength of the nC1 modified pastes was lower than that of the reference paste, certainly closely related to the chemistry and nanostructure of the OMMT itself. In fact, the smaller average pore diameter was delivered by nC3 followed by nC2, possibly because of the better exfoliation and dispersion. Both the apparent and bulk density at later ages tend to be the same for the three nC dispersions and approaching the reference paste. It is interesting to note that the total pore area (Figure 8-31) at day 28 is almost the same for the reference paste and for the nC2 and nC3 modified pastes, however, with the advancement of time, nC2 seems to have decreased the total pore area. It could be assumed that given the time the pozzolanic reaction advanced densifying the microstructure of the paste, possibly through the production of additional ettringite and C–S–H and/or C–A–H, in agreement with the TG analyses.

The comparative figures (Figure 8-31 to Figure 8-35) and the complete table of results (Table 8-1) are presented below:

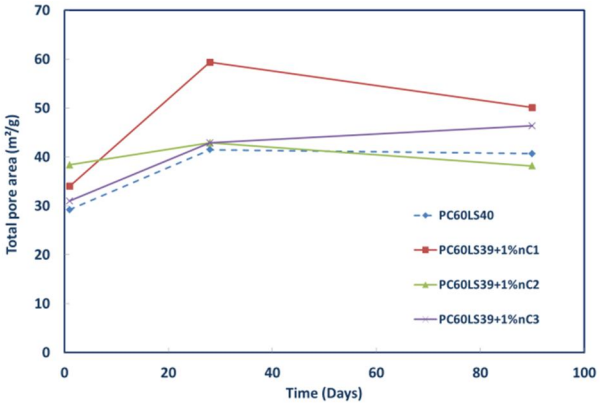

Figure 8-31: Effect of nC type on the total pore area of cement pastes

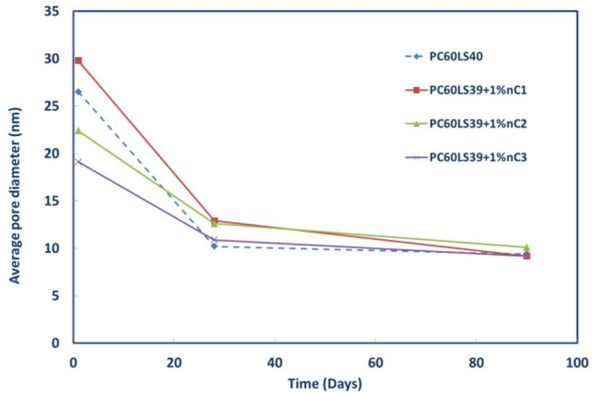

Figure 8-32: Effect of nC type on the average pore diameter of cement pastes

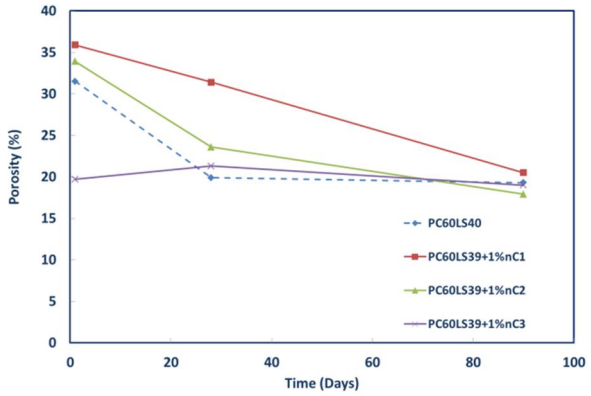

Figure 8-33: Effect of nC type on the porosity of cement pastes

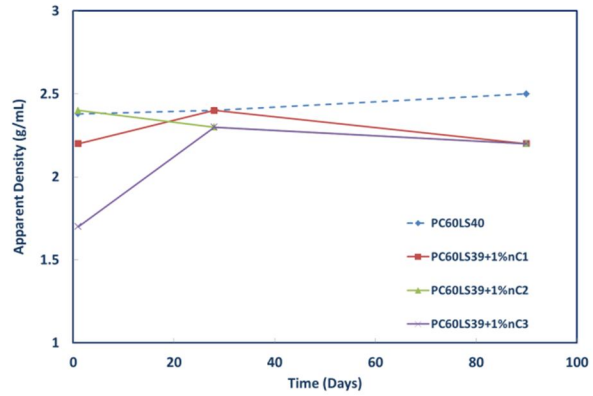

Figure 8-34: Effect of nC type on the apparent density of cement pastes

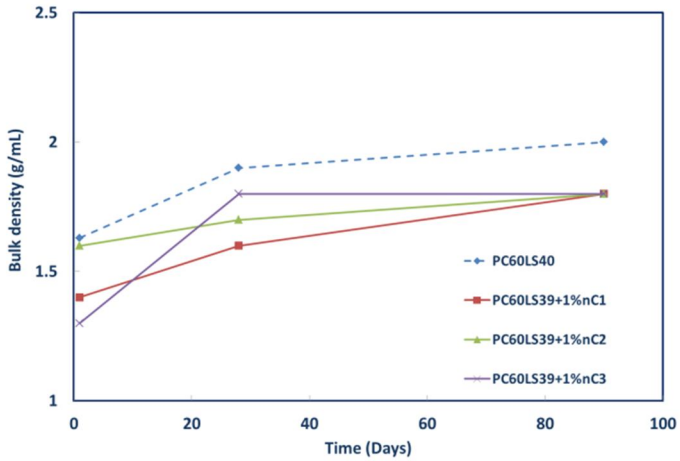

Figure 8-35: Effect of nC type on the bulk density of cement pastes

Table 8-1: Mercury Intrusion Data summary on PC60LS40

Mercury Intrusion Data Summary								
Paste	**$A_{pore-total}$ (m^2/g)**	**$F_{pore\ volume-med}$ (nm)**	**$F_{pore\ area-med}$ (nm)**	**r_{bulk} (g/mL)**	**$F_{pore-average}$ (nm)**	**$r_{apparent}$ (g/mL)**	**Porosity (%)**	**$V_{stem-used}$ (%)**
PC60LS40 – 1 Day	29.2	68.4	8.3	1.63	26.5	2.4	31.5	48
PC60LS39+ 1% nC1–1D	34.0	78.4	8.1	1.4	29.8	2.2	35.9	46
PC60LS39+1 %nC2–1D	38.4	55.6	7.8	1.6	22.4	2.4	33.9	38
PC60LS39+ 1% nC3–1D	31.0	38.1	7.2	1.3	19.1	1.7	19.7	40
PC60LS40 – 28 Days	41.5	13.7	7.0	1.9	10.2	2.4	19.9	30
PC60LS39+ 1%nC1–28D	59.4	18.6	6.8	1.6	12.9	2.4	31.4	50
PC60LS39+ 1%nC2–28D	42.9	17.4	7.7	1.7	12.6	2.3	23.6	38
PC60LS39+ 1%nC3–28D	42.9	13.4	7.7	1.8	10.9	2.3	21.3	33
PC60LS40– 90 Days	40.7	10.8	6.2	2.0	9.4	2.5	19.3	29
PC60LS39+ 1% nC1–90D	50.1	9.7	6.3	1.8	9.2	2.2	20.5	33
PC60LS39+ 1%nC2–90D	38.2	11.5	7.4	1.8	10.1	2.2	17.9	25
PC60LS39+ 1%nC3–90D	46.4	10.4	6.7	1.8	9.2	2.2	19.0	29

8.3 Cube compressive strength of mortars based on PC60LS40

Standard mortar cubes based on PC60LS40, denoted as M.PC60LS40, using CEMII-42.5R, were modified only with nC1 and nC2. The same trend observed for the cement pastes was also observed with the mortars; as can be observed in Figure 8-36, nC2 delivered higher compressive strength than nC1 and was further improved with the addition of LnS. It should be noted that a 2% nC content was preferred against the 1% nC content to ensure more homogeneous mixing.

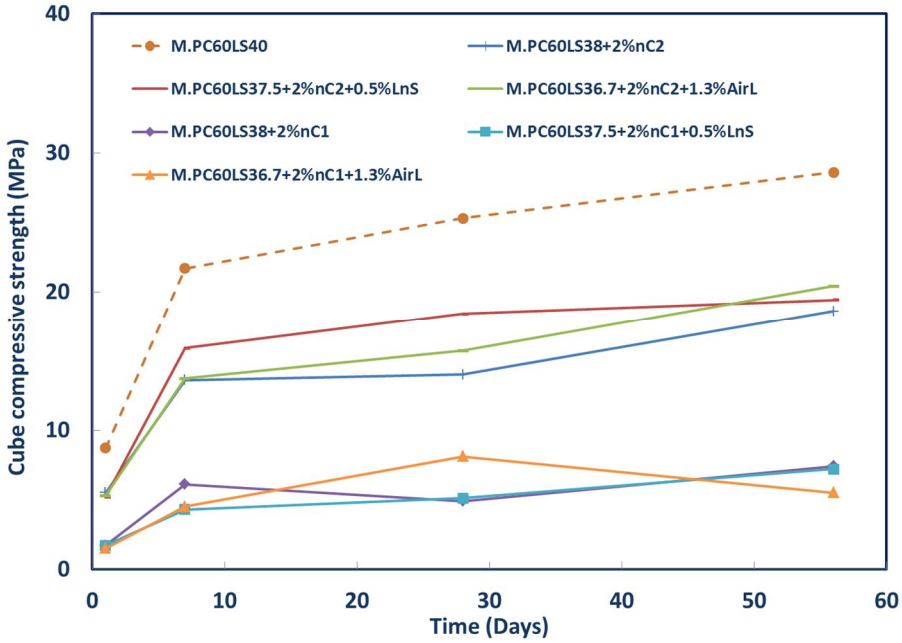

Figure 8-36: Cube compressive strength of nC and LnS modified mortars based on PC60LS40

8.3.1 Cube compressive strength and relative density of mortars based on PC100

A further series of mortars investigating the effect of nCs in combination with PC alone, was also prepared and tested, using CEMI-45R, in order to assess the potential of the organomodified dispersion nC2, the inorganic dispersion, nC3 and the organomodified powder nC4. Having already confirmed the poor performance of nC1 either within the paste or within the previously tested mortars, nC1 was not chosen to be further tested in these series. As shown in Figure 8-37, nC3 was the most stable and the only one offering a strength improvement after day 56, performance not reached even by the commercial nC4, although it is accredited that nC4 may have performed better if dispersed in the mix water before added to the binder. Still, however, the strengths achieved by the nC modification of the binder were lower than that of the reference mortar. One reason for this could be the increase in the total volume of pores due to the formation of conglomerates of nC within the volume of the binder (Kuo *et al.*, 2011), which is the case when OMMT was added. In fact, the inorganic dispersion seemed to be the only one providing (i) greater density than the reference mortar and nC2 and (ii) marginal variability in terms of standard deviation of density. It is interesting to note that for both nC2 and nC4 the higher concentrations (even at 5% by total mass of solids) favour lower standard deviation. This can be attributed to more homogeneous mixing (Figure 8-38). However, nC4, exhibited lower and varying density at all concentrations.

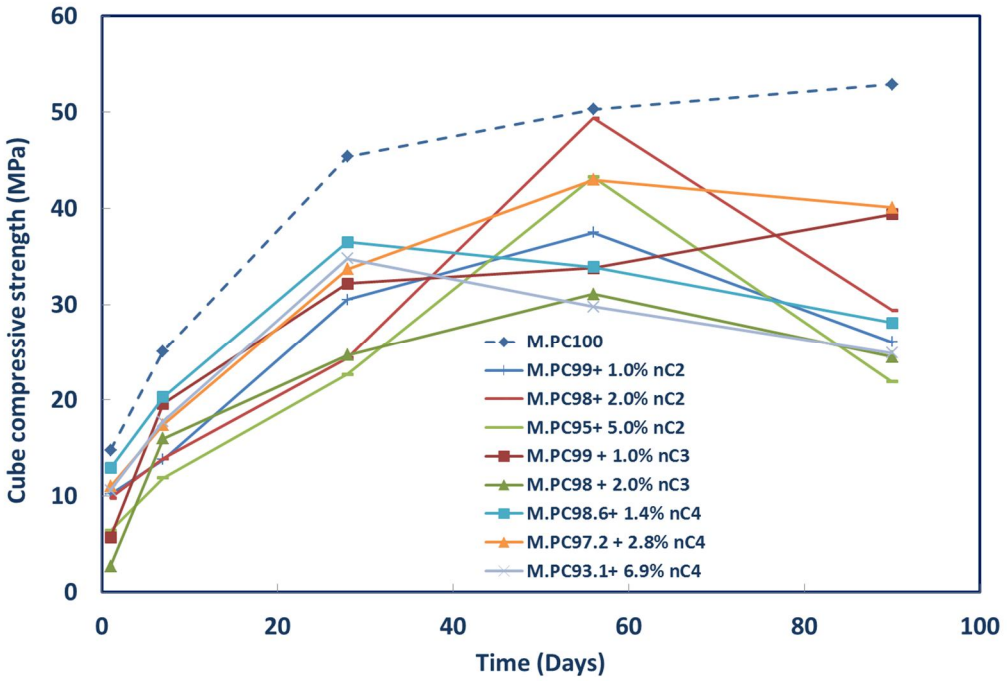

Figure 8-37: Cube compressive strength of nC modified mortars based on PC100

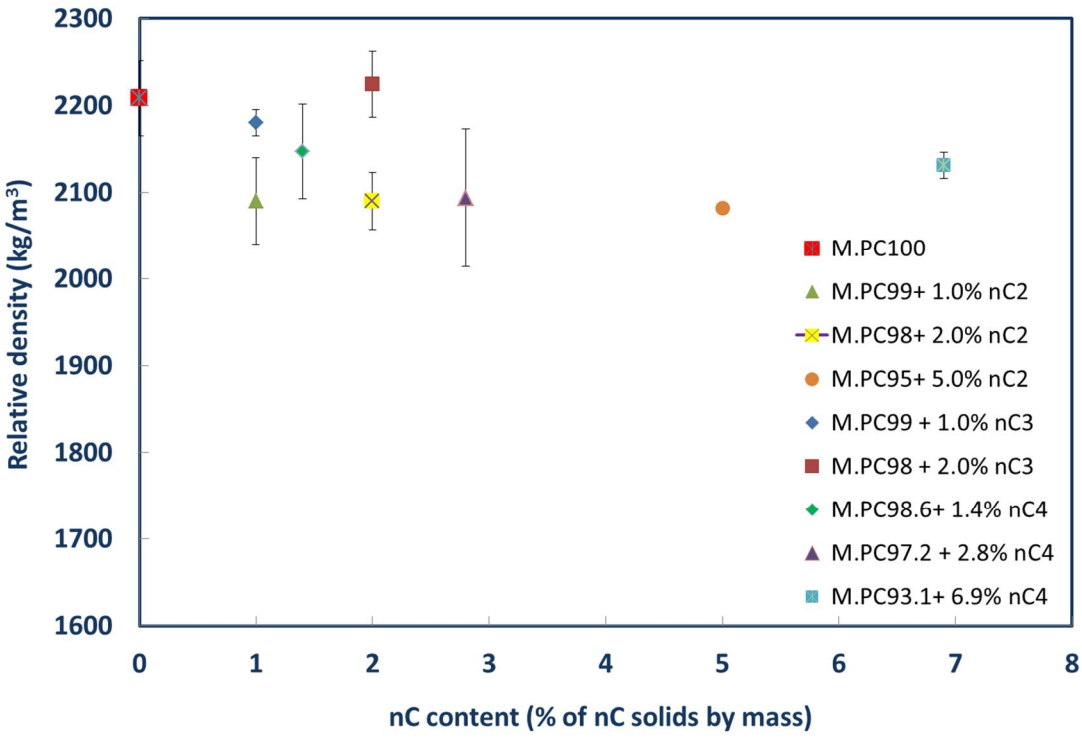

Figure 8-38: Long-term density of nC modified mortars based on PC100

8.4 Further discussion and conclusions

The results presented in this chapter have been interrelated and conclusions were made as to why the addition of nC slurries did not lead to the enhancement of the compressive strength. The potentials of the nC with respect to pozzolanic behaviour and particle packing abilities as expressed in terms of $Ca(OH)_2$ consumption, ettringite and C–S–H production, density and porosity were also discussed. Although past research suggested that MMT exhibit limited pozzolanic activity (Fernandez *et al.*, 2011) when MMT is intercalated or exfoliated it was proven that can act as a pozzolanic addition in cement. Furthermore, testing of the mortars helped in eradicating size effects and effects of autogeneous shrinkage and also pushed the envelope further by suggesting higher activation of the nC with the addition of another type of nanoparticle, that is to say nS.

9 NANOCLAY MODIFIED FIBRE CEMENT FORMULATIONS

9.1 Introductory section

In Chapter 3 it was discussed that the direction of the platelets in intercalated or exfoliated nanoclays may affect the load path and crack propagation within nanomodified pastes. Moreover, it has been argued that nC particles further exfoliate within the cement matrix, tending to disperse in one direction under stirring (He and Shi, 2008), rendering them possibly more suitable for flexural than compressive strength enhancement. To assess this hypothesis, three series of samples were prepared to be tested in flexure. The first one comprised of a non pozzolanic reference paste containing 3% PVA fibres and 2% superplasticizer, denoted as F.PC60LS40PVA3SP2 (F is for flexure). Of the three dispersions, nC1 was neglected due to the conglomeration observed in both the nC itself and the nC1 modified cement pastes. Adding to this, only the 1% nC content was investigated, taking into account the limitation identified in Chapter 6. nC2, nC3 and nC4 were, therefore, added at 1% by mass to the reference paste.

The second series was based on a pozzolanic paste for further improvements in flexural strength. The reference paste contained 60%PC, 20%LS, 20%FA 3% PVA fibres and 2% superplasticizer, denoted as F.PC60LS20FA20PVA3SP2. The two organomodified nC dispersions were added at four different levels; 0.5%, 1%, 2% and 4%, whereas the inorganic dispersion (nC3) and the organomodified powder (nC4) were only added at 1%.

Both series of specimens were prepared according to the specifications given in Chapter 4. The nC modified cement pastes were tested in flexure at different ages starting from day 7 and reaching day 90. This is the first study:

i. applied to cement pastes directly, rather than mortars;
ii. investigating the effect of hydrophilic or hydrophobic nC;
iii. comparing the effectiveness of nC in dispersions or in powder form;
iv. covering the flexural performance beyond day 28, an indeed more critical period.

Characterization of selected pastes allowed for more conclusions to be drawn.

A number of standard mortar cubes were also tested in compression in a final effort to explore any possible improvements within the new matrix (M.PC60LS20FA20 and M.PC60FA20).

The third series was based on the same pozzolanic paste that the second one was based on as well, but contained a higher PVA fibre content (4%), denoted as F.PC60LS20FA20PVA4SP2. No microstructural or chemical investigation was carried out, as it purely served as a demonstration of the potentials for future research.

9.2 Ternary nC modified fibre cement formulations

9.2.1 Flexural strength of fibre cement pastes based on F.PC60LS40PVA3SP2

The standard deviation was computed for all specimens but is not presented in the graphs for reasons of clarity. For the reference paste, F.PC6LS40PVA3SP2 and for the nC2 modified pastes, it ranged from 1 to 1.4. The addition of nC3 reduced the variation between 1.0 to 1.2 MPa, whereas the standard deviation of nC4 was approximately equal to 1.1 MPa. Hence, as in the case of nC modified pastes, the standard deviation was reduced with nC3.

It has been reported in past researches on other types of nanoparticles that they are expected to deliver higher flexural and tensile strength (Sobolev *et al.*, 2009b). Adding to this, a recent study on 1% nC addition to CEMI mortars showed an enhancement in the rate of strength gain for flexure (Hosseini *et al.*, 2014) with respect to rate of strength gain for compression. However, although comparison for compression was made at day 7, 28 and 91, the comparison for flexure was made between 7 and 28 days only and the matrix was oversimplified by containing solely PC and nC. What is important, though, is that nC performed better in flexure, attributed by the authors to better adhesion of the specific nanoparticles in the matrix.

As shown in Figure 9-1, given more curing time, the nC modified pastes outperformed the reference paste, in contrast to Hosseini *et al.* (2014) who suggested that the nC particles (just like nS particles) are more effective in the first seven days and their effectiveness reduces at middle ages (28 and 90 days). nC3 showed the highest flexural strength of all three. nC2 showed a lower strength at day 56, which could be attributed to bad compaction. If this was the case, then all three types of nC would not manage to maintain the strength gain after day 56, showing a relative reduction in flexural strength at day 90. It should also be noted that PVA fibres are highly hydrophobic, therefore the hydrophobic nature of nC1 and nC2 was possibly responsible for an inferior combination compared to nC3.

It is possible that with longer mixing time less amount of fibres, the nC modified specimens can be better compacted and consequently deliver even higher strengths.

Once again, it is of interest to note that the hydrophilic nC3 outperformed the hydrophobic one (nC2).

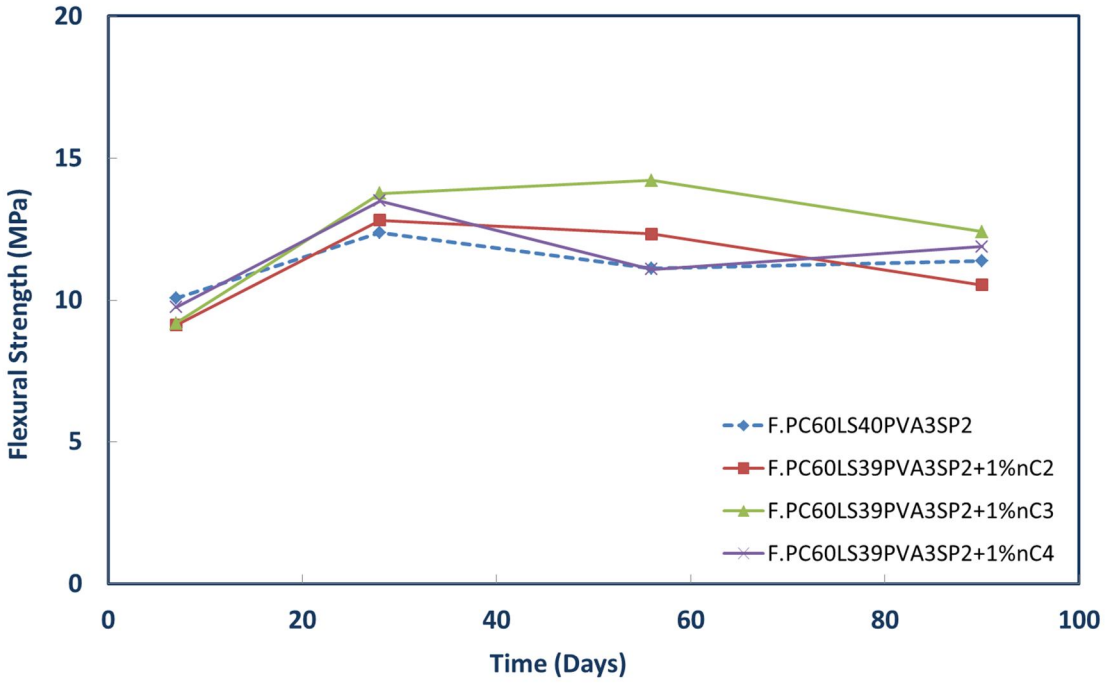

Figure 9-1 Flexural strength of 1% nC2, nC3 and nC4 modified fibre cement pastes based on F.PC60LS40PVA3SP2

9.2.2 Thermogravimetric and crystallographic analyses of fibre cement pastes based on F.PC60LS40PVA3SP2

For these series of fibre cement pastes, the 1% nC2, nC3 and nC4 content was analysed. It should be noted that, again, the amount of decomposing modifier and/or clay were deducted from the mass loss occurring at the 400-500°C temperature range and at the 600-800°C temperature range, respectively, as discussed in Chapter 6. In addition, PVA is expectd to decompose before 400°C (Gilman *et al.*, 1994). No consumption of $Ca(OH)_2$ seemed to have taken place (Figure 9-2). In addition, it can be claimed that no carbonation has occurred since the lines representing the nanomodified pastes are below that of the reference paste (Figure 9-3).

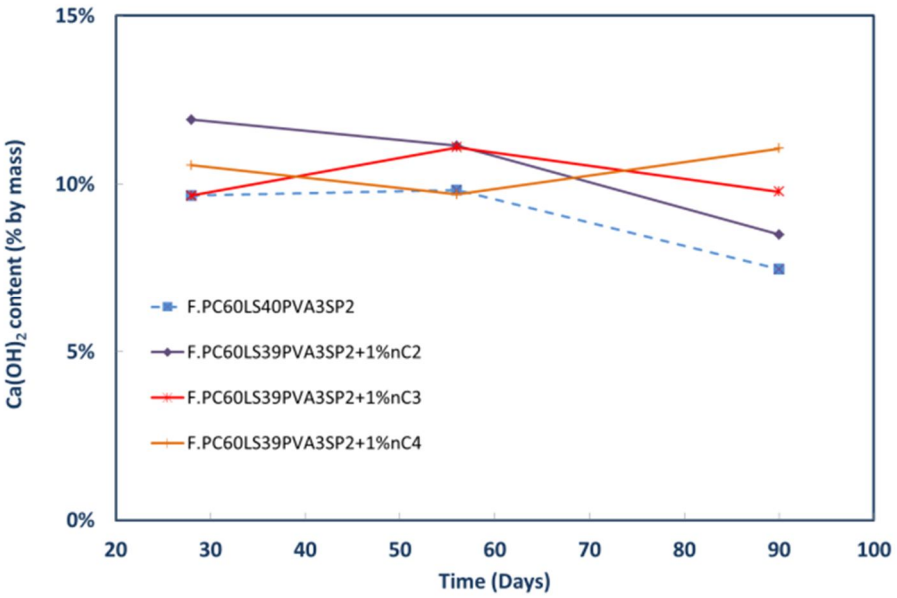

Figure 9-2: Effect of nC content and type on $Ca(OH)_2$ content of nC modified fibre cement pastes based on F.PC60LS40PVA3SP2

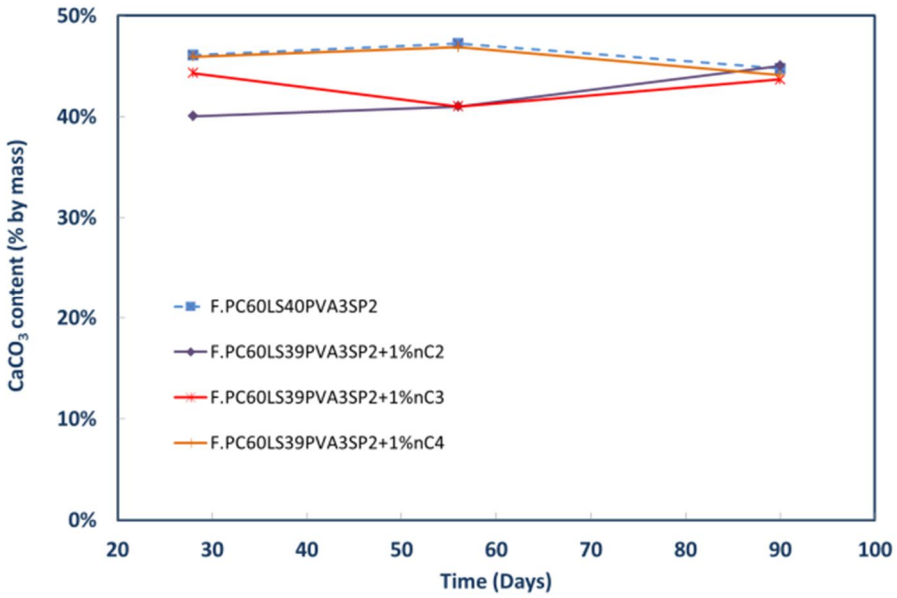

Figure 9-3: Effect of nC content and type on $CaCO_3$ content of nC modified modified fibre cement pastes based on F.PC60LS40PVA3SP2

For the reasons stated in Chapter 6, further analysis was carried out with respect to the temperature range within which ettringite and C–S–H decompose. As shown in Figure 9-4, Figure 9-5 and Figure 9-6, nC2 seemed to have generated greater quantities of ettringite (100-125°C) and C–S–H, with nC3 following, given the time. In full agreement with the flexural strength results, nC3 showed the greatest production of ettringite and C–S–H at day 90. Lastly, nC4 did not show much difference compared to the reference paste either in terms of TGA or in terms of flexural performance.

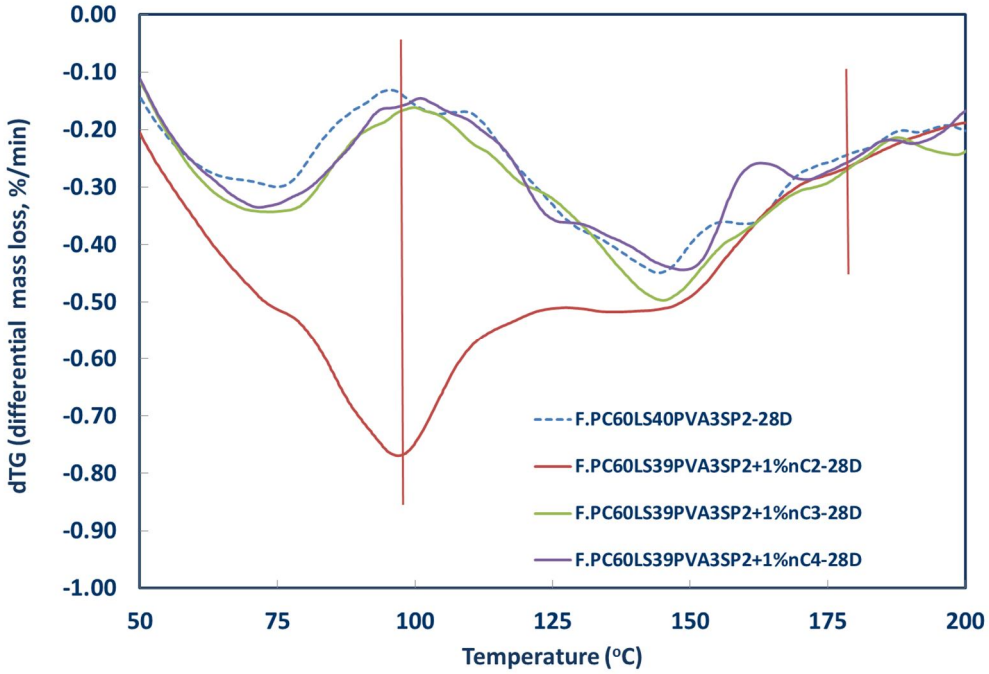

Figure 9-4: Differential mass loss between 100-200°C at Day 28

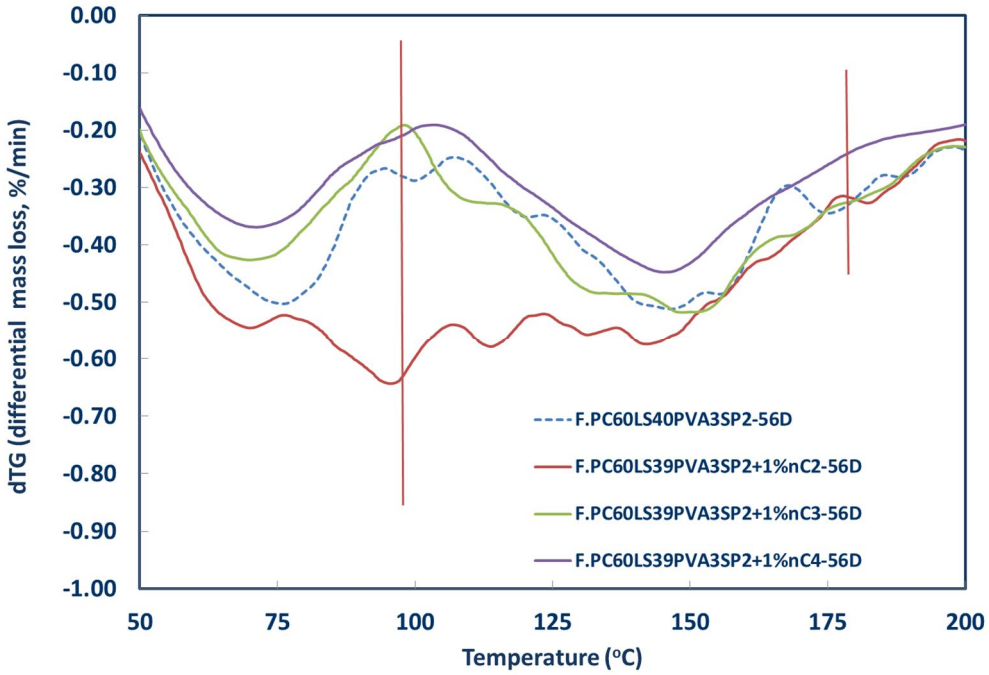

Figure 9-5: Differential mass loss between 100-200°C at Day 56

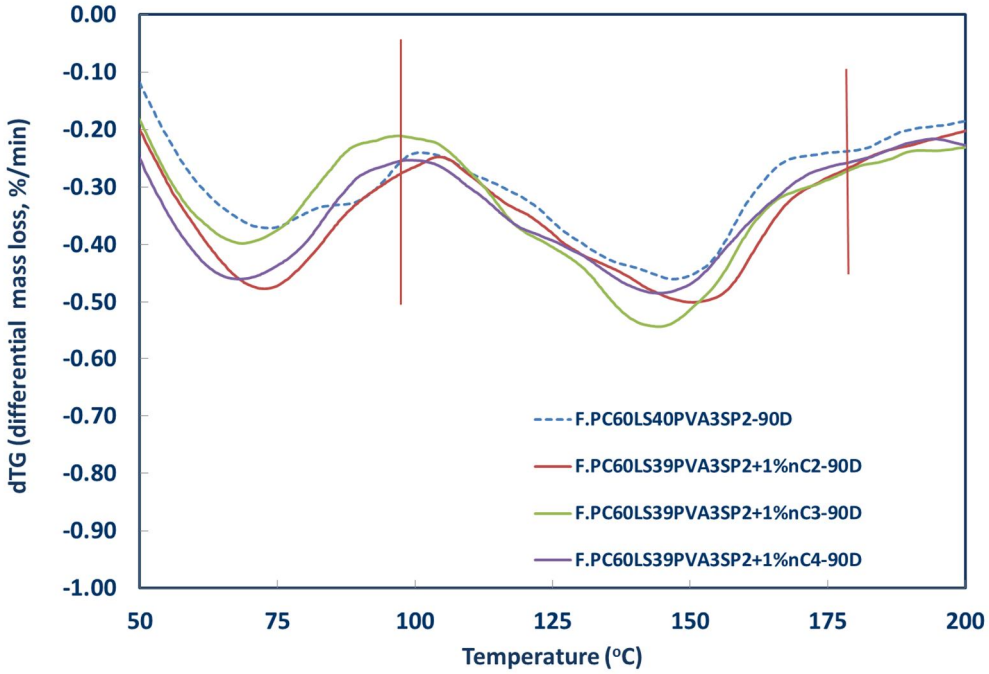

Figure 9-6: Differential mass loss between 100-200°C at Day 90

The fact that no significant $Ca(OH)_2$ consumption or carbonation had taken place was also confirmed by the XRD analyses executed indicatively on F.PC60LS40PVA3SP2 and the 1% nC3 and nC4 addition, as shown in Figure 9-7.

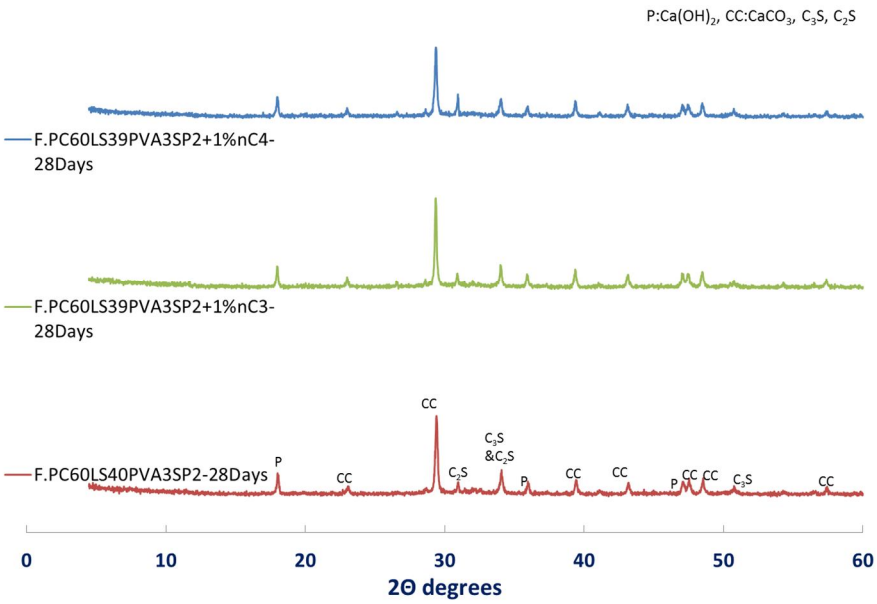

Figure 9-7: XRD pattern of nC modified fibre cement pastes at Day 28 – Effect of nC type

9.2.3 Relative density, pore structure and water permeability of fibre cement pastes based on F.PC60LS40PVA3SP2

Late age, (after month 3) relative density measurements were taken of the 1% nC modified fibre cement pastes. All measurements showed a very low standard deviation and similar values of relative density (Figure 9-8).

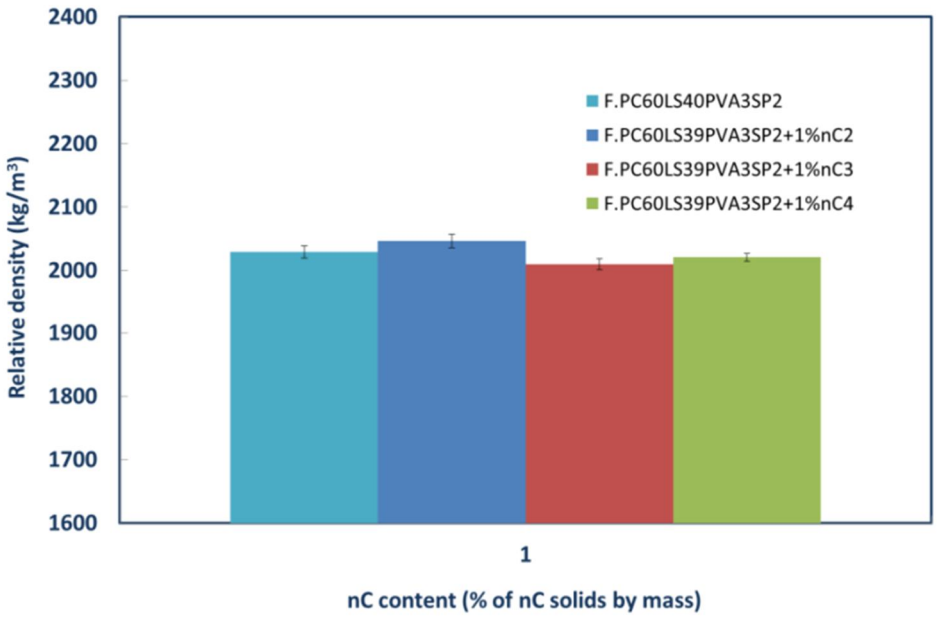

Figure 9-8: Effect of nC type (at 1% dosage) on Long-term relative density of nC modified fibre cement pastes based on F.PC60LS40PVA3SP2

For the fibre cement pastes based on F.PC60LS40PVA3SP2 only two representative samples were tested indicatively with the MIP and compared with the equivalent cement pastes, analysed in Chapter 6. These were the reference paste itself (F.PC60LS40PVA3SP2) and the 1% nC3 modified paste, F.PC60LS39PVA3SP2+1%nC3, both at day 28 (Table 9-1).

It can be seen that the total pore area, median volume pore diameter and porosity were increased. This can be attributed to the presence of the fibres. The apparent and bulk density, however, showed small fluctuations.

No further investigation of these series of fibre cement pastes was carried out, since the same cement pastes were already tested with MIP in Chapter 6.

Table 9-1: Mercury Intrusion Data summary comparison of PC60LS40 with F.PC60LS40PVA3SP2

Mercury Intrusion Data Summary								
Paste	**$A_{pore-total}$ (m^2/g)**	**$F_{pore\ volume-med}$ (nm)**	**$F_{pore\ area-med}$ (nm)**	**r_{bulk} (g/mL)**	**$F_{pore-average}$ (nm)**	**$r_{apparent}$ (g/mL)**	**Porosity (%)**	**$V_{stem-used}$ (%)**
F.PC60LS40PVA3SP2 – 28 Days	**45.8**	**76.8**	**5.1**	**1.6**	**18.9**	**2.4**	**34.1**	**50.0**
PC60LS40–28 Days	41.5	13.7	7.0	1.9	10.2	2.4	19.9	30.0
F.PC60LS39PVA3SP2+1%nC3 - 28 D	**51.2**	**29.1**	**5.5**	**1.7**	**14.1**	**2.5**	**30.6**	**37.0**
PC60LS39+1% nC3–28D	42.9	13.4	7.7	1.8	10.9	2.3	21.3	33.0

Water impermeability tests were carried out in accordance with BS EN 492:2012, with modifications accounting for the much smaller specimens used in this research as described in Chapter 3. As shown in Figure 9-9, in contrast to the state-of-the-art reported in Chapter 2, cement pastes modified by hydrophilic (nC3) or hydrophobic (nC2 and nC4) types of nC may present water permeability issues at later ages. Hence, particularly the OMMT should always be checked at later ages when water impermeability is a prerequisite.

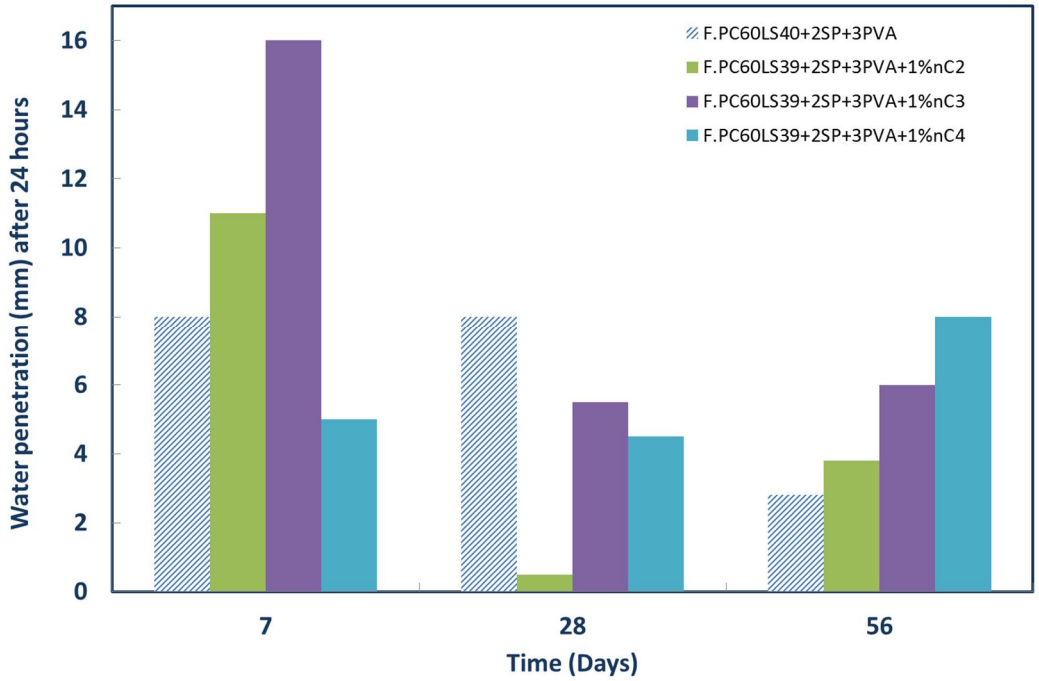

Figure 9-9: Effect of nC type (at 1% dosage) on the impermeability of nC modified fibre cement pastes based on F.PC60LS40PVA3SP2

9.3 Quaternary nC modified fibre cement formulations

9.3.1 Flexural strength of fibre cement pastes based on F.PC60LS20FA20PVA3SP2

The second series of specimens designed for flexure, comprised of 60% PC, 20% LS and 20% FA by total mass of binder. It can be seen in Figure 9-10 that nC1 could not deliver higher strengths compared to the reference paste at any dosage.

As shown in Figure 9-11, for nC2, only the 1% by mass addition offered the best results. The lowest, 0.5% by mass, nC dosage did not offer any flexural strength improvement, whereas the highest, 4%, dosage, proved to be the most detrimental.

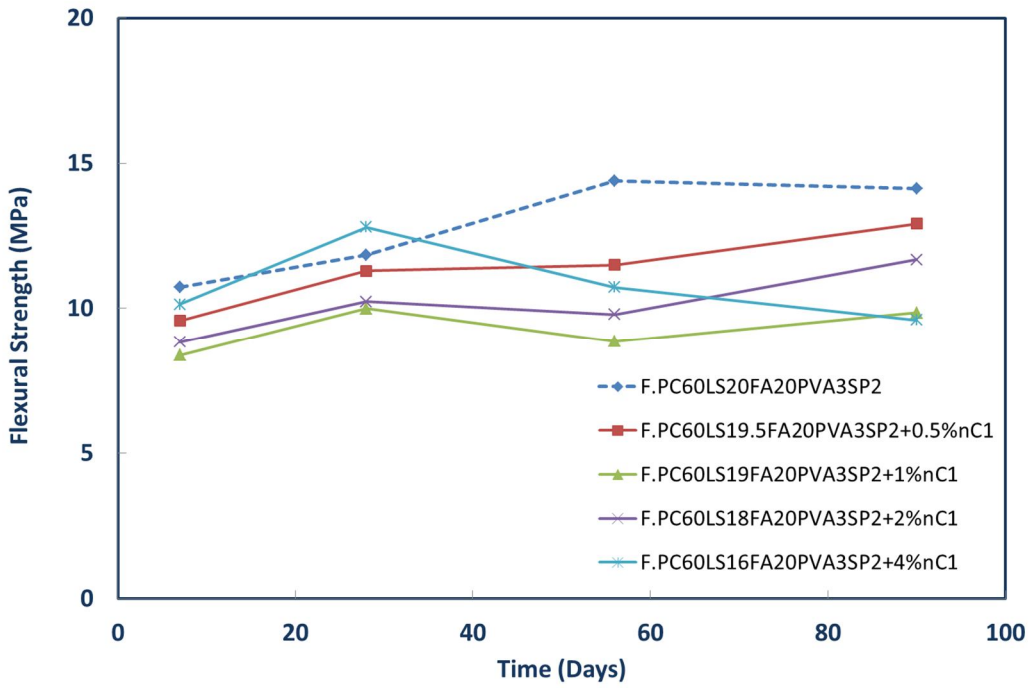

Figure 9-10: Flexural strength of nC1 modified fibre cement pastes based on F.PC60LS20FA20PVA3SP2

Lastly, as shown in Figure 9-12, which compares all nC at 1% by mass, the hydrophilic nC3, provided significant strength improvement, followed by nC4, which, however, showed a reduction in strength at later ages (90 days).

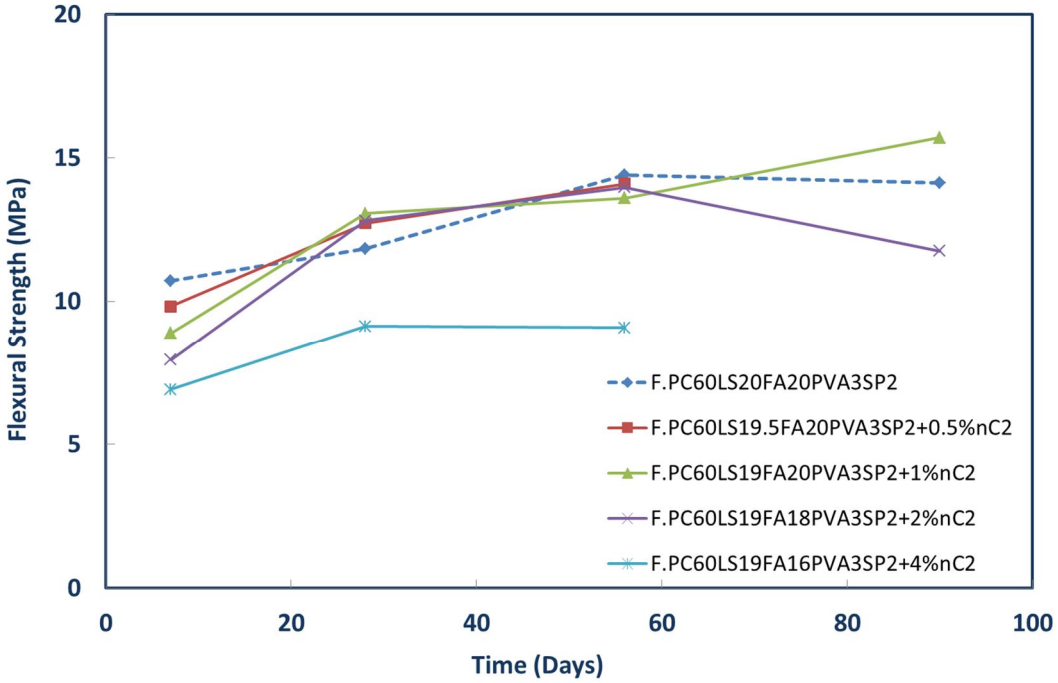

Figure 9-11: Flexural strength of nC2 modified fibre cement pastes based on F.PC60LS20FA20PVA3SP2

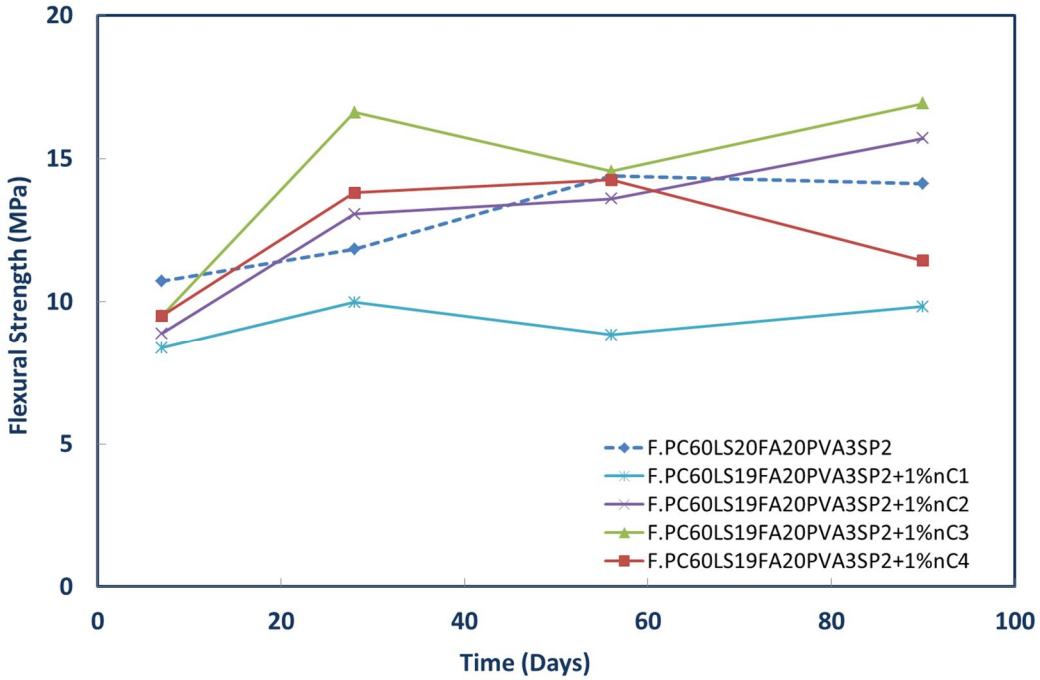

Figure 9-12: Flexural strength of 1% nC1, nC2, nC3 and nC4 modified fibre cement pastes based on F.PC60LS20FA20PVA3SP2

What is also worth noting is that the standard deviation for the reference paste ranged from 1 to 1.2 MPa. However it was similar for the nC1 and nC2 modified samples, reaching approximately 1.2 MPa, whereas for nC3 and nC4 it was again, much lower and equal to about 0.8 MPa.

9.3.2 Thermogravimetric and crystallographic analyses of fibre cement pastes based on F.PC60LS20FA20PVA3SP2

For the series based on F.PC60LS20FA20PVA3SP2, similar results to series based on F.PC60LS20FA20PVA3SP2 can be observed (Figure 9-13 and Figure 9-14). Carbonation of samples is consistent, therefore, not further elaborated upon.

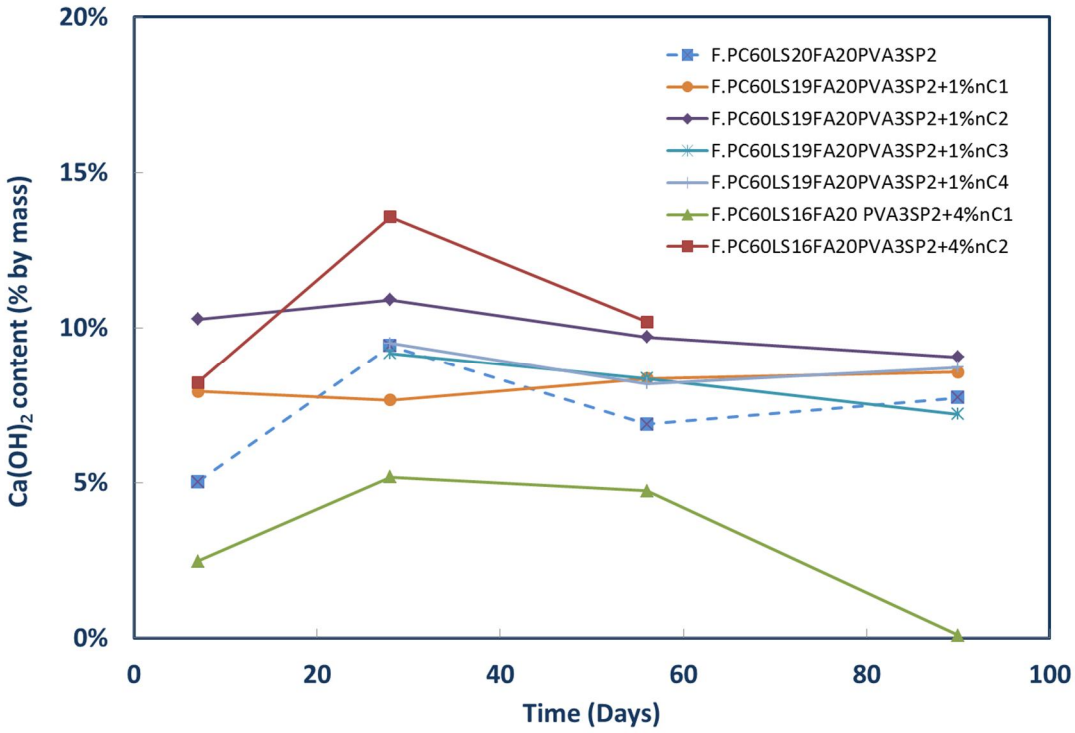

Figure 9-13: Effect of nC content and type on $Ca(OH)_2$ content of nC modified fibre cement pastes based on F.PC60LS20FA20PVA3SP2

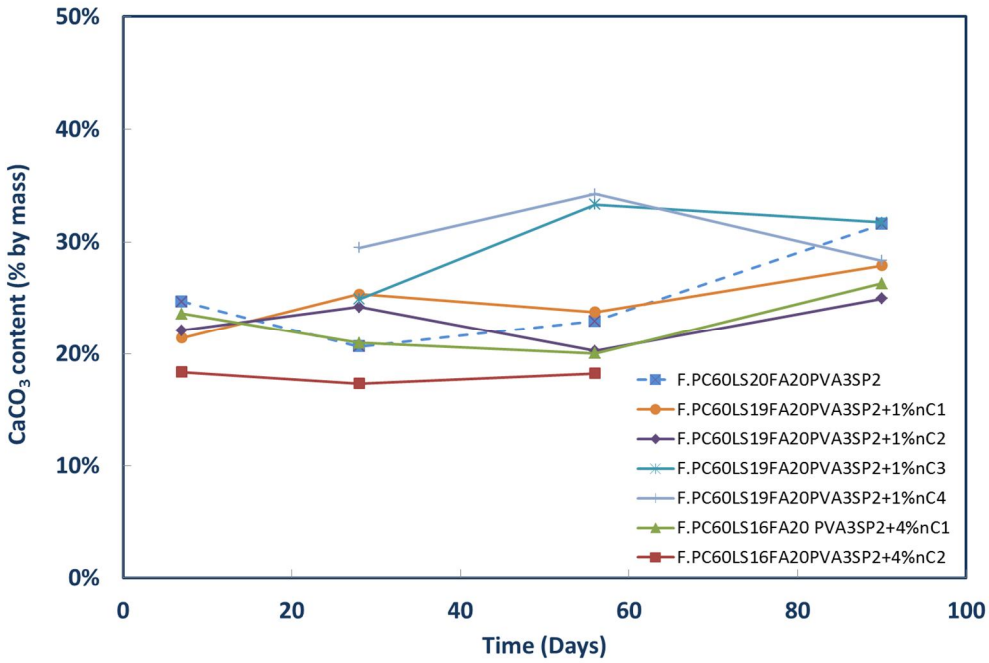

Figure 9-14: Effect of nC content and type on $CaCO_3$ content of nC modified fibre cement pastes based on F.PC60LS20FA20PVA3SP2

The pozzolanic performance was evaluated by TG analyses between approximately 100-180°C, at different ages, different nC types and percentages of nC content. As indicatively shown in Figure 9-15, in the first 28 days nC1 and nC3 had a more pronounced effect, whereas by day 90 (Figure 9–16) nC3 produced the greatest quantities of ettringite and C–S–H, followed by nC2 and nC1. The latter two, performed better at higher nC concentrations (4%) rather than 1%.

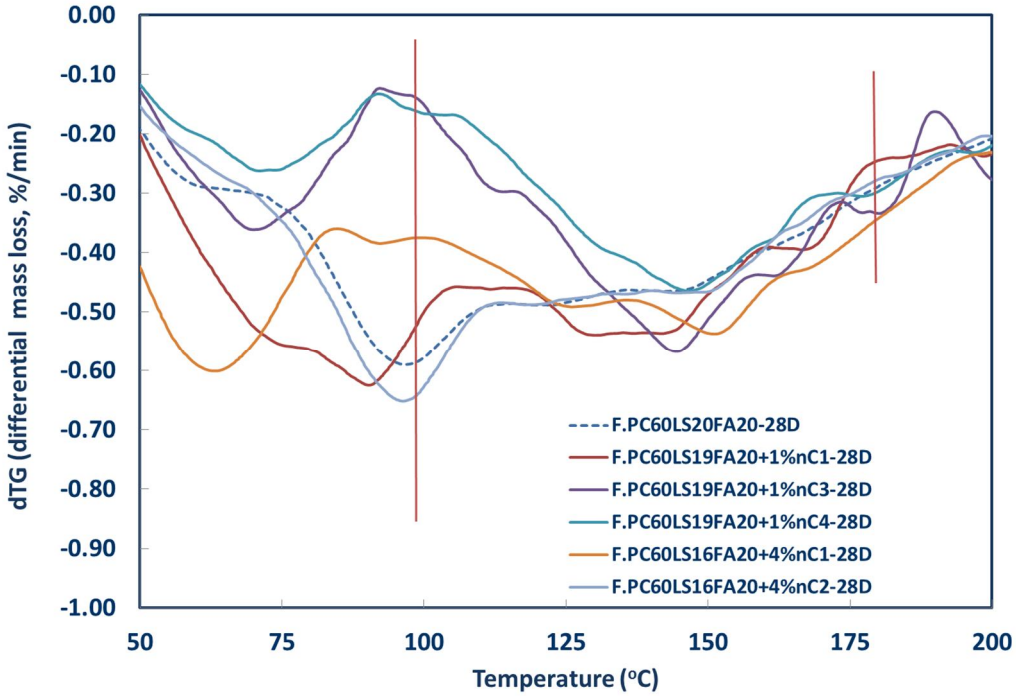

Figure 9-15: Differential mass loss between 100-200°C of nC modified fibre cements at Day 28

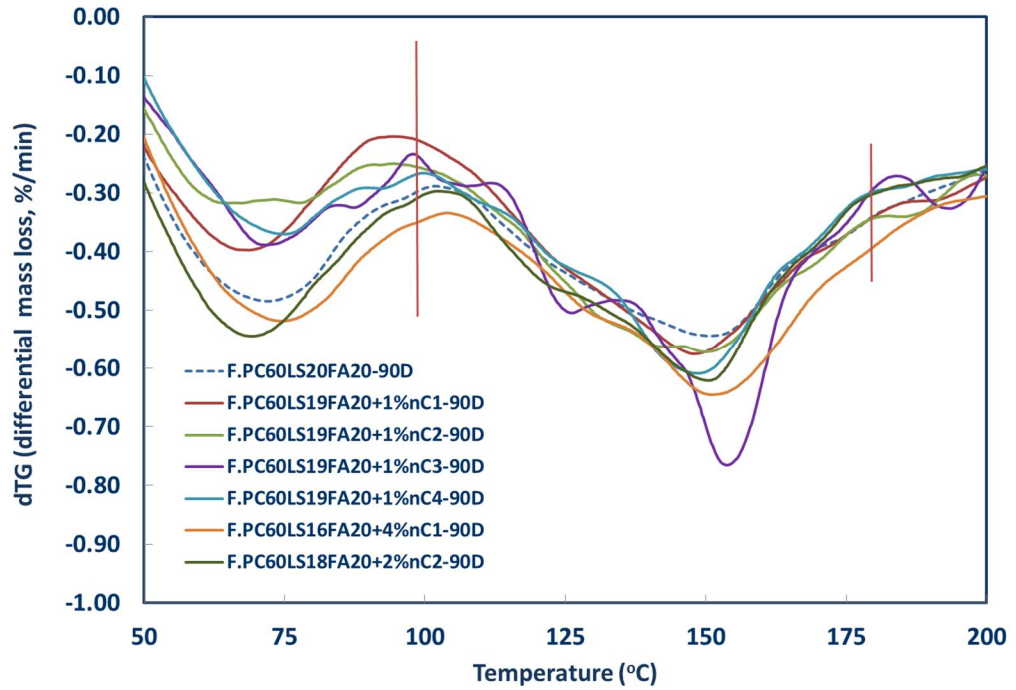

Figure 9-16: Differential mass loss between 100-200°C of nC modified fibre cements at Day 90

Since the consumption of $Ca(OH)_2$ could not be confirmed by TGA, XRD analyses were carried out for two different concentrations 1% and 4% of the organomodified nC. As early as seven days, the consumption of $Ca(OH)_2$ was confirmed (Figure 9-17) by both types of nC, even at the 4%. The nC1 or nC2 modified fibre pastes exhibited much lower intensity

$Ca(OH)_2$ diffraction peaks. Additionally, the intensity of the $CaCO_3$ seemed essentially the same.

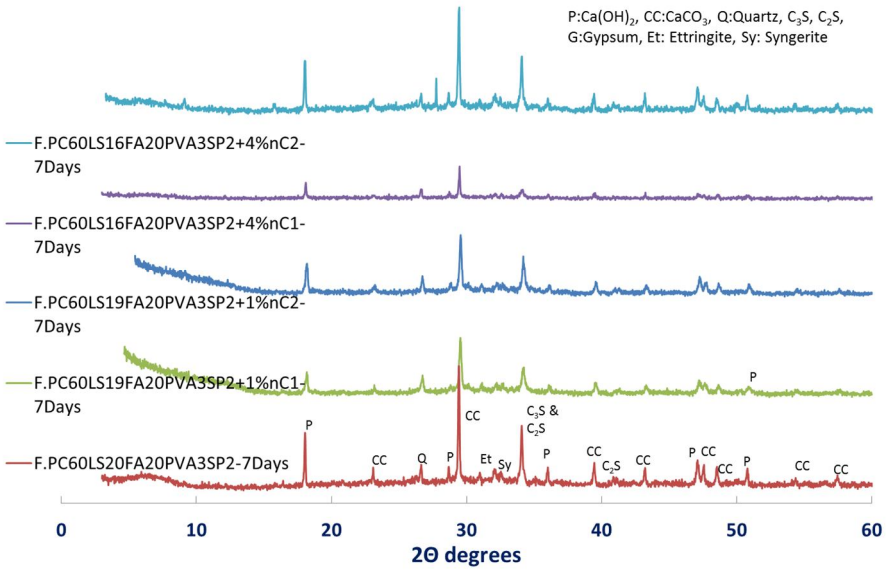

Figure 9-17: XRD pattern of nC modified fibre cement pastes at Day 7 – Effect of nC content and type

As the time advanced, the consumption of $Ca(OH)_2$ was more distinct (Figure 9-18).

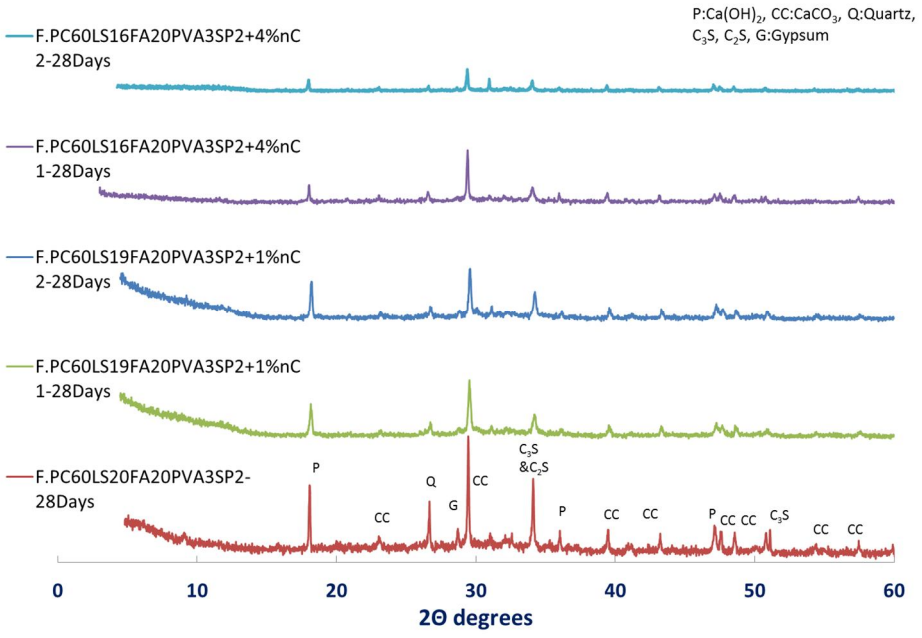

Figure 9-18: XRD pattern of nC modified fibre cement pastes at Day 28 – Effect of nC content and type

Lastly, as clearly shown in Figure 9-1, for the same amount of nC in the same reference paste, nC3 exhibited the greatest $Ca(OH)_2$ consumption. Therefore this reference fibre

cement paste seems to be exhibiting the best performance in terms of pozzolanic reactivity of the nC.

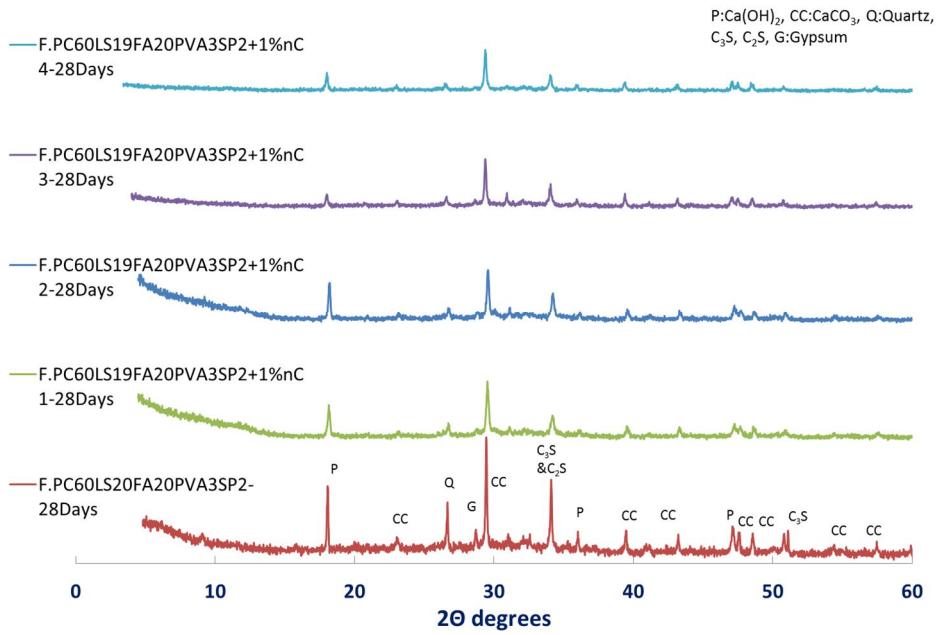

Figure 9-19: XRD pattern of 1% nC modified fibre cement pastes at Day 28 – Effect of nC type

9.3.3 Microstructural characterisation of fibre cement pastes based on F.PC60LS20FA20PVA3SP2

Figure 9–20 to Figure 9–25 constituted an investigation in the morphology of the nC modified fibre cement pastes based on F.PC60LS20FA20PVA3SP2. For this reason, the selected magnifications were primarily low. The reference paste (Figure 9–20) exhibited a grainy surface and clustering of materials probably due to the mixing which left localised voids. The reference paste looked very dense, overall and the fibres seemed to be dispersed in all directions, binding the paste. Some differences can be observed between the two nC types, nC1 and nC2 and the two nC dosages 1% and 4%. nC1. It can be claimed that nC2 and lower nC additions delivered denser pastes. A number of reacted FA particles were identified and circled. It can be supposed that nC1 made the formulation more brittle, a fact more evident at higher nC1 dosages (Figure 9–23 and Figure 9–24), in which microsized clusters of materials are predominant together with microcracks.

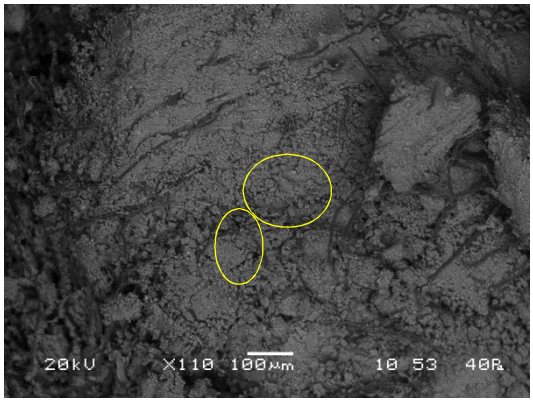

Figure 9-20: BSC micrograph of F.PC60LS20FA20PVA3SP2-28D - 110x

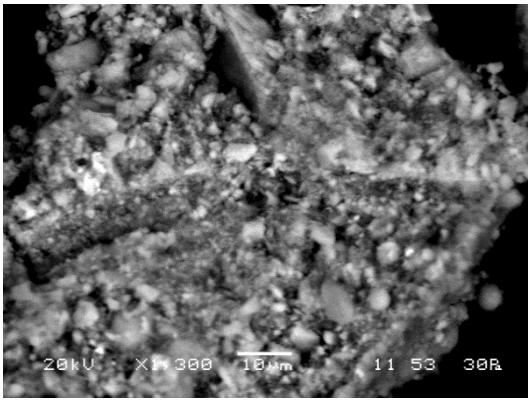

Figure 9-21: BSC micrograph of F.PC60LS19FA20PVA3SP2+1%nC1-28D - 1300x

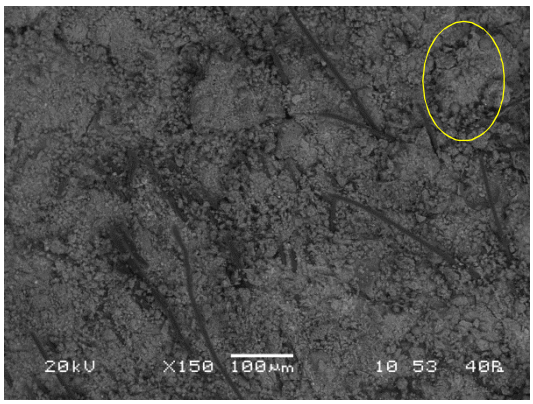

Figure 9-22: BSC micrograph of F.PC60LS19FA20PVA3SP2+1%nC2-28D-150x

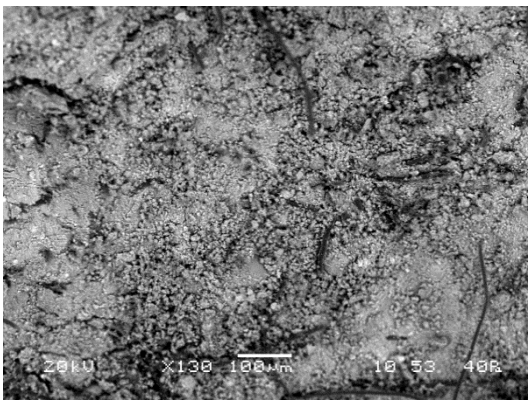

Figure 9-23: BSC micrograph of F.PC60LS16FA20PVA3SP2+4%nC1-28D - 130x

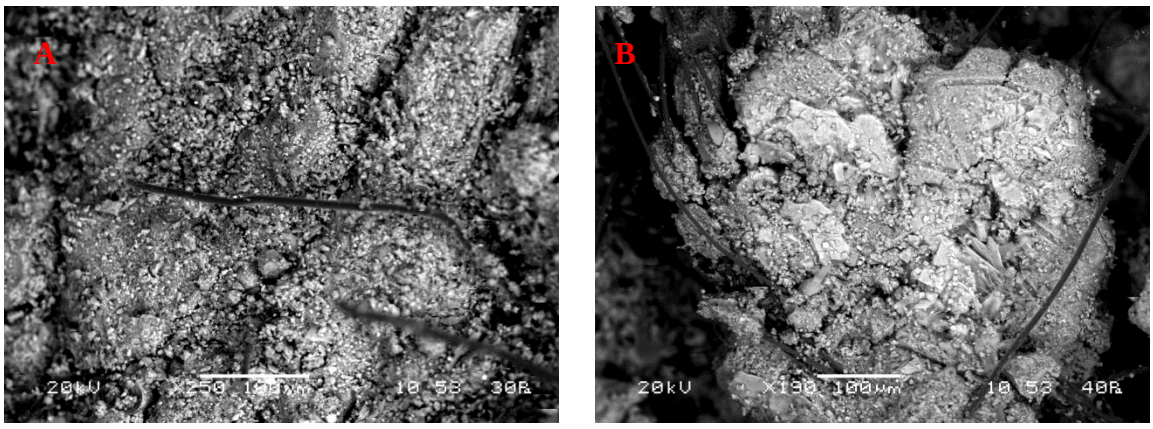

Figure 9-24: BSC micrograph of F. PC60LS16FA20PVA3SP2+4%nC1-28D- (A)250x and (B) 190x

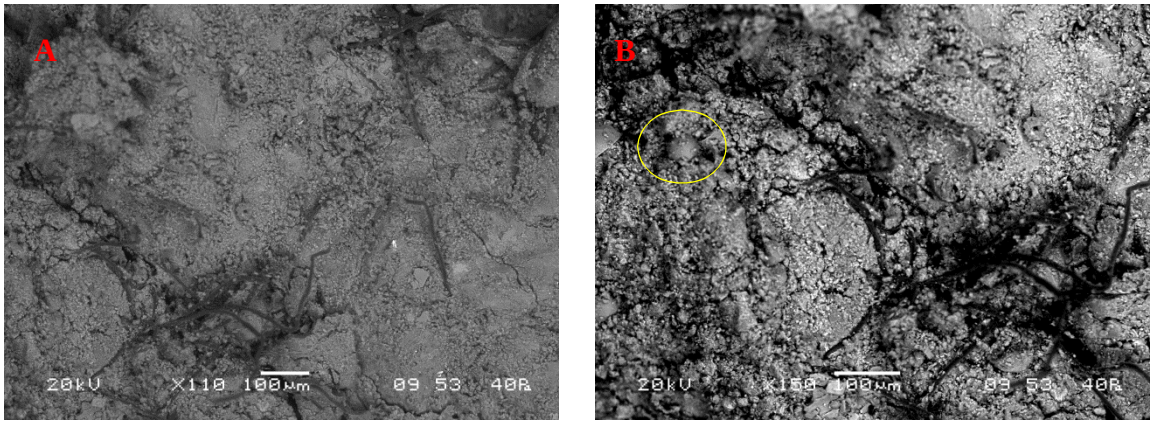

Figure 9-25: BSC micrograph of F. PC60LS16FA20PVA3SP2+4%nC2-28D- (A)110x and (B) 150x

9.3.4 Relative density pore structure and water permeability of fibre cement pastes based on F.PC60LS20FA20PVA3SP2

Late age (after month 3), relative density measurements were taken of the 1% nC modified fibre cement pastes. All measurements showed a very low standard deviation, particularly nC3 and nC4 and similar values of relative density for the 1% nC content (Figure 9-8). It is interesting to note that as the nC content increased the relative density decreased. This can be explained by the clustering of nC and fibre particles within the cement paste, which is consequently expected to increase the porosity, as also depicted by the BSC micrographs (Figure 9–23 to Figure 9–25).

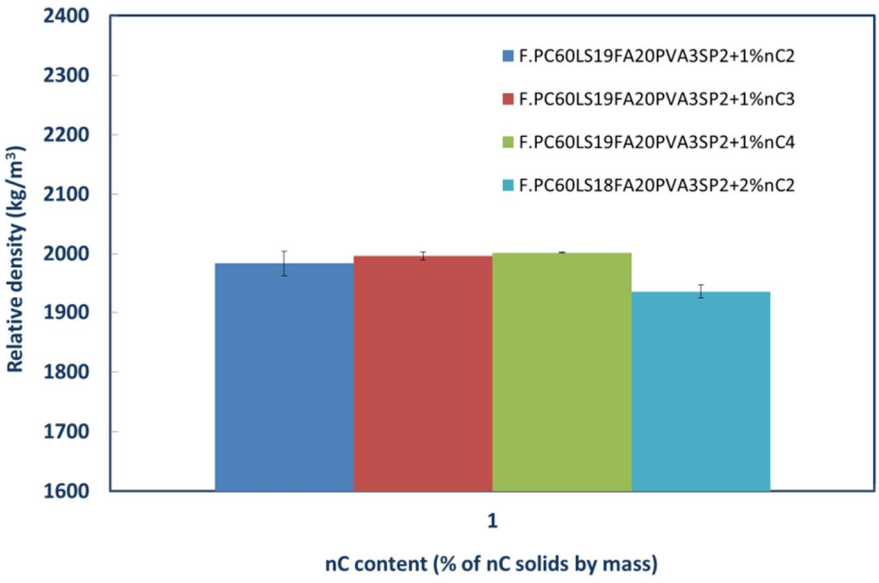

Figure 9-26: Effect of nC type and concentration on Long-term relative density of nC modified fibre cement pastes based on F.PC60LS20FA20PVA3SP2

In fact, MIP measurements carried out for the 1% and 4% nC content, showed that the addition of high quantities of nC, yielded an increase in the total pore area (Figure 9–27), the average pore diameter (Figure 9–28) and porosity (Figure 9–29) of fibre cement pastes. These results gave further justification to the hypothesis that nC addition must be limited to approximately 1%. Furthermore, it is interesting to note that the 1% nC3 modified fibre cement paste was the only nC modified sample that showed (i) higher bulk density than the reference paste and (ii) lower porosity than the reference paste at day 28. It is acknowledged, though, that later ages should be investigated with a number of techniques to ascertain these evidences. The complete set of MIP results is shown in Table 9-2.

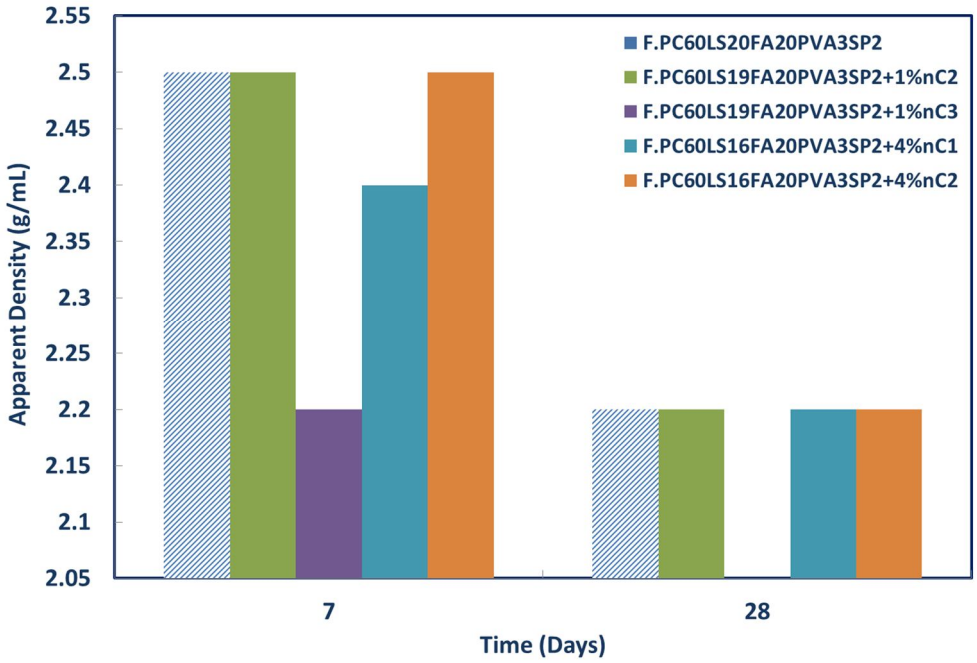

Figure 9-27: Effect of nC type on the total pore area of fibre cements

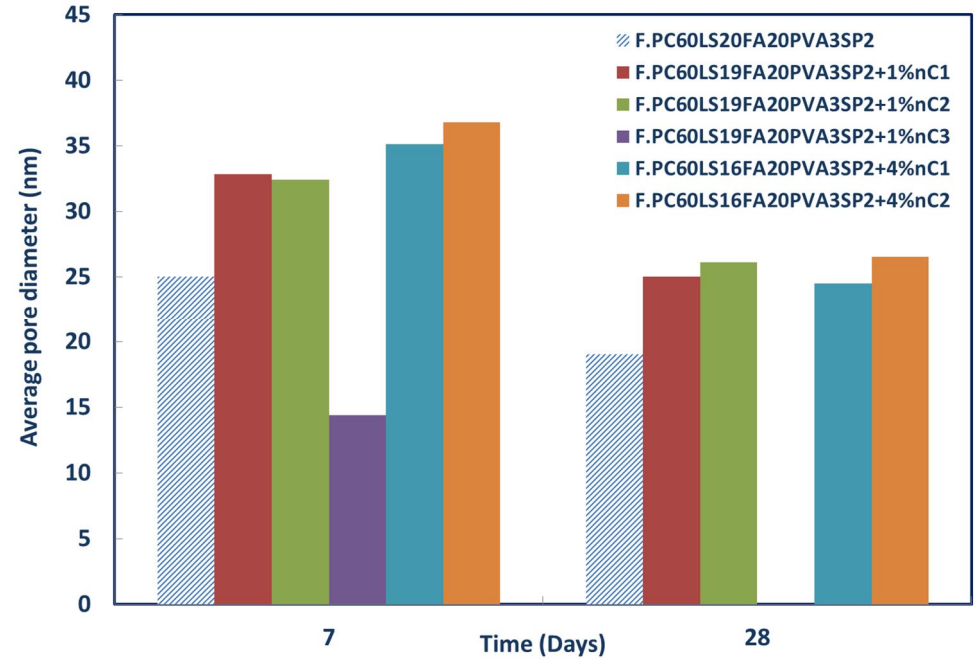

Figure 9-28: Effect of nC type on the average pore diameter of fibre cements

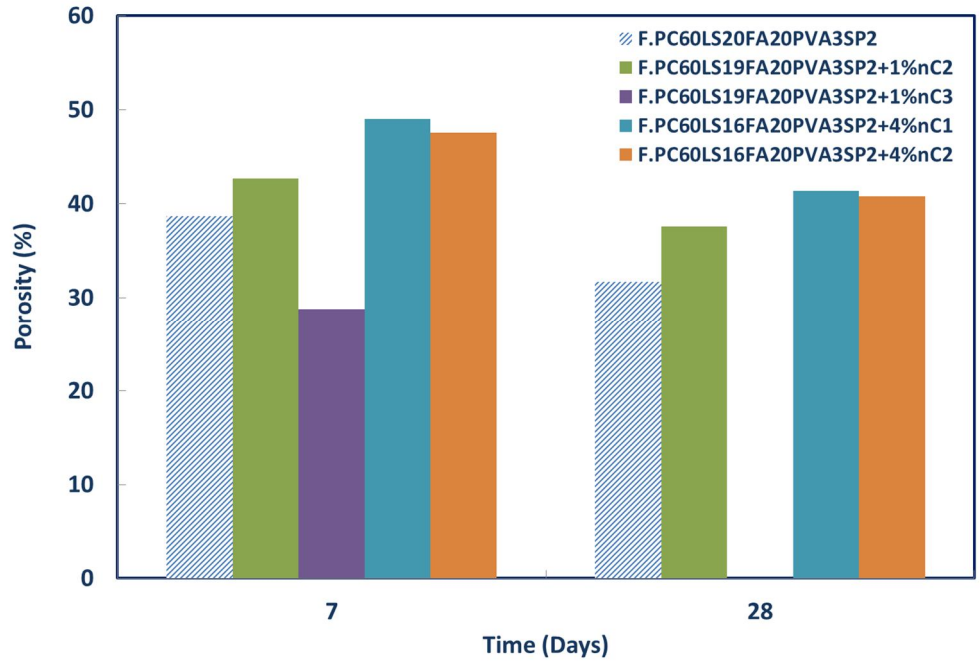

Figure 9-29: Effect of nC type on the porosity of fibre cements

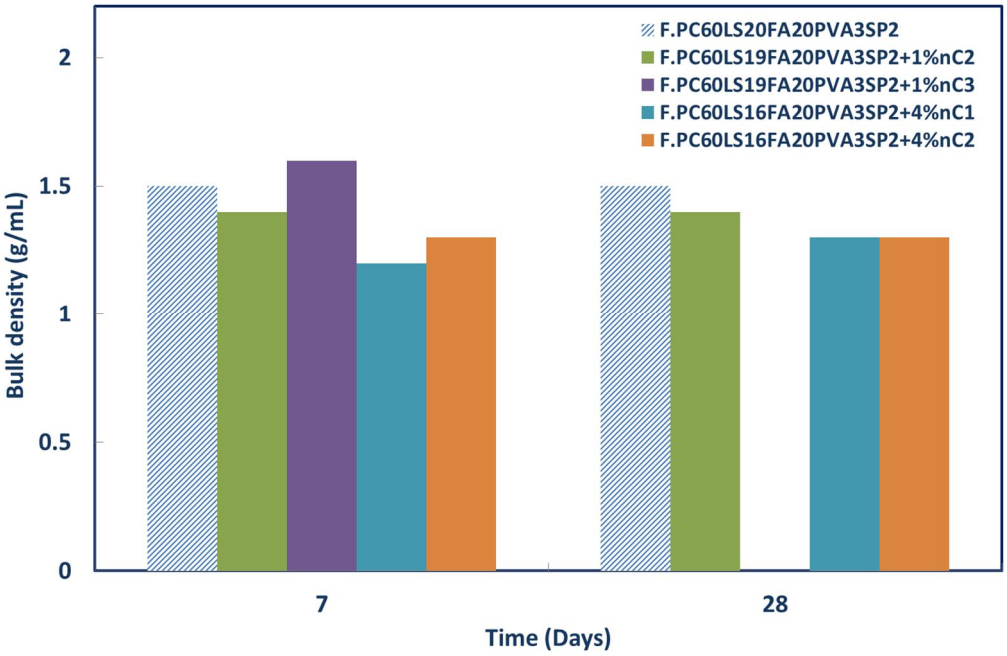

Figure 9-30: Effect of nC type on the bulk density of fibre cements

Table 9-2: Mercury Intrusion Data summary on PC60LS20FA20

Paste	$A_{pore-total}$ (m^2/g)	$\Phi_{pore\ volume-med}$ (nm)	$\Phi_{pore\ area-med}$ (nm)	r_{bulk} (g/mL)	$F_{pore-average}$ (nm)	$r_{apparent}$ (g/mL)	Porosity (%)	$V_{stem-used}$ (%)
PC60LS20FA20PVA 3SP2 – 7 Days	40.2	139.4	5.6	1.5	25.0	2.5	38.7	44
PC60LS19FA20PVA 3SP2+1%nC1–7D	37.7	382.2	6.8	x	32.8	x	1	49
PC60LS19FA20PVA 3SP2+1%nC2–7D	37.2	826.1	5.4	1.4	32.4	2.5	42.7	60
PC60LS16FA20PVA 3SP2+4% nC1-7D	45.1	1111.0	6.5	1.2	35.1	2.4	49.0	74
PC60LS16FA20PVA 3SP2+4%nC2 -7D	39.5	2142.9	5.8	1.3	36.8	2.5	47.6	71
PC60LS20FA20PVA 3SP2 – 28 Days	43.8	72.9	5.6	1.5	19.0	2.2	31.7	39
PC60LS19FA20PVA 3SP2+1%nC1-28D	42.1	341.6	6.2	x	25.0	x	1.0	47
PC60LS19FA20PVA 3SP2+1%nC2-28D	42.3	4119.9	5.6	1.4	26.1	2.2	37.6	52
PC60LS19FA20PVA 3SP2+1%nC3-28D	50.9	25.6	5.5	1.6	14.4	2.2	28.8	41
PC60LS16FA20PVA 3SP2+4%nC1-28D	51.6	607.1	6.0	1.3	24.5	2.2	41.4	66
PC60LS16FA20PVA 3SP2+4%nC2-28D	47.2	2300.7	5.7	1.3	26.5	2.2	40.8	59

Water impermeability tests were carried out for the nC modified fibre cement pastes based on F.PC60LS20FA20PVA3SP2, as before. As shown in Figure 9-31, the hypothesis suggesting that inorganic nC adsorbs more water is considered most possible, with the organoclays exhibiting better performance than the reference paste at early and at later ages. Once again, the higher nC concentrations are not effective, as was the case with the MIP analyses. These results are directly related to the flexural strength performance, as well, leading to the conclusion that higher nC dosages, create clusters, increase porosity and in total, add localised weaknesses in the volume of cement pastes.

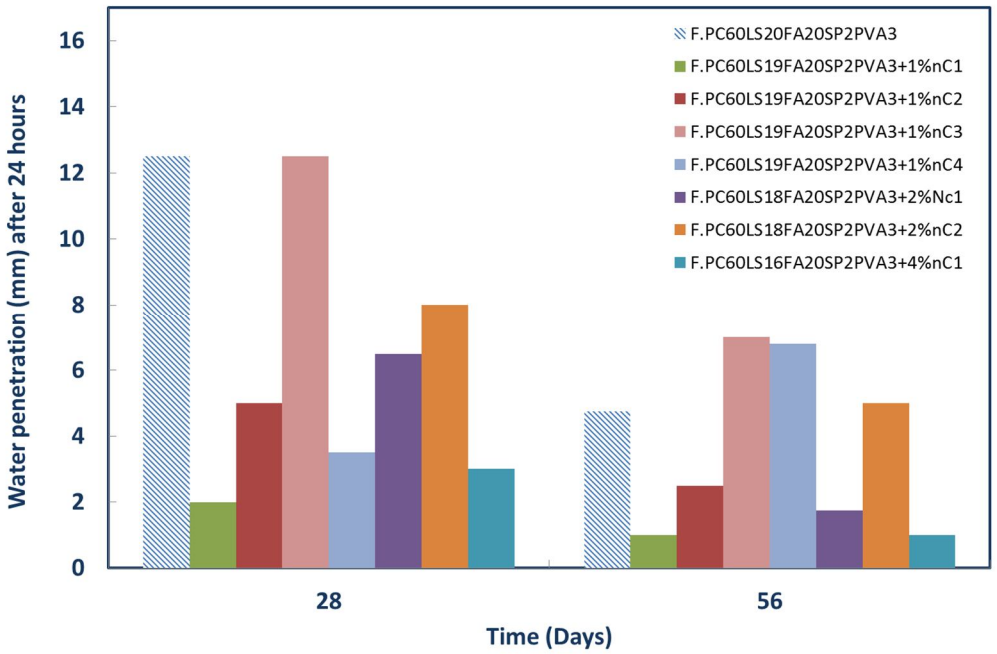

Figure 9-31: Effect of nC type and concentration on the impermeability of nC modified pastes based on F.PC60LS20FA20PVA3SP2

9.4 Cube compressive strength and relative density of mortars based on PC60LS20FA20

The compressive strength of mortar cubes produced using CEMI-45R, based on PC60LS20FA20 and denoted as M.PC60LS20FA20 was measured (Figure 9-32). The standard deviation of the compressive strength remained within 0.5 and slightly increased for the higher nC2 concentrations, as expected since the dispersion was highly viscous. The best performance was achieved for the lower nC4 concentration, followed by the nC4 and nS modified mortar. nC2 exhibited the lowest compressive strengths, however, best combination was given at 2% nC2 and 0.5% nS addition, as shown in Figure 9-32.

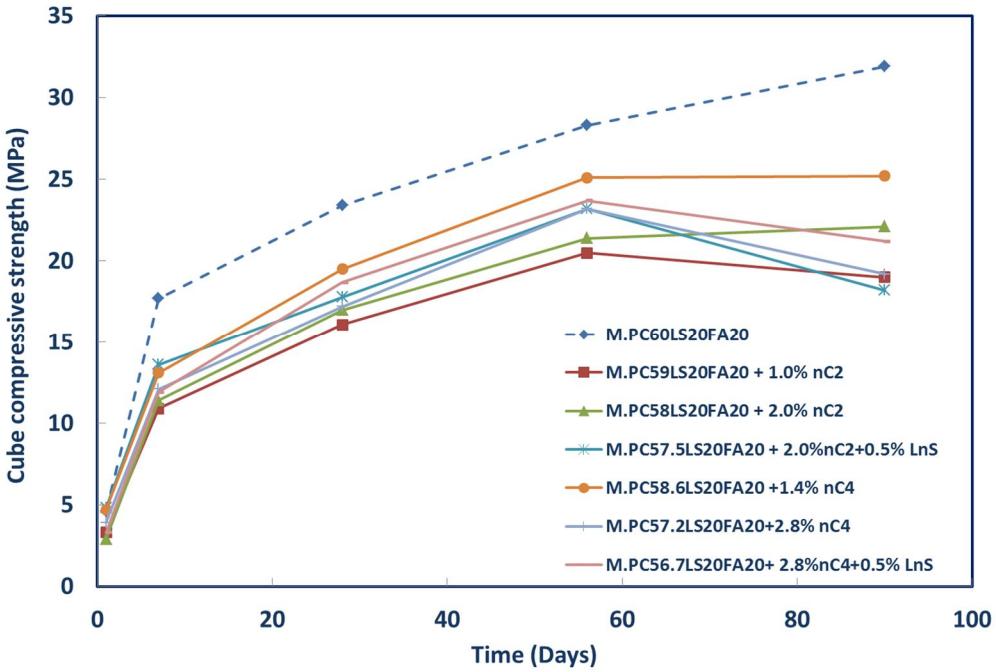

Figure 9-32: Cube compressive strength of nC2 or nC4 and LnS modified mortars based on PC60LS20FA20

The Long-term (after month 3) relative density measurements of the mortar cubes showed minor variation for nC2 and more significant for nC4 (Figure 9-36). The closest performance to the reference mortar was achieved by nC4. This is another indication as to why nC4 performed better in compression. The homogenous mixing and the compaction of the samples produced with nC4 was easier, due to the fact that it was added in powder form than in dispersion as nC1 to nC3. This, possibly lead to denser and more homogeneous mortars.

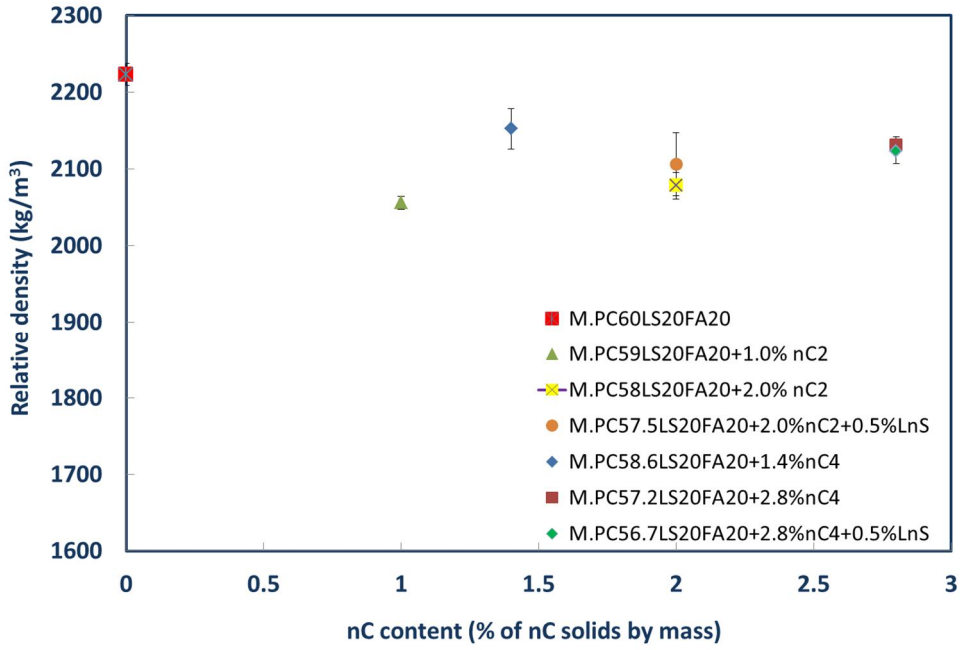

Figure 9-33: Long-term relative density of nC2 or nC4 and LnS modified mortars based on M.PC60LS20FA20

9.5 Cube compressive strength and relative density of mortars based on PC60FA40

One last series of mortars, produced using CEMI-45R, was tested in compression in an effort to investigate possible cooperation of high dosages of FA with nC particles. For this series, the reference mortar contained 60% PC and 40% FA and was denoted as M.PC60LS40. As shown in Figure 9-34 nC2 exhibited the poorest performance. The 2% concentration performed better than at 1%. Additional modification with LnS was more successful than plain nC2, particularly at later ages, as also discussed in Chapter 7, whereas the addition of very low dosage of GnS may be expected to deliver the best results if the w/b ratio is adjusted.

As shown in Figure 9-35 the hydrophilic nC3 dispersion performed better than the organomodified nC2 dispersion, the best combination being the one incorporating LnS, as well. The best combination in terms of compressive strength proved to be the one combining nC4 and LnS.

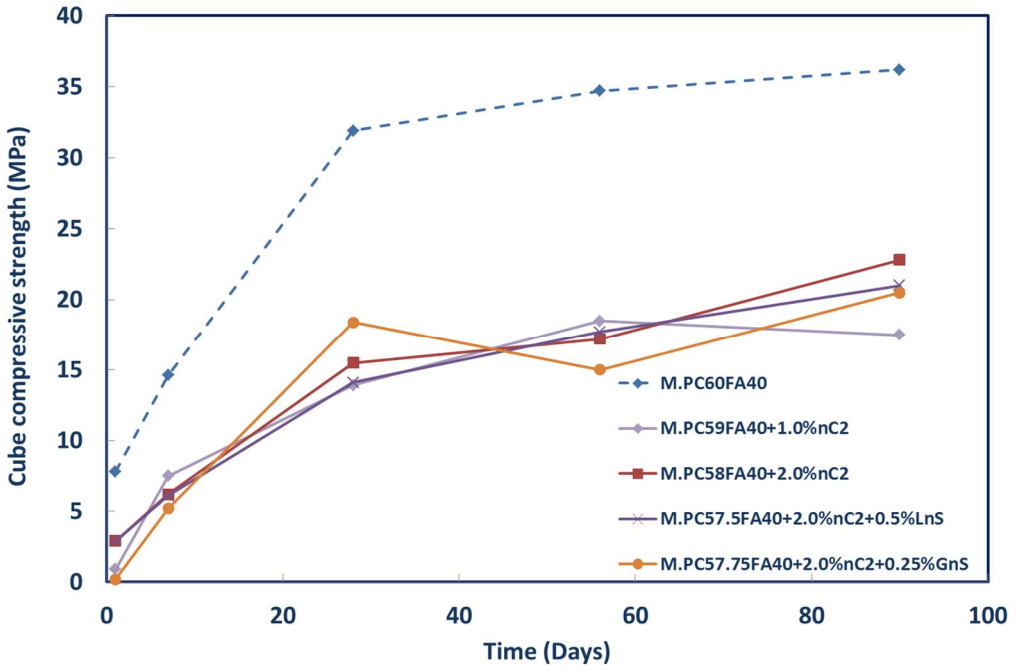

Figure 9-34: Cube compressive strength of nC2 and LnS or GnS modified mortars based on M.PC60FA40

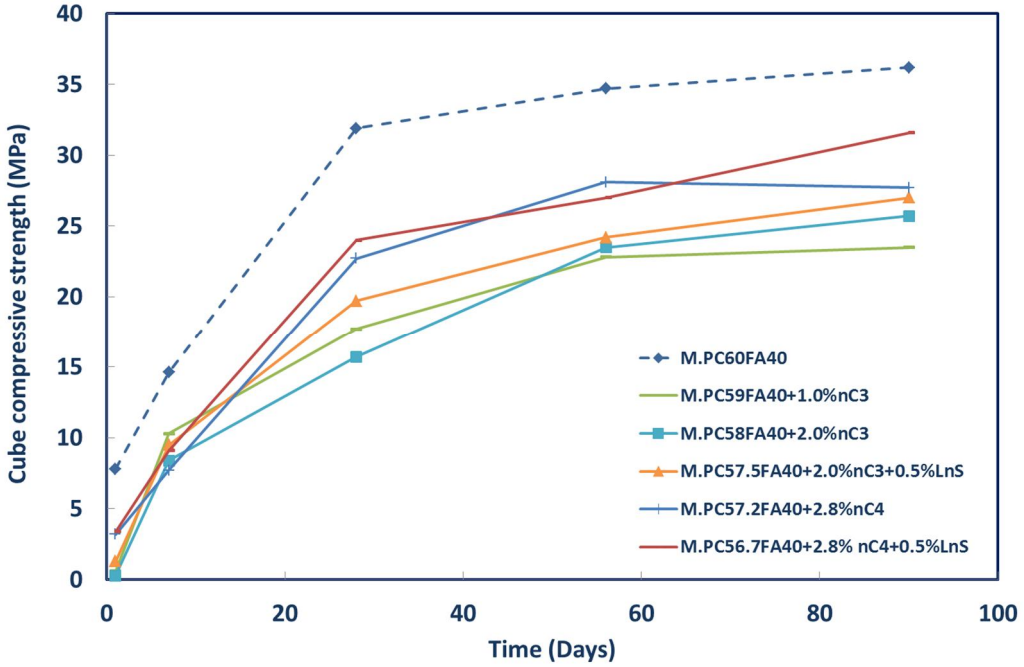

Figure 9-35: Compressive strength of nC3 or nC4 and LnS modified mortars based on PC60FA40

At this point, a comparison between the median compressive strength of the two mortar series was necessary. As shown in Table 9-3, the reference mortar M.PC60FA40 achieved higher strengths and higher strength gain rates than the reference mortar M.PC60LS20FA20. Additionally, all nC modified mortars based on M.PC60FA40 exhibited a strength gain after day 56, whereas the nC modified mortars based on M.PC60LS20FA20 exhibited a strength drop between day 56 and 90. However the rate of strength gain within the first 28 days of mortars was significantly lower for the mortars based on the 40% FA content than those based on the 20%FA+20%LS content.

Table 9-3: Comparison of median cube compressive strength of nC or nC and nS modified mortars

	DAY				
	1	7	28	56	90
	Strength (MPa)				
M.PC60LS20FA20	**4.6**	**17.7**	**23.4**	**28.3**	**31.9**
M.PC59LS20FA20 +1.0%nC2	**3.3**	**10.9**	**16.1**	**20.5**	**19**
M.PC58LS20FA20 +2.0%nC2	**2.9**	**11.4**	**17**	**21.4**	**22.1**
M.PC57.5LS20FA20+2.0%nC2+0.5% LnS	**4.8**	**13.6**	**17.8**	**23.2**	**18.2**
M.PC57.2LS20FA20+2.8%nC4	**3.9**	**12.1**	**17.2**	**23.2**	**19.2**
M.PC56.7LS20FA20+2.8%nC4+0.5% LnS	**3.3**	**11.9**	**18.7**	**23.7**	**21.2**

	DAY				
	1	7	28	56	90
	Strength (MPa)				
M.PC60FA40	**7.8**	**14.6**	**31.9**	**34.7**	**36.2**
M.PC59FA40+ 1.0%nC2	**0.9**	**7.5**	**13.9**	**18.5**	**17.5**
M.PC58FA40+ 2.0%nC2	**2.9**	**6.2**	**15.5**	**17.2**	**22.8**
M.PC57.5FA40 +2.0%nC2+0.5 %LnS	**2.9**	**6.1**	**14.1**	**17.7**	**21**
M.PC57.2FA40 +2.8%nC4	**3.2**	**7.7**	**22.7**	**28.1**	**27.7**
M.PC56.7FA40 +2.8%nC4+0.5 %LnS	**3.4**	**9.1**	**24**	**27**	**31.6**

Long-term (after month 3) relative density measurements (Figure 9-36) showed that nC3 can deliver denser mortars and that the supplementary nS addition does not cause any variation in terms of density within samples of the same combination, but can increase the density of the nC modified samples, even at higher nC dosages (e.g. M.PC58FA40+2.0%nC2 compared with M.PC57.5FA40+2.0%nC2+0.5%LnS or M.PC59.75FA40+0.25%GnS), bringing them close to the reference mortar.

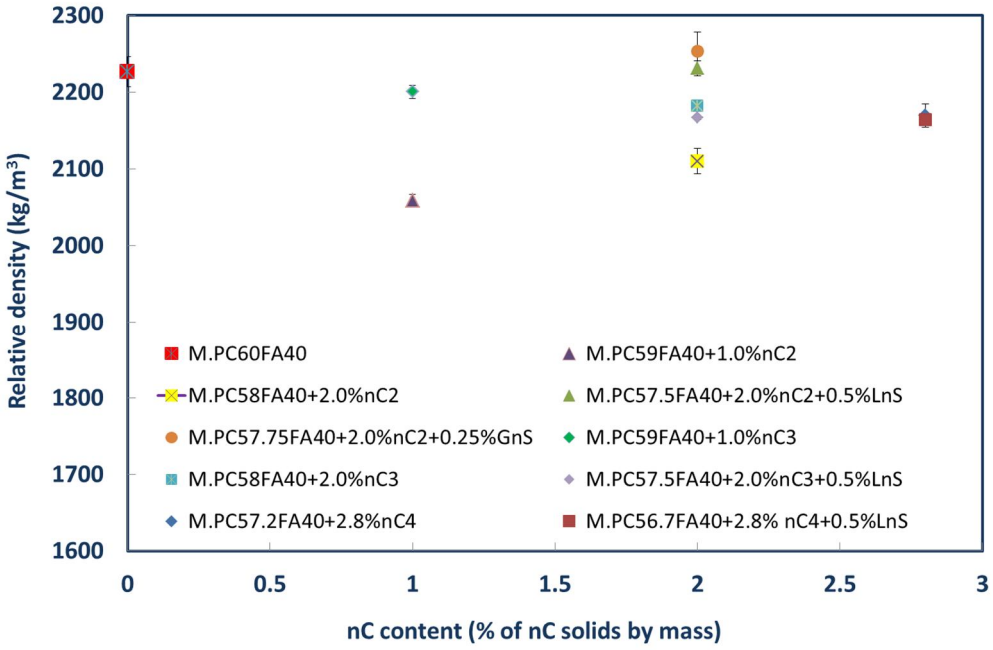

Figure 9-36: Long-term relative density of nC and LnS or GnS modified mortars based on M.PC60FA40

9.6 Quinary nC1 and LnS modified fibre cement formulations

These series constitute a demonstration of the potentials of the fibre cement formulations when nC is combined with LnS. In fact, even the less favourable nC dispersion, nC1 at 2% addition by mass, can offer flexural strength enhancement, as shown in Figure 9-37. Furthermore, once again, it can be observed that the 0.5% by mass LnS addition is more effective in terms of strength gain than the higher LnS addition, i.e. 1% by mass of binder. It is acknowledged that F.PC60LS20FA20PVA4SP2 is by no means a complete series if no later ages are studied and also a comparison between the effect of the difference nC dispersions.

The purpose of these series was to set the ground for the "further research" suggestions presented in the last chapter of this thesis. For this reason, no further investigations of these pastes have taken place at this stage.

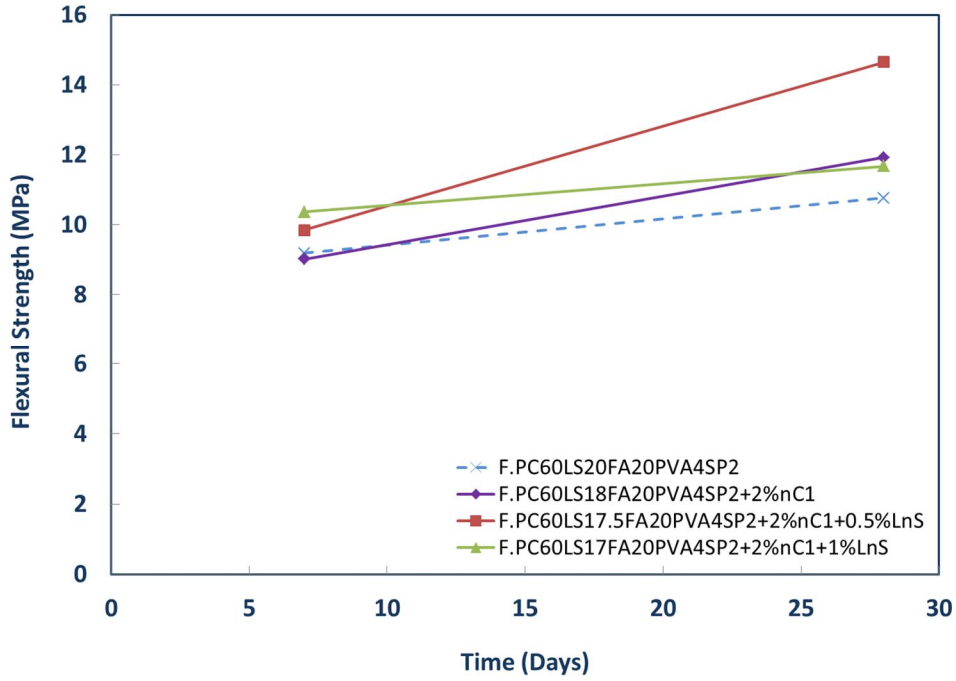

Figure 9-37: Flexural strength of nC1 and LnS modified fibre cement pastes based on F.PC60LS20FA20PVA4SP2

9.7 Conclusions

In the present chapter a successful application of the nC technology in cement pastes was presented with respect to:

- Flexural strength performance
- Late age behaviour
- Optimum nC content
- nC type

nC1 modified fibre pastes showed significantly higher $Ca(OH)_2$ consumption, but, the weakest performance in terms of strength. This can be again attributed to the limited exfoliation of the OMMT.

Both series of nC2 modified fibre pastes showed improved flexural performance, however, the difficulty of compaction of such pastes incorporating fibres and nC2 can lead to increased clustering of the various particles leading to greater strength variations.

The inorganic nC3 dispersion was proven to contribute to flexural strength enhancement through the pozzolanic reaction. However further research is required with respect to impermeability characteristics of pastes modified with nC3, as a tendency to adsorb water

was observed in pastes containing only PC and LS. nC modified pastes containing PC, LS and FA, showed enhanced performance by adsorbing less water than the reference paste but further research is required with respect to later age performance.

Lastly, testing of various mortars lead to the conclusion that nS can offer further improvements to nC modified binders. Different compositions of nC modified cements and mortars can yield significantly different mechanical performances and the advantages of two more reference binders were discussed in this chapter.

10 SUMMARY OF CONCLUSIONS & FUTURE RESEARCH

10.1 Summary

Detailed discussion and concluding remarks were presented in each chapter separately. The most important achievements with respect to the nS addition were: (i) the identification of an optimal nS content within ternary (PC/LS/nS), quaternary (PC/LS/FA/nS) and quinary (PC/LS/FA/μS/nS) formulations, (ii) the discovery of collaborating and antagonistic elements and dosages and their effect on strength and microstructure of the pastes, (iii) the enrichment of the knowledge on the hydration process and products and microstructure of such pastes.

The most important findings and achievements with respect to the nC addition were: (i) the in-depth analysis of the effect intercalation or exfoliation has on the nC itself and on its abilities when added to composite cement formulations, (ii) the correlation of the status of the platelets within the paste with the mechanical performance of the nanomodified cements, (iii) the study of the effect of three different types of nCs; organomodified and dispersed, inorganic and dispersed, organomodified and undispersed on the hydration and microstructure of cement pastes and (iii) the creation of successful combinations with intercalated nCs.

In this chapter the fundamental achievements of this research and the recommendation for future research are summarized below.

10.2 Achieved aims & objectives

10.2.1 To define the state of the art on the potentials of nanomodifications of cement pastes and main factors affected

In chapter 2 on understanding on the behaviour of the different pastes and on the parameters that affect the physical and chemical properties within the paste was established. The hydration characteristics and products of non-nanomodified pastes was discussed according to the state of the art and the expected effects of the nanomodification of cement pastes were presented according to the pre-existing literature. The major factors affected, cover the full range from the nanolevel to the macrolevel; in fact they were identified to be the C–S–H, morphology of the hydrated paste, porosity and compressive strength, as affected by enhanced pozzolanic reactions, nucleation site theory or enhanced particle packing and reduction of nanosized porosity. The main disagreements and disputes were identified and stressed. Moreover, lack of knowledge in the non-nanomodified composite cement formulations was also recognized.

10.2.2 To identify the debated issues with respect to the addition of nanosilica and nanoclay particles & to select the appropriate experimental tools to study the identified issues

In Chapter 2 a number of inconsistencies in current knowledge on nS and nC addition to cement pastes were identified. In fact, the optimum dosage of nanoparticles was unclear especially in blended or composite cement pastes, the pozzolanic nature of the nanoparticles was debated and the early and late age effects of the nanoparticles had never been covered in a single study over a number of different nanoparticle content additions. Furthermore, with respect to the nanoclays, it was clarified that the medium used to organomodify the nC has such an effect on the material itself that the nC's effect on cement paste has to be studied separately. Therefore, the nCs developed for the FIBCEM project had never been used before as additions in cement and all findings of this research would be presented for the first time ever. Additionally, the author in contrast to all pre-existing researches, which were in support of the organomodified clays, suggested that there were greater potentials in the use of inorganic clays, an area not previously investigated. For the first time a comparison between organomodified and undispersed nC, organomodified and dispersed nC and inorganic nC was designed to be analysed at different nC dosages and over a long period of time (from day one until six months).

10.2.3 To select the parameters to be studied with the experimental tools; and to carry out characterization and preliminary assessment of the potentials of the selected nanomaterials

In Chapter 3 a number of analytical tools were selected, for investigations on the identified factors affected with the addition of nanoparticles.

The two nS and three nC dispersions were characterized to the extent that predictions could be made with respect to their effect in different cement pastes.

With respect to the nCs, characterization was carried out in two phases of the material; the initial (in powder form) and the final (in a dispersion) showing the differences in composition and particle or crystal characteristics of the materials. Extensive thermal analyses assisted in the deeper understanding and decoding of the decomposition characteristics of the nCs. In addition, for the first time a separate study was devised to investigate the pozzolanic potentials of the nC dispersions. Lastly, another achievement, never presented before, was the development of a theory that related the exfoliation or intercalation of the nC with the condition of the platelets within the hydrating cement paste. Connection with the particle size distribution of the nC modified pastes and their compressive strength performance was also made.

More lessons learned:

- ✓ Optimizing blended or composite Portland cement pastes is an iterative process; for this it is essential that material characterisation is thorough.
- ✓ Poor initial dispersion of the nC can cause weak points in paste and premature failures in agreement with Birgisson and Dham (2011).
- ✓ The agglomeration observed could be also attributed to the high nC loading (15%) in the dispersion.
- ✓ Maybe less organic modifier for OMMT should have been used. Carbon seemed to be applying a critical barrier by covering the platelets, possibly not allowing them to react as intended. It is also possible that the excess of the organomodifier had a physical effect, as well, making the platelets agglomerate rather than keeping them apart. This is one of the reasons that the OMMT modified pastes performed less successfully in terms of compressive strength.
- ✓ The OMMTs were only intercalated. If they were exfoliated they may have performed better, as the charge would have made the platelets repulse each other and they, therefore, would have been individually available for reactions. In other words, their huge surface area would have been utilized.

10.2.4 To devise a sequence of formulations with which the various parameters will be investigated

Having identified the lack in knowledge on the composite cement blends, a series of formulations was designed covering from second order non-nanomodified pastes to fifth order nanomodified pastes. A unique casting technique with syringes was introduced and a mixing sequence for the successful addition of the nanoparticles to the cement blends was presented.

10.2.5 To obtain information on the behaviour of non-nanomodified blended cement formulations & identify possible competing constituents in high order cement formulations

In Chapter 5, the non-nanomodified pastes on which the research was based were introduced, analysed, compared and discussed. Three pastes were selected and analysed to become the reference pastes for the nanomodifications. Competing constituents and areas of improvements with the addition of the nanoparticles were identified.

10.2.6 To evaluate the effect the addition of nS has on the hydration, microstructure and mechanical properties of the blended cement formulations, as compared with the non-nanomodified ones & to identify the limits

In Chapter 6 the nS modified ternary cement formulations were studied. Analyses were carried out until month six. It was found that above 1% nS solids by mass, clustering occurs, leading to reductions in compressive strength over time. Most importantly, nS, was found to contribute to the strength gain of high (40%) LS content pastes.

More lessons learned:

- ✓ Pozzolanic activity was confirmed for LnS.
- ✓ Superplasticizers would have assisted with the better distribution of nanoparticles within the paste (Sobolev *et al.*, 2009b).
- ✓ 0.1 to 0.5% nS addition by mass is an optimal dosage for short and Long-term enhanced performance.
- ✓ It was also concluded that nS plays a role in the development of an enhanced microstructure.

In Chapter 7 the nS modified quaternary & quinary cement formulations were studied.

The optimisation of the other two selected reference pastes was achieved with the addition of nS particles in the quaternary combinations and the addition of nS and μS particles in the quinary combinations.

More lessons learned:

- ✓ Never before had such complex pastes (PC43LS20FA37 or PC60LS20FA20) been studied with the addition of nanoparticles at various contents and over different curing periods.
- ✓ PC43LS20FA37 nanomodified pastes should be studied for longer periods (reaching one year).
- ✓ 0.5% nS addition by mass is an optimal dosage for composite cement pastes, as well.
- ✓ nS and FA are competing materials when added in significant quantities
- ✓ The optimal point may pass in the presence of excessive nS particles

10.2.7 To evaluate the effect the addition of nC has on the hydration, microstructure and mechanical properties of the blended cement formulations, as compared with the non-nanomodified ones & to identify the limits

In Chapter 8, the first selected reference paste was modified with the addition of the three different nC dispersions. Analyses were carried out until month six. Although it was postulated by previous research that hydrophilic nCs should not be directly used in cement because they absorb water leading to catastrophic expansion (Kuo *et al.*, 2006), on the contrary it was proven that they can offer very advantageous solutions in terms of density, stability and microstructural enhancement. However, this research confirmed that, indeed, above 1% nC content clustering occurs creating microparticles of hydrated nC enhanced compounds. Clustering up of the nC particles was witnessed with various techniques (SEM, FESEM, MIP, density) and was largely responsible for the reductions in compressive strength.

More lessons learned:

- ✓ Pozzolanic activity was confirmed for both OMMT and inorganic nC.
- ✓ Superplasticizers would have assisted with the better distribution of nanoparticles within the paste (Sobolev *et al.*, 2009b).
- ✓ 1% nC addition by mass for cement pastes and to 2% for mortars is an optimal dosage for short and Long-term enhanced performance.
- ✓ The inorganic dispersion showed the best performance in terms of pozzolanic reactivity and porosity reduction.
- ✓ The nCs should be dilute in distilled water and stirred with a sonicator before added to mixer.
- ✓ Researchers should be particularly careful when stating if $Ca(OH)_2$ is being consumed by nC particles. The amount of the organomodifier should be stated as well as its temperature of decomposition so that to make sure that the mass loss stated, comprises the net value that indeed corresponds to the $Ca(OH)_2$ present.
- ✓ Despite the fact that the OMMTs were only intercalated, their shape provided some ductility to the cement paste, which was very important.

10.2.8 To extend the application to fibre cement pastes and analyse the effect on the three main parameters; hydration, microstructure and mechanical properties

In Chapter 9 a successful application of the nCs was achieved by incorporating them in quaternary & quinary fibre cement formulations. The addition of SP had a significant effect on all nCs. Even the OMMT performed better in flexure. Again, 1% nC by mass seemed to be the ideal dosage.

More lessons learned:

- ✓ Pastes should be investigated at later ages and performance should be ascertained over significant periods of times.
- ✓ Further research is required with the use of other techniques such as X-ray tomography (CT) scan to determine the absolute values of porosity, pore area and other parameters.
- ✓ PVA fibre content could be reduced to 2%. This would also make the surface of the samples be more level.
- ✓ Nano swelling may have taken place, filling the capillary pores (Farzadnia *et al.*, 2013). Nanoclays could fill, the possibly detectable by the MIP, LD C–S–H porosity (DeJong and Ulm, 2007), however further studies with different techniques should verify such hypothesis.
- ✓ Inorganic nanoclays may offer significant strength enhancement in cement pastes designed for flexure.

10.3 Future research

The abilities of the laboratories at the University of Bath have been fully utilized by the author. However, cutting edge science and research could be advanced with the following:

- ➢ The changes of particle size distributions in the nanomodified pastes could be studied with a particle size analyser.
- ➢ The kinetics of the early hydration reactions (acceleratory or retarding) of the nanomodified cement should be studied with isothermal conduction calorimetry.
- ➢ The study of chloride resistance particularly of the nC modified pastes due to their higher aluminium content.
- ➢ The exact phases decomposing in the pastes at different temperature ranges, particularly for the nC modified pastes whose chemistry is more complex could be detected and quantified by a TG analyser mounted with gas analyser. Moreover, if the TG analyser could test more than one sample at a time, the statistical accuracy would be improved.
- ➢ XRD with for quantitative analyses could provide reliable comparisons with the TG analyses.
- ➢ The C–S–H chain polymerization with the addition of the nanoparticles could be determined by solid state NMR.
- ➢ Changes in the C–S–H density could be detected with the help of an AFM mounted with a nanoindentation probe.
- ➢ The effect of nanoparticles on changes in the early-age properties with the help of vicat and calorimetry time tests should be defined.
- ➢ Changes in the pore structure could be assessed with Ar or N_2 porosimetry.

- It would be interesting to carry out rheology and consistency tests particularly with respect to the ability of the nanomodified pastes to be extruded.

It is possible that lowering the nC solids loading of dispersions could facilitate miscibility and therefore a separate study on the effect on nC solids content in the dispersions could test this hypothesis.

Moreover, in the case of mortars, lower than 0.5% concentrations should also be tried for standard mortars (w/b = 0.5), as in the past higher compressive strength have been achieved at 0.25% nC content (Kuo *et al.*, 2011). Further studies on the design of mortars with lower w/b ratios containing superplasticizers are expected to yield interesting results as a number of limitations can be eradicated:

- More coherent mortars can be delivered.
- Nanoparticles mobility could be enhanced avoiding clustering.
- Minimization of total porosity would be expected.
- Better pore size distribution should be maintained, since nanoparticles are better dispersed within the mass of mortars.

Furthermore, scaling up to concrete and particularly recycled aggregate concrete could create a new generation of highly sustainable concretes for structural applications.

Additionally, as discussed in chapter 7, with respect to the PC43LS20FA37 nanomodified pastes, an investigation by the nanoindentation method and a series of CT scans could shed more light in the relationship between, the densification of C–S–H in the presence of lower LnS contents and probable increase in porosity due to the presence of excessive LnS particles. Also, a PSD analyses verified by CT scans of the nanomodified PC/FA=1.16 pastes would elucidate the combined effect the high FA and nanoparticle content have on the pore size and total porosity.

A research programme on the properties of nanomodified - by a combination of nanoparticles - cements could yield very interesting results, taking into consideration the discussion on both nS and nC modified fibre cements, in Chapter 9.

Lastly, the most promising step would be the study of the addition of superplasticizers in the composite nanomodified cement pastes.

With demand for cement ever increasing particularly in the “emerging economies” of China and India and reduction of the environmental impact becoming an ethical obligation rather than an option, nanomodified cements can offer advanced solutions, providing better performing cementitious materials, increasing the durability and consequently the service life of structures, reducing the net environmental impact and fulfilling cement industry’s social responsibility for the future generations.

REFERENCES

Abell, A., Willis, K. & Lange, D. 1999. Mercury intrusion porosimetry and image analysis of cement-based materials. *Journal of colloid and interface science,* 211**,** 39-44.

Adamaki, V., 2015. Manufacturing and characterisation of Ti-suboxides for sensing and energy applications. PhD, University of Bath.

Al-Otaibi, S.F. 2012. Influence of nano-sio_2 on the properties of cement pastes. *NICOM 4: 4th International Symposium on Nanotechnology in Construction.* Agios Nikolaos, Crete, Greece.

Alizadeh, R., Beaudoin, J. & Raki, L. 2011. Mechanical properties of calcium silicate hydrates. *Materials and Structures,* 44**,** 13-28.

Alizadeh, R.A. 2009. *Nanostructure and engineering properties of basic and modified calcium-silicate-hydrate systems.* PhD, University of Ottawa.

Allen, A.J. & Thomas, J.J. 2007. Analysis of C–S–H gel and cement paste by small-angle neutron scattering. *Cement and Concrete Research,* 37**,** 319-324.

Allen, A.J., Thomas, J.J. & Jennings, H.M. 2007. Composition and density of nanoscale calcium-silicate-hydrate in cement. *Nat Mater,* 6**,** 311-316.

Aly, M., Hashmi, M.S.J., Olabi, A.G., Messeiry, M. & Hussain, A.I. 2011. Effect of nano clay particles on mechanical, thermal and physical behaviours of waste-glass cement mortars. *Materials Science and Engineering: A,* 528**,** 7991-7998.

Arivalagan, K., Ravichandran, S., Rangasamy, K. & Karthikeyan, E. 2011. Nanomaterials and its potential applications. *International Journal of ChemTech Research,* 3**,** 534-538.

ASTM 2012. C618-12a, standard specification for coal fly ash and raw or calcined natural pozzolan for use in concrete. ASTM International, West Conshohocken, PA, www.astm.org.

Balaguru, P. & Chong, K. Year. Nanotechnology and concrete: Research opportunities. *In:* Sobolev & Shah, eds. Session on "Nanotechnology of Concrete: Recent Developments and Future Perspectives", 2006 Denver, USA. American Concrete Institute, 15-28.

Barbhuiya, S.A., Gbagbo, J.K., Russell, M.I. & Basheer, P.A.M. 2009. Properties of fly ash concrete modified with hydrated lime and silica fume. *Construction and Building Materials,* 23**,** 3233-3239.

Barluenga, G., Palomar, I. & Puentes, J. 2012. Early age and hardened performance of cement pastes combining mineral additions. *Materials and Structures***,** 1-21.

Batra, M., Gotam, S., Dadarwal, P., Nainwani, R. & Sharma, M. 2011. Nano-clay as polymer porosity reducer: A review. *Journal of Pharmaceutical Science and Technology,* 3**,** 709-716.

BCA 2003. Guidance on the use of terms relating to cement and concrete.

BCA 2009. Fact sheet 18 [part 1] - embodied CO_2 of uk cement, additions and cementitious materials.

Beaudoin, J., R.F., F., J., B. & M., C. Year. Dependence of degree of silica polymerization and intrinsic mechanical properties of C–S–H on Ca/Si ratio. *In:* 8th Congr. Int. Quim. Cimento 1986. 337-342.

Bernal, J.D., Jeffery, J.W. & Taylor, H.F.W. 1952. Crystallographic research on the hydration of portland cement. A first report on investigations in progress. *Magazine of Concrete Research,* 4**,** 49-54.

Bhattarai, B. 2006. Mechanical properties of nanoclay based nanocomposites: A review. Pittsburg State University.

Bi, J., Pane, I., Hariandja, B. & Imran, I. 2012. The use of nanosilica for improving of concrete compressive strength and durability. *Applied Mechanics and Materials,* 204-208**,** 4059-4062.

Birgisson, B. & Dham, M. 2011. Optimization of clay addition for the enhancement of pozzolanic reaction in nano-modified cement paste. *In:* Gopalakrishnan, Birgisson, Taylor & Attoh-Okine (eds.) *Nanotechnology in Civil Infrastructure: A Paradigm Shift.* Springer Berlin Heidelberg.

Birgisson, B., Mukhopadhyay, A.K., Geary, G., Khan, M. & Sobolev, K. 2012. Nanotechnology in concrete materials - a synopsis. *Transportation Research Circular E-C170.* Washington, D.C.: Transportation Research Board.

Björnström, J., Martinelli, A., Matic, A., Börjesson, L. & Panas, I. 2004. Accelerating effects of colloidal nano-silica for beneficial calcium–silicate–hydrate formation in cement. *Chemical Physics Letters,* 392**,** 242-248.

Bonaccorsi, E., Merlino, S. & Kampf, A.R. 2005. The crystal structure of tobermorite 14 å (plombierite), a C–S–H phase. *Journal of the American Ceramic Society,* 88**,** 505-512.

Bonaccorsi, E., Merlino, S. & Taylor, H.F.W. 2004. The crystal structure of jennite, Ca9Si6o18(OH)6·8H_2O. *Cement and Concrete Research,* 34**,** 1481-1488.

Briell, B. 2000. Nanocomposite 2000 "nanoclays – counting on consistency". [Accessed 9-3-2013].

Brouwers, H.J.H. 2003. Chemical reactions in hydrated ordinary portland cement based on the work by powers and brownyard. *In:* Fisher (ed.) *15th Ibausil, International Conference on Building Materials (Internationale Baustofftagung).* Weimar, Germany: F.A. Finger-Institut fur Baustoffkunde

Brouwers, H.J.H. 2004. The work of powers and brownyard revisited: Part 1. *Cement and Concrete Research,* 34**,** 1697-1716.

Brouwers, H.J.H. 2005. The work of powers and brownyard revisited: Part 2. *Cement and Concrete Research,* 35**,** 1922-1936.

Brunauer, S. 1962. Tobermorite gel—the heart of concrete. *American Scientist,* 50**,** 210–229.

Brunauer, S., Mikhail, R.S. & Bodor, E.E. 1967. Some remarks about capillary condensation and pore structure analysis. *Journal of colloid and interface science,* 25**,** 353-358.

Bye, G. 2011. Portland cement. *In:* ICE (ed.) Third Edition ed. Great Britain: ICE Publishing.

BS EN 12390-7:2000: Testing hardened concrete. Density of hardened concrete.

BS EN 492:2012. Fibre-cement slates and fittings. Product specification and test methods.

Calabria-Holley, J., Paine, K. & Papatzani, S. 2014. Effects of nanosilica on the calcium silicate hydrates in portland cement-fly ash systems. *Advances in Cement Research,* 26**,** 1-14.

Camiletti, J., Soliman, A.M. & Nehdi, M.L. 2013. Effects of nano- and micro-limestone addition on early-age properties of ultra-high-performance concrete. *Materials and Structures,* 46**,** 881-898.

CEN 2000. Cement - part 1: Composition, specifications and conformity criteria for common cements.

Chang, T.P., Shih, J.Y., Yang, K.M. & Hsiao, T.C. 2007. Material properties of portland cement paste with nano-montmorillonite. *Journal of materials science,* 42**,** 7478-7487.

Chen, J.J., Sorelli, L., Vandamme, M., Ulm, F.-J. & Chanvillard, G. 2010. A coupled nanoindentation/sem-eds study on low water/cement ratio portland cement paste: Evidence for C–S–H /$Ca(OH)_2$ nanocomposites. *Journal of the American Ceramic Society,* 93**,** 1484-1493.

Commission, E. 2011. Commission recommendation of 18 october 2011 on the definition of nanomaterial. *2011/696/EU.* Brussels.

Cong, X. & Kirkpatrick, R.J. 1996a. 29si and 17o nmr investigation of the structure of some crystalline calcium silicate hydrates. *Advanced Cement Based Materials,* 3**,** 133-143.

Cong, X. & Kirkpatrick, R.J. 1996b. 29si mas nmr study of the structure of calcium silicate hydrate. *Advanced Cement Based Materials,* 3**,** 144-156.

Constantinides, G. & Ulm, F.-J. 2004. The effect of two types of C–S–H on the elasticity of cement-based materials: Results from nanoindentation and micromechanical modeling. *Cement and Concrete Research,* 34**,** 67-80.

Daimon, M., Abo-El-Enein, S.A., Rosara, G., Goto, S. & Kondo, R. 1977. Pore structure of calcium silicate hydrate in hydrated tricalcium silicate. *Journal of the American Ceramic Society,* 60**,** 110-114.

Dalir, H., Farahani, R.D., Nhim, V., Samson, B., Levesque, M. & Therriault, D. 2012. Preparation of highly exfoliated polyester-clay nanocomposites: Process-property correlations. *Langmuir*.

De Paiva, L.B., Morales, A.R. & Valenzuela Díaz, F.R. 2008. Organoclays: Properties, preparation and applications. *Applied Clay Science,* 42**,** 8-24.

De Weerdt, K., Haha, M.B., Le Saout, G., Kjellsen, K.O., Justnes, H. & Lothenbach, B. 2011a. Hydration mechanisms of ternary portland cements containing limestone powder and fly ash. *Cement and Concrete Research,* 41**,** 279-291.

De Weerdt, K., Kjellsen, K.O., Sellevold, E. & Justnes, H. 2011b. Synergy between fly ash and limestone powder in ternary cements. *Cement and Concrete Composites,* 33**,** 30-38.

DeJong, M.J. & Ulm, F.-J. 2007. The nanogranular behavior of C–S–H at elevated temperatures (up to 700°c). *Cement and Concrete Research,* 37**,** 1-12.

Dhir, R.K., El-Mohr, M.A.K. & Dyer, T.D. 1997. Developing chloride resisting concrete using pfa. *Cement and Concrete Research,* 27**,** 1633-1639.

Dhir, R.K., McCarthy, M.J. & Paine, K.A. 2002. *Use of fly ash to bs en 450 in structural concrete. Technology digest 1,* Camberley, UK: The Concrete Society.

Diamond, S. 2000. Mercury porosimetry: An inappropriate method for the measurement of pore size distributions in cement-based materials. *Cement and Concrete Research,* 30**,** 1517-1525.

Dyer, T.D. & Dhir, R.K. 2004. Hydration reactions of cement combinations containing vitrified incinerator fly ash. *Cement and Concrete Research,* 34**,** 849-856.

Dyer, T.D., Halliday, J.E. & Dhir, R.K. 1999. An investigation of the hydration chemistry of ternary blends containing cement kiln dust. *Journal of materials science,* 34**,** 4975-4983.

Elkady, H., I.Serag, M. & Elfeky, M.S. 2013. Effect of nano silica de-agglomeration, and methods of adding super-plasticizer on the compressive strength, and workability of nano silica concrete. *Civil and Environmental Research,* 3**,** 21-35.

Fares, G. & Khan, M.I. 2013. Nanosilica and its future prospects in concrete. *Advanced Materials Research,* 658**,** 50-55.

Farzadnia, N., Abang Ali, A.A., Demirboga, R. & Anwar, M.P. 2013. Effect of halloysite nanoclay on mechanical properties, thermal behavior and microstructure of cement mortars. *Cement and Concrete Research,* 48**,** 97-104.

Feldman, R.F. Year. Sorption and length-change scanning isotherms of methanol and water on hydrated portland cement. *In:* 5th ISCC, 1969. 53– 66.

Feldman, R.F. 1972a. Assessment of experimental evidence for models of hydrated portland cement. *Highway Research Record***,** 8-24.

Feldman, R.F. 1972b. Helium flow and density measurement of the hydrated tricalcium silicate - water system. *Cement and Concrete Research,* 2**,** 123-136.

Feldman, R.F., Carette, G.G. & Malhotra, V.M. 1990. Studies on mechanics of development of physical and mechanical properties of high-volume fly ash-cement pastes. *Cement and Concrete Composites,* 12**,** 245-251.

Feldman, R.F. & Sereda, P.J. 1968. A model for hydrated portland cement paste as deduced from sorption-length change and mechanical properties. *Matériaux et Construction,* 1**,** 509-520.

Fernandez, R., Martirena, F. & Scrivener, K.L. 2011. The origin of the pozzolanic activity of calcined clay minerals: A comparison between kaolinite, illite and montmorillonite. *Cement and Concrete Research,* 41**,** 113-122.

Fonseca, P.C., Jennings, H.M. & Andrade, J.E. 2011. A nanoscale numerical model of calcium silicate hydrate. *Mechanics of Materials,* 43**,** 408-419.

Gilman, J.W, VanderHart, D.L. & Kashiwagi, T.. Thermal decomposition chemistry of Poly(vinyl alcohol) . IN: Fire and Polymers II: Materials and Test for Hazard Prevention, American Chemical Society, ACS Symposium Series 599, August 21-26, 1994, Washington, DC

González-Teresa, R., Morales-Florez, V., Manzano, H. & Dolado, J.S. 2010. Modelos estructurales del empaquetamiento aleatorio de partículas esféricas de tobermorita: Una aproximación computacional sencilla-structural models of randomly packed tobermorite-like spherical particles: A simple computational approach. *Materiales de Construcción,* 60**,** 7-15.

Goodhew, P.J. 1975. *Electron microscopy and analysis / p. J. Goodhew,* London : New York: Wykeham Publications ; Springer-Verlag.

Grist, E., Paine, K., Heath, A. & Pinder, H. 2013. An investigation into the viability and benefits of modern hydraulic lime concretes. *In:* Dhir, Singh & Goel (eds.) *Innovations in concrete construction.* New Delhi: Excel India Publishers.

Gupta, S. 2014. Application of silica fume and nanosilica in cement and concrete-a review.

Hamid, S.A. 1981. The crystal structure of the 11å natural tobermorite $Ca2.25[Si_3O7.5(OH)1.5] \cdot 1H_2O$. *Zeitschrift für Kristallographie - Crystalline Materials,* 154**,** 189-198.

He, C., Makovicky, E. & Osbaeck, B. 1996. Thermal treatment and pozzolanic activity of Na- and Ca-montmorillonite. *Applied Clay Science,* 10**,** 351-368.

He, T., Shi, C., Li, G. & Song, X. 2012. Effects of superplasticizers on the carbonation resistance of C_3S and C_3A hydration products. *Construction and Building Materials,* 36**,** 954-959.

He, X. & Shi, X. 2008. Chloride permeability and microstructure of portland cement mortars incorporating nanomaterials. *Transportation Research Record: Journal of the Transportation Research Board,* 2070**,** 13-21.

Heath, A., Paine, K., Goodhew, S., Ramage, M. & Lawrence, M. 2013. The potential for using geopolymer concrete in the uk. *Proceedings of the Institution of Civil Engineers: Construction Materials,* 166**,** 195-203.

Hedley, C.B., Yuan, G. & Theng, B.K.G. 2007. Thermal analysis of montmorillonites modified with quaternary phosphonium and ammonium surfactants. *Applied Clay Science,* 35**,** 180-188.

Helmuth, R.A. 1965. *Dimensional changes and water adsorption of hydrated portland cement and tricalcium silicate.* MS thesis, Illinois Institute of Technology.

Hewlett, P.C. 2004. *Lea's chemistry of cement and concrete*: Butterworth-Heinemann.

Hosseini, P., Hosseinpourpia, R., Pajum, A., Khodavirdi, M.M., Izadi, H. & Vaezi, A. 2014. Effect of nano-particles and aminosilane interaction on the performances of cement-based composites: An experimental study. *Construction and Building Materials,* 66**,** 113-124.

Hou, P.-k., Kawashima, S., Wang, K.-j., Corr, D.J., Qian, J.-s. & Shah, S.P. 2013a. Effects of colloidal nanosilica on rheological and mechanical properties of fly ash–cement mortar. *Cement and Concrete Composites,* 35**,** 12-22.

Hou, P., Kawashima, S., Kong, D., Corr, D.J., Qian, J. & Shah, S.P. 2013b. Modification effects of colloidal nanosio_2 on cement hydration and its gel property. *Composites Part B: Engineering,* 45**,** 440-448.

Ipavec, A., Gabrovšek, R., Vuk, T., Kaučič, V., Maček, J. & Meden, A. 2010. Carboaluminate phases formation during the hydration of calcite-containing portland cement. *Journal of the American Ceramic Society,* 94**,** 1238-1242.

Jahromi, S.G., Andalibizade, B. & Vossough, S. 2010. Engineering properties of nanoclay modified asphalt concrete mixtures. *Arabian journal for science and engineering. Section B: Engineering,* 35**,** 90.

Jennings, H.M. 2000. A model for the microstructure of calcium silicate hydrate in cement paste. *Cement and Concrete Research,* 30**,** 101-116.

Jennings, H.M. 2004. Colloid model of C–S–H and implications to the problem of creep and shrinkage. *Materials and Structures,* 37**,** 59-70.

Jennings, H.M. 2008. Refinements to colloid model of C–S–H in cement: Cm-ii. *Cement and Concrete Research,* 38**,** 275-289.

Jennings, H.M., Bullard, J., Thomas, J.J., Andrade, J.E., Chen, J.J. & Scherer, G.W. 2008. Characterization and modeling of pores and surfaces in cement paste: Correlations to processing and properties. *J. Adv. Concr. Tech.,* 6**,** 5-29.

Jennings, H.M., Thomas, J.J., Gevrenov, J.S., Constantinides, G. & Ulm, F.-J. 2007. A multi-technique investigation of the nanoporosity of cement paste. *Cement and Concrete Research,* 37**,** 329-336.

Jo, B.-W., Kim, C.-H., Tae, G.-h. & Park, J.-B. 2007a. Characteristics of cement mortar with nano-SiO_2 particles. *Construction and Building Materials,* 21**,** 1351-1355.

Jo, B.W., Kim, C.H., Tae, G. & Park, J.B. 2007b. Characteristics of cement mortar with nano-SiO_2 particles. *Construction and Building Materials,* 21**,** 1351-1355.

Jones, R., McCarthy, M. & Newlands, M. 2011. Fly ash route to low embodied co_2 and implications for concrete construction. *World of coal Ash (WOCA) Conference* Denver, CO, USA.

Kantro, D.L., Brunauer, S. & Weise, C.H. 1962. Development of surface in the hydration of calcium silicates. Ii. Extension of investigations to earlier and later stages of hydration. *The Journal of Physical Chemistry,* 66**,** 1804-1809.

Kawashima, S., Hou, P., Corr, D.J. & Shah, S.P. 2012. Modifications of cement-based materials with nanoparticles. *Cement and Concrete Composites.*

Kawashima, S., Hou, P., Corr, D.J. & Shah, S.P. 2013. Modification of cement-based materials with nanoparticles. *Cement and Concrete Composites,* 36**,** 8-15.

Kuo, W.-Y., Huang, J.-S. & Yu, B.-Y. 2011. Evaluation of strengthening through stress relaxation testing of organo-modified montmorillonite reinforced cement mortars. *Construction and Building Materials,* 25**,** 2771-2776.

Kuo, W.Y., Huang, J.S. & Lin, C.H. 2006. Effects of organo-modified montmorillonite on strengths and permeability of cement mortars. *Cement and Concrete Research,* 36**,** 886-895.

Kurtis, K. 2007. Structure of the hydrated cement paste [online]. Atlanta, Georgia: School of Civil Engineering, Georgia Institute of Technology. Available from: http://people.ce.gatech.edu/~kk92/hcp.pdf [Accessed 16 February 2013].

Lam, L., Wong, Y. & Poon, C. 2000. Degree of hydration and gel/space ratio of high-volume fly ash/cement systems. *Cement and Concrete Research,* 30**,** 747-756.

Lawrence, R.M.H., Mays, T., Walker, P. & D'Ayala, D. 2006. The use of tg to measure different concentrations of lime in non-hydraulic lime mortars. *Journal of Thermal Analysis and Calorimetry,* 85**,** 377-382.

Lazaro, A., Brouwers, H.J.H., Quercia, G. & Geus, J.W. 2012. The properties of amorphous nano-silica synthesized by the dissolution of olivine. *Chemical Engineering Journal,* 211–212**,** 112-121.

LeBaron, P.C., Wang, Z. & Pinnavaia, T.J. 1999. Polymer-layered silicate nanocomposites: An overview. *Applied Clay Science,* 15**,** 11-29.

Lee, B.Y. & Kurtis, K.E. 2010. Influence of tio_2 nanoparticles on early c_3s hydration. *Journal of the American Ceramic Society,* 93**,** 3399-3405.

Li, G. 2004. Properties of high-volume fly ash concrete incorporating nano-SiO_2. *Cement and Concrete Research,* 34**,** 1043-1049.

Li, H., Xiao, H. & Ou, J. 2004a. A study on mechanical and pressure-sensitive properties of cement mortar with nanophase materials. *Cement and Concrete Research,* 34**,** 435-438.

Li, H., Xiao, H., Yuan, J. & Ou, J. 2004b. Microstructure of cement mortar with nano-particles. *Composites Part B: Engineering,* 35**,** 185-189.

Li, Z., Wang, H., He, S., Lu, Y. & Wang, M. 2006. Investigations on the preparation and mechanical properties of the nano-alumina reinforced cement composite. *Materials Letters,* 60**,** 356-359.

Lim, S., Mondal, P. & Cohn, I. 2012. Effects of nanosilica on thermal degradation of cement paste. *NICOM 4: 4th International Symposium on Nanotechnology in Construction.* Agios Nikolaos, Crete, Greece.

Lin, Z., Vivian, I.F. & Sobolev, K. 2012. Nano-engineered cements with improved early strength. *NICOM 4: 4th International Symposium on Nanotechnology in Construction.* Agios Nikolaos, Crete, Greece.

Lindgreen, H., Geiker, M., Krøyer, H., Springer, N. & Skibsted, J. 2008. Microstructure engineering of portland cement pastes and mortars through addition of ultrafine layer silicates. *Cement and Concrete Composites,* 30**,** 686-699.

Liu, X., Chen, L., Liu, A. & Wang, X. 2012. Effect of nano-$CaCO_3$ on properties of cement paste. *Energy Procedia,* 16, Part B**,** 991-996.

Lothenbach, B., Le Saout, G., Gallucci, E. & Scrivener, K. 2008. Influence of limestone on the hydration of portland cements. *Cement and Concrete Research,* 38**,** 848-860.

Lothenbach, B., Scrivener, K. & Hooton, R.D. 2011. Supplementary cementitious materials. *Cement and Concrete Research,* 41**,** 1244-1256.

Luckham, P.F. & Rossi, S. 1999. The colloidal and rheological properties of bentonite suspensions. *Advances in Colloid and Interface Science,* 82**,** 43-92.

Lukošiūtė, I. & Čėsnienė, J. 2012. Nanoclay modification report. D4.1. *FIBCEM project, Lietuvos Energetikos Institutas.*

Lukošiūtė, I. & Čėsnienė, J. 2013a. Modified nanoclays report. D4.2. *FIBCEM project, Lietuvos Energetikos Institutas.*

Lukošiūtė, I. & Čėsnienė, J. 2013b. Nanoclay developments report. D4.5. *FIBCEM project, Lietuvos Energetikos Institutas.*

Lukošiūtė, I. & Čėsnienė, J. 2013c. Report on the creation of modified nanoclays. D4.3. *FIBCEM project, Lietuvos Energetikos Institutas.*

Margalha, M., Silva, A., do Rosário Veiga, M., de Brito, J., Ball, R. & Allen, G. 2013. Microstructural changes of lime putty during aging. *Journal of Materials in Civil Engineering,* 25**,** 1524-1532.

McCarthy, M.J. & Dhir, R.K. 2005. Development of high volume fly ash cements for use in concrete construction. *Fuel,* 84**,** 1423-1432.

McCarthy MJ, Jones MR, Zheng L and Dhir RK (2008) New Approach to Fly Ash Processing and Applications to Minimise Wastage to Landfill. Final Report to Defra Project No WR0401, University of Dundee, UK.

Mendoza, O. & Tobón, J.I. 2013. An alternative thermal method for identification of pozzolanic activity in $Ca(OH)_2$ / pozzolan pastes. *Journal of Thermal Analysis and Calorimetry***,** 1-8.

Merlino, S., Bonaccorsi, E. & Armbruster, T. 2001. The real structure of tobermorite 11 angstrom: Normal and anomalous forms,od character and polytypic modifications *Eur. J. Mineral,* 13**,** 577–590.

Meyer, C. 2009. The greening of the concrete industry. *Cement and Concrete Composites,* 31**,** 601-605.

Mindess, S. & Young, J.F. 1981. *Concrete,* London: Englewood Cliffs ; London : Prentice-Hall

MIT 2013. Green paper: Improving concrete sustainability through alite and belite reactivity. MIT Concrete Sustainability Hub, Concrete Science Platform, http://www2.cement.org/exec2/PDFs/SN3228.pdf. ". [Accessed 9-7-2014].

Mondal, P., Shah, S.P., Marks, L.D. & Gaitero, J.J. 2010. Comparative study of the effects of microsilica and nanosilica in concrete. *Transportation Research Record*, 6-9.

Morsy, M., Alsayed, S. & Aqel, M. 2009. Effect of nano-clay on mechanical properties and microstructure of ordinary portland cement mortar. *International Journal of Civil & Environmental Engineering IJCEE-IJENS,* 10, 23-27.

MPA 2011. Specifying sustainable concrete.

Naden, B., Calabria-Holley, J. & Mitchels, J. 2013. Report on the dispersion of modified nanoclays. D4.4. *FIBCEM project, UK Materials Research Institute & University of Bath.*

Napierska, D., Thomassen, L.C., Lison, D., Martens, J.A. & Hoet, P.H. 2010. The nanosilica hazard: Another variable entity. *Part Fibre Toxicol,* 7, 39.

Nazari, A. & Riahi, S. 2010. Microstructural, thermal, physical and mechanical behavior of the self compacting concrete containing sio2 nanoparticles. *Materials Science and Engineering: A,* 527, 7663-7672.

Neville, A.M. 1995. *Properties of concrete,* England: Harlow : Longman Group

Nguyen, D.-T., Alizadeh, R., Beaudoin, J.J., Pourbeik, P. & Raki, L. 2014. Microindentation creep of monophasic calcium–silicate–hydrates. *Cement and Concrete Composites,* 48, 118-126.

Nguyen, D.-T., Alizadeh, R., Beaudoin, J.J. & Raki, L. 2013. Microindentation creep of secondary hydrated cement phases and C–S–H. *Materials and Structures,* 46, 1519-1525.

Nie, J., Ke, Y., Zheng, H., Yi, Y., Qin, Q., Pan, F. & Dong, P. 2012. Preparation and characterization of organo montmorillonite modified by a novel gemini surfactant. *Integrated Ferroelectrics,* 137, 67-76.

Nonat, A. & Lecoq, X. 1998. The structure, stoichiometry and properties of C–S–H prepared by C_3S hydration under controlled condition. *In:* Colombet, Zanni, Grimmer & Sozzani (eds.) *Nuclear magnetic resonance spectroscopy of cement-based materials.* Springer Berlin Heidelberg.

Oertel, T. 2013. *The influence of amorphous, sub-micrometer silica particles in cement pastes and mortars with very low water-to-cement ratios (ultra-high performance concrete).* PhD thesis, Universität Bayreuth.

Olivier, J.G.J., Janssens-Maenhout, G. & Peters, J.A.H.W. 2012. Trends in global co_2 emissions; 2012 report. The Hague: PBL Netherlands Environmental Assessment Agency: Ispra: Joint Research Centre.

Oltulu, M. & Sahin, R. 2011. Single and combined effects of nano-sio_2, nano-Al_2O_3 and nano-Fe_2O_3 powders on compressive strength and capillary permeability of cement mortar containing silica fume. *Materials Science and Engineering: A.*

Oltulu, M. & Şahin, R. 2014. Pore structure analysis of hardened cement mortars containing silica fume and different nano-powders. *Construction and Building Materials,* 53**,** 658-664.

Papadakis, V.G. 1999. Effect of fly ash on portland cement systems: Part i. Low-calcium fly ash. *Cement and Concrete Research,* 29**,** 1727-1736.

Papatzani, S., Paine, K. & Calabria-Holley, J. 2014. The effect of the addition of nanoparticles of silica on the strength and microstructure of blended portland cement pastes. *2014 International Concrete Sustainability Conference* Boston.

Papatzani, S., Paine, K. & Calabria-Holley, J. 2015. A comprehensive review of the models on the nanostructure of calcium silicate hydrates. *Construction and Building Materials,* 74**,** 219–234.

Papatzani, S. & Paine, K. Dispersed and modified montmorillonite clay nanoparticles for blended portland cement pastes: Effects on microstructure and strength. *In:* Fifth International Symposium on Nanotechnology in Construction (NICOM 5), 2015b Chicago. Springer - Accepted.

Pellenq, R.J.-M., Kushima, A., Shahsavari, R., Van Vliet, K.J., Buehler, M.J., Yip, S. & Ulm, F.-J. 2009. A realistic molecular model of cement hydrates. *Proceedings of the National Academy of Sciences,* 106**,** 16102-16107.

Pellenq, R.J.M., Lequeux, N. & van Damme, H. 2008. Engineering the bonding scheme in C–S–H: The iono-covalent framework. *Cement and Concrete Research,* 38**,** 159-174.

Peterson, V.K. 2003. *Diffraction investigations of cement clinker and tricalcium silicate using rietveld analysis.* PhD, University of Technology, Sydney.

Plassard, C., Lesniewska, E., Pochard, I. & Nonat, A. 2004. Investigation of the surface structure and elastic properties of calcium silicate hydrates at the nanoscale. *Ultramicroscopy,* 100**,** 331-338.

Plassard, C., Lesniewska, E., Pochard, I. & Nonat, A. Year. Intrinsic elastic properties of calcium silicate hydrates by nanoindentation. *In:* 12th International Congress on the Chemistry of Cement, 2007 Montreal, Canada.

Powers, T.C. 1965. Mechanism of shrinkage and reversible creep of hardened paste. *In:* International Conference on Structure of Concrete, 1965 London.

Powers, T.C. & Brownyard, T.L. 1946-7. Studies of the physical properties of hardened portland cement paste. Journal of American Concrete Institute, 43, pp. 101– 132, 249– 336, 469– 505, 549– 602, 669– 712, 845–880, 933–992.

Qing Ye, Zhang, Z., Kong, D. & Chen, R. 2007. Influence of nano-SiO_2 addition on properties of hardened cement paste as compared with silica fume. *Construction and Building Materials,* 21**,** 539-545.

Raki, L., Beaudoin, J. & Alizadeh, R. 2009. Nanotechnology applications for sustainable cement-based products. *Nanotechnology in Construction 3***,** 119-124.

Raki, L., Beaudoin, J., Alizadeh, R., Makar, J. & Sato, T. 2010. Cement and concrete nanoscience and nanotechnology. *Materials,* 3**,** 918-942.

Ramachandran, V.S. & Beaudoin, J.J. 2001. *Handbook of analytical techniques in concrete science and technology, principles, techniques, and applications,* New Jersey Noyes publications.

Ramachandran, V.S., Paroli, R.M., Beaudoin, J.J. & Delgado, A.H. 2002. *Handbook of thermal analysis of construction materials*: Noyes Publications/William Andrew Publishing.

Rashad, A.M. 2014. A comprehensive overview about the effect of nano-SiO_2 on some properties of traditional cementitious materials and alkali-activated fly ash. *Construction and Building Materials,* 52**,** 437-464.

Richardson, I.G. 2008. The calcium silicate hydrates. *Cement and Concrete Research,* 38**,** 137-158.

Richardson, I.G. & Groves, G.W. 1993. Microstructure and microanalysis of hardened ordinary portland cement pastes. *Journal of materials science,* 28**,** 265-277.

Ridi, F., Fratini, E. & Baglioni, P. 2011. Cement: A two thousand year old nano-colloid. *Journal of colloid and interface science,* 357**,** 255-264.

Ridi, F., Luciani, P., Fratini, E. & Baglioni, P. 2009. Water confined in cement pastes as a probe of cement microstructure evolution. *J. Phys. Chem.,* B 113**,** 3080–3087.

Sanchez, F. & Sobolev, K. 2010. Nanotechnology in concrete–a review. *Construction and Building Materials,* 24**,** 2060-2071.

Sapalidis, A.A., Katsaros, F.K. & Kanellopoulos, N.K. 2011. Pva/montmorillonite nanocomposites: Development and properties. *In:* Cuppoletti (ed.) *Nanocomposites and polymers with analytical methods.* InTech.

Sarris, E. & Constantinides, G. 2013. Finite element modeling of nanoindentation on c–s–h: Effect of pile-up and contact friction. *Cement and Concrete Composites,* 36**,** 78-84.

Scrivener, K. 2009. Nanotechnology and cementitious materials. *Nanotechnology in Construction 3***,** 37-42.

Scrivener, K.L., Füllmann, T., Gallucci, E., Walenta, G. & Bermejo, E. 2004. Quantitative study of portland cement hydration by x-ray diffraction/rietveld analysis and independent methods. *Cement and Concrete Research,* 34**,** 1541-1547.

Scrivener, K.L. & Kirkpatrick, R.J. 2008. Innovation in use and research on cementitious material. *Cement and Concrete Research,* 38**,** 128-136.

Selvam, R.P., Subramani, V.J., Murray, S. & Hall, K.D. 2009. Potential application of nanotechnology on cement based materials. Available: http://ww2.mackblackwell.org/web/research/ALL_RESEARCH_PROJECTS/2000s/2095/MBTC%202095-3004.pdf. ". [Accessed 9-5-2013].

Senff, L., Hotza, D., Repette, W.L., Ferreira, V.M. & Labrincha, J.A. 2010a. Effect of nanosilica and microsilica on microstructure and hardened properties of cement pastes and mortars. *Advances in Applied Ceramics,* 109**,** 104-110.

Senff, L., Hotza, D., Repette, W.L., Ferreira, V.M. & Labrincha, J.A. 2010b. Mortars with nano-sio2 and micro-sio2 investigated by experimental design. *Construction and Building Materials,* 24**,** 1432-1437.

Sinha Ray, S. & Okamoto, M. 2003. Polymer/layered silicate nanocomposites: A review from preparation to processing. *Progress in Polymer Science,* 28**,** 1539-1641.

Skinner, L.B., Chae, S.R., Benmore, C.J., Wenk, H.R. & Monteiro, P.J.M. 2010. Nanostructure of calcium silicate hydrates in cements. *Physical Review Letters,* 104**,** 195502.

Snellings, R., Salze, A. & Scrivener, K.L. 2014. Use of x-ray diffraction to quantify amorphous supplementary cementitious materials in anhydrous and hydrated blended cements. *Cement and Concrete Research,* 64**,** 89-98.

Sobolev, K., Flores, I., Hermosillo, R. & Torres-Martínez, L.M. 2006. Nanomaterials and nanotechnology for high-performance cement composites. *Proceedings of ACI Session on "Nanotechnology of Concrete: Recent Developments and Future Perspectives", Denver, USA*.

Sobolev, K., Flores, I., Torres-Martinez, L., Valdez, P., Zarazua, E. & Cuellar, E. 2009a. Engineering of sio_2 nanoparticles for optimal performance in nano cement-based materials. *NICOM 4: 4th International Symposium on Nanotechnology in Construction.* Agios Nikolaos, Crete, Greece.

Sobolev, K., Flores, I., Torres-Martinez, L.M., Valdez, P.L., Zarazua, E. & Cuellar, E.L. 2009b. Engineering of sio_2 nanoparticles for optimal performance in nano cement-based materials. *In:* Bittnar, Bartos, Němeček, Šmilauer & Zeman (eds.) *Nanotechnology in construction 3.* Springer Berlin Heidelberg.

Sobolev, K. & Gutiérrez, M.F. 2005a. How nanotechnology can change the concrete world: Part one of a two-part series. *American Ceramic Society Bulletin,* 84**,** 14.

Sobolev, K. & Gutiérrez, M.F. 2005b. How nanotechnology can change the concrete world: Part two of a two-part series. *American Ceramic Society Bulletin,* 84**,** 16-19.

Sobolev, K. & Sanchez, F. 2012. The application of nanoparticles to improve the performance of concrete. *NICOM 4: 4th International Symposium on Nanotechnology in Construction.* Agios Nikolaos, Crete, Greece.

Sobolev, K., Tabatabai, H., Zhao, J., Oliva, M.G., Flores-Vivian, I., Rivero, R., Rauf, R. & Muzenski, S. 2013. Superhydrophobic engineered cementitious composites for highway bridge applications: Technology transfer and implementation. University of Wisconsin-Milwaukee & University of Wisconsin-Madison.

Soin, A.V., Catalan, L.J.J. & Kinrade, S.D. 2013. A combined qxrd/tg method to quantify the phase composition of hydrated portland cements. *Cement and Concrete Research,* 48**,** 17-24.

Soleymani, F. 2012. Optimum content of sio_2 nanoparticles in concrete specimens. *Journal of American Science,* 8**,** 432-437.

Sorrentino, F. 2011. Chemistry and engineering of the production process: State of the art. *Cement and Concrete Research,* 41**,** 616-623.

Sprung, S. & Siebel, E. 1991. Assessment of the suitability of limestone for producing portland limestone cement (pkz). *Zem.–Kalk–Gips,* 44**,** 1-11.

Stefanidou, M. & Papayianni, I. 2012. Influence of nano-sio_2 on the portland cement pastes. *Composites Part B: Engineering,* 43**,** 2706-2710.

Supit, S. & Shaikh, F. 2014. Durability properties of high volume fly ash concrete containing nano-silica. *Materials and Structures***,** 1-15.

Taylor, H.F.W. 1950. Hydrated calcium silicates: Part i. Compound formation at ordinary temperatures. *J. Chem. Soc.***,** 3682-3690.

Taylor, H.F.W. 1986. Proposed structure for calcium silicate hydrate gel. *Journal of the American Ceramic Society,* 69**,** 464-467.

Tennis, P.D. & Jennings, H.M. 2000. A model for two types of calcium silicate hydrate in the microstructure of portland cement pastes. *Cement and Concrete Research,* 30**,** 855-863.

Thomas, J.J. & Jennings, H.M. 2006. A colloidal interpretation of chemical aging of the C–S–H gel and its effects on the properties of cement paste. *Cement and Concrete Research,* 36**,** 30-38.

Tishmack, J.K., Olek, J. & Diamond, S. 1999. Characterization of high-calcium fly ashes and their potential influence on ettringite formation in cementitious systems. *Cement, Concrete, and Aggregates,* 21**,** 82–92.

Uddin, F. 2008. Clays, nanoclays, and montmorillonite minerals. *Metallurgical and Materials Transactions A,* 39**,** 2804-2814.

Ulm, F.-J. 2012. Nano-engineering of concrete. *Arabian Journal for Science and Engineering,* 37**,** 481-488.

Urdan, T.C. 2010. *Statistics in plain english, third edition*: Taylor & Francis.

Utracki, L.A. 2004. *Clay-containing polymeric nanocomposites - volume 1,* Shawbury, Shrewsbury, Shropshire, SY4 4NR, United Kingdom: Rapra Technology Limited.

Vandamme, M., Ulm, F.-J. & Fonollosa, P. 2010. Nanogranular packing of C–S–H at substochiometric conditions. *Cement and Concrete Research,* 40**,** 14-26.

Vazquez, A., López, M., Kortaberria, G., Martín, L. & Mondragon, I. 2008. Modification of montmorillonite with cationic surfactants. Thermal and chemical analysis including cec determination. *Applied Clay Science,* 41**,** 24-36.

Vera-Agullo, J., Chozas-Ligero, V., Portillo-Rico, D., García-Casas, M., Gutiérrez-Martínez, A., Mieres-Royo, J. & Grávalos-Moreno, J. Year. Mortar and concrete reinforced with nanomaterials. *In:* Nanotechnology in Construction 3, May 31 to June 2, 2009 2009 Prague, Czech Republic. Springer-Verlag Berlin, 383-388.

Vogt, C. 2010. *Ultrafine particles in concrete - influence of ultrafine particles on concrete properties and application to concrete mix design.* PhD, Royal Institute of Technology

Vuk, T., Tinta, V., Gabrovšek, R. & Kaučič, V. 2001. The effects of limestone addition, clinker type and fineness on properties of portland cement. *Cement and Concrete Research,* 31**,** 135-139.

Wild, S. 2001. A discussion of the paper: Mercury porosimetry: An inappropriate method for the measurement of pore size distributions in cement-based materials. Author's reply. *Cement and Concrete Research,* 31**,** 1653-1656.

Wittmann, F.H. Year. The structure of hardened cement paste - a basis for a better understanding of the materials properties. *In:* Conf. on Hydraulic Cement Pastes: Their Structure and Properties, April 8-9 1976 Sheffield. 69-117

Wongkeo, W., Thongsanitgarn, P., Chindaprasirt, P. & Chaipanich, A. 2013. Thermogravimetry of ternary cement blends. *Journal of Thermal Analysis and Calorimetry***,** 1-12.

Xi, Y. 2006. *Synthesis, characterisation and application of organoclays.* Doctor of Philosophy, Queensland University of Technology.

Xi, Y., Martens, W., He, H. & Frost, R.L. 2005. Thermogravimetric analysis of organoclays intercalated with the surfactant octadecyltrimethylammonium bromide. *Journal of Thermal Analysis and Calorimetry,* 81**,** 91-97.

Xie, W., Gao, Z., Pan, W.-P., Hunter, D., Singh, A. & Vaia, R. 2001. Thermal degradation chemistry of alkyl quaternary ammonium montmorillonite. *Chemistry of Materials,* 13**,** 2979-2990.

Xu, A., Sarkar, S. & Nilsson, L.-O. 1993. Effect of fly ash on the microstructure of cement mortar. *Materials and Structures,* 26**,** 414-424.

Xu, A. & Sarkar, S.L. 1994. Microstructural development in high-volume fly-ash cement system. *Journal of Materials in Civil Engineering,* 6**,** 117-136.

Yang, T. 2006. *Afm study of the interactions between moisture and the surface of cementitious materials.* PhD, Swiss Federal Institute of Technology Zurich.

Ye, Q., Zhang, Z., Sheng, L. & Chen, R. 2006. A comparative study on the pozzolanic activity between nano-sio_2 and silica fume. *Journal of Wuhan University of Technology-Mater. Sci. Ed.,* 21**,** 153-157.

Ylmén, R. 2013. *Early hydration of portland cement- an infrared spectroscopy perspective complemented by calorimetry and scanning electron microscopy.* Doctoral thesis, Chalmers University of Technology.

Ylmén, R., Jäglid, U., Steenari, B.-M. & Panas, I. 2009. Early hydration and setting of portland cement monitored by ir, sem and vicat techniques. *Cement and Concrete Research,* 39**,** 433-439.

Zhang, J. & Scherer, G.W. 2011. Comparison of methods for arresting hydration of cement. *Cement and Concrete Research*.

Папатзани, С., Пэйн, К. & Калабрия-Холли, Д. 2014. Прочность и микроструктура цементного камня с добавками коллоидного sio_2 (strength and microstructure of colloidal nanosilica enhanced cement pastes (in russian)). *Цемент и его применение (Cement and its Applications),* 4**,** 80-85.

APPENDIX: PAPERS

1. **Papatzani S**, Paine K, Calabria-Holley J. 2015. A comprehensive review of the models on the nanostructure of calcium silicate hydrates. Construction and Building Materials; 74, 219–234. http://www.sciencedirect.com/science/article/pii/S0950061814011738
2. **Папатзани, С**., Пэйн, К. & Калабрия-Холли, Д. 2014. Прочность и микроструктура цементного камня с добавками коллоидного sio2 (strength and microstructure of colloidal nanosilica enhanced cement pastes (in russian)). Цемент и его применение (Cement and its Applications), 4, 80-85.

   http://opus.bath.ac.uk/41363

3. Calabria-Holley J, Paine K, **Papatzani S**. 2014 Effects of nanosilica on the calcium silicate hydrates in Portland cement-fly ash systems. Advances in Cement Research.;26:1-14. http://opus.bath.ac.uk/39310/
4. **Papatzani S**, Paine K, Calabria-Holley J, 2014 The effect of the addition of nanoparticles of silica on the strength and microstructure of blended Portland cement pastes. 2014 International Concrete Sustainability Conference, Boston. http://www.nrmcaevents.org/?nav=display&file=648
5. **Papatzani S**, Paine K. Dispersed and modified montmorillonite clay nanoparticles for blended Portland cement pastes: Effects on microstructure and strength. NICOM5, Chicago, 2015; Accepted.